What the Orne River tells about the former steelmaking activities : chemical and mineralogical investigations on sediments

Hussein Kanbar

University of Lorraine and the Lebanese University

Dissertation

in Geosciences

By

Hussein Jaafar KANBAR

What the Orne River tells about the former steelmaking activities: chemical and mineralogical investigations on sediments

Defense date: 11 July 2017

Jury members

Reviewer	Ms. Alexandra COURTIN-NOMADE, Professor, University of Limoges
Reviewer	Mr. Baghdad OUDDANE, Professor, University of Lille
Examiner	Mr. Christophe HISSLER, Dr, Senior researcher, Luxembourg Institute of Science and Technology
Examiner	Mr. Adib KFOURY, Associate professor, University of Balamand
Director	Mr. Frédéric VILLIERAS, Research director, CNRS-France, University of Lorraine
Co-director	Ms. Emmanuelle MONTARGES-PELLETIER, Researcher, CNRS-France, University of University
Director	Mr. Antoine EL SAMRANI, Professor, EDST, The Lebanese University
Co-director	Ms. Veronique KAZPARD, Professor, EDST, The Lebanese University
Invited member	Ms. Laurence MANSUY-HUAULT, Senior Lecturer, University of Lorraine
Invited member	Mr. Milad FAKHRY, Dr, CNRS-Lebanon

L'Université de Lorraine et l'Université Libanaise

Thèse

en Géosciences

Par

Hussein Jaafar KANBAR

Sur les traces de l'ancienne activité sidérurgique en Lorraine : chimie et minéralogie des sédiments de l'Orne

Soutenance publique le 11 juillet 2017

Membres du jury

Rapporteur	Mme. Alexandra COURTIN-NOMADE, Professeur, Université de Limoges
Rapporteur	M. Baghdad OUDDANE, Professeur, Université de Lille
Examinateur	M. Christophe HISSLER, Dr, Chargé de Recherche, Luxembourg Institute of Science and Technology
Examinateur	M. Adib KFOURY, Professeur associé, University of Balamand
Directeur	M. Frédéric VILLIERAS, Directeur de recherche, CNRS-France, Université de Lorraine
Co-directeur	Mme. Emmanuelle MONTARGES-PELLETIER, Chargée de Recherche, CNRS-France, Université de Lorraine
Directeur	M. Antoine EL SAMRANI, Professeur, EDST, l'Université Libanaise
Co-directeur	Mme. Veronique KAZPARD, Professeur, EDST, l'Université Libanaise
Invitée	Mme. Laurence MANSUY-HUAULT, Maître de conférences, Université de Lorraine
Invité	M. Milad FAKHRY, Dr, CNRS-Liban

ACKNOWLEDGEMENTS

This Ph.D. work was realized in “Laboratoire Interdisciplinaire des Environnements Continentaux (LIEC)”, Université de Lorraine, part of the “UMR 7360 CNRS-Université de Lorraine” research unit. I would like to thank the jury members for taking the time to be part of the defense and assess this work, namely Ms. Alexandra COURTIN-NOMADE, Mr. Baghdad OUDDANE, Mr. Adib KFOURY, Mr. Christophe HISSLER, Mr. Milad FAKHRY and Ms. Laurence MANSUY-HUAULT.

I would like to express my gratitude to all the people of LIEC-Charmois. First I would like to thank Ms. Mariam MOUSSA, whom I shared the office with for 22 months. Mr. Renaud GLEY (aka Monsieur GLEY) was always more than ready to help in the lab and on the field (even post-field work); whenever I had a question concerning the French language, he was always sought. Gratitude goes to Ms. Celine CAILLET and Mr. Yves WALDVOGEL, notably for the training on the laser grain size distribution analyzer and for discussions on the software. Ms. Isabelle BIHANNIC is acknowledged for her help with XRD (training, operation and mineral identification). Mr. Allan BAUER, who accompanied us on all sampling campaigns is appreciated. I also thank Mr. Fabrice FRAYSSE, who helped with the light microscope. Mr. Pierre-Yves ARNOULD, who was a lot of times stuck with some laptop/network troubles with me; even though it was not his job, he always shared his concerns and found solutions to the issues. Mr. Manuel PELLETIER, who was probably one of the first people who I came to know at LIEC; Manuel made my stay very comfortable, even before I arrived! Thank you. I would also like to express my gratitude to Ms. Nicole MAGNABOSCO and Ms. Tiffany GUYONNET. For all the Ph.D. students that I had the pleasure to meet, Mr. Mathieu LE MEUR, Mr. Fayez ABOHELOU, Mr. Romain PRESENT, Mr. Tareq ARRAJ and Ms. Marie-Laure BONIS. I always enjoyed a cup of coffee with my “coffee buddy” Mathieu, in which we would talk about results/techniques/work and non-work stuff. I also greatly thank my Friend Tareq and his wife Bushra for their hospitality during the last period of my stay in France. I also thank Ms. Manel KHEDRI and Ms. Marie GERARDIN who worked on some aspects of the sediments before my arrival, and Ms. Marie FRANCOISE-GERARD who helped during the main coring campaign. Mr. Patrick BILLARD and Mr. Michel PICON were also present during the same sampling campaign and are acknowledged. I would also like to thank Mr. Fabien THOMAS, the director of LIEC, for accepting me as a Ph.D. student in the lab and Mr. Frédéric VILLIÉRAS for accepting to be the director of this work.

A sincere appreciation from the heart to Ms. Emmanuelle MONTARGES-PELLETIER, co-director of this work. Despite her busy schedule, Emmanuelle always found time for planning and discussions regarding the work. I gained a lot of experience from the moments we spent together on the field, in the lab, during meetings, at synchrotron facilities, when submitting abstracts and finally on the corrections of the manuscript. I consider myself very lucky to have worked with her. I also would like to thank Ms. Laurence MANSUY-HUAULT who was present during all the sampling campaigns and even stayed for the long post-coring work. Ms. Catherine LORGEOUX, Ms. Delphine CATTELOIN, Mr. Quantin RAVALET and Mr. Valéry COLLIN, who worked on the organic fractions of the samples are also thanked. The gratitude extends to Mr. Benoit LOSSON, Mr. Luc MANCEAU and Ms. Claire DELUS, who were part of the multidisciplinary work on the Orne River. I am thankfulness to Ms. Francine TEDESCO and Ms. Christine FIVET, secretary office of Lorraine University. Christine was such a help from day one.

All the people who made my stay in France comfortable and enjoyable, especially the staff of the university restaurant at Vandœuvre-lès-Nancy (resto universitaire), who I saw on a daily basis for nearly two years; I greatly acknowledge their cheerful spirits! I also thank my Lebanese friends who I enjoyed their company in France, namely Ali KANSO, Hasan MOUSSA, Hasan HAJJ-ALI, Ramez SAAD, Sabrina SHOUMAN and Samer INATY.

I also give credit to a lot of people who were indirectly involved in the work: Ms. Lise SALSI for SEM sessions, Mr. Jaafar GHANBAJA and Ms. Sylvie MIGOT for TEM sessions, Mr. Marc DESMET for providing the Quadriraft that was used for coring, Mr. Alexandre FLAMMANG for preparing thin sections, Mr. Jean-Marie FISCHBACH, Mr. Frederic DIOT and Mr. Philippe MARION for XRF Niton gun training and sessions, Mr. Jerome MARIN from SARM for chemical analyses, and Ms. Justin PAOLI for ultra-thin section preparations.

I express my gratitude to Mr. Antoine EL SAMRANI (director) and Ms. Veronique KAZPARD (co-director) for agreeing to work on this joint Ph.D. program between the Lebanese University and University of Lorraine. I also thank Mr. Fawaz EL OMAR (dean of the doctoral school) and Mr. Fouad EL HAJJ-HASSAN (laboratory director) for accepting me as a student in their labs. I extend my gratitude to Mr. Ahmad Najib KOBAISSI (head of biology and environment department), who offered to help in many aspects of the work. I wish to thank all the students and staff members at the EDST (école doctorale des sciences et technologie) who made the stay at the lab comfortable. Thank you Ms. Nour HANNA, Ms.

Rana MHANNA, Ms. Rawaa AMMAR (aka magnificent BUILDER), Mr. Elias MAATOUK, Ms. Yara RAHME, Mr. Mohamad EL HAJJ, Ms. Ikram El HAJJ-HASSAN, Ms. Sarah HADDAD, Ms. Sahar RIHANE, Ms. Manal HOUHOU and Mr. Ali HAMMOUD.

For the funding programs, I thank ANR (MOBISED project, ANR-14-CE01-0019), the LTER-France and Region Lorraine through the research network of Zone Atelier Moselle (ZAM) and Long-Term Ecosystem Research (LTER) France for partially funding the work. I also thank ERASMUS-MUNDUS program and Ms. Delphine LAURANT (in charge of the project management). "This project has been funded with support of the European Commission. This manuscript reflects the view only of the author, and the Commission cannot be held responsible for any use which may be made of the information contained therein".

I would like to greet my siblings, Mahmoud, his wife Rana MONZIR and their kids Jaafar and Abbas, Soular and her husband Khalil SROUR and their kids Ibrahim, Zahraa, Hawraa and Haidar; Zahraa and her husband Alloushi IDRISS, their kids Hasan and Hussein; and my parents Jaafar and Samar. Finally, my friends, Beel, Smerson and Weelnem….. thanks a lot for the "*memories*" that we had, and the "*memories*" that are yet to come.

TABLE OF CONTENTS

ABBREVIATIONS AND ACRONYMS

µ-XRF	Micro-X-ray fluorescence
AMD	Acid mine drainage
ANC	Acid neutralizing capacity
AVS	Acid volatile sulfides
BF	Blast furnace
BFS	Blast furnace sludge
BOF	Basic oxygen furnace
BSE	Back-scattered electrons
BSi	Biogenic silica
CEC	Cation exchange capacity
CF	Contamination factor
CRPG	Centre de recherches pétrographiques et géochimiques
EAF	Electric arc furnace
EC	Electric conductivity
EDXS	Energy dispersion of X-ray spectroscopy
EF	Enrichment factor
EMPL	Établissement public de la métropole Lorraine
EPS	Extracellular polymeric substances
EU	European union
EXAFS	Extended X-ray absorption fine structure
FA	Fulvic acids
FESEM	Field-emission scanning electron microscopy
FNU	Formazin naphelometric units
ICP-MS	Inductively coupled plasma mass spectrometry
ICP-OES	Inductively coupled plasma optical emission spectrometry
I_{geo}	Geoaccumulation index
IRIS	Indicator of reduction in soil
LCF	Linear combination fitting
LDH	Layered double hydroxide
MTE	Metallic trace elements
OM	Organic matter
ORP	Oxidation reduction potential
PAH	Polycyclic aromatic hydrocarbon
PCB	Polychlorinated biphenyls
PLI	Pollution load index
ppm	Part per million
PVC	Polyvinyl chloride
Q25	1^{st} quartile
Q75	3^{rd} quartile
SAED	Selected area electron diffraction
SARM	Service d'analyse des roches et des minéraux
SEM	Scanning electron microscopy
SPM	Suspended particulate matter
spp.	Species (plural), the singular noun is sp.

STXM	Scanning transmission X-ray microscopy
TEM	Transmission electron microscopy
TSS	Total suspended solid
WWII	World war II
WWTP	Wastewater treatment plant
XANES	X-ray absorption near edge spectroscopy
XAS	X-ray absorption spectroscopy
XRD	X-ray diffraction
yr	Year
ZAM	Zone atelier Moselle

LIST OF TABLES

LIST OF FIGURES

LIST OF EQUATIONS

LIST OF SUPPLEMENTARY MATERIALS

GENERAL INTRODUCTION

Being non-degradable and causing risk to biota, the behavior and fate of metals in the environment are of great concern. Metals are mainly found in particulate phases (minerals), and to a lesser extent as dissolved and colloidal phases. Whatever the phase, metal introduction into the environment might be triggered by lithogenic as well as anthropogenic activities. Moreover, metal containing phases consequently reach water systems via surface run-off. In the river, particulate matter settles and forms sediments, preferentially at sites where water current slows down; otherwise, particles continue their way till they reach oceans/seas. Unfortunately, man-made activities violate the natural mineral/elemental cycles. For example, dams create preferential settling sites for waterborne particles; part of the severity emerges when metal rich particles settle in upstream zones of dams. Dams are usually built for human welfare, such as to create water reservoirs for agricultural needs and livestock, and to generate electricity. Industrial facilities might also need water sources, which are usually connected to the well-being of different production processes. Indeed, that was the case of the steelmaking facilities that were constructed in the Lorraine region during the last two centuries, notably near the Orne River (study site), where several small dams were built.

The Orne River is a tributary of the Moselle River and is located northeastern France. The vicinity of the Orne River was packed with mining and iron metallurgy, and most importantly steelmaking facilities. In addition to being a cooling source for blast furnaces, Orne water was used for cleaning procedures (e.g. for wet scrubbing of furnace smokes and dust); possible waste and by-product release into the Orne River is expected to have happened. Many sites along the Orne River course showed sediments that were mainly made from steelmaking wastes and by-products. In fact, the Orne River is well acknowledged as a highly polluted part of the Moselle River that still needs to be cleaned (Garcier, 2007). During the last decades of the previous century, part of the contaminated sediments was dredged; unfortunately, some contaminated sediments were subsequently remobilized further downstream. Eventually, only a relatively small river section was cleaned. Other contaminated deposits were not dredged, and the remobilized deposits are expected to have spread in the river and settled in other places, particularly upstream of dams. The maintenance and well-being of Orne River dams are expensive, especially since these structures are old and require constant management. In addition, the EU Water Framework Directive (adopted in 2000) proposed to remove any structures that would alter the natural river flow (EU Council, 2000). The problem arises here

since contaminated particulate matter that originated from former steelmaking facilities are present in some locations along the Orne River, especially upstream of dams.

Dam removal or modification will surely cause the remobilization and spreading of contaminated sediments; consequently, aquatic biota will be damaged and the river water might become useless, or even harmful for domestic, agricultural as well as industrial usage. Therefore, a detailed knowledge about sediment characteristics should be established, such as the mineralogical composition and chemical speciation, as well as the main metal carriers. The possible behavior can consequently be revealed. Indeed, sediments form storage zones for metals, which are found as heterogeneous mineral, organic and bio-organo-mineral complexes.

The thesis is part of a ZAM research project dedicated to study the impact of anthropogenic activities in the water compartments of Lorraine; an axis of the ZAM project focuses on the sedimentary archives that formed by the contribution of industrial activities and changing land use over the past years. The **objectives** of this study are to scan sediments along the course of the Orne River, to determine the variability of sediment characteristics and possible anthropogenic and lithogenic contributions, and to uncover deep sediments that might hold the fingerprint of former industrial activities. The objectives were realized by sediment characterization starting from bulk parameters, and ending at sub-micrometric and atomic levels, which will be revealed accordingly in the brief introductions of each chapter.

The manuscript is divided into 5 chapters. The first two chapters include the literature review and information about the sampling sites; the other three include results that are presented in the form of articles. Therefore, the “Materials and methods” section will be included accordingly in the chapters, instead of a distinct chapter.

Chapter 1: This chapter presents the **literature review**. The main notion evolves around the formation and cycle of particulate matter that form sediments, transport and settling mechanisms of suspended matter, importance of dams as sediment storage zones and natural flow disrupters, possible bio-geo-chemical transformations, and likely lithogenic and anthropogenic sources of metals and metal holding phases. Afterwards, the attention is shifted to river sediments, variation in grain size, dating techniques and the fate and behavior of metals, with special attention on Fe and Zn. The precipitation and dissolution of sulfides and oxy-hydroxides, and the association of metals to those phases are mainly discussed. Some methods used for mineralogical and chemical identification, such as X-ray, microscopic and

spectroscopic techniques are included. Finally, the role of variable physico-chemical parameters on the fate of metals is included.

Chapter 2: Since the contaminated deposits in the **Orne River** are sourced from former **steelmaking facilities**, a review on the **processes** that eventually form steel and different wastes and by-products is presented. The first part of the chapter is dedicated to the **Orne basin**, located in the Moselle basin, northeastern France. The Orne watershed is described in terms of **geology**, and the river is described in terms of **hydrology and physico-chemical parameters**. Then, the development of the main industrial facilities in the Orne area, mainly the steelmaking ones, is included. A few aerial images that were taken in the last century are also included to show the exact locations and the intense industrialization near the Orne River. Locations and dates of dredging are followed. Afterwards, a glimpse about the worldwide development of **iron mining** and **steelmaking** is given. This is then followed by the different steps that come before steelmaking, such coal combustion, coke production, iron mining and refining. The different raw materials, their mineralogical and chemical composition, the fate of metals, the products, and by-products used in each step are discussed. The focus is made on the sources, fate and released forms of Fe, Zn and Pb. Additionally, the composition and fate of the output materials, such as sludge, slag and dust particles are presented accordingly. The chapter then ends with information about the sampling sites (e.g. number and type of samples, the depths of sediment cores, coordinates and dates of collection), the context of the study and the objectives of the thesis.

Chapter 3: This chapter deals with **surface sediments** that were collected along the course of the Orne River. Since the Orne basin was heavily industrialized during the previous two centuries, and is currently urbanized, sediment samples were collected at different points to check if variation in sediment characteristics could be noted along the river course. Firstly, the chemical composition of Orne sediments as a function of grain size was revealed. Grain size parameters, water content and pH variations were then related to hydrodynamic conditions of the river. Afterwards, the variation in chemical and mineral composition was revealed to be mainly related to the lithology of the basin. The major crystalline mineralogy of bulk sediments was revealed by XRD, while micrometric and sub-micrometric crystalline, poorly crystalline and amorphous phases were identified by SEM and TEM. The nature of clay minerals was shown by oriented XRD patterns and TEM-EDXS. Since the Orne basin is relatively small on one hand, and did not show significant change in lithology on the other, the chemical

composition of Orne sediments were compared to sediments that were collected along the Moselle River, which is included in the *appendix to chapter 3*.

Most of the sediments presented in *chapter 3* were collected as cores. Even though the surface sediments were generally comparable in terms of chemical and mineralogical composition, deeper sediments showed some unique features. Despite the fact that several sediment cores were collected along the river course, the coming chapters include the sediments located upstream of the Beth dam, at Moyeuvre-Grande. Beth sediments clearly evidenced that the deposits originate from the former steelmaking facilities.

Chapter 4: The chapter presents data about sediments that had settled upstream of the Beth dam. Several cores were collected in the upstream zone of the dam, and the seriousness of the anthropogenic nature was well established in terms of chemical and mineralogical composition. First, ^{137}Cs and ^{210}Pb dating clearly evidenced that the sediments had not formed in conventional ways. The chemical composition showed that the surface sediments are mainly made from detrital material, while deeper layers showed unique characters. Indeed, the distinct **iron mineralogy** revealed by XRD, SEM and TEM was shown to be a fingerprint of deposits that originated from steelmaking wastes. Furthermore, that idea was mainly evidenced by Fe mineral species that were related to the materials used in the steelmaking processes in Lorraine (which was already presented in *chapter 2*), such as ferrospheres, goethite nanoparticles and Fe rich aluminosilicates. The last two were predominantly found in the contaminated sediments, mainly in the fine fractions. The weathering status of the unique Fe minerals was then discussed, based on what is known on the fate of steelmaking wastes in settling ponds and river systems. The exceptional structure of the Fe-aluminosilicates could eventually be used as a fingerprint of the weathered steelmaking wastes.

The distinctive status of the deposits that settled upstream the Beth dam demanded some elaboration on the dates of settling; this is included in *appendix to chapter 4.* Since conventional dating using ^{137}Cs and ^{210}Pb could not evidence the actual age of the sediments, a different approach was used, which mainly considered particle size distribution, major chemical composition and data of previous flood events.

Chapter 5: Being an element originated from former steelmaking facilities on one hand, and being evidenced in association to unique amorphous species, **zinc speciation** was discussed, mainly by SEM, TEM and X-ray absorption spectroscopy at the Zn K-edge. As expected in anoxic sediments, zinc was majorly carried by sulfides. Indeed, different zinc and

polymetallic sulfides (Fe-Zn and Fe-Zn-Pb) were evidenced by TEM. However, Zn was not exclusively associated to sulfides, rather, the predominant Fe-aluminosilicates (discussed in *chapter 4*) also demonstrated to be Zn carriers. Finally, XANES spectra at the Zn K-edge and linear combination fitting (LCF) showed that the main Zn carriers were sulfides (amorphous and crystalline), followed by Fe oxy-hydroxides and clay.

Finally, a *general discussion, conclusion, perspectives, recommendations* about sediment management, and a summarizing schema about the status of Beth sediments are presented.

I. CHAPTER 1: STATE OF THE ART

1. Interests of sediments in environmental studies

Sedimentary deposits in freshwater can form under natural and artificial conditions, in lotic (e.g. brooks, streams and rivers) and lentic (e.g. ponds, lagoons and lakes) water bodies. Sedimentation generally occurs when water current, which is loaded with suspended matter, slows down, which might be the case of estuaries, river junctions and dammed rivers (Naden, 2010). Indeed, those locations usually mark sedimentary archives that might have formed a few meters (more or less) of deposits during tens, hundreds, or even thousands of years. In some cases, tens of meters of sediments form in large lakes; an example is 12 meters of lacustrine sediments that had deposited during approximately 10 thousand years in Lake Ontario, Canada (Meyers, 2003). Therefore, sedimentary archives dating back to thousands or millions of years can be found in fresh water deposits (e.g. Kitagawa and van der Plicht, 1998; Sadori et al., 2013), but are more common in marine sediments, and might reach tens and hundreds of meters (e.g Fontugne and Duplessy, 1986; Løvlie et al., 1986). Sedimentary archives can provide various information. For example, deep marine sediments have been used for revealing past elemental cycles, such as Si using isotopic composition of biogenic silica ($\delta^{30}Si_{BSi}$) (Frings et al., 2016), mountain formation (Webb et al., 1984), climate modification (Petit et al., 1999), paleo-environmental records using carbon isotope ^{14}C (Voelker et al., 1998) and possible biological evolution, including humans during Paleolithic and Neolithic (Donges et al., 2011). Nonetheless, studies on fresh water sediments highlight relatively ancient history as well, i.e. more than 100 years (e.g. Komárek et al., 2008 and articles cited therein). Some of those studies focused on environmental history using palynology, organic and aquatic/macrophyte indications (Bertrand et al., 2013, 2012), climate change and impact of human activities on local environments (Meyers, 2003), and change in food web using organic fingerprints ($\delta^{15}N$ and $\delta^{13}C$) and planktonic organisms (Perga et al., 2010). Other studies concern more recent sediments, and focus on organic pollution history and sources (Bertrand et al., 2015; Heim and Schwarzbauer, 2013), and following trajectory and dynamics of pollutants due to flooding events (Dhivert et al., 2015a, 2015b). It should be noted that researches focusing on sedimentary archives as a tool for tracing metal input to the environment, such as marine, lake and stream sediments, peat bogs and soils, have been growing (Komárek et al., 2008). The manuscript will only concern riverine sedimentary deposits.

2. Sediment formation processes

Sediments are defined as the materials that settle (or sediment). In the case of rivers, sediments are composed of autochthonous[i] and allochthonous[ii] materials that settle in riverbeds. Moreover, sediments are mainly formed from weathering processes, such as erosion, degradation and bio-geo-chemical breakdown of rock materials. Therefore, biotic as well as abiotic processes are involved in sediment formation. Initially, continental weathering and rock erosion, at the rock-atmosphere interface, are considered the main sources of sedimentary materials (as well as soils). Weathering of rocks is mainly achieved by chemical and physical (i.e. mechanical) processes that can affect any type of rock (namely igneous[iii], metamorphic[iv] and sedimentary[v]) and transform part of relatively large rocks into fragments (called clasts, debris or detritus), which are initially and essentially minerals (inorganic). Those fragments, of finer nature with respect to the parent rocks, are more susceptible to weathering. Indeed, chemical weathering reactions take place on the surface of the materials; thus, explaining higher weathering rates for particles with higher surface area to volume ratio (Figure I-1). Most common reactions involved in weathering are hydration, hydrolysis, oxidation, reduction and carbonation. Part of the chemical weathering is achieved by biotic processes. Plant roots, fungi and lichens secrete organic acids that are involved in rock and rock fragment dissolution; microbes break down rock materials as well. Biotic processes are also involved in the physical weathering, such as the break-up and cracking of rocks by plant roots and burrowing animals (Marshak, 2011a; Négrel et al., 2014). It should be noted that the processes involved in weathering (i.e. chemical, mechanical, biotic and abiotic processes) are not independent, rather the processes are all involved in rock and rock fragment disintegration. With time, the products of the weathered materials form layers of soil on land (Marshak, 2011a; Velde, 1995); however, some of the fragments reach rivers via several pathways, such as land erosion, wind and surface run-off. In that case, and after a pathway prone to chemical, physical and bio-geo-chemical transformations, the waterborne fragments may deposit/settle/sediment in riverbeds and form sediments. In addition, organic matter, such as plant and animal debris, animal shells, microbial

[i] Materials that have formed or are originated in the same place where they are present.
[ii] Materials that have formed in or are originated from a place other than where they are present.
[iii] Rock formed from solidification and cooling of magma or lava.
[iv] Rock formed from physical and chemical transformation of any form of rock by heating and pressure.
[v] Rock formed by solidification and compaction of sediments.

colonies and biofilms are also part of the suspended and settled materials in rivers (Nichols, 2009a).

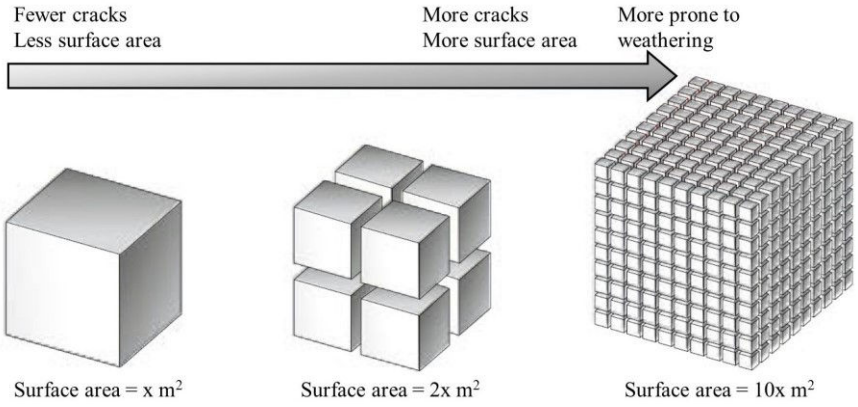

Figure I-1: The increase of surface area as a particle is more fragmented.
For the same volume, the surface area increases as more cracks or finer fragments are formed. Finer fragments will be more prone to weathering than coarser blocks.
Modified from Marshak (2011a).

The initially inorganic fragments sourced from parent rocks might form secondary minerals due to weathering, such as kaolinite, illite, chlorite and montmorillonite. Those minerals might be transformed into heterogeneous bio-organo-mineral complexes[vi] (Marshak, 2011a; Velde, 1995). The term bio-organo-mineral complex will be used to indicate that the formed flocs[vii] are rather heterogeneous and could contain biological, organic and mineralogical materials. In addition, flocs and aggregates of fine inorganic and organic particles, colloidal and/or amorphous matter occur in the water compartment and settle to form river sediments (Figure I-2). Flocs could represent a major percentage of the suspended material (Droppo and Ongley, 1994; Phillips and Walling, 1995). Diatoms, algae and bacterial colonies were proven to be a part of the bio-organo-mineral complexes in rivers as suspended matter and settled sediments (Dupont et al., 2001; Walling and Collins, 2016). Moreover, organic matter has an influential role on the formation of aggregates; for example, fulvic acids (FA), polysaccharides, algal exudates and bacterial polymeric fibers can coat and connect negative charges of colloids, consequently forming bridges or complexes of bio-organo-mineral materials (Droppo and Ongley, 1994; Wilkinson et al., 1997). Additionally, bio-organo-mineral aggregates might form from animals feces, such as from fish and zooplanktons (Dupont et al., 2001; Geesey et al., 1984). Consequently, biotic and abiotic processes carry on the (bio)-transformation[viii] and (bio)-degradation of the complexes with time.

[vi] Complex/aggregate/floc containing biological organisms (such as diatoms, algae and bacteria), organic and mineral phases.

[vii] A fluffy /woolly flocculent mass formed by flocculation, such as precipitation and aggregation.

[viii] The word (bio) is placed in parenthesis since the bio part of bio-transformation might be part of the transformation. In other words, (bio)-transformation could mean bio-transformation or transformation. The same principle applies to other terms similarly used in the text.

It should be noted that sediments and suspended matter generally mark natural and anthropogenic materials originated from watersheds. For example, the geological background of watersheds composed of carbonaceous formations will mark minerals with high carbonate contents, such as calcite and dolomite (Montargès-Pelletier et al., 2007), while those of argillaceous formation will mark clayey minerals, such as kaolinite, chlorite, montmorillonite, smectite and illite (Weaver, 1961). Some particles are introduced from water systems belonging to other watersheds located further upstream, while others are deposited in the basin from regions far from the watershed via wet and dry depositions (Thevenon et al., 2013). Therefore, autochthonous as well as allochthonous materials contribute to the formation of sediments. River sediments and suspended matter are eventually transported to seas and oceans; yet urbanization and industrialization has delimited sediment flux by forming reservoirs, which in many cases is done by constructing dams.

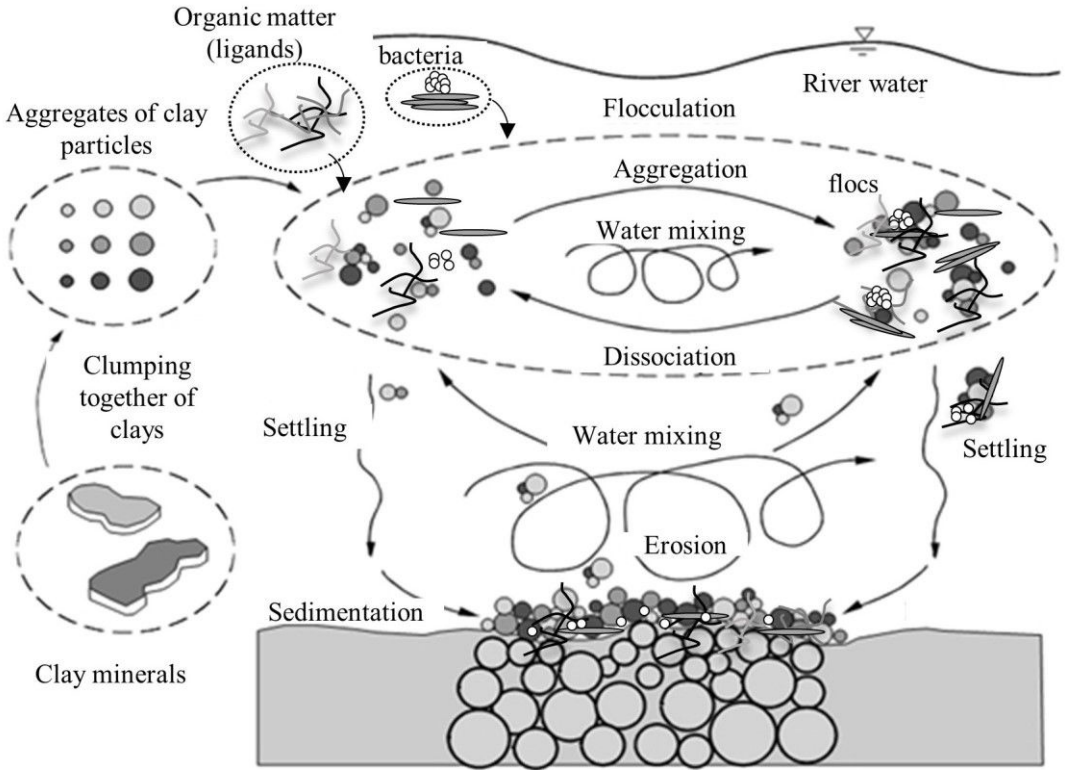

Figure I-2: Schematic representation on the formation of bio-organo-mineral complexes in river water and their settling to form sediments.
Clay particles, organic matter and bacteria form clumps/flocs in the water column. The formation and dissociation of clumps/flocs depends on the interaction between the particles as well as the water mixing. Particles are either suspended or settle to form sediments, depending on size and water hydrodynamics. Modified from Toorman and Berlamont (2016).

3. Particle transport and settling in rivers

Materials that are found in rivers can be divided into particulate, colloidal and dissolved fractions. The particulate fractions are roughly superior to 0.45 µm in diameter. The particulate fractions in river systems consist of boulders (> 256 mm), cobbles (64 – 256 mm), gravels

(composed of pebbles (4 – 64 mm) and granules (2 – 4 mm)), sands (0.064 – 2 mm), silts (2 – 64 µm) and clays (< 2 µm) (Fryirs and Brierley, 2012). It should be noted that clay minerals might be defined by sizes inferior to 2 (Hillier, 1995; Naden, 2010; Paterson, 2007) or 4 µm (Fryirs and Brierley, 2012; Nichols, 2009b; Robert, 2014; Sommerfield et al., 2007); therefore, the lower limit of silt might be either 2 or 4 µm. Moreover, the term clay is applied to the particles of sizes inferior to 2 µm (or 4 µm), and to the family of minerals that has similar chemical composition and crystal structural, such as smectites (Hillier, 1995). Riverbed material is generally composed of large boulders, cobbles and gravels, while the finer particles, such as sands, silts and clays might be part of riverbeds as well as suspended loads. Particles can be transported by rolling, saltation, traction (sliding on the riverbed, or simply referred as sliding (Fryirs and Brierley, 2012)), and as suspension in the water column (Figure I-3). Those represent the particulate phase in rivers, while dissolved phases and ions are transported in the water column. Additionally, colloidal phases, characterized by sizes between 1 nm and 1 µm, are part of the dissolved-particulate phase of rivers (Figure I-3). As mentioned in section *2*, the suspended solids and settled materials might undergo bio-geo-chemical transformations and weathering, therefore, the sizes of the materials are not constant. The sizes change during aggregation/disaggregation, complexation/de-complexation, precipitation/dissolution and sorption/desorption processes. It should be noted that the fractions deposited and transported do not necessarily depend on the size; water discharge (and water mixing) plays a major role

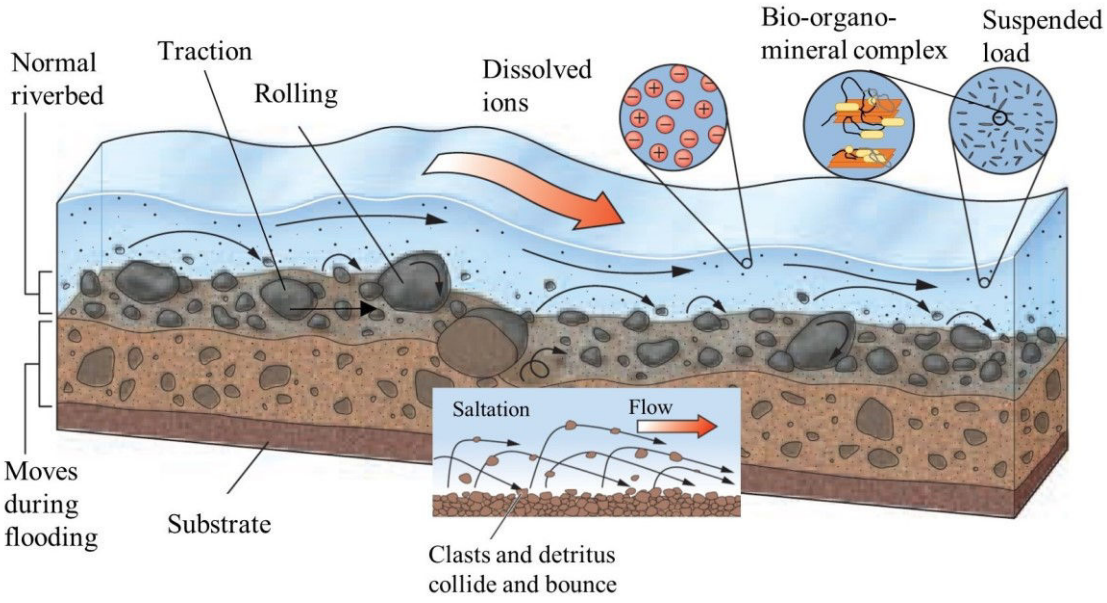

Figure I-3: Transport mode of river material.
The riverbed contains relatively coarse particles that might be rolled on the river floor or transported by suspension or saltation during flooding. Clasts, debris and detritus, of smaller sizes than the materials of the riverbed, might be transported in the river in suspension or via saltation. The suspended load contains the finest fractions, such as clays, colloids and bio-organo-mineral complexes. The dissolved phases and ions are transported in the river water. Schema modified from Marshak (2011a).

(Nichols, 2009a). Indeed, change in river hydrodynamics might cause coarse riverbed particles (e.g. boulders, cobbles and gravels) to roll or transport in the river, possibly as suspended materials during heavy inundations.

The main parameters that influence settling/transportation of grains are grain morphology (porosity, roughness or smoothness), riverbed morphology, clay content and organic ligands (which act as cohesive materials), density and viscosity of particles and fluid, temperature of the water, consolidation level, grain-grain interaction, grain sorting, electrochemical and surface tension forces, entrainment[ix] and shear stress[x] (Fryirs and Brierley, 2012; Naden, 2010; Robert, 2014). In controlled conditions, the settling velocity (also called fall velocity) is calculated by Stokes' law[xi]. The speed velocity is defined as the downward vertical motion of a particle in water, which is dependent on the size and density of the particle and fluid. The speed velocity is a major character that dictates the settling or transport of fine fractions in a suspension (Dupont et al., 2001; Naden, 2010; Robert, 2014). Nonetheless, in river systems, due to the heterogeneity of particle sizes and densities, the application of Stokes' law is rather difficult. Moreover, flow velocity and particle sizes are the key parameters in determining erosion, transportation and deposition of particles (as suspension or bedload) in rivers. Hence, the Hjulström diagram (Press and Siever, 1986), which is a simplified diagram coupling grain size (in mm) and flow velocity (in cm/s), would better describe the velocity at which different particles settle or transport (Figure I-4). It should be noted that the diagram is applicable for loose grains with diameter > 1 µm. Particles with one-dimension < 1 µm (colloids), organic matter (such as phytoplanktons and plant debris) and bio-organo-mineral complexes do not necessarily follow the Hjulström diagram. Furthermore, particles and colloids < 1 µm stay in suspension and do not settle, since they are subjected to Brownian motion[xii] (Robert, 2014). In addition to the direct correlation of flow velocity with the settling

[ix] Entrainment is the process where grains are detached from surrounding surfaces and consequently become prone to transportation. This process occurs via corrasion or cavitation. The former is a mechanical action caused by water on grain surface, while the latter is caused by different pressures applied on the grains, which causes collapse of the surface and detachment.

[x] The force applied perpendicular to the cross section of a particle that can cause its motion.

[xi] For silt and clay particles; i.e. particles < 64 µm: $V_0 = \frac{g(\rho_s - \rho)D^2}{18\mu}$; for gravels $V_0 = \sqrt{\frac{2}{3} D \frac{\rho_s - \rho}{\rho}}$. Where: V_0 is the settling velocity (m/s), g is the acceleration of gravity (m/s^2), D is the particle diameter (m), ρ_s and ρ are the densities of the particle and water/medium respectively (kg/m^3) and µ is the viscosity of the medium (kg/m/s).

[xii] Particles keep in motion due to their collision with fast moving atoms or molecules in the liquid (or gas).

and resuspension of river materials, dams are responsible for the decrease of water flow, which supports the settling of finer materials.

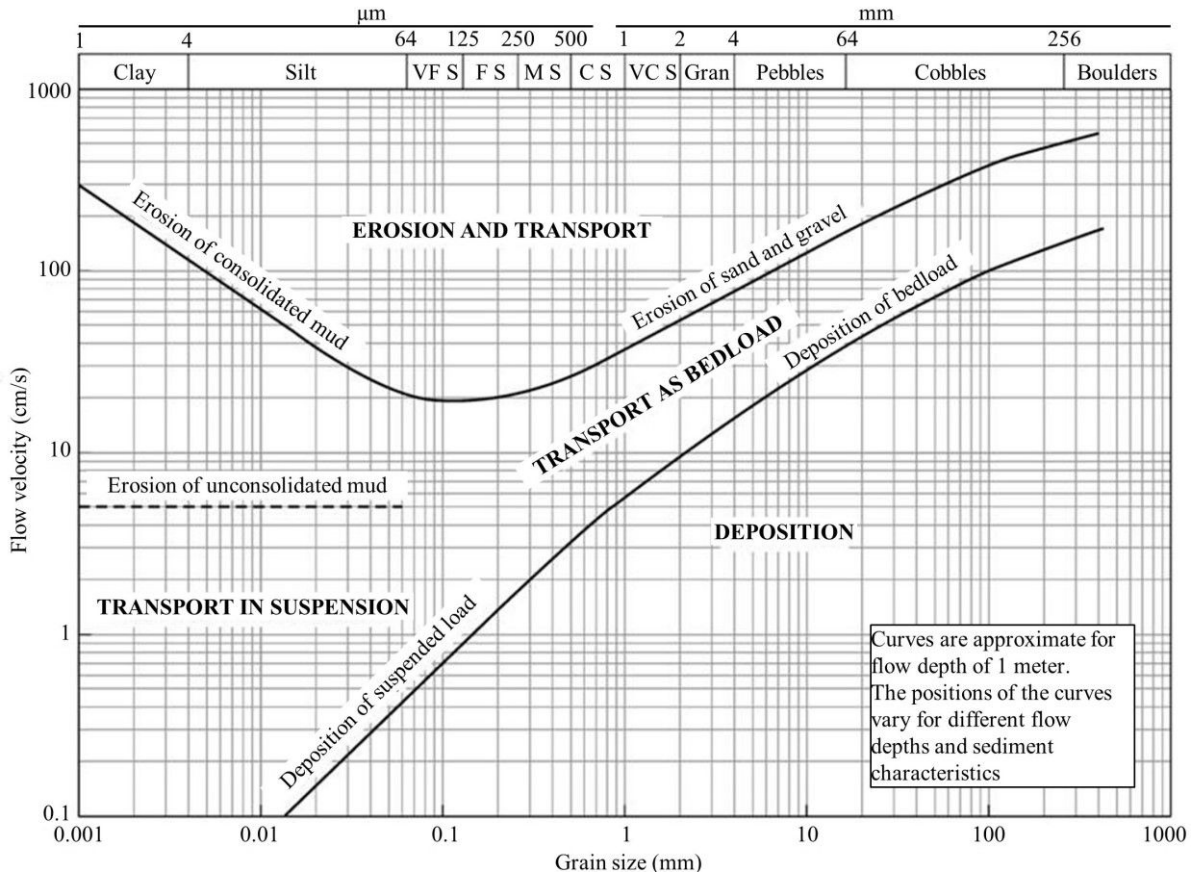

Figure I-4: Hjulström diagram showing the relationship between flow velocity, and settled and suspended particles. VF: very fine, S: sand, F: fine, M: medium, C: coarse, and Gran: granules. It should be noted that the clay fraction might also be considered as the fraction inferior to 4 µm (instead of 2 µm). Modified from Nichols (2009a).

3.1. Effects of dams on sedimentation

Dams are built for several reasons, such as fishing, agriculture, flood or water discharge control, generating electricity, cooling purposes for ovens/furnaces (e.g. for steelmaking facilities) and reserving water for drought periods. Fairly, dams are built in favor of human welfare, whereas the outcome on the environment might not be given the attention required. Upon dam construction, water hydrodynamics are modified, the collected water in the reservoir becomes static to some extent, meaning that oxygenation of the water becomes limited, evaporation increases, migration of fish is hindered and settling of suspended matter is favored; all which indicate disturbance of natural ecosystem and geochemical cycle (Babbitt, 2002; Bowman et al., 2002). For those reasons, the EU Water Framework Directive (adopted in 2000) strongly incites the European states to remove the engineered structures (including dams) that modify the natural functioning of rivers (EU Council, 2000). Nevertheless, socio-economic and ecological complications consequent to dam removal (and damming as well) should not be

overlooked on the welfare of the "natural" water flow. On the disturbance of sediment transport caused by damming, it is worth mentioning that on a study performed on 633 of the largest rivers and approximately 45,000 reservoirs, an estimation of 25 to 30% of the sediment flux was retained in reservoirs (Vörösmarty et al., 2003). Consequently, nutrient transport in fluvial systems is corrupted, mainly because nutrients are majorly held in the particulate fraction (Martin and Meybeck, 1979).

Damming enhances sedimentation by forming preferential sites for suspended matter settling due to reduced water flow. Therefore, archives of sediments develop upstream of dams, which create a suitable site for studies focusing on tracing recent history of land use via coring. Dams influence the size sorting of settled particles. Indeed, the particles that settle and form sediments (termed fluid mud in Figure I-5) are finer as approaching the dam (Fryirs and Brierley, 2012). The influence of dams on size sorting of suspended matter was seen till several kilometers before the dam (~ 5 km) (GEC, 2006; Snyder et al., 2004), depending on water flow velocity, river course morphology, coherence of aggregates and shearing stress (Fryirs and Brierley, 2012; Nichols, 2009a; Robert, 2014). Therefore, riverbeds nearest to dams are composed of finer particles, while grains become coarser further upstream (Figure I-5). The most recent deposit layer is found on the surface, while older deposits are overlaid by more recent sediments (overburden), thus causing consolidation of deep sediments and upward movement of pore water. Fluid mud layer is roughly considered as the layer prone to resuspension. The freshly deposited layer is considered as the zone of bioturbation, while the deepest consolidated zones are rather reserved and stored (according to Sommerfield et al., 2007). Consequently, and according to the size of the reservoir, riverbed morphology and transported material, the collected sediments might reach tons of what was previously being

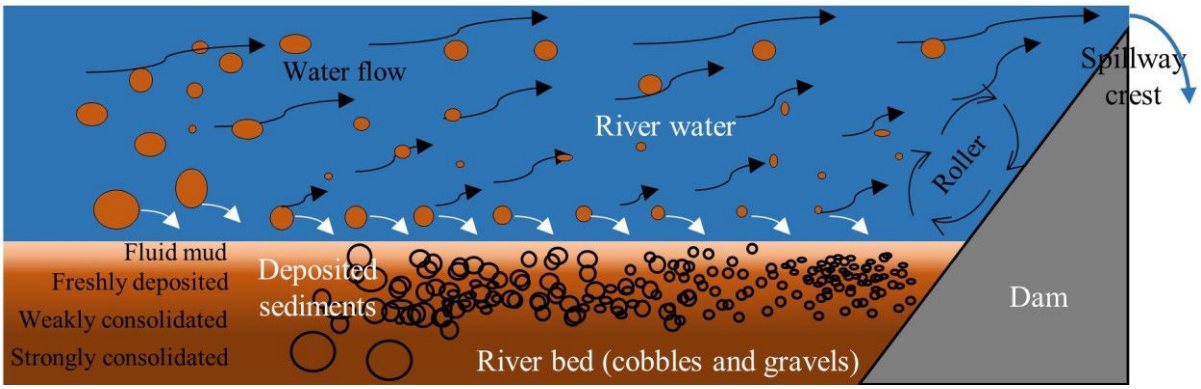

Figure I-5: Schematic representation of suspended materials and sediments, and their sizes in a reservoir zone. The water flow is shown as curved black arrows. Longer arrows indicate higher water flow. Coarser particles are transported as suspended matter at sites far from the dam where water flow is relatively high (with respect to zones nearer to the dam). The curved white arrows indicate settling of different sized suspended matter. Finer particles settle as approaching the dam. Consolidation of the settled sediments increase with depth.

transported in the river. The particularity of fine grains that settle upstream dams is important in the geochemical cycles (Martin and Meybeck, 1979). Indeed, since contaminants and metallic trace elements (MTE) are preferentially associated to and stored in fine fractions, settled materials upstream of dams are supposed to store masses of contaminated and metal laden sediments, especially in industrialized areas (e.g. Allan, 1986; Du Laing et al., 2007a).

3.2. Transformations of suspended matter and surface sediments

It was mentioned earlier in the text (sections *2* and *3*) that transformation (same as alteration) of river materials occur. These alterations may occur to suspended matter or sediments as pre- or post-depositional alterations, respectively. The post-depositional alterations included here take into consideration those occurring from hours to years (early diagenesis).

The process of suspended floc formation in freshwater systems is dependent on variable factors, such as water temperature and pH, major ions, dissolved and particulate organic carbon, suspended solid concentration, and bound microbial organisms and their exudates (Droppo and Ongley, 1994). The complexes found in river suspended matter and surface sediments (possibly flocs) play a role in chemical and biological dynamics of rivers on one hand, and on the fate of MTE and contaminants on the other (Allan, 1986; Walling, 2013). Contaminants can be associated and bound to surface complexes during or after floc formation (Droppo and Ongley, 1994). Furthermore, biological and bio-chemical transformations might change elemental speciation and/or contaminant fate (Taillefert et al., 2000). Thus, the materials present in river systems are subjected to changes, such as formation of (bio)-organo-mineral flocs or complexes. An example of a bio-organo-mineral floc is shown in Figure I-6. It should be noted that flocs might be held together by electrochemical forces and/or by sticky and filamentous materials associated with extracellular polymeric substances (EPS) (Lartiges et al., 2001; Walling and Collins, 2016). Therefore, and due to formation or dissociation of flocs, grain size is prone to variation.

Algal and bacterial exudates were shown to form EPS at the oxic – anoxic transition of a freshwater lake. Hydrous iron oxides formed aggregates with EPS, and the moiety (i.e. iron oxides bound to EPS) could further contain significant contents of lead. As a result, the formed bio-organo-mineral complexes precipitated and settled. Moreover, reductive dissolution of the formed complexes might cause Pb and Fe de-sorption or de-complexation from the bio-organo-mineral complex (Taillefert et al., 2000). Most common source of EPS are bacteria, benthic

organisms, such as micro-phyto-benthos, and microalgae (Paterson, 2001). Additionally, pre- and post-depositional transformations could be seen on the mineralogy. Indeed, the presence of organic compounds aid in the precipitation of mineral (or organo-mineral) phases in water columns (Wilkinson et al., 1997). For example, organically complexed ferrihydrite (by fulvic acids) aided in the precipitation and the formation of FA-hematite or FA-goethite complexes, according to FA concentrations and pH conditions (Kodama and Schnitzer, 1977).

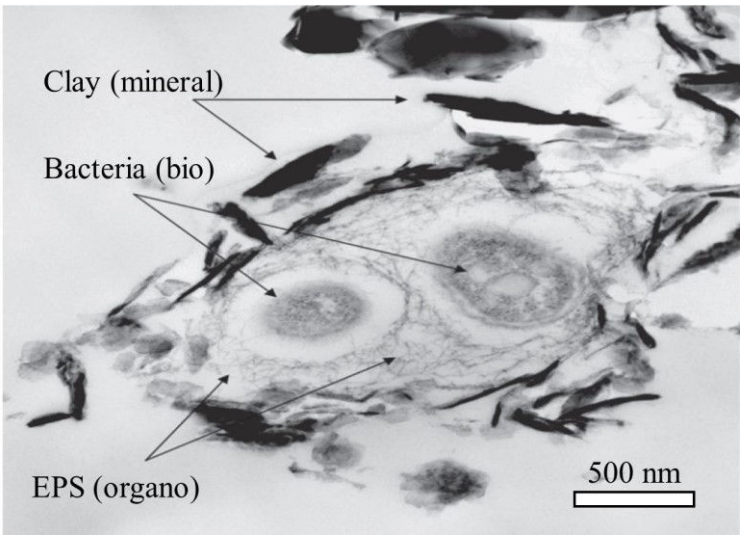

Figure I-6: Micro-image of a bio-organo-mineral complex/floc from suspended matter.
Modified from Walling and Collins (2016).

Sediments can physically be altered by consolidation (same as compaction) caused by gravity and the mass of the overburden (post-depositional alteration). Porewater is lifted from the consolidated subsurface sediments to lower consolidated surface sediments. As a result, density of the consolidated sediments increases and porosity decreases. Additionally, the critical shear stress increases and the possibility of sediment resuspension or remobilization is less likely to occur (Wheatcroft et al., 2007). Another effect of consolidation is uplifting of colloids and dissolved elements, such as MTE or contaminants, present in the porewater to surface sediments and consequently to the overlying water table. Indeed, metal sulfides were proven to be easily diffused from deep layers to surface sediments (Huo et al., 2015). As for some of the biological modifications, they are not merely biological, rather bio-physical and bio-chemical. An example about bio-physical alterations of deposited materials is compaction by benthic mass, bio-turbation mainly by macrofauna, and pelletization[xiii] of the muddy surface sediment. On the importance of pelletization and influence on grain size; the pellets of benthic organisms range in size from 200 µm to 1 mm in length on one hand, and are lighter, in terms of density, than the sand grains (which are similar in size with the pellets). Therefore, the bio-physical change alters critical shear stress, and consequently resuspension ability for the

[xiii] The repackaging of fine sediment particles into fecal pellets by organisms.

formed pellets. It should be noted that sometimes it is not possible to distinguish between different kinds of transformations or alterations. For example, the formation of flocs is a bio-chemical process that changes the size of aggregates (physical), and might change mineral and organic composition by degradation or dissolution. Finally, the transformations occurring to phases present in submerged river sediments, and mainly due to the development of anoxic conditions, will be discussed later in the chapter.

4. Origin of metallic elements in sediments

Sediment include major and trace elements. The major elements that are found in sediments, and Earth's crust to a larger extent, are aluminum (Al), calcium (Ca), iron (Fe), potassium (K), magnesium (Mg), manganese (Mn), phosphorous (P), sulfur (S), silicon (Si) and titanium (Ti). As for the trace elements[xiv], they are arsenic (As), barium (Ba), beryllium (Be), bismuth (Bi), cadmium (Cd), cobalt (Co), chromium (Cr), cesium (Cs), copper (Cu), gallium (Ga), germanium (Ge), hafnium (Hf), indium (In), molybdenum (Mo), niobium (Nb), nickel (Ni), lead (Pb), rubidium (Rb), antimony (Sb), tin (Sn), strontium (Sr), tantalum (Ta), thallium (Th), uranium (U), vanadium (V), tungsten (W), zinc (Zn) and zirconium (Zr); rare earth elements (REEs) including light lanthanides, which are cerium (Ce), lanthanum (La), europium (Eu), neodymium (Nd), samarium (Sm) and praseodymium (Pr); heavy lanthanides, which are dysprosium (Dy), erbium (Er), gadolinium (Gd), holmium (Ho), lutetium (Lu), terbium (Tb), thulium (Tm) and ytterbium (Yb), and the elements scandium (Sc) and yttrium (Y). These elements are naturally found in trace amounts, i.e. in the range of part per million (ppm; same as µg/g or mg/kg). The focus of the coming sections will be on some of the metals and the metalloid Si. The metal(oid)s are all the elements discussed above with the exception of P and S, which are non-metallic elements.

4.1. Geochemical background of metals

The geochemical background of an element/metal/compound is its content or concentration in a matrix (soil, sediment or water) that is not influenced by a defined incident, activity or source of pollution, but might be concerned with minor pollutions from everyday activities. The background contents depend on the topography, geology and geography of the site, and on physical, chemical and biological characteristics of the matrix (EPA, 2008). After

[xiv] The elements presented here are the ones that are included in this manuscript.

oxygen, the Earth's crust is mainly composed of Si, followed by Al and Fe (Marshak, 2011b). Magma that rises to form igneous rocks in the crust is mainly composed of Si, Al, Ca, Na, K, Fe and Mg (Marshak, 2011c). Nonetheless, trace metals are also a part of the magma and earth crust, and have contents lower than 0.1%. Upon magmatic rock formation (igneous rocks), metallic elements, such as Pb, Zn and Ni, substitute other elements via isomorphic substitution. Therefore, the formed crystal lattices might contain metals. The magma cools down upon reaching the Earth's surface and magmatic rocks are formed. At this stage, there remains some hot residual hydrothermal fluids; metals are mostly found there. Later, chemical reactions between the fluid and the rock may cause minerals to precipitate as ores. Example of formed ores are pyrite (FeS_2), arsenopyrite (FeAsS), magnetite (Fe_3O_4), hematite (Fe_2O_3), siderite ($FeCO_3$), sphalerite (ZnS) and galena (PbS). It should be noted that metals can also substitute (partly) each other in those ores, such as the partial substitution of Zn by Cd in sphalerite (Zn[Cd]S) (Bradl et al., 2005). With the geological processes (such as volcanism, mountain formation and erosion), metals follow a geochemical cycle and are heterogeneously distributed onto the Earth's surface. Erosion of continental crust may enrich streams and rivers with MTE. Moreover, weathering might dissolve part of the rocks or clasts to form metallic ions. Those ions can be transported via water currents and precipitate elsewhere.

4.2. Atmospheric deposition of metals

Weathering on the Earth's surface can cause particle transportation by wind. As a result, the airborne particles reach the Earth's crust by wet and dry depositions. However, airborne particles might also be deposited directly into water bodies, or can be leached to nearby water bodies via surface run-off. Volcanisms share a great part of introducing metals to the crust via atmospheric depositions (Bradl et al., 2005; Marshak, 2011b); anthropogenic activities, such as vehicular and industrial combustions, also lead to metal enrichment of the pedosphere and aquatic systems. Briefly, atmospheric depositions can mainly be connected to natural atmospheric depositions, such as volcanism and wind erosion, and anthropogenic input via combustion emissions (e.g. Nriagu, 1990a, 1990b; Zubovic et al., 1961).

4.2.1. Natural sources of atmospheric depositions

The most common natural atmospheric depositions responsible for MTE introduction on the surface of the Earth are volcanism, wind-borne soil particles, wind erosion, sea spray, biogenic activities and wild forest fire (some are presented in Table I-1). Volcanism is the main natural source for the release of some metals to the surface of the Earth, such as Cd, Cu, Fe,

Mo, Pb and Zn (Marshak, 2011c; Nriagu, 1989). Upon powerful volcanic eruptions, lava is sprayed into the air, freezes and forms volcanic ash, which can be transported by wind. For example, ashes released from a volcano that exploded in the Philippines in 1991 covered a 4000 km^2 area (Marshak, 2011b). Large particles, such as boulders, are also released to the atmosphere. On a compilation of some elements released from volcanic ash, the main composition was SiO_2 (61.7%), Fe (4.9%), Zn (79.8 mg/kg) and Cu (23/7 mg/kg) (Kobayashi and Shoji, 1976). The contents of some MTE (e.g. Zn and Cu) might be higher in some cases, depending on the minerals present in the volcanic tephra[xv], or initially in the magma. For example, Zn content was as high as 1089 mg/kg (~ 0.11%) in titanomagnetite tephra (Shoji et al., 1993); zinc can associate to the formed ash after deposition (Zubovic et al., 1961). In 1983, metal emissions from volcanism had been estimated to be 140 to 1500 tons of Cd, 540 to 6000 tons of Pb and 310 to 19000 tons of Zn (the median values are presented in Table I-1). Nonetheless, the emissions of those metals to the atmosphere via anthropogenic activities are ~ 6 (Cd), ~ 26 (Pb) and ~ 3 (Zn) fold higher than emissions caused by natural sources (Nriagu, 1989). Wind erosion on the Earth's crust, especially if loaded with airborne particles such as volcanic ash or dust, aid in the process of particle saltation, transport and weathering.

4.2.2. Anthropogenic sources of metals

A main part of MTE introduced to the pedosphere and aquatic systems is anthropogenic based. This has begun during prehistoric eras by firewood and the consequent spreading of fire ash. However, recent developments in the modern life boosted metal input onto the Earth's surface. Indeed, during the recent past, energy production, vehicular and industrial emissions increased metal input to the environment. For example, the large furnace stacks used in the XVI^{th} century had a great upgrade on metal release and dispersion into the environment (Nriagu, 1990b). Metals are commonly released to the surface of the Earth as particulate matter. Those metallic phases accumulate in surface soils and in settling sediment layers since they are non-degradable.

Leaded gasoline was first used in 1923, and the input of lead via deposition had increased till leaded gasoline started to be banned in the 70s or 80s (Nriagu, 1990a). As a result, the Pb contents in sediments archives can be linked to human activities, namely combustion of leaded gasoline. For instance, the content of lead in sediment layers and the banning of leaded gasoline,

[xv] Volcanic fragments, such as ash, dust and boulders.

and the consequent use of unleaded gasolines instead, could be followed in sediments of ponds, lakes and other water bodies, mainly those located nearby a road with high traffic jam. Combustion or emissions from vehicles and industrial activities, such as smelting of ores, coal burning and fuel combustion, could be followed in fresh water sediments for the last couple of hundreds of years (e.g. Eades et al., 2002; Farmer et al., 1997). Even though the major metal and isotope that is traced from engine exhaust is lead, other metals have also shown to be introduced and studied as well, such as Cd, Cu, Cs, Ni and Zn (Nriagu, 1996; Sezgin et al., 2004). Industrial activities also release MTE to the environment. In addition to the atmospheric depositions coming from vehicular and industrial emissions, MTE might also be introduced from manufacturing domestic tools, cars, buildings, high tech devices and cosmetics (Grossman, 2007). As a result, unwanted materials, wastewater, sludge and by-products, which might contain high MTE can reach surface water bodies due to surface leaching or underground water by infiltration. Finally, a summary of the metals released into the atmosphere via various natural and anthropogenic inputs are shown in Table I-1. It should be noted that for most metals, such as As, Cd, Cu, Pb and Zn, the anthropogenic atmospheric depositions were higher than the natural ones.

Table I-1: Metal inputs of worldwide emissions from natural and anthropogenic sources to the atmosphere.
The values presented in the table are the median values as calculated by Nriagu (1989) and compiled by Nriagu (1990b). The total contents (i.e. total natural and total anthropogenic; in kilotons/year) presented in the table are calculated from additional data that are not included in this table (those data can be found in the cited papers). The total values are rounded. For easier comparison between the total natural and anthropogenic metal contents, the higher values are indicated by bold numbers.

		Natural input (kilotons/year)			**Anthropogenic input (kilotons/year)**			
Element		Volcanos	Wind-borne soil particles	**Total natural**	Energy production	Mining, smelting and refining	Manufacturing processes	**Total anthropogenic**
Antimony	Sb	0.7	0.8	2.6	1.3	1.5	-	**3.5**
Arsenic	As	3.8	2.6	12.2	2.2	12.4	1.9	**19.0**
Cadmium	Cd	0.8	0.2	1.4	0.8	5.4	0.6	**7.6**
Chromium	Cr	15	27	**43**	13	-	17	31
Cobalt	Co	1.0	4.1	**6.1**	-	-	-	-
Copper	Cu	9	8	28	8	24	2	**35**
Lead	Pb	3.3	3.9	12.2	12.7	49.1	15.7	**332**
Manganese	Mn	42	221	**316**	12	3	15	38
Mercury	Hg	1.0	0.1	2.5	2.3	0.1	-	**3.6**
Molybdenum	Mo	0.4	1.3	3.0	-	-	-	-
Nickel	Ni	14	11	29	42	4	4	**52**
Selenium	Se	0.9	0.2	**10.3**	3.8	2.3	-	6.3
Vanadium	V	5.6	16.0	27.7	84	0.1	0.8	**86**
Zinc	Zn	10	19	45	17	72	33	**132**

4.3. Metal release due to mining activities

First, it should be noted that part of the metal release described here might be introduced into the environment via deposition (as discussed in the previous section *4.2.2*). Nonetheless, some ideas are included here since they are initially related to mining activities. Mining of metals began during the prehistoric eras (stone, bronze and iron ages), and developed to the relatively recent industrial period since the last few centuries. Mining, which is the process of extracting ores (rich in specific metals) from the Earth, is the first step of metal introduction to the surface of the Earth, namely soil, sediments and water bodies. Indeed, even if the ores are not further manipulated, i.e. smelted and extracted for metals, the ores are weathered, minerals are altered and metals are released to different compartments of the environment (e.g. Grgic et al., 2001). The targeted metals for extraction changed with time. Gold (6000 BC), copper (4200 BC) and silver (4000 BC) were the first metals to be extracted for coins and jewelry, followed by lead (3500 BC), tin (1750 BC), iron (1500 BC) and mercury (750 BC). Then, with the discovery of other metals (after the XIIIth century), such as arsenic, antimony, zinc and aluminum, the focus of smelting shifted towards them. It should be noted that different regions across the globe witnessed different periods of certain metal extraction, mainly because some metal ores are present in specific areas, and some metal extraction was more preferable than others (Aitchison, 1960; Han et al., 2002). Consequent to mining, the extracted ores or minerals are smelted to extract the targeted metals. Smelting processes have updated to include the utilization of large furnaces with tall stacks in the XVIth century and steam machines in the XVIIIth century. As a result, metal release into the environment boosted (Nriagu, 1990b). Nonetheless, it was not until the last century (industrial age) till the metal production started to exponentially increase (Han et al., 2002). Some of the metals that showed major production development during the last period of the last century are Cd, Cr, Cu, Ni, Pb and Zn (Figure I-7). As seen for most metals, the major increase in production happened between 1950 and 2000, except for lead, which decreased in the 70s – 80s, due to the banning of leaded gasoline (Nriagu, 1990a).

Metallurgy, involving mining, smelting, combustion of coal and petroleum, release of flue dust and ashes, and sludge disposal, is one of the main causes of metal enrichment to the land and water compartments. During mining, the ores are extracted from the inside of the

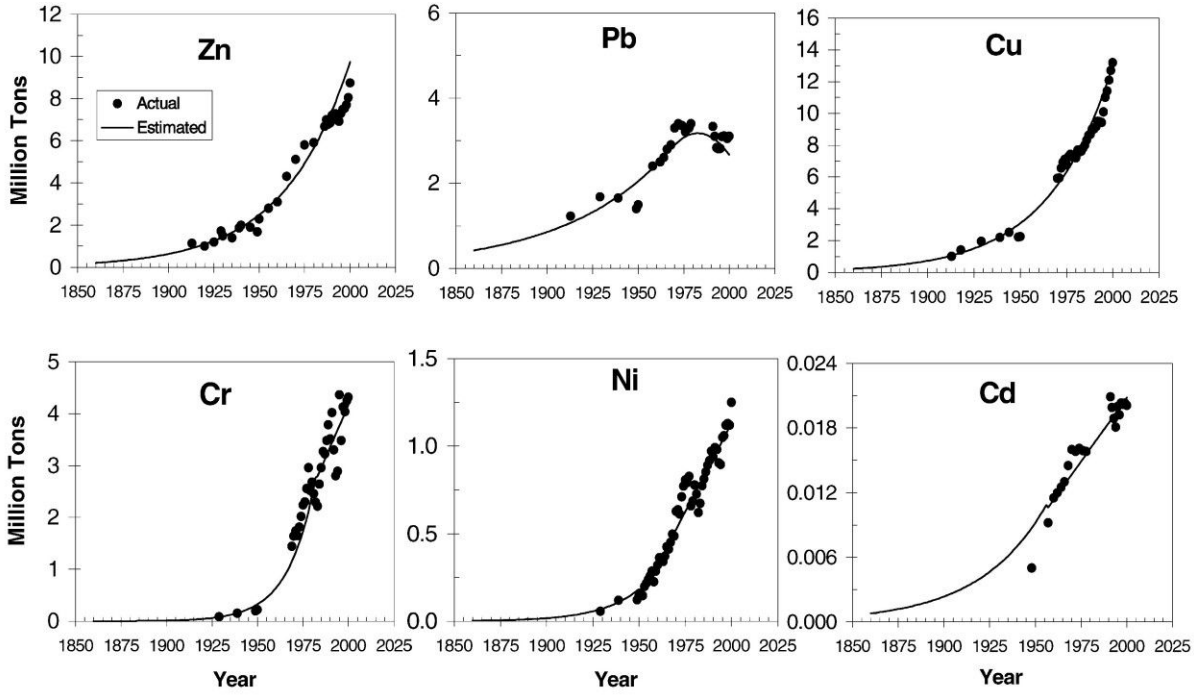

Figure I-7: Actual and estimated worldwide annual industrial metal production.
Source (Han et al., 2002).

Earth. Consequently, acid mine drainage[xvi] (AMD) may occur to sulfide containing minerals, since the ores are exposed to the environment (oxygen and humidity). Sulfide minerals are stable under anoxic conditions, however, they dissolve upon oxidation. As a result of sulfide dissolution, the pH of the leaching solution coming from the ores or stocked media (such as sludge stockpiles) drops and metals are released (B. Singh et al., 1999). Some of the sulfides that might cause AMDs are iron sulfides, such as pyrite and marcasite (FeS_2), copper sulfides, such as chalcocite (Cu_2S) and chalcopyrite ($CuFeS_2$), lead sulfide, such as galena (PbS), and zinc sulfide, such as sphalerite (ZnS) (Skousen et al., 1998). Some of the metals that are commonly released and pose a threat to the environment are As, Cd, Cu, Fe, Hg, Pb and Zn (Adriano, 2001a; Bradl et al., 2005; Gutiérrez et al., 2016). Additionally, the waste product remaining from mining are stocked as piles and could also create AMDs. Even though the waste products might not be as enriched as the metal ores, they might contain metals found in trace amounts, which usually represent the fraction that cannot be extracted. Indeed, metallurgic waste and by-products showed to enrich sediments as well as soils with metals. For example, metal contents of soils and sediments in areas near mining activities were in the range of 136 to 69000 mg/kg for Pb, 228 to 203000 mg/kg for Zn and 0.2 to 340 mg/kg for Cd

[xvi] The flow of leachate/water of acidic pH from the minerals that are exposed to oxidizing conditions.

(Gutiérrez et al., 2016 and articles cited therein). In addition, combustion of coal and petroleum release metals into the atmosphere, some in the form of fly ashes and flue dust. Sludge resulting from metallurgy also contribute to the input of metals into the environment. For example, sludge generated in metallurgy can be elevated with Zn, Cd, Fe and Cu, depending on the materials used during production (Das et al., 2007; Hansen and Tjell, 1982). Sludge wastes are in many cases stored in sedimentation ponds and might consequently be transported to water bodies and settle elsewhere, such as riverine sediments; metals might be leached from sludge wastes to nearby soils and water systems.

4.4. Metal input resulting from agricultural activities

Agriculture activities and consequent agro-chemical application increase metal input onto soils and aquatic media. Fertilizers, such as phosphate rock-based fertilizers, animal manures and other agro-chemicals (e.g. pesticides, herbicides and insecticides) are metal sources, such as As, Cd, Cr, Cu, Ni, Pb and Zn (Nicholson et al., 2003). Phosphate fertilizers, in addition to P, contain Cd and Zn (and other elements as well), mainly depending on the parent rock (Azzi et al., 2017). For example, fertilizers made from sedimentary rocks have higher Cd contents than magmatic ones. Indeed, magmatic based phosphate rocks are quasi-free from cadmium (Hansen and Tjell, 1982). Another source of metal in agricultural lands, and their vicinities, is pesticides. Metal-based pesticides are no longer used, however, former applications had accumulated metals, such as As, Hg and Pb (Nicholson et al., 2003). As for the application of manure, Cd, Co, Pb and Zn are some of the metals that might enrich the pedosphere, since some of dietary supplements given to animals contain those metals (Mahar et al., 2015 and articles cited therein). It should be noted that even though the agro-chemicals are applied and are accumulated in the pedosphere, part of these agro-chemicals might reach aquatic systems, including sediments. Major parts of metals are introduced into the environment as micro-particles with metals in the crystal lattice, or as organo-minerals or organo-metal compounds (Michalzik et al., 2007; Nicholson et al., 2003). A summary of worldwide metal input into aquatic systems, from various natural and anthropogenic activities, is summarized in Table I-2.

Table I-2: Metal input into aquatic systems.
The values presented in the table are the median values as calculated by Nriagu an Pacyna (1988) and compiled by Nriagu (1990b). The total values are rounded. Units are in kilotons/year.

Element		Domestic wastewaters	Electric power plants	Base metal mining and smelting	Manufacturing processes	Atmospheric deposition	Sewage discharges	Total input
Antimony	Sb	2.2	0.2	3.8	9.3	1.1	1.5	18
Arsenic	As	9.2	8.2	7.4	7	5.6	4.1	42
Cadmium	Cd	1.7	0.1	2	2.4	2.2	0.7	9.1
Chromium	Cr	46	5.7	12	51	9.1	19	143
Copper	Cu	28	13	14	34	11	12	112
Lead	Pb	6.8	0.7	7	14	100	9.4	138
Manganese	Mn	110	11	40	21	12	69	263
Mercury	Hg	0.3	1.8	0.1	2.1	2	0.16	6.5
Molybdenum	Mo	2.2	0.6	0.5	4.2	0.9	2.9	11
Nickel	Ni	62	11	13	7	10	11	114
Selenium	Se	4	18	12	4	1	2	41
Vanadium	V	2.3	0.3	0.6	0.5	26	3.5	33
Zinc	Zn	46	18	29	85	40	17	237

After introduction into water systems, part of the MTE phases is stored in sediments. However, as mentioned earlier (section *4.2.1*), atmospheric emissions, mainly from volcanism (natural) and mining, smelting and refining activities (anthropogenic), are among the main causes for metal introduction to the environment on one hand (Table I-1), and are the main sources of metal input into aquatic systems on the other (Table I-2). The metals introduced into aquatic systems can be in the form of dissolved phases, i.e. dissolved metals, such as in the case of wastewater treatment plant (WWTP) effluents (Karvelas et al., 2003). Finally, and after having presented the possible sources of metals present on the surface of the Earth, Table I-3 summarizes some of the main sources of the metals As, Cd, Cr, Cu, Fe, Ni, Pb and Zn.

Table I-3: Possible anthropogenic sources of the metals As, Cd, Cr, Cu, Fe, Ni, Pb and Zn introduced to the environment.
Compiled from Adriano (2001a), Bradl et al., (2005), Da Silva Oliveria et al., (2007), Karvelas et al., (2003), Mertens and Smolders (2013), Nicholson et al., (2003), Nriagu (1996, 1990a), Sezgin et al., (2004), Wang et al., (2005) and Yoon et al., (2012).

Metal	Sources
As	Additives to animal feed, wood preservative, ceramics, special glasses, agro-chemicals, sewage sludge, semiconductors, non-ferrous smelters, coal-fired generators, metallurgy and pyrometallurgy (smelting).
Cd	Ni/Cd batteries, anti-corrosive metal coatings, coil combustion, pigments, phosphate fertilizers, plastic industries, metallurgy (mining and smelting), vehicle combustion, WWTP effluent and sludge, coal combustion and agro-chemicals.
Cr	Stainless steel production, catalysts, pigments, textiles, leather tanning, agro-chemicals, paper industry, power plants, WWTP effluent and sludge, coal ash and metallurgy.
Cu	Wire production, electric apparatus, kitchenware, agro-chemicals, feed additive (growth promoter), metallurgy, WWTP effluent and sludge, vehicle combustion and coal combustion.
Fe	Cast iron, steel making, alloys, construction and iron metallurgy, and WWTP effluents and sludge.
Ni	Electroplating, alloy production, Ni/Cd batteries, electronics, automobiles, metallurgy, kitchen appliances, vehicle combustion, WWTP effluent and sludge, coal combustion and agro-chemicals.
Pb	Lead/acid batteries, pigments, glassware, ceramics, plastics, cable sheathings, pipes (PVC), metallurgy, steel industries, automobile exhaust, WWTP effluents and sludge, coal combustion and agro-chemicals.
Zn	Zn alloys (bronze), anti-corrosive metal coating, batteries, pipes (PVC), rubber industry, paints, textile, phosphate fertilizers, metallurgy, steelmaking, pyrometallurgical industries, coal residues, WWTP effluents and sludge, vehicle combustion and agro-chemicals.

5. Sediments: a reservoir of deposited materials and a record of industrial activities

Suspended particulate matters are suspended as long as the velocity of the particles are superior to the flow velocity, which is dependent on the grain size and density (section *3*). Otherwise, particulate matters settle and archives of sediments are formed. Therefore, different depths in the sedimentary archives might present specific periods of material settling. The sediments might contain lithogenic as well as anthropogenic materials. Moreover, the settled materials might be modified by bio-geo-chemical alterations, which further depend on the metal itself, metal content, metal species, physico-chemical condition of the hosting matrix and the original state of the metal/metal-bearing particles (Adriano, 2001b; Bradl et al., 2005; Du Laing et al., 2009, 2008b).

In many cases, industries are built near water systems, since river water might be used for production processes, cleaning purposes, wet scrubbing or wastewater discharge. As a result, metal bearing particles originating from the released effluents are transported as SPM or are settled and form sedimentary archives (e.g. Ayrault et al., 2012; Dhivert et al., 2015a, 2015b; Hudson-Edwards, 2003). For example, river sediments have been shown to contain historical information of anthropogenic sources, such as mining, smelting, chemical plants and automobile exhaust (e.g. Eades et al., 2002; Hudson-Edwards, 2003; Komárek et al., 2008; Lesven et al., 2008). Nonetheless, and due to legislations, the input of metals into the

environment is becoming limited or reduced, such as the banning of leaded gasoline that significantly decreased Pb in sediments that had settled recently (Ayrault et al., 2012; Ferrand et al., 2012; Nriagu, 1990a). Mining activities were shown to be main sources of metal introduction into the environment, notably into soils and sediments. As a result, sedimentary archives have shown elevated metal contents in comparison to background levels on one hand, and have shown the presence of foreign minerals that would not be found under natural conditions on the other. The mineralogy and geochemistry of metals is usually used to identify the past activities and waste materials (e.g. by-products), while the biological and organic fractions of the sediments, or the association of the metals to bio-organo-mineral complexes are more of interest for the transformed or aged materials in the post-depositional environment. Consequently, the possible transformations and alterations of the initially released metal bearing compounds can be observed in the deposited materials.

5.1. Contribution of grain sizes on the mineralogical and chemical composition

In river compartments, the finest fractions are the most attention-grabbing, especially for geochemical studies. Indeed, the fine clay and silt particles, according to their chemical and physical properties, have the highest metal scavenging ability on one hand (e.g. Acosta et al., 2011; Du Laing et al., 2007a), and are the most susceptible to be remobilized as SPM on the other (e.g. Robert, 2014; van der Veen et al., 2007). Moreover, metals can be scavenged by fine particles via different interactions, or the fine particles happen to be made from metal rich minerals (Walling, 2013). Conversely, coarse fractions might be more metal enriched than fine fractions; for example, metal enriched fine particles might form aggregates, which can be cemented by organic ligands, such as dissolved organic matter, salts and thin layers of water between individual particles (Nichols, 2009b; Parizanganeh, 2008). Another possibility is the presence of mining and milling deposits; those deposits might contain coarse grains enriched with metals, such as As, Cu, Fe, Pb and Zn (Moore et al., 1989). Other studies showed that sediments contaminated by mining (A. K. Singh et al., 1999) and milling (Vučnić Vasić et al., 2013) activities showed higher metal contents for the finer fractions. In addition, micro-environmental changes in sediments are also possible. For instance, the contents of metals and correlations to grain sizes were rather diverse in a 60 cm river sediment core (Maslennikova et al., 2012). In geochemical sedimentary studies, fractions inferior to 64 µm, i.e. only the clay and silt fractions, are generally analyzed for chemical composition (e.g. Dhivert et al., 2015b; Grosbois et al., 2012; Horowitz, 1991; Owens and Walling, 2002), others studies considered

the fractions inferior to 100 µm (e.g. Thévenot et al., 2007) or 75 µm (e.g. Jain, 2004). An alternative for using the fine fraction for elemental quantification is normalization by a major element (such as Al, Si and Fe) that is of lithogenic nature and has low variability if contamination occurs (more details regarding this issue will be discussed in sections *10.2.1* and *10.2.2*). Moreover, on a metal content – grain size study on estuary sediments, which evaluated 22 sediments and 16 elements, the metal contents were compared in the fractions < 20 µm and < 60 µm (Ackermann et al., 1983); higher contents were found in the finer fraction. For example, the fraction < 20 µm contained up to 5-fold higher metal contents (such as As, Cd, Fe, Pb and Zn) than the < 60 µm fraction. Several studies found that metals (such as As, Cu, Fe, Pb and Zn) were generally more enriched in the fine (< 63 µm) sediment fractions (e.g. Boateng, 2015; Prasad et al., 2006). Therefore, it is indefinite to robustly correlate sediment grain sizes with metal contents, rather the findings might be more suitable depending on the materials deposited in the river and sediment nature.

Grain sizes of sedimentary archives might also give indications about minerals present, and subsequently the elemental composition. For example, as quartz and feldspar (Na and K) usually belong to sand and coarse silt fractions (Velde, 1995), those fractions are expected to be enriched with Si, K and Na, especially if the sediments are of lithogenic nature. Indeed, on a study on chemical fractionation in sand, silt and clay, the first was the most enriched with Si, K and Na (Acosta et al., 2011), while other elements, such as Fe, were mainly found in the clay-sized particles, possibly as Fe-oxides (or oxy-hydroxides), since secondary Fe-oxide minerals have a clayey-silty texture (Hillier, 1995; Naden, 2010). Other elements, such as Pb and Zn, were mainly found in the clay-sized fraction, which might be explained by the adsorption of those metals by metal oxides or oxy-hydroxides; several studies have indicated the effectiveness of metal sorption by metal oxides (e.g Evans, 1991; Farley et al., 1997; Lynch et al., 2014).

6. Assessing the age of sediments using $^{210}Pb_{xs}$ and ^{137}Cs

Activities that were recorded in sedimentary archives might be revealed by knowing the age of the deposits (i.e. the time of settling). The age of sediments can be computed on the bases of excess lead isotope ($^{210}Pb_{xs}$) and ^{137}Cs. Those methods are used for sediments of lakes, rivers, oceans, seas, peatlands and ponds (e.g. Appleby and Oldfield, 1978; Cahill and Steele, 1986; Grosbois et al., 2012; Komárek et al., 2008; Lepage et al., 2015). With the half-life ($t_{1/2}$) of ^{210}Pb being 22 years, the age and sedimentation rate for the past 100 to 200 years can be

revealed. The uranium series (also called radium series) starts in the crust with the naturally occurring isotope ^{238}U, which later decays to ^{234}U, ^{230}Th and ^{226}Ra (Figure I-8). Afterwards, ^{226}Ra decays into the inert gas ^{222}Rn, which decays into ^{218}Po followed by ^{210}Pb. ^{210}Pb is then deposited onto the crust, via wet or dry deposition, is permanently fixed to soil particles (mainly fine ones), and eventually leaches to water bodies; this is considered as $^{210}Pb_{xs}$. The half-lives and series of decay are depicted in Figure I-8. Alternatively, ^{210}Pb might directly deposit into water bodies; or ^{226}Ra might be leached from surface erosion to water bodies where *in-situ* decay occurs (Figure I-8). The age of the sediments is then based on the decay of the $^{210}Pb_{xs}$ radionuclide. $^{210}Pb_{xs}$ can be used for sediment dating assuming that the ^{210}Pb input from the atmosphere is constant, the sediments have not been disturbed, and the $^{210}Pb_{xs}$ contents show a decrease with depth. Indeed, Pb decreases with depth due to the restricted use of Pb containing compounds and the improvement in environmental regulations (e.g. Ayrault et al., 2012; Ferrand et al., 2012; Nriagu, 1990a). If that was not the case, then the sediment layers might have been disturbed by benthic organisms or hydrodynamic variations, or anthropogenic materials that do not hold ^{210}Pb might had settled. Other Pb isotopes can also be used as proxies for tracing the sources of Pb, such as leaded and unleaded gasoline, coal combustion,

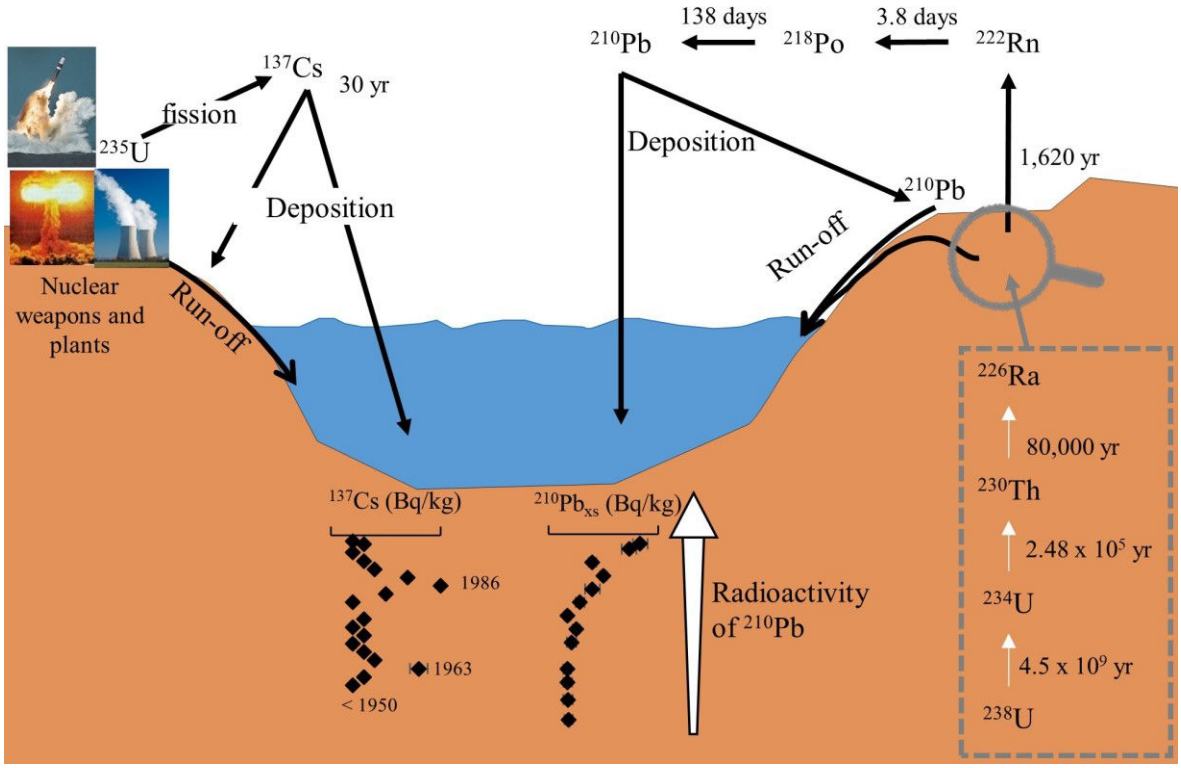

Figure I-8: Input of ^{210}Pb and ^{137}Cs into sediments.
^{210}Pb reaches the sediments as shown in the right part of the figure. The numbers near the arrows indicate half-lives; yr: year. Under perfect conditions, the $^{210}Pb_{xs}$ content decreases with depth (as indicated in this figure). To the left of the figure, possible sources of ^{137}Cs are shown. The peaks of ^{137}Cs are then linked to certain dates. ^{137}Cs and ^{210}Pb are fixed to soil particles (mostly fine) and are leached to water bodies where they settle.

metallurgy (such as sludge, slag and fumes/dust) and others (Komárek et al., 2008 and references cited therein).

Another method to determine sediment age is by ^{137}Cs. This method concerns sediments that had settled since the mid of the XXth century. ^{137}Cs is the fission product of ^{235}U (nuclear weapons) and has a 30-year half-life; the fallout of ^{137}Cs can then be used for calendar dating. ^{137}Cs is then fixed to soil particles, mainly fine clays, which consequently might reach water systems via surface leaching where they settle. The sediment dates are then known based mainly on the protrusion of 3 ^{137}Cs peaks; the first is linked to the thermonuclear and large-scale weapon tests in the 1950s, where the contents of ^{137}Cs started to be detected in sediments circa 1953/1954, the second is due to the maximum ^{137}Cs fallout in 1962/1963, and the third which is associated to the Chernobyl nuclear accident in Ukraine in 1986 (e.g. Grosbois et al., 2012; Loizeau et al., 2003). Indeed, the absence of ^{137}Cs indicates sediments that had settled before the 1950s, sediments that had formed from materials that do not carry ^{137}Cs, or sediments that had settled very recently. ^{137}Cs can be linked to other incidents as well, such as the Fukushima Dai-Ichi nuclear power plant incident in 2011 (Lepage et al., 2015). It should be noted that ^{137}Cs method provides certain dates (marker or calendar dates), while ^{210}Pb can be used for more detailed dating.

7. Fate of metals and minerals in river sediments

Metal behavior in river compartments dependents on physico-chemical conditions of sediments, river water and pore water (including pH and redox potential “Eh”), which in turn are translated on the chemical reactions that take place. Also, concentrations (or contents) of binding phases and dissolved elements, microbial communities, mineral constituents and time of interaction play a part in metal fate (e.g. Calmano et al., 1993b; Du Laing et al., 2009; Eggleton and Thomas, 2004).

In submerged river sediments, the redox potential and residence time of pore water play major roles in the fate and speciation of elements and minerals. In perennial river sediments, the deposits are always saturated with river water, thus anoxic conditions are well maintained, except for the top few millimeters (~5 mm), which might be the transition zone (moderately reduced) between the above lying oxic water table and the underlying anoxic deposits (Lesven et al., 2010; Matijević et al., 2007). In addition, prolonged durations of flooding events might have the same outcome on overbank sediments; i.e. chemical reactions and speciation of metals between overbank sediments and submerged sediments might be comparable. While still in the

water column, SPM is usually transported in oxic matrices, which gradually change upon sedimentation and subsequent covering with newer deposits (which was referred to as overburden in section *3.1* and *3.2*). Afterwards, anoxic conditions in the matrix start to prevail; physico-chemical parameters change accordingly. pH in sediments varies according to the organic by-products produced from organic matter decomposition, sulfate reduction and precipitation of sulfides and carbonates (e.g. Eggleton and Thomas, 2004). Microbial populations and their processes are also players in the fate of chemical species. Some of those microorganisms are denitrifying and Mn-, Fe- and S- reducing bacteria (Patrick and Delaune, 1972; Patrick and Jugsujinda, 1992). Therefore, possible variation in metal speciation might be caused by dissolution and/or (co)-precipitation reactions. The formed phases or minerals might be termed secondary minerals (e.g. secondary iron oxides or secondary zinc sulfides), since they form in the sediments (Hochella et al., 2005). The coming parts will discuss some metal sulfide and metal oxy-hydroxide precipitation processes.

7.1. Precipitation of metal sulfides in anoxic conditions: sulfidization

In anoxic matrices, precipitation and accumulation of metal sulfides are common (e.g. Du Laing et al., 2009; Eggleton and Thomas, 2004; Fanning and Fanning, 1989a). Metal sulfides are stable in anoxic conditions, and unstable under oxic conditions (depending on their crystallinity and age). As a result, metal sulfides have considerable roles on metal dynamics in sediments, especially those prone to varying redox potentials. The following paragraphs deal with the main steps and reactions that form metal sulfides in anoxic sediments.

The process of metal sulfide formation is called sulfidization (Fanning and Fanning, 1989a; Lowery and Wagner, 2012), which is analogous to sulfidation and pyritization, but were proposed by other researchers (Kettler et al., 1992; Rickard, 1973; Rodriguez and Hrbek, 1999). Decomposition of organic carbon in soils and sediments by microbial organisms is the first step (Eq. I-1), which is dependent on the carbon supply, redox potential and microbial population and activity. For example, an increase in redox potential might boost decomposition of organic material via microbial communities (Eggleton and Thomas, 2004). Moreover, organic carbon infiltration in the pore water encourages microbial activity (Byrne et al., 2013).

Eq. I-1: Organic matter decomposition $CH_2O + O_2 \rightarrow CO_2 + H_2O$

In river systems, sulfate naturally originates from degraded OM or from flooding water (Du Laing et al., 2007a), or may originate from anthropogenic activities, such as from impurities during the making of steel (Das et al., 2007; Yildirim and Prezzi, 2011). When

organic carbon is decomposed (via oxidation), other electron acceptors should be reduced to remain electrochemical neutrality; depending on the available species, pH and redox potential (Fiedler et al., 2007; Stumm and Morgan, 1996), the preferred first electron acceptor is oxygen or dioxygen O_2 (Eq. I-2).

Eq. I-2: Oxygen as an electron acceptor $$O_2 + 4H^+ + 4e^- \rightarrow 2H_2O$$

In oxygen depleted media, microbial populations switch to facultative and eventually strictly anaerobic respiration. Alternatively, other electron acceptors will be used, such as nitrate (NO_3^-), manganese oxides (MnO_2), iron oxides ($Fe(OH)_3$) in weakly and moderately reduced environments (~ 375 till ~ 0 mV) (Eq. I-3 till Eq. I-5), and sulfate (SO_4^{2-}) in highly reduced environments (~ 0 till ~ -400 mV) (Eq. I-6) (Du Laing et al., 2009; Fanning and Fanning, 1989a; Fiedler et al., 2007).

Eq. I-3: Nitrate reduction reaction $$NO_3^- + 2H^+ + 2e^- \rightarrow NO_2^- + H_2O$$

Eq. I-4: Manganese oxide reduction reaction $$MnO_2 + 4H^+ + 2e^- \rightarrow Mn^{2+} + 2H_2O$$

Eq. I-5: Iron oxide reduction reaction $$Fe(OH)_3 + 3H^+ + e^- \rightarrow Fe^{2+} + 3H_2O$$

It is important to note that the reactions mentioned above (Eq. I-3 till Eq. I-5) might happen at redox states others than those previously indicated, depending on pH values. For example, under flooding conditions, Fe reduction occurred at 300 mV when pH was 5, between 100 and 300 mV when pH was 6 – 7, and at -100 mV when pH was 8 (Gotoh and Patrick, 1974). The sensitivity to precipitation (and dissolution) according to pH is metal dependent. Manganese was shown to be reduced at higher redox potentials (200 – 300 mV) and faster than iron (Patrick and Henderson, 1981). However, after the reduction of metals, electrochemical neutrality in the highly anoxic sediments is reached by sulfate (SO_4^{2-}) reduction to sulfide species (H_2S or HS^-) (Eq. I-6).

Eq. I-6: Sulfate reduction reaction $$SO_4^{2-} + 10H^+ + 8e^- \rightarrow H_2S + 4H_2O$$

Another possible reaction that leads to the formation of sulfide species by sulfate reduction is methanogenesis, which is a final step of organic matter decomposition by anaerobic-respiration microbes, called methanogens (Eq. I-7).

Eq. I-7: Methanogenesis $$CH_3COOH \rightarrow CH_4 + CO_2$$

The produced methane gas might then be part of a reverse methanogenesis (also called anaerobic oxidation of methane), where sulfate is reduced to HS^- (Eq. I-8).

Eq. I-8: Reverse methanogenesis or anaerobic oxidation of methane

$$SO_4^{2-} + CH_4 \rightarrow HCO_3^- + HS^- + H_2O$$

By the processes (Eq. I-6 and Eq. I-8), sulfate in the aqueous phase (pore water in case of submerged sediments) forms sulfide species (H_2S and HS^-), depending on the redox conditions. Consequently, metal sulfides precipitate.

Sulfur in submerged sediments react with available metals, such as Fe, Mn, Cu, Zn and Pb, to form metal sulfides (Fanning and Fanning, 1989b; Stumm and Morgan, 1996). The metals released from reductive dissolution of metal oxy-hydroxides might be a part of the (co)-precipitated sulfides, mainly as Fe sulfides (this idea will be discussed in section *8.1*). Indeed, metals, such as Cd, Cu, Ni and Zn, that were released from Fe and Mn oxy-hydroxides by reductive dissolution might have been co-precipitated with Fe sulfides, or precipitated as metal sulfides; Cd, Cu, Ni and Zn were weakly pyritized, while Mn was found to be strongly pyritized (Billon et al., 2001; Huerta-Diaz et al., 1998). Therefore, sulfides other than iron do form, even though iron sulfides are the most common (Fanning and Fanning, 1989a). On a study on contaminated river sediments, sulfidization of the metals Cd, Cu and Zn was seen to be a competitive process (Simpson et al., 2000b). Sulfidization of Cd and Zn (CdS and ZnS respectively) showed to be more reactive than Cu (Cu_2S). It should be noted that the formation of CuS and Cu_2S is Cu concentration dependent; CuS formed at lower Cu concentrations than Cu_2S. Metals can also be co-precipitated in iron sulfides, such as chalcopyrite ($CuFeS_2$), which can be an intermediate in the formation of CuS (Parkman et al., 1999).

7.2. Dissolution of sulfide phases: sulfuricization

When oxic conditions predominate, oxidative dissolution of sulfides occur, and new minerals form; this is known as sulfuricization (Carson et al., 1982; Fanning and Fanning, 1989a). The idealized stages of sulfuricization encompass three steps, which are i. pre-sulfuricization, ii. actively sulfuricizing and iii. post-sulfuricization (Fanning and Fanning, 1989a). In oxygen free matrices (as submerged sediments), sulfides are quite stable. Those stable metal sulfides encompass the pre-sulfuricization step. Upon shifting to sub-oxic or oxic conditions, oxidative dissolution of metal sulfides occurs, and sulfuric acid is produced (actively sulfuricization). Unless carbonates buffer the medium and sulfuric acid reacts with silicates, pH will drop drastically. The capacity to buffer the medium depends, indirectly, on the oxygen supply and the rate of sulfuric acid formation. Thus silicates may partly or completely be decomposed by sulfuric acid, while other minerals might precipitate (Fanning

and Fanning, 1989a; Lowery and Wagner, 2012). Moreover, microbial activity accelerates the oxidation rate by up to 34-fold, in comparison to abiotic reactions (Lu and Wang, 2012). Some of the genera that are involved in the oxidation of metal sulfides are *Acidithiobacillus*, *Acidiphilium*, *Acidiferrobacter*, *Ferrovum*, *Leptospirillum, Alicyclobacillus*, *Sulfobacillus*, *Ferrimicrobium, Acidimicrobium* and *Ferrithrix* (Vera et al., 2013). Despite the fact that those genera are predominantly acidophilic, some are mesophilic and moderately thermophilic (Clark and Norris, 1996; Norris et al., 2000). In addition, amorphous, freshly precipitated and particularly fine metal sulfides are more prone to oxidative dissolution in comparison to crystalline, aged and coarse metal sulfides. Studies have shown that oxidative dissolution of freshly formed Fe mono-sulfides, and consequent adsorbed metal release, could happen at a minute scale (Eggleton and Thomas, 2004; Whiteley and Pearce, 2003). When sulfides are completely oxidized, the post-sulfuricization stage is reached. At that point, the pH of the medium is normally superior to 4, and sulfate minerals are formed, such as jarosite ($KFe^{3+}(SO_4)_2(OH)_6$) and gypsum ($CaSO_4.2H_2O$) (Fanning and Fanning, 1989a). In some cases, the pH of the medium may be alkaline due to the presence of secondary carbonates. Nonetheless, during the last stage, an acidic pH is usually associated, especially if jarosite minerals were present. AMD due to oxidative dissolution of metal sulfides is also considered as a main metal release (this issue was discussed in section *4.3*).

7.3. The fate of metals after anoxic sediments are re-oxidized

The oxidation of sediments might happen due to partial or complete resuspension caused by natural events and man-made activities. Natural events include pore water drainage or evaporation, which might be the case of winterbourne[xvii], ephemeral[xviii] and intermittent[xix] rivers, biotic disturbances (bioturbation) of surface sediments, which might be caused by benthic organisms (e.g. amphipods and fish) (Amato et al., 2016), and increase in water flow during flooding events. As for man-made activities, they include sediment dredging, land disposal, possible drainage of wetlands and boat activities (e.g. Calmano et al., 1993b; Du Laing et al., 2009; Simpson et al., 1998; Superville et al., 2014). However, metal sulfide dissolution is pH dependent. For example, oxidation of sulfides was found to be mainly a

[xvii] A stream that flows only or mostly in winter after heavy rains.
[xviii] A stream that flows for a very short time, mostly following precipitation or snowmelt.
[xix] Also called temporary rivers. A stream that ceases to flow every year or at least twice every five years. The stream might be ceased due to higher water demand or lower precipitation.

chemical process at elevated pH (~8), while it was a faster process at much lower pH values (~6.2), since the latter was mediated by microbes (Salomons et al., 1987). In addition, time of oxidation prevailing in the matrix plays a role in the metal sulfide dissolution processes. Some metal sulfides might be more stable than others and have different oxidation kinetics. For example, CuS and FeS_2 are less likely to be dissolved during short term resuspension, since they have slow oxidation kinetics (Caetano et al., 2003). Nevertheless, when metal sulfides dissolve, the Fe might be rapidly re-precipitated as Fe oxy-hydroxides (Du Laing et al., 2009), and other dissolved metals might (co)-precipitate as well (Caetano et al., 2003; Eggleton and Thomas, 2004).

7.3.1. Resuspension of metal-laden anoxic sediments

Numerous studies focused on the effect of resuspension of anoxic metal enriched sediments and revealed metal fate (e.g. Caetano et al., 2003; Calmano et al., 1993a, 1993b; Hirst and Aston, 1983; Simpson et al., 2000a, 1998; Vdović et al., 2006). The common findings were that sulfides are dissolved and metals are released upon oxidation, which are dependent on several factors, mainly pH and metal species, but also dissolved oxygen, biotic activity, redox potential, salinity, time of resuspension, temperature, sediment:water ratio, carbonate content (buffering capacity), shear stress and initial mineral phases and their stabilities. In some of those studies, metals, such as Cd, Cu, Pb and Zn, were found to change from sulfide phases to weaker bound carbonates and exchangeable fractions upon resuspension (Calmano et al., 1993b; Zoumis et al., 2001). In other studies, oxidation lead to increased metal release (Cu, Cd, Pb and Zn), especially since the sediments did not have a high acid neutralizing capacity (ANC) (or high buffering capacity). However, part of the released metals were re-(co)-precipitated after some time (> 4 – 5 days), depending on the metal (Calmano et al., 1993a, 1993b). On the ANC, it was seen as one of the major parameters that influenced metal release in a resuspension study. Indeed, ANC can control pH variation upon disturbance of anoxic sediments, as seen with higher ANC of clay rich samples (chlorites, smectites, and other phyllosilicates) over sandy ones (Cappuyns and Swennen, 2010). Finally, the main processes that are related to metal speciation in anoxic sediments are reductive precipitation of sulfides and reductive dissolution of metal oxy-hydroxides. On the contrary, oxidative sulfide dissolution and oxidative metal oxy-hydroxide precipitation are the main players in determining metal speciation in oxic conditions.

8. The case of Fe and Fe bearing minerals

The importance of the fate of iron and iron bearing minerals is due to its natural abundance in the environment, its role as metal holding phases, and its significant release from mineral and mining industries (e.g. Cummings et al., 2000, 1999). Iron is the forth abundant element on the Earth's crust (Marshak, 2011b). Some of the common iron minerals existing in sediments and soils are amorphous ferrihydrite and Fe oxy-hydroxides, crystalline oxides, such as hematite (Fe_2O_3), magnetite (Fe_3O_4) and wuestite (FeO), oxy-hydroxides, such as goethite (α-FeOOH), lepidocrocite (γ-FeOOH), akaganeite (β-FeOOH) and limonite ($FeO(OH).n(H_2O)$), and carbonates, such a siderite ($FeCO_3$). Moreover, iron sulfides (pyrite FeS_2) are common in anoxic conditions (Cornell and Schwertmann, 2003). The focus of the following sections will be on the precipitation and dissolution of iron species, namely Fe sulfides and Fe oxy-hydroxides.

8.1. The formation of iron sulfides under anoxic conditions

Even though various metal sulfides might form in anoxic conditions (section *7.1*), iron sulfides are the major ones, due to the reactivity of sulfides towards iron (Canfield et al., 1992). In addition, ferric iron is considered as the terminal electron acceptor for bacterial decomposition of organic matter (Tugel et al., 1986), microbial Fe reduction is an important metabolism in freshwater sediments (Jones et al., 1984), and iron is found in contents higher than other metals that might form sulfides (e.g. Mn, Cu, Zn and Pb). Iron sulfides form according to the simplified equation below (Eq. I-9).

Eq. I-9: Iron sulfide formation

$$3H_2S + 2FeOOH \rightarrow FeS + FeS_2 + H_2O$$

As a result, mono- and di-sulfides are formed (FeS and FeS_2, respectively). The reactions previously mentioned are not independent ones (Eq. I-1 to Eq. I-9), rather they represent individual reactions of a complex process that depends on the microbial communities, available elements, oxic/anoxic state and other aspects related to the matrix. A traditional idealized chemical reaction representing iron sulfide formation in highly anoxic conditions is shown in Eq. I-10 (Fanning and Fanning, 1989a; Pons et al., 1982).

Eq. I-10: Summarizing reaction producing pyrite

$$Fe_2O_3 + 4SO_4^{2-} + 8CH_2O + {}^1/_2\,O_2 \rightarrow 2FeS_2 + 8HCO_3^- + 4H_2O$$

Different end product species can be formed. For example, the possible iron sulfide minerals formed, sorted by increasing stability, are mackinawite (tetragonal FeS), greigite

(cubic Fe_3S_4), marcasite (orthorhombic FeS_2) and pyrite (isometric FeS_2); pyrite being the most abundant species (Billon et al., 2001; Fanning et al., 2010; Kurek, 2002; Rickard and Morse, 2005). The first two are quiet labile, and are considered as part of the acid volatile sulfides (AVS), which are dissolved very rapidly upon oxidation, while the latter two are relatively more stable. Furthermore, iron sulfide may initially be formed as mackinawite, and subsequent reactions give rise to greigite and pyrite (Billon et al., 2001; El Samrani et al., 2004; Fanning and Fanning, 1989a; Rickard, 1973). Iron sulfides might form from the reduction of several Fe species, such as iron oxides and oxy-hydroxides. Furthermore, freshly formed, poorly crystalline and fine-grained ferrihydrite phases are favorably reduced over aged and crystalline (older) iron oxides, such as hematite, goethite and magnetite (Brennan and Lindsay, 1998; Du Laing et al., 2009; Lynch et al., 2014).

8.1.1. The emergence and detection of framboïdal pyrites

The formed pyrite particles (FeS_2), each considered as a microcrystal, then form a spherical structure resembling a raspberry, which is “framboise” in French, hence the name framboïdal pyrite (Ohfuji and Rickard, 2005). The packing of the microcrystals is not necessarily spherical or framboïdal, yet it is a common form (Wilkin and Barnes, 1997). Several pathways have been shown to be responsible for the framboïdal structure. One is an abiotic and geomorphological self-organization of the microcrystals (Butler et al., 2000; Wilkin and Barnes, 1997), another one is nucleation and growth of microcrystals, which might be dependent on biogenic processes. Another pathway is the pre-existence of a spherical structure that is later filled with microcrystals (Rickard, 1970; Roberts, 2015). The pre-existing spherical structures might be algal cysts, such as *Tasmanites* (Schieber and Baird, 2001), remains of spherical organic globules, gaseous vacuoles (Rickard, 1970), fossilized bacterial colonies (Rickard, 1970; Wilkin and Barnes, 1997) or remains of plant vascular structures or cellular materials (Roberts, 2015).

Iron mono- and poly-sulfides were macroscopically (via black color formation) and microscopically visible after iron oxides were buried for 2 years in tidal marshes (Rabenhorst, 1990). However, other studies concluded that the transformation of ferric minerals (such as ferrihydrite and goethite) to iron sulfides is rather a quick process; using “indicator of reduction in soil, IRIS” tubes, only a couple of hours were sufficient to observe the change in color from orange-brown (iron oxide/oxy-hydroxides) to black (iron sulfide) (Fanning et al., 2010; Rabenhorst et al., 2010). The sulfides started to re-oxidize as soon as they were exposed to O_2

(Castenson and Rabenhorst, 2006). Total re-oxidization of Fe sulfide was visible after two hours of exposure to ambient atmosphere (Fanning et al., 2010).

The detection of sulfide phases is possible by light microscopy and scanning electron microscopy (SEM). Some of the common pyrite phases are shown in Figure I-9. It should be noted that framboïdal pyrites are distinguishable via optical microscopy, especially if samples are prepared as polished thin sections. Framboïdal pyrites are common in sediments where anaerobic oxidation of methane occurs (Xu, 2010) (see also Eq. I-7 – Eq. I-9 for the reactions). Studies performed in conditions similar to anoxic sediments showed that metals, such as Co, Cu, Mn, Pb, Zn and Cd, could be co-precipitated and adsorbed on metal sulfides (pyrite and mackinawite) during their formation (e.g. Arakaki and Morse, 1993; Lewis, 2010; Morse and Arakaki, 1993; Morse and Luther, 1999).

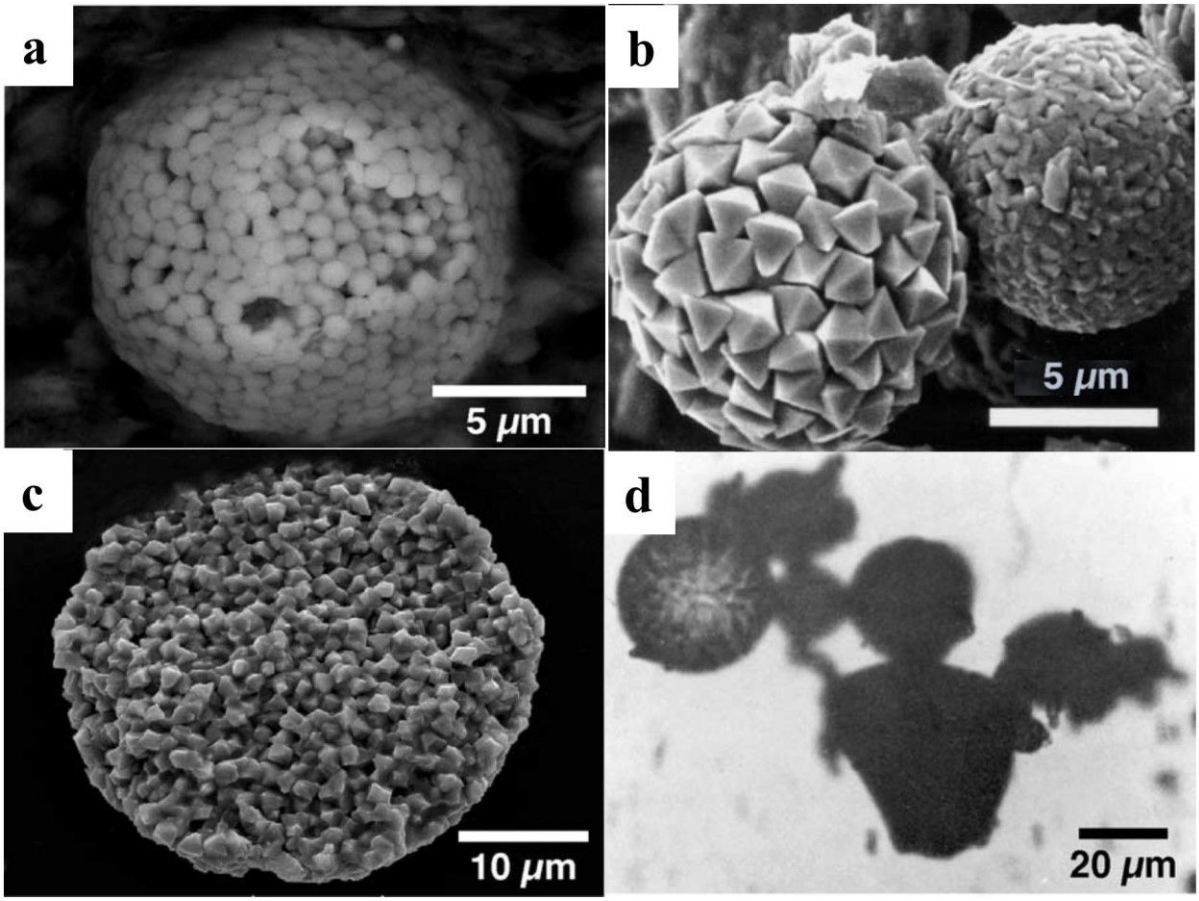

Figure I-9: Common framboïdal pyrites detected by microscopic tools.
a: SEM back-scattered electrons (BSE) micro-image of sub-spheroidal pyrite with cubo-octahedral microcrystals. b: SEM BSE micro-image of spherical pyrites with tetragonal microcrystals (left). c: SEM BSE micro-image of a disorganized framboïdal pyrite phase. d: optical microscope image (reflected light mode) showing a spherical framboïdal pyrite phase. Micro-images a, c and d are taken from Ohfuji and Rickard (2005), micro-image b is taken from Rabenhorst (2011).

8.2. Dissolution of iron sulfides upon oxidation of anoxic sediments

The sulfuricization processes were discussed in a previous section (see section *7.2*). Here, the sulfuricization of Fe is discussed, mainly pyrite. The precipitated pyrite formed by sulfidization (Eq. I-10) undergoes sulfuricization when oxic conditions prevail (Eq. I-11)

Eq. I-11: Pyrite sulfuricization reaction

$$FeS_2 + 3^{3}/_{4}O_2 + 3^{1}/_{2}H_2O \rightarrow 2H_2SO_4 + Fe(OH)_3$$

The produced sulfuric acid can further react with calcium released from carbonate minerals during dissolution to yield di-hydrated calcium sulfate (also known as gypsum) (Eq. I-12).

Eq. I-12: Gypsum formed from sulfuricization products

$$CaCO_3 + H_2SO_4 + H_2O \rightarrow CaSO_4.2H_2O + CO_2$$

Although the formation of minerals during sulfidization and sulfuricization can be rapid, the formed minerals can give insights on the processes that had taken place in those matrices (Fanning et al., 2010; Fanning and Fanning, 1989a). The degree of sulfuricization of metal sulfide is metal dependent. For example, the order of sulfuricization (or dissolution of metal sulfides) from the most soluble to least soluble is: Mn sulfides, Fe mono-sulfide (FeS), nickel sulfide (NiS), sphalerite (ZnS), cadmium sulfide (CdS), galena (PbS), cupper sulfide (CuS) and pyrite (FeS_2) (Du Laing et al., 2007b; Lynch et al., 2014). Finally, the binding of metals during sulfidization are temporal metal storage zones. In fact, metals released due to redox potential increase pose a threat to the aquatic life (Kelderman and Osman, 2007).

8.3. On the dissolution of sulfides and precipitation of Fe oxy-hydroxides

A common change that occurs after anoxic sediments oxidation is sulfide dissolution, which might be followed by Mn and Fe oxy-hydroxide precipitation (Du Laing et al., 2009; Lynch et al., 2014). Moreover, if anoxic sediments are exposed to air, due to partial draining and evaporation of pore water, iron sulfides dissolve and metals enrich the remaining pore water (Van den Berg et al., 1998). A noticeable amount of metals might be released from sulfide phases that had formed when the submerged sediments were still anoxic. Consequently, Fe and Mn oxy-hydroxides have the potential to scavenge those metals, since they are main metal carriers, such as Cd, Zn and Ni (Du Laing et al., 2009; Salomons et al., 1987).

8.4. Precipitation of Fe oxy-hydroxides

Formation of metal oxy-hydroxides is a common process in sediments. Metal oxy-hydroxide formation reduces metal concentrations by precipitation on one hand, and by

formation of surface coatings or co-precipitation with the formed oxy-hydroxides on the other. Oxidative precipitation and reductive dissolution of iron oxy-hydroxides take place in sediments (Humphries et al., 2010; Lynch et al., 2014 and articles cited therein). A study about dredging of contaminated sediments revealed that dissolved metal concentrations (Cd, Cu, Pb and Zn) increased upon oxidation, possibly due to the dissolution of metal sulfides. However, dissolved Fe concentrations rapidly decreased, while Mn, Ni and Co did not seem to be affected (Tack et al., 1998). Indeed, ferric iron hydrolysis occurs when pH is neutral or inferior to neutral. Therefore, in the former case, the dissolved iron could have been released due to the oxidative dissolution of Fe sulfides, which was coupled by fast episodes of pH decreases. Nonetheless, iron is rarely found in the dissolved phase in rivers, unless a significant drop of pH persists (Kosman, 2013). (Re)-precipitation of iron, possibly as oxy-hydroxides, might had happened via microbial populations, which is rather a quick process (starting from a few minutes); bacteria were shown to precipitate amorphous Fe phases via exopolymeric substances (Henry et al., 2013). The freshly formed oxy-hydroxides have higher scavenging ability than older (aged) and more crystalline forms. For example, freshly precipitated Mn and Fe oxy-hydroxides have 10-fold the capacity to bind metals than aged ones (Shuman, 1977). Indeed, freshly formed Fe oxy-hydroxides have high CEC; therefore, dissolved metals might form coatings onto the newly formed Fe oxy-hydroxides (Desbarats and Dirom, 2007; Lynch et al., 2014). Afterwards, the Fe oxy-hydroxides start to crystallize, and slow diffusion of the coating metals might occur (Axe and Trivedi, 2002; Farley et al., 1997). Some of the metals that were proven to be well scavenged by Fe oxy-hydroxides are Cd, Cu, Zn and Pb (Desbarats and Dirom, 2007; Evans, 1991). When Fe oxides become crystalline, metals can no longer incorporate into the structure (or at least only rarely and with slower kinetics). On a study on lead and nickel interaction with ferrihydrite, lead formed labile species with the sorbent, even more labile than nickel; during crystallization of iron oxides, nickel could be incorporated into the crystal, however, not without a delay in iron crystallization rate (Farley et al., 1997; Ford et al., 1999). Various iron phases are formed after Fe oxy-hydroxide precipitation, which are of higher crystallinity than the initial oxide or oxy-hydroxide formed, such as ferrihydrite, goethite, hematite and magnetite (Thompson et al., 2006). These processes are part of short term ageing that happen in sediments (Langmuir and Whittemore, 1971; Nordstrom and Alpers, 1999). Some metals are preferentially sorbed onto Fe oxy-hydroxides. For example, affinity for metal sorption onto ferric oxide followed the order of Pb, Cu, Zn and Cd (Desbarats and Dirom, 2005; Nordstrom and Alpers, 1999). In another study, Zn was more preferentially coated on ferric oxides (Burton et al., 2005). Moreover, the binding of metals is element

dependent (in addition to pH dependent); i.e. some metals might have higher sorption edges[xx] than others, which consequently reflects the mobility of the metals. For instance, Pb and Cu have lower sorption edges than Zn and Cd; therefore, the formers are more immobilized in natural sediments, while the others are more mobile (Galán et al., 2003; Lynch et al., 2014). Indeed, Pb is considered as a rather immobile element in sediments (e.g. Calmano et al., 1993a; Förstner, 1984; Gao et al., 2010). Lead could be highly scavenged (85% of the released metal) by Fe and Mn oxy-hydroxides after its release from sulfide phases, while other metals were significantly scavenged at lower percentages (30% of Cd, 34% of Zn and 53% of Cu) (Calmano et al., 1993a). Again, different conditions and initial sorbent interactions might lead to variable binding phases. In addition to Fe and Mn oxy-hydroxides as being binding phases for metals, carbonates, organic matter and clay phases (possibly with surface mineral coatings) are also metal carriers (Du Laing et al., 2009). For example, in the same study where Cd, Ni and Zn were found to be majorly bound to Fe and Mn oxy-hydroxides (Salomons et al., 1987), Cu was found to be mainly associated to organic matter.

On the particularity of metal – fine fraction interaction, part of the interaction is by Fe oxy-hydroxide coatings onto clay surfaces, since metal oxy-hydroxides initially have high CEC upon precipitation (Desbarats and Dirom, 2007; Lynch et al., 2014), and have high reactive sites on the relatively high specific surface area (Zhuang and Yu, 2002). In certain cases, where metals were seen to be more enriched in the fine fraction, sequential extraction revealed that those metals were mainly associated to Fe oxy-hydroxides (e.g. Prasad et al., 2006; A. K. Singh et al., 1999; Yao et al., 2015), possibly as coatings on clay minerals. On a study that compared metal contents in bulk sediment samples, and fractions superior and inferior to 63 µm, the metals associated to Fe and Mn oxides or oxy-hydroxides (reducible fraction) were highly found in the fine fraction (< 63 µm) (Boateng, 2015). Finally, a schematic representation showing some of the main interactions and processes in deposited riverine sediments is depicted in Figure I-10.

8.5. Iron in the context of mining and steelmaking

Iron ore mining, smelting, and pig iron and steel production are main sources for iron introduction into sediments (Das et al., 2007; Mansfeldt and Dohrmann, 2004; Van Herck et

[xx] The pH at which 50% of sorption occurs.

al., 2000). Other sources of iron are included in Table I-3. The iron bearing particles that enter the environment are various, depending on the initial iron ores and the processes and reactions taking place. During the production of pig iron (also called cast iron), iron ore is mined and smelted to extract iron; nonetheless, some forms of iron are not extractable, and therefore might remain in by-products and waste materials. Indeed, studies have shown that flue dusts (waste material), slag (by-product) and sludge (waste material) of blast furnaces might contain high iron contents (Das et al., 2007, 2002; Trinkel et al., 2016; Yildirim and Prezzi, 2011 and articles cited therein). For example, flue dusts might contain magnetite, wuestite and hematite (Das et al., 2002; Nyirenda, 1991); blast furnace sludge (BFS) might contain hematite, wuestite and magnetite (Mansfeldt and Dohrmann, 2004; Valentim et al., 2016; Vereš et al., 2010); and slag might contain hematite (Das et al., 2007; Yildirim and Prezzi, 2011).

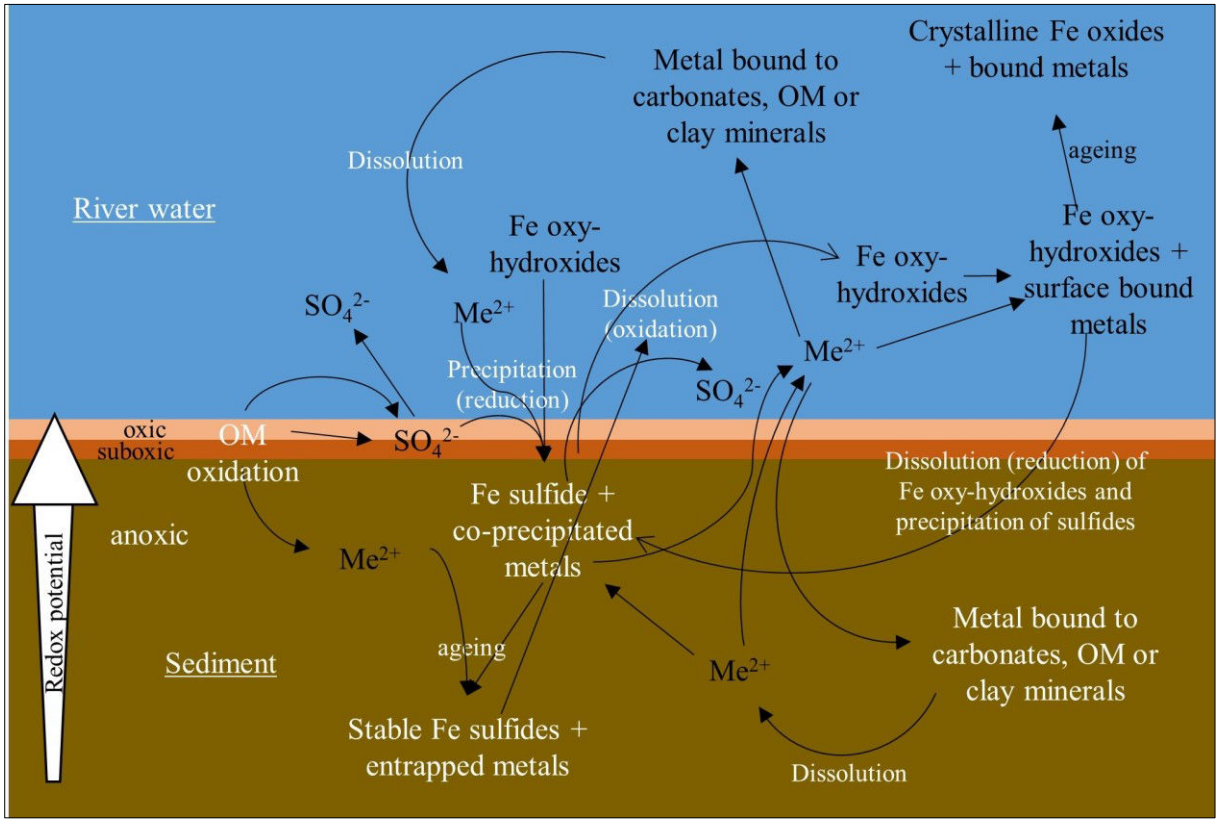

Figure I-10: Common precipitation and dissolution reactions that occur in river sediments.
The main processes presented above are the oxidative dissolution of Fe sulfides and oxidative precipitation of Fe oxy-hydroxides, and the reductive precipitation of Fe sulfides and reductive dissolution of Fe oxy-hydroxides. Co-precipitation of dissolved metals with Fe sulfides and Fe oxy-hydroxides might occur, especially during the initial periods of precipitation. Those metals might de-sorb from the phases upon Fe sulfide and Fe oxy-hydroxide dissolution. The schema is drawn according to the main Fe reactions, chiefly based on data of Du Laing et al., (2009) and Lynch et al., (2014).

On a study on the Minette iron ore, which was used for steel making in the Lorraine region in Northeastern France, the initial composition, weathered and formed minerals were discussed (Dagallier et al., 2002; Grgic et al., 2001). Minette is mainly composed of goethite

ooids, iron phyllosilicates (chamosite and berthierine), Fe-carbonate (siderite) and calcite. Upon contact with air, chamosite was completely transformed after ~ 80 years, and newly formed phases were detected, such as goethite nanogranules (Maitte et al., 2015); berthierine transformations that lead to incorporation of Fe and release of Si was also evidenced (Dagallier et al., 2002; Grgic, 2001; Grgic et al., 2013, 2002).

9. The case of Zn and Zn bearing minerals

Zinc is ubiquitously found in the environment as lithogenic minerals such as sphalerite and wurtzite (ZnS), smithsonite ($ZnCO_3$), hydrozincite ($Zn_5(CO_3)_2(OH)_6$), zincite (ZnO), Zn associated to ferrihydrite and hydrotalcite, and hemimorphite and willemite (Zn silicate) (e.g. Luxton et al., 2013; Manceau et al., 2004; Mertens and Smolders, 2013; Panfili et al., 2005). Zinc is associated to clay minerals as well, such as kaolinite, illite and montmorillonite, and to organic matter surfaces, which are weakly selective, reversible and pH dependent interactions (Mertens and Smolders, 2013; Pickering, 1980). The formation of Zn containing phyllosilicates, hydrozincite and Zn layered double hydroxides (LDH) are common in Zn rich matrices (e.g. Jacquat et al., 2009, 2008; Voegelin et al., 2005). In sediments, however, Zn minerals also precipitate, some of which are similar to lithogenic ones. Under anoxic conditions, Zn sulfides precipitate, i.e. secondary sulfides (Hochella et al., 2005). Zinc sulfides are neither as stable and reactive as Fe sulfides, nor as noticeable. Furthermore, precipitation of Zn phases is not common in river sediments, unless Zn contents or concentrations are high in sediments and porewater/river water, respectively.

9.1. The fate of zinc in submerged sediments

Zinc might co-precipitate during the first steps of iron sulfide formation (section *7.1*). In addition, substitution of Fe by Zn in iron framboïds was shown to happen when Zn contents are inferior to 1000 ppm. Moreover, spheroidal Zn sulfide framboïds were shown to precipitate when Zn contents were superior to 1000 ppm (Sawłowicz, 2000) in peat (Yoon et al., 2012), river sediments (Luther III et al., 1980) as well as suspended matter (Degens et al., 1972). The reactivity of Fe, over Zn, towards sulfide should be noted (Canfield et al., 1992); therefore, under the case of high Fe and Zn, Fe sulfide precipitation is still favored. In addition, amorphous Zn sulfides might be major Zn bearing minerals in suspended matter (Priadi et al., 2012). Iron mono-sulfides are considered as highly reactive phases, where they react with metals (such as Zn) according to the following reversible reaction (Eq. I-13) (Simpson et al.,

2000b). It should be noted that the reactions presented earlier regarding the formation of iron sulfides were irreversible (section *8.1*).

Eq. I-13: Zn reaction with iron mono-sulfide $Zn^{2+} + FeS \leftrightarrow ZnS + Fe^{2+}$

Dissolved Zn might originate from Fe oxy-hydroxide surfaces that had reductively dissolved. Since the formed Zn sulfides are not stable, they are considered as AVS (Hong et al., 2011; Peltier et al., 2005), which represent a part of the temporal metal holding phases under anoxia, and represent a source for metal release in oxic conditions. Moreover, reversible changes in Zn species from Zn associated to metal oxy-hydroxides or phyllosilicates towards sulfides (mainly ZnS) and smithsonite ($ZnCO_3$) happens during reducing conditions (Bostick et al., 2001). On the formation of secondary zinc sulfides, spheroidal micro-metric particles are biogenically formed by extracellular bio-mineralization (Moreau et al., 2004) within natural biofilms (Labrenz et al., 2000) (Figure I-11 a – b). Other Zn sulfides are made from finer particles and form clumps (Hochella et al., 2005). Those Zn sulfide phases have not been structurally ordered and lie within a film of Zn sulfides (Figure I-11 c). In addition, nano-particles of zinc sulfides also form in anoxic sediments (Figure I-11 d); those nano-particles are thought to had co-precipitated metals during their formation, like As and Pb, as suggested by small amounts of As and Pb in their structures (determined by EDXS). Selected area electron diffraction (SAED) patterns on those nano-particles were similar to sphalerite, therefore suggesting that those secondary sulfides are the precursors of sphalerite. It should be noted that Zn sulfide formation might also be an abiotic process, yet the biotic factor enhanced the crystallinity of the formed sulfides via carbonates present in the extracellular polymeric substances (Jain et al., 2015; Xu et al., 2016).

9.2. The fate of Zn under oxic conditions

Under oxic conditions, Zn might be associated to oxy-hydroxides (such as iron oxy-hydroxides). Furthermore, the association occurs at surface hydroxyl groups (Bradl et al., 2005; Evans et al., 2010; Stumm and Morgan, 1996) according to the reversible equation presented below (Eq. I-14), where ≡S–O represents the surface hydroxyl group of metal oxy-hydroxides or organic matter. The ≡S–O can also belong to clay minerals.

Eq. I-14: Zn sorption onto surface of metal oxy-hydroxide $\equiv S - OH + Zn^{2+} \leftrightarrow \equiv S - ZnO^{+} + H^{+}$

Some examples about Zn sorption onto Fe oxy-hydroxides were mentioned earlier in the text, where the scavenging ability of Fe oxy-hydroxides was discussed (section *8.4*). Indeed, amorphous Fe oxy-hydroxides were shown to be important zinc scavengers in river systems

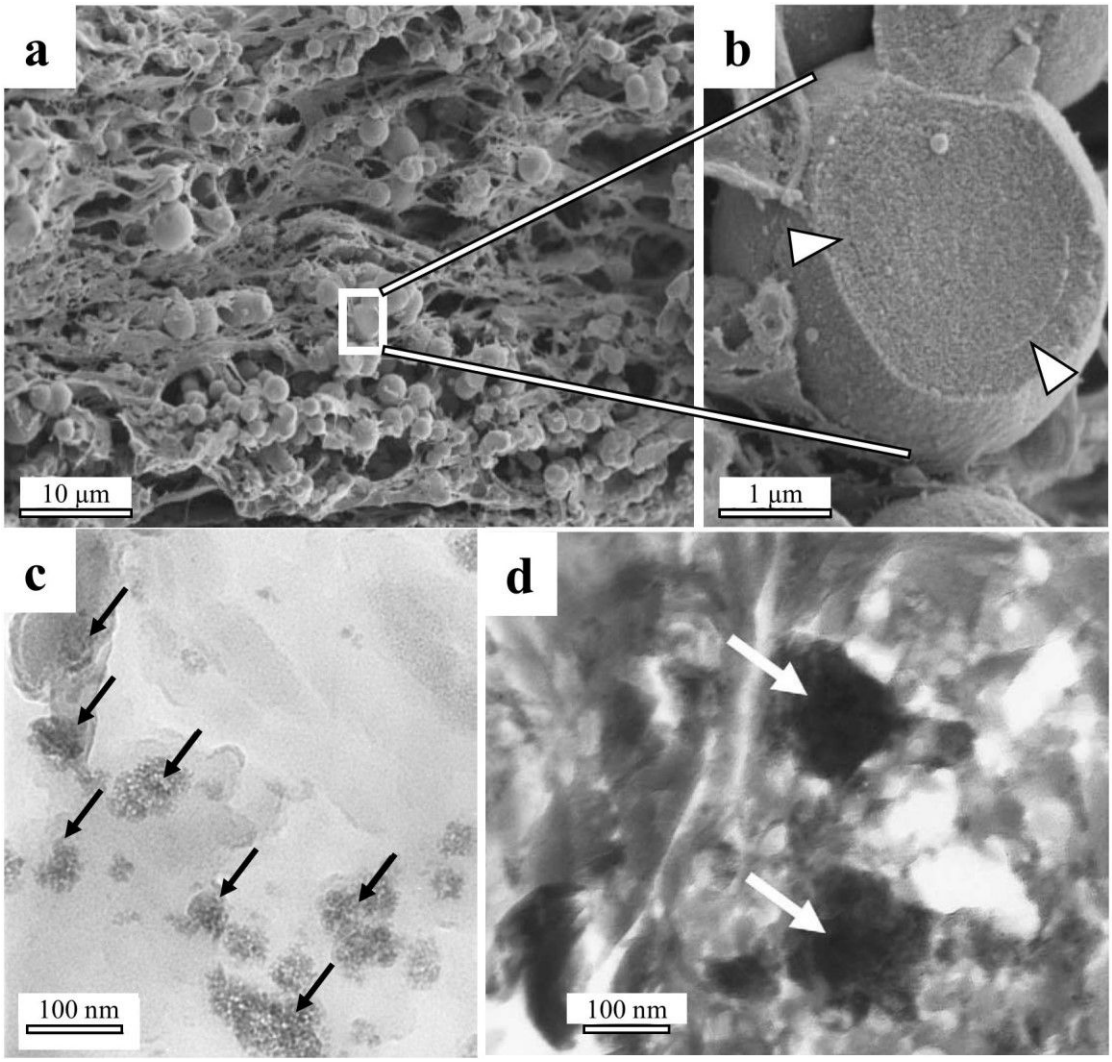

Figure I-11: Zn sulfide phases in anoxic matrices.
a and b: Field-emission scanning electron microscopy (FESEM) of spheroidal zinc sulfide particles (sphalerite) formed via sulfate reducing bacteria within a natural biofilm matrix. A zoom on a spheroidal micro-particle (in white rectangle) is shown in micro-image b: internal structure of a sphalerite particle showing concentric banding (white arrows), indicating their poly-crystalline character. c: TEM micro-image of clumps of fine zinc sulfides (black arrows) in a matrix of Zn sulfide film of various thicknesses (different shades of grey) that have formed in an anoxic riverbed. d: Circular/spherical Zn sulfide masses, also termed nano-particles (white arrows) with diffraction patterns similar to sphalerite. Those circular masses also contain minor amounts of Fe and Pb.
FESEM micro-images a and b are modified from Moreau et al., (2004). TEM micro-images c and d are modified from Hochella et al., (2005).

(e.g. Montargès-Pelletier et al., 2014) and in soils. Surface coating of Zn onto oxy-hydroxides, as well as organic matter and clay minerals, occur as Zn^{2+} (Mertens and Smolders, 2013); specific sorption of Zn species onto phyllosilicates also form (Isaure et al., 2002), mainly in sediments where Zn is enriched, such as settling ponds of industrial wastes (e.g. BFS) (Kretzschmar et al., 2012; Voegelin et al., 2005). In Zn rich oxic matrices, LDH and phyllosilicates are the main Zn bearing phases. These Zn containing phases could develop from ZnO as a function of time, as revealed by Voegelin et al., (2005). Indeed, ZnO was completed dissolved within several months (a little longer than 9 months) after zincite was introduced into

the soil. As a result, Zn majorly formed Zn-LDH and to a lesser extent Zn-phyllosilicates, while only a small fraction was associated to organic phases. On the formation or association and precipitation of Zn-LDH, some LDH like hydrotalcites are present in Zn rich soils on one hand (Manceau et al., 2004 and references cited therein; Panfili et al., 2005), and are efficient Zn scavengers on the other (Bellotto et al., 1996; Deja, 2002).

9.3. Fate of zinc released from steel industries

Similarly to Fe, Zn might be enriched in sludge and slag from steel industries (Das et al., 2007; Mansfeldt and Dohrmann, 2004; Van Herck et al., 2000). The main Zn species released from blast furnaces of steelmaking industries are oxides, yet they form sulfides after deposition under anoxia. Indeed, sphalerite could be found in piled and settled BFS, as detected by synchrotron XRD. Under atmospheric conditions, sulfide dissolution and Zn-LDH and phyllosilicate formation is possible (Kretzschmar et al., 2012), similar to the process discussed in section *9.2* and Eq. I-14). Other studies showed that the main Zn species released from smelters are franklinite ($ZnFe_2O_4$), willemite (Zn_2SiO_4), gahnite ($ZnAl_2O_4$), zincite, gunningite ($ZnSO_4.H_2O$), hardystonite ($CaZnSi_2O_7$) and hydrozincite (Jacquat et al., 2011; Luxton et al., 2013). Several factors play a role in the Zn species released from smelters, such as the raw materials used, temperature inside the smelters, sizes of the Zn containing particles and treatment of the materials released from the smelters (Besta et al., 2013; Trinkel et al., 2016, 2015). Zn rich particles might also be released from smelters and BFs as dust particles, which are in the form of ZnO or Zn-Fe ferrite spinel, yet small amounts of Zn might be found as sulfides and (alumino)-silicates (Nyirenda, 1991).

10. How to distinguish natural sediments from those that have been impacted by anthropogenic activities?

Firstly, visual inspection of sediments might give some indications about the nature. Furthermore, color might be an indicator of iron minerals. For example, blackish colored sediments might suggest the presence of reduced iron minerals (Fe sulfides), orangeish color might indicate Fe oxide minerals (goethite), dark red-brownish color might indicate ferrihydrite and reddish color might indicate hematite (Fanning et al., 2010; Rabenhorst et al., 2010; Thwaites, 2006). Additionally, grey-blackish color might also develop by anaerobic degradation of organic matter (Tyson, 1995). Texture, coupled with color in some cases, and presence of foreign materials or objects might reveal the occurrence of industrial wastes; the

presence of diatom skeletons, dwelling organisms, plant debris, mollusk shells and other indications of biota suggest an inhabitable medium for organisms, either when the materials were suspended in the river water or when they had settled. In the coming parts, some criteria are set to distinguish natural sediments from those that have been enriched with anthropogenic matter, namely in terms of geochemistry and mineralogy.

10.1. Geochemical composition and metal contents in sediments

The chemical composition of sediments might indicate whether they are impacted by anthropogenic activities. This is true for certain elements when found at elevated contents. For example, elevated Fe contents in sediments might be caused by deposits from iron metallurgy wastes and by-products, Zn might be introduced from Zn smelters and sewage sludge, and Pb might be introduced from lead batteries, coal burning, steel industries and automobile exhaust (also see Table I-3 for more sources of certain metals). Table I-4 shows some metal (Fe, Pb and Zn) contents for sediments that have been influenced by anthropogenic activities and are compared with metal contents (more or less) of natural sediments, sedimentary materials and continental crust.

The natural content is referred to as the geochemical background level or geochemical baseline. The term geochemical background was defined previously (section *4.1*). However, it should be noted that there is no precise comparison between metal contents in continental crusts (or soils) and river sediments, since sediments are formed from more than just weathered continental crust. Also, the natural background of sediments should be location dependent, since sediments forming at a specific site depend on the local geological background (see section *2*). Nonetheless, a rough comparison might be made between river sediments belonging to different locations, or between river sediments and continental crust to give a possibility of metal enrichment. A possible limitation for elemental content comparison between different sediment samples is the variation in grain size (e.g. Fukue et al., 2006); therefore, normalization of the anthropogenically introduced element is done by using a “lithogenic” element, such as Al, Si, Mn and Fe, to compensate for the variation in grain size. The idea about comparing metal contents in a sediment to the geochemical baseline on one hand, and the normalization to another element on the other will be dealt with in the coming parts.

Table I-4: Contents of Fe, Pb and Zn in anthropogenic matrices and geochemical backgrounds.
The sources of metal input into sediments that have been affected by anthropogenic activities are included in the table. For comparison, geochemical background levels (or relatively uncontaminated matrices) for the Moselle River sediments (Northeastern France), sedimentary materials (North France) and the upper continental crust are included and marked by γ.
The values presented in the cells are ranges which are indicated in the cited references. Some values are rounded for clearness.

Source of metal	Metal content			Reference
	Fe (%)	Pb (mg/kg)	Zn (mg/kg)	
Metallurgy (Zn and Pb smelters)	2	7300	3800	Vdović et al., (2006)
Mining and metallurgy	–	4 – 2396	28 – 2270	Zebracki (2008)
Metallurgy (Zn and Pb smelters)	1.2 – 4.1	11 – 19900	47 – 19600	Gabelle (2006)
Metallurgy (Zn and Pb smelters)	2.2 – 2.4	1850 – 12870	4590 – 7170	Lesven et al., (2010)
Mining and steelmaking*	11 - 38	61 – 727	1009 – 4521	Montargès-Pelletier et al., (2007)
Domestic discharge and industries (plant and metallurgy)	3.1 – 4.4	55.2 – 172	440 – 1900	Pekey (2006)
Urban, industrial (food) and shipping effluents	–	26 – 170	46 – 435	Soto-Jiménez and Páez-Osuna (2001)
γ Moselle surface sediments	0.5 – 4.3	26 – 107	25 – 214	Montargès-Pelletier, personal communication
γ Sedimentary materials in North France**	1.5 – 3.0	14 – 28	38 – 74	Sterckeman et al., (2006)
γ Continental crust	3.0 – 3.6	14 – 17	10 – 100	Martin and Meybeck (1979) and Alloway (2012)

– no values recorded.
γ Geochemical background level or uncontaminated matrices.
* The lower range represents the average minus the standard deviation, and the upper range represents the average plus the standard deviation.
** The values presented are the 1st and 3rd quartile.

10.2. Using factors and indices compared to the geochemical background to determine the degree of contaminated sediments

Different indices are used to quantify the contamination level, which are contamination factor (CF), enrichment factor (EF), pollution load index (PLI) and geoaccumulation index (I_{geo}). Indeed, several studies have used those factors and indices to study metal enriched sediments in vertical profiles of river sediments (e.g. Grosbois et al., 2012; Thevenon et al., 2013).

10.2.1. Contamination factor

Firstly, the CF is used to potentially indicate sediment (or matrix) enrichment with an element(s) of interest. The CF is calculated by the ratio of an elemental content found in a sample (of interest) to the content of the same element in a sample that has not been affected by anthropogenic activity (named background). The formula proposed by Hakanson (1980) is shown in Eq. I-15.

Eq. I-15: Contamination factor

$$CF = \frac{(El)_{sample}}{(El)_{background}}$$

Where CF is the contamination factor.
$(El)_{sample}$ is the content of an element of interest in the sample.
$(El)_{background}$ is the content of an element of interest in a sample that is not affected by anthropogenic metal enrichment.

However, the decision on the elemental background content might be tricky in some cases, especially in heterogeneous sediments that have various lithogenic contributions, have been affected by weathering, and where industrial by-products (sludge, dust, slag and others materials) have been introduced. Otherwise, the background content might be chosen from the upper continental crust, soil, or suspended matter (Martin and Meybeck, 1979; Viers et al., 2009; Wedepohl, 1995), depending on the sample of interest. Otherwise, the background level can be taken from samples located near the study site that are not influenced by anthropogenic activities (e.g. Sterckeman et al., 2006). In case of sediment cores, the lowest layer might be taken as background if it displays natural elemental contents and is sourced to deposits from pre-industrial times (e.g. Fukue et al., 2006; Thevenon et al., 2013). Seriousness of metal enrichment increases as CF increases. Values superior to 1.5 (Zhang and Liu, 2002) or 2 (Barakat et al., 2012) suggest that anthropogenic inputs are possible, while those inferior to 1.5 suggest lithogenic input. In addition, Hakanson (1980) proposed more detailed levels of contamination according to CF values shown in Table I-5.

Table I-5: Categories of contamination levels according to contamination factor.
According to Hakanson (1980).

Contamination Factor (CF)	Level of contamination
< 1	Low
1 - 3	Moderate
3 – 6	Considerable
> 6	Very high

10.2.2. Enrichment factor

Secondly, the EF is calculated similarly to CF, however, the elemental contents of the sample and the background are normalized by a reference element. The EF is calculated by the formula proposed by Ergin et al., (1991) and shown in Eq. I-16.

Eq. I-16: Enrichment factor

$$EF = \frac{(El/X)_{sample}}{(El/X)_{background}}$$

Where EF is the enrichment factor.
El is the content of an element.
X is the content of the reference element.
Sample is the sample of interest.
Background is a sample that is not affected by anthropogenic metal enrichment.

The background level was discussed in the previous section (section *10.2.1*). In many cases, the reference element is considered a major element that is representative of the geological background, is of low variability occurrences after metal deposition and is least affected by anthropogenic activities (Loska et al., 1997). Many studies have taken Al (Kłos et al., 2011; Matsunaga et al., 2014; Resongles et al., 2014), Si (Trzepla-Nabaglo et al., 2007), Mn (Shafie et al., 2013) or Fe (Aprile and Bouvy, 2008; Ghrefat et al., 2011) as reference. It is important to note that in some cases, such as the case of heterogeneous sedimentary materials, variations in the "reference" element might cause overestimation or underestimation of the enrichment factors. The values of the EF, according to Sutherland (2000), are then categorized into one of the levels found in Table I-6.

Table I-6: Categories of matrix according to enrichment factor. According to Sutherland (2000).

EF value	Significance
< 2	Depletion of mineral enrichment
2 – 5	Moderate enrichment
5 – 20	Significant enrichment
20 – 40	Very high enrichment
> 40	Extremely high enrichment

10.2.3. Geoaccumulation index

Thirdly, the I_{geo} is used to assess the enrichment level in sediments (and other matrices). The I_{geo} index is calculated by the following equation (Eq. I-17) proposed by Muller (1969).

Eq. I-17: Geoaccumulation index

$$I_{geo} = \mathrm{Log}_2\left(\frac{(El)_{sample}}{1.5(El)_{background}}\right)$$

Where I_{geo} is the geoaccumulation index.
El is the content of an element.
Sample is the sample of interest.
Background is a sample that is not affected by anthropogenic metal enrichment.

The coefficient 1.5 in the equation is a correction factor since the background contents of elements vary according to lithogenic variations. The level of contamination is later recognized according to the I_{geo} classes proposed by Muller (1981) and shown in Table I-7. The highest class or grade reflects up to a 100-fold enrichment with respect to the background.

Table I-7: Classes and contamination level of matrices according to the values of I_{geo}.
According to Muller (1981).

I_{geo} class	I_{geo} value	Contamination level
0	≤ 0	Background content
1	0 – 1	Uncontaminated
2	1 – 2	Uncontaminated – moderately contaminated
3	2 – 3	Moderately – strongly contaminated
4	3 – 4	Strongly contaminated
5	4 – 5	Highly contaminated
6	> 5	Extremely contaminated

10.2.4. Pollution load index

The previous calculation methods (CF, EF and I_{geo}) are used to determine the enrichment or contamination level of one element at a time. Pollution load index (PLI), however, includes more than one element. The PLI is calculated by using the CF of elements that were calculated according to Eq. I-15. Then, the PLI is calculated according to Tomlinson et al., (1980) presented in Eq. I-18.

Eq. I-18: Pollution load index

$$PLI = \sqrt[n]{CF_1 \times CF_2 \times CF_n}$$

Where PLI is the pollution load index.
CF is the contamination factor.
n is the number of elements.

The value of PLI then gives an estimation about the pollution load of the elements that are included in the equation. The value of the PLI would be one in case the elemental contents are exactly the same as the background contents; values above one indicate progressive increase in pollution load, according to Tomlinson et al., (1980).

10.3. Crystalline minerals as a criterion for lithogenic and anthropogenic matter differentiation

The mineralogical composition of sediments is generally related to watershed geology. Moreover, the presence of unexpected crystalline phases might indicate anthropogenic contributions. These minerals might be revealed by qualitative XRD analyses, under the condition of being well crystalline and constituting major phases. Indeed, the mineral(s) must comprise a few percentages of the sample in order to be detected in the diffractograms; the minimum content depends on crystal properties as well, and was recorded as an average between 0.5 and 5% (Luxton et al., 2013). Minerals found at percentages lower than 0.5 might be detected, while others higher than 5% might not, depending on the crystallinity of the minerals and the level of order in atom distribution within the crystal lattice. In river sediments of temperate regions, more specifically the Seine (Priadi et al., 2012), the Fensch (Montargès-

Pelletier et al., 2007) and the Moselle (Montargès-Pelletier et al., 2014) located in the northern and northeastern regions of France, the minerals quartz, calcite, dolomite, Na and K feldspars, illite and kaolinite are commonly detected. The presence of some minerals in soils (and sediments as well) might directly be related to their input source. For example, cerussite ($PbCO_3$), galena (PbS), smithsonite ($ZnCO_3$) and sphalerite (ZnS) might evidence the contributions from Zn smelters. Indeed, those minerals were proven to be originated from Zn smelters that have been transported by air to locations as far as 6.5 km (Vaněk et al., 2013). Additionally, anglesite ($PbSO_4$) was derived from Pb smelter emissions 4 km away from the site (Ettler et al., 2005); pyrite, galena and wurtzite (Zn,Fe)S were derived from Zn and Pb smelters (Boughriet et al., 2007); and anglesite, arsenosulvanite (Cu_3AsS_4), chalcopyrite ($CuFeS_2$), galena, plattnerite (PbO), tennantite ($(Cu,Fe)_{12}As_4S_{13}$) and quenselite ($PbMnO_2(OH)$) were derived from a Cu smelter as far as 12 km away from the site (Burt et al., 2003). Interestingly, in the last case, Pb and Cu minerals could be detected on the diffractogram (XRD) despite their "low contents"; lead ranged between 430 – 475 mg/kg (0.043 to 0.0475%) and copper content ranged between 590 – 1270 mg/kg (0.059 to 0.127%).

Iron bearing minerals might also be linked to certain industrial activities. For example, hematite, magnetite, wuestite and goethite might be sourced from iron mining (section *8.5*), wastes and by-products from steel industries (Das et al., 2002; Hudson-Edwards, 2003; Yildirim and Prezzi, 2011). Furthermore, some minerals can originate from lithogenic and anthropogenic activities. For example, quartz, calcite and dolomite can be originated from BF slag of steel industries (Yildirim and Prezzi, 2011 and references cited therein). In certain conditions, the predominance of a mineral might indicate the lithogenic or anthropogenic nature of sediments at the scale of bulk crystalline mineralogy; otherwise, complementary tools or analyses are crucial in revealing sediment nature.

10.4. Microscopic tools used in the investigation of sediment mineralogy at a sub-micrometric scale

Microscopic tools are used to reveal spatial resolution of micrometric particles that are beyond the limitations of XRD, such as poorly crystalline and amorphous phases, and phases (despite their crystallinity) that are found at low contents. As a result, the mineralogy and metal carriers of micrometric phases can be determined. Some of the common methods that are used to directly address mineralogical and chemical speciation are scanning and transmission electron microscopies (SEM and TEM, respectively), combined with semi-quantitative

elemental detection via EDXS (Energy dispersion of X-ray spectroscopy) through the detection of X-ray fluorescence, or combined with selective area electron diffraction (for TEM only, SAED). It should be noted that SEM and TEM reveal aspects of minerals at difference scales. Micrometric and sub-micrometric information can be produced by SEM and TEM, respectively. Furthermore, X-ray spectroscopy (XAS) reveals molecular information (by X-ray absorption near edge structure "XANES" and extended X-ray absorption fine structure "EXAFS"). For those reasons, the techniques mentioned above are in many cases combined in geochemical studies. Mineralogical and chemical speciation studies concerning sediments, suspended matter and soils regularly contain at least one of those techniques (e.g. Humphries et al., 2010; Isaure et al., 2002; Le Meur et al., 2016; Le Pape et al., 2014; Lesven et al., 2010; Montargès-Pelletier et al., 2014; Spadini et al., 2003).

SEM-EDX can be used to identify micrometric particles, despite of their origin (i.e. lithogenic or anthropogenic). For example, metal sulfides originating from Zn and Pb smelters, namely galena, sphalerite, pyrite, covellite (CuS), chalcopyrite and CdS, and natural clay/aluminosilicates were detected in Deûle River sediments (Lesven et al., 2010). Even though galena, pyrite and sphalerite were quantitatively evidenced by XRD, SEM added further information about some of those phases, such as sizes and shapes of pyrites (Figure I-12 a – b). Furthermore, SEM was used to visualize and identify different Fe bearing minerals in suspended particulate matter of a river highly influenced by steelmaking facilities (Montargès-Pelletier et al., 2014). In that case, iron bearing minerals were detected as micrometric particles of different shapes and sizes (Figure I-12 c – e), as well as nanoparticles. TEM can be used for the same objectives as SEM, however, the former is used to identify particles at finer resolutions, poorly crystalline and amorphous phases. It should be noted that SEM reveals surface properties of particles (shape and semi-quantitative elemental contents by EDXS), while TEM reveals not only the surface chemical composition, but also the integrated. In addition to the crystalline Fe bearing minerals detected by SEM (Figure I-12 c – e), poorly crystalline and amorphous Fe bearing minerals were revealed by TEM (Figure I-13 a – b). The variation in scale can clearly be seen between the SEM and TEM micro-images, where the first shows Fe bearing minerals in the range of few or tens of micrometers, while the latter shows Fe bearing minerals in the range of a few hundreds of nanometers. In another study, anthropogenic phases and their weathering by-products were seen in settling ponds belonging to steel wastes (Huot et al., 2014). Even though the circular and hairy/fibrous phases detected in micro-images a and b are similar in shape to those detected in micro-image c (Figure I-13),

EDXS revealed that they are certainly different. The fibrous aluminosilicates are thought to be weathering by-products of the spherical Si and Al glass-like phases (Figure I-13 c). In addition to microscopy, Mössbauer spectroscopy was also used in that study to detect various Fe bearing minerals, such as goethite, hematite and ferrihydrite, and Fe species (Fe^{2+} and Fe^{3+}).

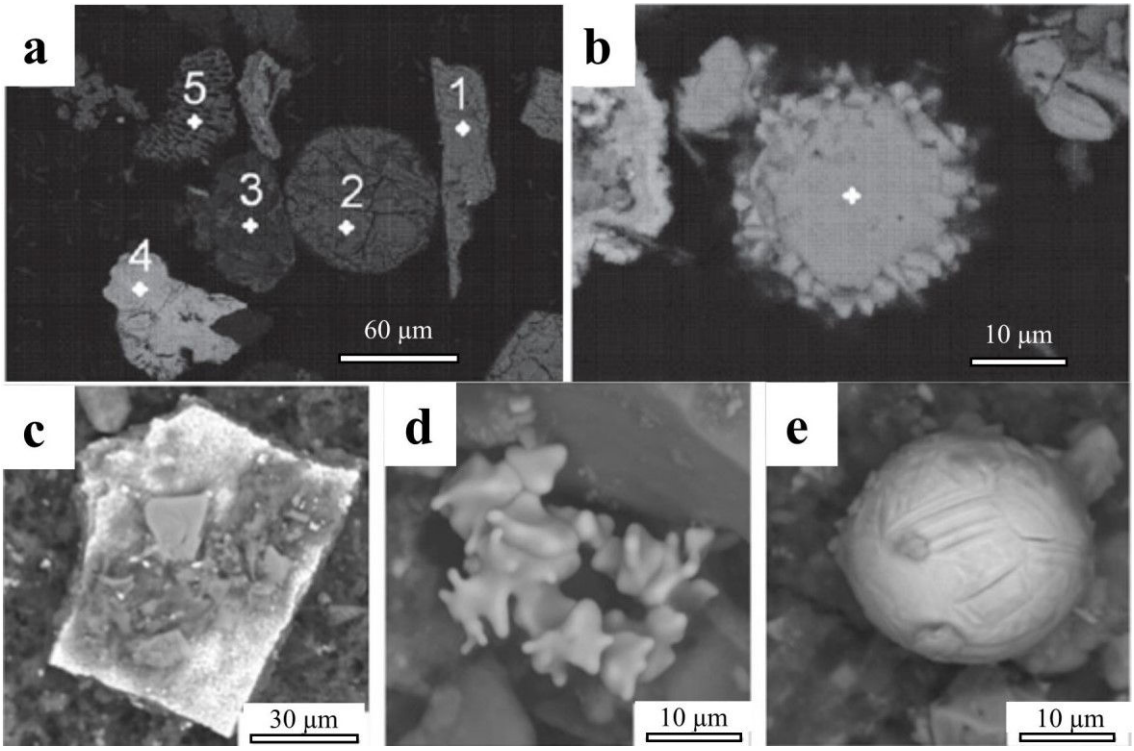

Figure I-12: SEM micro-images of river materials showing distinct phases.
a and b: SEM micro-images of heavy minerals of contaminated Deûle River sediments. a: 1: ZnS, 2 and 3: aluminosilicates, 4: PbS and 5: pyrite. b: pyrite. Note the various shapes and sizes of pyrite minerals. Modified from Lesven et al., (2010).
c – e: SEM micro-images of various Fe bearing particles collected from the Fensch River. Modified from Montargès-Pelletier et al., (2014).

Electron microscopies provide useful information about the diversity of minerals, yet an inconvenient is the relatively high detection limit. Indeed, trace element carriers might not be evidenced with such techniques if the content is lower than 1000 mg/kg (i.e. < 0.1%). Therefore, supplementary direct techniques, based on the use of synchrotron X-ray source, are commonly used to investigate solid speciation of trace metals. XAS (XANES and EXAFS) provides information about the local atomic environment (few Å) around an element. This spectroscopy is elementary selective and provides information about the oxidation state, the level of coordination and the number, nature and distances of closest neighbor elements. The spectra are more commonly interpreted on the basis of linear combination fitting (LCF) of well-known reference spectra (e.g. Isaure et al., 2002; Noël et al., 2014; Priadi et al., 2012). This spectroscopy can be performed at a global scale, on a centimeter sample or with the use of

spatially resolved X-ray beam (μ-XAS and μ-XRF). For example, Fe bearing minerals, such as goethite, ferrihydrite, lepidocrocite, Fe rich smectite and Fe rich serpentine, were quantified on the bases of XAS for mangrove sediments (Noël et al., 2014). Even though serpentine, smectite, goethite and pyrite were detected by XRD, the local atomic environment of Fe could only be shown by XAS.

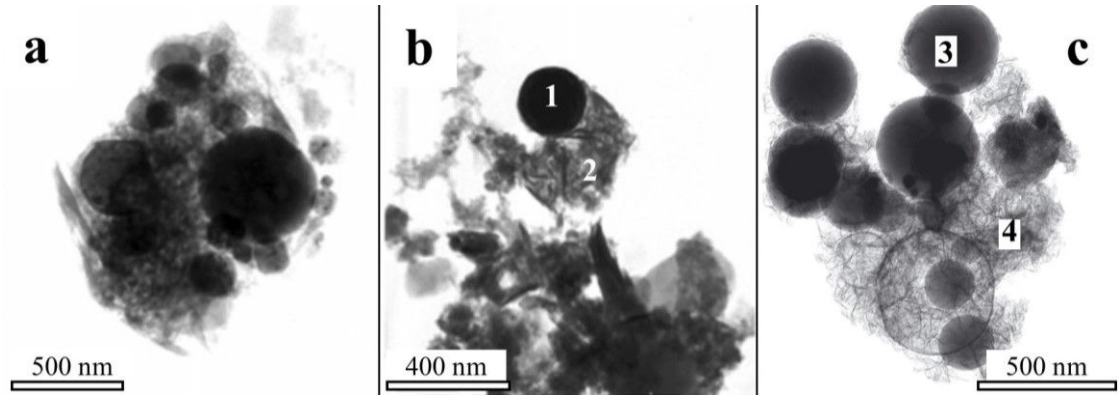

Figure I-13: TEM micro-images used to identify distinct phases at a sub-micrometric scale.
a and b: TEM micro-images of Fe rich aggregates of Fensch SPM. The spherical structures represent iron oxides. b: spherical iron oxides (1) and hairy Fe oxy-hydroxides (2). c: TEM micro-image of deposits from a settling pond containing wastes from steel industries. 3: glass-like and spherical aluminosilicates and 4: fibrous aluminosilicates.
Micro-images a and b are modified from Montargès-Pelletier et al., (2014). Micro-image c is modified from Huot et al., (2014).

Chemical speciation can also be approached via indirect techniques, such as sequential extraction, which was initially proposed by Tessier et al., (1979). Numerous studies have further modified and developed those extraction methods, such as modified time of extraction, concentration of extracting solution or proposing more extractions that would give more elemental bound phases (e.g. Förstner, 1984; Gao et al., 2010; Gómez Ariza et al., 2000; Okoro and Fatoki, 2012). Although being an indirect technique to reveal elements associated to different fractions, it is considered as a globally used technique. Nonetheless, sequential extractions might produce erroneous results (overestimated or underestimated values). Some of the shortcomings of sequential extraction are dissolution of non-target fraction(s), incomplete dissolution of target fraction(s), re-adsorption or re-precipitation of some target chemical species and change in oxidation state (Scheinost et al., 2002 and references cited therein). For example, acid soluble extraction step might release non-target fractions, such as metals bound to iron oxy-hydroxides. Furthermore, iron oxy-hydroxide phases might re-precipitate after dissolution, which might cause the scavenging of released (target) metals, causing underestimation. Another limitation of sequential extraction is non-targeted sulfide dissolution during the first steps of extraction, i.e. water soluble and exchangeable fractions

(Calmano et al., 2001; Gleyzes et al., 2002; Peltier et al., 2005). Therefore, prior knowledge on the composition of the sediment sample and coupling of sequential extraction with other techniques, such as XRD, SEM, TEM and XAS, might give better notions about the obtained results.

10.4.1. Complementarity between various techniques for mineral characterization

The methods presented above are usually used in a combined way. For example, XRD, SEM and Raman spectroscopy were used to study anthropogenic phases, such as metal sulfides and iron species in contaminated sediments (Lesven et al., 2010). Another study included XRD, SEM, TEM and Raman spectroscopy to study newly formed iron phases that were produced by bio-reduction (Maitte et al., 2015). Huot et al., (2014) used XRD, SEM, TEM and Mössbauer spectroscopy to study phases that have been transformed in a settling pond (of steelmaking wastes) over a period of 50 years. Going more into details about the complementarity of the techniques mentioned above; on a study on water, SPM and surface sediments collected from a highly polluted river, the Fensch, the increase of iron content in surface sediments and SPM samples was reflected by the detection of crystalline iron oxides (via XRD), such as hematite and wuestite; SEM and TEM-EDXS showed the structure and elemental composition of those iron phases. The Fe rich particles were concluded as zinc binding phases (microscopic analyses). Moreover, Fe oxidation state was revealed by scanning transmission X-ray microscopy (STXM) at the Fe $L_{2,3}$ edge (as Fe^{3+} and Fe^{2+}) and the binding phases of Zn were Fe-rich aggregates. Finally, by combining those techniques, the interaction between surface sediments and SPM, mainly for Fe and Zn, showed the importance of selective binding of Zn to Fe oxy-hydroxides, as well as selective remobilization of surface sediment phases (Montargès-Pelletier et al., 2014). In another study, SEM, TEM and EXAFS revealed the speciation of zinc in SPM samples across an urbanized stream (Le Pape et al., 2014). The preliminary mineralogical investigations should guide the choice of reference spectra that would be used for XAS.

Multiple techniques are also used to characterize one phase/mineral. For example, pyrite might be detected via XRD. However, SEM can give additional information (Figure I-9 a – d), such as size and type of structure (framboïdal, well organized sphere or disorganized) and arrangement of the domain properties of the framboïd (for example icosahedral domains) (Ohfuji and Akai, 2002). SEM can also reveal size, arrangement and structure of microcrystals,

such as octahedral, polyhedral, spherical, sub-spherical and cuboidal ones (Ohfuji and Rickard, 2005). It should be noted that dark field light microscope can also detect framboïdal pyrites and their sizes (Figure I-9 d). Furthermore, as metals might co-precipitate during the formation of the pyrites in anoxic conditions (e.g. Arakaki and Morse, 1993; Lewis, 2010; Morse and Arakaki, 1993; Morse and Luther, 1999), TEM might be further useful in revealing the bound metals in the framboïd microcrystals, rather than the whole framboïdal pyrite particle.

11. The parameters to follow to understand metal speciation in remobilized sediments

During sediment settling, consolidation of subsurface sediments occurs, which causes pore water to move to the more surface layers (see section *3.1*). Therefore, porosity and pore water volumes are affected by consolidation. Those two parameters, in addition to the bulk density, and their variations in the vertical profile of riverine sediments, are important factors to take in consideration when addressing erosion or remobilization of sediments (Sommerfield et al., 2007). Indeed, critical shear stress of fine grained sediments is dependent on consolidation level, porosity and bulk density, where sediments with higher porosity and lower consolidations are more susceptible to remobilization. In general, remobilization of the settled materials occurs when the vertical component of lift and drag created by the flow exceed frictional, cohesive and gravitational forces that hold grains in the riverbed (Dade et al., 1992). However, most of the studies related to sediment remobilization or resuspension were implemented at small scales or were theoretically based (Sommerfield et al., 2007 and references cited therein).

The interaction processes of metals with minerals, such as association/dissociation and precipitation/dissolution occurs in sediments according to various components and parameters. Some of the parameters are carbonates, CEC, complex size, microbial communities, mineral surface coatings, organic matter, pH, redox potential, salinity, sulfur, temperature, texture and plant population (e.g. Du Laing et al., 2009, 2007a). Actually, the interactions mentioned above do not solely depend on one parameter, rather a combination of parameters act as influencers upon sediment remobilization; therefore, a multi-parameter surveillance will help in understanding the fate of metals and metal bearing minerals.

11.1. Carbonates, period of flooding and pH

Period of flooding, or the endurance of a redox state (oxic or anoxic), controls metal and mineral speciation (Du Laing et al., 2009). On a study by Charlatchka and Cambier (2000), Fe and Mn oxy-hydroxides were reductively dissolved and pH declined upon flooding of the contaminated sediments. The reductive dissolution of those oxides released the bound metals Cd, Pb and Zn. Nonetheless, after a longer period of flooding (> 60 days), the metals co-precipitated as carbonates, instead of sulfides. Indeed, carbon precipitation occurs when sulfur concentrations are low (Du Laing et al., 2009). In addition, Ni was closely linked to the oxidation and reduction of Mn and Fe phases, which in turn was dependent on the flooding period. On a study by Du Laing et al., (2007b); after the flooding experiment commenced, Fe, Mn, Ni and Cr concentrations in the pore water increased, while those of Cd, Cu and Zn decreased. Moreover, after a couple of days under flooding conditions, Fe, Mn and Ni concentrations in pore water decreased, while those of Cd, Cu, Cr and Zn increased. The initial release of metals is linked to the reductive dissolution of the Fe and Mn oxy-hydroxides, which released Fe and Mn, and apparently the bound metals Ni and Cr, to the dissolved phase. After two days, however, Fe, Mn and Ni concentrations decreased, as did the redox potential, suggesting the formation of metal sulfides and possible (co)-precipitation of Mn and Ni. As for the initial decrease in Cd, Cu and Zn, they might have been directly bound to the precipitating metal sulfides or carbonates. When the redox potential dropped after a couple of days, concentrations of those metals increased in the pore water, which was caused by the dissolution of metal containing carbonates, and/or by the exchange of Ca cation with bound metals.

11.2. Carbonates, pH and sulfides

When pH in pore water drops (due to organic matter decomposition or AMD for example), the oxidative dissolution of sulfides occurs; the opposite is also true, i.e. oxidative dissolution of sulfides causes a drop in pH (also see section *7.2*). Nonetheless, at low pH, the negative binding sites on clay surfaces, organic matter and Fe and Al oxy-hydroxides are reduced, and sulfides and carbonates are prone to dissolution (Du Laing et al., 2009). Moreover, pH decline might be overcome by buffering if the matrix is rich in carbonates (Charlatchka and Cambier, 2000; Gambrell, 1994; Guo et al., 1997). In carbonate containing sediments, loss of carbonates (decalcification) might be a time bomb since metals are released when buffering capacity is absent (Van Den Berg and Loch, 2000). Carbonates might precipitate metals, thus

carbonate dissolution might be accompanied by releasing metals upon pH decrease (Du Laing et al., 2009).

11.3. Microbial communities, pH and redox potential

When anoxic sediments are re-oxidized, pH drops mainly due to metal sulfide dissolution, and some of the microbial communities boost (e.g. Förstner et al., 1989; Simpson et al., 1998). The drop in pH depends on the amount of dissolved sulfides and the buffering capacity of the matrix (Eggleton and Thomas, 2004). Nonetheless, some microbial communities might be responsible for oxidation processes, such as oxidative dissolution of Zn sulfides by *Thiobacillus ferrooxidans* and *T. thiooxidans* (Isaure et al., 2005). Those species are also involved in the iron oxide precipitation (Bradl et al., 2005; Ferris et al., 1989). Indeed, bacterial oxidative dissolution of Zn sulfides in dry sediments, or sediments with oxic conditions, released Zn to the percolating water, subsequently spreading Zn to a wider area.

11.4. Redox potential, salinity and sulfur

In anoxic conditions, increase in salinity increases desorption of metals in the absence of sulfides (Du Laing et al., 2009), otherwise stable metal sulfides form. Under oxic conditions, however, increasing salinity aids in the dissolution of Zn and Cd sulfides, which enhances metal release from particulate matter via metal exchange and formation of chloro-complexes (Du Laing et al., 2008a; Gerringa et al., 2001). On a study on dissolved Cd, Hg, Pb and Zn (Hahne and Kroontje, 1973), Cd, Cu and Cr (Gambrell et al., 1991), and Cd (Tipping et al., 1998), soluble metal-chloride complexes (chloro-complexations) formed when salts were present in the medium. Metals present in salts, such as Na, K, Ca and Mg, can compete with other metals (Tam and Wong, 1999). Indeed, higher Ca concentrations in solutions or porewater from salts (Tam and Wong, 1999) or amendments, such as phosphogypsum (Ammar et al., 2016), proved to cause metal release. Moreover, salts releasing monovalent cations, such as Na and K, are less competitive than bivalent ones, such as Ca and Mg (Khattak et al., 1989).

11.5. Period of resuspension, redox potential and salinity

On a laboratory study resembling contaminated sediment remobilization by a 250 days flooding using different salinities, metals were dissociated from particulate phase; metal concentrations increased in a salinity dependent manner. It should be noted that during the first days of resuspension (~ 20 days), the released metals are thought to have been re-adsorbed by Fe and Mn oxy-hydroxides, and thus low metal concentrations were detected. Indeed, the

solution was oxic for the first 20 days of the experiment. Afterwards, the redox potential became anoxic. Under that condition, Mn and Fe oxy-hydroxides dissolved, which lead to the de-complexation/release of the previously bound metals, which was translated as an increase in metal concentrations (Ni, Fe and Mn). Other metals behaved differently, such as Cd and Zn, which did not form complexes with Fe and Mn oxy-hydroxides; rather they became available during the first period of the resuspension experiment (Du Laing et al., 2008b). In another study, the oxidative dissolution of metal sulfides varied between metals at high salinities; Cd sulfide oxidative dissolution was higher than Zn under the same conditions. Even though CdS has lower solubility than ZnS, Cd is more prone to form dissolved chloro-complexes with Cd, which are more stable as salinity increases (Gerringa et al., 2001).

11.6. Organic matter and size of complex

Organic matter in sediments, such as plant litter and microbial exopolymers, can bind metals via ad- and ab-sorption, complexation and chelating (Alvim Ferraz and Lourençlo, 2000; Du Laing et al., 2006). Some organic matter fractions aid in metal mobility, such as when the organo-metal complex forms a dissolved phase (e.g. low – medium weight carboxylic acids, amino acids and fulvic acids). Indeed, several studies focused on organic matter as metal scavengers and mobilizers. Some of the studies focused on fulvic acid as scavengers of Cd, Co, Cu, Ni, Zn and Pb (Tipping et al., 1998), Cd, Cu, Pb and Zn (Wells et al., 1998), and Cu, Pb and Zn (Alvim Ferraz and Lourençlo, 2000). Moreover, larger organic complexes form particulate phases, which reduce metal mobility (Du Laing et al., 2009).

References

Ackermann, F., Bergmann, H., Schleichert, U., 1983. Monitoring of heavy metals in coastal and estuarine sediments - a question of grain-size: <20 µm versus <60 µm. Environ. Technol. Lett. 4, 317–328. doi:10.1080/09593338309384212

Acosta, J.A., Martínez-Martínez, S., Faz, A., Arocena, J., 2011. Accumulations of major and trace elements in particle size fractions of soils on eight different parent materials. Geoderma 161, 30–42. doi:10.1016/j.geoderma.2010.12.001

Adriano, D.C., 2001a. Trace Elements in Terrestrial Environments: Biogeochemistry, Bioavailability and Risks of Metals, 2nd ed. Springer, New York, NY. doi:10.1007/978-0-387-21510-5

Adriano, D.C., 2001b. Biogeochemical Processes Regulating Metal Behavior, in: Trace Elements in Terrestrial Environments. Springer New York, New York, NY, NY, pp. 29–59. doi:10.1007/978-0-387-21510-5_2

Aitchison, L., 1960. A History of Metals, Volume 1. MacDonald & Evans ; Interscience Publishers. Inc., London and New York.

Allan, R.J., 1986. The Role of Particulate Matter in the Fate of Contaminants in Aquatic Ecosystems. Inland Waters Directorate. Environment Canada, Ontario.

Alloway, B.J. (Ed.), 2012. Heavy Metals in Soils: Trace Metals and Metalloids in Soils and their Bioavailability, 3rd ed. Springer Science & Business Media.

Alvim Ferraz, M.C.M., Lourençlo, J.C.N., 2000. The Influence of organic matter content of contaminated soils on the leaching rate of heavy metals. Environ. Prog. 19, 53–58. doi:10.1002/ep.670190118

Amato, E.D., Simpson, S.L., Remaili, T.M., Spadaro, D.A., Jarolimek, C. V., Jolley, D.F., 2016. Assessing the effects of bioturbation on metal bioavailability in contaminated sediments by diffusive gradients in thin films (DGT). Environ. Sci. Technol. 50, 3055–3064. doi:10.1021/acs.est.5b04995

Ammar, R., Kanbar, H.J., Kazpard, V., Wazne, M., El Samrani, A.G., Amacha, N., Saad, Z., Chou, L., 2016. Role of phosphogypsum and NPK amendments on the retention or leaching of metals in different soils. J. Environ. Manage. 178, 20–29. doi:10.1016/j.jenvman.2016.04.042

Appleby, P.G., Oldfield, F., 1978. The calculation of lead-210 dates assuming a constant rate of supply of unsupported 210Pb to the sediment. CATENA 5, 1–8. doi:10.1016/S0341-8162(78)80002-2

Aprile, F.M., Bouvy, M., 2008. Distribution and enrichment of heavy metals in sediments at the Tapacurá River basin , northeastern Brazil. Brazilian J. Aquat. Sci. Technol. 12, 1–8.

Arakaki, T., Morse, J.W., 1993. Coprecipitation and adsorption of Mn(II) with mackinawite (FeS) under conditions similar to those found in anoxic sediments. Geochim. Cosmochim. Acta 57, 9–14. doi:10.1016/0016-7037(93)90463-7

Axe, L., Trivedi, P., 2002. Intraparticle surface diffusion of metal contaminants and their attenuation in microporous amorphous Al, Fe, and Mn oxides. J. Colloid Interface Sci. 247, 259–265. doi:10.1006/jcis.2001.8125

Ayrault, S., Roy-Barman, M., Le Cloarec, M.-F., Priadi, C.R., Bonté, P., Göpel, C., 2012. Lead contamination of the Seine River, France: Geochemical implications of a historical perspective. Chemosphere 87, 902–910. doi:10.1016/j.chemosphere.2012.01.043

Azzi, V., Kazpard, V., Lartiges, B., Kobeissi, A., Kanso, A., El Samrani, A.G., 2017. Trace metals in phosphate fertilizers used in eastern Mediterranean countries. Clean - Soil, Air, Water 45, 8. doi:10.1002/clen.201500988

Babbitt, B., 2002. What goes up, may come down. Bioscience 52, 656. doi:10.1641/0006-3568(2002)052[0656:WGUMCD]2.0.CO;2

Barakat, A., Baghdadi, M. El, Rais, J., Nadem, S., 2012. Assessment of heavy metal in surface sediments of Day River at Beni-Mellal Region , Morocco. Res. J. Environ. Earth Sci. 4, 797–806.

Bellotto, M., Rebours, B., Clause, O., Lynch, J., Bazin, D., Elkaïm, E., 1996. A reexamination of hydrotalcite crystal chemistry. J. Phys. Chem. 100, 8527–8534. doi:10.1021/jp960039j

Bertrand, O., Mansuy-Huault, L., Montargès-Pelletier, E., Faure, P., Losson, B., Argant, J., 2013. Recent vegetation history from a swampy environment to a pond based on macromolecular organic matter (lignin and fatty acids) and pollen sedimentary records. Org. Geochem. 64, 47–57. doi:10.1016/j.orggeochem.2013.09.008

Bertrand, O., Mansuy-Huault, L., Montargès-Pelletier, E., Losson, B., Argant, J., Ruffaldi, P., Etienne, D., Garnier, E., Dezileau, L., Faure, P., Michels, R., 2012. Molecular evidence for recent land use change from a swampy environment to a pond (Lorraine, France). Org. Geochem. 50, 1–10. doi:10.1016/j.orggeochem.2012.06.004

Bertrand, O., Mondamert, L., Grosbois, C., Dhivert, E., Bourrain, X., Labanowski, J., Desmet, M., 2015. Storage and source of polycyclic aromatic hydrocarbons in sediments downstream of a major coal district in France. Environ. Pollut. 207, 329–340. doi:10.1016/j.envpol.2015.09.028

Besta, P., Janovská, K., Samolejová, A., Beránková, A., Vozňáková, I., Hendrych, M., 2013. The cycle and effect of zinc in the blast-furnace process. Metalurgija 52, 197–200.

Billon, G., Ouddane, B., Laureyns, J., Boughriet, A., 2001. Chemistry of metal sulfides in anoxic sediments. Phys.

Chem. Chem. Phys. 3, 3586–3592. doi:10.1039/b102404n
Boateng, E., 2015. Distribution of Co, Cu and Pb in different Particle-size fractions of Polluted Zambian Wetland Sediments using the BCR Sequential Extraction Procedure. Ghent University.
Bostick, B.C., Hansel, C.M., La Force, M.J., Fendorf, S., 2001. Seasonal fluctuations in zinc speciation within a contaminated wetland. Environ. Sci. Technol. 35, 3823–3829. doi:10.1021/es010549d
Boughriet, A., Proix, N., Billon, G., Recourt, P., Ouddane, B., 2007. Environmental impacts of heavy metal discharges from a smelter in Deûle-canal sediments (northern France): concentration levels and chemical fractionation. Water. Air. Soil Pollut. 180, 83–95. doi:10.1007/s11270-006-9252-5
Bowman, M., Steve, H., Maclin, E., McClain, S., Sicchio, M., Souers, A., Graber, B., Johnson, S., 2002. Exploring dam removal: A decision-making guide. American Rivers and Trout Unlimited, Washington DC.
Bradl, H.B., Kim, C., Kramar, U., Stüben, D., 2005. Interaction of Heavy Metals, in: Heavy Metals in the Environment: Origin, Interaction and Remediation. Academic Press, pp. 28–164.
Brennan, E.W., Lindsay, W.L., 1998. Reduction and oxidation effect on the solubility and transformation of iron oxides. Soil Sci. Soc. Am. J. 62, 930–937. doi:10.2136/sssaj1998.03615995006200040012x
Burt, R., Wilson, M.A., Keck, T.J., Dougherty, B.D., Strom, D.E., Lindahl, J.A., 2003. Trace element speciation in selected smelter-contaminated soils in Anaconda and Deer Lodge Valley, Montana, USA. Adv. Environ. Res. 8, 51–67. doi:10.1016/S1093-0191(02)00140-5
Burton, E.D., Phillips, I.R., Hawker, D.W., 2005. Geochemical partitioning of copper, lead, and zinc in benthic, estuarine sediment profiles. J. Environ. Qual. 34, 263–273. doi:10.2134/jeq2005.0263
Butler, I., Rickard, D.T., Grimes, S., 2000. Framboidal pyrite: self organisation in the Fe-S system, in: An International Conference for Geochemistry. Oxford, U.K., U.K., pp. 276–277.
Byrne, P., Reid, I., Wood, P.J., 2013. Stormflow hydrochemistry of a river draining an abandoned metal mine: the Afon Twymyn, central Wales. Environ. Monit. Assess. 185, 2817–2832. doi:10.1007/s10661-012-2751-5
Caetano, M., Vale, C., Madureira, M.-J., 2003. Metal remobilisation during resuspension of anoxic contaminated sediment: short-term laboratory study. Water. Air. Soil Pollut. 143, 23–40. doi:10.1023/A:1022877120813
Cahill, R.A., Steele, J.D., 1986. Inorganic Composition and Sedimentation Rates of Backwater Lakes Associated with the Illinois River. Illininois State Geological Survey, Illinois.
Calmano, W., Förstner, U., Hong, J., Hong J., 1993a. Mobilization and Scavenging of Heavy Metals Following Resuspension of Anoxic Sediments from the Elbe River, Environnemental Geochemistry of Sulfide Oxidation, ACS Symposium Series. Umwelttechnik und Energiewirtschaft V-9, Washington, DC, DC. doi:10.1021/bk-1994-0550
Calmano, W., Hong, J., Förstner, U., 1993b. Binding and mobilization of heavy metals in contaminated sediments affected by pH and redox potential. Water Sci. Technol. 28, 223–235.
Calmano, W., Mangold, S., Welter, E., 2001. An XAFS investigation of the artefacts caused by sequential extraction analyses of Pb-contaminated soils. Fresenius' J. Anal. Chem. 371, 823–830. doi:10.1007/s00216-001-1106-9
Canfield, D.E., Raiswell, R., Bottrell, S.H., 1992. The reactivity of sedimentary iron minerals toward sulfide. Am. J. Sci. 292, 659–683. doi:10.2475/ajs.292.9.659
Cappuyns, V., Swennen, R., 2010. Oxidation of Anoxic Soils and Sediments: How Can We Evaluate the Risk of Heavy Metal Release?, in: Ramsey, G., McHugh, S. (Eds.), River Sediments. NOVA scientific publishers, pp. 77–101.
Carson, C.D., Fanning, D., Dixon, J.B., 1982. Alfisols and Ultisols with Acid Sulfate Weathering Features in Texas, in: Kittrick, J.A., Fanning, D.S., Hossner, L.R. (Eds.), Acid Sulfate Weathering. Soil Science Society of America, Madison, WI, pp. 127–146. doi:10.2136/sssaspecpub10.c8
Castenson, K.L., Rabenhorst, M.C., 2006. Indicator of reduction in soil (IRIS). Soil Sci. Soc. Am. J. 70, 1222–1226. doi:10.2136/sssaj2005.0130
Charlatchka, R., Cambier, P., 2000. Influence of reducing conditions on solubility of trace metals in contaminated soils. Water. Air. Soil Pollut. 118, 143–168. doi:10.1023/A:1005195920876
Clark, D.A., Norris, P.R., 1996. Acidimicrobium ferrooxidans gen. nov., sp. nov.: mixed-culture ferrous iron oxidation with Sulfobacillus species. Microbiology 142, 785–790. doi:10.1099/00221287-142-4-785
Cornell, R.M., Schwertmann, U., 2003. The Iron Oxides: Structure, Properties, Reactions, Occurrences and Uses, 2nd ed. John Wiley & Sons, Weinheim.
Cummings, D.E., Caccavo, F., Fendorf, S., Rosenzweig, R.F., 1999. Arsenic mobilization by the dissimilatory Fe(III)-reducing bacterium Shewanella alga BrY. Environ. Sci. Technol. 33, 723–729. doi:10.1021/es980541c
Cummings, D.E., March, A.W., Bostick, B., Spring, S., Caccavo, F., Fendorf, S., Rosenzweig, R.F., 2000. Evidence for microbial Fe(III) reduction in anoxic, mining-impacted lake sediments (Lake Coeur d'Alene, Idaho). Appl. Environ. Microbiol. 66, 154–162. doi:10.1128/AEM.66.1.154-162.2000
da Silva Oliveira, A., Bocio, A., Beltramini Trevilato, T.M., Magosso Takayanagui, A.M., Domingo, J.L., Segura-Muñoz, S.I., 2007. Heavy metals in untreated/treated urban effluent and sludge from a biological wastewater treatment plant. Environ. Sci. Pollut. Res. 14, 483–489. doi:10.1065/espr2006.10.355

Dade, W.B., Nowell, A.R.M., Jumars, P.A., 1992. Predicting erosion resistance of muds. Mar. Geol. 105, 285–297. doi:10.1016/0025-3227(92)90194-M

Dagallier, G., Grgic, D., Homand, F., 2002. Caractérisation minéralogique et microtexturale du vieillissement anthropique du minerai de fer lorrain. Comptes Rendus Geosci. 334, 455–462. doi:10.1016/S1631-0713(02)01783-2

Das, B., Prakash, S., Reddy, P.S.R., Biswal, S.K., Mohapatra, B.K., Misra, V.N., 2002. Effective utilization of blast furnace flue dust of integrated steel plants. Eur. J. Miner. Process. Environ. Prot. 2, 61–68.

Das, B., Prakash, S., Reddy, P.S.R., Misra, V.N., 2007. An overview of utilization of slag and sludge from steel industries. Resour. Conserv. Recycl. 50, 40–57. doi:10.1016/j.resconrec.2006.05.008

Degens, E.T., Okada, H., Honjo, S., Hathaway, J.C., 1972. Microcrystalline sphalerite in resin globules suspended in Lake Kivu, East Africa. Miner. Depos. 7, 1–12. doi:10.1007/BF00206891

Deja, J., 2002. Immobilization of Cr^{6+}, Cd^{2+}, Zn^{2+} and Pb^{2+} in alkali-activated slag binders. Cem. Concr. Res. 32, 1971–1979. doi:10.1016/S0008-8846(02)00904-3

Desbarats, A.J., Dirom, G.C., 2007. Temporal variations in the chemistry of circum-neutral drainage from the 10-Level portal, Myra Mine, Vancouver Island, British Columbia. Appl. Geochemistry 22, 415–435. doi:10.1016/j.apgeochem.2006.09.008

Desbarats, A.J., Dirom, G.C., 2005. Temporal variation in discharge chemistry and portal flow from the 8-Level adit, Lynx Mine, Myra Falls Operations, Vancouver Island, British Columbia. Environ. Geol. 47, 445–456. doi:10.1007/s00254-004-1175-0

Dhivert, E., Grosbois, C., Coynel, A., Lefèvre, I., Desmet, M., 2015a. Influences of major flood sediment inputs on sedimentary and geochemical signals archived in a reservoir core (Upper Loire Basin, France). Catena 126, 75–85. doi:10.1016/j.catena.2014.10.030

Dhivert, E., Grosbois, C., Rodrigues, S., Desmet, M., 2015b. Influence of fluvial environments on sediment archiving processes and temporal pollutant dynamics (Upper Loire River, France). Sci. Total Environ. 505, 121–136. doi:10.1016/j.scitotenv.2014.09.082

Donges, J.F., Donner, R. V, Trauth, M.H., Marwan, N., Schellnhuber, H.-J., Kurths, J., 2011. Nonlinear detection of paleoclimate-variability transitions possibly related to human evolution. PNAS 108, 20422–20427. doi:10.1073/pnas.1117052108

Droppo, I.G., Ongley, E.D., 1994. Flocculation of suspended sediment in rivers of southeastern Canada. Water Res. 28, 1799–1809. doi:10.1016/0043-1354(94)90253-4

Du Laing, G., De Meyer, B., Meers, E., Lesage, E., Van de Moortel, A., Tack, F.M.G., Verloo, M.G., 2008a. Metal accumulation in intertidal marshes: role of sulphide precipitation. Wetlands 28, 735–746. doi:10.1672/07-103.1

Du Laing, G., De Vos, R., Vandecasteele, B., Lesage, E., Tack, F.M.G., Verloo, M.G., 2008b. Effect of salinity on heavy metal mobility and availability in intertidal sediments of the Scheldt estuary. Estuar. Coast. Shelf Sci. 77, 589–602. doi:10.1016/j.ecss.2007.10.017

Du Laing, G., Rinklebe, J., Vandecasteele, B., Meers, E., Tack, F.M.G., 2009. Trace metal behaviour in estuarine and riverine floodplain soils and sediments: A review. Sci. Total Environ. 407, 3972–3985. doi:10.1016/j.scitotenv.2008.07.025

Du Laing, G., Van Ryckegem, G., Tack, F.M.G., Verloo, M.G., 2006. Metal accumulation in intertidal litter through decomposing leaf blades, sheaths and stems of Phragmites australis. Chemosphere 63, 1815–1823. doi:10.1016/j.chemosphere.2005.10.034

Du Laing, G., Vandecasteele, B., De Grauwe, P., Moors, W., Lesage, E., Meers, E., Tack, F.M.G., Verloo, M.G., Grauwe, P. De, 2007a. Factors affecting metal concentrations in the upper sediment layer of intertidal reedbeds along the river Scheldt. J. Environ. Monit. 9, 449–455. doi:10.1039/b618772b

Du Laing, G., Vanthuyne, D.R.J., Vandecasteele, B., Tack, F.M.G., Verloo, M.G., 2007b. Influence of hydrological regime on pore water metal concentrations in a contaminated sediment-derived soil. Environ. Pollut. 147, 615–625. doi:10.1016/j.envpol.2006.10.004

Dupont, J.-P., Guézennec, L., Lafite, R., Le Hir, P., Lesueur, P., 2001. Matériaux fins: le cheminement des particules en suspension. Editions Quae.

Eades, L.J., Farmer, J., MacKenzie, A.B., Kirika, A., Bailey-Watts, A.E., 2002. Stable lead isotopic characterisation of the historical record of environmental lead contamination in dated freshwater lake sediment cores from northern and central Scotland. Sci. Total Environ. 292, 55–67. doi:10.1016/S0048-9697(02)00026-8

Eggleton, J., Thomas, K. V., 2004. A review of factors affecting the release and bioavailability of contaminants during sediment disturbance events. Environ. Int. 30, 973–980. doi:10.1016/j.envint.2004.03.001

El Samrani, A.G., Lartiges, B.S., Ghanbaja, J., Yvon, J., Kohler, A., 2004. Trace element carriers in combined sewer during dry and wet weather: an electron microscope investigation. Water Res. 38, 2063–2076. doi:10.1016/j.watres.2004.01.029

EPA, 2008. Site contamination - Determination of background concentrations. EPA 838/08. Environmental

Protection Agency, Australia, Australia.
Ergin, M., Saydam, C., Baştürk, Ö., Erdem, E., Yörük, R., 1991. Heavy metal concentrations in surface sediments from the two coastal inlets (Golden Horn Estuary and İzmit Bay) of the northeastern Sea of Marmara. Chem. Geol. 91, 269–285. doi:10.1016/0009-2541(91)90004-B
Ettler, V., Vaněk, A., Mihaljevič, M., Bezdička, P., 2005. Contrasting lead speciation in forest and tilled soils heavily polluted by lead metallurgy. Chemosphere 58, 1449–1459. doi:10.1016/j.chemosphere.2004.09.084
EU Council, 2000. Directive 2000/60/EC of the European Parliament and of the Council of 23 October 2000 on the establishing a framework for Community action in the field of water policy.
Evans, D., 1991. Chemical and physical partitioning in contaminated stream sediments in the River Ystwyth, Mid-Wales. Environ. Geochem. Health 13, 84–92. doi:10.1007/BF01734299
Evans, L.J., Barabash, S.J., Lumsdon, D.G., Gu, X., 2010. Application of Chemical Speciation Modelling to Studies on Toxic Element Behaviour in Soils, in: Hooda, P.S. (Ed.), Trace Elements in Soils. John Wiley and Sons Ltd., Chichester, UK, UK, pp. 353–380.
Fanning, D., Fanning, M., 1989a. Sulfidization and Sulfuricization, in: Soil Morphology, Genesis and Classification. John Wiley and Sons Inc., New York, pp. 69–80.
Fanning, D., Fanning, M., 1989b. Mineral and Organic Matter Transformation, in: Soil Morphology, Genesis and Classification. John Wiley and Sons Inc., New York, pp. 29–41.
Fanning, D., Rabenhorst, M.C., Balduff, D., Wagner, D.P., Orr, R., Zurheide, P., 2010. An acid sulfate perspective on landscape/seascape soil mineralogy in the U.S. Mid-Atlantic region. Geoderma 154, 457–464. doi:10.1016/j.geoderma.2009.04.015
Farley, K.J., Ford, R.G., Bertsch, P.M., 1997. Changes in transition and heavy metal partitioning during hydrous iron oxide aging. Environ. Sci. Technol. 31, 2028–2033. doi:10.1021/es960824+
Farmer, J.G., MacKenzie, A.B., Eades, L.J., Kirika, A., Bailey-Watts, A.E., Centre, R., Estate, B., 1997. Influences on the extent and record of heavy metal pollution in sediment cores from Loch Tay in a mineralised area of Scotland. J. Geochemical Explor. 58, 195–202.
Ferrand, E., Eyrolle, F., Radakovitch, O., Provansal, M., Dufour, S., Vella, C., Raccasi, G., Gurriaran, R., 2012. Historical levels of heavy metals and artificial radionuclides reconstructed from overbank sediment records in lower Rhône River (South-East France). Geochim. Cosmochim. Acta 82, 163–182. doi:10.1016/j.gca.2011.11.023
Ferris, F.G., Tazaki, K., Fyfe, W.S., 1989. Iron oxides in acid mine drainage environments and their association with bacteria. Chem. Geol. 74, 321–330. doi:10.1016/0009-2541(89)90041-7
Fiedler, S., Vepraskas, M.J., Richardson, J.L., 2007. Soil Redox Potential: Importance, Field Measurements, and Observations, in: Advances in Agronomy. pp. 1–54. doi:10.1016/S0065-2113(06)94001-2
Fontugne, M.R., Duplessy, J.-C., 1986. Variations of the monsoon regime during the upper quaternary: Evidence from carbon isotopic record of organic matter in North Indian Ocean sediment cores. Palaeogeogr. Palaeoclimatol. Palaeoecol. 56, 69–88. doi:10.1016/0031-0182(86)90108-2
Ford, R.G., Kemner, K.M., Bertsch, P.M., 1999. Influence of sorbate-sorbent interactions on the crystallization kinetics of nickel- and lead-ferrihydrite coprecipitates. Geochim. Cosmochim. Acta 63, 39–48. doi:10.1016/S0016-7037(99)00010-1
Förstner, U., 1984. Chemical Forms and Reactivities of Metals in Sediments, in: Leschber, R., Davis, R.D., L'Hermite, P. (Eds.), Chemical Methods for Assessing Bio-Available Metals in Sludges and Soils. Elsevie, Münster, pp. 1–30.
Förstner, U., Ahlf, W., Calmano, W., 1989. Studies on the transfer of heavy metals between sedimentary phases with a multi-chamber device: Combined effects of salinity and redox variation. Mar. Chem. 28, 145–158. doi:10.1016/0304-4203(89)90192-8
Frings, P.J., Clymans, W., Fontorbe, G., De La Rocha, C.L., Conley, D.J., 2016. The continental Si cycle and its impact on the ocean Si isotope budget. Chem. Geol. 425, 12–36. doi:10.1016/j.chemgeo.2016.01.020
Fryirs, K.A., Brierley, G.J., 2012. Sediment Movement and Deposition in River Systems, in: Geomorphic Analysis of River Systems: An Approach to Reading the Landscape. Wiley-Blackwell Publishing, Ltd, Chichester, UK, pp. 81–115. doi:10.1002/9781118305454.ch6
Fukue, M., Yanai, M., Sato, Y., Fujikawa, T., Furukawa, Y., Tani, S., 2006. Background values for evaluation of heavy metal contamination in sediments. J. Hazard. Mater. 136, 111–119. doi:10.1016/j.jhazmat.2005.11.020
Gabelle, C., 2006. Etude de la contamination des sediments par les metaux dans les canaux et rivieres du nord de la France. Ph.D. thesis. Ecole Doctorale des Sciences de la Matiere, du Rayonnement et de l'Environnement. Universite de Lille, France.
Galán, E., Gómez Ariza, J.L., González, I., Fernández-Caliani, J.C., Morales, E., Giráldez, I., 2003. Heavy metal partitioning in river sediments severely polluted by acid mine drainage in the Iberian Pyrite Belt. Appl. Geochemistry 18, 409–421. doi:10.1016/S0883-2927(02)00092-6
Gambrell, R.P., 1994. Trace and toxic metals in wetlands—a review. J. Environ. Qual. 23, 883–891. doi:10.2134/jeq1994.00472425002300050005x

Gambrell, R.P., Wiesepape, J.B., Patrick, W.H., Duff, M.C., 1991. The effects of pH, redox, and salinity on metal release from a contaminated sediment. Water. Air. Soil Pollut. 57–58, 359–367. doi:10.1007/BF00282899

Gao, X., Arthur Chen, C.-T., Wang, G., Xue, Q., Tang, C., Chen, S., 2010. Environmental status of Daya Bay surface sediments inferred from a sequential extraction technique. Estuar. Coast. Shelf Sci. 86, 369–378. doi:10.1016/j.ecss.2009.10.012

Garcier, R.J., 2007. Rivers we can't bring ourselves to clean – historical insights into the pollution of the Moselle River (France), 1850–2000. Hydrol. Earth Syst. Sci. 11, 1731–1745. doi:10.5194/hess-11-1731-2007

GEC, 2006. Klamath River, Dam and Sediment Investigation. (Gathard Engineering Consulting), Seatle, Washington, USA.

Geesey, G. ll G., Alexander, G. V, Bray, R.N., Miller, A.C., 1984. Fish fecal pellets are a source of minerals for inshore reef communities. Mar. Ecol. Prog. Ser. 15, 19–25.

Gerringa, L.J.A., de Baar, H.J.W., Nolting, R.F., Paucot, H., 2001. The influence of salinity on the solubility of Zn and Cd sulphides in the Scheldt estuary. J. Sea Res. 46, 201–211. doi:10.1016/S1385-1101(01)00081-8

Ghrefat, H.A., Abu-Rukah, Y., Rosen, M.A., 2011. Application of geoaccumulation index and enrichment factor for assessing metal contamination in the sediments of Kafrain Dam, Jordan. Environ. Monit. Assess. 178, 95–109. doi:10.1007/s10661-010-1675-1

Gleyzes, C., Tellier, S., Astruc, M., 2002. Fractionation studies of trace elements in contaminated soils and sediments: A review of sequential extraction procedures. Trends Anal. Chem. 21, 451–467. doi:10.1016/S0165-9936(02)00603-9

Gómez Ariza, J.L., Giráldez, I., Sánchez-Rodas, D., Morales, E., 2000. Metal sequential extraction procedure optimized for heavily polluted and iron oxide rich sediments. Anal. Chim. Acta 414, 151–164. doi:10.1016/S0003-2670(00)00804-7

Gotoh, S., Patrick, W.H., 1974. Transformation of Iron in a Waterlogged Soil as Influenced by Redox Potential and pH. Soil Sci. Soc. Am. J. 38, 66–71. doi:10.2136/sssaj1974.03615995003800010024x

Grgic, D., 2001. Modélisation du comportement à court et à long terme des roches de la formation ferrifère lorraine. Lorraine University.

Grgic, D., Giraud, A., Auvray, C., 2013. Impact of chemical weathering on micro/macro-mechanical properties of oolithic iron ore. Int. J. Rock Mech. Min. Sci. 64, 236–245. doi:10.1016/j.ijrmms.2013.09.005

Grgic, D., Homand, F., Dagallier, G., 2002. Altération du minerai de fer dans les mines abandonnées de Lorraine. Rev. française géotechnique 49–60.

Grgic, D., Homand, F., Dagallier, G., 2001. Ageing of Lorraine (France) Abandoned Iron Mines, in: Rock Mechanics: A Challenge for Society. pp. 825–830.

Grosbois, C., Meybeck, M., Lestel, L., Lefèvre, I., Moatar, F., 2012. Severe and contrasted polymetallic contamination patterns (1900-2009) in the Loire River sediments (France). Sci. Total Environ. 435–436, 290–305. doi:10.1016/j.scitotenv.2012.06.056

Grossman, E., 2007. High tech trash: Digital devices, hidden toxics, and human health. Island Press, Washington.

Guo, T., DeLaune, R.D., Patrick, W.H., 1997. The influence of sediment redox chemistry on chemically active forms of arsenic, cadmium, chromium, and zinc in estuarine sediment. Environ. Int. 23, 305–316. doi:10.1016/S0160-4120(97)00033-0

Gutiérrez, M., Mickus, K., Camacho, L.M., 2016. Abandoned Pb--Zn mining wastes and their mobility as proxy to toxicity: A review. Sci. Total Environ. 565, 392–400. doi:10.1016/j.scitotenv.2016.04.143

Hahne, H.C.H., Kroontje, W., 1973. Significance of pH and chloride concentration on behavior of heavy metal pollutants: mercury(II), cadmium(II), zinc(II), and lead(II). J. Environ. Qual. 2, 444–450. doi:10.2134/jeq1973.00472425000200040007x

Hakanson, L., 1980. An ecological risk index for aquatic pollution control.a sedimentological approach. Water Res. 14, 975–1001. doi:10.1016/0043-1354(80)90143-8

Han, F.X., Banin, A., Su, Y., Monts, D.L., Plodinec, J.M., Kingery, W.L., Triplett, G.E., 2002. Industrial age anthropogenic inputs of heavy metals into the pedosphere. Naturwissenschaften 89, 497–504. doi:10.1007/s00114-002-0373-4

Hansen, J.A., Tjell, J.C., 1982. Sludge Application to Land - Overview of the Cadmium Problem, in: Davis, R., Hucker, G., L'Hermite, P. (Eds.), Environmental Effects of Organic and Inorganic Contaminants in Sewage Sludge. D. Reidel Publihing Company, Stevenage, pp. 91–112.

Heim, S., Schwarzbauer, J., 2013. Pollution history revealed by sedimentary records: a review. Environ. Chem. Lett. 11, 255–270. doi:10.1007/s10311-013-0409-3

Henry, R., Lo, M., Khoo, C., Zhang, H., Boysen, R.I., Picardeau, M., Murray, G.L., Bulach, D.M., Adler, B., 2013. Precipitation of iron on the surface of Leptospira interrogans is associated with mutation of the stress response metalloprotease HtpX. Appl. Environ. Microbiol. 79, 4653–4660. doi:10.1128/AEM.01097-13

Hillier, S., 1995. Erosion, Sedimentation and Sedientary Origin of Clays, in: Velde, B. (Ed.), Origin and Mineralogy of Clays. Springer Berlin Heidelberg, Berlin, Heidelberg, Heidelberg, pp. 162–219. doi:10.1007/978-3-662-12648-6

Hirst, J.M., Aston, S.R., 1983. Behaviour of copper, zinc, iron and manganese during experimental resuspension and reoxidation of polluted anoxic sediments. Estuar. Coast. Shelf Sci. 16, 549–558. doi:10.1016/0272-7714(83)90085-9

Hochella, M.F., Moore, J.N., Putnis, C. V, Putnis, A., Kasama, T., Eberl, D.D., 2005. Direct observation of heavy metal-mineral association from the Clark Fork River Superfund Complex: implications for metal transport and bioavailability. Geochim. Cosmochim. Acta 69, 1651–1663. doi:10.1016/j.gca.2004.07.038

Hong, Y.S., Kinney, K.A., Reible, D.D., 2011. Acid volatile sulfides oxidation and metals (Mn, Zn) release upon sediment resuspension: Laboratory experiment and model development. Environ. Toxicol. Chem. 30, 564–575. doi:10.1002/etc.411

Horowitz, A.J., 1991. A primer on sediment-trace element chemistry. Lewis Publishers.

Hudson-Edwards, K.A., 2003. Sources, mineralogy, chemistry and fate of heavy metal-bearing particles in mining-affected river systems. Mineral. Mag. 67, 205–217. doi:10.1180/0026461036720095

Huerta-Diaz, M.A., Tessier, A., Carignan, R., 1998. Geochemistry of trace metals associated with reduced sulfur in freshwater sediments. Appl. Geochemistry 13, 213–233. doi:10.1016/S0883-2927(97)00060-7

Humphries, M.S., Kindness, A., Ellery, W.N., Hughes, J.C., 2010. Sediment geochemistry, mineral precipitation and clay neoformation on the Mkuze River floodplain, South Africa. Geoderma 157, 15–26. doi:10.1016/j.geoderma.2010.03.010

Huo, S., Zhang, J., Yeager, K.M., Xi, B., Qin, Y., He, Z., Wu, F., 2015. Mobility and sulfidization of heavy metals in sediments of a shallow eutrophic lake, Lake Taihu, China. J. Environ. Sci. 31, 1–11. doi:10.1016/j.jes.2014.12.003

Huot, H., Simonnot, M.O., Watteau, F., Marion, P., Yvon, J., De Donato, P., Morel, J.-L., 2014. Early transformation and transfer processes in a Technosol developing on iron industry deposits. Eur. J. Soil Sci. 65, 470–484. doi:10.1111/ejss.12106

Isaure, M.-P., Laboudigue, A., Manceau, A., Sarret, G., Tiffreau, C., Trocellier, P., Lamble, G., Hazemann, J.-L., Chateigner, D., Arret, E.S., Iffreau, C.H.T., Su, L.P., Saclay, E. De, 2002. Quantitative Zn speciation in a contaminated dredged sediment by μ-PIXE, μ-SXRF, EXAFS spectroscopy and principal component analysis. Geochim. Cosmochim. Acta 66, 1549–1567. doi:10.1016/S0016-7037(01)00875-4

Isaure, M.-P., Manceau, A., Geoffroy, N., Laboudigue, A., Tamura, N., Marcus, M.A., 2005. Zinc mobility and speciation in soil covered by contaminated dredged sediment using micrometer-scale and bulk-averaging X-ray fluorescence, absorption and diffraction techniques. Geochim. Cosmochim. Acta 69, 1173–1198. doi:10.1016/j.gca.2004.08.024

Jacquat, O., Rambeau, C., Voegelin, A., Efimenko, N., Villard, A., Föllmi, K.B., Kretzschmar, R., 2011. Origin of high Zn contents in Jurassic limestone of the Jura mountain range and the Burgundy: evidence from Zn speciation and distribution. Swiss J. Geosci. 104, 409–424. doi:10.1007/s00015-011-0086-9

Jacquat, O., Voegelin, A., Kretzschmar, R., 2009. Soil properties controlling Zn speciation and fractionation in contaminated soils. Geochim. Cosmochim. Acta 73, 5256–5272. doi:10.1016/j.gca.2009.05.066

Jacquat, O., Voegelin, A., Villard, A., Marcus, M.A., Kretzschmar, R., 2008. Formation of Zn-rich phyllosilicate, Zn-layered double hydroxide and hydrozincite in contaminated calcareous soils. Geochim. Cosmochim. Acta 72, 5037–5054. doi:10.1016/j.gca.2008.07.024

Jain, C.K., 2004. Metal fractionation study on bed sediments of River Yamuna, India. Water Res. 38, 569–578. doi:10.1016/j.watres.2003.10.042

Jain, R., Jordan, N., Weiss, S., Foerstendorf, H., Heim, K., Kacker, R., Hübner, R., Kramer, H., van Hullebusch, E.D., Farges, F., Lens, P.N.L., 2015. Extracellular polymeric substances govern the surface charge of biogenic elemental selenium nanoparticles. Environ. Sci. Technol. 49, 1713–1720. doi:10.1021/es5043063

Jones, J.G., Gardener, S., Simon, B.M., 1984. Reduction of ferric iron by heterotrophic bacteria in lake sediments. Microbiology 130, 45–51. doi:10.1099/00221287-130-1-45

Karvelas, M., Katsoyiannis, A., Samara, C., 2003. Occurrence and fate of heavy metals in the wastewater treatment process. Chemosphere 53, 1201–1210. doi:10.1016/S0045-6535(03)00591-5

Kelderman, P., Osman, A.A., 2007. Effect of redox potential on heavy metal binding forms in polluted canal sediments in Delft (The Netherlands). Water Res. 41, 4251–4261. doi:10.1016/j.watres.2007.05.058

Kettler, R.M., Rye, R.O., Kesler, S.E., Meyers, P.A., Polanco, J., Russell, N., 1992. Gold deposition by sulfidation of ferrous Fe in the lacustrine sediments of the Pueblo Viejo district (Dominican Republic): the effect of Fe–C–S diagenesis on later hydrothermal mineralization in a Maar-Diatreme complex. Chem. Geol. 99, 29–50. doi:10.1016/0009-2541(92)90029-5

Khattak, R.A., Page, A.L., Jarrell, W.M., 1989. Mechanism of native manganese release in salt-treated soils. Soil Sci. Soc. Am. J. 53, 701–705. doi:10.2136/sssaj1989.03615995005300030009x

Kitagawa, H., van der Plicht, J., 1998. Atmospheric radiocarbon calibration to 45,000 yr B.P.: late glacial fluctuations and cosmogenic isotope production. Science (80-.). 279, 1187–1190. doi:10.1126/science.279.5354.1187

Kłos, A., Rajfur, M., Wacławek, M., 2011. Application of enrichment factor (EF) to the interpretation of results

from the biomonitoring studies. Ecol. Chem. Eng. S 18, 171–183.
Kobayashi, S., Shoji, S., 1976. Distribution of copper and zinc in volcanic ashes. Soil Sci. Plant Nutr. 22, 401–408. doi:10.1080/00380768.1976.10433002
Kodama, H., Schnitzer, M., 1977. Effect of fulvic acid on the crystallization of Fe(III) oxides. Geoderma 19, 279–291. doi:10.1016/0016-7061(77)90070-2
Komárek, M., Ettler, V., Chrastný, V., Mihaljevič, M., 2008. Lead isotopes in environmental sciences: A review. Environ. Int. 34, 562–577. doi:10.1016/j.envint.2007.10.005
Kosman, D.J., 2013. Iron metabolism in aerobes: managing ferric iron hydrolysis and ferrous iron autoxidation. Coord. Chem. Rev. 257, 210–217. doi:10.1016/j.ccr.2012.06.030
Kretzschmar, R., Mansfeldt, T., Mandaliev, P.N., Barmettler, K., Marcus, M.A., Voegelin, A., 2012. Speciation of Zn in blast furnace sludge from former sedimentation ponds using synchrotron X-ray diffraction, fluorescence, and absorption spectroscopy. Environ. Sci. Technol. 46, 12381–12390. doi:10.1021/es302981v
Kurek, E., 2002. Microbial Mobilization of Metals from Soil Minerals under Aerobic Conditions, in: Huang, P.M., Bollag, J.M., Senesi, N. (Eds.), Interactions Between Soil Particles and Microorganisms: Impact on the Terrestrial Ecosystem. John Wiley & Sons, Chichester, UK, pp. 189–226.
Labrenz, M., Druschel, G.K., Thomsen-Ebert, T., Gilbert, B., Welch, S.A., Kemner, K.M., Logan, G.A., Summons, R.E., Stasio, G. De, Bond, P.L., Lai, B., Kelly, S.D., Banfield, J.F., 2000. Formation of sphalerite (ZnS) deposits in natural biofilms of sulfate-reducing bacteria. Science (80-.). 290, 1744–1747. doi:10.1126/science.290.5497.1744
Langmuir, D., Whittemore, D.O., 1971. Variations in the Stability of Precipitated Ferric Oxyhydroxides, in: Hem, J.D. (Ed.), Non-Equilibrium Systems in Natural Water Chemistry. American Chemical Society, Washington DC, pp. 209–234. doi:10.1021/ba-1971-0106
Lartiges, B.S., Deneux-Mustin, S., Villemin, G., Mustin, C., Barrès, O., Chamerois, M., Gerard, B., Babut, M., 2001. Composition, structure and size distribution of suspended particulates from the Rhine River. Water Res. 35, 808–816. doi:10.1016/S0043-1354(00)00293-1
Le Meur, M., Montargès-Pelletier, E., Bauer, A., Gley, R., Migot, S., Barres, O., Delus, C., Villiéras, F., 2016. Characterization of suspended particulate matter in the Moselle River (Lorraine, France): evolution along the course of the river and in different hydrologic regimes. J. Soils Sediments 16, 1625–1642. doi:10.1007/s11368-015-1335-8
Le Pape, P., Quantin, C., Morin, G., Jouvin, D., Kieffer, I., Proux, O., Ghanbaja, J., Ayrault, S., 2014. Zinc speciation in the suspended particulate matter of an urban river (Orge, France): Influence of seasonality and urbanization gradient. Environ. Sci. Technol. 48, 11901–11909. doi:10.1021/es500680x
Lepage, H., Evrard, O., Onda, Y., Lefèvre, I., Laceby, J.P., Ayrault, S., 2015. Depth distribution of cesium-137 in paddy fields across the Fukushima pollution plume in 2013. J. Environ. Radioact. 147, 157–164. doi:10.1016/j.jenvrad.2015.05.003
Lesven, L., Gao, Y., Billon, G., Leermakers, M., Ouddane, B., Fischer, J.-C., Baeyens, W., 2008. Early diagenetic processes aspects controlling the mobility of dissolved trace metals in three riverine sediment columns. Sci. Total Environ. 407, 447–459. doi:10.1016/j.scitotenv.2008.08.033
Lesven, L., Lourino-Cabana, B., Billon, G., Recourt, P., Ouddane, B., Mikkelsen, O., Boughriet, A., 2010. On metal diagenesis in contaminated sediments of the Deûle river (northern France). Appl. Geochemistry 25, 1361–1373. doi:10.1016/j.apgeochem.2010.06.007
Lewis, A.E., 2010. Review of metal sulphide precipitation. Hydrometallurgy 104, 222–234. doi:10.1016/j.hydromet.2010.06.010
Loizeau, J.-L., Rozé, S., Peytremann, C., Monna, F., Dominik, J., 2003. Mapping sediment accumulation rate by using volume magnetic susceptibility core correlation in a contaminated bay (Lake Geneva , Switzerland). Eclogae Geol. Helv. 96, 73–79.
Loska, K., Cebula, J., Pelczar, J., Wiechuła, D., Kwapuliński, J., 1997. Use of enrichment, and contamination factors together with geoaccumulation indexes to evaluate the content of Cd, Cu, and Ni in the Rybnik water reservoir in Poland. Water. Air. Soil Pollut. 93, 347–365. doi:10.1023/A:1022121615949
Løvlie, R., Markussen, B., Sejrup, H.P., Thiede, J., 1986. Magnetostratigraphy in three Arctic Ocean sediment cores; arguments for geomagnetic excursions within oxygen-isotope stage 2–3. Phys. Earth Planet. Inter. 43, 173–184. doi:10.1016/0031-9201(86)90084-1
Lowery, D.L., Wagner, D.P., 2012. Geochemical impacts to prehistoric iron-rich siliceous artifacts in the nearshore coastal zone. J. Archaeol. Sci. 39, 690–697. doi:10.1016/j.jas.2011.10.035
Lu, X., Wang, H., 2012. Microbial oxidation of sulfide tailings and the environmental consequences. Elements 8, 119–124. doi:10.2113/gselements.8.2.119
Luther III, G.W., Meyerson, A.L., Krajewski, J.J., Hires, R., 1980. Metal sulfides in estuarine sediments. J. Sediment. Petrol. 50, 1117–1120.
Luxton, T.P., Miller, B.W., Scheckel, K.G., 2013. Zinc Speciation Studies in Soil, Sediment and Environmental Samples, in: Bakirdere, S. (Ed.), Speciation Studies in Soil, Sediment and Environmental Samples. CRC Press,

Taylor & Francis Groups, New York, pp. 433–477. doi:doi:10.1201/b15501-12
Lynch, S., Batty, L., Byrne, P., 2014. Environmental risk of metal mining contaminated river bank sediment at redox-transitional zones. Minerals 4, 52–73. doi:10.3390/min4010052
Mahar, A., Wang, P., Li, R., Zhang, Z., 2015. Immobilization of lead and cadmium in contaminated soil using amendments: A review. Pedosphere 25, 555–568. doi:10.1016/S1002-0160(15)30036-9
Maitte, B., Jorand, F.P.A., Grgic, D., Abdelmoula, M., Carteret, C., 2015. Remineralization of ferrous carbonate from bioreduction of natural goethite in the Lorraine iron ore (Minette) by *Shewanella putrefaciens*. Chem. Geol. 412, 48–58. doi:10.1016/j.chemgeo.2015.07.024
Manceau, A., Marcus, M.A., Tamura, N., Proux, O., Geoffroy, N., Lanson, B., 2004. Natural speciation of Zn at the micrometer scale in a clayey soil using X-ray fluorescence, absorption, and diffraction. Geochim. Cosmochim. Acta 68, 2467–2483. doi:10.1016/j.gca.2003.11.021
Mansfeldt, T., Dohrmann, R., 2004. Chemical and mineralogical characterization of blast-furnace sludge from an abandoned landfill. Environ. Sci. Technol. 38, 5977–5984. doi:10.1021/es040002+
Marshak, S., 2011a. Streams and Floods: The Geology of Running Water, in: Repcheck, J. (Ed.), Earth: Portrait of a Planet. WW Norton & Company, New York and London, pp. 582–619.
Marshak, S., 2011b. The Wrath of Vulcan: Volcanic Eruption, in: Repcheck, J. (Ed.), Earth: Portrait of a Planet. WW Norton & Company, New York and London, pp. 266–302.
Marshak, S., 2011c. Up from the Inferno: Magma and Igneous Rocks, in: Repcheck, J. (Ed.), Earth: Portrait of a Planet. WW Norton & Company, New York and London, pp. 152–182.
Martin, J.M., Meybeck, M., 1979. Elemental mass-balance of material carried by major world rivers. Mar. Chem. 7, 173–206. doi:10.1016/0304-4203(79)90039-2
Maslennikova, S., Larina, N., Larin, S., 2012. The effect of sediment grain size on heavy metal content. Lakes, Reserv. ponds 6, 43–54.
Matijević, S., Kušpilić, G., Kljaković-Gašpić, Z., 2007. The redox potential of sediment from the Middle Adriatic region. Acta Adriat. 48, 191–204.
Matsunaga, T., Tsuduki, K., Yanase, N., Kritsananuwat, R., Ueno, T., Hanzawa, Y., Naganawa, H., 2014. Temporal variations in metal enrichment in suspended particulate matter during rainfall events in a rural stream. Limnology 15, 13–25. doi:10.1007/s10201-013-0409-9
Mertens, J., Smolders, E., 2013. Zinc, in: Alloway, B.J. (Ed.), Heavy Metals in Soils: Trace Metals and Metalloids in Soils and Their Bioavailability. Springer Netherlands, pp. 465–493. doi:10.1007/978-94-007-4470-7_17
Meyers, P.A., 2003. Applications of organic geochemistry to paleolimnological reconstructions: a summary of examples from the Laurentian Great Lakes. Org. Geochem. 34, 261–289. doi:10.1016/S0146-6380(02)00168-7
Michalzik, B., Ilgen, G., Hertel, F., Hantsch, S., Bilitewski, B., 2007. Emissions of organo-metal compounds via the leachate and gas pathway from two differently pre-treated municipal waste materials – A landfill reactor study. Waste Manag. 27, 497–509. doi:10.1016/j.wasman.2006.02.018
Montargès-Pelletier, E., Duriez, C., Ghanbaja, J., Jeanneau, L., Falkenberg, G., Michot, L.J., 2014. Microscale investigations of the fate of heavy metals associated to iron-bearing particles in a highly polluted stream. Environ. Sci. Pollut. Res. 21, 2744–2760. doi:10.1007/s11356-013-2192-x
Montargès-Pelletier, E., Jeanneau, L., Faure, P., Bihannic, I., Barres, O., Lartiges, B.S., 2007. The junction of Fensch and Moselle rivers, France; mineralogy and composition of river materials. Environ. Geol. 53, 85–102. doi:10.1007/s00254-006-0621-6
Moore, J.N., Brook, E.J., Johns, C., 1989. Grain size partitioning of metals in contaminated, coarse-grained river floodplain sediment: Clark Fork River, Montana, U.S.A. Environ. Geol. Water Sci. 14, 107–115. doi:10.1007/BF01728502
Moreau, J.W., Webb, R.I., Banfield, J.F., 2004. Ultrastructure, aggregation-state, and crystal growth of biogenic nanocrystalline sphalerite and wurtzite. Am. Mineral. 89, 950–960. doi:10.2138/am-2004-0704
Morse, J.W., Arakaki, T., 1993. Adsorption and coprecipitation of divalent metals with mackinawite (FeS). Geochim. Cosmochim. Acta 57, 3635–3640. doi:10.1016/0016-7037(93)90145-M
Morse, J.W., Luther, G.W., 1999. Chemical influences on trace metal-sulfide interactions in anoxic sediments. Geochim. Cosmochim. Acta 63, 3373–3378. doi:10.1016/S0016-7037(99)00258-6
Muller, G., 1981. Schwermetallbelstung der sedimente des neckars und seiner nebenflusse: eine estandsaufnahme. Chem. Zeitung 105, 157–164.
Muller, G., 1969. Index of geoaccumulation in sediments of the Rhine River. Geological 2, 108–118.
Naden, P., 2010. The Fine-Sediment Cascade, in: Burt, T., Allison, R. (Eds.), Sediment Cascades: An Integrated Approach. John Wiley & Sons, West Sussex, pp. 271–305.
Négrel, P., Merly, C., Gourcy, L., Cerdan, O., Petelet-Giraud, E., Kralik, M., Klaver, G., van Wirdum, G., Vegter, J., 2014. Soil–Sediment–River Connections: Catchment Processes Delivering Pressures to River Catchments, in: Brils, J., Brack, W., Müller-Grabherr, D., Négrel, P., Vermaat, J.E. (Eds.), Risk-Informed Management of European River Basins. Springer Berlin Heidelberg, New York, Dordrecht, London, pp. 21–52.

doi:10.1007/978-3-642-38598-8_2
Nichols, G., 2009a. Introduction: Sedimentology and Stratigraphy, in: Sedimentology and Stratigraphy. Wiley-Blackwell, Oxford, UK, pp. 1–4.
Nichols, G., 2009b. Terrigenous Clastic Sediments: Gravel, Sand and Mud, in: Sedimentology and Stratigraphy. Wiley-Blackwell, Oxford, UK, UK, pp. 5–27.
Nicholson, F.A., Smith, S.R., Alloway, B.J., Carlton-Smith, C., Chambers, B.J., 2003. An inventory of heavy metals inputs to agricultural soils in England and Wales. Sci. Total Environ. 311, 205–219. doi:10.1016/S0048-9697(03)00139-6
Noël, V., Marchand, C., Juillot, F., Ona-Nguema, G., Viollier, E., Marakovic, G., Olivi, L., Delbes, L., Gelebart, F., Morin, G., 2014. EXAFS analysis of iron cycling in mangrove sediments downstream a lateritized ultramafic watershed (Vavouto Bay, New Caledonia). Geochim. Cosmochim. Acta 136, 211–228. doi:10.1016/j.gca.2014.03.019
Nordstrom, D.K., Alpers, C.N., 1999. Geochemistry of Acid Mine Waters, in: Plumlee, G.S., Logsdon, M.J. (Eds.), The Environmental Geochemistry of Mineral Deposits. Part A: Processes, Techniques, and Health Issues. Society of Economic Geologists, Littleton, CO, CO, pp. 133–160.
Norris, P.R., Burton, N.P., Foulis, N.A.M., 2000. Acidophiles in bioreactor mineral processing. Extremophiles 4, 71–76. doi:10.1007/s007920050139
Nriagu, J.O., 1996. A history of global metal pollution. Science (80-.). 272, 223–224. doi:10.1126/science.272.5259.223
Nriagu, J.O., 1990a. The rise and fall of leaded gasoline. Sci. Total Environ. 92, 13–28. doi:10.1016/0048-9697(90)90318-O
Nriagu, J.O., 1990b. Global metal pollution: poisoning the biosphere? Environ. Sci. Policy Sustain. Dev. 32, 7–33. doi:10.1080/00139157.1990.9929037
Nriagu, J.O., 1989. A global assessment of natural sources of atmospheric trace metals. Nature 338, 47–49. doi:10.1038/338047a0
Nriagu, J.O., Pacyna, J.M., 1988. Quantitative assessment of worldwide contamination of air, water and soils by trace metals. Nature 333, 134–139. doi:10.1038/333134a0
Nyirenda, R.L., 1991. The processing of steelmaking flue-dust: A review. Miner. Eng. 4, 1003–1025. doi:10.1016/0892-6875(91)90080-F
Ohfuji, H., Akai, J., 2002. Icosahedral domain structure of framboidal pyrite. Am. Mineral. 87, 176–180.
Ohfuji, H., Rickard, D.T., 2005. Experimental syntheses of framboids—a review. Earth-Science Rev. 71, 147–170. doi:10.1016/j.earscirev.2005.02.001
Okoro, H.K., Fatoki, O.S., 2012. A Review of Sequential Extraction Procedures for Heavy Metals Speciation in Soil and Sediments. J. Environ. Anal. Toxicol. 1, 1–9. doi:10.4172/scientificreports.181
Owens, P.N., Walling, D.E., 2002. Changes in sediment sources and floodplain deposition rates in the catchment of the River Tweed, Scotland, over the last 100 years: the impact of climate and land use change. Earth Surf. Process. Landforms 27, 403–423. doi:10.1002/esp.327
Panfili, F., Manceau, A., Sarret, G., Spadini, L., Kirpichtchikova, T., Bert, V., Laboudigue, A., Marcus, M.A., Ahamdach, N., Libert, M.F., 2005. The effect of phytostabilization on Zn speciation in a dredged contaminated sediment using scanning electron microscopy, X-ray fluorescence, EXAFS spectroscopy, and principal components analysis. Geochim. Cosmochim. Acta 69, 2265–2284. doi:10.1016/j.gca.2004.10.017
Parizanganeh, A., 2008. Grain Size Effect on Trace Metals in Contaminated Sediments along the Iranian Coast of the Caspian Sea, in: Sengupta, M., Dalwani, R. (Eds.), Proceedings of Taal 2007: The 12th World Lake Conference. pp. 329–336.
Parkman, R.H., Charnock, J.M., Bryan, N.D., Livens, F.R., Vaughan, D.J., 1999. Reactions of copper and cadmium ions in aqueous solution with goethite, lepidocrocite, mackinawite, and pyrite. Am. Mineral. 84, 407–419. doi:10.2138/am-1999-0326
Paterson, D.M., 2007. Hydrodynamics, in: Allan, R., Förstner, U., Salomons, W. (Eds.), Sediment Dynamics and Pollutant Mobility in Rivers: An Interdisciplinary Approach. Springer Science & Business Media, Berlin, pp. 67–116.
Paterson, D.M., 2001. The Fine Structure and Properties of the Sediment Surface, in: Boudreau, B.P., Jorgensen, B.B. (Eds.), The Benthic Boundary Layer. Transport Processes and Biogeochemistry. Oxford University Press, pp. 127–143.
Patrick, W.H., Delaune, R.D., 1972. Characterization of the oxidized and reduced zones in flooded soil. Soil Sci. Soc. Am. J. 36, 573–576. doi:10.2136/sssaj1972.03615995003600040024x
Patrick, W.H., Henderson, R.E., 1981. Reduction and reoxidation cycles of manganese and iron in flooded soil and in water solution. Soil Sci. Soc. Am. J. 45, 855–859. doi:10.2136/sssaj1981.03615995004500050006x
Patrick, W.H., Jugsujinda, A., 1992. Sequential reduction and oxidation of inorganic nitrogen, manganese, and iron in flooded soil. Soil Sci. Soc. Am. J. 56, 1071–1073. doi:10.2136/sssaj1992.03615995005600040011x
Pekey, H., 2006. The distribution and sources of heavy metals in Izmit Bay surface sediments affected by a

polluted stream. Mar. Pollut. Bull. 52, 1197–1208. doi:10.1016/j.marpolbul.2006.02.012
Peltier, E., Dahl, A.L., Gaillard, J.-F., 2005. Metal speciation in anoxic sediments: When sulfides can be construed as oxides. Environ. Sci. Technol. 39, 311–316. doi:10.1021/es049212c
Perga, M.-E., Desmet, M., Enters, D., Reyss, J.-L., 2010. A century of bottom-up- and top-down driven changes on a lake planktonic food web: A paleoecological and paleoisotopic study of Lake Annecy, France. Limnol. Oceanogr. 55, 803–816. doi:10.4319/lo.2010.55.2.0803
Petit, J.R., Jouzel, J., Raynaud, D., Barkov, N.I., Barnola, J.-M., Basile, I., Bender, M., Chappellaz, J., Davis, M., Delaygue, G., Delmotte, M., Kotlyakov, V.M., Legrand, M., Lipenkov, V.Y., Lorius, C., PÉpin, L., Ritz, C., Saltzman, E., Stievenard, M., 1999. Climate and atmospheric history of the past 420,000 years from the Vostok ice core, Antarctica. Nature 399, 429–436. doi:10.1038/20859
Phillips, J.M., Walling, D.E., 1995. An assessment of the effects of sample collection, storage and resuspension on the representativeness of measurements of the effective particle size distribution of fluvial suspended sediment. Water Res. 29, 2498–2508. doi:10.1016/0043-1354(95)00087-2
Pickering, W.F., 1980. Zinc Interaction with Soil and Sediment Components, in: Nriagu, J.O. (Ed.), Zinc in the Environment. Part 1. Ecological Cycling. John Wiley and Sons, pp. 71–112.
Pons, L.J., Van Breemen, N., Driessen, P.M., 1982. Physiography of Coastal Sediments and Development of Potential Soil Acidity, in: Acid Sulfate Weathering, SSSA Special Publication. Soil Science Society of America, pp. 1–18. doi:10.2136/sssaspecpub10.c1
Prasad, M.B.K., Ramanathan, A.L., Shrivastav, S.K., Anshumali, Saxena, R., 2006. Metal fractionation studies in surfacial and core sediments in the Achankovil River Basin in India. Environ. Monit. Assess. 121, 77–102. doi:10.1007/s10661-005-9108-2
Press, F., Siever, R., 1986. Earth, 4th ed. W.H. Freeman.
Priadi, C., Le Pape, P., Morin, G., Ayrault, S., Maillot, F., Juillot, F., Hochreutener, R., Llorens, I., Testemale, D., Proux, O., Brown, G.E., 2012. X-ray absorption fine structure evidence for amorphous zinc sulfide as a major zinc species in suspended matter from the seine river downstream of Paris, Ile-De-France, France. Environ. Sci. Technol. 46, 3712–3720. doi:10.1021/es2041652
Rabenhorst, M.C., 2011. Sulfidization : the origin of sulfides in our soils and sediments; University of Maryland.
Rabenhorst, M.C., 1990. Micromorphology of induced iron sulfide formation in a Chesapeake Bay (Usa) tidal marsh. Dev. Soil Sci., Developments in Soil Science 19, 303–310. doi:10.1016/S0166-2481(08)70342-8
Rabenhorst, M.C., Megonigal, J.P., Keller, J., 2010. Synthetic iron oxides for documenting sulfide in marsh pore water. Soil Sci. Soc. Am. J. 74, 1383–1388. doi:10.2136/sssaj2009.0435
Resongles, E., Casiot, C., Freydier, R., Dezileau, L., Viers, J.J., Elbaz-Poulichet, F., 2014. Persisting impact of historical mining activity to metal (Pb, Zn, Cd, Tl, Hg) and metalloid (As, Sb) enrichment in sediments of the Gardon River, Southern France. Sci. Total Environ. 481, 509–521. doi:10.1016/j.scitotenv.2014.02.078
Rickard, D.T., 1973. Sedimentary Iron Sulfide Formation, in: Dost, H. (Ed.), Proceedings of the International Symposium on Acid Sulphate Soils 13-20 August 1972, Wageningen, The Netherlands. Wageningen, pp. 28–65.
Rickard, D.T., 1970. The origin of framboids. Lithos 3, 269–293. doi:10.1016/0024-4937(70)90079-4
Rickard, D.T., Morse, J.W., 2005. Acid volatile sulfide (AVS). Mar. Chem. 97, 141–197. doi:10.1016/j.marchem.2005.08.004
Robert, A., 2014. Fluvial Sediments: Processes of Erosion and Transport, in: River Processes: An Introduction to Fluvial Dynamics. Routledge, London, pp. 51–90.
Roberts, A.P., 2015. Magnetic mineral diagenesis. Earth-Science Rev. 151, 1–47. doi:10.1016/j.earscirev.2015.09.010
Rodriguez, J.A., Hrbek, J., 1999. Interaction of sulfur with well-defined metal and oxide surfaces: unraveling the mysteries behind catalyst poisoning and desulfurization. Acc. Chem. Res. 32, 719–728. doi:10.1021/ar9801191
Sadori, L., Ortu, E., Peyron, O., Zanchetta, G., Vannière, B., Desmet, M., Magny, M., 2013. The last 7 millennia of vegetation and climate changes at Lago di Pergusa (central Sicily, Italy). Clim. Past 9, 1969–1984. doi:10.5194/cp-9-1969-2013
Salomons, W., de Rooij, N.M., Kerdijk, H., Bril, J., 1987. Sediments as a source for contaminants? Hydrobiologia 149, 13–30. doi:10.1007/BF00048643
Sawłowicz, Z., 2000. Framboids: from their origin to application. Wydawnictwo Oddziału Polskiej Akademii Nauk.
Scheinost, A.C., Kretzschmar, R., Pfister, S., Roberts, D.R., 2002. Combining selective sequential extractions, X-ray absorption spectroscopy, and principal component analysis for quantitative zinc speciation in soil. Environ. Sci. Technol. 36, 5021–5028. doi:10.1021/es025669f
Schieber, J., Baird, G., 2001. On the origin and significance of pyrite spheres in devonian black shales of North America. J. Sediment. Res. 71, 155–166.
Sezgin, N., Ozcan, H.K., Demir, G., Nemlioglu, S., Bayat, C., 2004. Determination of heavy metal concentrations in street dusts in Istanbul E-5 highway. Environ. Int. 29, 979–985. doi:10.1016/S0160-4120(03)00075-8

Shafie, N.A., Aris, A.Z., Zakaria, M.P., Haris, H., Lim, W.Y., Isa, N.M., 2013. Application of geoaccumulation index and enrichment factors on the assessment of heavy metal pollution in the sediments. J. Environ. Sci. Health. A. Tox. Hazard. Subst. Environ. Eng. 48, 182–190. doi:10.1080/10934529.2012.717810

Shoji, S., Nanzyo, M., Dahlgren, R., 1993. Productivity and Utilization of Volcanic Ash Soils, in: Volcanic Ash Soils: Genesis, Properties and Utilization. Elsevier, Amsterdam, pp. 209–251.

Shuman, L.M., 1977. Adsorption of Zn by Fe and Al hydrous oxides as influenced by aging and pH. Soil Sci. Soc. Am. J. 41, 703–706. doi:10.2136/sssaj1977.03615995004100040016x

Simpson, S.L., Apte, S.C., Batley, G.E., 2000a. Effect of short-term resuspension events on the oxidation of cadmium, lead, and zinc sulfide phases in anoxic estuarine sediments. Environ. Sci. Technol. 34, 4533–4537. doi:10.1021/es991440x

Simpson, S.L., Apte, S.C., Batley, G.E., 1998. Effect of short-term resuspension events on trace metal speciation in polluted anoxic sediments. Environ. Sci. Technol. 32, 620–625. doi:10.1021/es970568g

Simpson, S.L., Rosner, J., Ellis, J., 2000b. Competitive displacement reactions of cadmium, copper, and zinc added to a polluted, sulfidic estuarine sediment. Environ. Toxicol. Chem. 19, 1992–1999. doi:10.1002/etc.5620190806

Singh, A.K., Hasnain, S.I., Banerjee, D.K., 1999. Grain size and geochemical partitioning of heavy metals in sediments of the Damodar River - a tributary of the lower Ganga, India. Environ. Geol. 39, 90–98. doi:10.1007/s002540050439

Singh, B., Wilson, M.J., McHardy, W.J., Fraser, A.R., Merrington, G., 1999. Mineralogy and chemistry of ochre sediments from an acid mine drainage near a disused mine in Cornwall, UK. Clay Miner. 34, 301–317. doi:10.1180/claymin.1999.034.2.09

Skousen, J., Rose, A., Geidel, G., Foreman, J., Evans, R., Helloer, W., 1998. Handbook of Technologies for Avoidance and Remediation of Acid Mine Drainage. The National Mine Land Reclamation Center, West Virginia.

Snyder, N.P., Allen, J.R., Dare, C., Hampton, M.A., Schneider, G., Wooley, R.J., Alpers, C.N., Marvin-DiPasquale, M.C., 2004. Sediment grain-size and loss-on-ignition analyses from 2002 Englebright Lake coring and sampling campaigns. USGS, Santa Cruz, Menlo Park, Sacramento, USA.

Sommerfield, C.K., Ogston, A.S., Mullenbach, B.L., Drake, D.E., Alexander, C.R., Nittrouer, C.A., Borgeld, J.C., Wheatcroft, R.A., Leithhold, E.L., 2007. Oceanic Dispersal and Accumulation of River Sediment, in: Continental Margin Sedimentation. Blackwell Publishing Ltd., Oxford, UK, UK, pp. 157–212. doi:10.1002/9781444304398.ch3

Soto-Jiménez, M., Páez-Osuna, F., 2001. Cd, Cu, Pb, and Zn in lagoonal sediments from Mazatlán Harbor (SE Gulf of California): Bioavailability and geochemical fractioning. Bull. Environ. Contam. Toxicol. 66, 350–356. doi:10.1007/s001280012

Spadini, L., Bott, M., Wehrli, B., Manceau, A., 2003. Analysis of the major Fe bearing mineral phases in recent lake sediments by EXAFS spectroscopy. Aquat. Geochemistry 9, 1–17. doi:10.1023/B:AQUA.0000005608.69468.1e

Sterckeman, T., Douay, F., Baize, D., Fourrier, H., Proix, N., Schvartz, C., 2006. Trace elements in soils developed in sedimentary materials from Northern France. Geoderma 136, 912–929. doi:10.1016/j.geoderma.2006.06.010

Stumm, W., Morgan, J.J., 1996. Metal Ions in Aqueous Solutions: Aspects of Coordination Chemistry, in: Schnoor, J.L., Zehnder, A. (Eds.), Aquatic Chemistry: Chemical Equilibria and Rates in Natural Waters. A Wiley-Inerscience Publication, New York, pp. 252–349.

Superville, P.J., Prygiel, E., Magnier, A., Lesven, L., Gao, Y., Baeyens, W., Ouddane, B., Dumoulin, D., Billon, G., 2014. Daily variations of Zn and Pb concentrations in the Deûle River in relation to the resuspension of heavily polluted sediments. Sci. Total Environ. 470–471, 600–607. doi:10.1016/j.scitotenv.2013.10.015

Sutherland, R.A., 2000. Bed sediment-associated trace metals in an urban stream, Oahu, Hawaii. Environ. Geol. 39, 611–627. doi:10.1007/s002540050473

Tack, F.M.G., Singh, S.P., Verloo, M.G., 1998. Heavy metal concentrations in consecutive saturation extracts of dredged sediment derived surface soils. Environ. Pollut. 103, 109–115. doi:10.1016/S0269-7491(98)00107-9

Taillefert, M., Lienemann, C.-P., Gaillard, J.-F., Perret, D., 2000. Speciation, reactivity, and cycling of Fe and Pb in a meromictic lake. Geochim. Cosmochim. Acta 64, 169–183. doi:10.1016/S0016-7037(99)00285-9

Tam, N.F.Y., Wong, Y.S., 1999. Mangrove soils in removing pollutants from municipal wastewater of different salinities. J. Environ. Qual. 28, 556–564. doi:10.2134/jeq1999.00472425002800020021x

Tessier, A., Campbell, P.G.C., Bisson, M., 1979. Sequential extraction procedure for the speciation of particulate trace metals. Anal. Chem. 51, 844–851.

Thevenon, F., Alencastro, L.F. de, Loizeau, J.-L.L., Adatte, T., Grandjean, D., Wildi, W., Poté, J., De Alencastro, L.F., Loizeau, J.-L.L., Adatte, T., Grandjean, D., Wildi, W., Poté, J., 2013. A high-resolution historical sediment record of nutrients, trace elements and organochlorines (DDT and PCB) deposition in a drinking water reservoir (Lake Brêt, Switzerland) points at local and regional pollutant sources. Chemosphere 90, 2444–2452. doi:10.1016/j.chemosphere.2012.11.002

Thévenot, D.R., Moilleron, R., Lestel, L., Gromaire, M.-C., Rocher, V., Cambier, P., Bonté, P., Colin, J.-L., de Pontevès, C., Meybeck, M., 2007. Critical budget of metal sources and pathways in the Seine River basin (1994–2003) for Cd, Cr, Cu, Hg, Ni, Pb and Zn. Sci. Total Environ. 375, 180–203. doi:10.1016/j.scitotenv.2006.12.008

Thompson, A., Chadwick, O.A., Rancourt, D.G., Chorover, J., 2006. Iron-oxide crystallinity increases during soil redox oscillations. Geochim. Cosmochim. Acta 70, 1710–1727. doi:10.1016/j.gca.2005.12.005

Thwaites, R., 2006. Colors, in: Lal, R. (Ed.), Encyclopedia of Soil Science. CRC Press, pp. 303–306.

Tipping, E., Lofts, S., Lawlor, A., 1998. Modelling the chemical speciation of trace metals in the surface waters of the Humber system. Sci. Total Environ. 210–211, 63–77. doi:10.1016/S0048-9697(98)00045-X

Tomlinson, D.L., Wilson, J.G., Harris, C.R., Jeffrey, D.W., 1980. Problems in the assessment of heavy-metal levels in estuaries and the formation of a pollution index. Helgoländer Meeresuntersuchungen 33, 566–575. doi:10.1007/BF02414780

Toorman, E., Berlamont, J., 2016. Dynamics of mud transport [WWW Document]. URL http://www.coastalwiki.org/wiki/Dynamics_of_mud_transport (accessed 5.14.17).

Trinkel, V., Mallow, O., Aschenbrenner, P., Rechberger, H., Fellner, J., 2016. Characterization of blast furnace sludge with respect to heavy metal distribution. Ind. Eng. Chem. Res. 55, 5590–5597. doi:10.1021/acs.iecr.6b00617

Trinkel, V., Mallow, O., Thaler, C., Schenk, J., Rechberger, H., Fellner, J., 2015. Behavior of chromium, nickel, lead, zinc, cadmium, and mercury in the blast furnace — A critical review of literature data and plant investigations. Ind. Eng. Chem. Res. 54, 11759–11771. doi:10.1021/acs.iecr.5b03442

Trzepla-Nabaglo, K., Flocchini, R.G., Carvacho, O.F., 2007. PM 10 and PM 25 in ambient soil dust: elemental enrichment factor, in: European Aerosol Conference. pp. 9–14.

Tugel, J.B., Hines, M.E., Jones, G.E., 1986. Microbial iron reduction by enrichment cultures isolated from estuarine sediments. Appl. Environ. Microbiol. 52, 1167–1172.

Tyson, R. V., 1995. Origin and Nature of the Amorphous Group, in: Sedimentary Organic Matter: Organic Facies and Palynofacies. Springer Netherlands, Dordrecht, pp. 169–180. doi:10.1007/978-94-011-0739-6

Valentim, B., Shreya, N., Paul, B., Gomes, C.S., Sant'Ovaia, H., Guedes, A., Ribeiro, J., Flores, D., Pinho, S., Suárez-Ruiz, I., Ward, C.R., 2016. Characteristics of ferrospheres in fly ashes derived from Bokaro and Jharia (Jharkand, India) coals. Int. J. Coal Geol. 153, 52–74. doi:10.1016/j.coal.2015.11.013

Van Den Berg, G.A., Loch, J.P.G., 2000. Decalcification of soils subject to periodic waterlogging. Eur. J. Soil Sci. 51, 27–33. doi:10.1046/j.1365-2389.2000.00279.x

Van den Berg, G.A., Loch, J.P.G., Winkels, H.J., 1998. Effect of fluctuating hydrological conditions on the mobility of heavy metals in soils of a freshwater estuary in the Netherlands. Water. Air. Soil Pollut. 102, 377–388. doi:10.1023/A:1004920700598

van der Veen, A., Baborowski, M., Kraft, C., Kraft, J., Mages, M., Óvári, M., Von Tümpling, W., 2007. Dynamics of Heavy Metals and Arsenic – Hungarian Tisza River Sediments after Mining Spills in the Catchment Area, in: Sediment Dynamics and Pollutant Mobility in Rivers. Springer Berlin Heidelberg, Berlin, Heidelberg, Heidelberg, pp. 335–342. doi:10.1007/978-3-540-34785-9_8

Van Herck, P., Vandecasteele, C., Swennen, R., Mortier, R., 2000. Zinc and lead removal from blast furnace sludge with a hydrometallurgical process. Environ. Sci. Technol. 34, 3802–3808. doi:10.1021/es9910331

Vaněk, A., Chrastný, V., Komárek, M., Penížek, V., Teper, L., Cabala, J., Drábek, O., 2013. Geochemical position of thallium in soils from a smelter-impacted area. J. Geochemical Explor. 124, 176–182. doi:10.1016/j.gexplo.2012.09.002

Vdović, N., Billon, G., Gabelle, C., Potdevin, J.-L., 2006. Remobilization of metals from slag and polluted sediments (Case Study: The canal of the Deûle River, northern France). Environ. Pollut. 141, 359–369. doi:10.1016/j.envpol.2005.08.034

Velde, B., 1995. Geology of Clays, in: Velde, B. (Ed.), Origin and Mineralogy of Clays. Springer Berlin Heidelberg, Berlin, Heidelberg, pp. 1–7. doi:10.1007/978-3-662-12648-6

Vera, M., Schippers, A., Sand, W., 2013. Progress in bioleaching: fundamentals and mechanisms of bacterial metal sulfide oxidation—part A. Appl. Microbiol. Biotechnol. 97, 7529–7541. doi:10.1007/s00253-013-4954-2

Vereš, J., Jakabský, Š., Šepelák, V., 2010. Chemical, physical, morphological and structural characterization of blast furnace sludge. Diffus. Fundam. 12, 88–91.

Viers, J., Dupré, B., Gaillardet, J., 2009. Chemical composition of suspended sediments in World Rivers: New insights from a new database. Sci. Total Environ. 407, 853–868. doi:10.1016/j.scitotenv.2008.09.053

Voegelin, A., Pfister, S., Scheinost, A.C., Marcus, M.A., Kretzschmar, R., 2005. Changes in zinc speciation in field soil after contamination with zinc oxide. Environ. Sci. Technol. 39, 6616–6623. doi:10.1021/es047962g

Voelker, A.H.L., Sarnthein, M., Grootes, P.M., Erlenkeuser, H., Laj, C., Mazaud, A., Nadeau, M.-J., Schleicher, M., 1998. Correlation Of Marine C-14 Ages From the Nordic Seas With the Gisp2 Isotope Record - Implications For C-14 Calibration Beyond 25 Ka Bp, in: Nook, W.G., van der Plicht, J. (Eds.), Radiocarbon. pp. 517–534.

Vörösmarty, C.J., Meybeck, M., Fekete, B., Sharma, K., Green, P., Syvitski, J.P.M., 2003. Anthropogenic

sediment retention: major global impact from registered river impoundments. Glob. Planet. Change 39, 169–190. doi:10.1016/S0921-8181(03)00023-7

Vučnić Vasić, M., Kiurski, J., Aksentijević, S., Kozmidis-Luburić, U., 2013. Metal concentration and particle size distribution of stream and river water polluted from copper rolling mill industry. Int. J. Environ. Sci. Technol. 10, 923–930. doi:10.1007/s13762-013-0203-6

Walling, D.E., 2013. The evolution of sediment source fingerprinting investigations in fluvial systems. J. Soils Sediments 13, 1658–1675. doi:10.1007/s11368-013-0767-2

Walling, D.E., Collins, A.L., 2016. Fine Sediment Transport and Management, in: Gilvear, D.J., Greenwood, M.T., Thoms, Ma.C., Wood, P.J. (Eds.), River Science: Research and Management for the 21st Century. John Wiley & Sons, Ltd, Chichester, UK, UK, pp. 37–60. doi:10.1002/9781118643525.ch3

Wang, C., Hu, X., Chen, M.-L., Wu, Y.-H., 2005. Total concentrations and fractions of Cd, Cr, Pb, Cu, Ni and Zn in sewage sludge from municipal and industrial wastewater treatment plants. J. Hazard. Mater. 119, 245–249. doi:10.1016/j.jhazmat.2004.11.023

Weaver, C.E., 1961. Clay Mineralogy of the Late Cretaceous Rocks of the Washakie Basin, in: Symposium on Late Cretaceous Rocks, Wyoming and Adjacent Areas; 16th Annual Field. Wyoming Geological Association, pp. 148–154.

Webb, P.N., Harwood, D.M., McKelvey, B.C., Mercer, J.H., Stott, L.D., 1984. Cenozoic marine sedimentation and ice-volume variation on the East Antarctic craton. Geology 12, 287–291. doi:10.1130/0091-7613(1984)12<287:CMSAIV>2.0.CO;2

Wedepohl, K.H., 1995. The composition of the continental crust. Geochim. Cosmochim. Acta 59, 1217–1232. doi:10.1016/0016-7037(95)00038-2

Wells, M.L., Kozelka, P.B., Bruland, K.W., 1998. The complexation of "dissolved" Cu, Zn, Cd and Pb by soluble and colloidal organic matter in Narragansett Bay, RI. Mar. Chem. 62, 203–217. doi:10.1016/S0304-4203(98)00041-3

Wheatcroft, R.A., Wiberg, P.L., Alexander, C.R., Bentley, S.J., Drake, D.E., Harris, C.K., Ogston, A.S., 2007. Post-Depositional Alteration and Preservation of Sedimentary Strata, in: Continental Margin Sedimentation. Blackwell Publishing Ltd., Oxford, UK, UK, pp. 101–155. doi:10.1002/9781444304398.ch3

Whiteley, J.D., Pearce, N.J.G., 2003. Metal distribution during diagenesis in the contaminated sediments of Dulas Bay, Anglesey, N. Wales, UK. Appl. Geochemistry 18, 901–913. doi:10.1016/S0883-2927(02)00183-X

Wilkin, R.T., Barnes, H.L., 1997. Formation processes of framboidal pyrite. Geochim. Cosmochim. Acta 61, 323–339. doi:10.1016/S0016-7037(96)00320-1

Wilkinson, K.., Negre, J.-C., Buffle, J., 1997. Coagulation of colloidal material in surface waters: the role of natural organic matter. J. Contam. Hydrol. 26, 229–243. doi:10.1016/S0169-7722(96)00071-X

Xu, H., 2010. Synergistic Roles of Microorganisms in Mineral Precipitates Associated with Deep Sea Methane Seeps, in: Geomicrobiology: Molecular and Environmental Perspective. Springer Netherlands, Dordrecht, pp. 325–346. doi:10.1007/978-90-481-9204-5_15

Xu, J., Murayama, M., Roco, C.M., Veeramani, H., Michel, F.M., Rimstidt, J.D., Winkler, C., Hochella, M.F., 2016. Highly-defective nanocrystals of ZnS formed via dissimilatory bacterial sulfate reduction: A comparative study with their abiogenic analogues. Geochim. Cosmochim. Acta 180, 1–14. doi:10.1016/j.gca.2016.02.007

Yao, Q., Wang, X., Jian, H., Chen, H., Yu, Z., 2015. Characterization of the particle size fraction associated with heavy metals in suspended sediments of the Yellow River. Int. J. Environ. Res. Public Health 12, 6725–6744. doi:10.3390/ijerph120606725

Yildirim, I.Z., Prezzi, M., 2011. Chemical, mineralogical, and morphological properties of steel slag. Adv. Civ. Eng. 2011, 1–13. doi:10.1155/2011/463638

Yoon, S., Yáñez, C., Bruns, M.A., Martínez-Villegas, N., Martínez, C.E., 2012. Natural zinc enrichment in peatlands: Biogeochemistry of ZnS formation. Geochim. Cosmochim. Acta 84, 165–176. doi:10.1016/j.gca.2012.01.022

Zebracki, M., 2008. Devenir des polluants métalliques associés aux sédiments contaminés dans un cours d'eau en relation avec la dynamique sédimentaire. Ph.D. thesis. Rayonnements et Environnement. Université Paris-Sud XI, France.

Zhang, J., Liu, C.L., 2002. Riverine composition and estuarine geochemistry of particulate metals in China - Weathering features, anthropogenic impact and chemical fluxes. Estuar. Coast. Shelf Sci. 54, 1051–1070. doi:DOI 10.1006/ecss.2001.0879

Zhuang, J., Yu, G.-R., 2002. Effects of surface coatings on electrochemical properties and contaminant sorption of clay minerals. Chemosphere 49, 619–628. doi:10.1016/S0045-6535(02)00332-6

Zoumis, T., Schmidt, A., Grigorova, L., Calmano, W., 2001. Contaminants in sediments: remobilisation and demobilisation. Sci. Total Environ. 266, 195–202. doi:10.1016/S0048-9697(00)00740-3

Zubovic, P., Stadnichenko, T., Sheffey, N.B., 1961. Geochemistry of minor elements in coals of the Northern Great Plains Coal Province. Geolgical Surv. Bull. 58.

II. CHAPTER 2: A REVIEW ON THE ORNE WATERSHED AND STEELMAKING PROCESSES: PAST ACTIVITIES AND SAMPLING SITES

This chapter focuses on the description of the Orne watershed and the Orne River, the main industrial activities that had emerged in the Orne basin, and the sampling sites. Firstly, the geology of the Orne watershed and the hydrology of the Orne River are described. This is followed by the discussion on steelmaking processes in the Orne basin, mainly the operation and closure of the facilities. Finally, the sampling sites are described and the objectives are stated.

1. Geology of the Orne Watershed, a tributary of the Moselle River

The Orne River is a tributary of the Moselle River. The Moselle River has a drainage area of 28,280 km^2, with more than 50% of the basin and most of the river heads in France, 15% of the basin in Luxembourg, and the rest in Germany. The Moselle flows 544 km starting from France, through Luxembourg, before its confluence with the Rhine River at Koblenz, Germany. The Rhine River then passes through the Netherlands and finally reaches the North Sea after a 329 km course (AERM, 2000; Garcier, 2007). The destination of suspended matter and remobilized sediments of the Orne River are of interest since they might be transported along the watercourse between the Orne River and the North Sea. The focus is made on the Orne River, since this study focuses on sediments that had settled at several stations along its course.

The Orne River is located in northeastern France, drains a 1,268 km^2 watershed and flows 90 km before the confluence with the Moselle River at Richemont (Figure II-1 a; refer to the caption for the location of Richemont). The geology of the watershed can be divided into two main parts, a clayey (marl) depression in the Woëvre region (marked white in Figure II-1 a) and a calcareous plateau at the Pays-Haut region (marked grey). In the Woëvre region, the watercourse of the Orne and tributaries start from the late Jurassic epoch, which is made from easily eroded soft marl, while the downstream part consists of a limestone plateau belonging to the Bajocian age (middle Jurassic). The marl and calcareous plateaus of the Orne basin, in addition to the geological formation of the ferriferous basin of Lorraine, are shown in Figure II-2. Nowadays, the Woëvre region is mainly agricultural, includes forests and to a lesser

degree some rural/urban agglomerations (Figure II-1 b). As for the Pays-Haut region, which starts at Jarny (beginning of grey zone in Figure II-1 a), it is calcareous in nature; however, it is also rich with iron minerals (oolitic ironstone; Figure II-2 b). The Pays-Haut region, although containing agricultural and forest areas, shows urbanized accumulations and some industrially

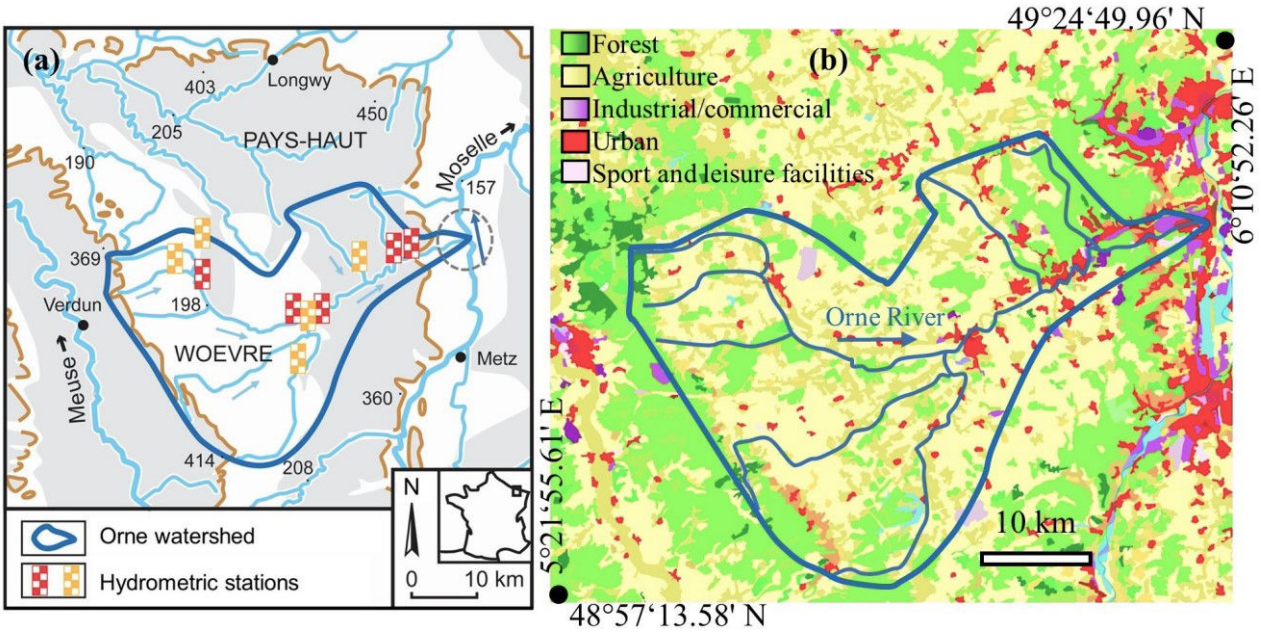

Figure II-1: The Orne watershed showing the Orne River, tributaries and land cover.
a: The insert on the lower right shows the location of the Orne watershed in France (northeastern). The direction of the river course is shown by blue arrows. The confluence of the Orne River with the Moselle River at Richemont is indicated by a dotted grey circle. The Woëvre region is marked by a white color, and the Pays-Haut region is marked by a grey color. Numbers on the map indicate altitudes (in meters). Hydrometer stations of red and white color record data on the Orne River, those of orange and white color record data on Orne tributaries. Image modified from the map created by Benoit Losson, on the basis of data provided by the French National Institute of Geography IGN, www.geoportail.gouv.fr.
b: Orne watershed with the water systems and the land cover. Adapted from www.geoportail.gouv.fr with Corine Land Cover (2006).

active areas (Figure II-1 b), especially in the east zone of the watershed, and more precisely near the banks of the Orne River (AERM, 2000; Bonnefoy and Bourg, 1984). Furthermore, oolitic ironstones (minette) were deposited in the Briey basin (located in Luxembourg and northern Lorraine) and in the smaller basin of Nancy (central Lorraine) in the late Toarcian and early Aalenian ages of the Jurassic period, i.e. approximately 175 million years ago (Teyssen, 1984). The iron ores could be found at depths inferior to 250 meters in Lorraine (Figure II-2 b), which constituted of successive Fe rich mineral layers (Grgic et al., 2002). Therefore, the region between Meuse and Moselle was mined for iron in the past.

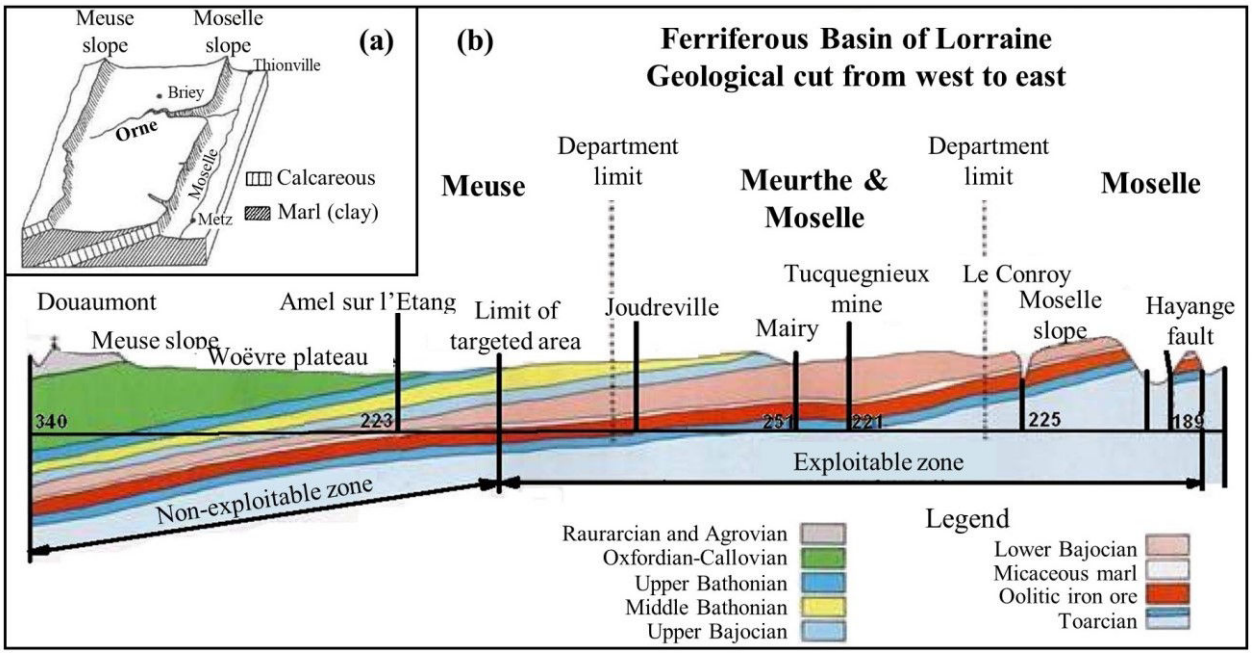

Figure II-2: Geology of the Orne basin
a: Basic geological map of the Orne River section showing marl (clayey) and calcareous plateaus in the Meuse-Moselle region. Modified from Bonnefoy and Bourg (1984). b: A detailed geological map of the ferriferous basin of Lorraine. Modified from Picon (2014) and the personal page of Francois Xavier Bibert (www.bibert.fr).

2. Hydrology and physico-chemical parameters of the Orne River

The water discharge in the Orne River and tributaries is measured at several stations (Figure II-1 a). The water discharge, in addition to other data, at the Rosselange hydrometer station has been recorded since 1968. The discharge values are measured at an hourly basis and recalculated as a daily average (EauFrance, 2016). From 49 years of data that had been collected between 1968 and 2016 (Figure II-3), the highest water discharges were measured during the winter period (December to April), while they were significantly lower throughout the other months, especially from July till September, where the discharge was circa 3 m^3/s. Additionally, the variation in water discharge is relatively high throughout the winter, which comes natural due to precipitation at the beginning of winter and snow melting afterwards. Water discharge variation during the summer period is rather small (as seen by the small error bars in Figure II-3). The hydrometer station at Rosselange also collects data on physico-chemical parameters, as well as mineral and organic matter composition (SIERM, 2017). Some of those parameters and chemical composition are shown below. It should be noted, however, that the collected data were not measured at a daily basis; also, the measured parameters and

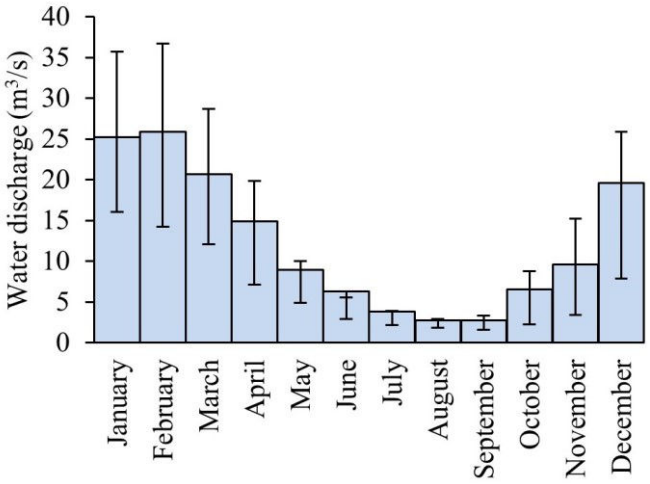

Figure II-3: Hydrograph of the Orne River at Rosselange with monthly average values between 1968 and 2016.
For better representation of the values during the 49 years, the negative and positive error bars represent the 1st and 3rd quartiles (or Q25 and Q75), respectively. Data collected from (EauFrance, 2016).

chemicals in the river have not necessarily been collected at the same dates. The temperature variation between 2007 and 2015 is shown in Figure II-4, and averaged 11.6 ± 4 °C, with 50% of the values ranging between 8.6 and 15°C, as indicated by the 1st and 3rd quartile values (Table II-1). As for the water discharge, and as previously described, it was higher during the winter period, which could be seen as an opposite trend with respect to temperature. The total suspended solids (TSS), turbidity (in formazin naphelometric units "FNU") and dissolved iron showed similar trends, which is expected due to the remobilization of sediments and material input due to run-off during rainy periods. The quartiles, average values and standard deviations of the parameters presented in Figure II-4 are shown in Table II-1. Furthermore, from the values of dissolved Fe and water discharge, it might be suggested that iron input increases during higher water flow, which might be caused by Fe mineral dissolution from the remobilized particles (e.g. Fe rich minerals), or from surface leachates. The pH of the river water is slightly basic, and ranges between 7.6 – 7.7 (Q25 – Q75, respectively) with an average of 7.7 ± 0.2 (Figure II-5 and Table II-1). The electric conductivity (EC) showed temporal trends, with lower values during winter periods; indeed, EC and temperature followed similar trends. The high values might also be explained by higher dissolved elements (chlorine, sulfate, calcium, sodium and potassium), as seen by similar trends for those elements with EC (Figure II-5).

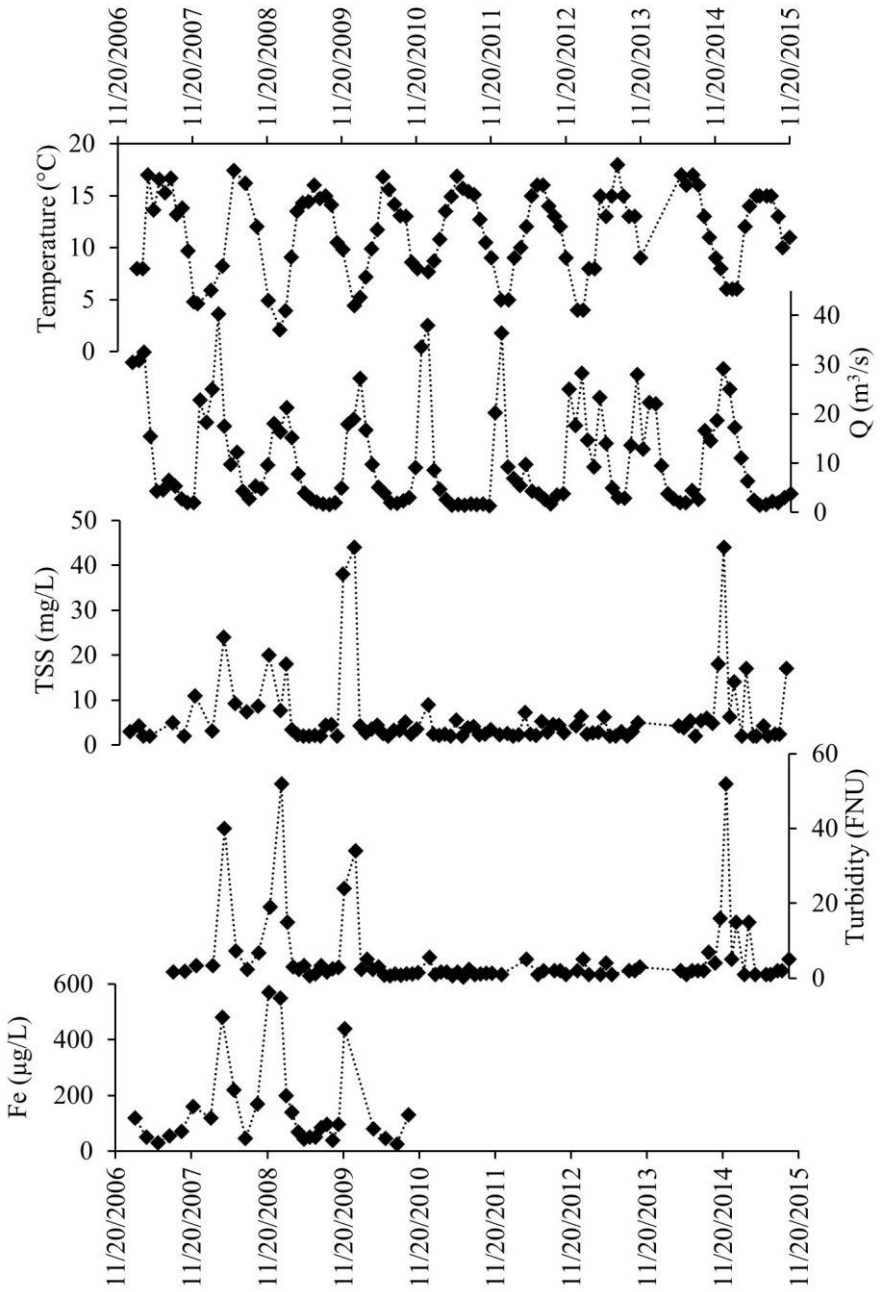

Figure II-4: Variation of temperature (°C), water discharge (m^3/s), TSS (mg/L), turbidity (FNU) and dissolved Fe (µg/L) of Orne River water at Rosselange.
The graphs are plotted using the data collected between 2007 and 2015 from the Rhin-Meuse database (SIERM, 2017).

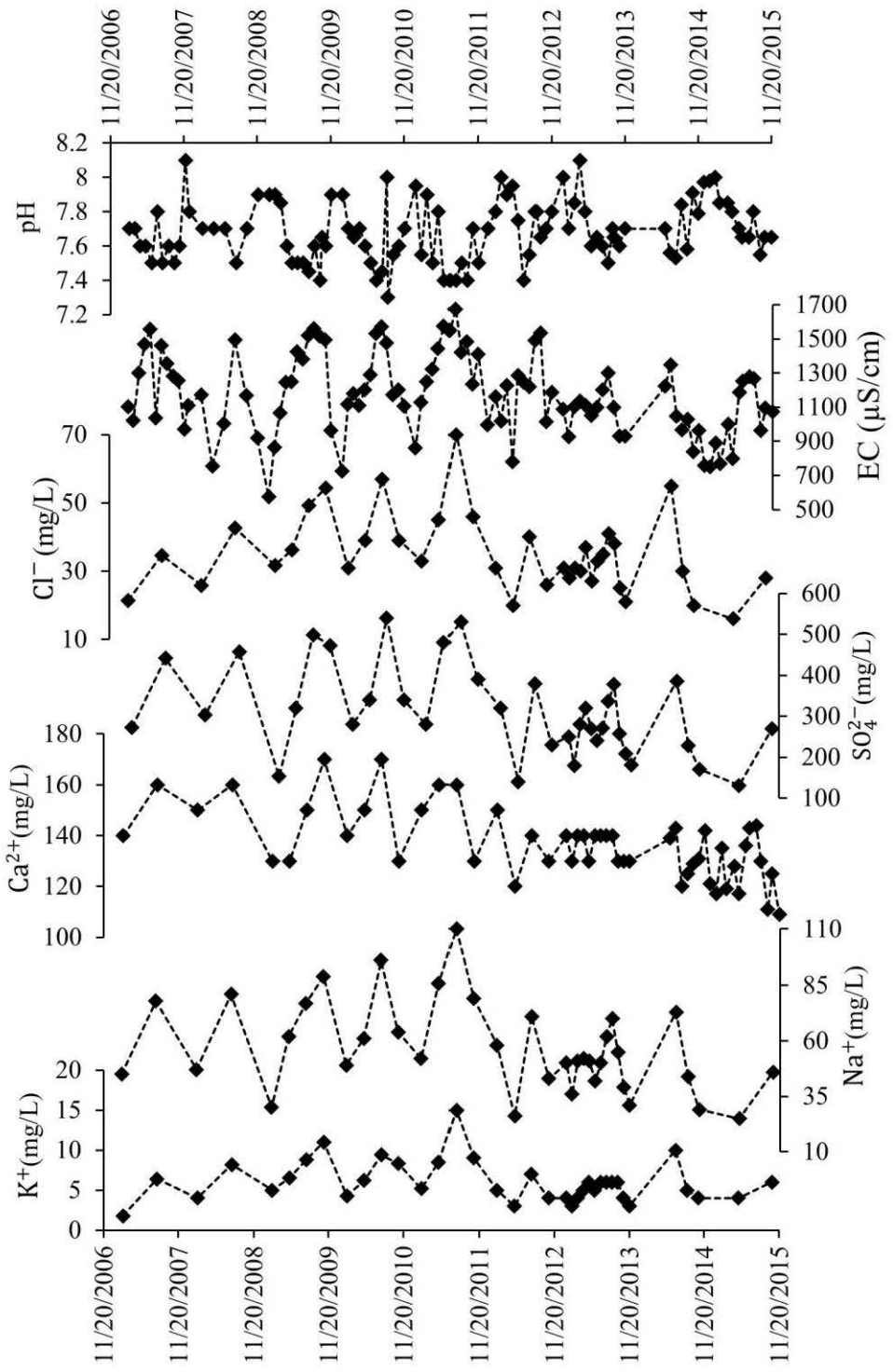

Figure II-5: Variation of pH, electric conductivity (EC), chlorine, sulfate, calcium, sodium and potassium of Orne River water at Rosselange.
The graphs are plotted using the data collected between 2007 and 2015 from the Rhin-Meuse database (SIERM, 2017).

Table II-1: Summary of physico-chemical data and dissolved chemicals collected at Rosselange.
The 1st and 3rd quartiles (Q25 and Q75, respectively), averages and standard deviations were calculated according to the data collected from SIERM (2017).

	Q25	Q75	Average	Standard deviation
Temp (°C)	8.6	15.0	11.6	4.0
Q (m^3/s)	2.7	17.3	9.8	9.3
TSS (mg/L)	2.3	5.4	6.0	7.9
Turbidity (NFU)	1.1	4.0	5.5	10.1
Fe (µg/L)	50	163	152	156
pH	7.6	7.8	7.7	0.2
EC (µS/cm)	1017	1316	1174	235
Cl^- (mg/L)	28	40	35	11
SO_4^{2-}(mg/L)	240	380	312	109
Ca^{2+}(mg/L)	130	143	137	14
Na^+ (mg/L)	44	71	57	20
K^+ (mg/L)	4.0	7.0	6.0	2.6

3. The evolution of iron and steelmaking

Iron mining and smelting began more than 3 millennia ago (~ 1500 BC) (Aitchison, 1960; Trinkel et al., 2015), however, with upgraded machinery in the XVIIIth century, iron (and other metals) mining and smelting extremely increased (Nriagu, 1990). The extraction of iron ore and the production of crude steel greatly increased since the last period of the XXth century in major countries worldwide, such as Brazil, Australia, China and India. For other countries, the production decreased in the 90s, such as Russia, Ukraine and countries of Europe (Figure II-6: a – i). It should be noted that a great part of the extracted iron ores from Australia, Brazil, India and China were exported, therefore explaining the high extraction of iron ore and low crude steel production. The opposite is true for Japan, which imported iron ores for the production of steel (Yellishetty et al., 2010). Moreover, iron ore extraction had increased worldwide since the 50s, which is also expected to rise for the coming years (Figure II-6 j). In France, pig iron and steel production flourished in the Moselle River basin, northeastern France (Garcier, 2007; Picon, 2014). Since those industries consume water, they were constructed near water systems. Some rivers, such as the Fensch, the Orne, Bievre, petite Roselle and Alzette, passed through areas that were highly active with iron mining and steelmaking (see Figure II-7 for the area in northeastern France). However, the iron industries transformed into steelmaking in the late XIXth. Another gain of having lotic water systems near the industries is having a possible dumping site. Back then, the function of the river as a natural self-purification system was overrated (Garcier, 2007). Nonetheless, Prof. Léon Poincaré (Nancy University) pointed out to

the severity of the wastes resulting from those industries on the environment, and claimed that those wastes would be more devastating than discharges resulting from industrial wastewater

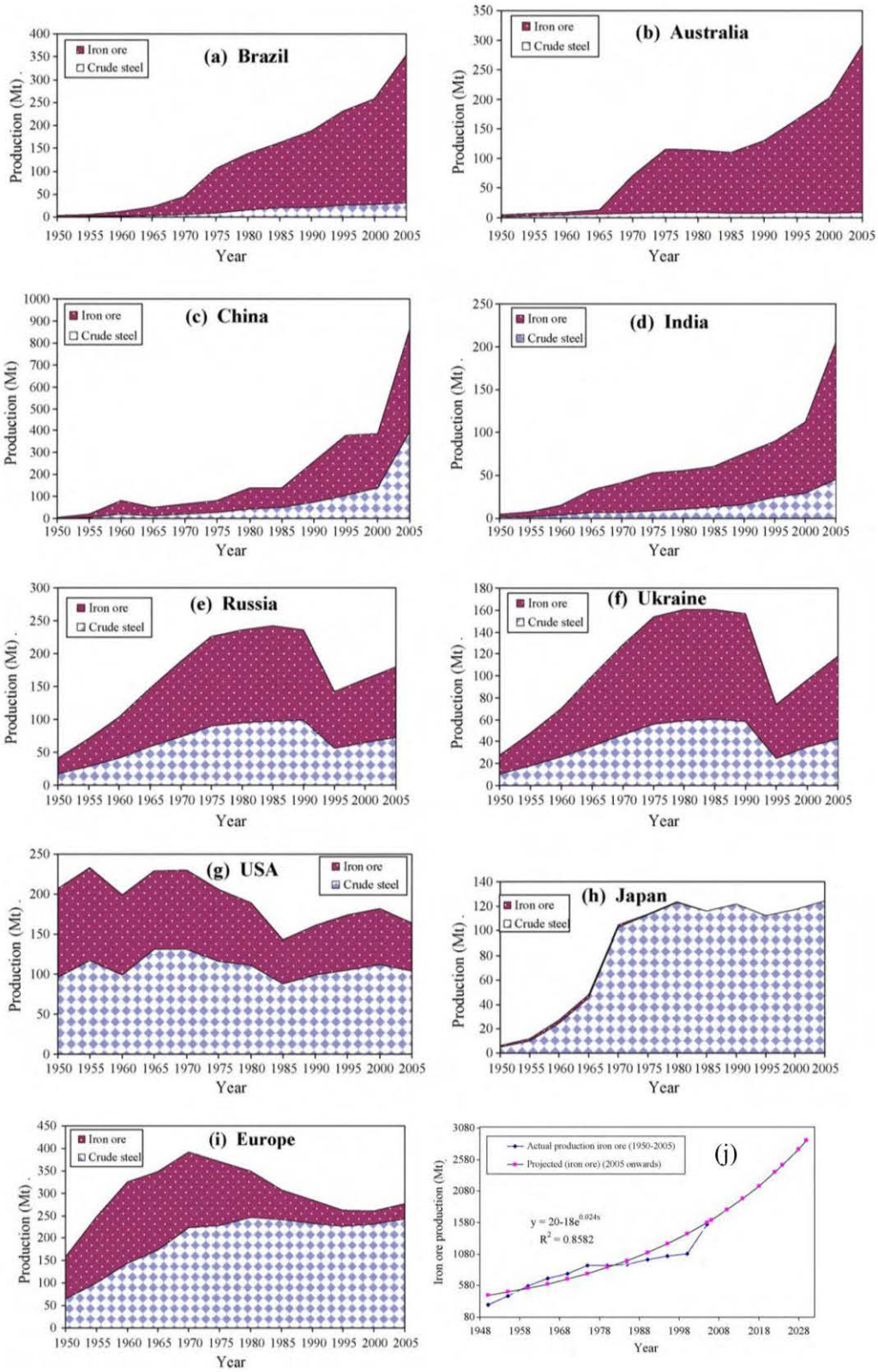

Figure II-6: Extraction of iron ore and production of crude steel in major countries.
a – i: iron ore extraction and steel production for different countries; j: the actual and projected iron production in the world for the last few decades.
Modified from Yellishetty et al., (2010).

(Poincaré, 1886). Industrial activities in the Lorraine area also included coal and salt mining (Figure II-7). The focus on the coming parts will be on the steelmaking processes, the by-products and wastes formed, their mineral and chemical composition, and their fate.

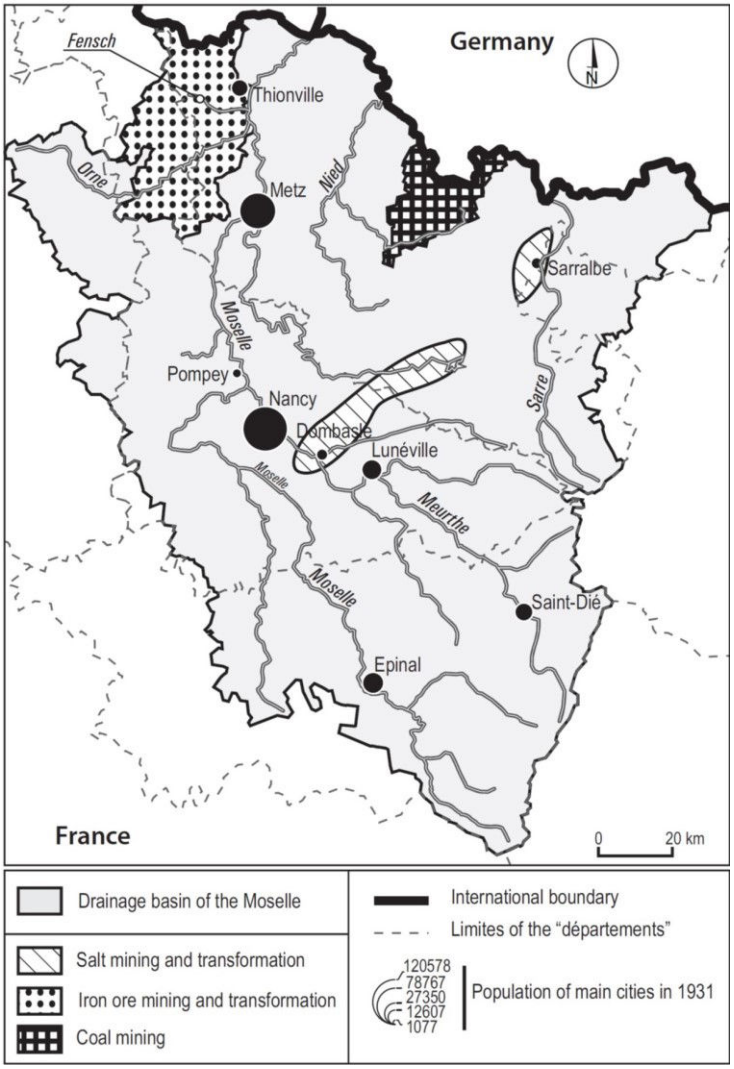

Figure II-7: Map of the French part of the Moselle basin showing the locations were mining activities were conducted.
The Fensch and Orne Rivers, located on the top left of the map flow in areas where iron mining and transformations were conducted. Source (Garcier, 2007).

4. Industrial development near the Orne River

During the 1870s, the production of iron and steel had increased worldwide, including France. Moreover, Lorraine was ranked the second most steel producing region in the world in the XXth century, which flourished after the mid XXth century, i.e. a little after WWII (Worldsteel Association, 2016; Yellishetty et al., 2010). The 1870s witnessed transformation of the Orne River basin; the activities that had previously focused on agriculture were becoming more industrial. From those transformations are socio-environmental ones, which

showed the emergence and development of iron, salt and coal mining, followed by steel production (Garcier, 2007; Picon, 2014). In Lorraine, the modern[xxi] steelmaking industry had begun in the 1870s, when local pig iron industries transformed into steelmaking industries after the process of dephosphoration emerged. Indeed, industries were built near rivers so that the water can be used as cooling sources (e.g. for blast furnaces). In addition to the industrial wastewaters released to the Orne River (and Moselle River), or tributaries, urban wastewaters were also released without treatment between 1870 and 1950 (during the active years of steelmaking industries), which seriously impacted the water quality of the river. As a result, the Orne River was characterized as one of the "rivers we can't bring ourselves to clean"[xxii], as indicated by Mr. Romain GARCIER (2007). Figure II-8 shows a model about the pollution level and its development in case pollution controls might be enacted. That case might be applied to the Moselle River in general, and the Orne River in particular.

Unfortunately, the part B – C1 of the model might fit the case of the Orne River, at least to some extent, since during the XIXth century, it was thought that the river could act as a self-purification system for the wastes released, therefore little control was made. Another cause

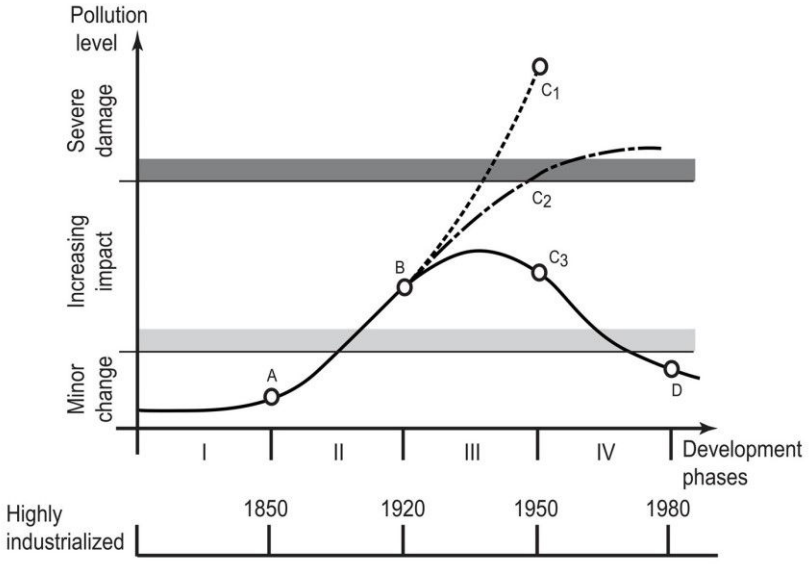

A: Pollution increase linear with population increase (rural society).
A – B: Exponential increase of pollution with industrialization.
B – C1: No pollution control enacted.
B – C2: Some controls installed (e.g., mechanical sewage treatment)
B – C3: Effective controls consistently employed (e.g., mechanical-biological wastewater treatment).
C3 – D: Recovery of pollution situation to a tolerable environmental status due to effective source control and/or tertiary treatment of effluents.

Figure II-8: Model of pollution occurrence applied on the Moselle basin. Modified from Garcier (2007) after Meybeck et al., (1992).

[xxi] Which is similar to the iron industry nowadays, which uses basic oxygen furnaces (also see section *7* of this chapter).

[xxii] The influence of the industrial activities (such as iron mining, steel making and coal mining) that were active in the last two centuries are still held in the sediments; therefore, the rivers are yet to be cleaned from the anthropogenic deposits.

that resulted in little or no control of the effluents in Lorraine was the feeling that advances in sciences and technology would rise up to the occasion and no real threats were considered, especially since scientific technology was incorporated in the pig iron and steelmaking industries (Garcier, 2007).

4.1. Steelmaking facilities and outcome on the Orne River area

The minette ironstone was exploited in the Lorraine region, therefore pig iron production, and later on steelmaking, developed rapidly during the 1870s; as a result, artificializing of the region started, such as the installation of the first blast furnaces at Jœuf in 1882, which closed in 1969, and the planning of a steelmaking plant in Homécourt in 1898 (Picon, 2014). Figure II-9 shows a couple of aerial images taken near the Orne River, which show the strong signature of industrialization, namely at Homécourt and Jœuf. Moreover, around twenty mines were located in the Orne basin after the 1870s, and coking industries were built in the 1920s; all which had severe impacts on the aquatic compartment (Garcier, 2007). Coupled to that development, the population also increased, mainly between 1880 and 1910 (Picon, 2014). Due to the requirements of the industries and mining sites, the landscape was changed, natural river courses were re-directed, river channels were rectified, railroads were built, and dams, embankments[xxiii] (levees) and weirs[xxiv] were constructed, and sediments were dredged (Garcier, 2007; Picon, 2014). One of the dams that were built was the Beth dam, located in Moyeuvre-Grande, which is still present today. Two blast furnaces were installed on the left bank of the Orne River in Jœuf between 1958 and 1964. It should be noted that during the building of blast furnaces, the transport of equipment and vehicles also introduced changes to the area downstream where the blast furnaces were installed. Another modification was the demolition and re-building of the Beth dam in Moyeuvre-Grande in 1959/1960 (Picon, 2014). One of the reasons that steelmaking activities was common in Lorraine was because at Jarny, which is located between Boncourt and Moineville (Figure II-10), was rich in exploitable iron ores (the Minette ironstone; see also Figure II-2 b); another reason was the presence of rolling mills and blast furnaces near the Orne River, including the area from Homécourt till Moyeuvre-Grande,

[xxiii] A raised platform built above the surface of the immediate surrounding land to redirect or prevent flooding of a river.

[xxiv] A barrier across the width of a river that pools water upstream and allows water flow over it and continue the path downstream.

which was considered as an agglomeration of steelmaking industries upstream the Moyeuvre

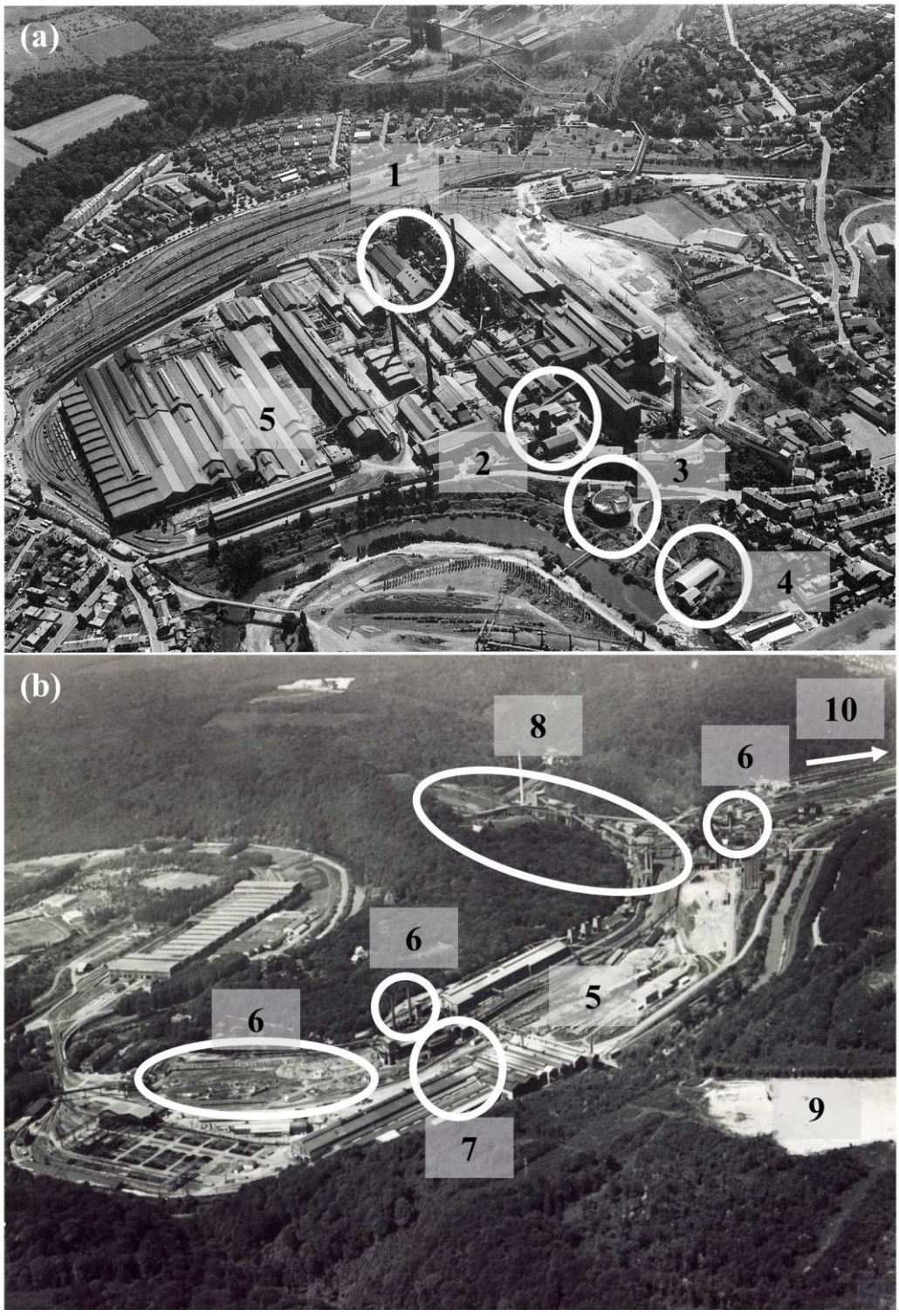

Figure II-9: Aerial images belonging to the Orne River basin showing industrial facilities that were installed near the river.
a: aerial image of the pig iron and steelmaking complexes at Homécourt taken on 1974. 1: preserved hall, 2: power plant, 3: settling tank, 4: pumping station, and 5: industrial area.
b: aerial image of the industrial steelmaking complex at Jœuf taken on 1975. 5: industrial area, 6: blast furnaces, 7: rolling mills, 8: mining site, 9: quarry, and 10: towards the Beth dam.
Images modified from Picon (2014) according to a: Établissement Public de la Métropole Lorraine (EMPL), and b: Sacilor, Hayange photo Library, 1975.

dam, also known as Beth dam (Ministère de l'Environnement, 1985; Teyssen, 1984).

Accompanying the development of steelmaking industries and iron, salt and coal mines that were built near the Orne River, was the deposition of waste materials (by-products and wastewaters) into the river. Therefore, a few dredging activities were recorded with the purpose of cleaning the riverbed from those deposits on one hand, and to widen the river's horizontal section on the other (Garcier, 2007). Massive deforestations and transport of metal rich deposits (such as sludge and slag) to river water also occurred (see Figure II-11 for the deforestation caused by dredging). One dredging activity took place in 1967, which included the riverbed between Homécourt and Jœuf (at Sainte Anne region; Figure II-10). Unfortunately, it was noted that some shuttle trucks transported through waste heaps, which caused some truck to slip and a bulldozer to sink, which caused a delay in the work; the materials of the heaps were also remobilized due to that action. Another dredging activity was recorded further upstream of the first dredging activity and took place between 1972 and 1981. The riverbed sediments of the Orne River between Olley and Boncourt were dredged (see Figure II-10 for the locations of

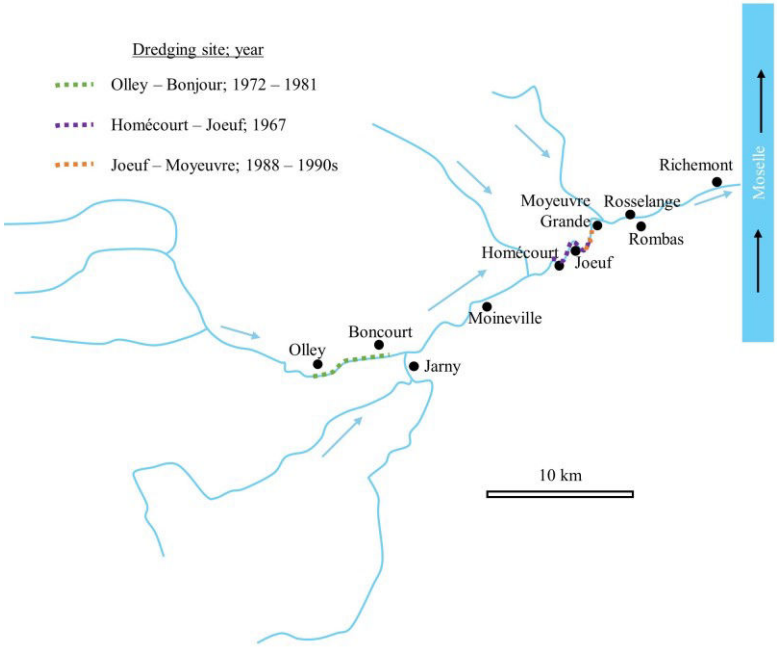

Figure II-10: The Orne River and main tributaries showing some cities of interest and dredged sections of the river.
Map was built based on the map created by Benoit Losson on the basis of data provided by the French National Institute of Geography IGN, www.geoportail.gouv.fr, and the communities indicated by Système d'information sur l'eau Rhin-Meuse (SIERM, 2017).

cities on the map). Due to those dredging activities, and others, the pollution load in the Orne River (as well as the Moselle River) is difficult to establish. Therefore, undisturbed settling

ponds or river sediments that had collected materials throughout the years of the industrial activity might be hard to locate.

In 1977, there was a temporal shutting down of industrial activities in the Orne basin, which re-emerged in the early 80s, such as the case in Jœuf; other industries remained closed, such as the coking plant at Homécourt in 1981 (Picon, 2014). However, the activity at Jœuf stopped in 1988. Due to this re-emergence, a three year study (January 1982 – December 1984) on the hydrological characteristic, physico-chemical parameters and metal contents and concentrations in several along the Orne River course was conducted (Ministère de l'Environnement, 1985). The study estimated the metal loads transported in parts of the Orne River by measuring metal contents in the suspended matter as well as the dissolved concentrations; the studied metals were Fe, Zn, Cr, Cu and Pb. The total metal loads flowing in the River were calculated according to the following: the metal content of the SPM was multiplied by the TSS to indicate the metal load transported in the river (i.e. X µg of particulate metal per liter of river water; µg/L). Then, that value was added to the dissolved metal concentration to indicate the total metal load in a volume of water; which is consequently multiplied by the water discharge to estimate the metal load transported in the river per time (i.e. Kg/day or tons/day). For example, the estimated metal releases were thousands of tons of Fe and tens of tons of Zn between 1982 and 1984. The metal contents in the suspended matter ranged between 174 and 64189 mg/kg for Zn (average 6568 mg/kg) and 1.8 and 39.4% for Fe (average 6.9%) (Ministère de l'Environnement, 1985). Moreover, it should be noted that this study only showed a relatively narrow investigation about the metals present and transported in the river, since industrial and urban wastes (and wastewater) had been released into the Orne River long before this study (for example between the years 1870 and 1950, as mentioned in

Figure II-11: A section of the Orne River at Jœuf showing the river before (left) and after (right) dredging that took place between the 80s and 90s of the XXth century.
Images from Martinois (2014).

section *4*). Some of the possible sources of metallic elements are run off from slag heaps, sludge waste, furnace by-products (flue dust or fly ash), cinder and fuel. Due to the re-emergence of the industries in the 80s, another dredging activity was proposed, especially since the first two did not include the areas downstream of Jœuf. Indeed, a dredging was arranged in 1988 to include that area. About 48,000 m^3 of deposits were removed in the Moyeuvre area, including obviously iron rich deposits (which could be identified by the reddish colored mud) which could be found as deposits of more than one meter in some cases. Finally, the dredging from Jœuf till the city of Moyeuvre was finished in the 90s. It should be noted that high amounts of sediments still remained in the riverbed.

Some of the devices installed near the Orne watercourse were removed in the late 80s. For example, coke ovens were removed from Homécourt between 1984 and 1985, after they ceased in 1981. Nonetheless, steelmaking industries in the area between Jœuf and Moyeuvre were closed in 1988. Since waste management was absent, or at least not developed, during the periods where the industries were active (Garcier, 2007), metal rich particles might have settled along the Orne River course, especially in areas upstream of dams, which usually are suitable sites for sediment settling.

Finally, steelmaking processes can generally be divided into two main steps. The first is the production of molten iron[xxv] via blast furnaces (BF), and the second is the further purification and removal of carbon and other impurities produced from the first step to produce steel.

5. The production of pig or cast iron

The main materials that are used for pig iron production are coke, crude (raw) iron ore and limestone.

5.1. Coal combustion, coke production, and mineralogical and chemical composition

Coal used in the production of iron and steel making is majorly composed of carbon (~90%), but also contains metals, such as As (13 – 2000 mg/kg), Cd (0.07 – 0.18 mg/kg), Cr (10 – 1000 mg/kg), Cu (1 – 49 mg/kg), Pb (16 – 60 mg/kg), V (10 – 1000 mg/kg), Mo (0.3 –

[xxv] Same as pig iron.

30 mg/kg) and Ni (3 – 50 mg/kg) (Bradl et al., 2005; Groen and Craig, 1994; Peacey and Davenport, 1979; Xu et al., 2003). Coal is then heated (carbonization[xxvi]) in ovens under oxygen deficient atmosphere to produce coke. Coke is then left to cool before its usage in BFs. The gas produced in the making of coke is also used as a fuel in the making of sinter[xxvii] (iron rich clinker) and to heat the air for blast furnaces. During the production of coke, and before its usage in the pig iron production or steel making, by-products are formed; those by-products are metal rich and might be released to nearby water systems. Indeed, wastewaters released from coking plants contain organic pollutants, such as aromatic, phenolic, heterocyclic and polycyclic hydrocarbons (such as PAHs), some which are toxic and carcinogenic (Biache et al., 2013, 2008). Different organic markers could be linked to coal burning and coke production (e.g. Faure et al., 2007; Jeanneau et al., 2006). Furthermore, inorganic materials can also be associated to coal burning and coke production, such as sulfur, cyanide, ammonium and ammonia. Ashes released from coke production include silicates, such as quartz, cristobalite, mullite, Ca and Mn silicates, feldspars and metakaolinite, and oxides and oxy-hydroxides such as ferrospheres (e.g. magnetite, magnesioferrite and hematite) and lime and rutile (Vassilev and Vassileva, 1996; Zhao et al., 2006). Indeed, ferrospheres are a major component of fly ashes. Some SEM micro-images of fly ash released during coal combustion are shown in Figure II-12. Even though Fe is the main element in those ferrospheres, their composition varies according to morphology, since different morphologies of ferrospheres are caused by different chemical and mineralogical composition (Sharonova et al., 2015). In addition, sulfate rims could also be detected on ferrospheres, which in turn might control metal fate, possibly by co-precipitation and dissolution (Brownfield, 2002). The produced ashes also contain MTE, such as As, Cd, Cr, Pb, Zn and V (Xu et al., 2003). One of the main anthropogenic sources of vanadium is coke plants, which is released via heat combustion of coal and ash release since V is not volatile (Groen and Craig, 1994; Helble and Sarofim, 1993; López-Antón et al., 2011). A main V containing mineral associated to coke combustion is ferrovanadium, which is released from iron and steel industries (Huang et al., 2015; Moskalyk and Alfantazi, 2003).

[xxvi] Turn into carbon by burning.

[xxvii] Sinter is produced from fine raw iron ore, coke particles, sand-sized limestone and numerous other steel plant waste materials that contain some iron, such as scrap.

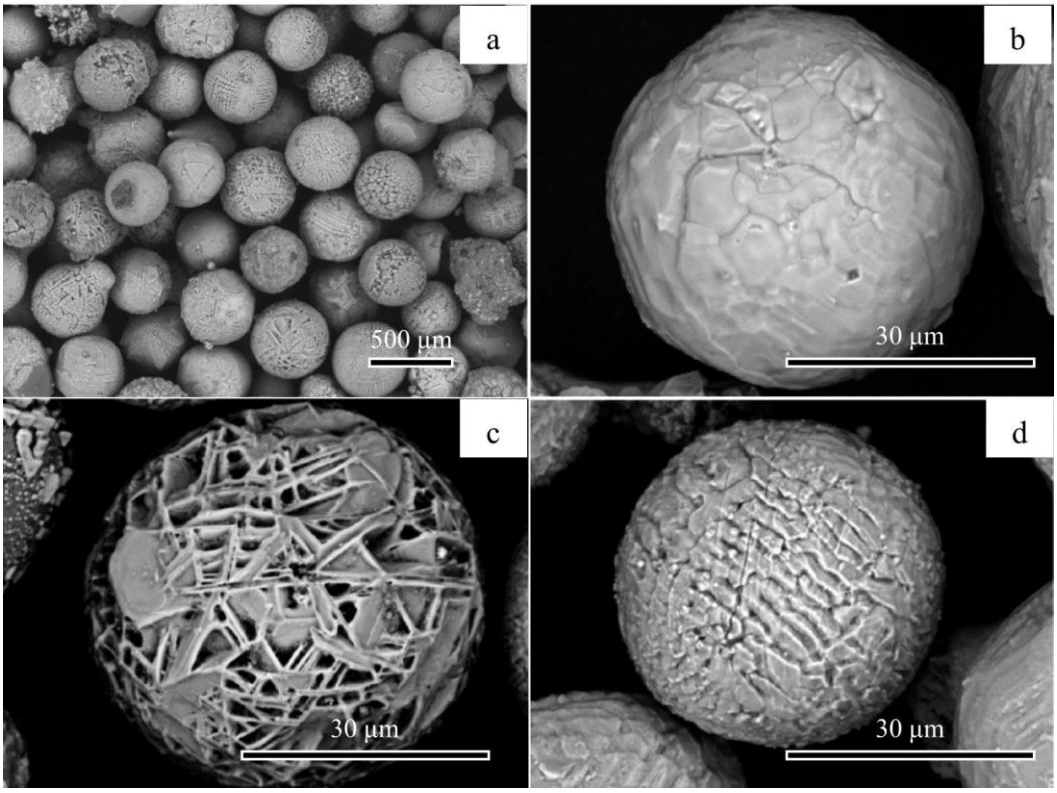

Figure II-12: SEM micro-images of polished sections of fly ash recovered from coal combustion. a: a general view of ferrospheres showing various surface morphologies, b: a single block ferrosphere, c: a plate-like ferrosphere, and d: a ferrosphere with dendritic magnetite. Micro-images modified from Sharonova et al., (2015).

5.2. Iron ore used in Lorraine steelmaking facilities

The main material used in the making of pig iron is Fe ore. An example of a crude iron ore is the Minette ironstone (also called Lothingren, according to Teyssen (1984) and Maitte et al., (2015)), which was used in the steelmaking industries in Lorraine. Minette is mainly composed of goethite ooids, Fe carbonates (siderite) and iron phyllosilicates (berthierine and chamosite), the last two act as a cohesive assembly which fill the spaces between goethite ooids (Figure II-13). Analyses of minette ores from several horizons in the Landres-Amermont basin in Lorraine showed that the main minerals are goethite (37 – 54%), siderite (5 – 13%), ankerite (1 – 2%), chamosite (10 – 30%), calcite (5 – 23%), quartz (1 – 18%) and phosphate (0.1 – 1.4%). Furthermore, the chemical composition of the oolitic limonite was SiO_2 (4 – 5%), Al_2O_3 (3 – 8%), Fe_2O_3 (20 – 72%), FeO (0.1 – 15%), MnO (0.1 – 0.5%), MgO (0.4 – 2.9%), CO (5 – 27%), TiO_2 (~ 0.1%), P_2O_5 (0.7 – 3.7%) and S (0.09 – 0.40%) (James, 1966). SEM-EDX analyses of goethite ooids collected from Lorraine (Malavillers and Jœuf) were mainly characterized by 70% FeO (total iron) , 9% SiO_2, 11% Al_2O_3, 3% MgO and 3 – 7% P_2O_5 (Grgic et al., 2002).

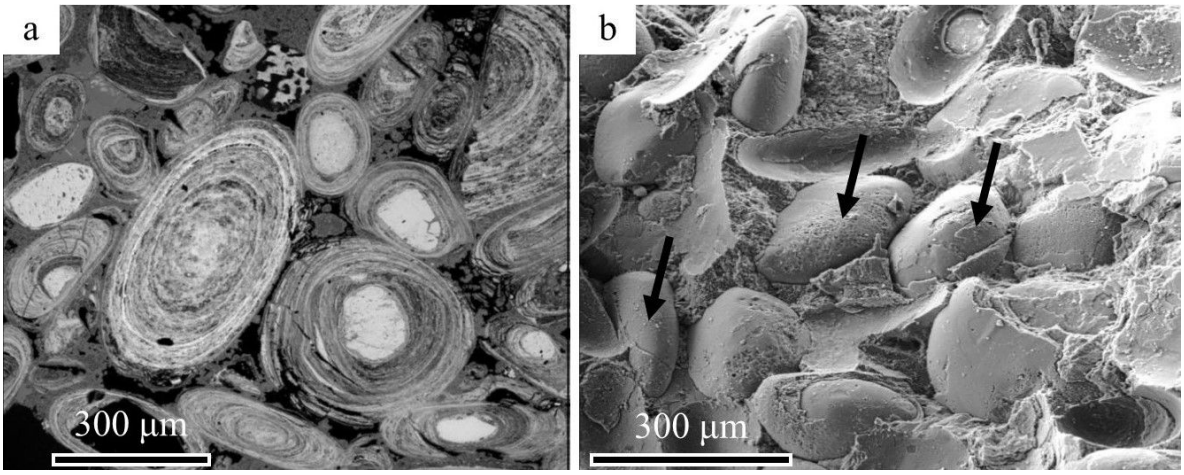

Figure II-13: SEM micro-images of minette iron ore.
a: SEM micro-image of a polished section showing concentric layers of goethite. b: SEM micro-image showing goethite ooids (black arrows) with siderite and iron phyllosilicate assembly between the ooids. Modified from Grgic et al., (2002).

6. Processes occurring in blast furnaces

The raw materials, which are Fe rich material, coke and lime, are introduced in the blast furnace for the production of pig iron (Figure II-14 a). It should be noted that the Fe material can be raw Fe ores, pellets or sinter (including scrap[xxviii]). Sinter is formed by the addition of iron ore and coke in the blast furnace. Inside the blast furnace, hot air blast is injected through the nozzles (called tuyeres), hence the name blast furnace. At this stage, the temperature of the BF is approximately 2200°C. Coal or oil might be introduced in the blast furnace to further raise the temperature and to reduce the requirement of coke. As a consequence, chemical reduction and iron melting from the sinter and iron ores takes place; therefore, a pool of liquid iron is formed at the bottom of the furnace (called hearth). As for the added limestone, it is combusted into lime and carbon dioxide (Figure II-14 b); the former then combines with impurities, such as Si_2O, Al_2O_3 and MgO, and molten rock (residues from iron ore, sinter and scrap) and forms a liquid called slag. Slag is lighter than the molten iron that is collected at the hearth, and therefore floats on top (Figure II-14 a). The molten iron formed at the hearth is then tapped into ladles; at that stage, the iron is called pig iron or cast iron. Additionally, the slag formed on the surface of the molten iron is removed through a taphole (also known as slag notch) located at the bottom of the furnace (Figure II-14 a). As the process of pig iron

[xxviii] Iron waste materials that can be used in metal reprocessing, such as parts of vehicles and buildings. The range of metal contents depend on the materials, and therefore are highly variable; for example, paints, rubber and plastic materials enrich BF components with impurities.

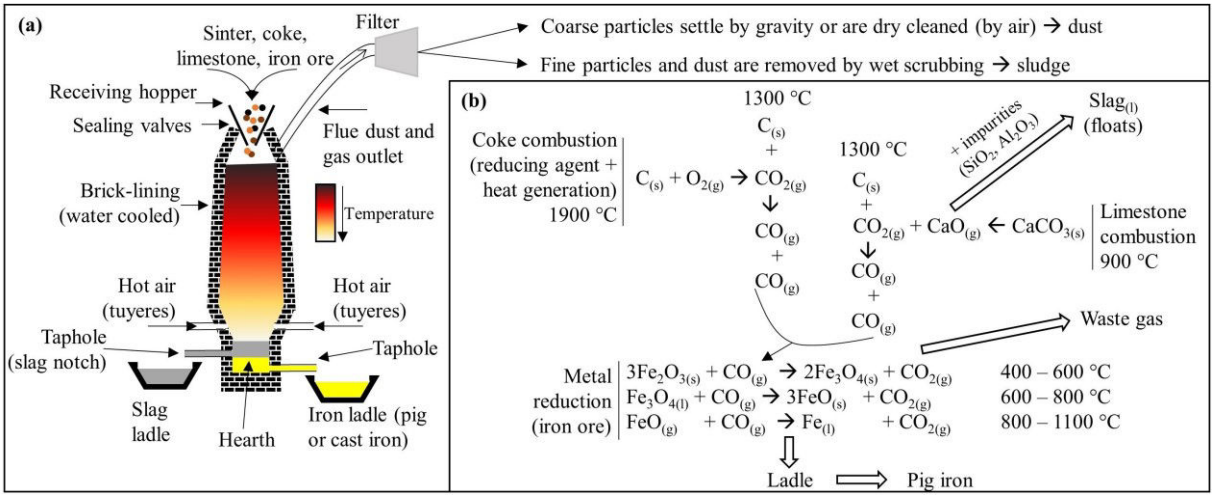

Figure II-14: Schema of a blast furnace (a) and main chemical reactions taking place (b).
a: The blast furnace with the main parts and the product (cast or pig iron), the by-product (slag) and wastes (flue dust and sludge). b: The main chemical reactions of limestone, coke and iron ore taking place in the blast furnace to produce pig iron and slag. The temperatures indicated in the schema represent gas temperatures. Schema drawn according to Peacey and Davenport (1979), Trinkel et al., (2015) and Yildirim and Prezzi (2011).

production in the BF is a continuous process, addition of raw materials is also continuous. Some of the main processes (chemical reactions) taking place in BFs are shown in Figure II-14 b. Producing pig iron might go on without stop for more than ten years, depending on the resistivity of the heat-resistant brick lining and the availability of the raw materials used. Afterwards, the lining is replaced and the process continues. However, the produced iron that is collected from BFs contains impurities, such as sulfur, phosphorous, manganese and silicon. The next step might be the reduction of the impurities and the processing of pig iron into steel.

7. Steelmaking: production of steel from pig iron

Steel can be made from iron scrap or from the hot pig iron produced in BFs, or a mixture of both. The chemical composition varies according to the type of steel required. The process commences with the pouring of molten iron in a furnace (called converter or vessel). Previously, the common converters or furnaces used were the Thomas-Gilchrist converter and the open hearth furnaces (known as the Siemens-Martin process) invented in the XIXth century. The common furnaces used nowadays are basic oxygen furnaces (BOF) and electric arc furnaces (EAF) (Davison and Owens, 2012; Peacey and Davenport, 1979; Yildirim and Prezzi, 2011), which refine metal iron into steel. In the BOF, high purity oxygen is blown at very high pressures just above the surface of the molten iron to remove carbon impurities. Oxygen reacts with carbon and other unwanted elements which results in the formation of slag on the surface of molten iron (see Figure II-14 b for possible reactions). Carbon is then released as carbon monoxide (which can be re-used as fuel; same as the re-use of gas from the combustion of coke

in section *5.1*). In addition, lime, metal scrap and hot pig iron are added to control temperature. Lime and dolomite (also referred to as fluxes) are also added to remove unwanted products (Yildirim and Prezzi, 2011), such as Si_2O, Al_2O_3 and MgO, which results in slag formation (similar to the reaction seen in Figure II-14 b). The converter is then tilted so that slag is removed from the top of the molten steel via a taphole. Afterwards, the molten steel is tapped into a ladle. At that stage, the carbon content should typically be 0.04%, while it initially was ~ 4% in pig iron. As for the process of EAF, the outcomes are the same. However, on the contrary to BOF, only scrap metals are used in EAF. Also, an advantage of using EAF over BOF is the more precise control over the composition of the formed material. Afterwards, the steel is casted to form the required shapes, mainly as billets[xxix], blooms[xxx] and slabs[xxxi] (Davison and Owens, 2012). The casted steel (as well as iron) might be covered with a protective layer of zinc to prevent rusting, which is called galvanization. A summarizing schema representing iron and steelmaking is shown in Figure II-15. Finally, whether BOF or EAF was used in steelmaking, it should be noted that the by-products from the crude iron and

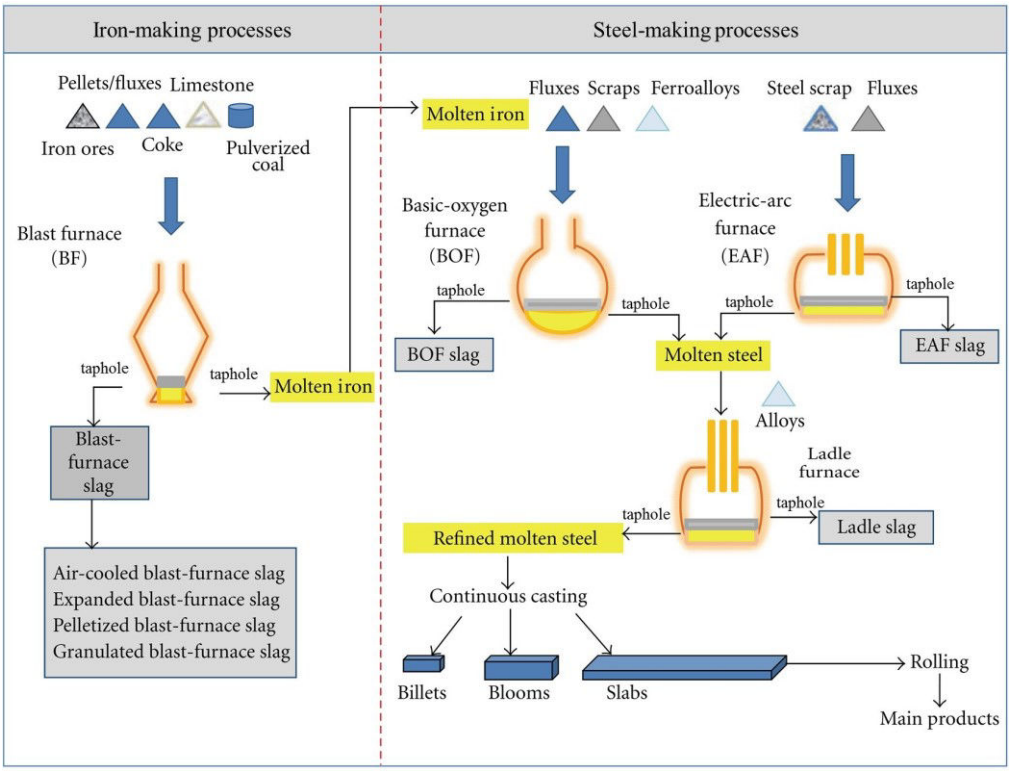

Figure II-15: Schema of iron and steelmaking processes.
The boxes filled with grey color represent slag phases. The boxes filled with yellow color represent iron/steel phases. Modified from Yildirim and Prezzi (2011).

[xxix] A steel piece that has a square or circular cross section.
[xxx] Same as billet, but with a rectangular cross section.
[xxxi] A slab is a thinner and wider bloom.

steel production are slag (90%), and the waste materials are dust (collected in filters) and sludge (collected in gas scrubbers).

8. Sources and fate of metals inside the blast furnace

Iron and steel industries are major sources of iron input into the environment; nonetheless, MTE, such as As, Cr, Cd, Ni, Zn and Pb are also released (e.g. Das et al., 2007, 2002; Kretzschmar et al., 2012; Mansfeldt and Dohrmann, 2004; Trinkel et al., 2016, 2015). The following paragraphs will deal with the sources of Fe, Zn and Pb, and their fate in BFs. The focus is made on those metals due to their predominance as mineral species (as it will be seen in the coming chapters). Additionally, Fe and Zn might be nutrients for living organisms (dependent on their speciation).

8.1. Iron fate in blast furnaces

During the making of pig iron or steel, some Fe might not be extracted and remain in the by-products or wastes, while the majority is transformed into liquid iron. In addition to goethite as an Fe bearing mineral used in the steelmaking processes in Lorraine (which is the main constituent of the minette ironstone), other forms of Fe bearing minerals include hematite (Fe_2O_3), ilmenite ($FeTiO_3$), magnetite (Fe_3O_4), siderite ($FeCO_3$) and pyrite (FeS_2) (Peacey and Davenport, 1979; Yellishetty et al., 2010 and articles cited therein). Part of the fate of Fe inside the blast furnace was depicted in Figure II-14 b. Iron minerals are gradually reduced to eventually form molten Fe. For example, hematite is reduced via carbon monoxide to yield magnetite and carbon dioxide at relatively low temperatures in BFs (400 – 600°C). At higher temperatures, and deeper in the BF, magnetite is further reduced by CO and ferrous oxide (wurtzite if well crystalline) is formed. Towards the hearth, where the temperature is the highest, liquid iron is formed, which is then tapped to ladles (as discussed in section *6*). In case iron sulfide minerals were used as Fe ore, they are oxidized in the furnace; as a result, magnetite might form (Lauf et al., 1982; Thorpe et al., 1984), which continuous the steps mentioned above (i.e. reduction to form wuestite and liquid/molten iron). Furthermore, part of the iron escapes the blast furnace as dust and fly ash, or remains inside the BF as slag.

8.2. Zinc cycle in blast furnaces

On a monitoring study about the input of zinc into BFs, it was seen that Zn is mainly originated from the raw materials used, such as sinter, scrap, coke and treated slag/sludge, and also to a lesser extent from limestone and coal. Zinc is very difficult to remove during steel

production, especially in the sinter production stage, since Zn is not volatile and concentrates in the formed dust/sludge and slag. Zinc is mainly introduced into BFs as oxides and carbonates, and to a lesser extent as sulfides (Besta et al., 2013; Trinkel et al., 2015). Since slag contains carbonates, it can be re-used in the blast furnace to remove impurities; sludge might also be re-used in BFs. In case Zn was introduced into BFs as oxides, it is reduced by means of CO at temperatures ranging between 800 and 1000°C to form Zn gas, which is rapidly oxidized by CO to form Zn oxide (ZnO) again (Figure II-16). However, after reaching lower levels in the BF, ZnO is reduced to metallic Zn at temperatures between 900 and 1300°C. Since metallic Zn is of lower density, it moves upward in the furnace where it oxidizes again, and the cycle continuous. Additionally, zinc and zinc oxide might react with sulfur to form Zn sulfides, or Zn is introduced into BFs as sulfides; in either case, Zn sulfide is reduced and ZnO is produced, and the cycle of ZnO, as presented above, continuous. Zn sulfides might be reduced by means of CaO, produced from the combustion of limestone for example (see reaction of limestone in the blast furnace in Figure II-14 b) (Besta et al., 2013; Trinkel et al., 2015). Zinc is then released from BFs mainly from the top gas dust and then concentrates in the sludge after wet scrubbing of flue dust (Trinkel et al., 2015 and references cited therein). Sludge (e.g. Kretzschmar et al., 2012) and dust (e.g. Sobanska, 1999) might contain trace amounts of Zn as sulfides, such as wurtzite and sphalerite. Nonetheless, the main Zn species released from BFs are silicates (and phyllosilicates), such as hemimorphite ($Zn_4Si_2O_7(OH)_2.H_2O$) and willemite (Zn_2SiO_4), oxides,

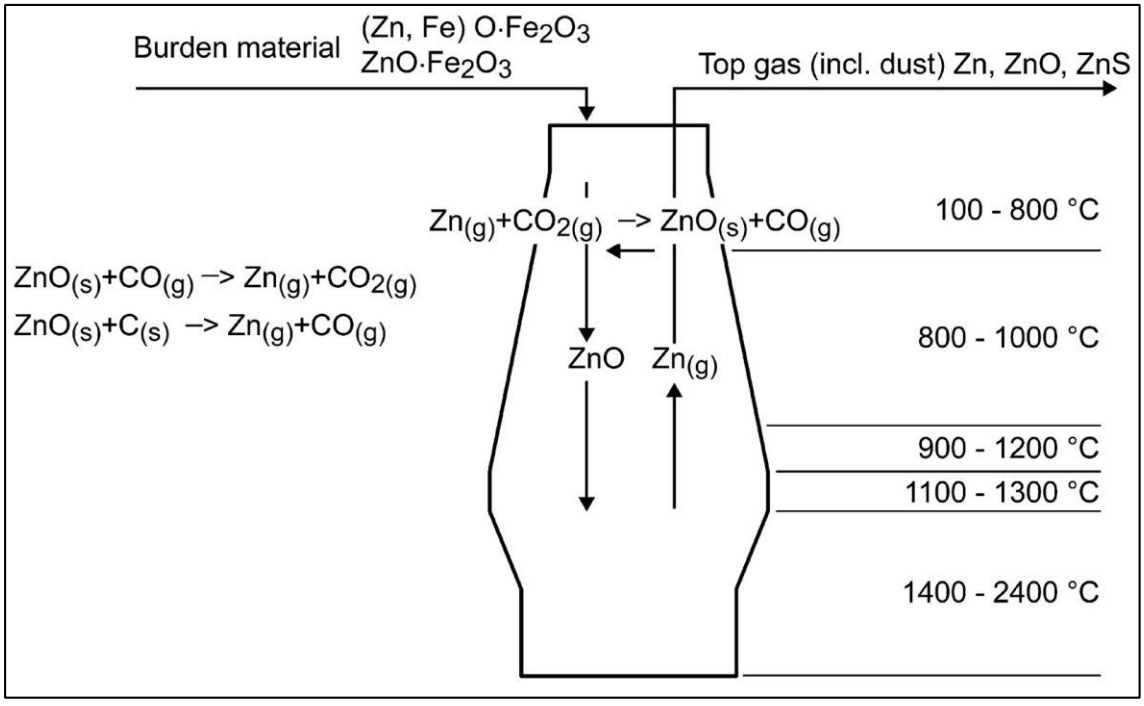

Figure II-16: Zinc cycle in blast furnace.
The temperatures included in the figure represent gas temperatures. Image modified from Trinkel et al., (2015) on the basis of Deike and Hillmann (1999).

such as franklinite ($ZnFe_2O_4$) and zincite (ZnO), and carbonates, such as smithsonite ($ZnCO_3$) (e.g. Isaure et al., 2002; Kretzschmar et al., 2012; Luxton et al., 2013; Manceau et al., 2000; Mansfeldt and Dohrmann, 2004; Nachtegaal et al., 2005; Ndiba et al., 2008; Trung et al., 2011; Van Damme et al., 2010; Van Herck et al., 2000).

8.3. Lead cycle in blast furnaces

During the production of steel, lead is majorly introduced to BFs from iron ore (or sinter) and scrap. The main forms of Pb that enter BFs are oxides (PbO) and sulfides (PbS and $PbSO_4$) (Trinkel et al., 2015 and references cited therein). Lead, similar to Zn, also follows a cycle in the different locations in BFs. The introduced lead minerals (oxides and sulfides) reach the hearth, where temperature is the highest; lead minerals are reduced by CO and H_2 to produce liquid metallic lead (Figure II-17). However, lead reduction might occur starting from relatively low temperatures (~ 400°C). Also, and at temperatures ranging between 400 and 700°C, lead oxide might react with SiO_2 to produce lead silicate ($PbSiO_4$), or might be reduced to form lead sulfides at temperatures between 650 and 900°C (the equations are found in Figure II-17). Lead then rises to the top of the BF, where it condenses again due to lower temperatures. Furthermore, the same cycle applies to Pb sulfides, where PbS is reduced at high temperatures at the bottom of the BF. Lead is majorly released from BFs as molten metal, gas dust and slag, and mainly as oxides and sulfides (Trinkel et al., 2015 and references cited therein).

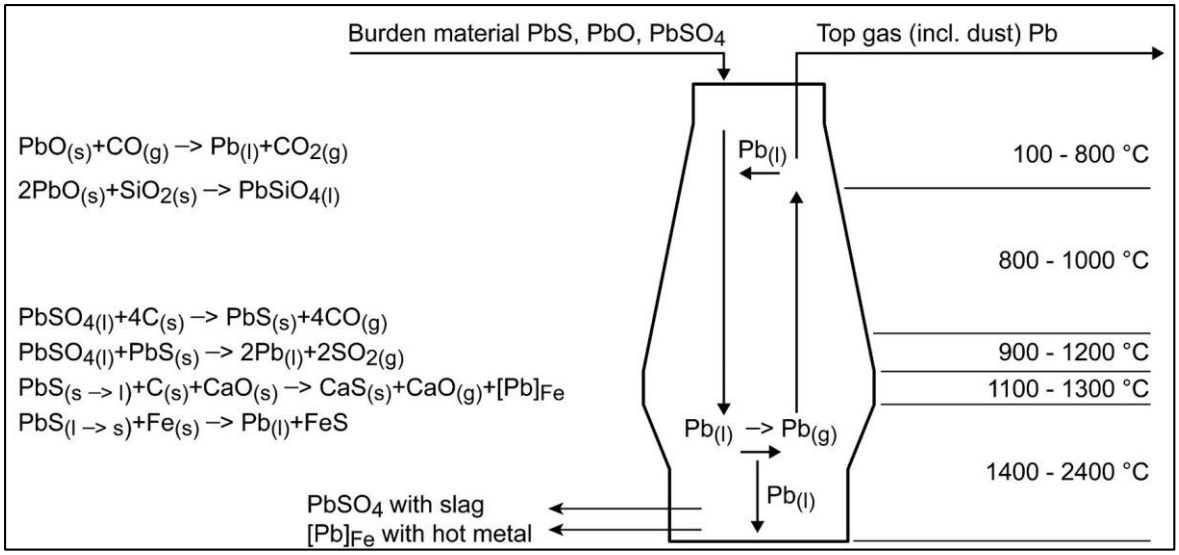

Figure II-17: Lead cycle in blast furnaces.
The temperatures included in the figure represent gas temperatures.
Image modified from Trinkel et al., (2015) on the basis of Chernousov et al., (2011).

9. The output materials of blast furnaces: composition and fate

As mentioned earlier, slag forms on the surface of the molten iron, while dust is collected in filter bags positioned at the top of the blast furnace, and sludge is generated after wet scrubbing (or wet cleaning) of dust particles (Das et al., 2007; Davison and Owens, 2012; Korpa and Mudron', 2006; Trinkel et al., 2016). Slag represents 90% of the produced materials during iron and steelmaking, while the other percentage represents pig iron, steel, dust and sludge. Some of the by-products might be re-used, which will be included in the coming sections.

9.1. Slag composition and usage

Slag is the biggest fraction of the materials that result from the making of pig iron and steel. The chemical composition of slag varies according to the raw materials used, however, a general range of contents is 24 – 60% CaO, 2 – 20% SiO_2, 1 – 22% Al_2O_3, 0.5 – 15% MgO, 1 – 38% Fe_2O_3, 0.1 – 0.8% SO_3, 0.1 – 6% MnO, 0.3 – 2% TiO_2 and 0 – 3.3% P_2O_5 (see table 1 in Yildirim and Prezzi, 2011). Moreover, various crystalline minerals are found in slag, such as portlandite ($Ca(OH)_2$), srebrodolskite (Ca_2Fe2O_5), merwinite ($Ca_3Mg(SiO_4)_2$), larnite (Ca_2SiO_4), calcite ($CaCO_3$), manganoan calcite ($(Ca,Mn)CO_3$), lime (CaO), dolomite ($CaMg(CO_3)_2$), wollastonite ($CaSiO_3$), periclase (MgO), pentahydrite ($MgSO_4.5H_2O$), monticellite ($CaMgSiO_4$), hematite (Fe_2O_3), magnesite ($MgCO_3$), and finally wuestite (FeO), which might be of high contents in steelmaking slag, especially if they are rich in Fe (Yildirim and Prezzi, 2011 and references cited therein). It should be noted that sediments (or other matrices) containing slag cannot merely be identified by chemical composition (Al or Si contents for example), rather complementary techniques need to be employed to identify unique minerals or phases usually occurring in slag, such as circular glass like phases (Figure I-13). In many cases, slag is re-used in BFs as a CaO or Fe source. Nonetheless, slag re-use or recycle in BFs might be limited enriched with metals (such as As and Zn) or non-metals (mainly S and P). In that case, metal recovery from slag is possible (Das et al., 2007; Mansfeldt and Dohrmann, 2004). Slag might also be re-used in areas others than steelmaking, such as construction materials (e.g. cement, silica, glass and bricks), soil amendments and fertilizers (Das et al., 2007; Peacey and Davenport, 1979; Wei et al., 2014). It is important to notice that slag that is tapped from BFs can be treated differently. For example, slag might be air-cooled, expanded, pelletized or granulated (Figure II-15); as a result, aggregates of different densities form. The formed slag depends on how it is cooled and solidified on one hand, and how the

by-product is intended to be used on the other. Slag pellets are used in cement industries (unless they contain high Fe contents), expanded slag is used in construction, and pulverized slag might be used as soil amendments for growing fruits and vegetables (Das et al., 2007; Maslehuddin et al., 2003; Palomo et al., 2014). Alternatively, if the usage of slag aggregates is discouraged, for example due to undesirable chemical contents, slag might be stocked as piles or heaps, i.e. slagheaps, used road sub-base materials, or might be discharged into flowing water systems. Therefore, slag particles might be transported to surface waters, or might weather and cause metal leaching, possibly to groundwater. Slag might form sub-micrometric (< 1 μm) glass like droplets that are rich in Pb and Zn sulfides; dissolution of those phases from dumpsites or in water systems can cause undesirable metal enrichment to river compartments (water and sediment) as well as biota (e.g. Das et al., 2007; Ettler et al., 2001; Houben et al., 2013; Sobanska et al., 2016; Vanaecker et al., 2014). Bio-alterations might also be a part of the metal fate in slag, either as metal mobilizers or immobilizers (van Hullebusch et al., 2015).

9.2. Dust particles emitted from blast furnaces

Dust particles (also termed fly ash and flue dust) are emitted from BFs and are collected in filters (called dust bags), following the same pathway of the gases that escape BFs (Figure II-14 a). It should be noted that fly ashes could have various origins, such as from coal combustion (section *5.1*) and iron melting (section *6*). The particle size and chemical composition depend on the raw materials used and the processes undergoing in BFs. The sizes are usually inferior to 210 μm (Kiventerä et al., 2016; Leimalm et al., 2010), and the chemical content is roughly 50 – 51% Fe_2O_3, 3 – 8% SiO_2, 2 – 5% Al_2O_3, 2 – 5% CaO, 0.9 – 1.5% MgO, 190 – 240 mg/kg Pb and 280 – 420 mg/kg Zn. In some steelmaking industries, metal content was recorded to be significantly higher. For example, the contents of Pb and Zn could reach as much as 4.4 and 8.8%, respectively, in dust particles collected from a Chinese steel plant (Zhou et al., 2013). Iron rich dust might be re-used in the furnace; however, due to the possible high metal contents, such as Pb and Zn, recycling of flue dust particles in BFs is usually discouraged, which consequently becomes an environmental concern. Indeed, the presence of metals, such as As, Cd, Pb and Zn, might cause operational problems, such as damaging the lining of the furnace or tuyeres (Trinkel et al., 2016 and references cited therein). Some of the common minerals detected in the emitted dusts from BFs are magnetite (Fe_3O_4), hematite (Fe_2O_3), quartz (SiO_2), wuestite (FeO) and gehlenite ($Ca_2Al_2SiO_7$) (Das et al., 2007, 2002). However, a great part of the emitted dust particles is treated to make the dust re-usable in the furnace, such as passing the dust through a cyclone (dry treatment) where Zn and Pb rich particles are separated

from the Fe and C rich particles; the latter fraction is re-used in the furnace (Korpa and Mudron', 2006), while the former metal rich fraction is dumped into the environment. Other treatments include cleaning systems using water (gas or wet scrubbing); the formed sludge is deposited in tanks and left to settle (i.e. settling tanks or settling ponds). In other words, sludge is left to settle so that metal rich particles are more concentrated in the solid fraction, rather than in the liquid fraction as suspension, which will make the treatment of the sludge more efficient and practical (Kiventerä et al., 2016). The chemical and mineralogical composition of dust particles and sludge might be similar; therefore, it is typical to include the chemical content, mineralogical composition and fate of dust and sludge particles in the same context.

9.3. Sludge composition and fate

The chemical and mineral composition of flue dust, which becomes sludge after wet scrubbing, was discussed in the previous section; this section discusses formed sludge. It should be noted that sludge is formed from the making of iron (from blast furnaces) and steel (steel converters). The major composition of sludge is iron oxides (50 – 80% Fe_2O_3) and coke fines (carbon), and minor components are silicon (1 – 5%), aluminum (0.3 – 5%), calcium (4 – 11%), potassium (1.22%), magnesium (0.3 – 1.3%) and manganese (0.1 – 0.6%) oxides, as well as trace metals (Das et al., 2007; Kretzschmar et al., 2012; Mansfeldt and Dohrmann, 2004). Moreover, some of the common minerals in sludge are magnetite, hematite, quartz, wuestite, gehlenite, calcite, dolomite, graphite, kaolinite, muscovite, siderite, maghemite and iron cyanide (Das et al., 2007, 2002; Kretzschmar et al., 2012; Mansfeldt and Dohrmann, 2004). Again, the chemical composition and grain size of sludge and flue dust particles are dependent on the materials that are introduced into BFs. For example, on a study that characterized the chemical composition of differently size-fractionated sludge particles (with cut-off sizes of 20, 40, 63, 100 and 250 µm), carbon was mainly associated to the relatively coarse fractions (> 100 µm), while Fe, Pb, Cd and Zn were more enriched in the fine particles (Trinkel et al., 2016). Furthermore, metals might condense on surface of particles, similarly to the presence of sulfate rim coating ferrospheres (Brownfield, 2002). Indeed, Zn, Pb and Cd contents in sludge were significantly correlated to the surface over volume ratio of sludge particles (Trinkel et al., 2016). As discussed in the previous section, dust (and also wet scrubbed dust, i.e. sludge) might be re-used in BFs under certain conditions (see section *9.2*). It should be noted that high contents of iron, in case of flue dust, is found as hematite, and can be re-used in the furnace (Das et al., 2007). Nonetheless, as undesirable metals might be associated to ferrospheres of fly ash and other sludge particles, sludge re-use in the furnace is limited, unless chemical separation is

done, which might be economically disagreeable. Metals might be removed from sludge before re-usage via selective leaching, ion exchanger, froth flotation[xxxii] and others (Das et al., 2007). Anionic exchangers were successfully used to remove Zn and Pb from BFS (Van Herck et al., 2000). Otherwise, BFS might be treated as wastes, and is stocked as piles or left to settle in settling ponds or is released into flowing water systems (e.g. Das et al., 2007; Kretzschmar et al., 2012; Mansfeldt and Dohrmann, 2004).

Storing of sludge in settling tanks, sedimentation ponds and landfills might create environmental concerns, mainly due to weathering processes, such metal release caused by bio-chemical transformations or alterations (Kretzschmar et al., 2012; Mansfeldt and Dohrmann, 2004; Van Herck et al., 2000; van Hullebusch et al., 2015). On a study on sludge weathering in a sedimentation pond from pig iron production, Zn was released from BFs mainly as ZnO. However, after some decades had passed (~ 30 – 80 years), sludge was weathered in the pond, zinc oxides could hardly be detected due to transformations, and Zn became incorporated into octahedral sheets of phyllosilicates, hydrozincite and LDH (Jacquat et al., 2008; Kretzschmar et al., 2012). Another study proved that the complete weathering of ZnO and the formation of other Zn species, mainly Zn phyllosilicates, LDH and hydrozincite occurred after 9 months; no noticeable transformations of Zn species could be seen afterwards in the 4 year study (Voegelin et al., 2005). In another study, weathering of silicon and aluminum from silico-calcic glass like phases, that were introduced from iron making industries, was suggested to occur in settling ponds. As a result, fibrous allophane-like aluminosilicates precipitated (Huot et al., 2014). Moreover, the fate of metals and metal bearing particles released from sludge might be different in case they are leached to water systems and deposited as sediments, where precipitation of metal sulfides might happen (see chapter *I*, sections *7.1* and *8.1*).

10. Locations of the sampling sites along the course of the Orne River

Several sediment samples were collected along the course of the Orne River, mainly between Homécourt (the most upstream site is BARB; Figure II-18) and Moyeuvre-Grande (labeled BETH in Figure II-18), in addition to a site located approximately 1 km before the confluence with the Moselle River, which is Richemont (labelled RICH in Figure II-18). An inventory of the collected samples is found in Table II-2. Sediment samples were mainly

[xxxii] Selective separation of hydrophobic materials from hydrophilic ones.

collected via coring using a piston corer (or Beeker corer); sediment cores near the bank were collected while on land; a floating platform (Quadriraft, from Marc Desmet, GECO laboratories, Tours University) was used for sediments that were submerged with relatively high water columns (~ 1 – 2 meters) such as the case of BETH1402 (see Figure II-19) and HOM1403. Some of the surface sediment samples were collected via scooping (scoop and dredges) and fractionated using the wet sieving method with the corresponding river water,

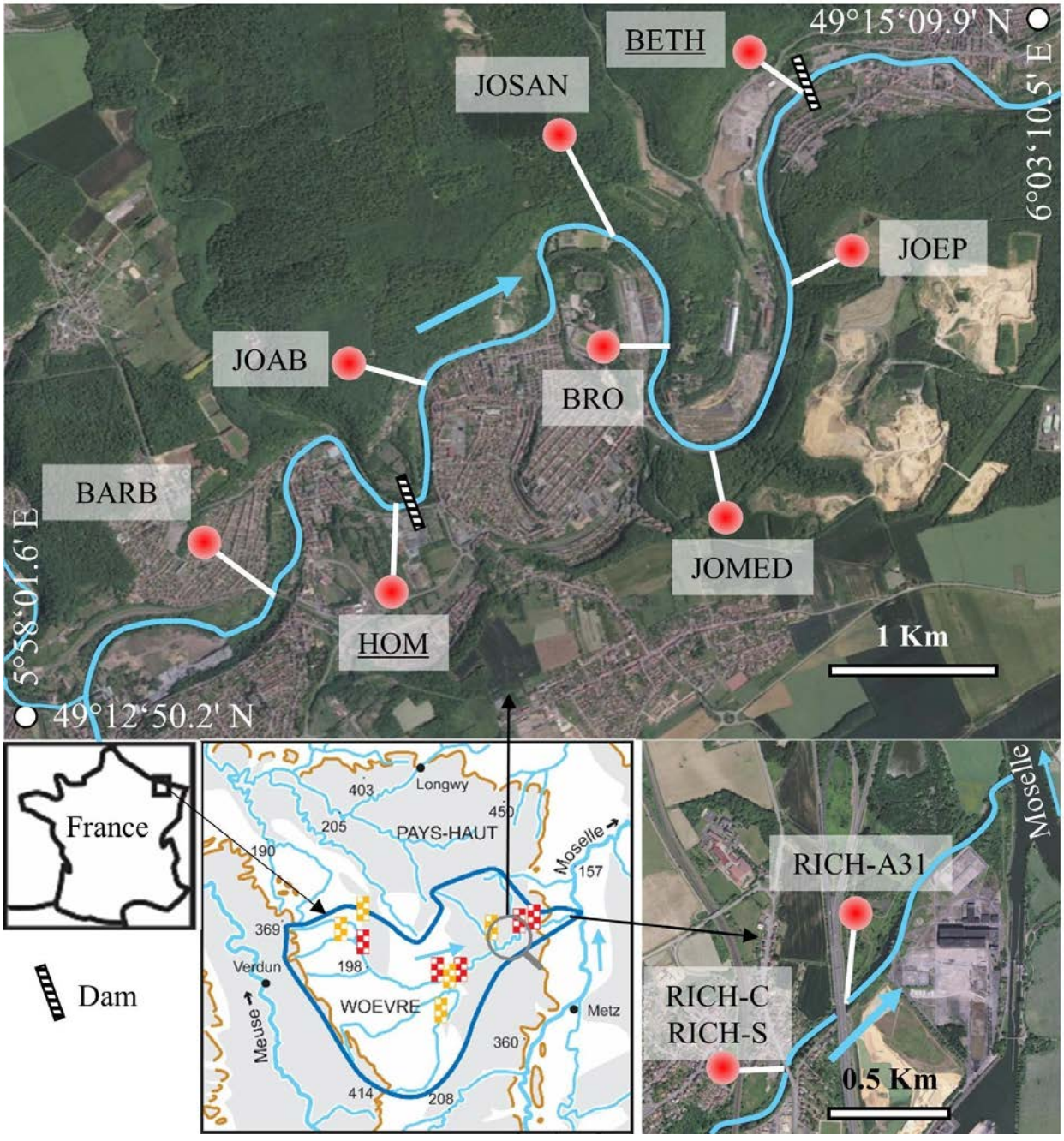

Figure II-18: Locations of the sediments that were collected along the course of the Orne River.
The map of the Orne watershed (lower left) is modified from the map created by Benoit Losson, on the basis of data provided by the French National Institute of Geography IGN, www.geoportail.gouv.fr. Other maps were collected from www.geoportail.gouv.fr. Sites located upstream of dams are underlined (i.e. BETH and HOM).

namely samples collected on 08 and 09 April 2013 (i.e. 20130408 and 20130408 in Table II-2, highlighted in light gold). The sediment samples were then separated into fractions with cut-off sizes of 2 mm, 250 µm and 50 µm. As for the sediment cores (highlighted in light blue in Table II-2), they were sectioned into layers of various thicknesses. Therefore, grain size separation was not possible, due to the relatively small amount of each layer. In addition, the grain sizes were rather homogeneous throughout the vertical layers of the sediments, with the exception of the sediment cores JOSAN15C1, JOSAN15C2 and JOSAN15C3. Only the surface sediments of those cores will be discussed. However, after the cores were retrieved from the submerged sediments, Styrofoam was put on top of the cores (including surface layer) to prevent surface layer disturbance; the Styrofoam was pushed gently inside the top of the

Figure II-19: The area upstream the Beth dam, Moyeuvre-Grande, and collection of a sediment core using a floating platform (quadriraft).
a: The upstream zone of the Beth dam; Orne River at Moyeuvre-Grande. Image taken on 10 July 2013, when the water level of river was low due to the maintenance. b: same location as a, but image taken on 05 June 2015, where the water level was high (flooding event). c and d: an example on sediment coring using a floating platform and a Beeker corer. Images c and d were taken on 26 February 2014 (BETH1402 core).

core, which caused the removal of the water layer above the sediments. Rubber tube end caps were put on the bottom end of the cores (which contain the deepest sediment layers). Afterwards, the cores were either cut on site (case of JOSAN15C1), or transported back to the laboratory in a vertical position where sectioning took place. Although keeping the sediment core in a vertical position might cause consolidation of the sediments, it was done to reduce the circulating of pore water. An example on the collection of a sediment core using a beeker corer and a floating platform (Quadriraft) is shown in Figure II-19. The quadriraft was used in the sediment collection upstream the Beth dam at Moyeuvre-Grande (BETH1402) and upstream the Homécourt dam (HOM1403), due to the controlled water flow, which makes the usage of a floating platform practical. Those sites are expected to have higher sediment load (as seen in Figure II-19 a). Finally, the importance of the sites come from the fact that the Orne river course was highly influenced by past steel industries (section *4*), and also because the dam is planned to be completely or partially modified or removed in the coming decades, which will cause the settled sediments to be remobilized.

Table II-2: An inventory of the sediment samples collected along the Orne River course.
Names, labels, coordinates, type and features of the sediment samples collected along the course of the Orne River.
The samples are placed in the table according to their locations in the course of the Orne River (downstream gradient).

Site name	Label of site	Longitude (E)	Latitude (N)	Elevation (m)	Type	Label of core	Diameter of core (mm)	Depth of core (cm)	Date
Jœuf Barbusse	BARB	5°59'23.8"	49°13'12.0"	177	SS				20130408
		5°59'25.0"	49°13'13.5"	177	SC	BARB1401	90	34	20140120
		5°59'24.7"	49°13'13.4"	177	SC	BARB1501	90	24	20150106
Jœuf Homécourt	HOM	6°00'01.7"	49°13'30.3"	176	SC	HOM1401	90	12	20140120
		6°00'01.7"	49°13'30.3"	176	SC	HOM1402	90	15	20140120
		5°59'56.8"	49°13'30.9"	176	SC*	HOM1403	60	63	20140318
Jœuf Abattoir	JOAB	6°00'08.2"	49°13'53.4"	174	SS				20130408
		6°00'08.5"	49°13'52.1"	174	SC	JOAB1401	90	22	20140120
		6°00'08.9"	49°13'52.4"	174	SC	JOAB1501	60	9.25	20160106
Jœuf Sainte Anne	JOSAN	6°00'59.9"	49°14'22.6"	174	SS			0.5	20150215
		6°01'00.8"	49°14'22.6"	174	SC	JOSAN15C1	60	19	20150215
		6°01'00.6"	49°14'22.6"	174	SC	JOSAN15C2	90	36	20150215
		6°01'00.6"	49°14'22.6"	174	SC	JOSAN15C3	90	51.5	20150215
Jœuf Brochetiere	BRO	6°01'20.3"	49°14'00.3"	174	SC	BRO1507	60	38	20150722
Jœuf Mediatheque	JOMED	6°01'32.8”	49°13'42.0"	173	SC	JOMED1507	60	~40	20150722
Jœuf Europipe	JOEP	6°01'51.8"	49°14'01.5"	173	SC	JOEP1503	90	41.5	20150330
Moyeuvre-Grande: Beth dam	BETH	6°01'55.0"	49°14'47.0"	171	SC	BETH1301	90	77	20130710
		6°01'55.0"	49°14'47.0"	171	SC	BETH1302	90	96	20130710
		6°01'55.3"	49°14'46.5"	171	SC*	BETH1402	60	131	20140226
		6°01'57.2"	49°14'48.6"	171	SC	BETH1507	60	18	20150722
Richemont near the city (1)	RICH-C	6°10'11.7"	49°16'38.7"	155	SS				20130409
Richemont near the sewer (1)	RICH-S	6°10'12.0"	49°16'40.6"	155	SS				20130409
Richemont near route A31	RICH-A31	6°10'22.2"	49°16'48.1"	154	SS				20130409

SS: surface sediment.
SC: sediment core.
Date: Year, month, day (YYYYMMDD).
Note: The bottom of the JOMED1507 sediment core collapsed, so the length is not precise, hence ~ 40 cm.
*: Sediment cores were collected via a floating platform.

11. Context of the study

The Zone Atelier Moselle (ZAM), with the laboratories of the Centre National de la Recherche Scientifique (CNRS), Institut National de la Recherche Agronomique (INRA), Agence Nationale de Sécurité sanitaire de l'alimentation, de l'Environnement et du travail (ANSES) and Université de Lorraine, structure the work on the protection of water resources of the Moselle River and tributaries, including the Orne River. The aims of the ZAM project are to comprehend the impact of anthropogenic activities on the quality of the aquatic compartment of Lorraine, and to make the scientific knowledge available for the implementation of prevention strategies and remediation techniques. The ZAM project focuses on 4 axes (Figure II-20), three of which are built on the basis of geography, which are i: forest water of the upstream part of the Vosges, ii: rural water of the plain, and iii: urban and industrial water in the Moselle basin; and one which is concerned with the history of the area, i.e. iv: sedimentary archives, which includes temporal variations caused by different land use over the past years (ZAM, 2017).

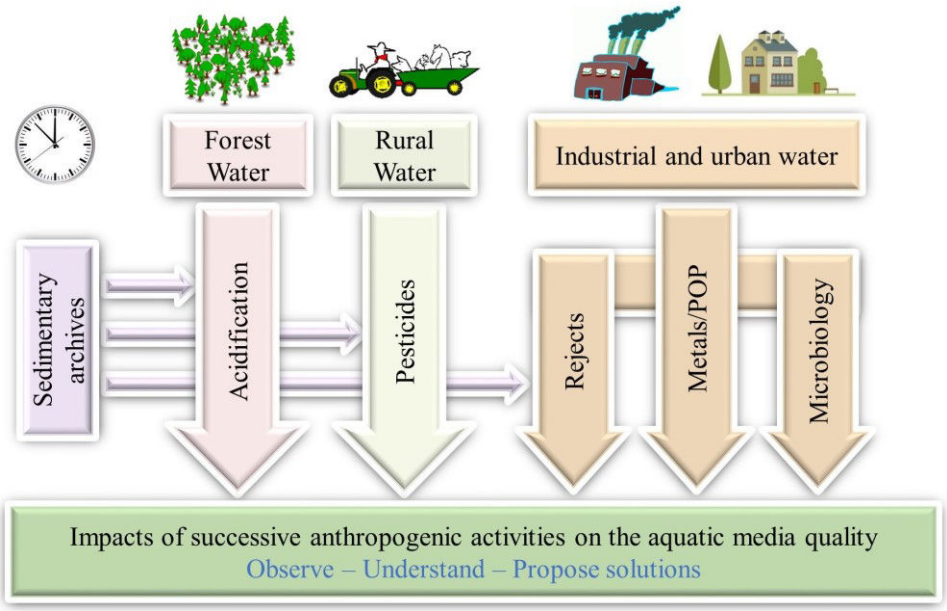

Figure II-20: Schema summarizing the activities and axes of the ZAM project.
POP: particulate organic phosphorus.
Translated from French and modified from ZAM (2017).

Another project which is partially concerned with the Orne River is MOBISED (Modelling of the reMOBilization of SEDiments and the release of associated contaminants), proposed by the Agence Nationale de la Recherche (ANR). The project is effectuated between Luxembourg Institute of Science and Technology (LIST) and Université de Lorraine. The MOBISED project aims to reveal the fate of contaminants after the remobilization of sediments

that have been highly impacted by mining and industrial activities, namely in the northeastern region of France (including the Orne River). Furthermore, controlled experiments are planned to be done after the multidisciplinary work reveals the properties of the river, such as a detailed description of the hydroclimatology, hydrodynamics and bed morphology; in addition, chemical, mineralogical, organic and microbial composition of river sediments and suspended matter will be characterized at global, micrometric, sub-micrometric and molecular levels (This Ph.D. work will be concerned with the chemical composition and the mineralogy of Orne surface and subsurface sediments). Afterwards, metallic, organic and bacterial species fate upon sediment remobilization will be studied in controlled experiments (LIST, 2017). The results will provide solid findings for environmental management (sediment and river). The findings will also give a notion about contaminant status in case a dam is removed, which is the case of the Beth dam located in Moyeuvre-Grande, which is planned to be removed in the coming years.

Several studies have been effectuated in the Orne River so far. An ecological study on biological richness, including insects, macro-invertebrates and micro-organisms, showing the impact of metal rich sediments on the ecological life was effectuated by Catteau (2015). Although not definitive, the macro-invertebrate and biological communities varied between different sites, especially sites upstream and downstream of dams. The spatial and temporal variations of PAHs were also studied by AbuHelou (2016). Another study evaluated the level of antibiotic resistance markers in microbial communities of Orne sediments (Mahou, 2015). However, this thesis focuses on the mineralogical and chemical part of Orne River sediments.

12. Objectives of the study

As a brief summary, industrial wastes and by-products were released into the Orne River during the last two centuries, when mining, pig iron and steelmaking activities were active. Since metal laden deposits (wastes and by-products) were introduced into the river as particulate matter, some of them have certainly settled along the river course. During flooding events, remobilization of settled materials occurs (as indicated by turbid river water in Figure II-19 b), some of which might be metal laden. In addition, the dam at Moyeuvre-Grande (Beth dam) is planned to be removed, which will definitely cause remobilization of the materials that had settled in the upstream part of the dam. In the Orne River, there has not been a study that had focused on the settled materials, their sources, mineralogy, chemical composition,

speciation and variation with depth and along the river course. For those reasons, this study was conducted.

The objectives of this thesis are to unravel the nature of surface sediments that had deposited at various points along the Orne River, to follow the mineralogical and chemical composition, to give details about the variation of sediments (grain size, chemical composition and thorough bulk to sub-micrometric mineralogical identification) attributed by lithogenic weathering, land use, land cover, urbanization and former industrial activities. The inventory of Orne sediments might then mark the sites where the fingerprints of the former steelmaking activities are located. Then, sediment cores collected in the upstream area of the Beth dam, located at Moyeuvre-Grande, are characterized. Indeed, the Beth dam is thought to have caused sediment accumulation in the upstream zone since it was reconstructed in 1959/1960. The aims are to characterize the sediments that had settled upstream of the Beth dam, to identify the minerals of lithogenic and anthropogenic sources, to follow the possible transformation of anthropogenic or industrial phases in the vertical sediment profile, and to identify the major Fe bearing species. Zinc speciation is then determined to reveal the possible fate of Zn in the submerged sediments of Beth after being deposited for decades, and to evidence the major Zn carriers using multiple X-ray and spectroscopic techniques.

References

AbuHelou, F., 2016. Spatial and temporal variations of the occurrence and distribution of polycyclic aromatic compounds in a river system affected by past industrial activities. Ph.D. thesis. Geosciences. Lorraine University.

AERM, 2000. Débits mensuels d'étiage et modules. vol. 3 : bassin de la moselle aval (sarre inclus). Agence de l'Eau Rhin-Meuse.

Aitchison, L., 1960. A History of Metals, Volume 1. MacDonald & Evans ; Interscience Publishers. Inc., London and New York.

Besta, P., Janovská, K., Samolejová, A., Beránková, A., Vozňáková, I., Hendrych, M., 2013. The cycle and effect of zinc in the blast-furnace process. Metalurgija 52, 197–200.

Biache, C., Faure, P., Mansuy-Huault, L., Cébron, A., Beguiristain, T., Leyval, C., 2013. Biodegradation of the organic matter in a coking plant soil and its main constituents. Org. Geochem. 56, 10–18. doi:10.1016/j.orggeochem.2012.12.002

Biache, C., Mansuy-Huault, L., Faure, P., Munier-Lamy, C., Leyval, C., 2008. Effects of thermal desorption on the composition of two coking plant soils: Impact on solvent extractable organic compounds and metal bioavailability. Environ. Pollut. 156, 671–677. doi:10.1016/j.envpol.2008.06.020

Bonnefoy, D., Bourg, A., 1984. Estimation du fond géochimique naturel dans les sols et évaluation du niveau de pollutions dues aux activités humaines : cas du bassin versant de l'Orne, affluent de la Moselle. Beuilly-sur-Seine.

Bradl, H.B., Kim, C., Kramar, U., Stüben, D., 2005. Interaction of Heavy Metals, in: Heavy Metals in the Environment: Origin, Interaction and Remediation. Academic Press, pp. 28–164.

Brownfield, M.E., 2002. Characterization and modes of occurrence of elements in feed coal and fly ash - an integrated approach, U.S. Geological Survey fact sheet-038-02.

Catteau, A., 2015. Evaluation de l'état écologique prérestauration d'un cours d'eau industriel. Master thesis. LIEC. Université de Lorraine.

Chernousov, P.I., Golubev, O. V., Petelin, A.L., 2011. Phosphorus, lead, and arsenic in blast-furnace smelting. Metallurgist 55, 242–250. doi:10.1007/s11015-011-9418-2

Das, B., Prakash, S., Reddy, P.S.R., Biswal, S.K., Mohapatra, B.K., Misra, V.N., 2002. Effective utilization of blast furnace flue dust of integrated steel plants. Eur. J. Miner. Process. Environ. Prot. 2, 61–68.

Das, B., Prakash, S., Reddy, P.S.R., Misra, V.N., 2007. An overview of utilization of slag and sludge from steel industries. Resour. Conserv. Recycl. 50, 40–57. doi:10.1016/j.resconrec.2006.05.008

Davison, B., Owens, G.W., 2012. Steel designers' manual, 7th ed. Wiley-Blackwell.

Deike, R., Hillmann, C., 1999. Metallurgie-Das Verhalten von Zink beim Recycling von eisenhaltigen Stauben und Schlammen-Eisenhaltige Staube und Schlamme konnen gut uber den Sinter-und Hochofenprozess wiederverwertet werden. Stahl und Eisen 119, 53–60.

EauFrance, 2016. Banque Hydro [WWW Document]. Le Serv. public d'information sur l'eau. Ministère l'Ecologie, du Développement Durable l'Energie. URL http://www.hydro.eaufrance.fr/ (accessed 5.28.16).

Ettler, V., Legendre, O., Bodénan, F., Touray, J.-C., 2001. Primary phases and natural weathering of old lead–zinc pyrometallurgical slag from Příbram, Czech Republic. Can. Mineral. 39, 873–888.

Faure, P., Mansuy-Huault, L., Su, X., 2007. Alkanes and hopanes for pollution source apportionment in coking plant soils. Environ. Chem. Lett. 5, 41–46. doi:10.1007/s10311-006-0066-x

Garcier, R.J., 2007. Rivers we can't bring ourselves to clean – historical insights into the pollution of the Moselle River (France), 1850–2000. Hydrol. Earth Syst. Sci. 11, 1731–1745. doi:10.5194/hess-11-1731-2007

Grgic, D., Homand, F., Dagallier, G., 2002. Altération du minerai de fer dans les mines abandonnées de Lorraine. Rev. française géotechnique 49–60.

Groen, J.C., Craig, J.R., 1994. The inorganic geochemistry of coal, petroleum, and their gasification/combustion products. Fuel Process. Technol. 40, 15–48. doi:10.1016/0378-3820(94)90033-7

Helble, J.J., Sarofim, A.F., 1993. Trace element behavior during coal combustion. Am. Chem. Soc. Div. Fuel Chem. Prepr. 38, 257–264.

Houben, D., Couder, E., Sonnet, P., 2013. Leachability of cadmium, lead, and zinc in a long-term spontaneously revegetated slag heap: implications for phytostabilization. J. Soils Sediments 13, 543–554.

Huang, J.-H., Huang, F., Evans, L., Glasauer, S., 2015. Vanadium: global (bio)geochemistry. Chem. Geol. 417, 68–89. doi:10.1016/j.chemgeo.2015.09.019

Huot, H., Simonnot, M.O., Watteau, F., Marion, P., Yvon, J., De Donato, P., Morel, J.-L., 2014. Early transformation and transfer processes in a Technosol developing on iron industry deposits. Eur. J. Soil Sci. 65, 470–484. doi:10.1111/ejss.12106

Isaure, M.-P., Laboudigue, A., Manceau, A., Sarret, G., Tiffreau, C., Trocellier, P., Lamble, G., Hazemann, J.-L.,

Chateigner, D., Arret, E.S., Iffreau, C.H.T., Su, L.P., Saclay, E. De, 2002. Quantitative Zn speciation in a contaminated dredged sediment by μ-PIXE, μ-SXRF, EXAFS spectroscopy and principal component analysis. Geochim. Cosmochim. Acta 66, 1549–1567. doi:10.1016/S0016-7037(01)00875-4

Jacquat, O., Voegelin, A., Villard, A., Marcus, M.A., Kretzschmar, R., 2008. Formation of Zn-rich phyllosilicate, Zn-layered double hydroxide and hydrozincite in contaminated calcareous soils. Geochim. Cosmochim. Acta 72, 5037–5054. doi:10.1016/j.gca.2008.07.024

James, H.L., 1966. Chemistry of the Iron-Rich Sedimentary Rocks, in: Fleisher, M. (Ed.), Data of Geochemistry. US Government Printing Office, Washington, pp. W1–W61.

Jeanneau, L., Faure, P., Montargès-Pelletier, E., Ramelli, M., 2006. Impact of a highly contaminated river on a more important hydrologic system: changes in organic markers. Sci. Total Environ. 372, 183–192. doi:10.1016/j.scitotenv.2006.09.021

Kiventerä, J., Leiviskä, T., Keski-Ruismäki, K., Tanskanen, J., 2016. Characteristics and settling behaviour of particles from blast furnace flue gas washing. J. Environ. Manage. 172, 162–170. doi:10.1016/j.jenvman.2016.02.037

Korpa, L., Mudron', Y., 2006. System for cleaning blast-furnace gas in the blast-furnace shop at the VSZh Koshitse combine. Metallurgist 50, 379–383. doi:10.1007/s11015-006-0092-8

Kretzschmar, R., Mansfeldt, T., Mandaliev, P.N., Barmettler, K., Marcus, M.A., Voegelin, A., 2012. Speciation of Zn in blast furnace sludge from former sedimentation ponds using synchrotron X-ray diffraction, fluorescence, and absorption spectroscopy. Environ. Sci. Technol. 46, 12381–12390. doi:10.1021/es302981v

Lauf, R.J., Harris, L.A., Rawlston, S.S., 1982. Pyrite framboids as the source of magnetite spheres in fly ash. Environ. Sci. Technol. 16, 218–220. doi:10.1021/es00098a009

Leimalm, U., Lundgren, M., Ökvist, L.S., Björkman, B., 2010. Off-gas dust in an experimental blast furnace. Part 1: characterization of flue dust, sludge and shaft fines. ISIJ Int. 50, 1560–1569. doi:10.2355/isijinternational.50.1560

LIST, 2017. MOBISED [WWW Document]. Model. remobilisation SEDiments release Assoc. Contam. URL https://www.list.lu/en/project/mobised/ (accessed 1.1.17).

López-Antón, M.A., Díaz-Somoano, M., Ochoa-González, R., Martínez-Tarazona, M.R., 2011. Distribution of trace elements from a coal burned in two different spanish power stations. Ind. Eng. Chem. Res. 50, 12208–12216. doi:10.1021/ie2018542

Luxton, T.P., Miller, B.W., Scheckel, K.G., 2013. Zinc Speciation Studies in Soil, Sediment and Environmental Samples, in: Bakirdere, S. (Ed.), Speciation Studies in Soil, Sediment and Environmental Samples. CRC Press, Taylor & Francis Groups, New York, pp. 433–477. doi:doi:10.1201/b15501-12

Mahou, A., 2015. Evaluation du niveau d'antibiorésistance dans les communautés microbiennes de l'eau et des sédiments de l'Orne. M1 thesis. Laboratoire de Chimie Physique et Microbiologie pour l'Environnement (LCPME). Université de Lorraine.

Maitte, B., Jorand, F.P.A., Grgic, D., Abdelmoula, M., Carteret, C., 2015. Remineralization of ferrous carbonate from bioreduction of natural goethite in the Lorraine iron ore (Minette) by *Shewanella putrefaciens*. Chem. Geol. 412, 48–58. doi:10.1016/j.chemgeo.2015.07.024

Manceau, A., Lanson, B., Schlegel, M.L., Hargé, J.C., Musso, M., Eybert-Bérard, L., Hazemann, J.-L., Chateigner, D., Lamble, G.M., 2000. Quantitative Zn speciation in smelter-contaminated soils by EXAFS spectroscopy. Am. J. Sci. 300, 289–343. doi:10.2475/ajs.300.4.289

Mansfeldt, T., Dohrmann, R., 2004. Chemical and mineralogical characterization of blast-furnace sludge from an abandoned landfill. Environ. Sci. Technol. 38, 5977–5984. doi:10.1021/es040002+

Martinois, R., 2014. Histoire d'Orne. France.

Maslehuddin, M., Sharif, A.M., Shameem, M., Ibrahim, M., Barry, M.., 2003. Comparison of properties of steel slag and crushed limestone aggregate concretes. Constr. Build. Mater. 17, 105–112. doi:10.1016/S0950-0618(02)00095-8

Meybeck, M., Chapman, D., Helmer, R., 1992. An Introduction to Water Quality, in: Chapman, D. (Ed.), Water Quality Assessments - A Guide to Use of Biota, Sediments and Water in Environmental Monitoring. UNESCO/WHO/UNEP, pp. 1–21.

Ministère de l'Environnement, 1985. Repartition et passage de polluants metalliques dans divers compartiments inertes et vivants d'un cours d'eau. Premiere partie: Estimation du degre de pollution metallique de l'eau, des matiere en suspension et des sediments de l'Orne, affluent de la Mose. Metz.

Moskalyk, R.R., Alfantazi, A.M., 2003. Processing of vanadium: a review. Miner. Eng. 16, 793–805. doi:10.1016/S0892-6875(03)00213-9

Nachtegaal, M., Marcus, M.A., Sonke, J.E., Vangronsveld, J., Livi, K.J.T., van Der Lelie, D., Sparks, D.L., 2005. Effects of in situ remediation on the speciation and bioavailability of zinc in a smelter contaminated soil. Geochim. Cosmochim. Acta 69, 4649–4664. doi:10.1016/j.gca.2005.05.019

Ndiba, P., Axe, L., Boonfueng, T., 2008. Heavy metal immobilization through phosphate and thermal treatment of dredged sediments. Environ. Sci. Technol. 42, 920–926. doi:10.1021/es072082y

Nriagu, J.O., 1990. Global metal pollution: poisoning the biosphere? Environ. Sci. Policy Sustain. Dev. 32, 7–33. doi:10.1080/00139157.1990.9929037

Palomo, A., Krivenko, P., Kavalerova, E., Maltseva, O., Garcia-Lodeiro, I., Kavalerova, E., Maltseva, O., Fernández-Jiménez, A., 2014. A review on alkaline activation: new analytical perspectives. Mater. Construcción 64, e022. doi:10.3989/mc.2014.00314

Peacey, J.G., Davenport, W.G., 1979. The Iron Blast Furnace: Theory and Practice, 1st ed. Pergamon Press, Oxford; New York.

Picon, M., 2014. Autour de l'Orne industrieuse : paysages industriels hérités. Université de Lorraine, Environmental Engineering. <dumas-01110255>.

Poincaré, É.L., 1886. Traité d'hygiène industrielle: à l'usage des médecins et des membres des conseils d'hygiène. Masson.

Sharonova, O.M., Anshits, N.N., Fedorchak, M.A., Zhizhaev, A.M., Anshits, A.G., 2015. Characterization of ferrospheres recovered from high-calcium fly ash. Energy & Fuels 29, 5404–5414. doi:10.1021/acs.energyfuels.5b01618

SIERM, 2017. Système d'information sur l'eau Rhin-Meuse. Données des eaux superficielles [WWW Document]. EauFrance, Minist. l'environnement, l'energie la mer. URL http://rhin-meuse.eaufrance.fr/ (accessed 1.1.17).

Sobanska, S., 1999. Etude de la spéciation du plomb et du zinc dans des poussières industrielles et dans un sol contaminé: Approche par méthodes spectroscopiques. University of Lille, France.

Sobanska, S., Deneele, D., Barbillat, J., Ledésert, B., 2016. Natural weathering of slags from primary Pb–Zn smelting as evidenced by Raman microspectroscopy. Appl. Geochemistry 64, 107–117. doi:10.1016/j.apgeochem.2015.09.011

Teyssen, T., 1984. Sedimentology of the Minette oolitic ironstones of Luxembourg and Lorraine: a Jurassic subtidal sandwave complex. Sedimontology 31, 195–211. doi:10.1111/j.1365-3091.1984.tb01959.x

Thorpe, A.N., Senftle, F.E., Alexander, C.C., Dulong, F.T., 1984. Oxidation of pyrite in coal to magnetite. Fuel 63, 662–668. doi:10.1016/0016-2361(84)90163-7

Trinkel, V., Mallow, O., Aschenbrenner, P., Rechberger, H., Fellner, J., 2016. Characterization of blast furnace sludge with respect to heavy metal distribution. Ind. Eng. Chem. Res. 55, 5590–5597. doi:10.1021/acs.iecr.6b00617

Trinkel, V., Mallow, O., Thaler, C., Schenk, J., Rechberger, H., Fellner, J., 2015. Behavior of chromium, nickel, lead, zinc, cadmium, and mercury in the blast furnace — A critical review of literature data and plant investigations. Ind. Eng. Chem. Res. 54, 11759–11771. doi:10.1021/acs.iecr.5b03442

Trung, Z.H., Kukurugya, F., Takacova, Z., Orac, D., Laubertova, M., Miskufova, A., Havlik, T., 2011. Acidic leaching both of zinc and iron from basic oxygen furnace sludge. J. Hazard. Mater. 192, 1100–1107. doi:10.1016/j.jhazmat.2011.06.016

Van Damme, A., Degryse, F., Smolders, E., Sarret, G., Dewit, J., Swennen, R., Manceau, A., 2010. Zinc speciation in mining and smelter contaminated overbank sediments by EXAFS spectroscopy. Geochim. Cosmochim. Acta 74, 3707–3720. doi:10.1016/j.gca.2010.03.032

Vanaecker, M., Courtin-Nomade, A., Bril, H., Laureyns, J., Lenain, J.-F., 2014. Behavior of Zn-bearing phases in base metal slag from France and Poland: A mineralogical approach for environmental purposes. J. Geochemical Explor. 136, 1–13. doi:10.1016/j.gexplo.2013.09.001

Van Herck, P., Vandecasteele, C., Swennen, R., Mortier, R., 2000. Zinc and lead removal from blast furnace sludge with a hydrometallurgical process. Environ. Sci. Technol. 34, 3802–3808. doi:10.1021/es991033l

van Hullebusch, E.D., Yin, N.-H., Seignez, N., Labanowski, J., Gauthier, A., Lens, P.N.L., Avril, C., Sivry, Y., 2015. Bio-alteration of metallurgical wastes by *Pseudomonas aeruginosa* in a semi flow-through reactor. J. Environ. Manage. 147, 297–305. doi:10.1016/j.jenvman.2014.09.018

Vassilev, S. V, Vassileva, C.G., 1996. Mineralogy of combustion wastes from coal-fired power stations. Fuel Process. Technol. 47, 261–280. doi:10.1016/0378-3820(96)01016-8

Voegelin, A., Pfister, S., Scheinost, A.C., Marcus, M.A., Kretzschmar, R., 2005. Changes in zinc speciation in field soil after contamination with zinc oxide. Environ. Sci. Technol. 39, 6616–6623. doi:10.1021/es047962g

Wei, Y.-L., Lin, C.-Y., Cheng, S.-H., Wang, H.P., 2014. Recycling steel-manufacturing slag and harbor sediment into construction materials. J. Hazard. Mater. 265, 253–260. doi:10.1016/j.jhazmat.2013.11.049

Worldsteel Association, 2016. Crude steel production [WWW Document]. URL https://www.worldsteel.org/media-centre/press-releases.html

Xu, M., Yan, R., Zheng, C., Qiao, Y., Han, J., Sheng, C., 2003. Status of trace element emission in a coal combustion process: a review. Fuel Process. Technol. 85, 215–237. doi:10.1016/S0378-3820(03)00174-7

Yellishetty, M., Ranjith, P.G., Tharumarajah, A., 2010. Iron ore and steel production trends and material flows in the world: is this really sustainable? Resour. Conserv. Recycl. 54, 1084–1094. doi:10.1016/j.resconrec.2010.03.003

Yildirim, I.Z., Prezzi, M., 2011. Chemical, mineralogical, and morphological properties of steel slag. Adv. Civ. Eng. 2011, 1–13. doi:10.1155/2011/463638

ZAM, 2017. Zone Atelier: Bassin de la Moselle [WWW Document]. La Zo. Atelier Moselle. URL http://apps.ensic.inpl-nancy.fr/Zam/index_fr.html

Zhao, Y., Zhang, J., Sun, J., Bai, X., Zheng, C., 2006. Mineralogy, chemical composition, and microstructure of ferrospheres in fly ashes from coal combustion. Energy & Fuels 20, 1490–1497. doi:10.1021/ef060008f

Zhou, Y., Ning, X., Liao, X., Lin, M., Liu, J., Wang, J., 2013. Characterization and environmental risk assessment of heavy metals found in fly ashes from waste filter bags obtained from a Chinese steel plant. Ecotoxicol. Environ. Saf. 95, 130–136. doi:10.1016/j.ecoenv.2013.05.026

III. CHAPTER 3: CHEMICAL AND MINERALOGICAL COMPOSITION OF SURFACE SEDIMENTS: VARIATION ACCOUNTED BY LITHOLOGY, LAND USE AND FORMER INDUSTRIAL ACTIVITIES

Abstract

River sediments were collected along the course of the Orne River, northeastern France. The Orne is a sub-basin of the Moselle watershed and was highly impacted by industrial activities during the last two centuries. The objectives of this study are to show the effect of grain size variation on the chemical and mineralogical composition on one hand, and to evidence chemical and mineralogical variations induced by dam, lithology, land cover, land use and former industrial activities on the other. Therefore, several surface sediment samples were collected along the river course. Part of the collected sediments were divided into 3 fractions of different sizes; the chemical composition was determined for each. For the other sediments, grain size properties, water content, pH, and chemical and mineralogical composition were determined. The mineralogical composition was shown at a bulk scale using XRD, and at finer scales using oriented slides, SEM and TEM. The lithogenic nature of the sediments could be followed by major elements (Si, Al and Ca), rare earth elements (REEs) and mineralogy. Bulk mineralogy of the sediments was rather similar from a qualitative point of view. Furthermore, distinct clay minerals, identified as interlayered illite/smectite clays, were identified by TEM. The influence of urbanization and former industries was noticed by elevated Zn, Pb, Fe and P contents in surface sediments. Iron was associated to clay minerals, and was also found as poorly defined and nanoparticles of oxy-hydroxides (possibly as clay coatings), sulfides (framboïdal pyrite), (poly)metallic sulfides and hairy aluminosilicates. The last two were only detected at the end of the densely urbanized area of the Orne River. Effect of urbanization/domestic activities, were also evidenced by elevated P and Zn contents, and the presence of some phases, such as calcium phosphate. Finally, the signature of urbanization, industrialization, as well as lithogenic fingerprints, could be followed along the Orne River course.

Keywords: *Orne River, Surface sediment, grain size, chemical composition, mineralogy, microscopy, interlayered clays.*

1. Introduction

River surface sediments mark the most recent settled materials, such as surface run-off, land erosion, bedrock weathering and remobilized river particles (e.g. Négrel et al., 2014). If sediments are submerged, they also act as storage zones for waterborne chemicals and compounds, which might come from natural as well as anthropogenic sources. Some of the chemicals/compounds are phosphates, nitrates, pesticides, metal(loid)s, minerals, organic phases, microbiological and bio-organo-mineral complexes (e.g. Fox et al., 2016 and references therein; Lovley and Chapelle, 1995; Tomohiko Isobe et al., 2001). Settling and remobilization of waterborne particles majorly depend on water discharge, sediment consolidation level, cohesion, grain morphology, sorting and size (Naden, 2010; Nichols, 2009a; Robert, 2014). Variation in chemical and mineralogical composition of sediments along a river course might be attributed to change in land use, bedrock geology, land cover and river hydrodynamics. In addition to posing socio-economic and environmental concerns, river hydrodynamics are certainly modified upon dam construction (Babbitt, 2002; Wang et al., 2005). One of the alterations caused by dam construction is modification of natural biogeochemical cycles (e.g. carbon, silicon, iron, nitrogen, organic matter and phosphorous) (e.g. Kondolf et al., 2014; Martin and Meybeck, 1979; Wildi, 2010). Alterations might be direct, such as selective settling induced by reduced water flow, or when particulate matter transport is hindered by dams. Otherwise, alterations might be indirect, such as when the redox conditions, salinity, temperature, water flow and pH change in reservoir zones due to higher residence time of river water (Friedl and Wüest, 2002). Under natural conditions, sediments are mainly composed of terrigenous clastic deposits that have formed by weathering and breakdown of lithogenic materials, such as silicates (including quartz, illite and kaolinite) and carbonates (such as calcite), which are mainly eroded from bedrock. Carbonates might also be originated from invertebrate shells and diatoms (Nichols, 2009a). For example, the mineralogical composition of sediments was used to determine the source of weathered materials of Jurassic and Cretaceous formations (Dokuz and Tanyolu, 2006). Additionally, anthropogenic activities can be marked by chemical and mineralogical composition of sediments (Dhivert et al., 2016, 2015b; Van Damme et al., 2010), either by introducing minerals that are markers of anthropogenic activities, or by metal-enriched enrichment, such as Zn sourced from Zn smelters or Fe sourced from steelmaking or iron metallurgy (e.g. Lesven et al., 2010). Suspended particulate matter (SPM), as well as sediments, might reveal the nature of introduced materials. Waterborne particles, however, might be introduced from land or

remobilized from the sediments. In our case, the submerged river sediments lie in an area of different lithology/land cover, and in a region that was formerly occupied with steelmaking facilities. Nonetheless, the steelmaking facilities stopped in 1988, and the industrialized zones were dismantled and cleaned; yet, the downstream part of the area remains marked by urban agglomerations (Corine Land Cover 2012). The objectives of this study are to i) characterize the surface sediments along the course of the Orne River in terms of chemical and mineralogical composition, ii) reveal the variation directly accounted by grain size and indirectly by change in river hydrodynamics caused by dams, and iii) show the possibility of marking geological formation, land use, land cover and former anthropogenic activities.

2. Materials and Methods

2.1. Study area and sampling sites

The Orne watershed is a sub-basin of the Moselle watershed and is located northeastern France. The Orne River flows 90 km in the 1,226 km^2 watershed before its confluence with the Moselle River, which in turn is a tributary of the Rhine River. The Orne watershed can be divided into two main regions, a clayey depression in the Woëvre region (marked white in Figure III-1 a), and a calcareous plateau at the Pays-Haut region (marked grey in Figure III-1 a). The detrital input in Orne sediments can mainly be distinguished between those two regions. In the Woëvre region, the watercourse starts from the upper Jurassic epoch, which is made from easily eroded soft marl; thus, the contribution of clay and carbonate minerals (such as calcite, dolomite and aragonite) to sediments might be expected. The downstream part consists of a limestone plateau belonging to the Bajocian age (middle Jurassic), which might explain the contributions of illite, kaolinite, swelling and non-swelling interlayered clays and calcium carbonate minerals (Guillet et al., 1984; Jacquat et al., 2011). The Woëvre region is mainly agricultural, includes forests and to a lesser extent some rural/urban agglomerations. As for the Pays-Haut region, which starts near Jarny (beginning of grey zone in Figure III-1 a), it is calcareous in nature. However, it also includes the iron ore rich Aalenian formation (see section *1* of Chapter *II*). Carbonate and iron rich minerals might thus be found as a result of erosion and weathering (Bonnefoy and Bourg, 1984; Teyssen, 1984). The Pays-Haut region, although containing agricultural and forest areas, shows urbanized clusters and some industrially active areas (Figure III-1 b), especially in the east zone of the watershed, and more precisely near the banks of the Orne River (Corine Land Cover, 2012).

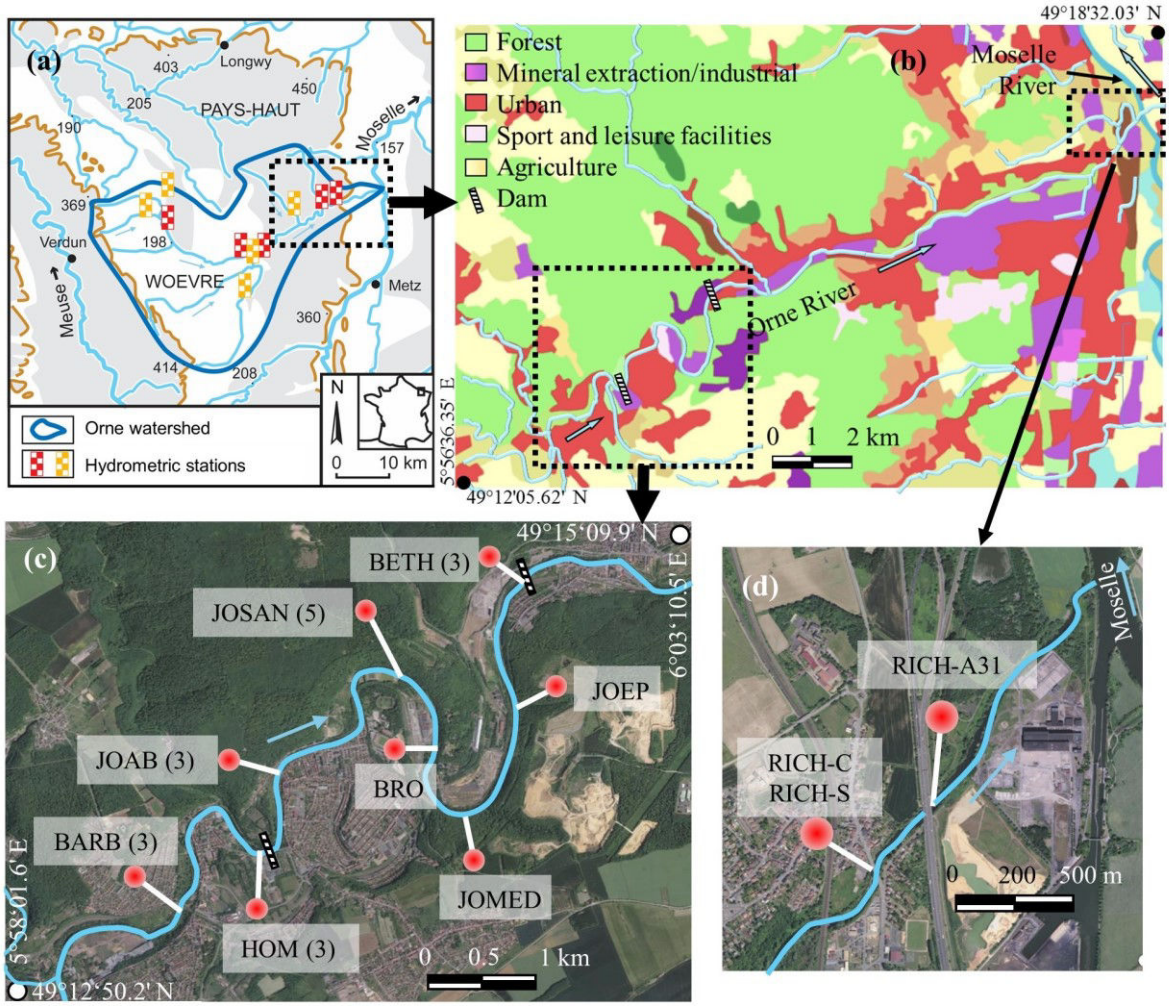

Figure III-1: The Orne watershed and the locations of the collected sediments.
a: The Orne watershed located northeastern France and the Orne River flowing towards the northeast. Map was created by Benoit Losson on the basis of the data provided by the French National Institute of Geography IGN, www.geoportail.gouv.fr. Red marked hydrometric stations collect data from the Orne River, while yellow ones collect data from Orne River tributaries. b: Section of the Orne basin with land cover and land use (Corine Land Cover, 2012). c and d: Satellite images of parts of the Orne River showing the locations of the collected sediments. The numbers in brackets represent the number of samples taken at the site. Whenever there is no number, only one sample was taken. Images modified from the map provided by www.geoportail.gouv.fr.

The Orne watershed was intensively impacted by steelmaking activities during the last two centuries. Industrial activities started to decrease in the mid-1970s, and then stopped in 1988 (Pederson, 2004). The area between BARB and BETH, was very active in iron metallurgy and steelmaking during the XIXth and XXth century (see Figure III-1 c for locations of BARB and BETH). Two dams are located in that area, namely Beth (at Moyeuvre-Grande; the sample is named BETH) and Homécourt (HOM); which were used to create artificial water reservoirs for cooling blast furnaces of the steelmaking facilities (Garcier, 2007). Waste products from the steelmaking facilities could be evidenced in sedimentary archives.

In this study, 11 sampling sites were chosen along the course of the Orne River, which are BARB, HOM, JOAB, JOSAN, BRO, JOMED, JOEP, BETH, RICH-S, RICH-C and RICH-

A31 (Figure III-1 c and d). For better representation of the sediments, more than one sample was collected from most sites (indicated in brackets in Figure III-1 c and compiled in Table III-1). The first sampling site is at Homécourt (labelled BARB in Figure III-1 c) and the most downstream station is Richemont (labelled RICH-A31). BARB marks the end of the agricultural zone and the start of the urban zone, and RICH-A31 marks the end of approximately 21 km densely urbanized area (starting from BARB) and lies about 1.3 km before the confluence with the Moselle River. More details about the sampling sites are found in Table III-1.

2.2. Sediment preparation for analyses

Sediments were collected during 2013, 2014 and 2015 campaigns. The samples from the 2013 campaigns were collected from BARB, JOAB, RICH-S, RICH-C and RICH-A31 (Figure III-1: c – d). Those sediments were collected by scooping the surface layers and were wet-sieved using the adjacent river water. The cut-off sizes were 2 mm, 250 µm and 50 µm. The different fractions were then frozen, freeze-dried and ground using an agate mortar and pestle. Consequently, the grain size influence on the chemical composition was determined. Those sediments will be termed "fractionated" in the coming sections. The second set of sediment samples was collected from BARB, HOM, JOAB, JOSAN, BRO, JOMED, JOEP and BETH, and were analyzed as "bulk" samples. The bulk sediment samples were mainly collected via coring, using a piston corer or Beeker corer. Some cores were collected on a floating platform (Quadriraft, from Marc Desmet, GEHCO laboratories, Tours University), such as BETH and HOM, due to a relatively high water column above the sediments. Other cores were collected near the river bank, while on land or a few steps within the river (case of BARB, JOAB, JOSAN, BRO, JOMED and JOEP). The surface layers were then taken, mainly 0 – 2 cm. More details were presented elsewhere (chapter *II*, section *10*). A small aliquot of the sediments was frozen at -80°C for microscopic and spectroscopic analyses. Additionally, a part of each sample was put in pre-weighed containers, frozen, freeze-dried and an aliquot was ground using an agate mortar and pestle for chemical and mineralogical analyses.

Table III-1: An inventory of the surface sediment samples collected along the course of the Orne River.
The samples are placed in the table according to their locations in the course of the Orne River (downstream gradient).

Site (number of samples)	Sample name	Longitude (E)	Latitude (N)	Elevation (m)	Thickness (cm)	Notes
Homécourt Barbusse (3)	BARB	5°59'25.0"	49°13'13.5"	177	2 and 5*	Site surrounded by urban areas (left and right side of the river) and located upstream the urban area at Homécourt. The site is located in the influence zone of the Homécourt dam. Samples were collected a few tens of meters before the bridge at Henry Barbusse street. RS.
Homécourt dam (3)	HOM	6°00'01.7"	49°13'30.3"	176	2 and 5*	Samples located upstream (< 200 m) of the Homécourt dam. Forest area on the left side and industrial/mining area on the right side. That site was highly active with steelmaking industries, mainly between the 1870s and the 1950s. LS.
Jœuf Abattoir (3)	JOAB	6°00'08.5"	49°13'52.1"	174	1.5 and 12.5*	Site contains forest areas on the left side of the river; site is located at the entrance of Jœuf city. Samples were collected a few tens of meters upstream the bridge in 2015, and downstream the bridge in 2013 (near Abattoir street). LS.
Jœuf Sainte Anne (5)	JOSAN	6°00'59.9"	49°14'22.6"	174	0.5	Left side of the river includes forests; right side includes former sport/leisure facilities. RS.
Jœuf Brochetiere (1)	BRO	6°01'20.3"	49°14'00.3"	174	2.5	Left side of the river contains forests, while the right side includes industries. The site is located in the influence zone of the Beth dam. RS.
Jœuf Mediatheque (1)	JOMED	6°01'32.8"	49°13'42.0"	173	1	Right side of the river contains forests, while the left side includes industries. The site adjoins the former Europipe site. LS.
Jœuf Europipe (1)	JOEP	6°01'52.9"	49°14'01.5"	173	2	The site is located downstream the former Europipe site (and others). RS.
Moyeuvre-Grande (3)	BETH	6°01'55.7"	49°14'47.5"	171	2	Sediments were collected < 200 m upstream of the Beth dam. The area is industrial, with railroads to the right side of the river. RS.
Richemont near the sewer (1)	RICH-S	6°10'12.0"	49°16’40.6"	155	na	Sampling site is located near RICH-C, but closer to the left bank and close to a sewer outlet. LS.
Richemont near the city (1)	RICH-C	6°10'11.7"	49°16'38.7"	155	na	Site located at the end of highly urbanized and industrial areas. Sampling site is under the bridge (nationale street), which lies a couple of hundred meters downstream a wastewater treatment plant. LS.
Richemont near route A31 (1)	RICH-A31	6°10'22.3"	49°16'47.1"	154	na	Sampling site is located under the bridge of A31 highway, which is located downstream a combined sewer outflow. LS.

na: not measured. For those samples, the sediment samples were scooped, so the thicknesses could not be measured.
*: Visual aspect of the surface layer, 5 or 12.5 cm, was rather similar throughout that depth, therefore the sediment is relatively thicker than other sediments.
RS: Sediment sample(s) collected from the right side of the river.
LS: Sediment sample(s) collected from the left side of the river.
Note: Multiple sediments belonging to the same site do not have the same exact coordinates, but are close to each other. Even though the samples at each site might not be identical, they will be treated together in an attempt to have a representative view from each site. Exact coordinated for all samples are included in chapter *II*, Table II-2.

2.3. Particle size distribution, water content and pH

For the fractionated samples, the percentage of each grain size fraction was calculated by dividing the mass of each fraction by the total sediment mass (freeze-dried samples were used for the calculations). The fractions superior to 2 mm (gravels), which consist of granules (2 – 4 mm) and pebbles (4 – 64 mm), will not be of interest since those particles are not reactive metal carriers. As for the bulk sediment samples, the water contents were calculated according to the percentage of mass loss after freeze-drying. Furthermore, dried and non-ground samples of the freeze-dried fractions were used for particle size distribution (PSD), provided by laser diffraction measurements (Sympatec GmbH, LIEC). Sediment clumps were gently disaggregated using a plastic spatula to avoid change in particle grain size. A homogeneous fraction was then inserted into the Succel dispersing unit (containing distilled water), where it was ultra-sonicated for 1 minute during circulation. This was followed by duplicate measurements, each of 1 minute. Whenever the measurements were not reproducible, more measurements were performed. The results were then provided by Helos software. The main data produced where the percentiles (D_i, {i = 10, 16, 50, 84, 90 and 99}). The following parameters were used to describe the grain sizes of the bulk sediments: the median or D_{50} (in μm), sorting or spreading (σ) of the sizes around the average, skewness (Sk) to determine the symmetry (or lack of symmetry) of the population, and kurtosis (K) to determine the sharpness of the grain population with respect to the average. The bases of calculations are found elsewhere (Blott and Pye, 2001). Also, the pH and redox potential of the sediments were measured *in-situ* using an HI 99121 pH meter (from Hanna) equipped with an HI 1292 pH electrode, and an HI 9126 pH/ORP meter (from Hanna) equipped with a platinum-Ag/AgCl redox potential electrode (from QIS).

2.4. Chemical composition of the sediments

The fractionated sediment samples (BARB, JOAB, RICH-S, RICH-C and RICH-A31) and bulk samples (BARB, HOM, JOAB, JOSAN, BRO, JOMED, JOEP and BETH) were analyzed for chemical composition (at the SARM; Service d'Analyse des Roches et des Minéraux – CRPG, Vandœuvre-lès-Nancy). The freeze-dried and ground sediments were used. Major elements were quantified by inductively coupled plasma optical emission spectrometry (ICP-OES, iCap 6500 ThermoFisher); trace elements were quantified by inductively coupled plasma mass spectrometry (ICP-MS, X7 ThermoFisher); and total carbon (TC) and loss on ignition (LoI) were calculated by the procedures developed at the SARM (Carignan et al., 2001).

For each sample, a powdered aliquot (300 mg) is fused with ultrapure $LiBO_2$ (900 mg) in a Pt crucible at 980°C. The fusion glass is then cooled at room temperature and dissolved in 1 M HNO_3-H_2O_2 (~ 0.5% v/v)-glycerol (~ 10% v/v) mixture. H_2O_2 helps to stabilize elements (e.g. Ti) and glycerol is used to "wet" the sample before the introduction in the ICP-MS machine. Consequently, the solution was quantified for major elements (Al, Ca, Fe, K, Mg, Mn, P, S, Si and Ti), trace elements (As, Ba, Be, Bi, Cd, Co, Cr, Cs, Cu, Ga, Ge, Hf, In, Mo, Nb, Ni, Pb, Rb, Sb, Sn, Sr, Ta, Th, U, V, W, Zn and Zr), and rare earth elements (REEs) including light lanthanides (Ce, La, Eu, Nd, Sm and Pr), heavy lanthanides (Dy, Er, Gd, Ho, Lu, Tb, Tm and Yb) and Sc and Y. All analytical methods were subject to quality assurance and quality control (QC/QA) procedures using certified reference materials. Indeed, for each set of 25 to 30 samples, a blank ($LiBO_2$) and 5 international reference materials of different compositions were also passed after being subjected to the same protocol (Carignan et al., 2001). The limits of detection and uncertainty for measurements on solid and liquid samples are included in the supplementary materials SM III-1 and SM III-2, respectively. Total carbon was measured with a carbon-sulfur analyzer (Leco SC144 DRPC) after measurement of the emitted carbon dioxide caused by HCl attack, and loss on ignition (LoI) was calculated by the mass loss after ignition at 1000°C.

2.5. Mineralogy of sediments

2.5.1. Major and crystalline minerals of bulk sediments and clay-sized particles

The mineralogy of sediments was determined using X-ray diffraction (XRD). A D8 Advance Bruker diffractometer with a Co $K_{\alpha 1}$ radiation source operated at 35 kV and 45 mA (λ = 1.7902 Å) was used. The diffraction patterns were collected on the angular range (2θ) of 3 – 64°, with a 0.034° angle step and a 3 sec collecting time. Furthermore, the clay-sized sediments particles were separated and clay minerals were identified through oriented preparations. For that purpose, 2 to 5 g of dry sediment from each sample (according to availability) was stirred in 120 – 150 ml ultrapure water. HCl solution (1 M) was used to remove carbonates. This was monitored by pH variation after adding drops of HCl; the increase in pH after HCl addition indicates buffering capacity, i.e. presence of carbonates. The sample was then left on the stirrer for 2 to 3 hours to disaggregate. The solution was then centrifuged at 20,000 g for 15 min to remove the solution (Sorvall Evolution RC lab centrifuge). Ultrapure water was then added to the sediments and centrifuged again to remove remaining HCl traces. This step was repeated 3-times so that excess chloride was removed (the chloride concentration

was monitored by electric conductivity). The sediment fraction was then mixed with 200 ml ultrapure water, ultra-sonicated for 1 to 2 minutes and stirred for approximately 30 min to 1 hour. The suspension was then left 32 minutes to settle before the top 3 cm suspension was sampled (according to Stokes' law). This sample contains the clay-sized particles. The suspension was then centrifuged at 34,000 g for 15 minutes; the supernatant was discarded, and the remaining particles were spread on glass slides; well oriented clay particles form on the glass slides since the basal planes tend to be parallel to the glass slide. All glass slides were left to dry under ambient temperature. For each sample, one glass slide was left as it was (i.e. just dried at room temperature and named air dried "AD"), another was saturated with ethylene glycol vapor (named EG), and the last was heated at 550°C for 4 hours. Consequently, the three glass slides, containing the clay fractions were analyzed by XRD using a 2θ range between 3 and 40°, a 0.034° angle step and 3 sec collection time per angular position.

2.5.2. Sub-micrometric mineral analyses of Orne sediments

Crystalline, poorly crystalline and amorphous phases at a sub-micrometer scale were identified by scanning and transmission electron microscopies. Micrometric particles were identified and characterized using the scanning electron microscope (SEM) Hitachi S-4800 equipped with a Kevex 4850-S energy dispersive X-ray spectrometer (EDXS) (GeoRessources laboratory, Vandœuvre-lès-Nancy). HOM and BETH samples were analyzed by SEM. Freeze-dried sediment grains were adhered onto metallic holders with carbon tape and were carbon coated. For obtaining finer particles for SEM investigations, sediment-ultrapure water suspensions were filtered; the filter was then dried and carbon coated onto metallic holders. The accelerating voltage was set to 15 kV. For EDXS, the acquisition time was set to 60 seconds.

Transmission electron microscopy (TEM) was used to investigate amorphous and poorly crystalline phases at a sub-micrometric scale. A CM200 Philips TEM with 200 kV accelerating voltage coupled with an EDXS in Jean Lamour Institute was used (Department of Microscopy, Université de Lorraine, Nancy, France). For the fractionated sediments, only the finest fractions (< 50 µm) were used for TEM analyses. BARB, HOM, BETH, JOAB, RICH-C and RICH-A31 were analyzed by TEM. One or two milligrams of each sample that were frozen at -80°C were suspended in ethanol and exposed to ultrasound for 10 minutes to disperse the aggregates. A drop of the suspension was then put on a carbon coated copper grid and left to evaporate.

EDX spectra were recorded on selected areas using the nano-probe device, and the acquisition time was set for 50 or 70 seconds, depending on the particles' thicknesses.

3. Results

3.1. Chemical composition as a function of grain size

The fractionated sediment samples (namely BARB, JOAB, RICH-S, RICH-C and RICH-A31), showed great grain size variability, especially between the first three on one hand, and the latter two on the other (Figure III-2; pie charts). BARB, JOAB and RICH-S samples contained an average of 43% (± 6) of grains inferior to 50 µm, while the other samples, namely

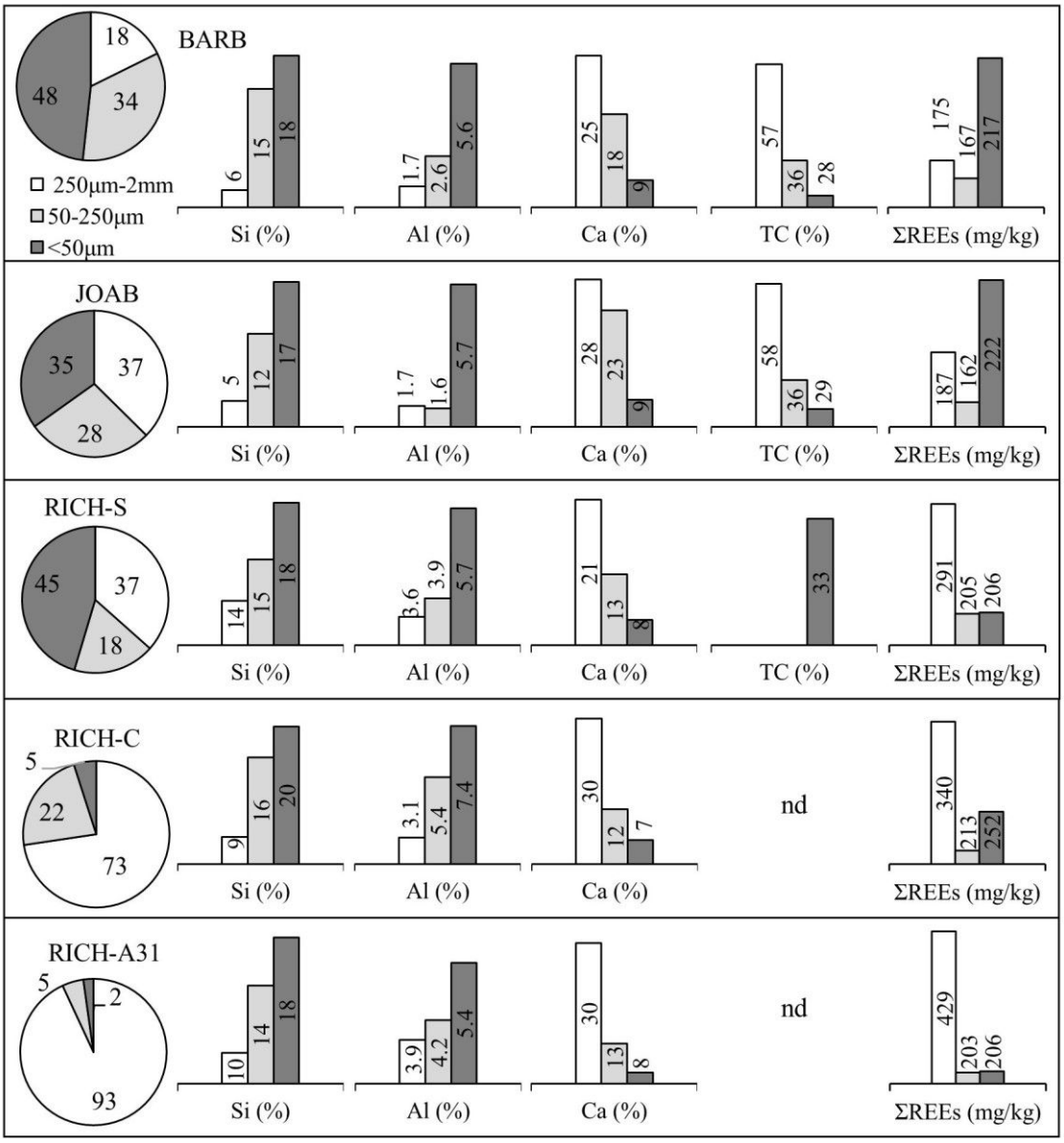

Figure III-2: Grain sizes, and contents of major elements (Si, Al and Ca in %), TC (in %) and ΣREEs (in mg/kg) of the fractionated sediments.
Percentages of grain size fractions were calculated after wet sieving and are presented as pie charts.
nd: data not available.

RICH-C and RICH-A31, were mainly composed of medium to coarse sands (250 µm – 2 mm). The very fine and fine sand fraction (50 – 250 µm), and silt-clay fraction (< 50 µm) were only slightly present in RICH-A31. The chemical composition was different for the fractionated samples. For all the samples, the finest fraction (i.e. < 50 µm) was mostly enriched with Al and Si, followed by the 50 – 250 µm and then the 250 µm – 2 mm fractions (Figure III-2). The same applies for Na, Ti and K, with an exception for Na in RICH-S (SM III-3). The REEs (Lu, Tm, Tb, Ho, Eu, Yb, Er, Dy, Gd, Sm, Sc, Pr, Y, La, Nd and Ce) are a coherent group of elements in terms of charge, ionic radius and site coordination, and are generally introduced together into the environment (McLennan and Taylor, 2012). In addition, the REEs followed a similar trend in the different fractions, and were significantly correlated at a 99% confidence level (SM III-4), therefore, the sum of REEs (ΣREEs) will be subsequently used (Figure III-2). Ca, total carbon (TC) and ΣREEs, in addition to the aforementioned elements (Si, Al, Na, Ti and K), are supposed to be inherited from pedogenic or lithogenic sources; i.e. they fingerprint the contribution of detrital materials that run-off from the watershed. It should be noted that those elements can also come from anthropogenic sources (e.g. Si and Al can be sourced from slag; REEs can be sourced from electronic appliances). According to the land use, land cover and the geology of the Orne watershed, the elements Si, Al, Ti, REEs, K and Na in Orne surface sediments are mostly anticipated to come from lithogenic contributions. The coarsest grains (250 µm – 2 mm) were enriched with Ca and TC for all the samples, suggesting a strong contribution of carbonates in the coarser fraction; this is indicated by 2.0- to 4.5-fold higher contents in the 250 µm – 2 mm fraction with respect to the < 50 µm fraction. Some TC contents were not determined, but it is thought that TC contents in the different fractions are similar to Ca, since they have similar pathways in the environment (Whiting and Stamm, 1995). The variation of ΣREEs in different fractions could be differentiated between BARB and JOAB on one hand (highest in the < 50 µm fraction), and the samples collected at Richemont on the other (highest in the 250 µm – 2 mm fractions, similar to Ca). Although the objective of the fractionated samples was to see the variation of chemical composition in different fractions, it is worth noting that the contents of Si and Al were rather similar in the same fraction for the different samples, as indicated by relatively low standard deviations. The average Si contents are 8.5 ± 3.3, 14.5 ± 1.6 and 17.9 ± 0.8% for the fractions 250 µm – 2 mm, 50 – 250 µm and < 50 µm, respectively; and the average Al contents are 2.8 ± 1.9, 3.6 ± 1.3 and 5.9 ± 0.7% for the fractions 250 µm – 2 mm, 50 – 250 µm and < 50 µm, respectively.

Similar to ΣREEs, the elements Fe, As and Zn showed a different correlation with grain sizes between BARB and JOAB on one hand, and RICH-S, RICH-C and RICH-A31 on the other. In this case, the finest fraction was mostly enriched with those elements for BARB and JOAB, while the 50 – 250 µm fraction was, in general, mostly enriched for the other 3. Other trace elements also showed a general increase in the finer fractions, such as Pb and Cr (Figure III-3), and Mo, Cs, Hf, Rb, Ga, Nb, Cu and Ni (SM III-5). Indeed, the variation could be distinguished by a several fold difference (for example, up to 4-fold for Fe and Pb). Finally, the variation in grain size and chemical composition might be explained by detrital and anthropogenic contributions from the watershed on one hand, and by river hydrodynamics that influence sediment remobilization and SPM settling on the other. The total chemical contents

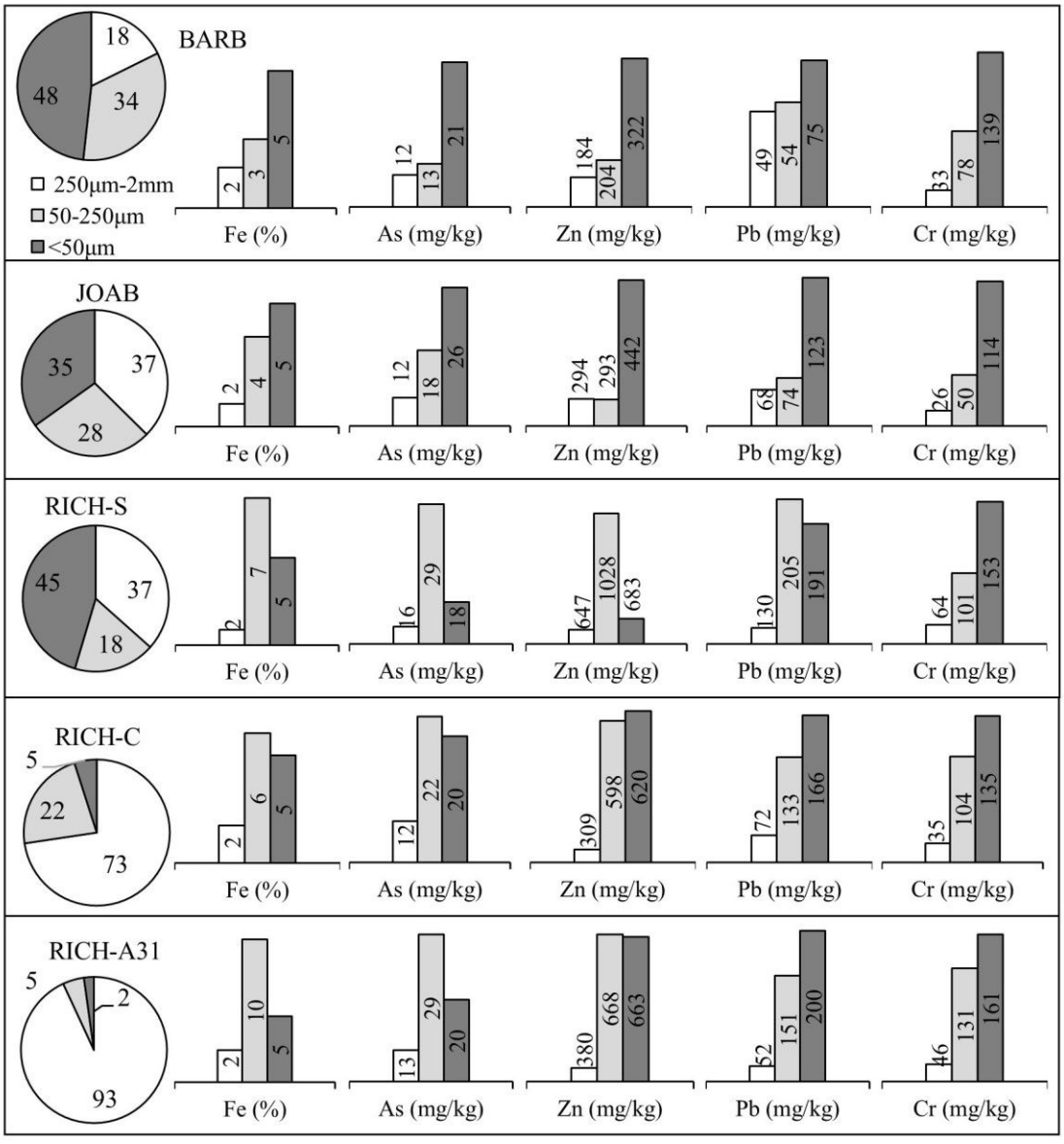

Figure III-3: Grain sizes and contents of Fe (in %), and As, Zn, Pb and Cr (in mg/kg) of the fractionated sediments.
The pie charts are the same as presented in the previous figure.

for the samples that were collected along the course of the Orne will be discussed in the coming sections.

3.2. Grain size variation, water content and pH of Orne sediments

The 50th percentile (D_{50}) and other grain parameters of the sediments, namely sorting (σ), skewness (Sk) and kurtosis (K), as well as the grain size distributions are shown in Figure III-4 (a – e). BARB is located 1.8 km upstream of the Homécourt dam and JOEP is located 1.1 km upstream of the Beth dam (Figure III-1 c); both samples are made of relatively fine deposits (Figure III-4 a, average D_{50} = 27 ± 1 µm). HOM and BETH samples showed comparable D_{50} values (average 32 ± 1 µm) and are both located within 200 m upstream dams. Those samples, namely BARB, HOM, JOEP and BETH, lie in the influence zones of dams, where the water current is reduced and forms a nearly uniform flow. It should be noted that the influence zone of the dam at Homécourt extends approximately 100 m before BARB, and that of the Beth dam (at Moyeuvre-Grande) extends approximately 300 m before JOSAN (Luc Manceau and Benoit Losson, personal communication, from water velocity measurements). The influence zone of dams can reach a few kilometers in the upstream sense (e.g. GEC, 2006; Snyder et al., 2004). That zone depends on water flow velocity, river course morphology, coherence/consistency of aggregates and shearing stress (Fryirs and Brierley, 2012; Nichols, 2009b; Robert, 2014). When compared to JOAB, JOSAN, BRO and JOMED, the other sediments were finer (Figure III-4 a). In addition, the change in grain size properties (σ, Sk and K) was noticed as the samples tend to become closer to the dams (i.e. from BARB to HOM and from JOEP to BETH). Indeed, the very poorly sorted, symmetric, mesokurtic, and almost bimodal distributions of BARB and JOEP became better sorted, finely skewed, leptokurtic and more centered/unimodal (in terms of distribution) for HOM and BETH (Figure III-4: b – e); at this stage, this might be explained by the change in river hydrodynamics induced by the dams. As for the other sediments, i.e. JOAB till JOMED, the median grain size increased in a significant manner and the sorting became more homogeneous.

The water contents of the sediments are shown in Figure III-4 f. The highest water contents were seen for sediments located upstream the dams (i.e. HOM and BETH; average 71 ± 1%), while lowest water contents were seen for JOAB and JOEP (average 53 ± 1%). In addition, and similarly to the change in sediment grain size parameters from BARB to HOM and from JOEP to BETH (Figure III-4: a – e), water content also followed a trend, which

increased towards the dam. Variation in water content might be caused by consolidation, grain size variation, grain sorting, and organic and carbon contents.

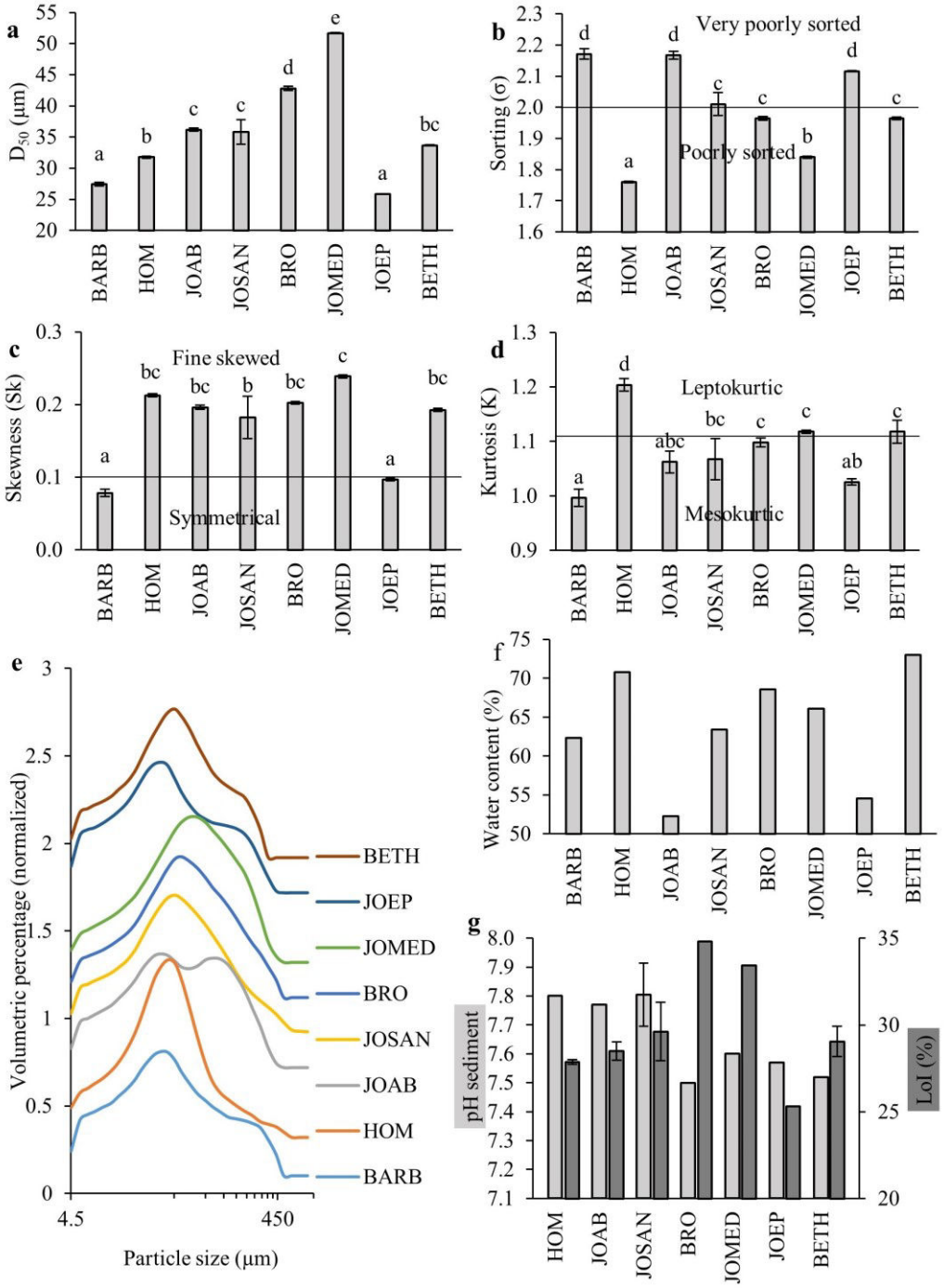

Figure III-4: Grain size parameters, water content, pH and LoI for bulk surface sediments (from BARB till BETH).
a: D_{50} (µm), b: sorting (σ), c: skewness (Sk), d: kurtosis (K), and e: volumetric grain size (grain size distribution) of surface sediments. Plotted histograms are the means (of the duplicate measurements) and standard deviations. Bars within a graph that do not share a letter indicate significant differences according to Duncan's multiple range test ($\alpha = 0.05$). f: water content (%) and g: pH and LoI (%) values for the sediments.

A slight pH variation was recorded between HOM, JOAB and JOSAN on one hand (average 7.80 ± 0.09), and BRO, JOMED, JOEP and BETH (average 7.55 ± 0.04) on the other (Figure III-4 g). Those slight pH variations might be explained by variation in organic and carbonate composition of the sediments. Moreover, metals might be selectively released from sediments with lower pH, noticeably during sediment resuspension (Eggleton and Thomas, 2004; Li et al., 2013). pH variation in sediments might be related to organic matter content. Indeed, BRO and JOMED showed the highest LoI values (34.8 and 33.4%, respectively), as well as TC (as it will be seen in Figure III-5 a), and had relatively low pH values (Figure III-4 g). The redox potential of surface sediments was measured for BARB (124 mV), HOM (8.1 mV), JOSAN (-44 mV), BRO (-102 mV), JOMED (-104 mV), JOEP (86 mV) and BETH (-79 mV). Those values represent moderately reduced conditions (Fiedler et al., 2007 and references cited therein), as it would be expected for submerged river sediments.

3.3. Chemical composition of sediments

Elements whose major sources are expected to be anthropogenic were normalized by Al. Al was used for normalization since it is considered as a conservative element, is derived from lithogenic contributions, and consequently has negligible anthropogenic input (in the case of Orne surface sediments). Other reasons for using Al is to overcome the variation in grain size, since aluminosilicates are considered as important metal carriers and reflect granular variability (Loring and Rantala, 1992). The contents of the major elements K, Al, Si and Ca, REEs, TC, and Al normalized Zn, Pb, Fe and P are shown in Figure III-5 a. Similar to the case of the fractionated sediments, ΣREEs will be used (significant correlations between REEs is shown in SM III-6). The major elements K, Al and Si, and ΣREEs (also Na, data not shown) showed similar trends along the course of the river and were significantly correlated in most cases ($P < 0.01$, SM III-7); HOM and RICH were the most enriched, while JOMED was the most depleted, with a 1.5, 1.7 and 1.3-fold variation for K, Al and ΣREEs, respectively, between the maximum and minimum values. Si contents showed clear trends along the river course, with a minimum at JOMED. Those elements (i.e. K, Al, Si and ΣREEs) reveal detrital contributions. It should be noted that the geological formation changes from argillaceous in the Woëvre region to calcareous in the Pays-Haut region (see Figure III-1 a for locations of the regions), which might cause a variation of detrital contributions to surface sediments. Indeed, Ca and TC contents (also Mn and Mg, data not shown) followed a different trend than the previously mentioned group of elements (Figure III-5 a). The left side of the river is made from forest

areas, and leaching of soil particles is expected. Consequently, Ca and carbonate rich particle introduction to the river sediments, especially via surface leaching of fine grains, is anticipated.

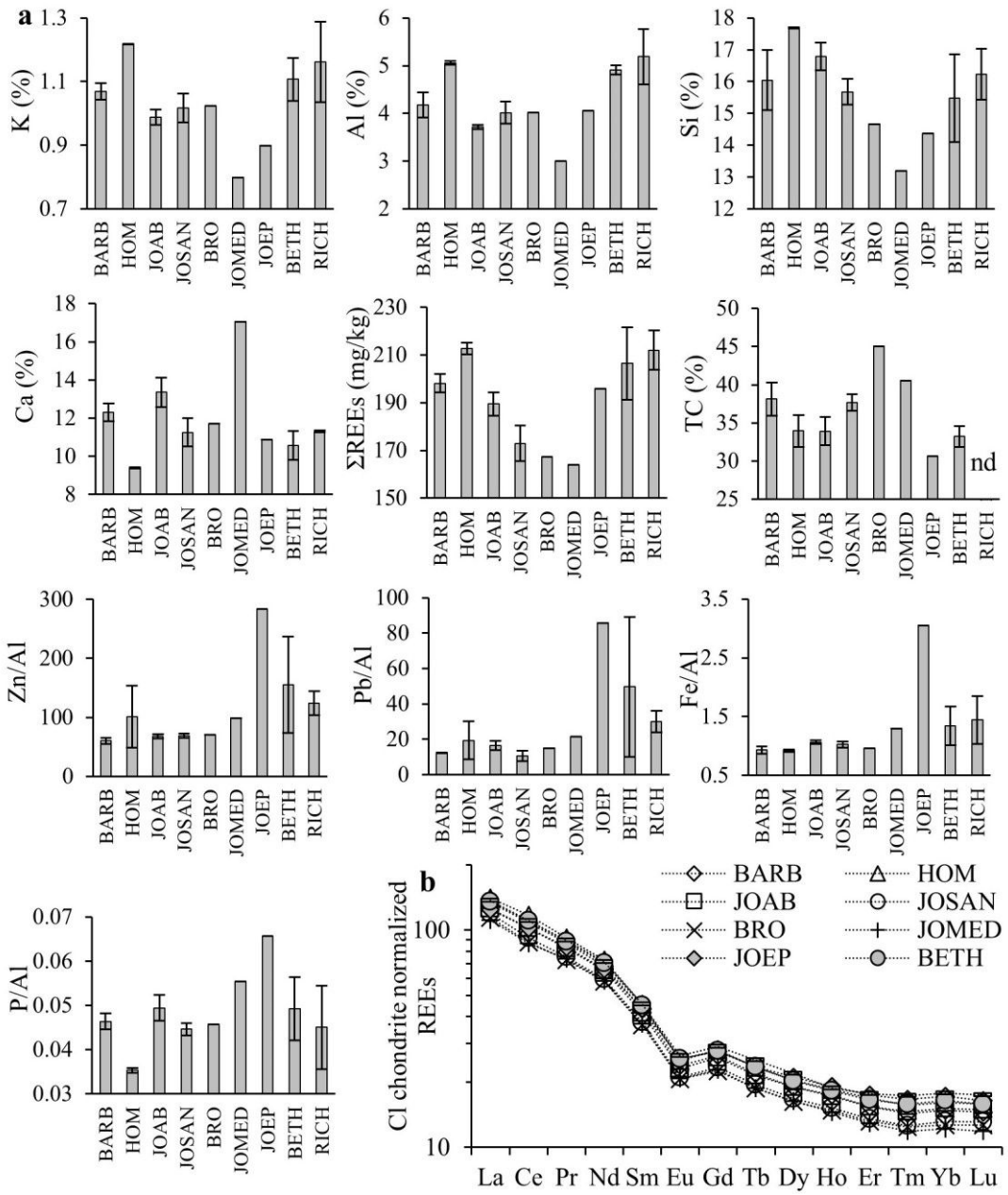

Figure III-5: Chemical composition and normalized REEs of bulk sediments collected along the course of the Orne River.
a: Variation of K (%), Al (%), Si (%), Ca (%), ΣREEs (mg/kg), TC (%) and Al normalized Zn, Pb, Fe and P. Averages and standard deviations are plotted when several sediment samples were collected. b: Cl chondrite normalized REEs showing a smooth trend except for a negative Eu anomaly.

Furthermore, Al normalized Zn, Pb and Fe had similar evolutions along the course of the Orne River. It should be noted that the trends of metal contents, whether normalized or not, were similar along the river course; therefore, the metal content itself, without referring to the normalized value, might be used in some cases. With the exception of HOM, which had

relatively elevated Zn and Pb contents (also seen by high Zn/Al and Pb/Al), the samples from BARB till JOMED had relatively low Fe, Zn and Pb contents. The average contents of the non-normalized values from BARB till JOMED were 3.9 ± 0.12% for Fe, 71 ± 17 mg/kg for Zn, and 56 ± 8 mg/kg for Pb; JOEP was the most enriched with those metals, even after Al normalization, indicating the anthropogenic contribution of the exceptionally fine particles. Therefore, the fine character of JOEP sediments might be related, to a big extent, to the nature of the sediments, and not to the change in river hydrodynamics caused by the dam. Indeed, metal enriched JOEP sediments can be related to the former steelmaking industries located in Jœuf (SM III-8). Fe, Zn and Pb contents in surface sediments showed rather high variations for Beth sediments (upstream the dam), as seen by the relatively high standard deviations (Figure III-5 a). The surface sediments were certainly influenced by highly contaminated materials evidenced a few centimeters below the surface (at 3 cm from a sample collected upstream the Beth dam). The contents of Fe, Zn and Pb then varied in the downstream sense, i.e. from JOEP towards RICH-A31, mainly due to change in the nature of the sediments, but also possibly due to variation in land use. Phosphorus showed a trend similar to Fe, Pb and Zn, and was significantly correlated to the first two (SM III-7). Phosphorous might be introduced by urban and domestic effluents, as well as agricultural practices. P contents slightly changed between BARB and JOMED (average P content 0.18% ± 0.1), while the stations further downstream (JOEP till RICH) were more enriched and had an average P content of 0.25% ± 0.02. Also, variation of detrital elements (K, Al, Si and REEs) and elements linked to anthropogenic activities (Zn, Pb, P and slightly Fe) was noticed between JOMED and RICH. The Cl chondrite normalized REEs contents can be used for sediment identification (Taylor and McLennan, 1985). The normalized profile demonstrated a smooth trend, except for the normalized Eu values (Figure III-5 b).

3.4. Mineralogy of Orne River sediments

3.4.1. Major crystalline minerals, bulk samples and clay fractions

The major crystalline mineral phases detected in Orne sediments were rather similar (from BARB till RICH); the focus will be made on the samples from BARB till BETH. The most prominent minerals detected by XRD were quartz, calcite and phyllosilicates (Figure III-6), as it would be expected in Orne sediments (according to lithology). Some samples showed higher diffraction lines for quartz, mainly JOAB, JOSAN, JOMED and JOEP (insert "a" of Figure III-6); JOAB, JOMED and JOEP also exhibited higher calcite diffraction lines.

Although Ca content, TC and calcite intensity peak (XRD) might behave similarly (as observed for JOMED), the intensity does not give robust findings. Therefore, the diffraction line intensity might only be used in a semi-quantitative way in this case. Iron minerals were also detected. Goethite (α-FeOOH) was mainly identified by the diffraction line at 4.18 Å and the secondary diffraction line at 2.69 Å. Goethite was detected in BETH and JOEP. The 2.69 Å diffraction line was displayed in almost all samples, but more clearly in JOMED, JOEP and BETH. The peak at 4.18 Å was not clearly detected in JOMED, therefore a mineral other than goethite might be responsible for the 2.69 Å diffraction line. The peak at 2.69 or 2.70 Å, or the relatively broad 2.69 – 2.70 Å peak, is also the primary diffraction line of hematite (Fe_2O_3, 2.69 Å) and pyrite (FeS_2, 2.70 Å); due to the relatively low peak intensity of the primary diffraction line, the secondary lines were hardly detected on the diffractograms. Two other iron minerals,

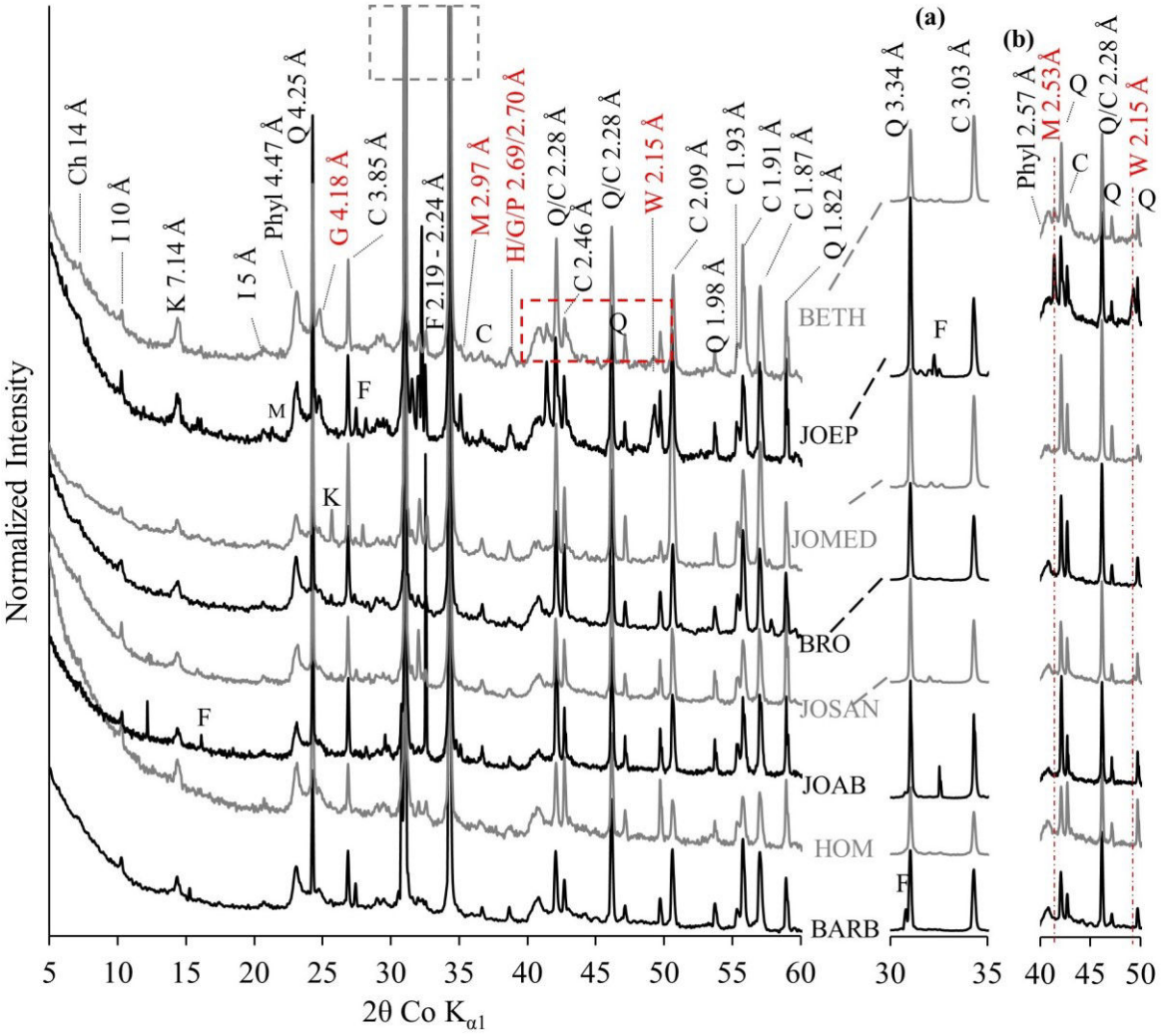

Figure III-6: XRD patterns for surface sediments of the Orne River.
Ch: chlorite, I: illite, K: kaolinite, Phyl: phyllosilicate, Q: quartz, G: goethite, C: calcite, F: feldspar, M: magnetite, P/H: pyrite/hematite, and W: wuestite. The insert (a) highlights on the main diffraction lines of quartz and calcite (dotted grey rectangle); the insert (b) highlights on magnetite and wuestite (dotted red rectangle). *The diffractograms are vertically packed as they appear in the course of the Orne River.*

which are magnetite (Fe_3O_4, mainly by 2.53 Å) and wuestite (FeO, mainly by 2.15 Å), were seen in BETH and JOEP, with higher intensity peaks for the latter (insert "b" of Figure III-6). Finally, the XRD patterns of the sediments showed the presence of primary silicate minerals (quartz and feldspars), secondary weathered silicate minerals, such as phyllosilicates (kaolinite and illite), carbonate minerals (calcite), and iron minerals (oxides, oxy-hydroxides and sulfides).

In addition to the bulk XRD analyses, oriented preparations of clay fractions were analyzed by XRD to identify clay minerals (Figure III-7). Kaolinite, illite and chlorite are non-swelling clays, thus the interlayer space does not increase upon saturation with ethylene glycol, and the diffraction line of *(001)* plane remains at ~ 7.16, 10 and 14 Å, respectively. Since kaolinite is not stable at temperatures higher than 500°C, the 7.16 Å peak disappears after thermal treatment; kaolinite and illite are evidenced in all the sediments (Figure III-7). The 14 Å band, being broader than the other diffraction peaks, may have various or multiple assignments. Indeed, chlorite and smectite, which are respectively TOTO and TOT clays could be evidenced in the sediments according to the presence of the 14.2 Å peak in the patterns of

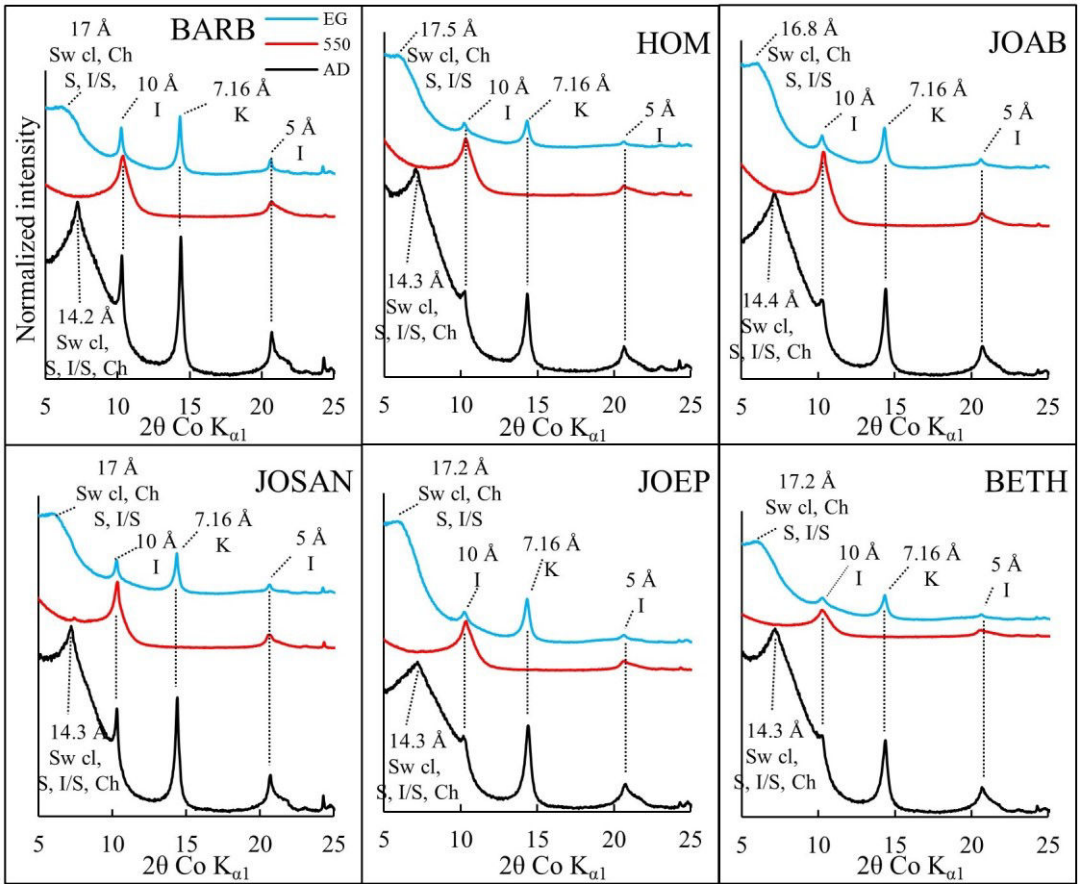

Figure III-7: Oriented XRD patterns for clay particles of Orne River surface sediments.
Sw cl: swelling clays, Ch: chlorite, S: smectite, I: Illite, I/S: interlayered illite/smectite, and K: kaolinite.

the air-dried slides. The shifting of the 14 Å peak towards a broad ~ 17 Å peak with ethylene glycol treatment indicates the presence of swelling clays. The swelling appears to be unequal as the band at 17Å is broader; there is a continuous band between 14 and 18 Å, suggesting the presence of non-swelling clays and above all interlayered clays, displaying swelling and non-swelling layers in same particles (for instance illite/smectite or I/S interlayered clays).

3.4.2. Micrometric to sub-micrometric investigations of surface sediments (SEM and TEM)

SEM and TEM observations on surface sediments were conducted to reveal the mineral composition at resolutions finer than XRD; i.e. crystalline, poorly crystalline and amorphous phases. The major detected micrometric phases were diatom skeletons and detrital material. The detected diatom skeletons were spotted as intact frustules of various shapes and sizes, as slightly degraded or weathered frustules, or as amorphous silica, which is thought to be the product of frustule weathering (Figure III-8: a – d). Other phases that could be readily identified in the sediments were quartz, calcite and clay minerals (Figure III-8: e and f), which roughly constituted 12, 21 and 24%, respectively, of the analyzed particles (SEM observations). Even though the clay particles could not be identified at this scale/level, it is worth pointing out that their major components were Si and Al, and other detectable elements were Fe, Mg and K.

TEM observations revealed variable clay minerals (Figure III-9), mostly identified as interlayered (same as interstratified) clays. The main criteria that were used to characterize the clay particles were elemental composition (EDXS data, such as Si:Al ratios and atomic percentages of K and Mg) and shape (as defined or cloudy shape). Si:Al ratios close to 1 and the absence of K and Mg indicate kaolinite, a TO clay; however, EDXS spectra rarely evidenced pristine kaolinite. Nonetheless, kaolinite is surely present in the samples, as evidenced by XRD and oriented slides (Figure III-6 and Figure III-7). Most of the clay particles showed Si:Al ratios higher than 1 and close to 2 (Table III-2), a feature of TOT phyllosilicates, such as illite and smectites (e.g. montmorillonite). Montmorillonite is a dioctahedral smectite, mainly aluminous for the octahedral sheet (4 octahedral sites per unit cell) and siliceous for the tetrahedral sheet (8 tetrahedral sites per unit cell, Si:Al slightly higher than 2.0 and about 0.5-1 octahedral site is occupied by cations other than Al (such as Mg and Fe)); high Si:Al ratios (~ 2), low atomic percentages of K and Ca, and relatively higher atomic percentages of Mg and Fe in the clay particles, therefore, suggest the occurrence of montmorillonite. Moreover, most of the particles identified as clays had a cloudy feature; that feature is commonly encountered

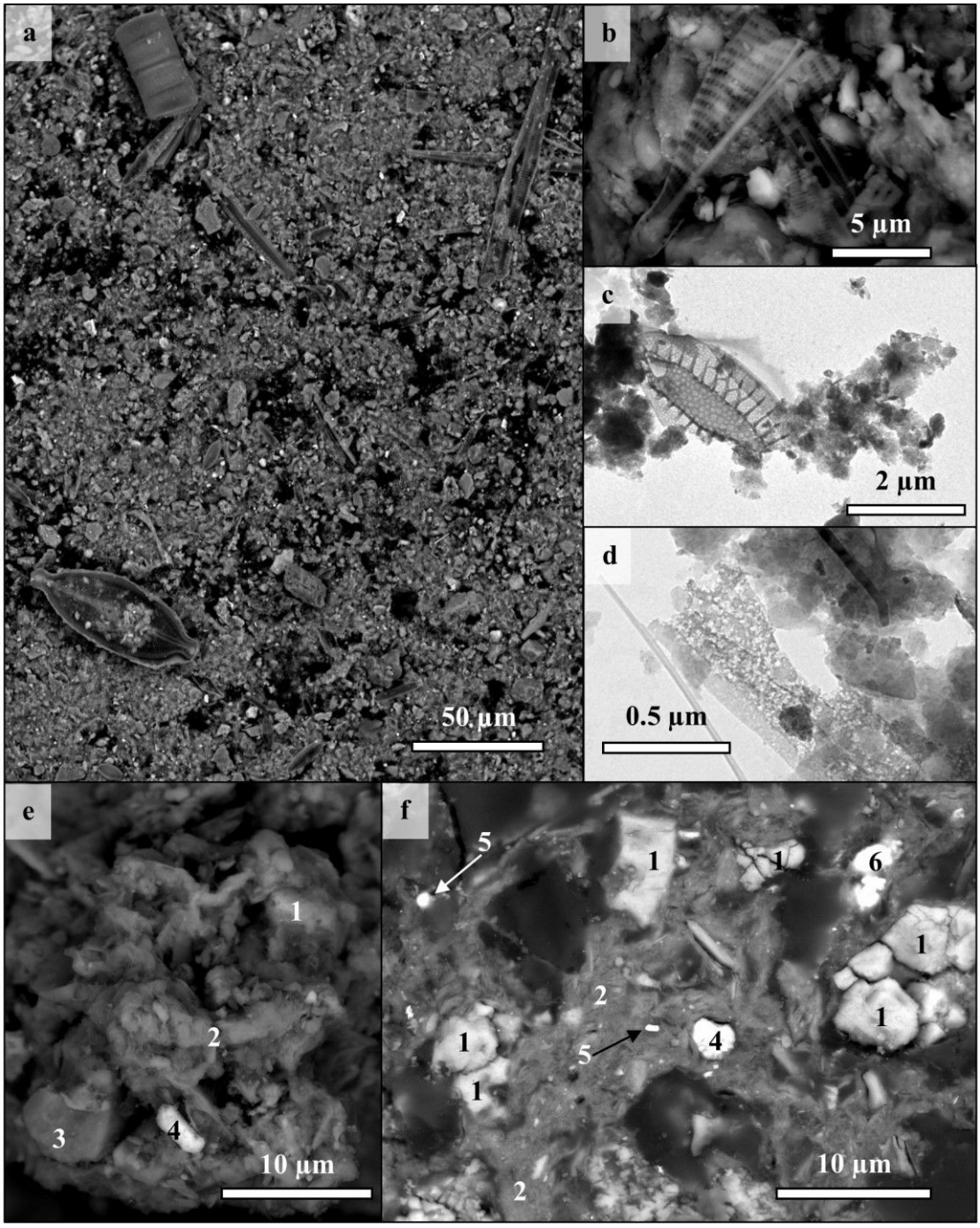

Figure III-8: SEM and TEM micro-images showing diatom skeletons and the main phases in Orne River surface sediments.
SEM Back-scattered electrons (BSE) micro-image of a: a wide scale view showing intact diatom skeletons or frustules (BETH) and b: more or less weathered diatom frustules (BETH), c: TEM micro-image of a weathered diatom skeleton (RICH-C), and d: amorphous silica produced by the weathering of diatom skeleton (HOM). e: SEM BSE micro-image showing 1: calcite, 2: clay particle mainly composed of Si and Al, and contains traces of Mg, K and Fe, 3: quartz (SiO_2), and 4: Fe oxy-hydroxide particle (BETH). f: SEM BSE micro-image showing 1: calcite, 2: clay, 4: Fe oxy-hydroxide, 5: pyrite microcrystal (FeS_2) and 6: zinc sulfide particle (HOM).

in smectite clays (Figure III-9). Using TEM, illite is observed as defined structures; potassium is an interlayer cation present between the TOT planes of the phyllosilicate. This indicates the predominance of interlayered illite/smectite clays in the surface sediments of the Orne River.

The heterogeneity of the clay particles (labelled as C in Table III-2) is partially explained by various Si/(Al+Fe+Mg) ratios; Al, Fe and Mg being components of the tetrahedral layers, lower ratios indicate higher contribution of tetrahedral sheets, such is the case of mixed or

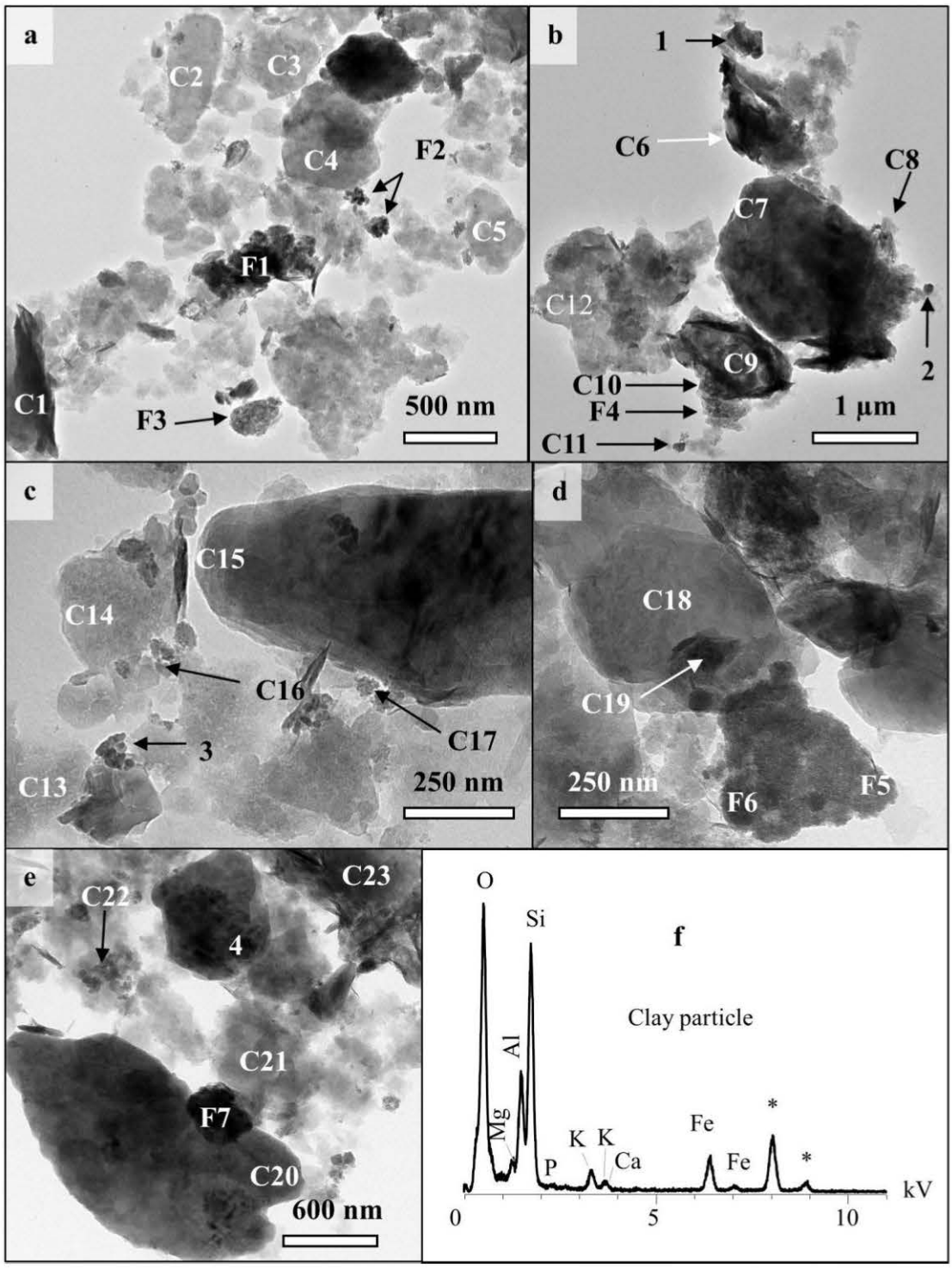

Figure III-9: TEM micro-images for Orne surface sediments.
a – e: Micro-images representing sediments of JOAB (a and b), BARB (c), RICH-C (d) and HOM (e). The particles labelled by a number preceded by a C are identified as clays (mainly interlayered I/S), those preceded by an F are identified as Fe oxy-hydroxides. The EDXS data are compiled in Table III-2. f: a typical EDX spectrum of the predominant clay particles encountered in the sediments. Asterisks on the spectrum indicate the emission lines of copper, which are due to the contribution of the TEM grid, a carbon coated copper grid.

interlayered clays (e.g. smectites). It should be noted that illite, smectite and I/S clays were already evidenced by XRD (Figure III-7). Finally, the exact nature of clay minerals was hard to determine due to the evident superimposition of different kinds of clay minerals, even at the nanoprobe scale.

Table III-2: Atomic percentages of particles revealed by TEM (Figure III-9).
Highlighted in blue are clays, and highlighted in pale orange are Fe minerals.

	Atomic percentages (%)											Ratios		
	Ca	**O**	**Si**	**Al**	**K**	**Mg**	**Fe**	**S**	**P**	**Ti**	**Mn**	**Si:Al**	**Si/ (Al+Fe+Mg)**	**O/Fe**
C1	0.6	63	19.4	11.2	1.0	2.2	2.2					1.7	1.2	
C2	0.1	65	18.7	13.0	1.3	1.3	0.9					1.4	1.2	
C3	0.2	65	18.2	12.6	0.9	1.4	2.0					1.4	1.1	
C4	0.1	64	23.1	10.7	0.1	1.2	1.0					2.2	1.8	
C5	0.1	63	24.2	10.1	0.5	1.2	1.3					2.4	1.9	
C6	0.2	64	20.1	11.3	0.5	1.9	1.9					1.8	1.3	
C7		70	15.9	12.7	0.2	1.0	0.2					1.3	1.2	
C8	0.4	62	18.3	12.1	0.8	2.0	4.4					1.5	1.0	
C9	0.5	65	17.2	13.3	0.5	1.6	1.7		0.2			1.3	1.0	
C10	0.4	64	14.5	10.8	0.4	1.6	7.9		0.3			1.3	0.7	
C11	0.4	64	18.0	9.6	1.0	1.9	5.1		0.1			1.9	1.1	
C12	0.2	63	19.2	14.0	0.5	1.6	1.4					1.4	1.1	
C13	0.4	66	17.6	10.7	1.4	1.8	2.0					1.7	1.2	
C14	0.9	69	15.1	11.3	2.1	0.7	1.2					1.3	1.2	
C15	0.1	61	20.7	14.5	0.3	1.6	1.8			0.1		1.4	1.2	
C16	1.1	63	15.2	9.9	0.8	1.8	7.8			0.1		1.5	0.8	
C17	0.4	65	17.3	12.8	0.5	1.3	3.3					1.4	1.0	
C18		68	20.8	11.0								1.9	1.9	
C19	0.2	59	17.2	13.2		1.6	9.2			0.1		1.3	0.7	
C20		64	22.8	11.6	0.2	0.9	0.3					2.0	1.8	
C21	0.1	59	22.2	13.6	1.0	1.7	2.2					1.6	1.3	
C22	0.3	57	23.4	11.6	1.7	2.6	2.9	0.5	0.2	0.2		2.0	1.4	
C23	0.1	60	21.5	11.2	1.9	2.5	2.7					1.9	1.3	
F1	0.6	66	7.3	5.4	0.4	1.0	18.3	0.1	0.5		0.3	1.3		3.6
F2	0.3	68	3.1	3.3	0.2	0.6	23.3		0.3		0.5	0.9		2.9
F3	0.9	60	3.0	5.2	0.1	0.8	26.7	0.2	0.7	1.9	0.4	0.6		2.3
F4	0.8	66	6.6	5.3	0.2	0.5	19.6		0.6			1.2		3.4
F5	2.0	67	3.4	1.5		0.3	24.3	0.4	1.1			2.2		2.8
F6	1.8	67	6.0	2.8	0.3	0.6	19.7	0.5	1.0			2.2		3.4
F7	0.5	58	9.4	7.2	0.5	0.8	23.0		0.7			1.3		2.5
1	34.2	66	0.1			0.1								
2	1.0	70	7.1	4.1	0.4	0.7	3.9			12.6		1.7		
3	0.2	64	29.2	2.2	0.1	0.5	3.7							
4		62	14.3	8.9		0.6	0.6			13.9		1.6		

In addition to the Fe included in the structure of clay minerals, other particles that were mainly composed of Fe, i.e. Fe bearing particles, were detected by SEM and TEM. Iron bearing particles were seen via SEM as defined sub-micrometric oxy-hydroxides (Figure III-8: e and f), and via TEM as oxy-hydroxides of poorly defined particles, well defined nanoparticles, and associated to clay particles (Figure III-9). In the last case, however, it was sometimes difficult to ascertain if Fe oxy-hydroxides are associated to the clay structure (as a surface coating), or

are superimposed onto the clay particles. The evidenced iron nanoparticles were circular to rod-like in shape, and had cross sections ranging between 10 to 30 nm, while the non-defined Fe oxy-hydroxide particles were generally inferior to 250 nm in dimension (length of section).

Less frequently, SEM and TEM-EDXS evidenced TiO_2 particles, iron sulfides (pyrite microcrystals), and sub-micrometric zinc sulfides (Figure III-8 f). Framboïdal pyrites could be observed in the sediments of HOM (Figure III-10 a and b). Other distinct phases were detected in RICH sediments, namely hairy Fe rich aluminosilicates and polymetallic sulfides (Figure III-10 c). The polymetallic (Fe, Zn and traces of Pb) sulfides were seen as fluffy nanoparticles (few tens of nm); the atomic percentage of Zn was higher than Fe (~ 15, 6.8 and 6.0% for Zn, Fe and S, respectively). The couple polymetallic sulfides were seen to be embedded, or at least

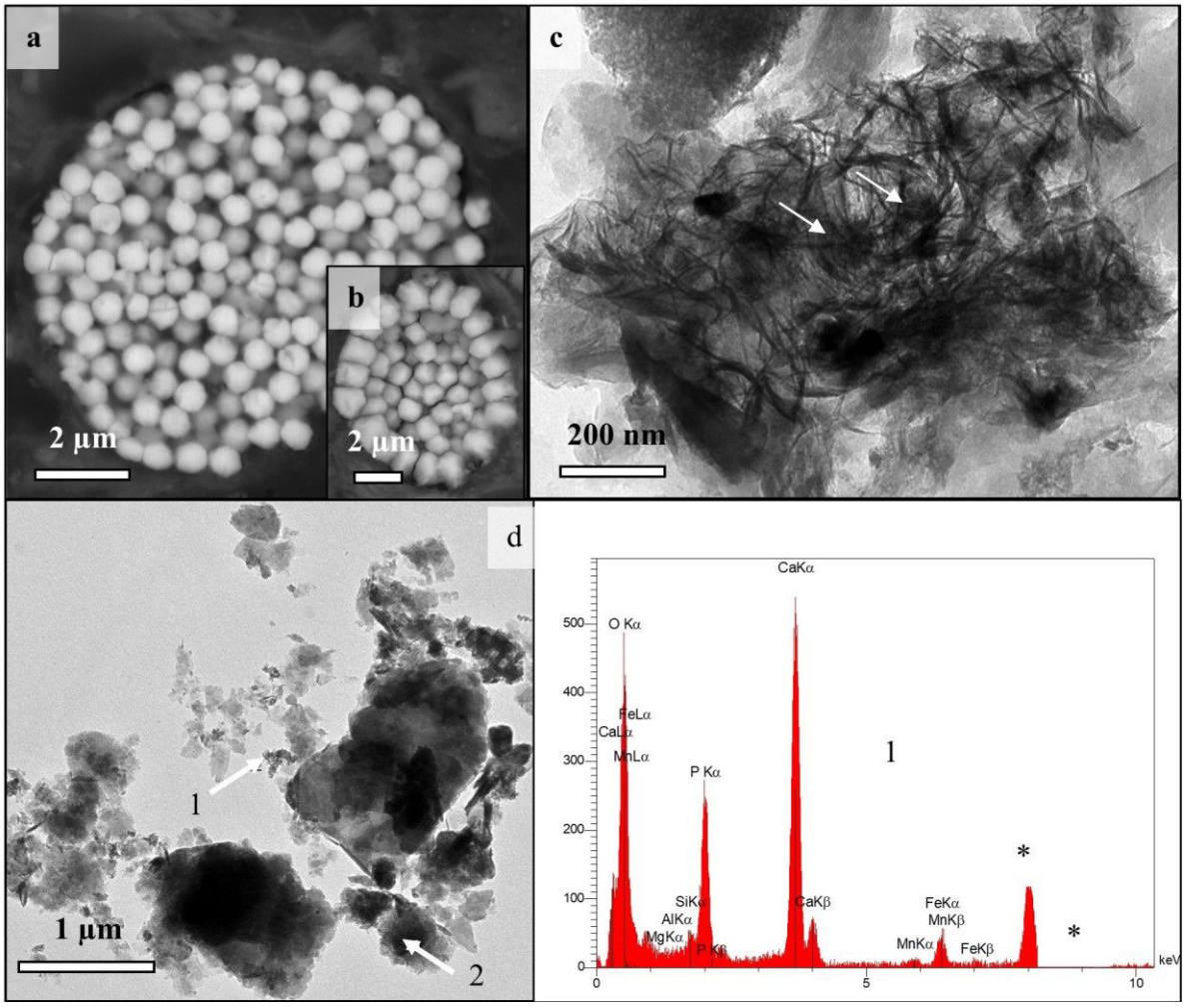

Figure III-10: Electron microscope images of surface sediments.
a and b: SEM BSE micro-images of framboïdal pyrite phases with octahedral to spheroidal microcrystals (HOM). c: TEM micro-image showing polymetallic sulfides (indicated by arrows) in hairy Fe-aluminosilicate phases (RICH). d: TEM micro-image showing 1: phosphate rich particle identified as apatite with the corresponding EDX spectrum, and 2: interlayered I/S (RICH). Asterisks on the spectrum indicate the emission lines of copper, which are due to the contribution of the TEM grid, a carbon coated copper grid.

lying, in the hairy Fe-aluminosilicate phase. Those particular Fe-aluminosilicates were characterized by an Al:Si ratio of 0.58, while atomic percentage of Fe was approximately 7.5%. It should be noted that such Fe-aluminosilicates were also predominant in metal rich sediments highly impacted by former steelmaking facilities (Fe > 20%, Zn > 2000 mg/kg), starting at least from 3 cm depth. Furthermore, calcium phosphate rich phases were detected in RICH, which is located in the upstream zone of the Orne River (Figure III-10 d). That phase was identified as apatite.

4. Discussion

4.1. Influence of grain size on the chemical and mineralogical composition of sediments

The sediments that were collected along the course of the Orne River showed variable chemical composition for different grain fractions (Figure III-2 and Figure III-3). The chemical composition, especially of major elements, is highly dependent on the origin of the sediments; the origin in turn is related to the geological formation of the basin, land use and input from anthropogenic materials (Adriano, 2001). In addition, grain sizes of sediments are supposed to strongly influence the chemical composition. Even though there was a distinction between the fractionated and bulk sediments in the previous sections, they will be partially discussed in a conjoint way. The fine grains (< 50 µm) were the main Si, Al and K carriers in Orne surface sediments (Figure III-2 and SM III-3). Indeed, that was also seen for the bulk sediments, where HOM contained relatively low D_{50} values (Figure III-4 a), and were mostly enriched with Si, Al and K (Figure III-5 a), while the opposite was true for JOMED (i.e. high D_{50} and low Si, Al and K contents). Those elements are generally found in secondary minerals that form after weathering/dissolution/breakdown of primary silicate minerals, and that constitute most of the sedimentary rocks in the studied area. The higher contents of those elements in the fine fractions can be explained by the predominance of clay minerals (e.g. phyllosilicates). The relatively coarser grain sizes of JOSAN, BRO and JOMED were translated by higher diffraction line intensities for calcite and quartz (Figure III-6), which might be attributed to the presence of relatively coarse quartz and calcite minerals in the coarse silt and sand grains. SEM micro-images showed quartz and silicate phases, in addition to diatoms (Figure III-8), indicating the detrital/natural aspect of the surface sediments.

4.2. Particle size properties and water content

In the influence zone of dams, suspended particles are sorted according to size; in the close vicinity of dams, fine particles settle in particularly low hydrodynamic conditions, enhancing the parallel orientation of clay particles. Therefore, the voids present between the particles are reduced. The fine character of Orne surface sediments (i.e. D_{50} values) was similar to other sediments collected in upstream zones of dams (e.g. Ammar et al., 2015; Dhivert et al., 2015a, 2015b). Fine particles that are transported after segregation of aggregates might be deposited at places where shear stress and water discharge decrease (Shrestha et al., 2014); as a result, mesokurtic and wide-ranged sediment particles form (e.g. very poorly sorted grains), consisting of either a spread population or a multimodal one (Lisle, 1989). Indeed, that might be applied to BARB, JOAB and JOEP (Figure III-4 a and e). Under natural hydrodynamic conditions, where water discharge fluctuates, sediments are usually characterized by a wide range of grain sizes, heterogeneity, asymmetrical and poorly sorted grains (Ramanathan et al., 2009; Robert, 2014), which are partially explained by the variation of river flow characteristics (Baruah et al., 1997). The particularity of the fine grain sizes of the sediments could also be evidenced through their water content. Fine particles have high surface areas and are mainly composed of clay particles, which could retain more water than silt and sand particles; this was seen for BETH and HOM sediments (Figure III-4 a and f). In the case of Orne surface sediments, the overlying water column is generally low (approximately 1 m), except for locations in the direct upstream zones of the dams (namely HOM and BETH), where the water column might reach approximately 4 meters (Losson and Manceau, from echo sounder data of the riverbed profiles). Higher water columns are expected to cause higher consolidation levels and consequently reduce surface sediment remobilization. Furthermore, the behavior of sediments can be distinguished between coarse and fine grains. Coarse grains have densities higher than clay particles, therefore causing overburden, and reducing water content and possibility of remobilization; on the other hand, fine particles have higher cohesion, which is common for clay particles (Naden, 2010). In either case, once sediments are remobilized, finer particles (the case of HOM, JOEP and BETH) are relatively more easily transported in the river course. Since BETH and HOM are located upstream of dams and are relatively fine/clayey, cohesion is thought to be higher. Indeed, fine particles stick together, partly via thin films of water between the individual particles, form aggregates and tend to mobilize together. Once settled, the cohesive clay aggregates are rather preserved (i.e. do not remobilize), unless strong hydrodynamic variations cause the disruption of the steady states of the sediments (Nichols,

2009a). The lowering remobilization capacity is further supported by relatively higher water levels above HOM and BETH sediments.

Even in the relatively small river of the Orne, physical (grain parameters) and chemical (trace and major elements) characteristics of the sediments were variable. The variability is partially explained by the dams at Homécourt and Moyeuvre-Grande (downstream HOM and BETH, respectively). Another explanation would be the variability in water hydrodynamics and riverbeds along the river course, where water with low flow (e.g. at a river turn), and bumpy (e.g. due to large blocks of rocks/trees) and vegetated riverbed enhance sedimentation. Coarser particles are therefore preferentially settled near or after river turns, before dams, and in areas near vegetated banks. Indeed, JOMED is located at a river turn, and therefore explains, at least partially, the relatively high D_{50} values (it should be noted that other deciles were also significantly higher than other samples; data not shown).

4.3. Variation of chemical and mineralogical composition of Orne sediments and possible sources

4.3.1. Detrital elements and clay mineralogy

The major source of Si, Al, Ca, K, Mg and Na is lithogenic contribution from the geological formation and surface run-off. The decrease in Si contents from HOM till JOMED might be linked to the modification of substratum from marl to limestone (from the Woëvre to the Pays-Haut region; Figure III-1 a), which might also be seen by the apparent Ca increase and REEs decrease (Figure III-5). Common REEs minerals are phosphates (e.g. monazite and xenotime), silicates (e.g. gadolinite and allanite) and carbonates (e.g. bastnaesite and parisite); nonetheless, those minerals are not included in the geology of the Orne basin. Therefore, other possible sources can be proposed, such as metal alloys, hybrid engines, magnets, petroleum refining, smart phones, laptop (and accessories), and others (Haque et al., 2014 and articles cited therein). Another possibility would be agricultural practices. The Orne area includes agricultural lands in the upstream reach of the sampling sites. Furthermore, REEs used in agriculture are adsorbed by soil and sediment particles (Hu et al., 2006). Al and K trends from HOM till JOMED were similar to Si, with higher contents for HOM and lower contents for JOMED. Moreover, and as indicated in section *3.1*, the presence of higher Si, Al and K contents in the < 50 μm fraction (Figure III-2 and SM III-3), and the higher Si, Al and K contents in samples of fine grain sizes (D_{50}), such as in the case of HOM and BETH (Figure III-4 a and Figure III-5 a), might indicate that those elements are majorly found in secondary clay minerals.

The variations in Si and Al contents are explained by grain sizes; similar contents were found for the same fraction for different sediments (Figure III-2). Fine sediments are preferentially transported for further distances in the river course; the finest fractions were seen to be enriched with some major and trace metals (Figure III-2, Figure III-3, SM III-3 and SM III-5), thus highlighting the seriousness of chemical cycle (such as Si, Fe and K) modification upon sediment remobilization. Mineral modifications might occur along the transport cascade; i.e. before reaching water bodies (on land), when suspended in the water and after sedimentation. The detected phyllosilicates by XRD were kaolinite, illite, chlorites, smectites and interlayered illite/smectite clays (Figure III-6 and Figure III-7). Even though the 10 Å peak was identified as illite, the same peak also evidences naturally occurring interlayered illite/smectite (Dong, 2005; Heller-Kallai and Kalman, 1972), as predominantly detected by TEM-EDXS (Figure III-9 and Table III-2). Interlayered illite/smectite particles are rather common in fine-grained sediments (Srodon, 1981). Moreover, only few kaolinite platelets were observed by TEM. The interlayered clay minerals were detected in approximately 30% of the analyzed samples (n = 220). Those clay minerals are quite common in river SPM of the French part of the Moselle Watershed (Le Meur et al., 2016, fig. A4), and in the geological layers of the Callovo-Oxfordian belonging to the Jurassic sedimentary rocks in the Woëvre region, upstream the sampling sites (Rivard et al., 2013).

4.3.2. Carbonates and REEs

The TC content represents the organic and inorganic fractions; the former being lower (roughly 1 – 2%) than the latter (roughly 30 – 40%) (Meybeck, 1982; Seiter et al., 2004). Some of the inorganic carbonate minerals detected in sediments and soils are calcite, dolomite and aragonite. Carbonate materials can be used to trace the contribution of natural (e.g. plant and rock debris) and foreign (e.g. pharmaceuticals) materials. Additionally, the carbon content might represent allochthonous as well as autochthonous materials, depending on the source. The variation in carbonate contents (TC) along Orne River sediments can be explained by biomass production and degradation; the inorganic part depends more on mineralization, depositional process at variable river flow conditions and land contribution (Meyers, 2003). BRO, which showed the highest TC content and one of the coarsest fraction, might therefore mark weathering or soil erosion. REEs were majorly found in the coarse fractions for RICH-S, RICH-C and RICH-A31 (Figure III-2) for which carbonates appeared to dominate. This might indicate that REEs are associated to carbonaceous rocks and carbonate minerals. Indeed, carbonates were proven to be major REEs hosts in sediments (Hogarth et al., 1985; McLennan

and Taylor, 2012). This idea is further supported by sediments that were collected from the Moselle River, where REEs and Ca contents followed similar trends (the idea is developed in the appendix by referring to data from Moselle sediments, see section *IV*). Finally, the inclined normalized Eu value is usually witnessed in riverine sediments. That anomaly indicates the highly differentiated sources of the samples (Taylor and McLennan, 1985), and scarce present of feldspars (Singh, 2010, 2009; Singh and Rajamani, 2001).

4.3.3. Metallic elements and contribution of anthropogenic deposits

In the XIXth and XXth centuries, when steelmaking facilities were active Lorraine, it was evidenced that by-products and wastes were dumped into nearby small streams (Garcier, 2007; Jeanneau et al., 2008, 2007, 2006; Jeanneau and Faure, 2010; Ministère de l'Environnement, 1985; Montargès-Pelletier et al., 2007). In addition, steelmaking wastes, especially sludge that forms after wet scrubbing of furnace smokes, are deposited in settling ponds, or form bank/overbank deposits (Huot et al., 2014; Mansfeldt and Dohrmann, 2004). The steelmaking facilities gradually closed in the Orne basin in the last century, and the final facility was shut down in 2007 (the final steelmaking site was at Gandrange, close to Richemont). HOM, JOEP and BETH sediments mark elevated metal contents (Figure III-5), which are clearly related to steelmaking and industrial activities on one hand, and lessen the lithogenic nature of the surface sediments on the other. Those fine deposits are originated from blast furnace sludge (BFS), therefore explaining high metal contents. In some rivers, high chemical contents were used to trace previous activities, such as Zn in Riou Mort River, where sediments were polluted by Zn smelters (Sivry et al., 2008), Fe, Zn, Pb and PAHs in the Fensch and Orne Rivers, due to steelmaking activities (Jeanneau et al., 2008, 2007, 2006; Jeanneau and Faure, 2010; Montargès-Pelletier et al., 2014, 2007), and Zn and Pb in the Deûle River, due to smelting and mining activities (Lesven et al., 2010; Louriño-Cabana et al., 2011). In the case of Orne sediments, Zn, Pb and Fe could be used to trace the former steelmaking facilities. That was mainly seen for JOEP and BETH, which showed elevated metal contents, similar to Fensch sediments. Nevertheless, sediments from the Fensch River, which drains a valley majorly influenced by steelmaking industries, were more enriched with Fe, Zn and Pb than Orne sediments (Montargès-Pelletier et al., 2014) (refer to the appendix for detailed information, section *IV*). Several reasons are proposed for this relatively lower contributions in Orne sediments; i. the first is that the Fensch basin mainly drains a densely industrialized and urbanized area, while the Orne watershed contains forests (26.5%), agricultural (67%) and urban (6%) lands; ii. the Fensch watershed region witnessed mining and steelmaking activities

until 2006, while most steelmaking facilities were stopped in the Orne watershed in 1988; iii. the Fensch River is smaller than the Orne (15.2 and 90 km in length, respectively), with lower average water discharge (2 m^3/s and 12.2 m^3/s for the Fensch and Orne, respectively) and smaller watershed area (82 and 1226 km^2 for Fensch and Orne, respectively) (Le Meur et al., 2016; Montargès-Pelletier et al., 2007). For those reasons, the fingerprints of steelmaking wastes are more prominent in Fensch sediments, while lithogenic input might be more detectable in Orne sediments.

4.3.4. Particularity of Fe and Fe bearing phases in Orne sediments

The metal enrichment of Orne sediments caused by steelmaking facilities was discussed in the previous section; nonetheless, iron introduction into Orne sediments might also be explained by the Aalenian geological formation present in the upstream zone of the Orne River (which is also located around Moyeuvre). The Orne basin includes the deposited "Minette" ironstone of the Toarcian/Aalenian ages, belonging to the lower/middle Jurassic epochs (Grgic et al., 2013; Teyssen, 1984). Additionally, during the last years of prehistoric and early historic periods, i.e. during the iron age (11th till 6th century BC), Europe witnessed Fe as the major toolmaking material; that caused the introduction of Fe rich materials to the surface of the earth (Leroy et al., 2015). In more recent times, the Orne Valley was active with mining (iron), smelting and steelmaking, which peaked during the XXth century (Freyssenet, 1979; Garcier, 2007). Therefore, Fe rich materials were introduced into the Orne River from various origins, such as iron ore extraction, sintering, waste release and run off and remobilization of Fe rich wastes. JOEP is located a few dozens of meters downstream the Europipe site, where a set of five blast furnaces were formerly located (Freyssenet, 1979). The released wastes from the furnaces, such as sludge that results from wet scrubbing of furnace smokes, might still be stored in that area, not necessarily as surface or subsurface sediments, but as overbank sediments. Wuestite and magnetite, mainly detected in JOEP and BETH, are some of the fingerprints of the former steelmaking facilities in the Orne watershed.

Fe sulfide minerals were also observed, such as framboïdal pyrites in HOM (Figure III-10 a and b). The framboïdal pyrites might have formed in the lower part of this 0 – 2 cm layer (i.e. 0.5 – 2 cm for example), since the oxic state of the sediment layer inferior to 0.5 cm, if submerged in water, usually marks the start of the anoxic zone (Lesven et al., 2010; Matijević et al., 2007). The river hydrology is modified and the turbulence effects are strongly reduced upstream dams, giving similar settling features to lakes; this might have enhanced sulfide

formation. It should be noted that sulfide formation requires a series of reactions, which start by degradation of organic carbon (via oxidation), followed by reduction of nitrate, manganese and iron (depending on the redox conditions) and sulfate reduction to sulfide species, such as pyrite (Fanning et al., 2010; Fanning and Fanning, 1989). The measured redox potentials for different surface sediments might be related to the previously mentioned point. Nonetheless, it should be noted that the few dozens of micrometers of surface sediments in contact with the overlying water might be concerned, and not the collected sediment samples that reached more than a centimeter.

4.3.5. Phosphorous contents and land cover

Phosphorous is transported to river systems either as dissolved or particulate phases; in the former case, phosphorous is adsorbed by soil or sediment particles (Nichols, 2009c; Søndergaard et al., 2003). Once found as particulate phase, P is diffused into pore water or water column after the decomposition of organic and inorganic compounds (Maassen et al., 2003), which might cause eutrophication in waters with low flow, such as the case of HOM and BETH. P release is enhanced after sediment remobilization, especially with increasing temperatures (Søndergaard et al., 1992). Due to the relatively low water flow of HOM and BETH, induced by the dams, increase of water temperature is expected during summer. Enrichment of sediment with particulate P might be linked to the magnitude of P release from agricultural activities and from sewage plants. The release is not necessarily particulate, however, precipitation and formation of particulate P might happen in the river. The Orne River drains 821 km^2 of agricultural lands (67% of the Orne watershed), possibility explaining the contribution of P, such as a result of using phosphate fertilizers (Azzi et al., 2017). Furthermore, sediments enriched with P might also be due to urban influence. Indeed, high P contents were detected in downstream sediments of the Orne River (after BETH). An increase of P contents in the river gradient was also seen in rivers with similar catchment areas (1932 and 930 km^2 for Aire and Calder Rivers, respectively, while that of the Orne is 1226 km^2). JOEP, BETH, and especially RICH, lie at the end of an urbanized zone (Figure III-1 b); therefore, run-off having high P contents might have settled at those sites. In addition, Zn and P showed comparable trends in Orne sediments (Figure III-5 a); Zn might be associated to phosphate minerals from WWTP effluents (Houhou et al., 2009b). In addition, particulate P might be associated to Fe oxy-hydroxides, carbonates and apatite (Søndergaard et al., 2003); that could be seen by similar contents of P and carbonates in the surface sediments (Figure III-5). A distinct calcium phosphate particle was observed in RICH (Figure III-10 d), which was

suggested to be apatite, due to the Ca:P atomic percentage ratio of 1.7 (Houhou et al., 2009a). Richemont lies at the end of the urbanized zone of the Orne valley (Figure III-1 b), and is located nearly 400 m downstream a WWTP and a few dozens of meters downstream a combined sewer overflow. Calcium phosphate phases were previously evidenced in SPM of the Moselle River (Le Meur et al., 2016) as well, and were assigned to domestic or urban inputs into surface waters. Those urban fingerprints held by RICH are probably due to the urbanized site in the city of Gandrange, which is located on the left side of the Orne River. Apatite can also form from animal bone materials, indicating a non-anthropogenic source. Nonetheless, its presence only in the urbanized area suggests anthropogenic origin. Moreover, WWTP effluents, containing biologically active microbes, will modify the initial status of chemicals. WWTPs are found approximately 1 and 0.4 km upstream of BETH and RICH, respectively. Since carbonates and P followed different trends along the river course (Figure III-5 a), they are thought to have originated from different sources, or are at least not correlated in their introduction pathway.

Finally, the impact of dams as natural suspended matter hinders should not be overlooked as influencers of SPM transport, sediment remobilization, and consequently chemical and mineralogical composition of sediments. Indeed, chemical balance in river-ocean transport were shown to be corrupted by damming (Viers et al., 2009). The deposited particles, especially those forming surface sediments, can be used as a proxy for identifying source(s), which might be done via lithogenic materials or distinct anthropogenic markers. Lastly, due to the variation in chemical and mineralogical composition of BETH and RICH sediments (which are ~ 11 km apart), more stations should be studied between these two sites. Consequently, the point of chemical and mineralogical change, caused by urbanization or former/present industrial activities, might be detected.

5. Conclusion

An inventory of the chemical and mineralogical characteristics of river sediments in part of the Orne watershed was effectuated. The role of dams as modifiers of grain sizes and properties was partially evidenced. Dams also influence minerals that settle accordingly. From the surface sediments collected along the course of the Orne River, the variation in chemical composition was explained by grain size, geological formation, land cover, and current and previous land use. Furthermore, the mineralogical composition was followed by bedrock erosion of the surrounding lithology. The lithogenic character of the sediments was tracked by

Si, Ca, Al, K and REEs, and by certain minerals (such as quartz, calcite and clays). Even more, clays with distinct, yet heterogeneous, morphology were recognized using TEM. The clays were mainly identified as interlayered clays, mostly illite/smectite, as per their chemical composition detected by TEM-EDXS, while only few kaolinite platelets were evidenced. On the other hand, former industrial activities were marked by metal enriched surface sediments (such as Fe, Zn and Pb). Increasing P contents demonstrated the urbanization gradient along the river course or the contribution of agricultural practices. The enrichment of elements, such as Fe, Zn, Pb and P, was mainly detected in JOEP and sites further downstream. The presence of iron minerals is partially due to the previous mining and metallurgical activities, such as wuestite, magnetite, goethite and Fe-aluminosilicates. Additionally, Fe-aluminosilicates, which are possible metal scavengers, contained distinct phases, such as (poly)metallic sulfides. Nevertheless, more stations should be taken, especially in the area between BETH and RICH to better determine the transition of sediment characteristics along the Orne River course. In addition, an ongoing study on the isotopic signatures of Zn and Pb of SPM, surface and subsurface sediments of the Orne River are underway to relate those three parts and see their correlations, possibly at different flow regimes.

6. Supplementary Material

Limites de détermination* et incertitudes**

Dosage des éléments traces
(ICP-MS X7 ThermoFisher)

	>50 ppm	>10 ppm	>1 ppm	>0,1 ppm	>0,01 ppm	* Limites déterm. ppm
As	<5%	<10%	**			1,50
Ba	<5%	<10%	**			1,60
Be	<5%	<10%	**			0,40
Bi		<5%	<10%	**		0,10
Cd		<5%	<15%	**		0,12
Ce		<5%	<10%	**		0,14
Co	<5%	<10%	<15%	**		0,40
Cr	<5%	<10%	**			4,00
Cs		<5%	<10%	**		0,10
Cu	<5%	<10%	**			5,00
Dy			<5%	<10%	<15%	0,01
Er			<5%	<10%	**	0,01
Eu				<5%	<10%	0,005
Ga		<5%	<8%	**		0,20
Gd				<5%	<10%	0,013
Ge		<5%	<8%	**		0,15
Hf		<5%	<10%	<15%	**	0,03
Ho			<5%	<10%	**	0,002
In			<5%	**		0,07
La			<5%	<10%	**	0,09
Lu				<5%	<10%	0,003

	>50 ppm	>10 ppm	>1 ppm	>0,1 ppm	>0,01 ppm	* Limites déterm. ppm
Mo		<5%	<10%	**		0,50
Nb		<5%	<10%	<15%	**	0,09
Nd			<5%	<10%	**	0,06
Ni	<5%	**				5,00
Pb		<5%	<10%	**		0,70
Pr			<5%	<10%	**	0,015
Rb		<5%	<10%	**		0,40
Sb		<5%	<10%	**		0,20
Sm			<5%	<10%	**	0,015
Sn	<5%	<10%	<15%	**		0,45
Sr	<5%	<10%	**			2,00
Ta		<5%	<10%	<15%	**	0,01
Tb				<5%	10%	0,003
Th		<5%	<10%	<15%	**	0,06
Tm			<5%	<10%	**	0,001
U	<5%	<10%		<15%	**	0,03
V	<5%	<10%	**			0,70
W	<5%	<10%	<15%	**		0,25
Y		<5%	**			0,20
Yb			<5%	<10%	**	0,007
Zn	<10%	**				11,00
Zr	<8%	<15%	**			1,00

Dosage des éléments majeurs et Sc
(ICP-OES iCap 6500 ThermoFisher)

Oxydes %	>10%	>5%	>1%	>0,5%	>0,1%	>0,05%	>0,01%	>0,005%	* Limites déterm. %
SiO_2	<1%		<5%			<15%	**		0,02
Al_2O_3	<1%			<10%		<15%	**		0,02
Fe_2O_3			<2%		<5%	<15%	**		0,02
MnO			<1%		<5%		<10%	**	0,0002
MgO		<2%	<5%			<10%	**		0,015
CaO		<2%		<5%		<15%	**		0,03
Na_2O		<2%		<5%		<15%	**		0,01
K_2O		<2%		<5%	<10%	<15%	**		0,01
TiO_2				<5%	<10%	**			0,02
P_2O_5			<5%		<10%	**			0,04
					>50 ppm	>20 ppm	>10 ppm	>1 ppm	* L.D. ppm
Sc					<5%		<15%	**	1,00

* La limite de détermination (L.D.) est calculée comme étant 6 fois l'écart type absolu sur 100 mesures de blancs de préparation.

** L'incertitude sur la mesure est calculée pour 200 mg d'échantillon préparé. Elle devient importante (>25 %) sur une plage de concentration située entre la limite de détermination et la plus faible concentration pour laquelle un pourcentage d'erreur est indiqué.

Calculs effectués pour 5 matériaux géochimiques de référence en analyse de routine sur une période de 12 mois (n = 300 par matériau).

SARM
CRPG-CNRS : 15 rue Notre Dame des Pauvres, BP20, 54501 Vandoeuvre-lès-Nancy, France
Tél : 33 (0)3 83 59 42 41 ; Fax : 33 (0)3 83 51 17 98

SM III-1: Limits of detection and uncertainty for elements using ICP-MS and ICP-OES (solid fraction). Values reported by SARM–CRPG, Vandœuvre-lès-Nancy, France.

Analyses des eaux naturelles et lixiviats

Limites de détermination et incertitudes*

Dosage des éléments traces

ICP-MS 7700x Agilent

	>100 µg/L	>10 µg/L	>1 µg/L	>0,1 µg/L	>0,01 µg/L	* Limites déterm. µg/L
Al	<5%	<15%	**			0,60
Ba	<5%		<10%	**		0,025
Be	<5%	<15%	<20%	**		0,03
Bi		<5%	<10%	<20%	**	0,003
Cd	<10%		<20%	**		0,007
Co	<5%	<10%		<20%	**	0,013
Cr	<5%	<15%	**			0,09
Cs		<5%	<10%	**		0,002
Cu		<5%	<15%	**		0,03
Ga		<5%	<8%	<20%	**	0,003
In			<10%	<20%	**	0,002
Mn			<10%	**		0,15
Ni	<5%	<10%	**			0,90
Pb		<5%	<10%	**		0,01
Rb		<10%	<20%	**		0,007
Sr	<5%	<10%	**			0,06
Th		<5%	<10%	<15%	**	0,003
U	<5%		<10%	<20%	**	0,002
V	<5%		<15%	**		0,04
Y		<15%	<20%	**		0,002
Zn		<10%	<20%	**		1

	>100 ng/L	>10 ng/L	>1 ng/L	* Limites déterm. ng/L
La	<10%	<15%	**	3,0
Ce	<15%	<20%	**	6,5
Pr	<5%	<10%	**	2,0
Nd	<10%	<15%	**	4,5
Sm	<5%	<10%	**	4,0
Eu	<5%	<5%	**	1,5
Gd	<10%	<15%	**	3,5
Tb	<15%	<20%	**	1,5
Dy	<10%	<20%	**	2,5
Ho	<15%	<20%	**	1,0
Er	<10%	<20%	**	2,5
Tm	<5%	<15%	**	1,0
Yb	<5%	<15%	**	3,0
Lu	<10%	<20%	**	1,5

Dosage des éléments majeurs et mineurs

ICP-OES iCap6500 ThermoFisher

	> 10 mg/L	> 1 mg/L	> 0,5 mg/L	> 0,1 mg/L	> 0,01 mg/L	* Limites détermin. (mg/L)
Si	<5%			<10%	**	0,05
Al		<10%	<15%	**		0,06
Fe	<2%		<5%	<20%	**	0,03
Mn			<5%	<15%	**	0,01
Mg		<5%	<10%	<15%	**	0,04
Ca	<2%	<5%	<15%	**		0,10
Na		<5%	<10%	<15%	**	0,03
K		<5%	<10%	<25%	**	0,08
Ti		<5%	<10%	**		0,10
P	<5%	<15%	**			0,50

* La limite de détermination (L.D.) est calculée comme étant 6 fois l'écart type absolu sur 30 mesures de blancs.

** L'incertitude sur la mesure est calculée à partir de solutions de référence internationales analysées brutes et diluées. Elle devient importante (>30%) sur une plage de concentration située entre la limite de détermination et la plus faible concentration pour laquelle un pourcentage est indiqué.

SARM
CRPG-CNRS : 15 rue Notre Dame des Pauvres, BP20, 54501 Vandoeuvre-lès-Nancy, France
Tél : 33 (0)3 83 59 42 41 ; Fax : 33 (0)3 83 51 17 98

SM III-2: Limits of detection and uncertainty for elements using ICP-MS and ICP-OES (liquid fraction). Values reported by SARM–CRPG, Vandœuvre-lès-Nancy, France.

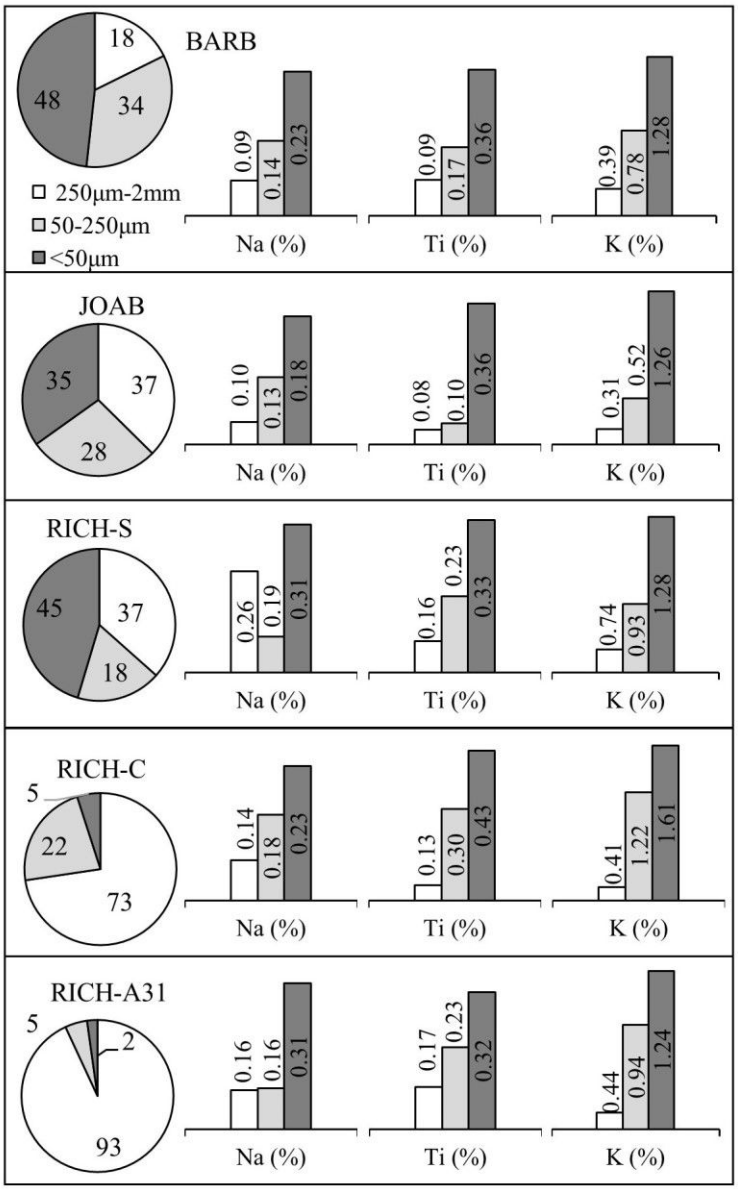

SM III-3: Grain size and contents of major elements for different fractions of Orne surface sediments.
Grain size variations are shown as pie charts and major elements (Na, Ti and K, in %) are shown as histograms. The finest fractions were mostly enriched with the presented elements.

SM III-4: Spearman's correlation coefficients (ρ, n = 15) for the REEs of the fractionated sediment samples.
The REEs are Lu, Tm, Tb, Ho, Eu, Yb, Er, Gd, Dy, Sm, Sc, Pr, Y, La, Nd and Ce. The fractionated samples are BARB, JOAB, RICH-S, RICH-C and RICH-A31.

		Tm	Tb	Ho	Eu	Yb	Er	Dy	Gd	Sm	Sc	Pr	Y	La	Nd	Ce
Lu	ρ	.972**	.953**	.975**	.943**	.971**	.966**	.948**	.948**	.975**	.908**	.907**	.977**	.894**	.935**	.880**
	P	.000	.000	.000	.000	.000	.000	.000	.000	.000	.000	.000	.000	.000	.000	.000
Tm	ρ		.975**	.998**	.939**	.995**	.998**	.970**	.953**	.928**	.871**	.837**	.979**	.825**	.869**	.821**
	P		.000	.000	.000	.000	.000	.000	.000	.000	.000	.000	.000	.000	.000	.000
Tb	ρ			.979**	.979**	.964**	.971**	.996**	.989**	.946**	.832**	.796**	.971**	.779**	.832**	.775**
	P			.000	.000	.000	.000	.000	.000	.000	.000	.000	.000	.001	.000	.001
Ho	ρ				.946**	.989**	.996**	.975**	.957**	.939**	.875**	.843**	.979**	.829**	.871**	.825**
	P				.000	.000	.000	.000	.000	.000	.000	.000	.000	.000	.000	.000
Eu	ρ					.932**	.936**	.982**	.989**	.950**	.821**	.800**	.961**	.793**	.829**	.779**
	P					.000	.000	.000	.000	.000	.000	.000	.000	.000	.000	.001
Yb	ρ						.993**	.954**	.950**	.925**	.850**	.839**	.986**	.832**	.882**	.818**
	P						.000	.000	.000	.000	.000	.000	.000	.000	.000	.000
Er	ρ							.964**	.954**	.918**	.871**	.832**	.971**	.821**	.861**	.811**
	P							.000	.000	.000	.000	.000	.000	.000	.000	.000
Dy	ρ								.982**	.943**	.839**	.793**	.964**	.775**	.821**	.782**
	P								.000	.000	.000	.000	.000	.001	.000	.001
Gd	ρ									.946**	.821**	.796**	.964**	.786**	.832**	.761**
	P									.000	.000	.000	.000	.001	.000	.001
Sm	ρ										.868**	.907**	.961**	.889**	.936**	.879**
	P										.000	.000	.000	.000	.000	.000
Sc	ρ											.936**	.825**	.921**	.900**	.932**
	P											.000	.000	.000	.000	.000
Pr	ρ												.846**	.993**	.986**	.986**
	P												.000	.000	.000	.000
Y	ρ													.839**	.896**	.825**
	P													.000	.000	.000
La	ρ														.979**	.979**
	P														.000	.000
Nd	ρ															.964**
	P															.000

ρ: Spearman's rho, same as Spearman's correlation coefficient.
P: *P* value. The *P* value is the probability of finding the observed results when the null (H_0) hypothesis is true. H_0: there does not exist a correlation between X and Y.
**: Correlation is significant at the 0.01 level (2-tailed), which is the case for all REEs.
For clarity, cells are highlighted according to the ρ range (0.7 – 0.8 in blue and 0.8 – 0.9 in green), while values greater than 0.9 are not highlighted.

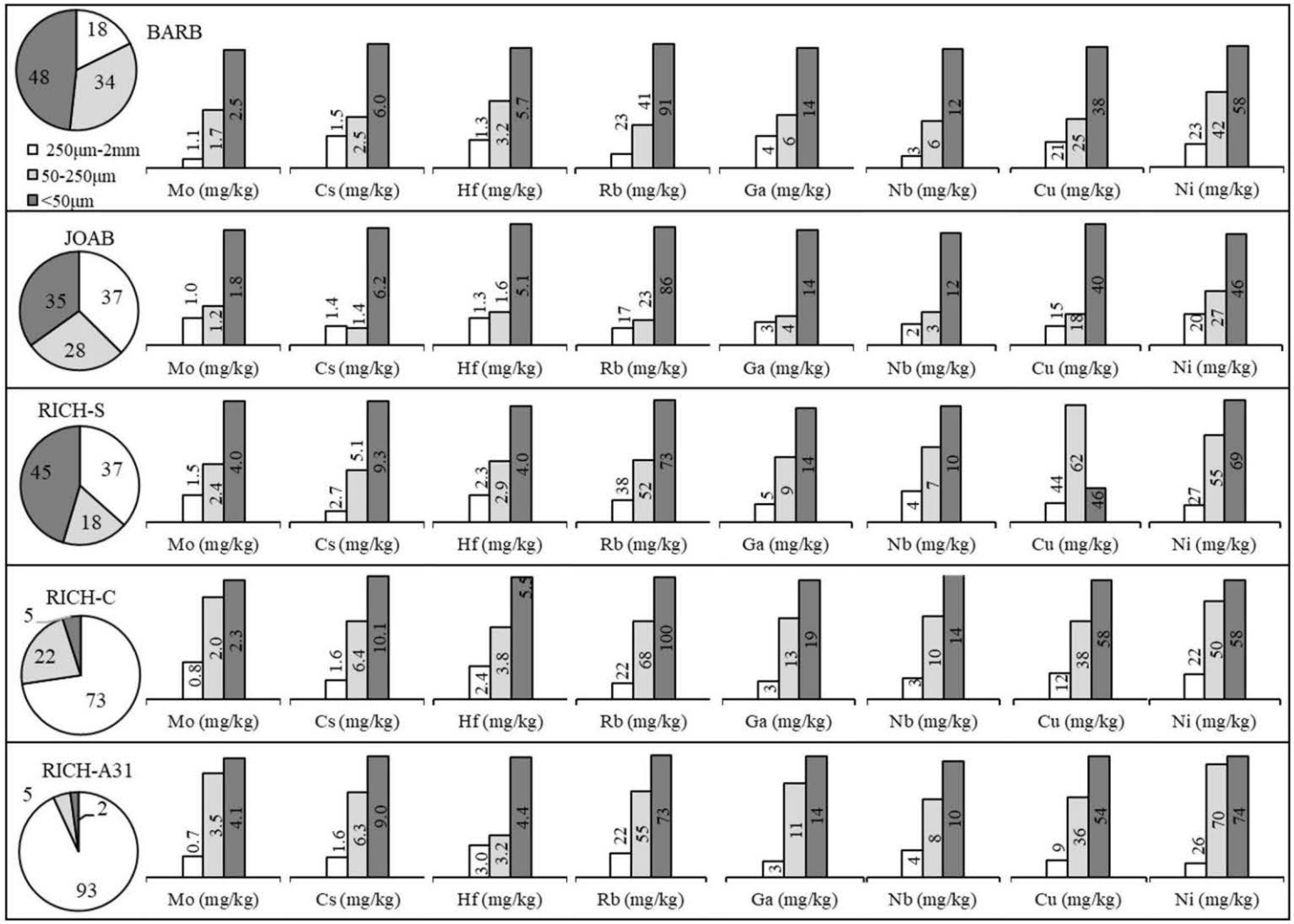

SM III-5: Trace elements of the fractionated sediments that showed to be mostly found in the finest fraction.
The presented elements are Mo, Cs, Hf, Nb, Rb, Ga, Nb, Cu and Ni (in mg/kg).

SM III-6: Spearman's correlation coefficients (ρ, n = 18) for the REEs of the bulk sediments.
The REEs are Lu, Tm, Tb, Ho, Eu, Yb, Er, Gd, Dy, Sm, Sc, Pr, Y, La, Nd and Ce. The samples are BARB, HOM, JOAB, JOSAN, BRO, JOMED, JOEP, BETH and RICH.

		Tm	Tb	Ho	Eu	Yb	Er	Dy	Gd	Sm	Sc	Pr	Y	La	Nd	Ce
Lu	ρ	.994**	.969**	.950**	.961**	.973**	.979**	.983**	.940**	.899**	.838**	.843**	.971**	.785**	.851**	.814**
	P	.000	.000	.000	.000	.000	.000	.000	.000	.000	.000	.000	.000	.000	.000	.000
Tm	ρ		.971**	.955**	.975**	.983**	.983**	.988**	.940**	.903**	.853**	.837**	.969**	.773**	.847**	.800**
	P		.000	.000	.000	.000	.000	.000	.000	.000	.000	.000	.000	.000	.000	.000
Tb	ρ			.948**	.975**	.934**	.965**	.981**	.979**	.965**	.817**	.926**	.992**	.882**	.930**	.895**
	P			.000	.000	.000	.000	.000	.000	.000	.000	.000	.000	.000	.000	.000
Ho	ρ				.934**	.911**	.961**	.955**	.905**	.907**	.759**	.849**	.940**	.796**	.856**	.839**
	P				.000	.000	.000	.000	.000	.000	.000	.000	.000	.000	.000	.000
Eu	ρ					.955**	.948**	.971**	.950**	.938**	.867**	.878**	.959**	.812**	.889**	.827**
	P					.000	.000	.000	.000	.000	.000	.000	.000	.000	.000	.000
Yb	ρ						.957**	.961**	.897**	.853**	.877**	.773**	.926**	.699**	.789**	.725**
	P						.000	.000	.000	.000	.000	.000	.000	.001	.000	.001
Er	ρ							.990**	.948**	.899**	.811**	.841**	.967**	.785**	.847**	.812**
	P							.000	.000	.000	.000	.000	.000	.000	.000	.000
Dy	ρ								.963**	.920**	.812**	.864**	.977**	.804**	.870**	.827**
	P								.000	.000	.000	.000	.000	.000	.000	.000
Gd	ρ									.971**	.787**	.946**	.977**	.915**	.950**	.913**
	P									.000	.000	.000	.000	.000	.000	.000
Sm	ρ										.783**	.983**	.950**	.950**	.988**	.959**
	P										.000	.000	.000	.000	.000	.000
Sc	ρ											.715**	.782**	.636**	.729**	.649**
	P											.001	.000	.005	.001	.004
Pr	ρ												.917**	.983**	.998**	.983**
	P												.000	.000	.000	.000
Y	ρ													.880**	.920**	.895**
	P													.000	.000	.000
La	ρ														.979**	.979**
	P														.000	.000
Nd	ρ															.979**
	P															.000

ρ: Spearman's rho, same as Spearman's correlation coefficient.
P: *P* value. The *P* value is the probability of finding the observed results when the null (H_0) hypothesis is true. H_0: there does not exist a correlation between X and Y.
**: Correlation is significant at the 0.01 level (2-tailed), which is the case for all REEs.
For clarity, cells are highlighted according to the ρ range (0.6 – 0.7 in orange, 0.7 – 0.8 in blue, 0.8 – 0.9 in green), while values greater than 0.9 are not highlighted.

SM III-7: Spearman's correlation coefficients (n = 18) for chemical contents of bulk sediments collected along the course of the Orne River.

		Al	Si	Ca	ΣREEs	TC	Zn/Al	Pb/Al	Fe/Al	P/Al
K	ρ	.841**	.662**	-.587*	.686**	-.238	-.084	-.100	-.484*	-.758**
	P	.000	.003	.010	.002	.342	.742	.693	.042	.000
Al	ρ		.401	-.806**	.740**	-.486*	.288	.296	-.176	-.446
	P		.099	.000	.000	.041	.247	.233	.484	.064
Si	ρ			-.263	.641**	-.358	-.309	-.232	-.426	-.720**
	P			.291	.004	.145	.213	.354	.078	.001
Ca	ρ				-.441	.326	-.311	-.176	.077	.419
	P				.067	.187	.210	.484	.760	.083
ΣREEs	ρ					-.748**	.162	.315	-.049	-.309
	P					.000	.521	.203	.848	.213
TC	ρ						-.573*	-.633**	-.380	-.048
	P						.013	.005	.119	.850
Zn/Al	ρ							.893**	.695**	.349
	P							.000	.001	.156
Pb/Al	ρ								.678**	.502*
	P								.002	.034
Fe/Al	ρ									.609**
	P									.007

ρ: Spearman's rho, same as Spearman's correlation.
P: *P* value. The *P* value is the probability of finding the observed results when the null (H_0) hypothesis is true. H_0: there does not exist a correlation between X and Y.
*: correlation is significant at the 0.05 level (highlighted in orange).
**: correlation is significant at the 0.01 level (highlighted in blue).
For clarity, significant correlations at the 0.05 level are highlighted in orange, those significantly correlated at the 0.01 level are highlighted in blue.

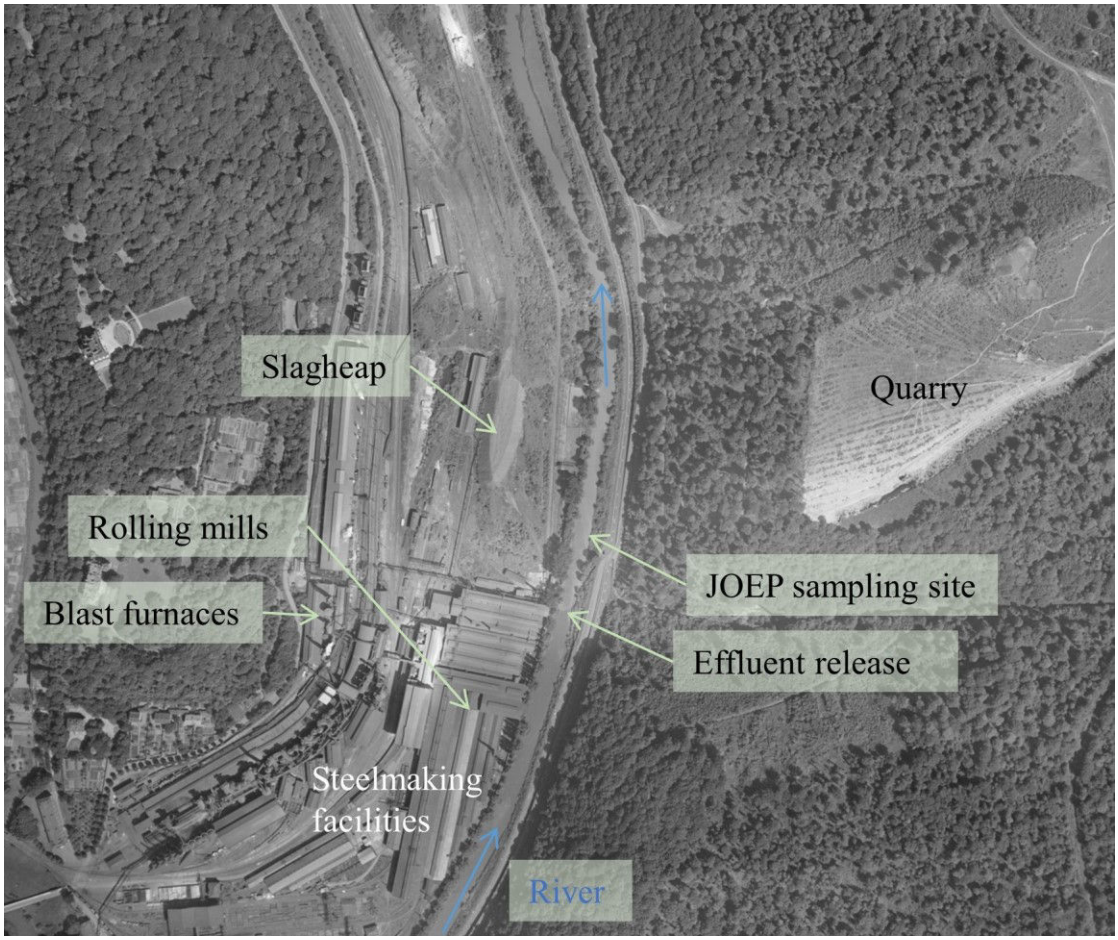

SM III-8: Aerial view of Moyeuvre-Grande near the site where JOEP was sampled.
The image was taken in 1950 (IGN 1950, reference IGNF_PVA_1-0__1950-07-09__C93PHQ8301_1950_CDP3759_0018). The image shows the change in the color of the river water after the site where effluents were released upstream the JOEP sampling site. The image also shows some steelmaking facilities that were active during that period.

References

Adriano, D.C., 2001. Trace Elements in Terrestrial Environments: Biogeochemistry, Bioavailability and Risks of Metals, 2nd ed. Springer, New York, NY. doi:10.1007/978-0-387-21510-5

Ammar, R., Kazpard, V., Wazne, M., El Samrani, A.G., Amacha, N., Saad, Z., Chou, L., 2015. Reservoir sediments: a sink or source of chemicals at the surface water-groundwater interface. Environ. Monit. Assess. 187, 4791. doi:10.1007/s10661-015-4791-0

Azzi, V., Kazpard, V., Lartiges, B., Kobeissi, A., Kanso, A., El Samrani, A.G., 2017. Trace metals in phosphate fertilizers used in eastern Mediterranean countries. Clean - Soil, Air, Water 45, 8. doi:10.1002/clen.201500988

Babbitt, B., 2002. What goes up, may come down. Bioscience 52, 656. doi:10.1641/0006-3568(2002)052[0656:WGUMCD]2.0.CO;2

Baruah, J., Kotoky, P., Sarma, J.N., 1997. Textural and geochemical study on river sediments: a case study on the Jhanji River. Indian Assoc. Sedimentol. 16, 195–206.

Blott, S.J., Pye, K., 2001. GRADISTAT: A grain size distribution and statistics package for the analysis of unconsolidated sediments. Earth Surf. Process. Landforms 26, 1237–1248. doi:10.1002/esp.261

Bonnefoy, D., Bourg, A., 1984. Estimation du fond géochimique naturel dans les sols et évaluation du niveau de pollutions dues aux activités humaines : cas du bassin versant de l'Orne, affluent de la Moselle. Beuilly-sur-Seine.

Carignan, J., Hild, P., Mevelle, G., Morel, J., Yeghicheyan, D., 2001. Routine analyses of trace elements in geological samples using flow injection and low pressure on-line liquid chromatography coupled to ICP-MS: A study of geochemical reference materials BR, DR-N, UB-N, AN-G and GH. Geostand. Geoanalytical Res. 25, 187–198. doi:10.1111/j.1751-908X.2001.tb00595.x

Dhivert, E., Grosbois, C., Courtin-Nomade, A., Bourrain, X., Desmet, M., 2016. Dynamics of metallic contaminants at a basin scale - Spatial and temporal reconstruction from four sediment cores (Loire fluvial system, France). Sci. Total Environ. 541, 1504–1515. doi:10.1016/j.scitotenv.2015.09.146

Dhivert, E., Grosbois, C., Coynel, A., Lefèvre, I., Desmet, M., 2015a. Influences of major flood sediment inputs on sedimentary and geochemical signals archived in a reservoir core (Upper Loire Basin, France). Catena 126, 75–85. doi:10.1016/j.catena.2014.10.030

Dhivert, E., Grosbois, C., Rodrigues, S., Desmet, M., 2015b. Influence of fluvial environments on sediment archiving processes and temporal pollutant dynamics (Upper Loire River, France). Sci. Total Environ. 505, 121–136. doi:10.1016/j.scitotenv.2014.09.082

Dokuz, A., Tanyolu, E., 2006. Geochemical constraints on the provenance, mineral sorting and subaerial weathering of Lower Jurassic and Upper Cretaceous clastic rocks of the eastern Pontides, Yusufeli (Artvin), NE Turkey. Turkish J. Earth Sci. 15, 181–209.

Dong, H., 2005. Interstratified illite-smectite: a review of contributions of TEM data to crystal chemical relations and reaction mechanisms. Clay Sci. 12, 6–12.

Eggleton, J., Thomas, K. V., 2004. A review of factors affecting the release and bioavailability of contaminants during sediment disturbance events. Environ. Int. 30, 973–980. doi:10.1016/j.envint.2004.03.001

Fanning, D., Fanning, M., 1989. Sulfidization and Sulfuricization, in: Soil Morphology, Genesis and Classification. John Wiley and Sons Inc., New York, pp. 69–80.

Fanning, D., Rabenhorst, M.C., Balduff, D., Wagner, D.P., Orr, R., Zurheide, P., 2010. An acid sulfate perspective on landscape/seascape soil mineralogy in the U.S. Mid-Atlantic region. Geoderma 154, 457–464. doi:10.1016/j.geoderma.2009.04.015

Fiedler, S., Vepraskas, M.J., Richardson, J.L., 2007. Soil Redox Potential: Importance, Field Measurements, and Observations, in: Advances in Agronomy. pp. 1–54. doi:10.1016/S0065-2113(06)94001-2

Fox, G.A., Purvis, R.A., Penn, C.J., 2016. Streambanks: A net source of sediment and phosphorus to streams and rivers. J. Environ. Manage. 181, 602–614. doi:10.1016/j.jenvman.2016.06.071

Freyssenet, M., 1979. La sidérurgie française : 1945 – 1979, l'histoire d'une faillite, les solutions qui s'affrontent. Savilli, <halshs-00165640>, Paris.

Friedl, G., Wüest, A., 2002. Disrupting biogeochemical cycles - Consequences of damming. Aquat. Sci. 64, 55–65. doi:10.1007/s00027-002-8054-0

Fryirs, K.A., Brierley, G.J., 2012. Sediment Movement and Deposition in River Systems, in: Geomorphic Analysis of River Systems: An Approach to Reading the Landscape. Wiley-Blackwell Publishing, Ltd, Chichester, UK, pp. 81–115. doi:10.1002/9781118305454.ch6

Garcier, R.J., 2007. Rivers we can't bring ourselves to clean – historical insights into the pollution of the Moselle River (France), 1850–2000. Hydrol. Earth Syst. Sci. 11, 1731–1745. doi:10.5194/hess-11-1731-2007

GEC, 2006. Klamath River, Dam and Sediment Investigation. (Gathard Engineering Consulting), Seatle, Washington, USA.

Grgic, D., Giraud, A., Auvray, C., 2013. Impact of chemical weathering on micro/macro-mechanical properties

References

of oolithic iron ore. Int. J. Rock Mech. Min. Sci. 64, 236–245. doi:10.1016/j.ijrmms.2013.09.005

Guillet, B., Burtin, G., Delcroix, P., Gury, M., 1984. Le fer des calcaires et des terra fusca des plateaux lorrains (France). Pedologie 3, 301–318.

Haque, N., Hughes, A., Lim, S., Vernon, C., 2014. Rare earth elements: overview of mining, mineralogy, uses, sustainability and environmental impact. Resources 3, 614–635. doi:10.3390/resources3040614

Heller-Kallai, L., Kalman, Z.H., 1972. Some naturally occurring illite-smectite interstratifications. Clays Clay Miner. 20, 165–168. doi:10.1346/CCMN.1972.0200308

Hogarth, D.D., Hartree, R., Loop, J., Solberg, T.N., 1985. Rare-earth element minerals in four carbonatites near Gatineau, Quebec. Am. Mineral. 70, 1135–1142.

Houhou, J., Lartiges, B.S., Hofmann, A., Frappier, G., Ghanbaja, J., Temgoua, A., 2009a. Phosphate dynamics in an urban sewer: A case study of Nancy, France. Water Res. 43, 1088–1100. doi:10.1016/j.watres.2008.11.052

Houhou, J., Lartiges, B.S., Montarges-Pelletier, E., Sieliechi, J., Ghanbaja, J., Kohler, A., 2009b. Sources, nature, and fate of heavy metal-bearing particles in the sewer system. Sci. Total Environ. 407, 6052–6062. doi:10.1016/j.scitotenv.2009.08.019

Hu, Z., Sparovek, G., Haneklaus, S., Schnug, E., 2006. Rare Earth Elements, in: Lal, R. (Ed.), Encyclopedia of Soil Science. CRC Press, pp. 1437–1441. doi:10.1081/E-ESS-120015983

Huot, H., Simonnot, M.O., Watteau, F., Marion, P., Yvon, J., De Donato, P., Morel, J.-L., 2014. Early transformation and transfer processes in a Technosol developing on iron industry deposits. Eur. J. Soil Sci. 65, 470–484. doi:10.1111/ejss.12106

Isobe, T., Nishiyama, H., Nakashima, A., Takada, H., 2001. Distribution and behavior of nonylphenol, octylphenol, and nonylphenol monoethoxylate in Tokyo metropolitan area: Their association with aquatic particles and sedimentary distributions. Environ. Sci. Technol. 35, 1041–1049. doi:10.1021/es001250i

Jacquat, O., Rambeau, C., Voegelin, A., Efimenko, N., Villard, A., Föllmi, K.B., Kretzschmar, R., 2011. Origin of high Zn contents in Jurassic limestone of the Jura mountain range and the Burgundy: evidence from Zn speciation and distribution. Swiss J. Geosci. 104, 409–424. doi:10.1007/s00015-011-0086-9

Jeanneau, L., Faure, P., 2010. Quantification of fossil organic matter in contaminated sediments from an industrial watershed: Validation of the quantitative multimolecular approach by radiocarbon analysis. Sci. Total Environ. 408, 4251–4256. doi:10.1016/j.scitotenv.2010.06.002

Jeanneau, L., Faure, P., Jardé, E., 2007. Influence of natural organic matter on the solid-phase extraction of organic micropollutants: Application to the water-extract from highly contaminated river sediment. J. Chromatogr. A 1173, 1–9. doi:10.1016/j.chroma.2007.09.080

Jeanneau, L., Faure, P., Montarges-Pelletier, E., 2008. Quantitative multimolecular marker approach to investigate the spatial variability of the transfer of pollution from the Fensch River to the Moselle River (France). Sci. Total Environ. 389, 503–513. doi:10.1016/j.scitotenv.2007.09.023

Jeanneau, L., Faure, P., Montargès-Pelletier, E., Ramelli, M., 2006. Impact of a highly contaminated river on a more important hydrologic system: changes in organic markers. Sci. Total Environ. 372, 183–192. doi:10.1016/j.scitotenv.2006.09.021

Kondolf, G.M., Gao, Y., Annandale, G.W., Morris, G. regory L., Jiang, E., Zhang, J., Yongtao, C., Carling, P., Fu, K., Guo, Q., Hotchkiss, R., Peteuil, C., Sumi, T., Wang, H.-W., Wang, Z., Wei, Z., Wu, B., Wu, C., Yang, C.T., 2014. Sustainable sediment management in reservoirs and regulated rivers: Experiences from five continents. Earth' s Futur. 2, 256–280. doi:10.1002/2013EF000184.of

Le Meur, M., Montargès-Pelletier, E., Bauer, A., Gley, R., Migot, S., Barres, O., Delus, C., Villiéras, F., 2016. Characterization of suspended particulate matter in the Moselle River (Lorraine, France): evolution along the course of the river and in different hydrologic regimes. J. Soils Sediments 16, 1625–1642. doi:10.1007/s11368-015-1335-8

Leroy, M., Merluzzo, P., Mahé-Le Carlier, C., Benoit, P., 2015. Archéologie du fer en Lorraine : minette et production du fer en bas fourneaux dans l'antiquité et au Moyen-Age. Fensch Vallée editions, Knutange.

Lesven, L., Lourino-Cabana, B., Billon, G., Recourt, P., Ouddane, B., Mikkelsen, O., Boughriet, A., 2010. On metal diagenesis in contaminated sediments of the Deûle river (northern France). Appl. Geochemistry 25, 1361–1373. doi:10.1016/j.apgeochem.2010.06.007

Li, H., Shi, A., Li, M., Zhang, X., 2013. Effect of pH, temperature, dissolved oxygen, and flow rate of overlying water on heavy metals release from storm sewer sediments. J. Chem. 2013, 1–11. doi:10.1155/2013/434012

Lisle, T.E., 1989. Sediment transport and resulting deposition in spawning gravels, north coastal California. Water Resour. Res. 25, 1303–1319. doi:10.1029/WR025i006p01303

Loring, D.H., Rantala, R.T.T., 1992. Manual for the geochemical analyses of marine-sediments and suspended particulate matter. Earth-Science Rev. 32, 235–283. doi:10.1016/0012-8252(92)90001-A

Louriño-Cabana, B., Lesven, L., Charriau, A., Billon, G., Ouddane, B., Boughriet, A., 2011. Potential risks of metal toxicity in contaminated sediments of Deûle river in Northern France. J. Hazard. Mater. 186, 2129–2137. doi:10.1016/j.jhazmat.2010.12.124

Lovley, D.R., Chapelle, F.H., 1995. Deep subsurface microbial processes. Rev. Geophys. 33, 365–381.

References

doi:10.1029/95RG01305

Maassen, S., Röske, I., Uhlmann, D., 2003. Chemical and microbial composition of sediments in reservoirs with different trophic state. Int. Rev. Hydrobiol. 88, 508–518. doi:10.1002/iroh.200310596

Mansfeldt, T., Dohrmann, R., 2004. Chemical and mineralogical characterization of blast-furnace sludge from an abandoned landfill. Environ. Sci. Technol. 38, 5977–5984. doi:10.1021/es040002+

Martin, J.M., Meybeck, M., 1979. Elemental mass-balance of material carried by major world rivers. Mar. Chem. 7, 173–206. doi:10.1016/0304-4203(79)90039-2

Matijević, S., Kušpilić, G., Kljaković-Gašpić, Z., 2007. The redox potential of sediment from the Middle Adriatic region. Acta Adriat. 48, 191–204.

McLennan, S.M., Taylor, S.R., 2012. Geology, Geochemistry, and Natural Abundances of the Rare Earth Elements, in: Atwood, D.A. (Ed.), The Rare Earth Elements: Fundamentals and Applications. Wiley, New York, pp. 1–19.

Meybeck, M., 1982. Carbon, nitrogen, and phosphorus transport by world rivers. Am. J. Sci. 282, 401–450. doi:10.2475/ajs.282.4.401

Meyers, P.A., 2003. Applications of organic geochemistry to paleolimnological reconstructions: a summary of examples from the Laurentian Great Lakes. Org. Geochem. 34, 261–289. doi:10.1016/S0146-6380(02)00168-7

Ministère de l'Environnement, 1985. Repartition et passage de polluants metalliques dans divers compartiments inertes et vivants d'un cours d'eau. Premiere partie: Estimation du degre de pollution metallique de l'eau, des matiere en suspension et des sediments de l'Orne, affluent de la Mose. Metz.

Montargès-Pelletier, E., Duriez, C., Ghanbaja, J., Jeanneau, L., Falkenberg, G., Michot, L.J., 2014. Microscale investigations of the fate of heavy metals associated to iron-bearing particles in a highly polluted stream. Environ. Sci. Pollut. Res. 21, 2744–2760. doi:10.1007/s11356-013-2192-x

Montargès-Pelletier, E., Jeanneau, L., Faure, P., Bihannic, I., Barres, O., Lartiges, B.S., 2007. The junction of Fensch and Moselle rivers, France; mineralogy and composition of river materials. Environ. Geol. 53, 85–102. doi:10.1007/s00254-006-0621-6

Naden, P., 2010. The Fine-Sediment Cascade, in: Burt, T., Allison, R. (Eds.), Sediment Cascades: An Integrated Approach. John Wiley & Sons, West Sussex, pp. 271–305.

Négrel, P., Merly, C., Gourcy, L., Cerdan, O., Petelet-Giraud, E., Kralik, M., Klaver, G., van Wirdum, G., Vegter, J., 2014. Soil–Sediment–River Connections: Catchment Processes Delivering Pressures to River Catchments, in: Brils, J., Brack, W., Müller-Grabherr, D., Négrel, P., Vermaat, J.E. (Eds.), Risk-Informed Management of European River Basins. Springer Berlin Heidelberg, New York, Dordrecht, London, pp. 21–52. doi:10.1007/978-3-642-38598-8_2

Nichols, G., 2009a. Terrigenous Clastic Sediments: Gravel, Sand and Mud, in: Sedimentology and Stratigraphy. Wiley-Blackwell, Oxford, UK, UK, pp. 5–27.

Nichols, G., 2009b. Introduction: Sedimentology and Stratigraphy, in: Sedimentology and Stratigraphy. Wiley-Blackwell, Oxford, UK, pp. 1–4.

Nichols, G., 2009c. Biogenic, Chemical and Volcanic Sediments, in: Sedimentology and Stratigraphy. Wiley-Blackwell, Oxford, UK, pp. 28–43.

Pederson, J.P., 2004. International Directory of Company Histories. St James Press, Detroit.

Ramanathan, A.L., Rajkumar, K., Majumdar, J., Singh, G., Behera, P.N., Santra, S.C., Chidambaram, S., 2009. Textural characteristics of the surface sediments of a tropical mangrove Sundarban ecosystem India. Indian J. Mar. Sci. 38, 397–403.

Rivard, C., Montargès-Pelletier, E., Vantelon, D., Pelletier, M., Karunakaran, C., Michot, L.J., Villiéras, F., Michau, N., 2013. Combination of multi-scale and multi-edge X-ray spectroscopy for investigating the products obtained from the interaction between kaolinite and metallic iron in anoxic conditions at 90 °C. Phys. Chem. Miner. 40, 115–132. doi:10.1007/s00269-012-0552-6

Robert, A., 2014. Fluvial Sediments: Processes of Erosion and Transport, in: River Processes: An Introduction to Fluvial Dynamics. Routledge, London, pp. 51–90.

Seiter, K., Hensen, C., Schröter, J., Zabel, M., 2004. Organic carbon content in surface sediments - Defining regional provinces. Deep. Res. Part I Oceanogr. Res. Pap. 51, 2001–2026. doi:10.1016/j.dsr.2004.06.014

Shrestha, P., Su, S., James, S., Shaller, P., Doroudian, M., Firstenberg, C., Thompson, C., 2014. Conceptual site model for Newark Bay—Hydrodynamics and sediment transport. J. Mar. Sci. Eng. 2, 123–139. doi:10.3390/jmse2010123

Singh, P., 2010. Geochemistry and provenance of stream sediments of the Ganga River and its major tributaries in the Himalayan region, India. Chem. Geol. 269, 220–236. doi:10.1016/j.chemgeo.2009.09.020

Singh, P., 2009. Major, trace and REE geochemistry of the Ganga River sediments: Influence of provenance and sedimentary processes. Chem. Geol. 266, 242–255. doi:10.1016/j.chemgeo.2009.06.013

Singh, P., Rajamani, V., 2001. REE geochemistry of recent clastic sediments from the Kaveri floodplains, southern India: Implication to source area weathering and sedimentary processes. Geochim. Cosmochim. Acta

References

65, 3093–3108. doi:10.1016/S0016-7037(01)00636-6
Sivry, Y., Riotte, J., Sonke, J.E., Audry, S., Schäfer, J., Viers, J., Blanc, G., Freydier, R., Dupré, B., 2008. Zn isotopes as tracers of anthropogenic pollution from Zn-ore smelters The Riou Mort–Lot River system. Chem. Geol. 255, 295–304. doi:10.1016/j.chemgeo.2008.06.038
Snyder, N.P., Allen, J.R., Dare, C., Hampton, M.A., Schneider, G., Wooley, R.J., Alpers, C.N., Marvin-DiPasquale, M.C., 2004. Sediment grain-size and loss-on-ignition analyses from 2002 Englebright Lake coring and sampling campaigns. USGS, Santa Cruz, Menlo Park, Sacramento, USA.
Søndergaard, M., Jensen, J.P., Jeppesen, E., 2003. Role of sediment and internal loading of phosphorus in shallow lakes. Hydrobiologia 506–509, 135–145. doi:10.1023/B:HYDR.0000008611.12704.dd
Søndergaard, M., Kristensen, P., Jeppesen, E., 1992. Phosphorus release from resuspended sediment in the shallow and wind-exposed Lake Arreso, Denmark. Hydrobiologia 228, 91–99.
Srodon, J., 1981. X-ray identification of randomly interstratified illite-smectite in mixtures with discrete illite. Clay Miner. 16, 297–304.
Taylor, S.R., McLennan, S.M., 1985. The Continental Crust: Its Composition and Evolution. Blackwell Scientific Pub.,Palo Alto, CA.
Teyssen, T., 1984. Sedimentology of the Minette oolitic ironstones of Luxembourg and Lorraine: a Jurassic subtidal sandwave complex. Sedimontology 31, 195–211. doi:10.1111/j.1365-3091.1984.tb01959.x
Van Damme, A., Degryse, F., Smolders, E., Sarret, G., Dewit, J., Swennen, R., Manceau, A., 2010. Zinc speciation in mining and smelter contaminated overbank sediments by EXAFS spectroscopy. Geochim. Cosmochim. Acta 74, 3707–3720. doi:10.1016/j.gca.2010.03.032
Viers, J., Dupré, B., Gaillardet, J., 2009. Chemical composition of suspended sediments in World Rivers: New insights from a new database. Sci. Total Environ. 407, 853–868. doi:10.1016/j.scitotenv.2008.09.053
Wang, G., Wu, B., Wang, Z.Y., 2005. Sedimentation problems and management strategies of Sanmenxia Reservoir, Yellow River, China. Water Resour. Res. 41, 1–17. doi:10.1029/2004WR003919
Whiting, P.J., Stamm, J., 1995. The hydrology and form of spring-dominated channels. Geomorphology 12, 233–240. doi:10.1016/0169-555X(95)00006-Q
Wildi, W., 2010. Environmental hazards of dams and reservoirs, NEAR Curriculum in Natural Environmental Science. Terre Environ. 88, 187–197.

IV. APPENDIX TO CHAPTER 3: CHEMICAL COMPOSITION OF SEDIMENTS OF THE MOSELLE RIVER AND TRIBUTARIES

1. Introduction

In the previous *chapter,* several Orne River sediments were described. The chemical and mineralogical composition was discussed according to the lithology of the watershed, former activities and land use. Possible sources of the chemicals and minerals were also indicated. Orne River sediments will be compared to sediments of the Moselle River and tributaries. At the scale of the Moselle watershed, the varying contributions of lithology, land cover and land use on sediment chemical composition can be revealed. Therefore, the aim of this appendix is to show the contribution of land use, land cover and lithology on the chemical composition of sediments located in the Moselle River on one hand, and to compare them to sediments of the Orne River and other tributaries on the other.

2. Study area and sampling sites

The Moselle River 544 km long, it starts from France, passes through Luxembourg and then joins the Rhine River at Koblenz, Germany. The Rhine River then passes through the Netherlands and finally reaches the North Sea after a path of circa 329 km. The Moselle River watershed has a 28,280 km^2 area; more than 50% of the basin and most of the river heads are located in France, 15% of the basin in Luxembourg, and the rest in Germany (Garcier, 2007). Several samples were collected in the Moselle watershed, some of which belong to the Moselle River, and others that belong to tributaries. Sediments were collected from Jarménil, Dinozé, Thaon les Vosges and Tonnoy (most upstream part of the Moselle River); Pont Saint Vincent (Madon River, before the confluence with the Moselle River); Méreville and Liverdun (Moselle River); Bouxiéres (Meurthe River, a Moselle River tributary located downstream the city of Nancy); Millery, Jouy and Ay sur Moselle (Moselle River, located upstream the confluence with the Orne River); Moselle River before the confluence with the Fensch River (Moselle-Up-Fensch); Florange (Fensch River, a Moselle River tributary); and Catennom and Sierck (Moselle River, most downstream sites) (Figure IV-1). Those sediments were collected during 2003 – 2004 sampling campaigns.

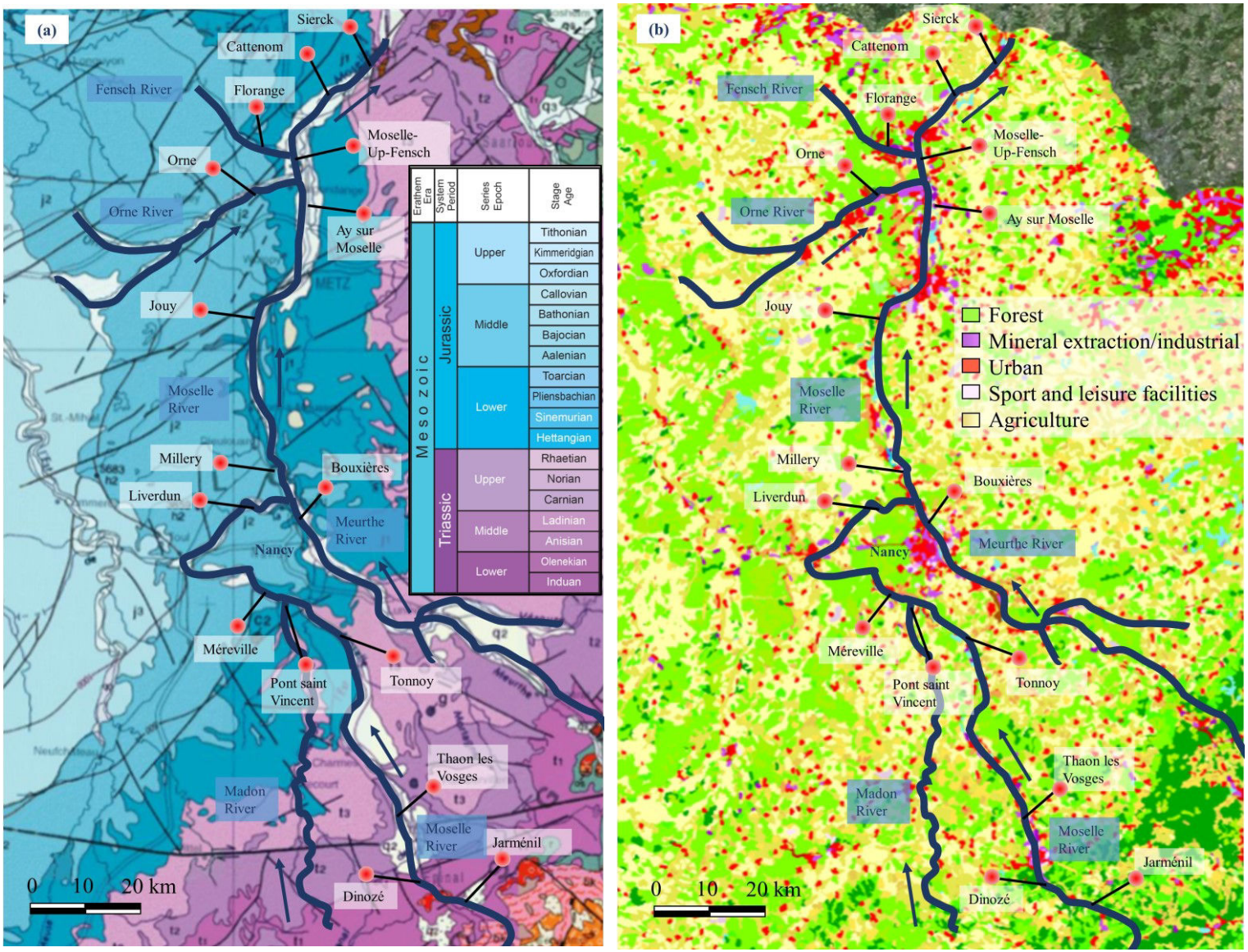

Figure IV-1: Geology (a) and land use (b) maps of the French part of the Moselle watershed.
The maps were created on the basis of data provided by the French National Institute of Geography "IGN", www.geoportail.gouv.fr. and Corine Land Cover 2006.
It should be noted that not all Moselle tributaries are included in the maps.

3. Sediment preparation for analyses

Grab surface sediments were collected from the sites mentioned above. The samples were wet sieved on site using adjacent river water (to include only the < 2 mm fraction), frozen, freeze-dried, ground and analyzed for chemical composition. A fraction < 50 µm was also sieved on site; however, those data won't be discussed. Chemical composition of the 0 – 2 mm fraction of the samples was determined similarly to Orne sediments (presented in the previous *chapter*); i.e. according to Carignan et al., (2001).

4. Chemical composition of sediments of the Moselle River and tributaries

The chemical composition of sediments collected from the Moselle River and some tributaries, including the Orne River, will be discussed according to lithology, land use and land cover. The lithology is variable along the course of the Moselle River, especially between Jarménil (JAR), Dinozé (DIN), Thaon les Vosges (TLV) and Tonnoy (TON) on one hand, and Méreville (MER), Liverdun (LIV), Millery (MIL), Jouy (JOY), Ay sur Moselle (ASM), Cattenom (CAT) and Sierck (SIE) on the other (the abbreviations are also included in Table IV-1). The first samples of the Moselle River (JAR till TON) are located in the geological formation made from dolostone (rock made from dolomite), shales/claystones (compressed clays and silt minerals) and evaporites (rock resulting from salt water evaporation), which had formed in the late Triassic period (~ 220 Ma) (Figure IV-1 a). As a result, sediments that had formed from the weathering of the basin's lithology are expected to be enriched with K, Al and Si (from shale and evaporite erosion and weathering). Indeed, K, Si and to a lesser extent Al, showed to be mostly enriched in the sediments located in the most upstream part of the Moselle River (Figure IV-2 and Table IV-1), which then decreased for the sediments located in the downstream part. For example, K contents decreased from 3.6 to 1.7% and Si decreased from 39 to 29% between the most upstream and most downstream sediments; indicating that the fingerprint, of the weathered materials from the late Triassic formation, faded along the Moselle River course. After Tonnoy, the Moselle River flows in the Jurassic formation; lower Jurassic to the right of the Moselle River and middle Jurassic to the left (Figure IV-1 a). As the formation is mainly made from carbonaceous substratum, the sediments that have formed from substratum weathering should be relatively enriched with Ca, in comparison to samples found in the upstream zone. Indeed, Ca contents started to protrude after Tonnoy, while sediments JAR till TON showed only slight Ca contents (Table IV-1). The increase of Ca comes natural

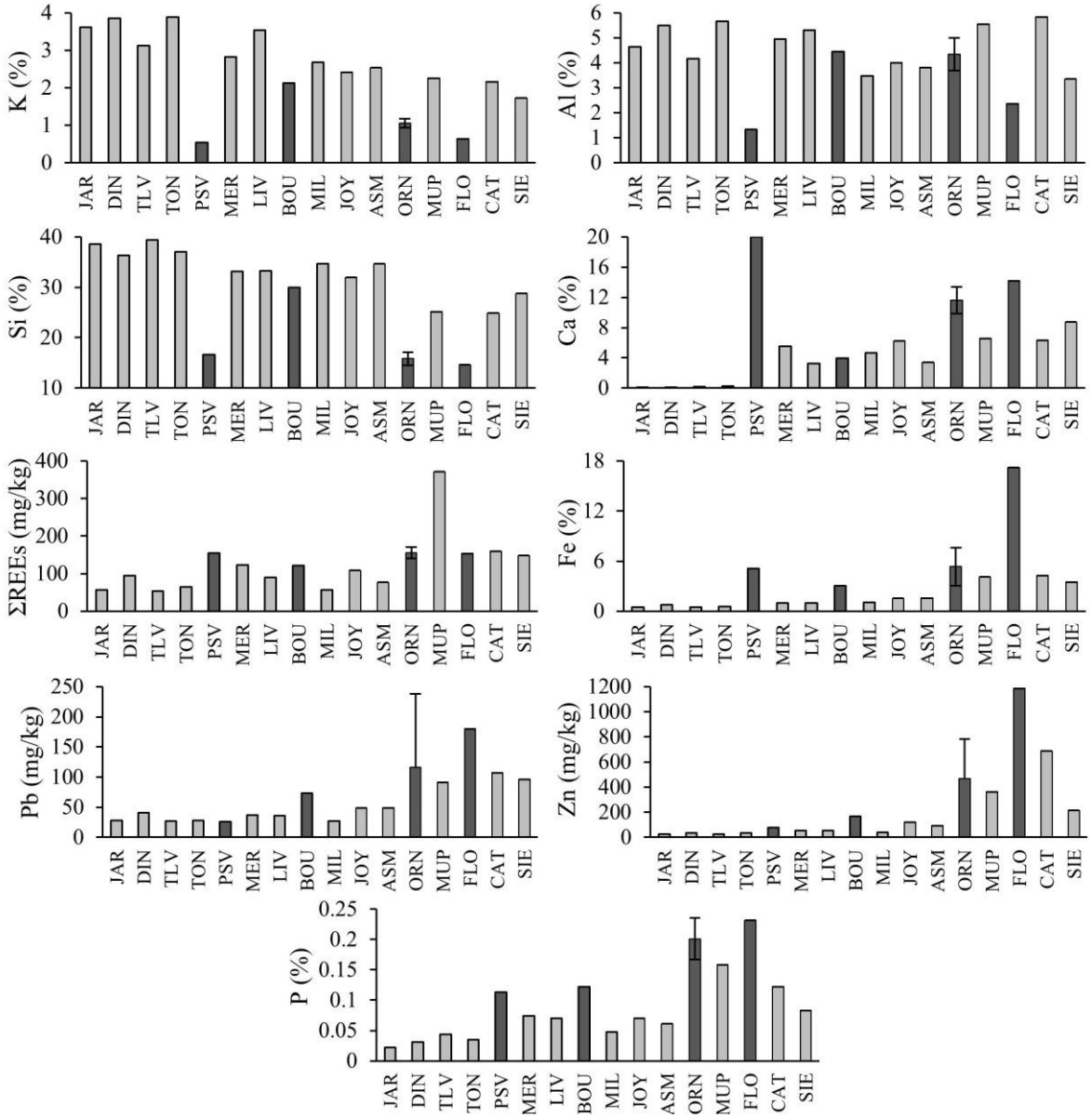

Figure IV-2: Chemical composition of sediments of the Moselle River and tributaries.
The contents of K (%), Al (%), Si (%), Ca (%), REEs (mg/kg), Fe (%), Pb (mg/kg), Zn (mg/kg) and P (%) for Moselle River sediments are indicated in grey, those of tributaries are indicated in black. For clearer visualization of low contents, the same chemical composition values are compiled in Table IV-1.

due to the weathering of the carbonaceous materials of the Jurassic environment. This is mainly seen in the sediment collected from the tributaries, namely PSV (just before the confluence with the Moselle River), ORN and FLO. Additionally, sediments of those tributaries generally showed lower K and Si values in comparison to Moselle sediments, which, again, is due to the change in geological formation. Moreover, K and Si contents in sediments after the confluence with tributaries showed lower values (e.g. decrease of K and Si from TON to MER, after the confluence with PSV). That decrease might be explained by the input of K and Si poor sediments from the tributaries to the Moselle River, or by the fading contribution of the upstream zone (JAR to TON) of the Moselle River.

In addition, REEs showed a general increase in the downstream course. Land cover and land use also influence the chemical composition of sediments. The carbonaceous waters coming from PSV might carry agricultural fingerprints (Figure IV-1 b), especially since REEs were also enriched in PSV. Despite the usage of REEs to reveal lithogenic inputs caused by erosion of parent materials (Wen et al., 2014), they might be introduced into sediments as a result of agricultural practices (Hu et al., 2006), and are also found as phosphate (e.g. monazite and xenotime), silicate (e.g. gadolinite and allanite) and carbonate minerals (e.g. bastnaesite and parisite) (Haque et al., 2014). In the case of Moselle sediments, the contents of REEs followed a behavior similar to calcium, which could be seen by a common trend between REEs and Ca, mainly between PSV and ORN (Figure IV-2). Indeed, parisite is a REE rich carbonate, and the possibility of REEs diffusion in calcite (Cherniak, 1998; Terakado and Masuda, 1988) might suggest that at least part of the REEs are carried as carbonates. The possibility of REEs association to phosphate minerals is not excluded, since REEs and P contents also showed common trends (Figure IV-2). The aforementioned elements were used to indicate lithogenic contributions, mainly based on the geological formations of the region.

The sediment samples collected from the tributaries, namely BOU, ORN and FLO, showed enriched Pb, Zn and P contents; those sediments are found in urbanized areas, such as the city and suburbs of Nancy (Figure IV-1 b). Those elements are introduced from anthropogenic inputs, such as domestic waters and industrial effluents (Adriano, 2001; Meybeck, 1982; Owens and Walling, 2002). Being smaller sized rivers, Pb, Zn and P inputs into tributary sediments might be more prominent than Moselle River sediments. In other words, the same contribution might be less prominent in Moselle River sediments due to dilution of the metal content by the introduction of lithogenic materials. It should be noted that Orne River sediments had varying metal contents along the river course, which explain the relatively high standard deviations in Figure IV-2, mainly for Zn and Pb (the variation was elaborated in the previous *chapter*). Fe can be included in the previously discussed elements. Moreover, the case of Fe is more specific, since the area in the Orne and Fensch watersheds were active with steelmaking facilities; which stopped in 1988 in the studied Orne River section and 2006 in the Fensch River region. Indeed, ORN and FLO were the most Fe-enriched sediments. Another possible source of Fe in sediments is the weathering of the Aalenian formation located in the Pays-Haut region in the Orne and Fensch watersheds (Bonnefoy and Bourg, 1984; Teyssen, 1984).

Table IV-1: Chemical composition of sediments of the Moselle River and tributaries.
The contents of K (%), Al (%), Si (%), Ca (%), ΣREEs (mg/kg), Fe (%), Pb (mg/kg), Zn (mg/kg) and P (%) for Moselle River sediments and tributaries (highlighted) are compiled. The data presented in the table are the same as those plotted in Figure IV-2.

Sample name and abbreviation		K (%)	Al (%)	Si (%)	Ca (%)	ΣREEs (mg/kg)	Fe (%)	Pb (mg/kg)	Zn (mg/kg)	P (%)
Jarménil	JAR	3.6	4.7	39	0.1	57	0.5	28	26	0.02
Dinozé	DIN	3.9	5.5	36	0.1	95	0.7	41	35	0.03
Thaon les Vosges	TLV	3.1	4.2	39	0.2	53	0.5	27	26	0.04
Tonnoy	TON	3.9	5.7	37	0.3	65	0.6	28	33	0.03
Pont saint Vincent	PSV	0.5	1.3	17	20.0	154	5.1	26	78	0.11
Méreville	MER	2.8	4.9	33	5.5	123	1.0	37	54	0.07
Liverdun	LIV	3.5	5.3	33	3.2	90	1.0	36	55	0.07
Bouxières	BOU	2.1	4.5	30	3.9	121	3.1	74	170	0.12
Millery	MIL	2.7	3.5	35	4.6	57	1.1	27	39	0.05
Jouy	JOY	2.4	4.0	32	6.2	108	1.5	49	122	0.07
Ay sur Moselle	ASM	2.5	3.8	35	3.4	77	1.6	49	93	0.06
Orne	ORN	1.1 ± 0.1	4.3 ± 0.7	16 ± 1	11.6 ± 1.9	156 ± 15	5.3 ± 2.3	117 ± 121	467 ± 316	0.20 ± 0.03
Moselle-UP-Fensch	MUP	2.3	5.6	25	6.6	371	4.1	91	362	0.16
Florange	FLO	0.6	2.4	15	14.2	153	17.2	180	1187	0.23
Cattenom	CAT	2.2	5.8	25	6.4	159	4.3	107	686	0.12
Sierck	SIE	1.7	3.4	29	8.7	148	3.5	97	214	0.08

5. Conclusion

The chemical composition of sediments collected along the course of the Moselle River and tributaries were determined. The possible introduction of elements was discussed according to the geology of the area, land use and land cover. It was shown that the lithogenic contribution could easily be seen, mainly in the most upstream zone of the Moselle River and by the gradual fading of K, Al and Si contents in the downstream zone on one hand, and by the protrusion of Ca contents downstream Tonnoy on the other. That variation is mainly explained by the change in geological formation from Triassic to Jurassic. The influence of urbanization could also be seen by the chemical composition of sediments, mainly by increasing contents of Pb, Zn and P in tributary sediments belonging to urbanized zones, such as BOU (Meurthe River) located downstream the city and suburbs of Nancy. Iron might also be related to urbanization and industrialization, more precisely to the former steelmaking facilities that were active in the Orne and Fensch watersheds. Finally, it is important to recognize the geological formation, land use and land cover when the chemical, as well as mineralogical, composition of sediments is to be revealed.

References

Adriano, D.C., 2001. Trace Elements in Terrestrial Environments: Biogeochemistry, Bioavailability and Risks of Metals, 2nd ed. Springer, New York, NY. doi:10.1007/978-0-387-21510-5

Bonnefoy, D., Bourg, A., 1984. Estimation du fond géochimique naturel dans les sols et évaluation du niveau de pollutions dues aux activités humaines : cas du bassin versant de l'Orne, affluent de la Moselle. Beuilly-sur-Seine.

Carignan, J., Hild, P., Mevelle, G., Morel, J., Yeghicheyan, D., 2001. Routine analyses of trace elements in geological samples using flow injection and low pressure on-line liquid chromatography coupled to ICP-MS: A study of geochemical reference materials BR, DR-N, UB-N, AN-G and GH. Geostand. Geoanalytical Res. 25, 187–198. doi:10.1111/j.1751-908X.2001.tb00595.x

Cherniak, D.J., 1998. REE diffusion in calcite. Earth Planet. Sci. Lett. 160, 273–287.

Garcier, R.J., 2007. Rivers we can't bring ourselves to clean – historical insights into the pollution of the Moselle River (France), 1850–2000. Hydrol. Earth Syst. Sci. 11, 1731–1745. doi:10.5194/hess-11-1731-2007

Haque, N., Hughes, A., Lim, S., Vernon, C., 2014. Rare earth elements: overview of mining, mineralogy, uses, sustainability and environmental impact. Resources 3, 614–635. doi:10.3390/resources3040614

Hu, Z., Sparovek, G., Haneklaus, S., Schnug, E., 2006. Rare Earth Elements, in: Lal, R. (Ed.), Encyclopedia of Soil Science. CRC Press, pp. 1437–1441. doi:10.1081/E-ESS-120015983

Meybeck, M., 1982. Carbon, nitrogen, and phosphorus transport by world rivers. Am. J. Sci. 282, 401–450. doi:10.2475/ajs.282.4.401

Owens, P.N., Walling, D.E., 2002. The phosphorus content of fluvial sediment in rural and industrialized river basins. Water Res. 36, 685–701. doi:10.1016/S0043-1354(01)00247-0

Terakado, Y., Masuda, A., 1988. The coprecipitation of rare-earth elements with calcite and aragonite. Chem. Geol. 69, 103–110. doi:10.1016/0009-2541(88)90162-3

Teyssen, T., 1984. Sedimentology of the Minette oolitic ironstones of Luxembourg and Lorraine: a Jurassic subtidal sandwave complex. Sedimontology 31, 195–211. doi:10.1111/j.1365-3091.1984.tb01959.x

Wen, X.-Y., Huang, C.-M., Tang, Y., Gong-Bo, S.-L., Hu, X.-X., Wang, Z.-W., 2014. Rare earth elements: a potential proxy for identifying the lacustrine sediment source and soil erosion intensity in karst areas. J. Soils Sediments 14, 1693–1702. doi:10.1007/s11368-014-0928-y

V. CHAPTER 4: IRON MINERALOGY AS A FINGERPRINT OF FORMER STEELMAKING ACTIVITIES IN RIVER SEDIMENTS

Hussein Jaafar Kanbar[a,b,c*], Emmanuelle Montargès-Pelletier[a,b*], Benoit Losson[d], Isabelle Bihannic[a,b], Renaud Gley[a,b], Allan Bauer[a,b], Frederic Villieras[a,b], Luc Manceau[d], Antoine G El Samrani[c], Veronique Kazpard[c], Laurence Mansuy-Huault[a,b]

[a] CNRS, LIEC (Laboratoire Interdisciplinaire des Environnements Continentaux), LTER Zone Atelier Moselle, 54500 Vandœuvre-lès-Nancy, France.
[b] Université de Lorraine, LIEC (Laboratoire Interdisciplinaire des Environnements Continentaux), UMR 7360, 54500 Vandœuvre-lès-Nancy, France.
[c] Research and Analysis Platform for Environmental Sciences (PRASE), Doctoral School of Sciences and Technology (EDST); Faculty of Sciences; Lebanese University, P.O. 5, Rafic Hariri Campus, 1003 Hadat, Lebanon.
[d] Université de Lorraine, LOTERR, UFR SHS-Metz, Ile du Saulcy, CS60228, 57045 Metz cedex 01, France.
* Corresponding authors: Hsen.kanbar@gmail.com; emmanuelle.montarges@univ-lorraine.fr

Published in the journal of *Science of the Total Environment, Volume 599-600, pp:* 540-553; https://dx.doi.org/10.1016/j.scitotenv.2017.04.156

Abstract

Submerged sediment cores were collected upstream of a dam in the Orne River, northeastern France. This dam was built in the context of steelmaking to constitute a water reservoir for blast furnace cooling and wet cleaning of furnace smokes. The dam also enhanced sediment deposition in the upstream zone. This study was performed to unravel the contamination status of sediments and to evidence possible contribution sources. The sediment layers were analyzed for water content, grain size, chemical composition, crystalline phases at a bulk scale and poorly crystalline and amorphous phases at a sub-micrometer scale. Visual aspect, texture, color, and chemical and mineralogical analyses showed that the settled sediments were mainly composed of fine black matter, certainly comprising steelmaking by-products or wastes. Those materials were highly enriched with Fe, Zn, Pb and other trace metals, except for a relatively thin layer of surficial sediments that had settled more recently. Bulk mineralogy revealed crystalline iron minerals, such as magnetite, goethite, wuestite and pyrite, in the deep layers of the sediment cores. Furthermore, microscopic investigations evidenced the presence of ferrospheres, goethite nanoparticles and newly formed Fe-aluminosilicates; all

originating from the former steelmaking facilities. The variation of iron mineralogy, combined with specific chemical profiles and other sediment features, demonstrate different contributions that constitute the sediment deposit. Furthermore, chemical and mineralogical features of goethite and Fe-aluminosilicates could be used as a fingerprint for such contaminated sediments.

Keywords: *Sediment archives, Steelmaking sludge, Iron mineralogy, Fe-aluminosilicates.*

1. Introduction

River sediments are recognized as reservoirs of various pollutants, such as chemicals (e.g. nitrates, pesticides, medical drugs, organic micropollutants and metals) and microbes (e.g. viruses, bacteria and parasites) (Droppo et al., 2009; Grabowski et al., 2011 and references therin; Heise and Förstner, 2007; Hudson-Edwards et al., 2008). Furthermore, surface waters are often common receptacles of anthropogenic pollutants from diverse origins, which once combined to particulate matter, might settle and enrich the sediment compartment. A concern could arise if contaminated sediments are then translocated downstream, which might be caused by specific seasonal or hydroclimatic events (Droppo et al., 2009). It is also commonly assumed that the contaminants in sediments can be several orders of magnitude higher than in overlying water, and consequently constitute a threat for stream quality (Cappuyns et al., 2006; Simpson et al., 1998). In European and North-American countries, studies dealing with sediment cores have shown that contaminant inputs into sediments were maximized in the 1960s, and then decreased due to the improvement in environmental regulations (Ayrault et al., 2012; Dhivert et al., 2016; Ferrand et al., 2012; Wakeham et al., 2004).

Northern and northeastern France had been very active with mining (such as iron, coal and salt) and metallurgical (such as Zn and Fe) activities during the last century (Lesven et al., 2010; Lourino-Cabana et al., 2010; Montargès-Pelletier et al., 2014, 2007, Sterckeman et al., 2002, 2000). Industrial facilities were commonly established close to rivers to ensure a water source for cooling of furnaces. This was the case in Lorraine, where several rivers in the Moselle watershed, like the Orne, Fensch and Rosselle Rivers, were physically, chemically and biologically modified by steelmaking activities, including iron ore mining and coke production (Garcier, 2007; Picon, 2014). Because they were strongly impacted by the industrial activity, those small valleys were referred to as “steelmaking valleys”. Waste products, furnace smokes, dust and sludge from wet cleaning of furnace smokes had been introduced in the aqueous media, transported as suspended particulate matter (SPM) or stored more or less definitely in river sediments. The possible metal release due to resuspension upon flooding (Vdović et al., 2006; Zebracki, 2008) or sediment dredging (Lesven et al., 2010), as well as selective remobilization of metal bearing phases (Montargès-Pelletier et al., 2014) were studied and reported to evidence the possible impact of contaminated sediments. Furthermore, polluted sediment remobilization was shown to cause socioeconomical, ecological and environmental problems (e.g. Fernandes et al., 2016; Macklin et al., 1997; Maclin and Sicchio, 1999). For example, the

removal of the Fort Edward Dam (Hudson River) caused the remobilization of polluted sediments for tens of kilometers in the downstream region. As a result, more than 40 distinct "polluted sites" had formed and the biota and water quality were severely damaged for a period of nearly thirty years (Maclin and Sicchio, 1999).

Many studies focused on speciation and evolution of elements in contaminated river sediments (e.g. Roberts et al., 2002; Spadini et al., 2003; Sterckeman et al., 2000; Van Damme et al., 2010; Zeng et al., 2013), or the speciation of metals in weathered blast furnace sludge from landfills or ponds (e.g. Huot et al., 2013; Kretzschmar et al., 2012; Mansfeldt and Dohrmann, 2004). In order to understand the fate of steelmaking by-products, there is a need for detailed knowledge of the raw materials used, the processes undertaken, and the possible ageing and transformations taking place within the sediment matrix. Therefore, this study focuses on the mineralogy of river sediments that have accumulated upstream of a dam in an area that was highly influenced by steelmaking processes during the last century. The objectives of the study are to i) characterize the sediments that had settled upstream of the dam, ii) identify the layers and phases of lithogenic and anthropogenic sources and iii) follow the Fe-bearing mineral species in the vertical sediment profile. For that purpose, the present study investigates global parameters, chemical composition, as well as iron mineralogy of the sediments. The objectives are attained by using a combination of techniques, mainly X-ray diffraction and scanning and transmission electron microscopies.

2. Materials and Methods

2.1. Study area

During the XXth century, steelmaking activities were very intense in the Lorraine region, and in 1938, as much as 67% of the total French steel was produced in Lorraine. In 1974, when the French steel production was at its maximum (25 million tons per year "Mt/yr"), the production in Lorraine was about 8 Mt/yr. The steel or iron basin in Lorraine covered a 60 km long and 40 km wide area, subdivided into several compartments, one of which was the Orne valley. The Orne River, a tributary of the Moselle River, flows in northeastern France (Figure V-1 a), is 90 km long, has a drainage basin of 1,226 km^2, and displays a mean discharge of 12.2 m^3/s at the junction with the Moselle River. Several small sized dams were built in the Orne River to create water reservoirs for industrial purposes. The production of steel encountered the highest expansion period from 1954 to 1960. Thus, at the end of the 50's, two new blast furnaces were installed on the left bank of the Orne River, located within the limits

of Moyeuvre-Grande city area, and close to the iron mine of Jœuf «Mine du Haut Fond» (Figure V-1 b). Those two blast furnaces were active from 1960 until 1988, with a steel production of about 1.3 Mt/yr (Freyssenet, 1979). In the same period, Beth dam was built to provide high volumes of water for the general functioning of steelmaking facilities (Figure V-1 b and Supplementary Material "SM V-1"). Two other sets of blast furnaces were previously installed along the Orne River, one set at the exit of Jœuf city (active from 1882 to 1970), and another set in the center of Moyeuvre-Grande city (active from 1918 to 1975) (Figure V-1 b). The blast furnaces were fed with ore extracted from the nearby iron mine; the ore was partially sintered before its introduction in furnaces (about 64% in 1967), producing about 2.4 Mt/yr.

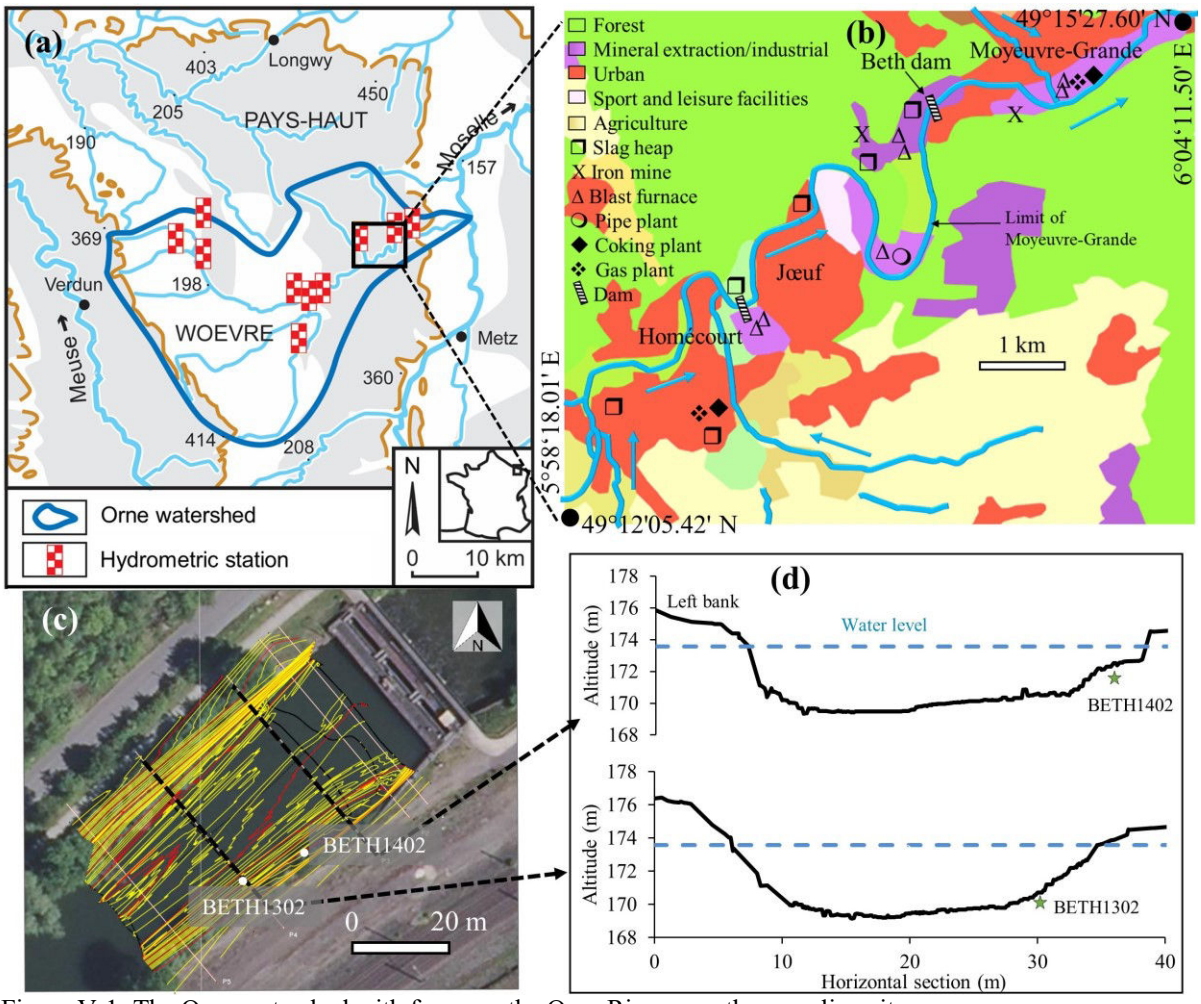

Figure V-1: The Orne watershed with focus on the Orne River near the sampling site.
a: The Orne watershed located northeastern France. Map created on the basis of data provided by the French National Institute of Geography IGN, www.geoportail.gouv.fr, b: the Orne River section that was studied, the land use established in 2006 (Corine Land Cover 2006) and the former locations of industrial facilities, c: the upstream zone of Beth dam showing the locations of BETH1302 and BETH1402 cores (white dots), the altitude lines (yellow and red lines are drawn as intervals of 0.2 m and 1 m variation in altitude, respectively), the measurement lines (in black) and the horizontal sections of the river where the profiles of the riverbed were produced (dashed black lines), which are shown in "d"; the profiles were produced using an echo sounder.

Generally speaking, for this part of the Orne valley, the steelmaking activities and related industrial activities (iron mining, coke and gas production) resulted in a strong contamination of soils and aqueous media, with the spreading of materials enriched in iron, other metallic elements and persistent organic pollutants, such as polycyclic aromatic hydrocarbons (PAHs). In 1988, dredging of the Orne River was performed from Jœuf to Moyeuvre, stopping at the limit of Moyeuvre city area. Thus, the dredging operation removed most of the highly contaminated sediments (Garcier, 2007; Picon, 2014), but did not concern the sediment deposits in the upstream part of the Beth dam. This dam should be partially modified or completely removed in the coming decade, with consequent questioning about the fate of the highly anthropogenic sediments located near the right bank of the river.

2.2. Sediment coring

Three sediment cores were collected at distinct locations upstream of the Beth dam. The lengths of the cores were 96 (BETH1302), 131 (BETH1402) and 18 cm (BETH1507). The submerged sediments were cored with a piston corer (or Beeker corer) directly from the bank (in July 2013, the dam was emptied for three days), or from a floating platform (2014 and 2015 coring, Quadriraft from GEHCO laboratory, Tours University, France). BETH1402 and BETH1302 cores were 2 and 4 m away from the right bank, respectively (Figure V-1: c – d). Most analyses were performed on BETH1402 core (131 cm). In addition, the purpose of the third core (BETH1507) was to check the thickness of recent sediments lying above the highly contaminated ones by steelmaking waste on one hand, and also to estimate the longitudinal extent of this sedimentary deposit.

2.3. Sample preparation for analyses

The collected sediment cores were sealed from air and transported back to the laboratory in a vertical position. It should be noted that the visual aspect of BETH1402 core was rather homogeneous along the 131 cm of extracted matter, with no eye detectable variation along the sediment profile, except for brown colored materials found at the surface (11 cm). Furthermore, the uppermost 2 cm layer was highly loose and muddy, and thus was taken as the surface layer. Afterwards, 3 cm thick layers were taken. For each layer, a small aliquot was frozen at -80°C for microscopic and spectroscopic analyses; another aliquot was put in pre-weighed containers, frozen, freeze-dried and a part was ground using an agate mortar and pestle.

2.4. Physical properties of sediments

For each layer, the water content was calculated by the difference in mass between the fresh and the freeze-dried samples. Also, a raw aliquot (not ground) of the freeze-dried sample was used to determine the particle size distribution (PSD) by laser diffraction (Sympatec GmbH, LIEC). The sample was gently disaggregated using a plastic spatula and introduced into the Sucell dispersing unit (containing distilled water) where the sample was circulating and being ultra-sonicated for 60 seconds. Duplicate or triplicate measurements were performed to improve the measurement quality. The particle size distribution was then presented as volumetric percentage as a function of particle diameter. In addition, the percentiles (D*i*) of the particles were calculated using Helos software. D_i is the i^{th} percentile, i.e. the particle's diameter at which *i* % of the particles in the sample is smaller than D_i (in µm).

2.5. Sediment dating, measurements of ^{137}Cs and excess ^{210}Pb

Dating of sediment layers was performed using the ^{210}Pb and ^{137}Cs methods (Appleby and Oldfield, 1992; Radakovitch et al., 1999; Robbins and Edgington, 1975). Freeze-dried and powdered sediment samples were packed into 15 or 60 ml (depending on the sediment quantity available) pre-tared polyethylene specimen cups and sealed. ^{137}Cs (661.6 keV) and ^{210}Pb (46.5 keV) activities were determined by gamma spectrometry using the seven very low-background coaxial N- and P-type GeHP detectors (Canberra/Ortec) available at the LSCE (Laboratoire des Sciences du Climat et de l'Environnement, CEA CNRS, UVSQ, Gif sur Yvette, France). "Excess" ^{210}Pb ($^{210}Pb_{xs}$) activity was calculated by subtracting the supported activity (determined using two ^{238}U daughters, i.e. ^{214}Pb, by taking the average count number at 295.2 and 351.9 keV, and ^{214}Bi at 609.3 keV) from the total activity of ^{210}Pb (Le Cloarec et al., 2011; Lepage et al., 2015). Those analyses were carried out on eleven layers of the BETH1302 core.

2.6. Chemical composition of sediments

The freeze-dried and ground aliquots were used for semi-quantitative element analyses using a Niton X-ray fluorescence (XRF) gun (Thermo Scientific Niton XL3t GOLDD+ Analyzer from GeoRessources laboratory, Vandœuvre-lès-Nancy, France) (SM V-2 a). XRF and PSD results were used to select the layers for the precise determination of major and trace elements. Major and trace elements were detected by inductively coupled plasma optical emission spectrometry (ICP-OES, iCap 6500 ThermoFisher) and inductively coupled plasma mass spectrometry (ICP-MS, X7 ThermoFisher), respectively. The quantified major elements

were Al, Ca, Fe, K, Mg, Mn, P, Si and Ti (major elements), trace elements were As, Ba, Be, Bi, Cd, Co, Cr, Cs, Cu, Ga, Ge, Hf, In, Mo, Nb, Ni, Pb, Rb, Sb, Sn, Sr, Ta, Th, U, V, W, Zn and Zr, and rare earth elements (REEs) were Ce, Eu, La, Nd, Sm and Pr (light lanthanides), Dy, Er, Gd, Ho, Lu, Tb, Tm and Yb (heavy lanthanides), and Sc and Y; in addition, total carbon, organic carbon and sulfur were also quantified. Those analyses were performed at SARM (Service d'Analyse des Roches et des Minéraux – CRPG, Vandœuvre-lès-Nancy, France) and all analytical methods were subject to QC/QA procedures using certified reference materials (Carignan et al., 2001).

2.7. Mineralogy of sediments

2.7.1. Bulk and major mineral phases detected by XRD

X-ray diffraction (XRD) analyses were performed on ground sediment layers to determine the major crystalline phases. A D8 Advance Bruker diffractometer with a Co $K_{\alpha 1}$ radiation source, operated at 35 kV and 45 mA (λ = 1.7902 Å), was used. XRD patterns were collected on the angular range (2θ) of 3 – 64°, with a 0.034° step size and a 3 sec collecting time. All layers were subjected to XRD analyses, and for clearness purpose, only relevant patterns are presented.

Furthermore, fine particles of sediment layers (from 11 till 131 cm) were also investigated from a mineralogical point of view. Indeed, the fingerprint of the former steelmaking industries was shown to be held in the fine particles (as it will be revealed later in the text). That fine fraction is most prone to be remobilized for farther distances under different scenarios, such as high water flow, flooding, dredging and modifying or removing the Beth dam. The fine fraction was extracted from the bulk sample by suspending 1 g of dry and non-ground sample in 200 ml ultrapure water for 30 minutes. Then, ultrasound was applied for 5 – 15 minutes to separate the aggregates, stirred for a few seconds, and left for 4 hours to settle. The supernatant was centrifuged at 34000 g for 15 minutes, and the resulting solid sample was prepared on glass slides to identify the major crystalline phases of the < 2 µm fraction. Due to the low amount of the fine material recovered, the XRD patterns were only obtained on oriented preparations.

2.7.2. Millimetric to sub-micrometric analyses: light microscope, SEM and TEM

For light microscope observations, a slide of each sediment layer was prepared by dropping a few milliliters of sediment-ultrapure water mixture on a glass slide, which was dried

using a hot plate. Light microscope observations were conducted to visualize certain particles and phases, such as diatom skeletons, and what later turned out to be distinct iron minerals and framboïdal pyrites. The last two phases were detected using dark field mode. In addition, 30 µm thick polished thin sections were prepared for several layers of BETH1402 sediment core (GeoRessources laboratory, Vandœuvre-lès-Nancy, France). Dried and non-ground samples were used to prepare thin sections for the layers 0 – 2 cm, 14 – 17 cm, 38 – 41 cm, 62 – 65 cm, 104 – 107 cm and 125 – 128 cm. The thin sections were later visualized under a light microscope.

Micrometric particles were identified and characterized using the scanning electron microscopy (SEM) Hitachi S-4800 equipped with a Kevex 4850-S energy dispersive X-ray spectrometer (EDXS) (GeoRessources laboratory, Vandœuvre-lès-Nancy, France). Dried sediment particles were taped on metallic holders with carbon tape and were carbon coated. The following layers were analyzed by SEM: 0 – 2 cm, 8 – 11 cm, 11 – 14 cm, 14 – 17 cm, 41 – 44 cm and 125 – 128 cm. In addition, thin section of the layer 125 – 128 cm was also observed via SEM. The accelerating voltage was set to 15 kV; when a better resolution was required, the accelerating voltage was set to 3 kV. For EDXS, the acquisition time was set to 60 seconds.

Transmission electron microscopy (TEM) was used to investigate amorphous and poorly crystalline phases at a sub-micrometric scale. A CM200 Philips TEM with 200 kV accelerating voltage coupled with an EDXS was used in Jean Lamour Institute (Department of Microscopy, Université de Lorraine, Nancy, France). The samples frozen at -80°C were used for TEM investigations. One to two milligrams of the raw sample were suspended in ethanol and exposed to ultrasound for 10 minutes to disperse the particles. Afterwards, a drop from the suspension was put on a carbon coated copper grid and left to evaporate. EDX spectra were recorded on selected areas using the nano-probe device (25 nm probe), and acquisition time was set to 50 or 70 seconds, depending on the particle's thickness. Selective area electron diffraction (SAED) patterns were collected for certain nanoparticles, which were predominantly observed in TEM micro-images. The following sediment layers were analyzed using TEM: 0 – 2 cm, 2 – 5 cm, 5 – 8 cm, 11 – 14 cm, 14 – 17 cm, 41 – 44 cm, 62 – 65 cm, 104 – 107 cm and 125 – 128 cm. Furthermore, TEM was also used to investigate the fine fraction (as prepared in section *2.7.1*).

3. Results

3.1. Visual description, water content and grain size of the sediments

For all sediment cores, a clear distinction could be made between two types of settled materials; the top layers appeared to be brown colored materials, overlying black and fine sediments. This was observed for the three cores collected in the upstream area of the Beth dam. The thickness of the brownish surface sediments varied as follow: 28 cm for BETH1302, 11 cm for BETH1402 and 3 cm for BETH1507. For BETH1402 sediments, the water contents of the brownish, loose and muddy top layers (0 – 8 cm) were the highest (~ 73%), while the water content significantly dropped at the end of the brown zone (8 – 11 cm) (Figure V-2 a). Water content further dropped to reach a minimum of 47% at 68 cm, and finally displayed two slightly increasing trends for layers 68 – 110 cm and 110 – 131 cm. This modification of water content could also be due to sediment compaction resulting from gravity coring. Moreover, the sediment layers showed D_{50} values ranging between 11 and 34 µm (Figure V-2 b). The size of the carried and subsequently deposited material is relatively fine, not only due to the abatement of water flow influenced by the dam (Fryirs and Brierley, 2012), but also likely related to the industrial origin of the black material. For the top 26 cm sediments, D_{50} and D_{90} values decreased with depth; then relatively coarser particles were detected at 29 – 35 cm depth, with a maximum at 33.5 cm (layer 32 – 35 cm). Fluctuations of particle sizes were also noticed between 35 and 68 cm. The last section of this core (68 – 131 cm) contained the finest particles (D_{50} values were as low as 11 µm), except for the relatively coarser fraction of 107 – 116 cm. The layer at 110 cm depth marked a start of a new sub-zone as evidenced by water content

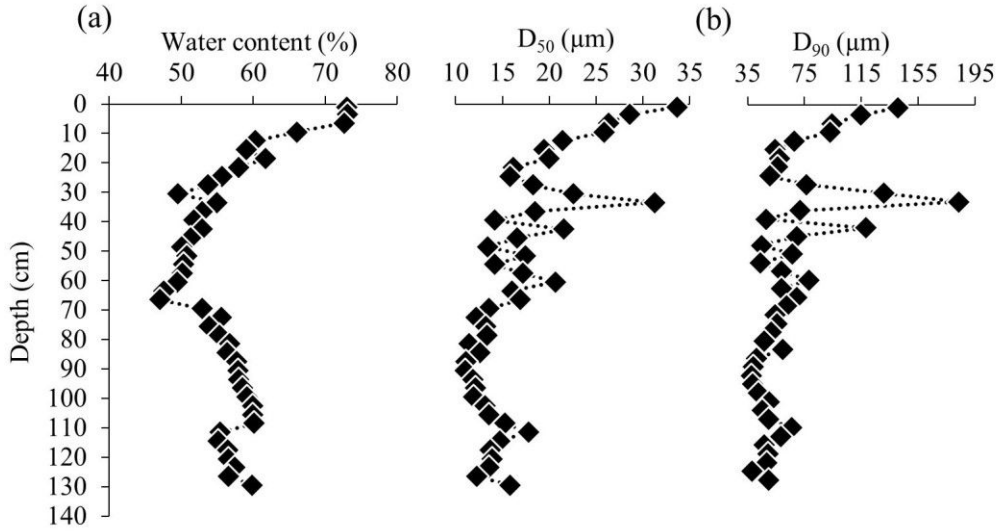

Figure V-2: Variation of a: water content (in %) and b: D_{50} and D_{90} values (in µm) of sediment particles for BETH1402.

evolution (Figure V-2: a – b). On the basis of water content and grain size analyses (Figure V-2), three units could be distinguished in the sediment core, which are 0 – 11 cm, 11 – 68 cm and 68 – 131 cm.

3.2. Dating of Beth sediments

The measurements of ^{137}Cs and ^{210}Pb are reported in Figure V-3. Due to similarity of major element contents between the cores BETH1302 and BETH1402, we assumed that the dating results presented for BETH1302 could be applied to BETH1402 (SM V-2 b). The measurements were considered to be rather unsucessful due to the relatively low counting of ^{137}Cs and the absence of $^{210}Pb_{xs}$ decrease with depth. Indeed, it was not possible to estimate a sedimentation rate on the basis of those $^{210}Pb_{xs}$ values. Such a method is commonly used to date recent sediment archives assuming that the sedimentation rate is constant. In the studied case, the sedimentation dynamics were likely disturbed by the dam functioning and the industrial use of river waters.

The ^{137}Cs measurement in the Beth sediments evidenced the presence of this radionuclide all along the profile, without displaying any peak as it is usually reported. Two peaks were expected, one due to atmospheric nuclear bomb tests (from 1954 to 1963 with a maximum of ^{137}Cs atmospheric deposition in 1963), and a second maximum due to the Chernobyl nuclear plant accident in 1986.

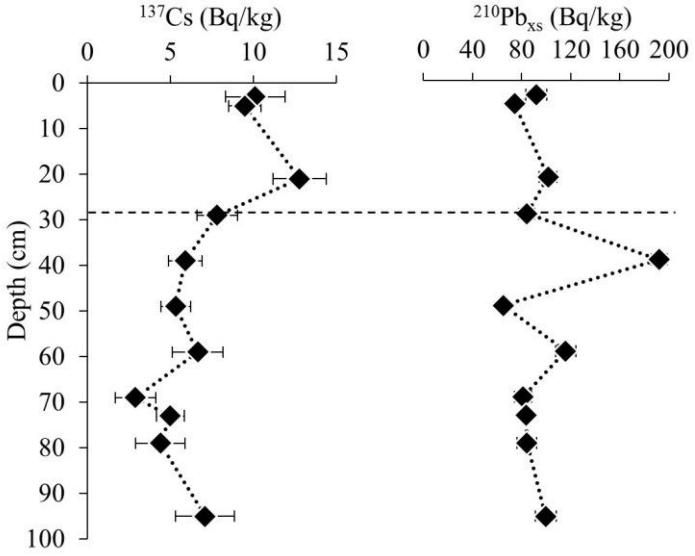

Figure V-3: Radionuclide vertical profiles for $^{210}Pb_{xs}$ and ^{137}Cs. The dashed line marks the limit between brown (top) and black (deep) sediments of BETH1302.

Assuming that the atmospheric emissions of ^{137}Cs ceased in 1963, we can suppose that the Beth sediments had majorly settled after the beginning of atmospheric nuclear tests (1954). The expected peak of Chernobyl nuclear plant explosion did not show up either. The presence of ^{137}Cs suggests that the sediments are younger than 1954 which is consistant with the date of Beth dam building. The atmospheric depositions of ^{137}Cs are strongly scavenged by clay minerals (Lepage et al., 2015; Sawhney, 1972). Those soil constituents are subsequently

transported to streams and rivers during rain events. The clay-size fraction (< 2 μm) of river suspended particulate matter was expected to be particularly enriched in ^{137}Cs, and the ^{137}Cs content in sediments is definitely depending on the settling rate of those fine particles. ^{137}Cs measurements confirmed the age of sediments but a precise age model could not be established. Taking into account the ^{137}Cs contents and the activity period of the blast furnaces, we assumed that the vertical profile covered the period from 1960 to 2014, and that brown sediments, constituting the top of the core, started to settle after the steelmaking activities stopped in 1988. The absence of ^{210}Pb decrease with depth on the other hand might be assigned to the modification of river hydrodynamics and sedimentation regime.

3.3. Chemical composition of sediments as a function of depth

The vertical variations of Si, La, Ca and Fe contents in the sediment core are shown in Figure V-4 a. The vertical profiles of light lanthanides other than La (which are Ce, Nd and Pr), major elements K, Na, Ti and Al, and trace element Zr are plotted in SM V-3. It should be noted that Si, K, Na, Al, Ti, Zr and light lanthanides (La, Ce, Nd and Pr) followed a similar trend in the profile of BETH1402 core, and were subsequently classified into one group, referred to as Si group. Indeed, all those cited elements were significantly correlated to one another (Pearson correlation coefficient "PCC" or Pearson's R ~ 0.9, SM V-4). From the vertical profiles of this first set of elements, 4 units could clearly be defined, which are 0 – 11 cm, 11 – 44 cm, 47 – 68 cm and 68 – 131 cm (indicated as I, II, III and IV, respectively, in Figure V-4). The first unit (between 0 and 11 cm) was the most enriched with elements of the Si group, suggesting a strong contribution of materials originating from erosion in the watershed; the other units showed an increasing trend from 11 till 41 cm, a peak at 44 – 47 cm, a slight decreasing trend for 47 – 68 cm, and a quasi-stable content for the last unit (68 – 131 cm). The layer 44 – 47 cm displayed a striking discontinuity for all elements and was therefore considered as an individual layer. Furthermore, the contents of the lanthanides (La, Ce, Nd and Pr) in the 44 – 47 cm layer were very close to those measured in unit I (Figure V-4 a and SM V-3). Although Si, K and Al contents were high for the 44 – 47 cm layer, they did not reach the respective ranges of unit I. Ca contents were relatively high for the 41 – 44 and 44 – 47 cm layers (9.8 and 9.4%, respectively), and similar to lanthanides, the contents were as high as in surface sediments (unit I). Another distinctive sediment feature is the particularly high Fe contents (between 15 and 29%), related to the iron mining and steelmaking activities in the vicinity of the river (Figure V-4 a). It is worth mentioning that Fe contents in the lower units (II till IV) were 3 to 5 fold higher than in the surface unit (unit I). Such high Fe contents were

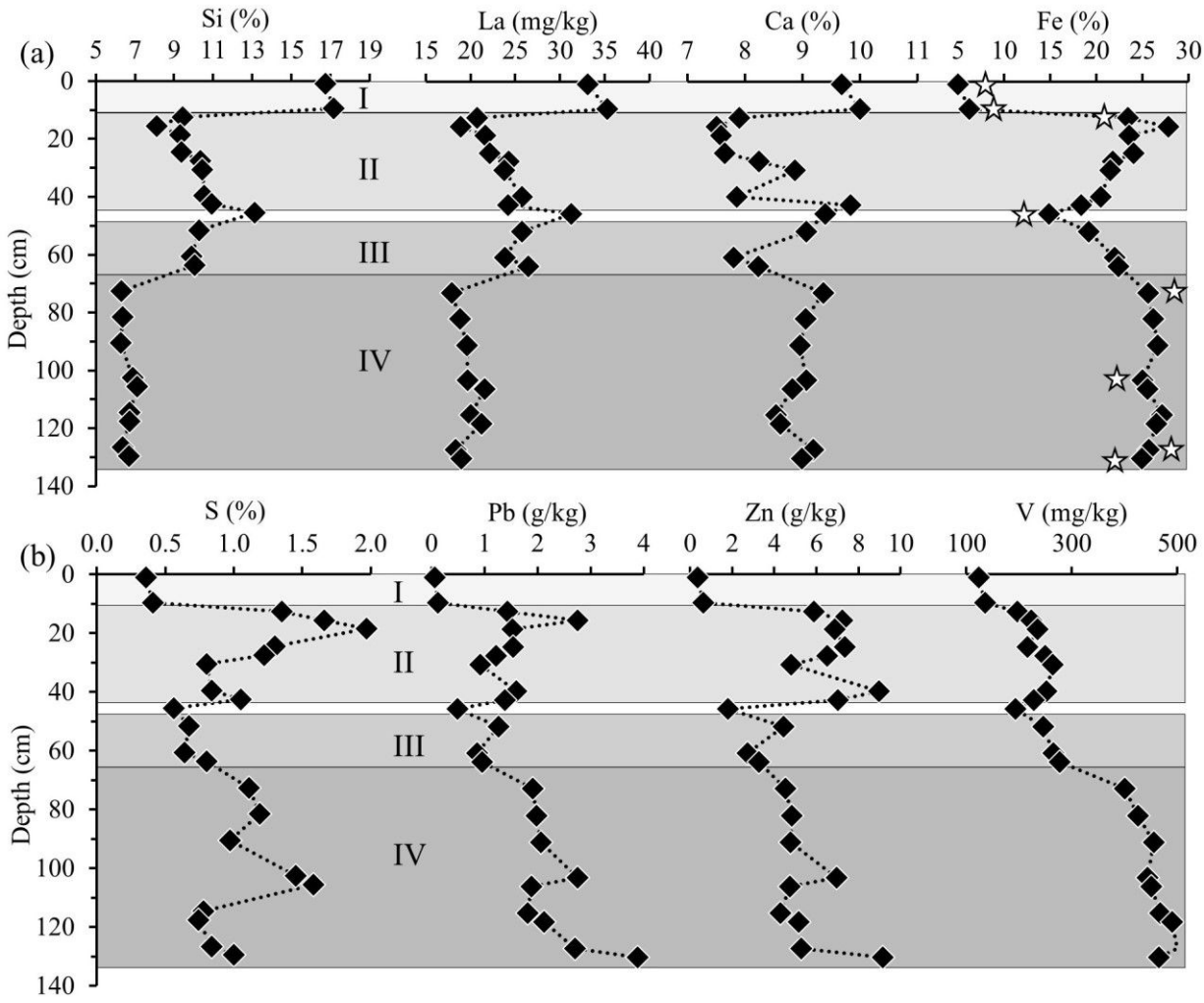

Figure V-4: Variation of chemical composition in the vertical profile of BETH1402.
The profiles of a: Si (%), La (mg/kg), Ca (%) and Fe (%) and b: total sulfur (S in %), Pb (g/kg), Zn (g/kg) and V (mg/kg) as a function of depth for the sediment layers of BETH1402 core. The units 0 – 11 cm, 11 – 44 cm, 47 – 68 cm and 68 – 131 cm are indicated by I, II, III and IV respectively. In the Fe profile, stars are put near the layers for which XRD patterns are presented in the following figure.

also encountered in the other cores. Fe variation is clearly opposite to the first group of elements with PCC close to -1 (SM V-4), and showed a global increase with depth. This allows us to define the group of Si, K, Na, Ti, Al, Zr and light lanthanides (La, Ce, Nd and Pr) as a lithogenic group. Those elements mainly originate from watershed surface weathering and soil erosion, and thus reflect the geological background.

Similarly to iron contents in BETH1402 core, total sulfur, Mn, Mg, P, As, Cd, Co, Cr, Cu, Mo, Ni, Pb, Sc, Sb, Sn, V, W and Zn contents were less enriched in the 0 – 11 cm unit; some of them are plotted in Figure V-4 b (see also SM V-3). Indeed, total sulfur, Cr, Zn and Pb showed similar behavior and were significantly correlated ($P < 0.05$), except for Cr and Pb ($P = 0.159$). Furthermore, those elements were also correlated to Fe ($P < 0.01$) (SM V-4). As for Pb and Zn, the start of the second unit (i.e. layer 11 – 14 cm) showed a great increase in

their contents. The high contents of the "trace" metals Pb (0.1 – 0.4%) and Zn (0.1 – 0.9%) in the black sediments (11 – 131 cm) eliminate the term "trace" and highlight on the level of sediment contamination. In our case, enrichment factors for Pb and Zn reached as much as 77 and 35 respectively (Al was taken as the "conservative" element and the recently deposited 0 – 2 cm layer was taken as reference for the calculation of enrichment factors, i.e. 68 mg/kg for Pb and 349 mg/kg for Zn). However, none of the measured elements could be considered as a conservative element in the case of Beth sediments. Therefore, the differentiation between the lithogenic nature of unit I and the other units (II till IV) is obvious, without a real need of enrichment factor calculation. In such contaminated sediments, aluminum normalization was not relevant due to the drastic decrease of this element with depth (SM V-3).

Other trace elements showed relatively striking contents in BETH1402 sediments. Indeed, V profile displayed a relatively continuous increase with depth (Figure V-4 b) and was strongly correlated with Mn ($P < 0.01$, PCC = 0.956, SM V-4). Finally, the four units (as seen in Figure V-4 a) could also be distinguished for the elements presented in Figure V-4 b (such as total sulfur, Zn and Pb) and SM V-3. Those four units certainly demonstrate a modification of steelmaking activities and processes, and/or a modification of the nature of steelmaking wastes poured into the Orne waters. Iron being the major element brought to the river by former industrial activities, investigations about its status in the sediments are presented in the following paragraphs.

3.4. Mineralogy of sediments

3.4.1. Major crystalline minerals

The major crystalline phases were studied through the qualitative analysis of XRD patterns. The sediment cores BETH1302, BETH1402 and BETH1507 showed the same mineralogical composition, and only BETH1402 sediment layers will be discussed here. For clarity, the XRD patterns of distinct layers, namely 0 – 2 cm, 8 – 11 cm, 11 – 14 cm, 44 – 47 cm, 68 – 71 cm, 95 – 98 cm, 125 – 128 cm and 128 – 131 cm, are shown in Figure V-5. Major crystalline phases, such as quartz, calcite and phyllosilicates were revealed by XRD. The evolution of major elements could be related to the evolution of some major crystalline phases. Indeed, a great diminution of quartz peaks (reflections at 3.34 Å and 4.26 Å) could be related to the simultaneous decrease of Si contents from the surficial brown sediments (unit I) to the underlying black sediments (Figure V-4 a and insert of Figure V-5). Even more, the relatively higher diffraction line intensity for quartz in layer 44 – 47 (insert of Figure V-5) is coupled to

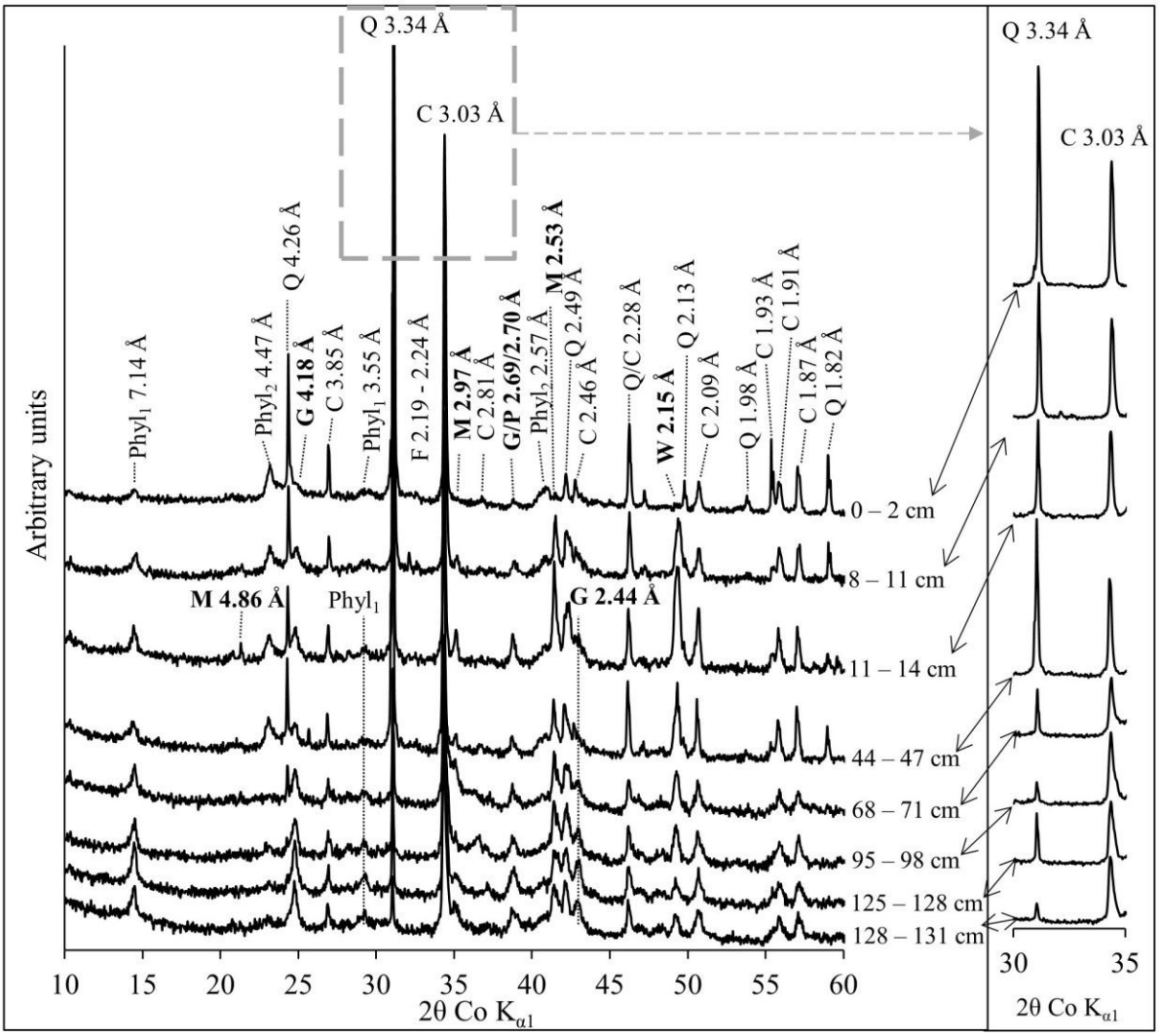

Figure V-5: XRD patterns of selected BETH1402 sediment layers.
XRD patterns of selected BETH1402 sediment layers. Phyl: phyllosilicates (including $Phyl_1$ and $Phyl_2$, which are treated differently; see text for more information), Q: quartz, G: goethite, C: calcite, M: magnetite, P: pyrite, W: wuestite. Iron minerals are labelled bold. The insert on the right shows the variation of quartz and calcite peak intensities with depth.

an increase in lithogenic elements, and a decrease in iron and most of the trace elements (Figure V-4). In addition, diffraction line intensities of quartz indicated a significant decrease between the 125 – 128 cm and 128 – 131 cm layers, while Si content appeared rather constant.

Calcite diffraction lines (3.03 Å and 3.85 Å) evolved similarly to quartz, showing maximum intensities in the first unit and in the 44 – 47 cm layer; and finally a decreasing trend with depth. Even though the Ca contents followed the trend displayed by calcite occurrence in the top unit of the core (and for the specific layer 44 – 47 cm), it was not completely correlated to carbonate occurrence as evidenced by XRD. Phyllosilicates were also detected with the basal reflections *001* and the *hkl* reflections (4.47 and 2.57 Å; denoted by $Phyl_2$ in Figure V-5). Although phyllosilicates and clay minerals were mainly present in the 0 – 2 cm layer of unit I, and slightly present in deeper layers, the intensity of the peak centered at 7.14 Å, assigned to

d(*001*) plane of TO clay, seemed to increase with depth and therefore will be treated differently, along with the diffraction line at 3.55 Å (denoted by $Phyl_1$ in Figure V-5). Indeed, the diffraction line at 3.55 Å is related to that of 7.14 Å, which is clearly visible in the XRD patterns of layers inferior to 14 cm. The increase of the 7.14 and 3.55 Å peaks were also evidenced for BETH1302 sediment core (SM V-5). The apparent increase of the peak at 7.14 Å is not associated with the other expected *hkl* lines for phyllosilicates (referred to as $Phyl_2$ on Figure V-5) and the lines at 4.47 and 2.57 Å are hardly detected for layers deeper than 60 cm. The respective intensities of *001* and *hkl* reflections are due to the particle orientation and are commonly anti-correlated. The fine character of sediments as well as the depletion in quartz and calcite minerals, might enhance the orientation of platelets along the c-axis, and thus favor the *00l* reflections including the *001*.

XRD patterns of BETH1402 sediments were particularly fingerprinted by iron oxides (wuestite FeO and magnetite Fe_3O_4), iron oxy-hydroxide (goethite α-FeOOH) and iron sulfide (pyrite FeS_2) (bold type labels on the XRD patterns in Figure V-5). The general shape of the XRD pattern was strongly modified as soon as the brown siliceous unit from 0 to 11 cm was exceeded. Indeed, peaks of iron minerals, namely goethite (4.18, 2.69 and 2.44 Å), magnetite (2.97 Å and 2.53 Å), pyrite (2.70 Å) and wuestite (2.15 Å), became more obvious at a depth of 11 cm (see XRD pattern for the 11 – 14 cm layer in Figure V-5). The main diffraction peak of pyrite and a secondary diffraction peak for goethite are very close to one another (2.70 Å and 2.69 Å respectively), thus the evidenced broad peak at 2.69 – 2.70 Å can be assigned to both iron bearing phases. Nonetheless, goethite and pyrite are certainly both present in the deep sediment layers, due to high iron content and anoxic conditions. Goethite could clearly be detected in the layers 8 – 11 cm and 11 – 14 cm, and the goethite diffraction lines developed in the unit IV (layers 68 – 131 cm). Magnetite and wuestite diffraction lines developed in layer 8 – 11 cm, with highest intensities in the layers 11 – 14 cm and 89 – 92 cm, and then decreased with depth. This decrease of iron oxide diffraction lines, mainly observed by wuestite diffraction line (2.15 Å), was combined with an increase of the diffraction line at 7.14 Å, as well as an increase of the diffraction lines of the main iron oxy-hydroxide detected in the 11 – 131 cm zone via XRD, i.e. goethite at 4.18, 2.69 and 2.44 Å.

3.4.2. Identification of main mineral phases using microscopic tools

Since XRD is sensitive to major crystalline minerals only, supplementary techniques were used to study the mineralogy of less abundant, poorly crystalline and amorphous phases.

Those findings will reveal other Fe-minerals and metal bearing phases. Using multiple microscopic techniques (SEM and TEM), the upper layer (0 – 2 cm) was shown to be mainly composed of clay particles. On the basis of EDX spectra, those clays were identified to be predominantly illite, smectite and interlayered illite/smectite, while only few particles of kaolinite could be detected. The different clay minerals were identified on the basis of Si:Al, Si:K and Si:Mg ratios, as well as particle morphology. The samples also displayed quartz and iron oxides and oxy-hydroxides associated to clay or carbonate particles (Figure V-6). Furthermore, many diatom skeletons could be observed by SEM and light microscopy in the surface sediment layer (0 – 2 cm). This zone exhibited features of natural sediments, originating from soil erosion and biological production. However, although the iron content is not particularly high in that layer, about 50% of the particles analyzed via TEM-EDXS contained iron with atomic percentages above 15%.

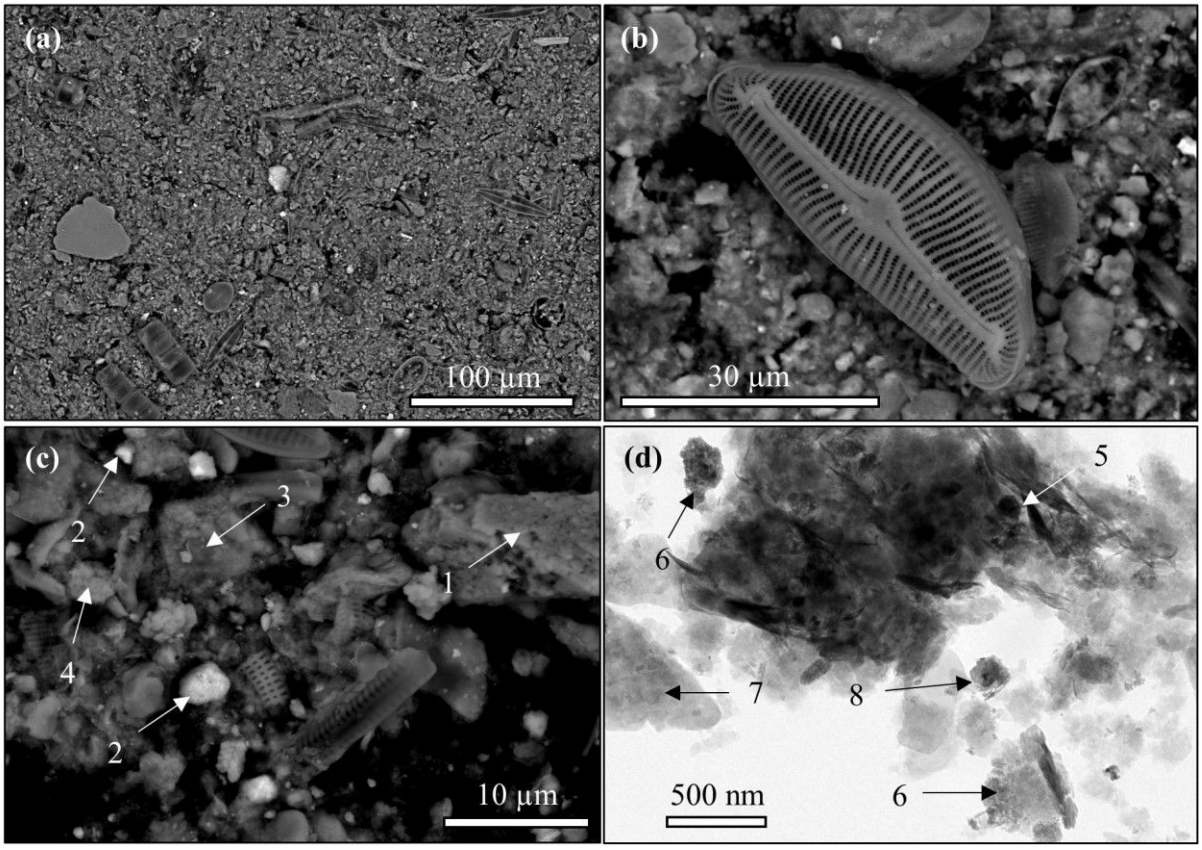

Figure V-6: Micro-images for the surface 0 – 2 cm layer of BETH1402 core.
a, b and c: SEM back-scattered electrons (BSE) micro-images showing a large field of view of the sediment sample, displaying numerous diatom skeletons (a and b), and evidencing: 1: calcite, 2: iron oxy-hydroxide, 3: interlayered illite-smectite and 4: calcite. d: TEM micro-image showing: 5: TiO_2 particle associated with clay (interlayered illite-smectite), 6: iron oxy-hydroxide, 7: interlayered illite-smectite, and 8: TiO_2 and iron oxy-hydroxide.

From 5 to 11 cm, few polymetallic sulfides and Ca-phosphate particles could be detected, suggesting a possible contribution of underlying sediments due to coring, or a contribution of

urbanized surface leaching or urban sewer network (El Samrani et al., 2004; Houhou et al., 2009). Furthermore, for units II till IV, EDXS evidenced the prevalence of iron particles in terms of number and content. For layers inferior to 11 cm, clay particles were also present, but strongly less predominant as compared to the first unit. Diatom skeletons were still evidenced in the 11 – 131 cm zone, suggesting that the industrial-borne materials were transported by the river and mixed with waterborne particles before settling. The general aspect of particles in the deeper sediments was strongly modified, as it could be expected from the chemical composition (Figure V-4 and SM V-3). From EDXS analysis, iron seemed to be ubiquitous and detected in more than 90% of analyzed particles.

3.4.3. Iron minerals: crystalline, poorly crystalline and amorphous phases

For the layers inferior to 11 cm, distinct iron minerals were observed by microscopic tools (Figure V-7: a – b). The iron minerals ranged between 10 and 30 µm in diameter and were recognized as ferrospheres. Some of the ferrospheres displayed dendritic magnetite crystals in cracks (Figure V-7: a – b). Iron sulfides were also evidenced by microscopic observations (Figure V-7: c – d). Indeed, framboïdal pyrites were detected via light microscopy and SEM. Those minerals were detected starting from 5 cm, and were observed until the bottom of the core (131 cm). Most of the framboïdal pyrites were 10 µm in diameter. Nonetheless, a few particles as small as 5 µm, and as large as 20 µm, in diameter were also seen. Layers 14 – 26 cm and 41 – 65 cm contained the highest number of framboïdal pyrites (light microscopy observations).

At higher spatial resolution, iron nanoparticles were evidenced in most of the sediment layers by TEM (Figure V-8 a). Their cross sections ranged in size from 7 to 39 nm, with an average of 20 ± 8.2 nm. Even though they were detected starting from 5 cm depth, those nanoparticles were abundant in all investigated layers below 11 cm (TEM observations); and the corresponding EDX spectra evidenced an atomic ratio O:Fe close to 2 (Table V-1). Similar iron nanoparticles, in shape, size and composition, were also detected in the local iron ore and were identified as goethite (FeOOH, O:Fe = 2) (SM V-6). The main Fe ore used for steelmaking in Lorraine, also called “Minette” or Loth, was a ferri-arenite, mainly composed of goethite ooids, iron phyllosilicates (chamosite and berthierine), Fe-carbonate or siderite and calcite (Dagallier et al., 2002). SEM observations unraveled the presence of oolitic phases in the sediments, where they appeared as weathered goethite ooids (SM V-6 b). Therefore, on the basis of the presence of goethite clearly evidenced by XRD (Figure V-5), the identification of

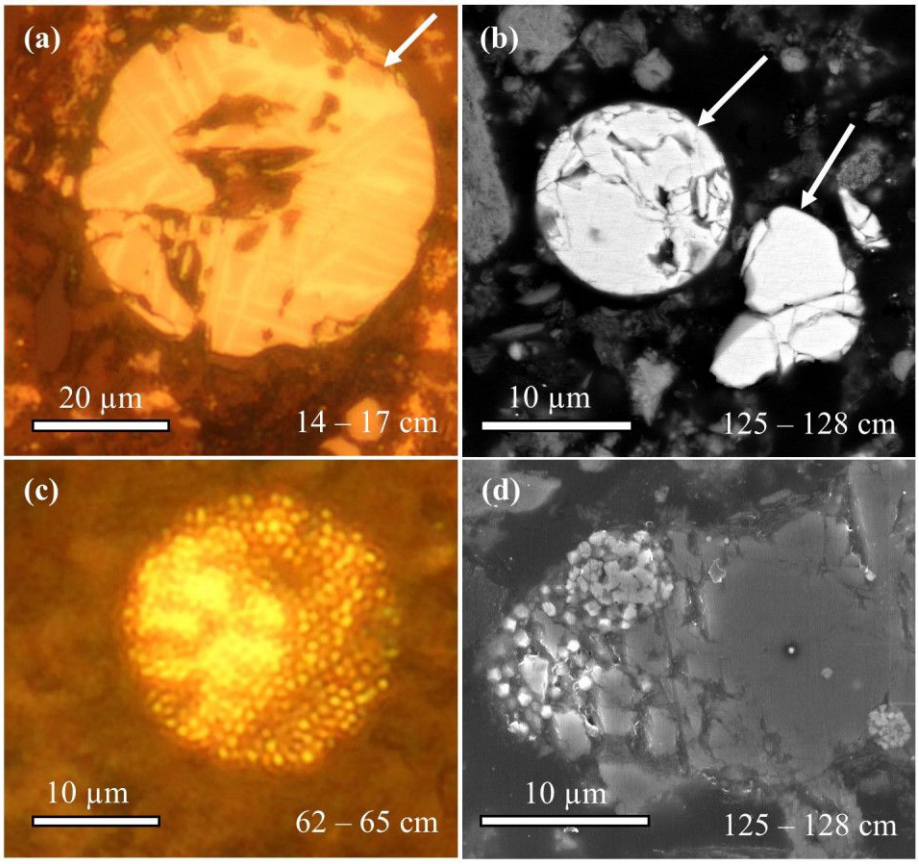

Figure V-7: Distinct iron minerals observed by light microscope and SEM.
a: Light microscope image of layer 14 – 17 cm (thin section) showing a ferrosphere with dendritic magnetite in cracks (dark field mode). b: SEM BSE micro-image of layer 125 – 128 cm (thin section) showing a ferrosphere and distinct iron oxide fragments. c: Light microscope image (dark field) of layer 62 – 65 cm (thin section) showing a framboïdal pyrite. d: SEM SE micro-image of layer 125 – 128 cm (thin section) showing a framboïdal pyrite with octahedral microcrystals.

goethite nanoparticles with TEM SAED (Figure V-8 a), and due to the strong similarity with goethite grains in iron ore "Minette de Lorraine" (SM V-6), those nanoparticles were assigned to goethite grains, and were assumed as a fingerprint of iron ore contribution to the sediments. Another predominant phase evidenced by TEM was hairy structured iron rich aluminosilicates (Figure V-8 b), hereafter named Fe-aluminosilicates. Those phases were mainly detected in the sediments below 11 cm. The main constituents of those phases are O, Si, Al and Fe, while the minor ones are Ca and Mg. Those phases were recognized by an Al:Si atomic ratio of 0.5 ± 0.2, and an Fe:Si atomic ratio of 0.9 ± 0.3 (Table V-1). Those phases were particularly predominant in layers deeper than 60 cm, such as the layer 104 – 107 cm (Figure V-8 b).

In most cases, the hairy Fe-aluminosilicate phases displayed darker rings (Figure V-8 c), strongly suggesting that those Fe-aluminosilicates resulted from the weathering of circular or spherical entities. Furthermore, the dark ring was shown to include nano-grains of polymetallic

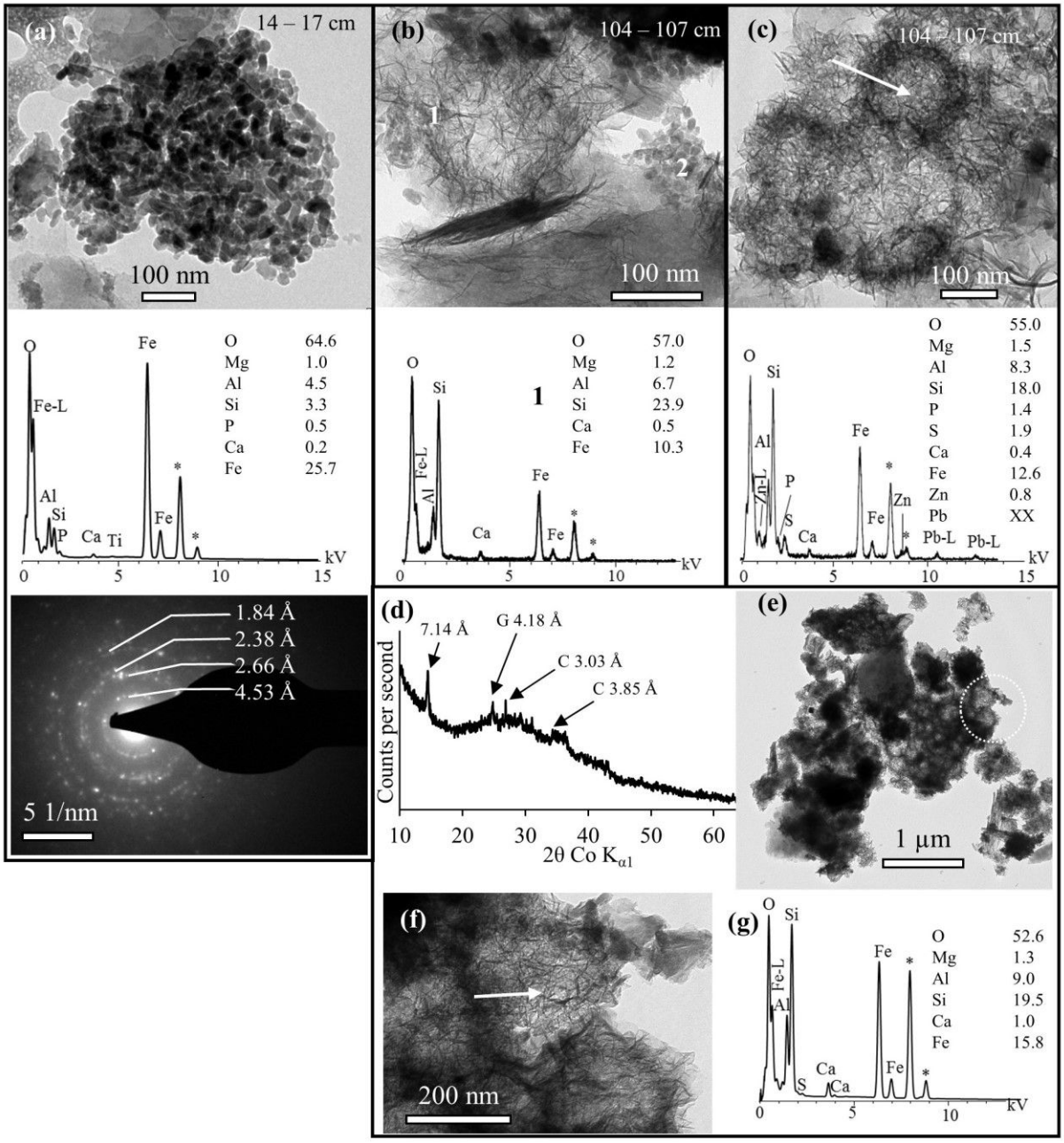

Figure V-8: TEM micro-images and corresponding EDX spectra of iron phases.
a: Goethite nanoparticles in layer 14 – 17 cm with corresponding EDX spectrum, atomic percentages and SAED pattern. b: Fe-aluminosilicates in layer 104 – 107 cm (1) with corresponding EDX spectrum and goethite nanoparticles (2). c: hairy aluminosilicate phases marked by dark rings of Zn-Pb sulfides (104 – 107 cm). Due to the presence of S, Pb signal is not correctly fitted, therefore the atomic percentage is not given for Pb. d – g: Mineralogy of the selected fine fraction of the metal laden layers of BETH1402 core. d: XRD pattern showing the main crystalline constituent to be a mineral of interplanar distance 7.14 Å. e and f: TEM micro-images showing hairy iron rich aluminosilicate phases and g: corresponding EDX spectrum. The micro-image e shows an aggregate of circular structures; the micro-image f shows a zoomed section of micro-image e (dotted white circle). The hairy phases are associated with rings of fluffy grains, assigned to polymetallic (Zn-Pb) sulfides. Asterisks on the EDX spectra indicate the emission lines of copper, which are due to the contribution of the TEM grid, a carbon coated copper grid.

(Zn, Pb and Fe) sulfides. Such a feature was even more evident for the fine fraction of the deep sediment layers (below 11 cm), which was analyzed by XRD and TEM-EDXS (Figure V-8: d – g). The diffraction reflection corresponding to basal plane *001* (7.14 Å) was more evident for

the fine fraction, in comparison to the bulk sample, supporting the predominance of phyllosilicates. The same pattern also suggests a light decrease in goethite and other iron oxides in the sample (Figure V-8 d). TEM observations revealed the predominance of the hairy iron-rich aluminosilicates in the fine fraction of BETH1402 sediments (Figure V-8: e – f) as well as the presence of few grains of goethite, polymetallic sulfides and few platelets of clay minerals.

Table V-1: Atomic percentages and atomic ratios (average ± standard deviation) of the elements constituting goethite nanoparticles and Fe-aluminosilicates

	Atomic percentages (%)				Atomic ratios		
Phase	O	Si	Al	Fe	O/Fe	Al/Si	Fe/Si
Goethite nanoparticles (n = 20)	63.3 ± 2.7	–	–	30.5 ± 2.4	2.1 ± 0.2	–	–
Fe-aluminosilicates (n = 44)	50.9 ± 5.8	18.9 ± 3.9	9.7 ± 2.0	15.1 ± 3.9	–	0.5 ± 0.2	0.9 ± 0.3

Those hairy aluminosilicates, particularly enriched in iron, were apparently related to the 7.14 Å diffraction line that increased with depth (Figure V-5). The hairy phases might be assigned to TO phyllosilicates, constituted of one octahedral and one tetrahedral layer, resulting in basal spacings close to those of TO phyllosilicates. Furthermore, the hairy Fe-aluminosilicates, or crumpled paper structures, display a three-dimensional aggregate of rings or empty spheres (Figure V-8: c and e). Again, the EDX spectra showed that the darker rings underlying the circular entities were made of Zn-Pb (or Zn-Pb-Fe) sulfides, and thus strongly suggest that the same processes or a combination of related processes were at the origin of Fe-aluminosilicate and polymetallic sulfide formation within the sediments.

4. Discussion

4.1. Industrial and natural contributions to the sediment deposits

From historical data and ^{137}Cs measurements, we assumed that the 120 cm black materials (11 – 131 cm) had settled during the industrial activity period, i.e. from 1960 to 1988. We also presumed that the bottom of the deposits was reached at 131 cm, and that no material was eroded during that period. The estimated sedimentation rate is about 4.7 cm per year, which is more than ten times the sedimentation rate measured in fish ponds located in the Moselle watershed (Bertrand et al., 2012). This estimated sedimentation rate should be put against the activity of the steelmaking site. Indeed, the blast furnaces and the sintering plant were reported to produce 1.3 Mt/yr and 2.4 Mt/yr, respectively (Freyssenet, 1979). The top of the core might represent the materials that had deposited between 1988 and 2014; the estimated sedimentation rate (0.42 cm/year) would then be closer to what was measured in Lachaussee and Lansquenet

ponds (Bertrand et al., 2012). Considering those numbers, it was difficult to establish an age model for BETH sediments as the main part of the deposits was directly influenced by steel production, and not by natural sedimentation dynamics. The relatively low thickness of the recent sediment deposit (11 cm only for 26 years) might also be attributed to the erosion of settled materials during the flood event of 1993 (50-year flood, with a 318 m^3/s maximum flow measured). Further investigations on this sediment deposit, including year to year monitoring should bring more detailed explanations about sedimentation dynamics.

4.1.1. Natural contributions in Beth sediment deposits

First of all, unit I (0 – 11 cm) of the settled materials displayed lithogenic nature. The detrital character was evidenced not only by the distinct brown color and relatively higher contents of detrital elements (Figure V-4 a and SM V-3), but also by XRD and microscopic tools. Indeed, the predominance of detrital minerals, such as quartz, calcite, illite and smectite, and diatom skeletons (Figure V-5 and Figure V-6) were clearly evidenced. The contents of REEs evidence the geochemical background (Hu et al., 2006; Wen et al., 2014). Nonetheless, since the deposited materials were highly influenced by steelmaking wastes in our case, only the light lanthanides La, Ce, Nd and Pr were used to fingerprint the detrital contributions. Indeed, the contents of light REEs were anticorrelated to Fe, Zn and Pb (SM V-4). In addition, the high Si and Ca contents in the first unit were assigned to the erosion of argillaceous surface layers of the Woëvre region (Figure V-1 a), and the detrital crystalline minerals (quartz and calcite) were shown to be commonly transported in the Moselle River and its tributaries (Le Meur et al., 2016; Montargès-Pelletier et al., 2007). In the deeper sediments (inferior to 11 cm), the contribution of detrital elements and minerals, and diatom skeletons could still be evidenced, but significantly less than the first unit; therefore, indicating the combined contributions of natural SPM and steelmaking wastes in the deposited materials.

4.1.2. Industrial contributions to the sediments, ferrous and non-ferrous materials

The origin of the sediment particles between 11 and 131 cm depth can be undoubtedly related to former steelmaking activities. The investigation of sediment mineralogy revealed, or at least suggested, different and distinct units in the sediment profile, certainly related to diverse periods of activity in the vicinity of the Beth dam. The main iron phases detected in the layers below 11 cm were goethite, magnetite, wuestite, pyrite, Fe-aluminosilicates and (poly)metallic sulfides (XRD, SEM and TEM). The mineral phases evidenced in the sediments below 11 cm resulted from different outputs of steelmaking processes as well as likely weathering processes

within the sediment profile. Different sources of iron were present on the site, such as iron ore, cast iron, iron scraps, sludge from wet cleaning of furnace smokes, and fly ash from the sintering plant, blast furnaces or converters (see SM V-1 for machineries that were installed upstream of the dam).

At elevated temperatures inside blast furnaces (1200 to 1600°C), some elements are volatilized, others are associated to furnace smokes; both are partially evacuated from blast furnaces. This is the case for Zn and Pb (Trinkel et al., 2016, 2015). In Lorraine steelmaking facilities, furnace smokes were cleaned through a wet procedure (wet scrubbing), resulting in sludge with particularly high contents of metallic elements (such as Pb and Zn), which partly explains the high contents of those elements in the 11 – 131 cm layers (Figure V-4). Furthermore, sludge cannot be re-used in blast furnaces if enriched with metals, such as Pb and Zn (few hundred mg/kg to a few %) (Das et al., 2007, 2002; Kretzschmar et al., 2012); therefore, sludge is piled or dumped in settling ponds (Mansfeldt and Dohrmann, 2004). In settling ponds, supplementary reactions occur due to the presence of water and atmospheric gases, which result in mineralogical transformations, mainly hydration and carbonatation. Another industrial contribution to the sediments can be expected from slagheap exploitation. Besides the production of metallic iron, the by-product slag is formed, which is rich in Si, Ca, Al and Mg (ore constituents), and forms glass-like phases. As the molten slag is channeled out of the blast furnace, it is rapidly quenched with water, which results in the formation of granular material, which were stored as slagheaps near the Orne River (Figure V-1 b). Only few of those granulated materials could be seen as spheres of Si, Al and Mg (SM V-7). Those glass-like phases can display different shapes and sizes, depending on the cooling speed, and can form (sub)-micrometric to meter size blocks (Sobanska et al., 2016; Vassilev and Vassileva, 1996).

Vanadium had retained our attention because it was one of the trace elements that increased with depth, particularly in the last two units (units III and IV in Figure V-4 b), while other trace metals fluctuated, such as Zn and Pb, or were quite steady, such as Ni and Co (SM V-3). Vanadium is known to be relatively concentrated in fossil fuels, with values up to 1000 mg/kg in petroleum and 100 mg/kg in coal (Groen and Craig, 1994; Xu et al., 2003). Upon combustion, and particulary coke production from coal, high contents of V (up to 0.1%) are majorly associated to emitted ashes, since V is not volatile (Helble and Sarofim, 1993; López-Antón et al., 2011). Usually, V is used as a tracer of oil in petroleum basins. In the context of the Orne River, the steelmaking industry produced coke in facilities located in Homécourt and Moyeuvre-Grande (Figure V-1 b). The presence of such high V contents in the sediments could

be assigned to coke production, while the decrease of V contents from the bottom up might be due to the progressive decline of coke production in the 1980's, which was followed by the dismantling of the Homécourt facilities, while steel production at Moyeuvre-Grande was still active until 1988.

The iron ore demonstrated to be one of the sources of iron in Beth sediments since the nanometric sized grains of goethite are particularly similar to those found in the Minette iron ore (Figure V-8 a and SM V-6). Furthermore, few parts of oolites were evidenced with SEM (SM V-6 b). The fine grain size distribution of the settled sediments strongly suggests that part of the materials that had settled in the riverbed were mainly originating from blast furnace smokes, with or without wet cleaning, and enriched with micro-particles and nano-particles, such as ferrospheres. Such ferrospheres are very common in coal combustion, fly ash, unburnt fuel from ferrous metallurgy and by-products from blast furnaces (Huang et al., 2015; Moskalyk and Alfantazi, 2003), and were shown to have dendritic magnetite crystals in their cracks (Valentim et al., 2016; Zhao et al., 2006). Moreover, quenching of molten iron results in the formation of ferrospheres (Sokol et al., 2002). Indeed, ferrospheres are also common in metallurgical wastes and were already evidenced in suspended matter and sediments of a neighboring river affected by steelmaking (Montargès-Pelletier et al., 2014). Additionally, and from a mineralogical point of view, crystalline minerals, such as wuestite and magnetite, are formed during the release of furnace smokes and partly constitute fly ash (Sharonova et al., 2013; Valentim et al., 2016).

4.2. Evolution of the iron minerals

The formation of crystalline framboïdal pyrites in Fe and S rich sediments commonly occurs in anoxic conditions (Wilkin and Barnes, 1997), and was expected in our case (Figure V-7: c – d). However, since iron was majorly detected as distinct phases and highly linked to steelmaking activities, the variation of iron mineralogy could be considered as a fingerprint of the industrial activity in the vicinity of the dam. On a study concerning a neighboring river, the Fensch River, which also witnessed intense steelmaking activities, the mineralogy of sediments and suspended particulate matter had revealed the occurrence of numerous spherical iron oxides. Those phases, more or less weathered, covered a wide size range and were directly related steelmaking (Montargès-Pelletier et al., 2014, 2007). SPM and sediments were collected while the steel industry was still active. Ferrospheres of various sizes were observed in sediments and SPM of the Fensch River and were spatially associated to Fe-aluminosilicates

(Montargès-Pelletier et al., 2014). Moreover, spherical entities were also evidenced in sludge settling ponds by Huot et al., (2014), but their chemical composition was close to that of slag, i.e. mainly constituted of Al and Si. Indeed, those light elements originate from the pristine ore after their separation from iron in blast furnaces or sintering plants. Weathering of those glassy slag particles or iron oxide spheres resulted into the formation of the hairy aluminosilicates identified as crumpled paper or hairy structures, referred to as "allophane-like" by Huot et al., (2014). The chemical composition of the hairy aluminosilicates depends on the type of industry (Zn or Fe metallurgy for example), raw materials used, sludge and other by-products (e.g. Kretzschmar et al., 2012; Mansfeldt and Dohrmann, 2004). In addition, the composition of hairy aluminosilicates might be influenced by weathering processes. In BETH1402 sediments, only few iron oxide spheres (ferrospheres) were detected at the light microscopy scale (i.e. from few microns to several tens of microns) (Figure V-7: a – b), thus suggesting the contribution of fly ashes or sludge to the sediments. Those spheres were not evidenced at the sub-micrometric scale (TEM), as it was the case for Fensch sediments and SPM (Montargès-Pelletier et al., 2014). Only the ghost of the spherical shape is suggested by the spatial organization of newly formed Fe-aluminosilicates, (Figure V-8: c and e). The high Fe contents of the hairy phases and the spherical voids that appear to structure their aggregates strongly call for a relationship between those Fe-phases and expected ferrospheres.

The processes resulting in the formation of Fe-aluminosilicates were not identified with precision, and due to the various origins of iron in the sediments, several hypotheses need to be debated. Indeed, the presence of such Fe-aluminosilicates could be assigned to iron ore contribution, since the Minette contains iron-rich phyllosilicates, such as chamosite and berthierine (Dagallier et al., 2002). In addition, crumpled paper-like phases, similar to Fe-aluminosilicates, were shown to be the bio-reduction products of Minette iron ore minerals (Maitte et al., 2015). Although the hairy aluminosilicates were microscopically similar (between this study and Maitte et al., (2015)), the crumpled paper-like phases showed lower Fe contents in the case of BETH1402 sediments (Maitte, personal communication). Similar Fe-aluminosilicates were also identified in the case of controlled experiments, where the interaction between metal iron and purified clay was studied (Rivard et al., 2013); the composition of the resulted phase was close to berthierine minerals, with typical basal spacing at 7.13 Å. The starting material is likely to be the ferrospheres (evidenced by light microscopy and SEM), which is mainly iron made, and is constituted of a mixture of wuestite and magnetite, as suggested by the Fe:O ratios. However, the possible sources of the light elements, Si and Al,

are more than a few. The presence of slagheaps, and thus the possible introduction of silico-calcic spheres in the sludge might be one possibility; but since Si and Al drastically decreased below 11 cm depth (Figure V-4 a and SM V-3), the contribution of slag to the sediments should be minor. The contribution of clay minerals, naturally occurring as suspended particles in the Orne waters, detrital quartz and diatom skeletons can also be retained as supplementary explanations. Indeed, diatom frustules are constituted of amorphous silica, which is supposed to be more reactive than phyllosilicates or quartz. In an attempt to characterize the weathering products of industrial sludge on one hand, and to decipher the contributions of natural and iron ore minerals that constitute the sediments and SPM of Orne River on the other, we reported the atomic proportions of Fe, Al and Si (that were determined by EDXS) in a ternary diagram (Figure V-9). On the basis of this Fe-Al-Si diagram on Orne River sediments (hairy Fe-aluminosilicates), Fensch River SPM (hairy Fe-aluminosilicates), iron ore particles (Fe-clays), and natural clays evidenced majorly in the top layers of BETH1402, there is a clear distinction between the newly formed Fe-aluminosilicates and the Fe-clays constituting the iron ore. Iron

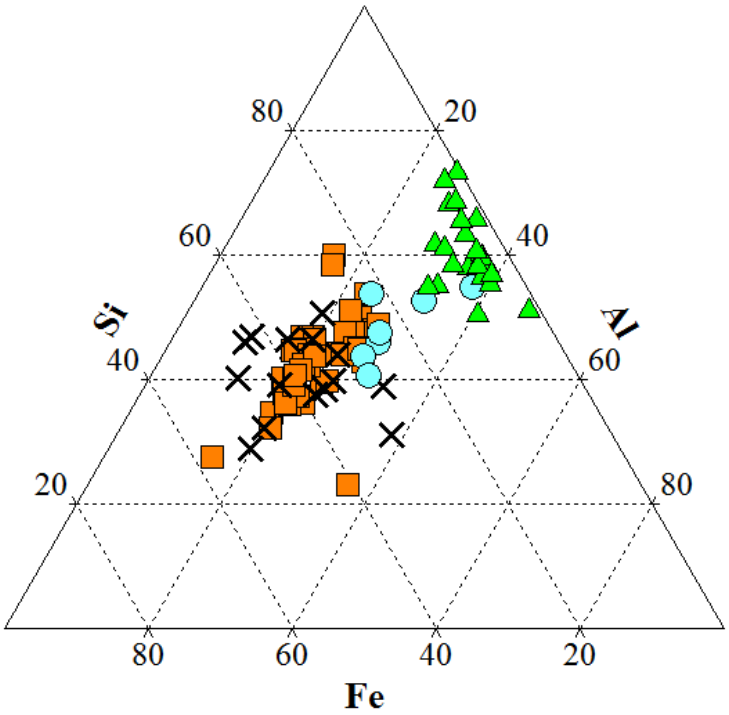

Figure V-9: Ternary diagram showing the atomic percentages of Fe, Al and Si measured by TEM-EDXS.
Included in the ternary diagram are the Fe-aluminosilicates particles from BETH1402 sediments (■, n = 44), similar hairy structures observed in the SPM from a neighboring steel river, the Fensch River, (✕, n = 15) (Montargès-Pelletier et al., 2014), Fe-clays from the iron ore, Minette de Lorraine (●, n = 7), and clays evidenced in the top layers of the sediment core (▲, n = 24).

content is higher in the Fe-aluminosilicates for sediments and SPM collected from the steel rivers (Orne and Fensch Rivers, respectively). In addition, there is an overlapping of newly formed Fe-aluminosilicates and Fe-clays from iron ore, which is certainly due to the presence of iron ore (Dagallier et al., 2002) in the sediments. However, the ternary diagram also demonstrates the distinction between the Fe-aluminosilicates and naturally occurring clays, which are mainly interlayered clays (illite/smectite) with lower iron contents. Si:Al atomic ratios were calculated for the same series of EDXS data, and showed only small variations, i.e., Si:Al was 2.0 ± 0.5 for Fe-aluminosilicates, 1.8 ± 0.5 for autochthonous clays and 1.65 ± 0.3 for Fe-clays of the iron ore. From the few EDX spectra acquired on silico-aluminous slag particles (SM V-7), Si:Al ratio is noticeably higher than 2.0, and reached as much as 3.2 for one particle. Although the number of micro-analyses is not sufficient to certainly evidence the contribution of slag particles to the formation of the Fe-aluminosilicates, we propose that several sources of Si and Al, including slag particles, were involved in the formation of these hairy phases. The weathering of the ferrospheres might have begun on land, and continued in sediments, after having mixed with natural suspended matter in the water column. Finally, Figure V-10 shows a schematic summary of the formation of Fe-aluminosilicates. At this stage,

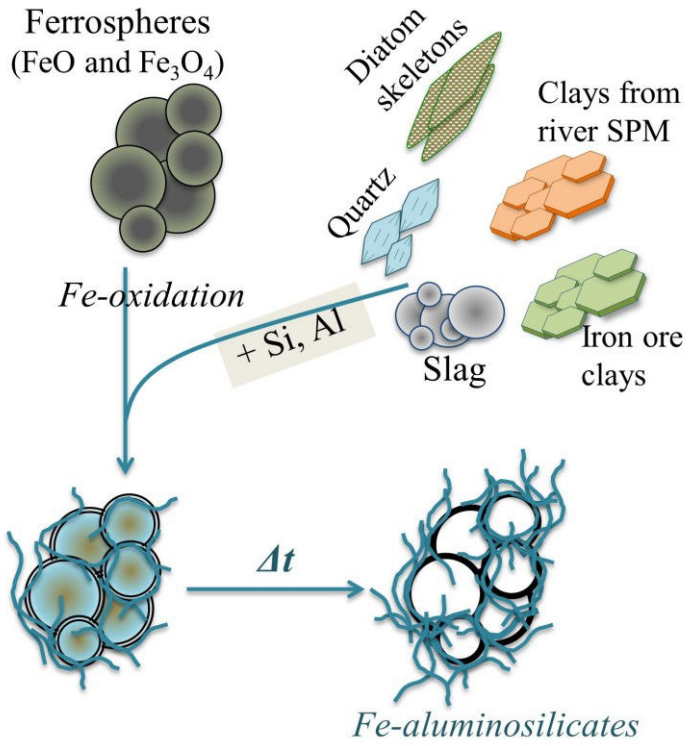

Figure V-10: Schematic representation on the hypothesis of hairy Fe-aluminosilicate formation.
Iron in the ferrospheres is oxidized and reacts with Al and Si from different sources (clays, diatom skeletons and quartz naturally occurring in the Orne River, Fe rich clays from the iron ore and slag particles) to form hairy Fe-aluminosilicates with time.

it is not really possible to identify the chemical mechanism(s) and the bacterial metabolism(s) involved in such mineralogical transformation(s), but we can still imagine some hypothetical processes on the basis of what is known about metal corrosion (e.g. Liu et al., 2015).

5. Conclusion

The vertical profile of contaminated river sediments in a former steelmaking area was investigated using grain size, chemical composition and mineralogical examination at bulk and sub-micrometric scales. The investigation of sediment mineralogy brought new interpretations on the chemical profiles with depth. The sedimentary materials were obviously characterized by iron rich minerals emitted from steelmaking facilities in the area upstream of the dam. The detected iron rich phases were goethite, magnetite, wuestite, pyrite and newly formed Fe-aluminosilicates, the former fingerprinting the iron ore and the four last minerals from the steelmaking sludge, more or less aged and weathered. Additional investigations on slagheap samples will compare the weathering processes on land and should unravel the specificity of weathering processes within the sediments. In this study, Fe-aluminosilicate was shown to be the predominant phase in the fine fraction of the contaminated sediments. Fe-aluminosilicates could also be used as markers in sediments and suspended particulate matter that have been influenced by steelmaking wastes. Moreover, the specific tridimensional organization of Fe-aluminosilicates, having polymetallic sulfides as crowns, further support the idea that those phases can be used as tracers for sediment remobilization in riverine systems. Nonetheless, the fate of the formed polymetallic sulfides remains unknown, but it is thought that sulfide dissolution and metal (Fe, Zn and Pb) release is a possible scenario upon sediment remobilization, which might be caused by floods, or dam modification or removal (Simpson et al., 2000). Studies concerning Zn, Pb and Ni isotopes are underway on Orne suspended matter and vertical layers of BETH1402 sediments to reveal different sources of the anthropogenic materials that had settled upstream the dam.

6. Supplementary Materials

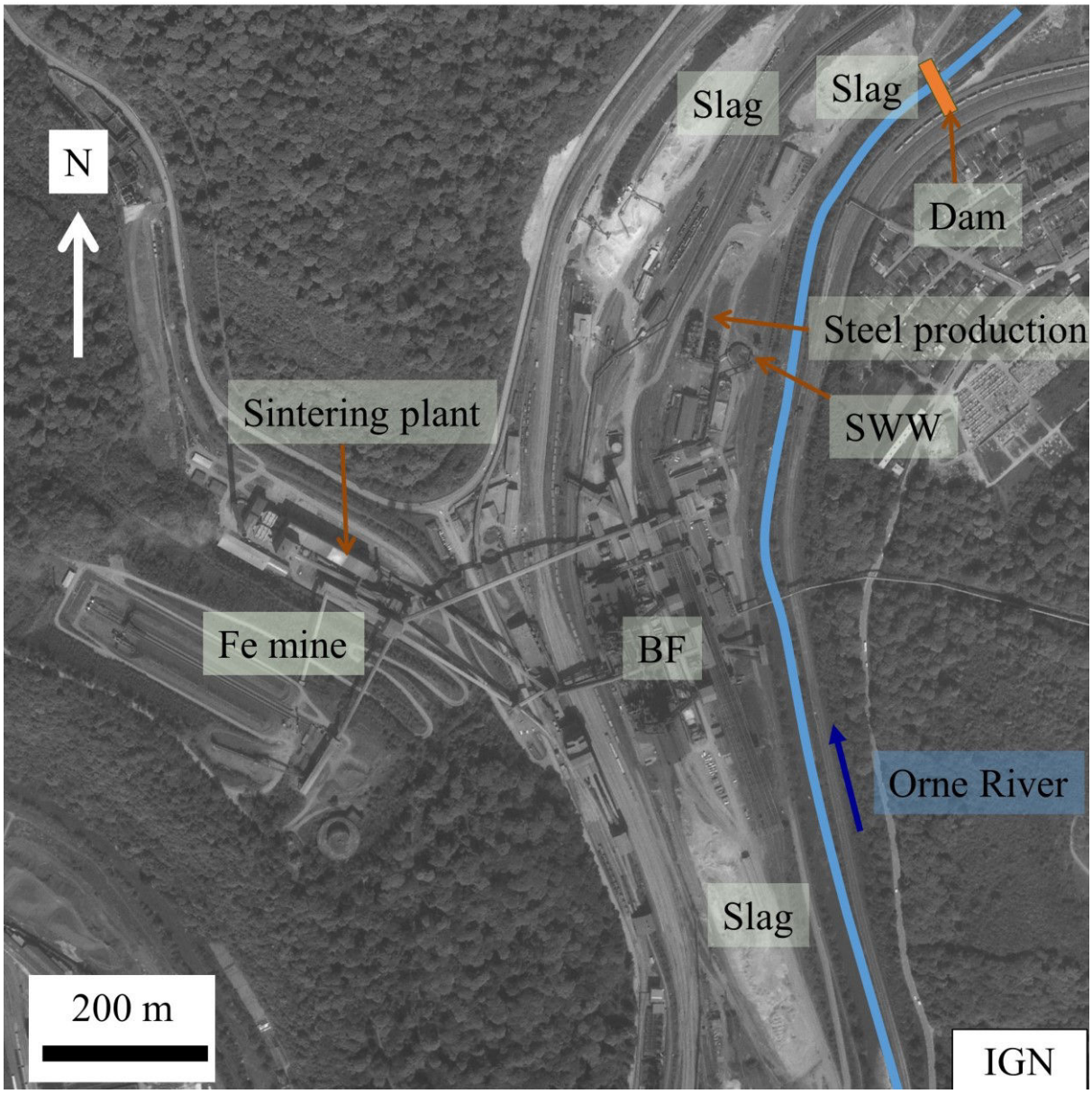

SM V-1: Aerial view of steelmaking facilities located in the very upstream zone of the Beth dam at Moyeuvre-Grande.
The image was taken approximately 32 years before the study (IGN 1982 – picture reference IGNF_PVA_1-0__1982-05-13__C3112-0011_1982_F3112-3512_0070). The image shows the Beth dam, and the locations of slagheaps, steel production, settling tank for wastewater (SWW), blast furnaces (BF), iron mine (Fe mine), sintering plant and the Orne River.

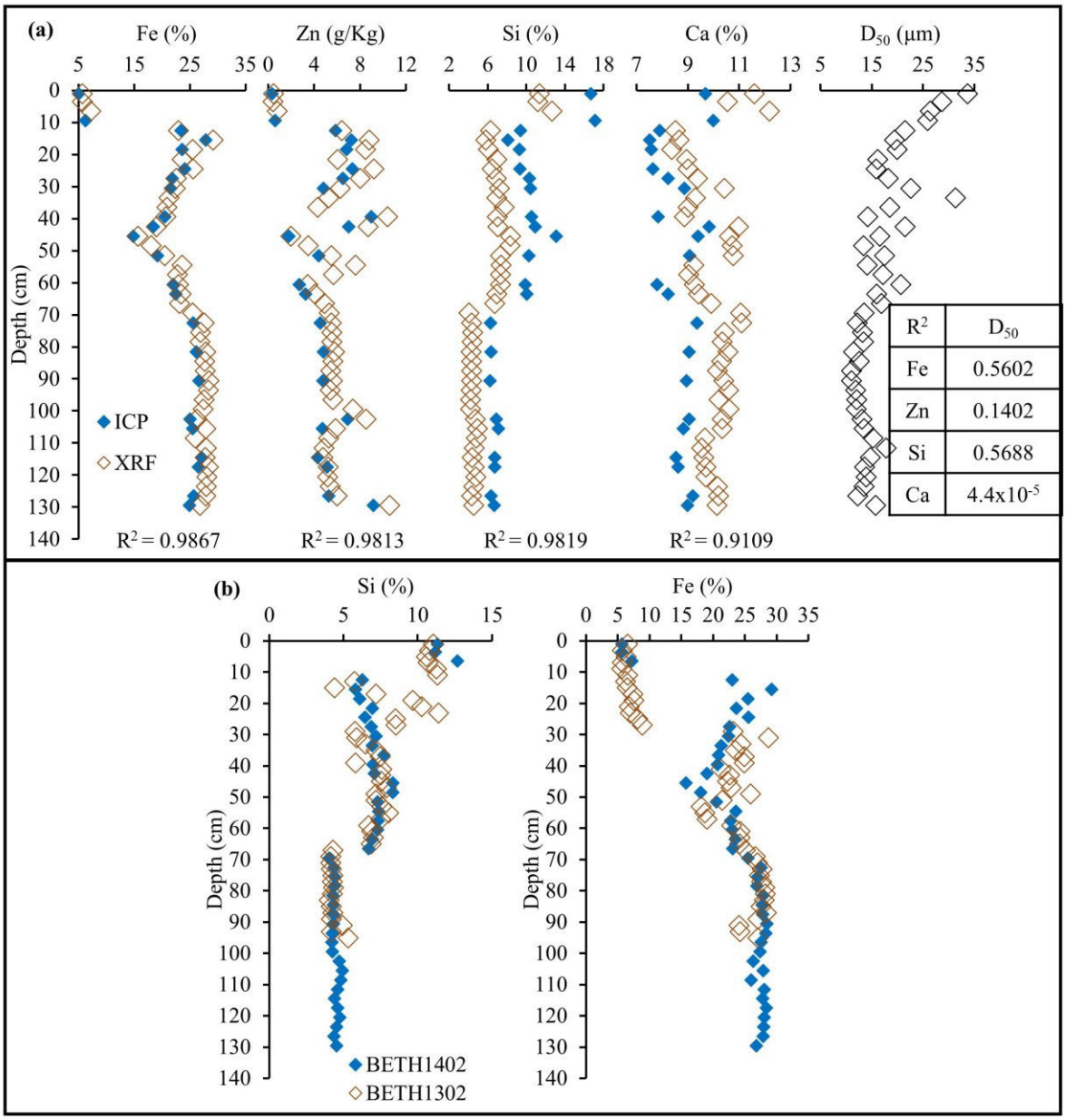

SM V-2: Using XRF data as a reliable technique for chemical composition.
a: Variation of Fe (%), Zn (g/Kg), Si (%) and Ca (%) contents (according to XRF and ICP data), and D_{50} values (µm) in the vertical profile of BETH1402 sediments. b: Comparison between Si and Fe contents (%) in BETH1302 and BETH1402 cores (according to XRF data).

a: A comparison was made between the contents of the elements Fe, Zn, Si and Ca obtained from the XRF gun (Thermo Scientific Niton XL3t GOLDD+ Analyzer from GeoRessources laboratory, Vandœuvre-lès-Nancy, France) and ICP-OES (for Fe, Si and Ca) and ICP-MS (for Zn). XRF measurements were performed on all the layers of BETH1402 core (as well as BETH1302 core). On the basis of XRF and grain size data, we selected several layers to determine their chemical composition by ICP-OES (for major elements) and ICP-MS (for trace elements), according to the procedures developed by Carignan et al., (2001). Fe contents were very alike between the semi-quantitative XRF measurements and ICP-OES, Zn

contents were less alike, while Si and Ca XRF contents were slightly underestimated and overestimated, respectively. Nevertheless, the contents of the elements revealed by XRF and ICP were significantly correlated (R^2 = 0.9867 for Fe, 0.9813 for Zn, 0.9819 for Si and 0.9109 for Ca; indicated at the bottom of the figures), and had similar trends in the vertical profile. Therefore, the XRF gun could be used as a reliable semi-quantitative technique to determine the chemical composition. As a result, we plotted the Fe and Si contents for all layers of BETH1302 and BETH1402 using the XRF data (elaborated in the below paragraph; part b). However, the chemical composition was not correlated to the particle size, as seen by poor correlations between D_{50} and the elements (see the table in the D_{50} figure). The poor or absence of correlation is most probably related to the complexity of the sediments; i.e. the contribution of various anthropogenic and lithogenic materials that had formed the sediments.

b: Fe and Si contents produced from the XRF gun for the layers of BETH1302 and BETH1402. The contents for both cores are superimposed and showed similar trends, especially in the deep layers. Consequently, the dating data of BETH1302 sediment core could be applied to BETH1402. It should be noted that the deposits of BETH1302 and BETH1402 also showed similar mineralogical composition (SM V-5 and Figure V-5).

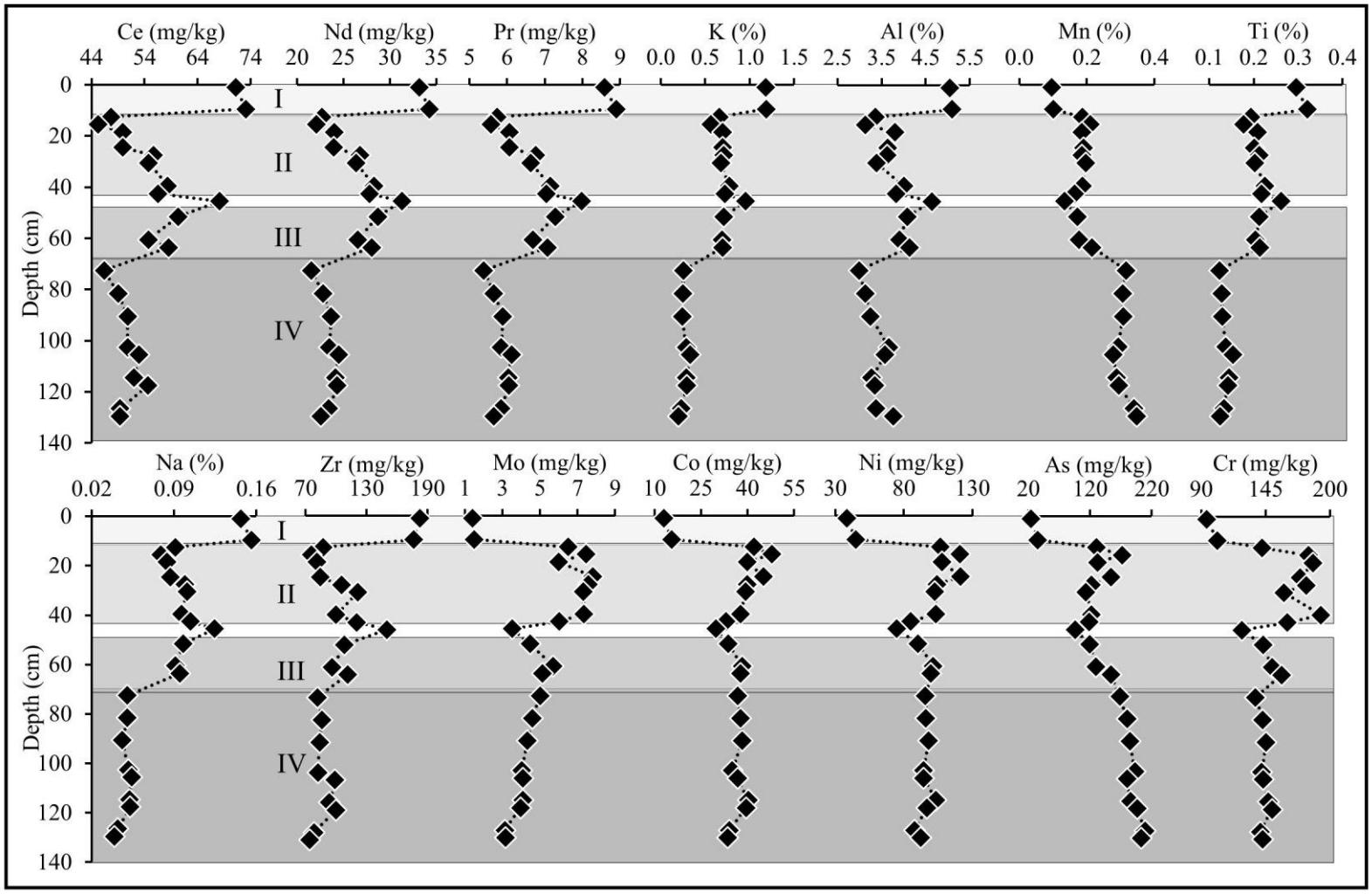

SM V-3: Chemical composition as a function of depth in BETH1402.
Variation of the light lanthanides Ce, Nd and Pr (in mg/kg), major elements K, Al, Mn, Ti and Na (in %), and trace elements Zr, Mo, Co, Ni, As and Cr (in mg/kg) as a function of depth for the sediment layers of BETH1402 core. The units 0 – 11 cm, 11 – 44 cm, 47 – 68 cm and 68 – 131 cm are indicated by I, II, III and IV respectively.

SM V-4: Pearson correlation coefficient for the elements in the sediment layers of BETH1402 core (n = 23).

		Al	Ca	K	Na	Ti	La	Ce	Pr	Nd	Zr	Zn	Pb	V	Fe	S	As	Mn	Mo	Ni	Co	Cr
Si	PCC	.898**	.295	.968**	.979**	.981**	.956**	.885**	.938**	.923**	.913**	-.569**	-.819**	-.849**	-.960**	-.510*	-.969**	-.912**	-.238	-.695**	-.723**	-.390
	P	.000	.171	.000	.000	.000	.000	.000	.000	.000	.000	.005	.000	.000	.000	.013	.000	.000	.275	.000	.000	.066
Al	PCC		.371	.832**	.824**	.873**	.940**	.926**	.934**	.926**	.853**	-.555**	-.659**	-.637**	-.921**	-.553**	-.811**	-.741**	-.484*	-.773**	-.815**	-.486*
	P		.082	.000	.000	.000	.000	.000	.000	.000	.000	.006	.001	.001	.000	.006	.000	.000	.019	.000	.000	.019
Ca	PCC			.086	.181	.154	.360	.502*	.428*	.434*	.557**	-.473*	-.177	.099	-.510*	-.521*	-.273	.000	-.725**	-.795**	-.757**	-.752**
	P			.696	.409	.482	.091	.015	.042	.039	.006	.023	.418	.655	.013	.011	.207	.999	.000	.000	.000	.000
K	PCC				.990**	.992**	.907**	.796**	.877**	.860**	.814**	-.472*	-.839**	-.937**	-.872**	-.387	-.952**	-.976**	-.030	-.511*	-.545**	-.196
	P				.000	.000	.000	.000	.000	.000	.023	.000	.000	.000	.068	.000	.000	.893	.013	.007	.371
Na	PCC					.987**	.923**	.824**	.898**	.883**	.859**	-.521*	-.858**	-.919**	-.894**	-.441*	-.966**	-.965**	-.065	-.560**	-.583**	-.257
	P					.000	.000	.000	.000	.000	.000	.011	.000	.000	.000	.035	.000	.000	.767	.006	.003	.236
Ti	PCC						.942**	.848**	.918**	.903**	.852**	-.507*	-.837**	-.893**	-.899**	-.429*	-.949**	-.955**	-.114	-.574**	-.606**	-.245
	P						.000	.000	.000	.000	.000	.014	.000	.000	.000	.041	.000	.000	.604	.004	.002	.260
La	PCC							.971**	.987**	.982**	.942**	-.645**	-.828**	-.722**	-.939**	-.618**	-.901**	-.837**	-.349	-.732**	-.751**	-.440*
	P							.000	.000	.000	.000	.001	.000	.000	.000	.002	.000	.000	.103	.000	.000	.036
Ce	PCC								.982**	.984**	.950**	-.683**	-.760**	-.558**	-.920**	-.716**	-.821**	-.714**	-.500*	-.815**	-.822**	-.539**
	P								.000	.000	.000	.000	.000	.006	.000	.000	.000	.000	.015	.000	.000	.008
Pr	PCC									.999**	.943**	-.636**	-.804**	-.676**	-.942**	-.669**	-.885**	-.807**	-.382	-.765**	-.784**	-.444*
	P									.000	.000	.001	.000	.000	.000	.000	.000	.000	.072	.000	.000	.034
Nd	PCC										.938**	-.636**	-.801**	-.652**	-.929**	-.683**	-.869**	-.792**	-.382	-.760**	-.777**	-.438*
	P										.000	.001	.000	.001	.000	.000	.000	.000	.072	.000	.000	.037
Zr	PCC											-.737**	-.806**	-.610**	-.943**	-.664**	-.876**	-.741**	-.469*	-.841**	-.832**	-.599**
	P											.000	.000	.002	.000	.001	.000	.000	.024	.000	.000	.003
Zn	PCC												.724**	.286	.627**	.631**	.563**	.416*	.600**	.694**	.649**	.759**
	P												.000	.186	.001	.001	.005	.048	.002	.000	.001	.000
Pb	PCC													.734**	.753**	.488*	.865**	.838**	.072	.487*	.487*	.304
	P													.000	.000	.018	.000	.000	.743	.018	.018	.159
V	PCC														.706**	.160	.870**	.956**	-.224	.272	.311	.011
	P														.000	.466	.000	.000	.304	.209	.149	.960
Fe	PCC															.600**	.930**	.789**	.453*	.856**	.880**	.576**
	P															.002	.000	.000	.030	.000	.000	.004
S	PCC																.455*	.289	.507*	.641**	.625**	.582**
	P																.029	.180	.014	.001	.001	.004
As	PCC																	.921**	.153	.648**	.676**	.357
	P																	.000	.487	.001	.000	.095
Mn	PCC																		-.096	.392	.420*	.098
	P																		.662	.064	.046	.658
Mo	PCC																			.813**	.786**	.871**
	P																			.000	.000	.000
Ni	PCC																				.989**	.834**
	P																				.000	.000
Co	PCC																					.796**
	P																					.000

PCC: Pearson correlation coefficient, same as Pearson's R.
P: *P* value. The *P* value is the probability of finding the observed results when the null hypothesis (H_0) is true. H_0: there does not exist a correlation between X and Y.
**: Correlation is significant at the 0.01 level (2-tailed).
*: Correlation is significant at the 0.05 level (2-tailed).

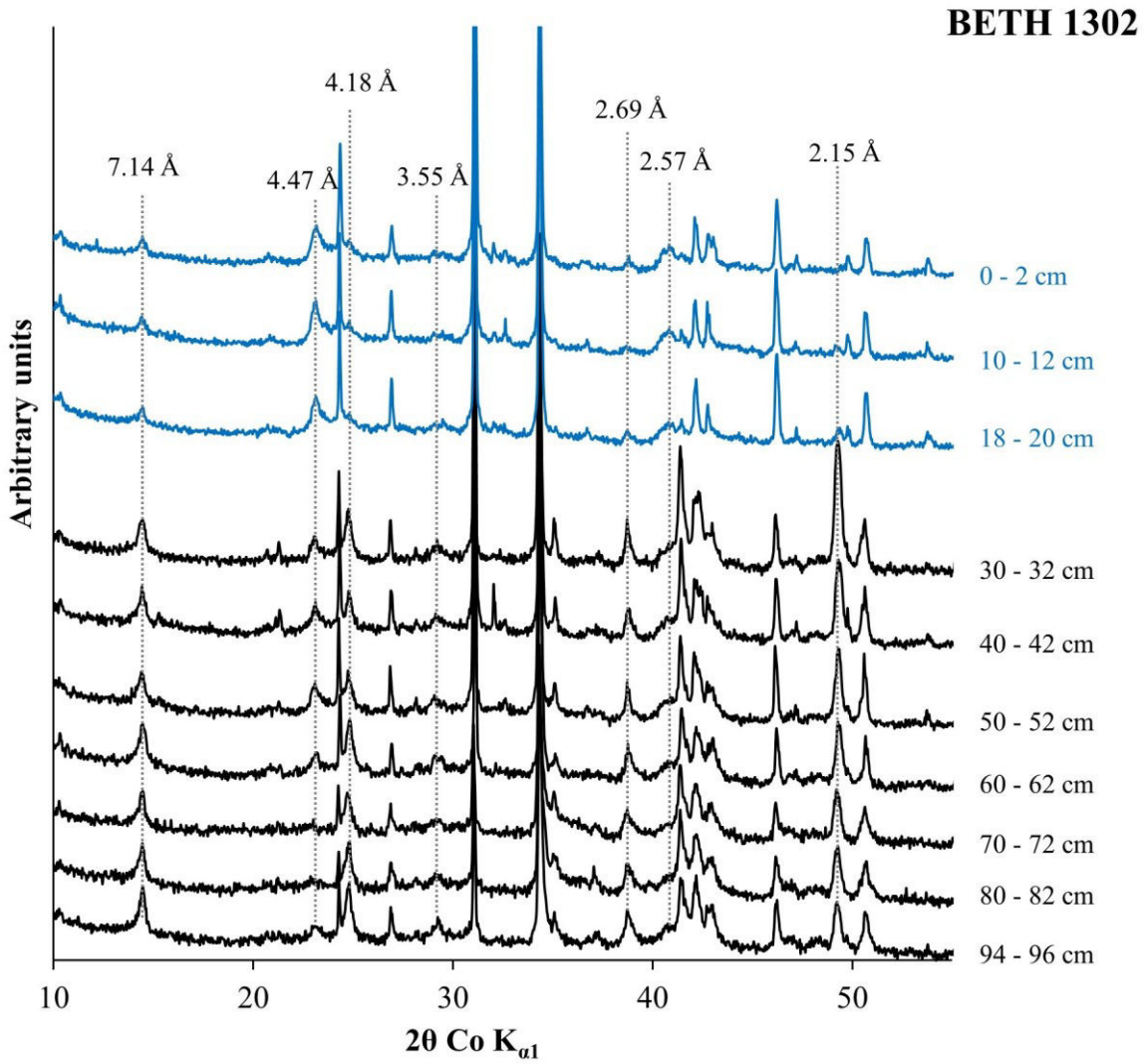

SM V-5: XRD patterns of BETH1302 sediments.
Similar diffraction line trends to BETH1402 sediments (Figure V-5) are shown. The XRD patterns of BETH1302 layers showed, as a function of depth: i. an increase of the 7.14 Å diffraction line, which was assigned to a newly formed aluminosilicate (with basal plane *001* of phyllosilicate) and was particularly enriched in iron, ii. an increase of goethite peaks at 4.18 and 2.69 Å, and iii. a decrease of hkl diffraction lines of phyllosilicates at 4.47 and 2.57 Å. The blue diffractograms represent sediment samples of lithogenic nature, while the black diffractograms belong to the materials mainly composed of steelmaking waste (black deposits).

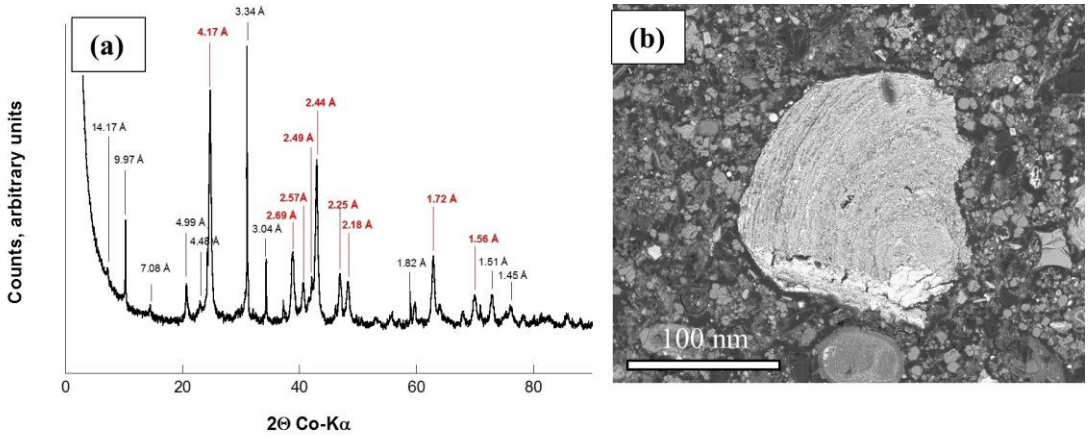

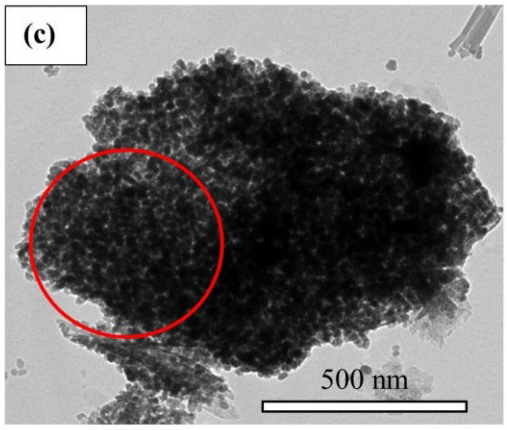

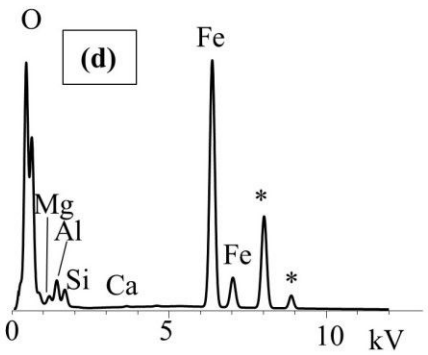

(e)	K factor	Atomic percentage	Emission line
O	1.7628	67.4	Kα
Mg	0.7624	1.1	Kα
Al	0.7314	2.7	Kα
Si	0.6924	1.8	Kα
P	0.7440	<0.1	Kα
Ca	0.7732	<0.1	Kα
Fe	1.0	27	Kα

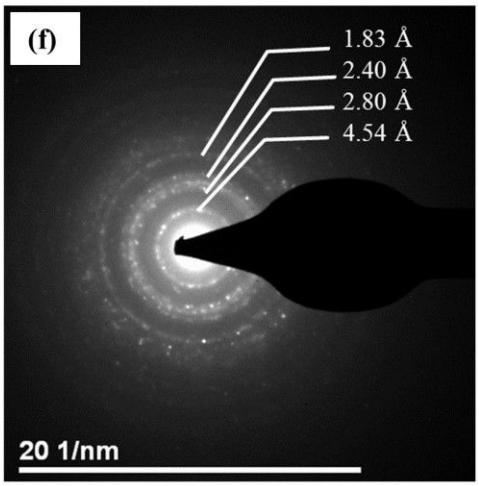

SM V-6: Identification of the iron nanogranules as goethite
a: XRD pattern of "Minette" iron ore; marked in red are the diffraction lines of goethite; b: SEM BSE micro-image of a weathered iron ooid seen in the sediments of the Orne River; c: TEM micro-image of goethite nanogranules of the Minette ore, d: corresponding EDX spectrum, e: table summarizing the TEM-EDXS data and f: SAED pattern. Asterisks on the EDX spectra (d) indicate the emission lines of copper, which are due to the contribution of the TEM grid, a carbon coated copper grid.

TEM micro-images of the Minette ore showed the predominance of circular Fe-bearing nanoparticles (SM V-6 c). EDXS revealed that those nanoparticles had an O:Fe ratio of 2.1 ± 0.2 (Table V-1 in the main text), indicating Fe oxy-hydroxide (FeOOH). Furthermore, since XRD patterns of the "Minette" sample showed diffraction lines for goethite (mainly 4.17 and 2.44 Å), these FeOOH particles were identified as goethite particles (SM V-6 a). Finally, TEM SAED on aggregates provide a typical pattern of polycrystalline material (SM V-6 f). Electron

diffraction resulted in several rings that were assigned to diffraction distances. Several aggregates were tested and all provided similar SAED patterns. Also a similar electron diffraction pattern was obtained from Fe oxy-hydroxides particles in Beth sediments. From particle size and morphology, EDXS and SAED data, we could demonstrate that the nanoparticles detected in BETH1402 sediments (Figure V-8 a in the main text), are fingerprints of the Minette ore that was used for making steel in Lorraine.

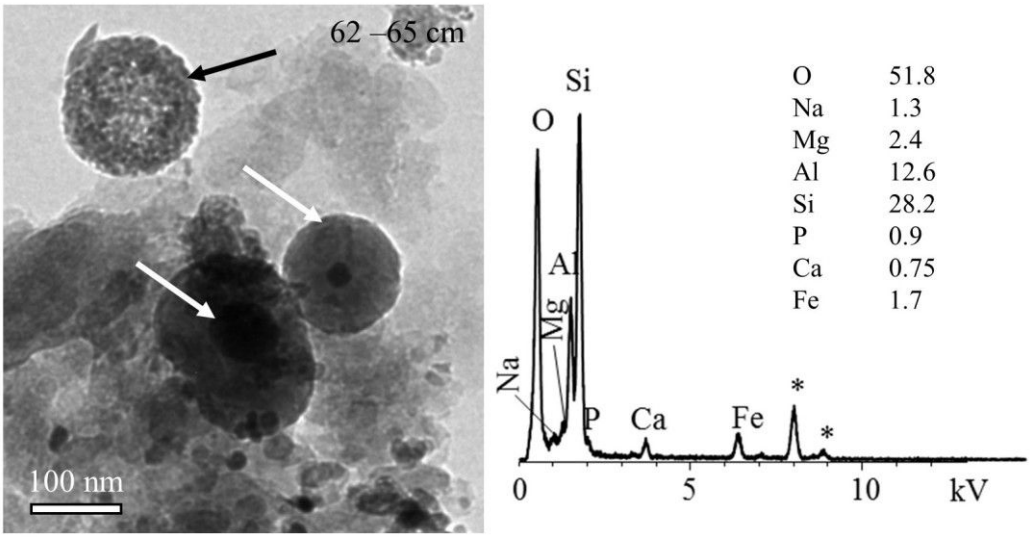

SM V-7: TEM micro-image of silico-calcic glass phases that were detected in the sediments of BETH1402 with a corresponding EDX spectrum

References

Appleby, P.G., Oldfield, F., 1992. Applications of Lead-210 to Sedimentation Studies, in: Ivanovich, M., Harmon, R.S. (Eds.), Uranium-Series Disequilibrium: Applications to Earth, Marine, and Environmental Sciences. Clarendon Press, Oxford, p. 910.

Ayrault, S., Roy-Barman, M., Le Cloarec, M.-F., Priadi, C.R., Bonté, P., Göpel, C., 2012. Lead contamination of the Seine River, France: Geochemical implications of a historical perspective. Chemosphere 87, 902–910. doi:10.1016/j.chemosphere.2012.01.043

Bertrand, O., Mansuy-Huault, L., Montargès-Pelletier, E., Losson, B., Argant, J., Ruffaldi, P., Etienne, D., Garnier, E., Dezileau, L., Faure, P., Michels, R., 2012. Molecular evidence for recent land use change from a swampy environment to a pond (Lorraine, France). Org. Geochem. 50, 1–10. doi:10.1016/j.orggeochem.2012.06.004

Cappuyns, V., Swennen, R., Devivier, A., 2006. Dredged river sediments: Potential chemical time bombs? A case study. Water, Air, Soil Pollut. 171, 49–66. doi:10.1007/s11270-005-9012-y

Carignan, J., Hild, P., Mevelle, G., Morel, J., Yeghicheyan, D., 2001. Routine analyses of trace elements in geological samples using flow injection and low pressure on-line liquid chromatography coupled to ICP-MS: A study of geochemical reference materials BR, DR-N, UB-N, AN-G and GH. Geostand. Geoanalytical Res. 25, 187–198. doi:10.1111/j.1751-908X.2001.tb00595.x

Dagallier, G., Grgic, D., Homand, F., 2002. Caractérisation minéralogique et microtexturale du vieillissement anthropique du minerai de fer lorrain. Comptes Rendus Geosci. 334, 455–462. doi:10.1016/S1631-0713(02)01783-2

Das, B., Prakash, S., Reddy, P.S.R., Biswal, S.K., Mohapatra, B.K., Misra, V.N., 2002. Effective utilization of blast furnace flue dust of integrated steel plants. Eur. J. Miner. Process. Environ. Prot. 2, 61–68.

Das, B., Prakash, S., Reddy, P.S.R., Misra, V.N., 2007. An overview of utilization of slag and sludge from steel industries. Resour. Conserv. Recycl. 50, 40–57. doi:10.1016/j.resconrec.2006.05.008

Dhivert, E., Grosbois, C., Courtin-Nomade, A., Bourrain, X., Desmet, M., 2016. Dynamics of metallic contaminants at a basin scale - Spatial and temporal reconstruction from four sediment cores (Loire fluvial system, France). Sci. Total Environ. 541, 1504–1515. doi:10.1016/j.scitotenv.2015.09.146

Droppo, I.G., Liss, S.N., Williams, D., Nelson, T., Jaskot, C., Trapp, B., 2009. Dynamic existence of waterborne pathogens within river sediment compartments. Implications for water quality regulatory affairs. Environ. Sci. Technol. 43, 1737–1743. doi:10.1021/es802321w

El Samrani, A.G., Lartiges, B.S., Ghanbaja, J., Yvon, J., Kohler, A., 2004. Trace element carriers in combined sewer during dry and wet weather: an electron microscope investigation. Water Res. 38, 2063–2076. doi:10.1016/j.watres.2004.01.029

Fernandes, G.W., Goulart, F.F., Ranieri, B.D., Coelho, M.S., Dales, K., Boesche, N., Bustamante, M., Carvalho, F.A., Carvalho, D.C., Dirzo, R., Fernandes, S., Galetti Jr, P.M., Millan, V.E.G., Mielke, C., Ramirez, J.L., Neves, A., Rogass, C., Ribeiro, S.P., Scariot, A., Soares-Filho, B., 2016. Deep into the mud: ecological and socio-economic impacts of the dam breach in Mariana, Brazil. Nat. Conserv. 14, 35–45. doi:10.1016/j.ncon.2016.10.003

Ferrand, E., Eyrolle, F., Radakovitch, O., Provansal, M., Dufour, S., Vella, C., Raccasi, G., Gurriaran, R., 2012. Historical levels of heavy metals and artificial radionuclides reconstructed from overbank sediment records in lower Rhône River (South-East France). Geochim. Cosmochim. Acta 82, 163–182. doi:10.1016/j.gca.2011.11.023

Freyssenet, M., 1979. La sidérurgie française : 1945 – 1979, l'histoire d'une faillite, les solutions qui s'affrontent. Savilli, <halshs-00165640>, Paris.

Fryirs, K.A., Brierley, G.J., 2012. Sediment Movement and Deposition in River Systems, in: Geomorphic Analysis of River Systems: An Approach to Reading the Landscape. Wiley-Blackwell Publishing, Ltd, Chichester, UK, pp. 81–115. doi:10.1002/9781118305454.ch6

Garcier, R.J., 2007. Rivers we can't bring ourselves to clean – historical insights into the pollution of the Moselle River (France), 1850–2000. Hydrol. Earth Syst. Sci. 11, 1731–1745. doi:10.5194/hess-11-1731-2007

Grabowski, R.C., Droppo, I.G., Wharton, G., 2011. Erodibility of cohesive sediment: The importance of sediment properties. Earth-Science Rev. 105, 101–120. doi:10.1016/j.earscirev.2011.01.008

Groen, J.C., Craig, J.R., 1994. The inorganic geochemistry of coal, petroleum, and their gasification/combustion products. Fuel Process. Technol. 40, 15–48. doi:10.1016/0378-3820(94)90033-7

Heise, S., Förstner, U., 2007. Risk assessment of contaminated sediments in river basins—theoretical considerations and pragmatic approach. J. Environ. Monit. 9, 943–952. doi:10.1039/b704071g

Helble, J.J., Sarofim, A.F., 1993. Trace element behavior during coal combustion. Am. Chem. Soc. Div. Fuel Chem. Prepr. 38, 257–264.

Houhou, J., Lartiges, B.S., Hofmann, A., Frappier, G., Ghanbaja, J., Temgoua, A., 2009. Phosphate dynamics in an urban sewer: A case study of Nancy, France. Water Res. 43, 1088–1100. doi:10.1016/j.watres.2008.11.052

Hu, Z., Sparovek, G., Haneklaus, S., Schnug, E., 2006. Rare Earth Elements, in: Lal, R. (Ed.), Encyclopedia of Soil Science. CRC Press, pp. 1437–1441. doi:10.1081/E-ESS-120015983

Huang, J.-H., Huang, F., Evans, L., Glasauer, S., 2015. Vanadium: global (bio)geochemistry. Chem. Geol. 417, 68–89. doi:10.1016/j.chemgeo.2015.09.019

Hudson-Edwards, K.A., Macklin, M.G., Brewer, P.A., Dennis, I.A., 2008. Assessment of Metal Mining-Contaminated River Sediments in England and Wales. Environment Agency, Bristol, UK.

Huot, H., Simonnot, M.-O., Marion, P., Yvon, J., De Donato, P., Morel, J.-L., 2013. Characteristics and potential pedogenetic processes of a Technosol developing on iron industry deposits. J. Soils Sediments 13, 555–568. doi:10.1007/s11368-012-0513-1

Huot, H., Simonnot, M.O., Watteau, F., Marion, P., Yvon, J., De Donato, P., Morel, J.-L., 2014. Early transformation and transfer processes in a Technosol developing on iron industry deposits. Eur. J. Soil Sci. 65, 470–484. doi:10.1111/ejss.12106

Kretzschmar, R., Mansfeldt, T., Mandaliev, P.N., Barmettler, K., Marcus, M.A., Voegelin, A., 2012. Speciation of Zn in blast furnace sludge from former sedimentation ponds using synchrotron X-ray diffraction, fluorescence, and absorption spectroscopy. Environ. Sci. Technol. 46, 12381–12390. doi:10.1021/es302981v

Le Cloarec, M.-F., Bonte, P.H., Lestel, L., Lefèvre, I., Ayrault, S., 2011. Sedimentary record of metal contamination in the Seine River during the last century. Phys. Chem. Earth, Parts A/B/C 36, 515–529. doi:10.1016/j.pce.2009.02.003

Le Meur, M., Montargès-Pelletier, E., Bauer, A., Gley, R., Migot, S., Barres, O., Delus, C., Villiéras, F., 2016. Characterization of suspended particulate matter in the Moselle River (Lorraine, France): evolution along the course of the river and in different hydrologic regimes. J. Soils Sediments 16, 1625–1642. doi:10.1007/s11368-015-1335-8

Lepage, H., Evrard, O., Onda, Y., Lefèvre, I., Laceby, J.P., Ayrault, S., 2015. Depth distribution of cesium-137 in paddy fields across the Fukushima pollution plume in 2013. J. Environ. Radioact. 147, 157–164. doi:10.1016/j.jenvrad.2015.05.003

Lesven, L., Lourino-Cabana, B., Billon, G., Recourt, P., Ouddane, B., Mikkelsen, O., Boughriet, A., 2010. On metal diagenesis in contaminated sediments of the Deûle river (northern France). Appl. Geochemistry 25, 1361–1373. doi:10.1016/j.apgeochem.2010.06.007

Liu, H., Fu, C., Gu, T., Zhang, G., Lv, Y., Wang, H., Liu, H., 2015. Corrosion behavior of carbon steel in the presence of sulfate reducing bacteria and iron oxidizing bacteria cultured in oilfield produced water. Corros. Sci. 100, 484–495. doi:10.1016/j.corsci.2015.08.023

López-Antón, M.A., Díaz-Somoano, M., Ochoa-González, R., Martínez-Tarazona, M.R., 2011. Distribution of trace elements from a coal burned in two different spanish power stations. Ind. Eng. Chem. Res. 50, 12208–12216. doi:10.1021/ie2018542

Lourino-Cabana, B., Lesven, L., Billon, G., Proix, N., Recourt, P., Ouddane, B., Fischer, J.C., Boughriet, A., 2010. Impacts of metal contamination in calcareous waters of Deûle River (France): Water quality and thermodynamic studies on metallic mobility. Water. Air. Soil Pollut. 206, 187–201. doi:10.1007/s11270-009-0095-8

Macklin, M.G., Hudson-Edwards, K.A., Dawson, E.J., 1997. The significance of pollution from historic metal mining in the Pennine orefields on river sediment contaminant fluxes to the North Sea. Sci. Total Environ. 194–195, 391–397. doi:10.1016/S0048-9697(96)05378-8

Maclin, E., Sicchio, M., 1999. Dam Removal Success Stories, Restoring Rivers through Selective Removal of Dams that Don't Make Sense. American Rivers, Friends of the Earth, & Trout Unlimited, Washington, DC.

Maitte, B., Jorand, F.P.A., Grgic, D., Abdelmoula, M., Carteret, C., 2015. Remineralization of ferrous carbonate from bioreduction of natural goethite in the Lorraine iron ore (Minette) by *Shewanella putrefaciens*. Chem. Geol. 412, 48–58. doi:10.1016/j.chemgeo.2015.07.024

Mansfeldt, T., Dohrmann, R., 2004. Chemical and mineralogical characterization of blast-furnace sludge from an abandoned landfill. Environ. Sci. Technol. 38, 5977–5984. doi:10.1021/es040002+

Montargès-Pelletier, E., Duriez, C., Ghanbaja, J., Jeanneau, L., Falkenberg, G., Michot, L.J., 2014. Microscale investigations of the fate of heavy metals associated to iron-bearing particles in a highly polluted stream. Environ. Sci. Pollut. Res. 21, 2744–2760. doi:10.1007/s11356-013-2192-x

Montargès-Pelletier, E., Jeanneau, L., Faure, P., Bihannic, I., Barres, O., Lartiges, B.S., 2007. The junction of Fensch and Moselle rivers, France; mineralogy and composition of river materials. Environ. Geol. 53, 85–102. doi:10.1007/s00254-006-0621-6

Moskalyk, R.R., Alfantazi, A.M., 2003. Processing of vanadium: a review. Miner. Eng. 16, 793–805. doi:10.1016/S0892-6875(03)00213-9

Picon, M., 2014. Autour de l'Orne industrieuse : paysages industriels hérités. Université de Lorraine, Environmental Engineering. <dumas-01110255>.

Radakovitch, O., Charmasson, S., Arnaud, M., Bouisset, P., 1999. ^{210}Pb and Caesium accumulation in the Rhône delta sediments. Estuar. Coast. Shelf Sci. 48, 77–92. doi:10.1006/ecss.1998.0405

Rivard, C., Montargès-Pelletier, E., Vantelon, D., Pelletier, M., Karunakaran, C., Michot, L.J., Villiéras, F., Michau, N., 2013. Combination of multi-scale and multi-edge X-ray spectroscopy for investigating the products obtained from the interaction between kaolinite and metallic iron in anoxic conditions at 90 °C. Phys. Chem. Miner. 40, 115–132. doi:10.1007/s00269-012-0552-6

Robbins, J.A., Edgington, D.N., 1975. Determination of recent sedimentation rates in Lake Michigan using Pb-210 and Cs-137. Geochim. Cosmochim. Acta 39, 285–304. doi:10.1016/0016-7037(75)90198-2

Roberts, D.R., Scheinost, A.C., Sparks, D.L., 2002. Zinc speciation in a smelter-contaminated soil profile using bulk and microspectroscopic techniques. Environ. Sci. Technol. 36, 1742–1750. doi:10.1021/es015516c

Sawhney, B.L., 1972. Selective sorption and fixation of cations by clay minerals: a review. Clays Clay Miner. 20, 93–100. doi:10.1346/CCMN.1972.0200208

Sharonova, O.M., Anshits, N.N., Anshits, A.G., 2013. Composition and morphology of narrowly sized ferrospheres isolated from various types of fly ash. Inorg. Mater. 49, 586–594. doi:10.1134/S0020168513060113

Simpson, S.L., Apte, S.C., Batley, G.E., 2000. Effect of short-term resuspension events on the oxidation of cadmium, lead, and zinc sulfide phases in anoxic estuarine sediments. Environ. Sci. Technol. 34, 4533–4537. doi:10.1021/es991440x

Simpson, S.L., Apte, S.C., Batley, G.E., 1998. Effect of short-term resuspension events on trace metal speciation in polluted anoxic sediments. Environ. Sci. Technol. 32, 620–625. doi:10.1021/es970568g

Sobanska, S., Deneele, D., Barbillat, J., Ledésert, B., 2016. Natural weathering of slags from primary Pb–Zn smelting as evidenced by Raman microspectroscopy. Appl. Geochemistry 64, 107–117. doi:10.1016/j.apgeochem.2015.09.011

Sokol, E. V, Kalugin, V.M., Nigmatulina, E.N., Volkova, N.I., Frenkel, A.E., Maksimova, N. V, 2002. Ferrospheres from fly ashes of Chelyabinsk coals: chemical composition, morphology and formation conditions. Fuel 81, 867–876. doi:10.1016/S0016-2361(02)00005-4

Spadini, L., Bott, M., Wehrli, B., Manceau, A., 2003. Analysis of the major Fe bearing mineral phases in recent lake sediments by EXAFS spectroscopy. Aquat. Geochemistry 9, 1–17. doi:10.1023/B:AQUA.0000005608.69468.1e

Sterckeman, T., Douay, F., Proix, N., Fourrier, H., 2000. Vertical distribution of Cd, Pb and Zn in soils near smelters in the North of France. Environ. Pollut. 107, 377–389. doi:10.1016/S0269-7491(99)00165-7

Sterckeman, T., Douay, F., Proix, N., Fourrier, H., Perdrix, E., 2002. Assessment of the contamination of cultivated soils by eighteen trace elements around smelters in the north of France. Water. Air. Soil Pollut. 135, 173–194. doi:10.1023/A:1014758811194

Trinkel, V., Mallow, O., Aschenbrenner, P., Rechberger, H., Fellner, J., 2016. Characterization of blast furnace sludge with respect to heavy metal distribution. Ind. Eng. Chem. Res. 55, 5590–5597. doi:10.1021/acs.iecr.6b00617

Trinkel, V., Mallow, O., Thaler, C., Schenk, J., Rechberger, H., Fellner, J., 2015. Behavior of chromium, nickel, lead, zinc, cadmium, and mercury in the blast furnace — A critical review of literature data and plant investigations. Ind. Eng. Chem. Res. 54, 11759–11771. doi:10.1021/acs.iecr.5b03442

Valentim, B., Shreya, N., Paul, B., Gomes, C.S., Sant'Ovaia, H., Guedes, A., Ribeiro, J., Flores, D., Pinho, S., Suárez-Ruiz, I., Ward, C.R., 2016. Characteristics of ferrospheres in fly ashes derived from Bokaro and Jharia (Jharkand, India) coals. Int. J. Coal Geol. 153, 52–74. doi:10.1016/j.coal.2015.11.013

Van Damme, A., Degryse, F., Smolders, E., Sarret, G., Dewit, J., Swennen, R., Manceau, A., 2010. Zinc speciation in mining and smelter contaminated overbank sediments by EXAFS spectroscopy. Geochim. Cosmochim. Acta 74, 3707–3720. doi:10.1016/j.gca.2010.03.032

Vassilev, S. V, Vassileva, C.G., 1996. Mineralogy of combustion wastes from coal-fired power stations. Fuel Process. Technol. 47, 261–280. doi:10.1016/0378-3820(96)01016-8

Vdović, N., Billon, G., Gabelle, C., Potdevin, J.-L., 2006. Remobilization of metals from slag and polluted sediments (Case Study: The canal of the Deûle River, northern France). Environ. Pollut. 141, 359–369. doi:10.1016/j.envpol.2005.08.034

Wakeham, S.G., Forrest, J., Masiello, C.A., Gélinas, Y., Alexander, C.R., Leavitt, P.R., 2004. Hydrocarbons in Lake Washington sediments. A 25-year retrospective in an urban lake. Environ. Sci. Technol. 38, 431–439. doi:10.1021/es0343149

Wen, X.-Y., Huang, C.-M., Tang, Y., Gong-Bo, S.-L., Hu, X.-X., Wang, Z.-W., 2014. Rare earth elements: a potential proxy for identifying the lacustrine sediment source and soil erosion intensity in karst areas. J. Soils Sediments 14, 1693–1702. doi:10.1007/s11368-014-0928-y

Wilkin, R.T., Barnes, H.L., 1997. Formation processes of framboidal pyrite. Geochim. Cosmochim. Acta 61, 323–339. doi:10.1016/S0016-7037(96)00320-1

Xu, M., Yan, R., Zheng, C., Qiao, Y., Han, J., Sheng, C., 2003. Status of trace element emission in a coal combustion process: a review. Fuel Process. Technol. 85, 215–237. doi:10.1016/S0378-3820(03)00174-7

Zebracki, M., 2008. Devenir des polluants métalliques associés aux sédiments contaminés dans un cours d'eau en

relation avec la dynamique sédimentaire. Ph.D. thesis, Université Paris-Sud XI, France.
Zeng, T., Arnold, W.A., Toner, B.M., 2013. Microscale characterization of sulfur speciation in lake sediments. Environ. Sci. Technol. 47, 1287–1296. doi:10.1021/es303914q
Zhao, Y., Zhang, J., Sun, J., Bai, X., Zheng, C., 2006. Mineralogy, chemical composition, and microstructure of ferrospheres in fly ashes from coal combustion. Energy & Fuels 20, 1490–1497. doi:10.1021/ef060008f

VI. APPENDIX TO CHAPTER 4: SEDIMENTATION UPSTREAM THE BETH DAM

1. Introduction

This appendix deals with information that was presented in the previous chapter/article but was not included for publication reasons. Even though the previous chapter/article showed that Beth sediments have not formed under conventional sedimentation processes, as indicated by ^{137}Cs and $^{210}Pb_{xs}$ findings, we interpret data that might be useful to generate an age model for Beth sediments (i.e. the sediments that had settled upstream the dam). This approach was developed by using particle size distribution (PSD), past flood information, major elements and the history of the steelmaking facilities. It should be noted that the chemical composition used in this section is based on XRF measurements (Thermo Scientific Niton XL3t GOLDD+ Analyzer from GeoRessources laboratory, Vandœuvre-lès-Nancy, France), since all the layers were analyzed by XRF; while the chemical composition of only 23 layers (out of 44) was determined by ICP-OES and ICP-MS (see SM V-2 of the previous chapter where XRF data was proven to be representative of the actual contents in the case of Beth sediments).

2. Recapture of the sediments upstream the Beth dam

In the coming parts, non-conventional methods will be used to suggest the age of the sediments. The Beth dam was built in 1959/1960. Consequently, the sediments found in the upstream zone of the dam had surely deposited after 1960. During that period (60s), steelmaking facilities were active along the Orne River, including the area from Homécourt to Moyeuvre-Grande (Freyssenet, 1979; Thouvenin, 1981), which extends nearly 10 km upstream of the Beth dam. The dam was constructed mainly to store water for steelmaking facilities (blast furnaces). BETH1402 sediment core was 131 cm long, and the 11 – 131 cm deposits were fingerprinted by steelmaking wastes, as proven by enriched chemical contents and mineral speciation, mainly by Fe and Fe minerals, respectively (as revealed by ICP-OES for the first, and XRD, SEM and TEM for the latter). As a result, the 120 cm deposits are surely originated from steelmaking wastes. The steelmaking facilities stopped in 1988. Consequently, the deposits had settled over a maximum period of 28 years (i.e. between 1960 and 1988). It should be noted that the sediments found upstream the dam can be deeper than 131 cm, depending on the location. Indeed, a 210 cm sediment core was collected in 2017 (named

BETH1701[xxxiii]). The 5 – 210 cm deposits of BETH1701 showed sediments highly enriched in Fe (Fe contents ranged between 15 and 30%), similar to the 11 – 131 cm deposits of BETH1402. Therefore, the major part of the sediments is clearly fingerprinted by steelmaking deposits, except for a relatively thin surficial layer. That layer ranged between 3 and 28 cm, depending on the distance of the sediment with respect to the right bank as well as the distance away from the dam.

If the sedimentation rate were to be calculated for the 11 – 131 cm deposits of BETH1402, it would roughly be 4.3 cm/yr (that of BETH1701 would be 7.3 cm/yr). However, steel production was not constant during that period (Freyssenet, 1979); therefore, the proposed sedimentation rate is not precise, yet it gives an idea about the high and certainly unnatural value. For example, steel production was approximately 6 million tons per year "Mt/yr" in 1954, 11.6 Mt/yr in 1960, 17 My/yr in 1965 and 33 My/yr in 1977 (Freyssenet, 1979). As a result, waste products and consequent release into the river should vary as well. As for the surface 11 cm layer of BETH1402, it had a lithogenic nature, which was also revealed by chemical composition and mineral speciation (detrital material). Those 11 cm deposits would then have settled after 1988 and before the sampling date (2014), i.e. 0.42 cm/yr; which is similar to the sedimentation rates found in fish ponds in the upstream area of the sampling site (Bertrand et al., 2012). That hypothesis would be true if we assumed that sedimentation was continuous and there was no erosion or resuspension of the settled materials during that period. Moreover, the surface sediments of lithogenic nature were 28 cm for BETH1302 and 5 cm for BETH1701; which would roughly suggest a 1 and 0.2 cm/yr sedimentation rate, respectively. The variation in the thickness of lithogenic (detrital) surficial deposits is clear (3 cm for BETH1507, 5 cm for BETH1701, 11 cm for BETH1402 and 28 cm for BETH1302). This difference is due to the variation in riverbed profile. Indeed, the riverbed is of peculiar shape at BETH1302, with a slope followed by a flat surface, which promotes settling (Figure VI-1).

[xxxiii] Between December 2016 and January 2017, the dam was opened, the water level was low and the sediments could be easily sampled; therefore, sediments were cored. Only general information was collected for BETH1701 (XRF and PSD).

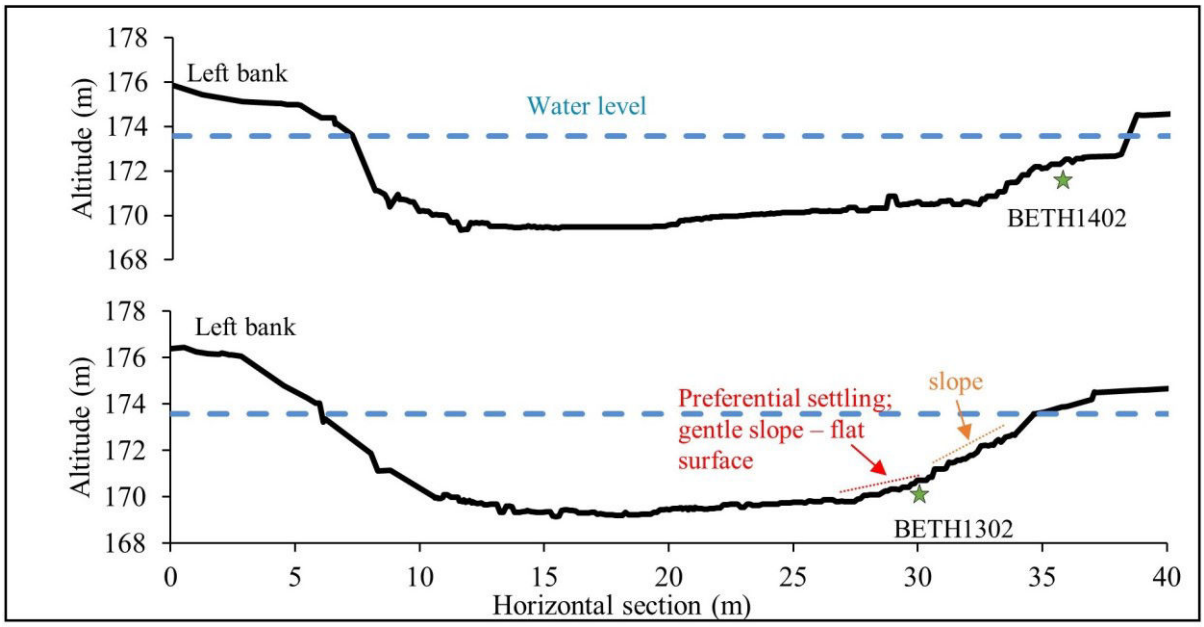

Figure VI-1: Sections of the Orne River where BETH1402 and BETH1302 cores were collected. The profiles were produced using an echo sounder (by Luc Manceau and Benoit Losson).

The recorded water discharge in the Orne River is generally between 13 and 35 m^3/s during the winter period (see chapter *II*, Figure II-3). Moreover, several flood events were documented since the 1970s, which are compiled in Table VI-1. The water discharge during the floods is several fold higher than the average. The change in river hydrodynamics is, therefore, a likely factor for sediment remobilization. During a flood, settled particles are remobilized in case the flow force exceeds the forces of the immersed mass of the grain and cohesion, which is termed threshold shear stress for initial motion (Robert, 2014). After a flood, and when the water flow goes back to normal, the relatively coarse grains will start to settle first, which are followed by finer particles. Accordingly, fine particles are remobilized and coarser grains settle in the riverbed (Di Francesco et al., 2016). This approach, along with the major contents (Si, Fe and Ca) will be used to link past flood events in BETH1402 sediment layers in the following sections.

3. An insight about Beth deposits

The water discharge is reduced in the Beth dam influence zone, therefore explaining the particularly fine nature of BETH1402 sediments. The fine grain sizes are also due to the nature of the deposited materials that are fingerprinted by steelmaking wastes. The coarsest particles that remobilize due to a flood might settle upstream the influence zone. Furthermore, and according to the D_{50} and D_{90} values of BETH1402 sediments (10 – 34 µm and 35 – 190 µm, respectively; see chapter *V*, Figure V-2) the deposits had formed as a result of uniform settling

(Passega, 1964, 1957). Generally, all sediment layers are poorly sorted, and most are finely skewed, except for the layers 29 – 35 cm, 41 – 44 cm, 68 – 74 cm and 80 – 86 cm, which had more of a symmetrical distribution, according to Blott and Pye (2001).

Table VI-1: Major flood events recorded in the Orne River since 1970.
Data compiled by Claire Delus on the basis of the database provided by EauFrance (2016).

Date (month/year)	Water discharge (m^3/s)	Flood volume (Mm^3)	Type of flood
02/1970	133	56	2
05/1970	159	37	4
02/1977	175	35	3
01/1979	164	32	2
02/1979	155	78	3
02/1980	156	58	3
10/1981	239	41	1
12/1982	177	42	3
04/1983	207	58	4
05/1983	212	54	4
02/1984	181	81	2
01/1986	138	66	3
03/1988	207	72	3
01/1993	160	25	3
12/1993	292	222	2
01/1995	227	97	2
02/1997	195	32	2
10/1998	149	44	1
12/1999	140	92	2
03/2001	167	69	2
12/2001	188	34	3
02/2002	144	45	2
12/2010	175	37	3
02/2016	121	32	2

Mm^3: million m^3
1: Flood occurring after the dry season or low water flow; mainly in the fall.
2: Flood occurring during the wet season or high water flow; mainly in the winter.
3: Flood occurring during mild weather, when it rains or when ice/snow melts after temperatures reach positive values (in °C).
4: Flood occurring at the end of high flow period; in the mid-end of the spring.

From the sediments that had deposited first (i.e. the deepest layers of BETH1402), the contents of the major elements showed slight changes between 119 and 131 cm, and did not follow the same trend as D_{50} (Figure VI-2). It should be noted that the metal contents are based on XRF measurements. The grain size was relatively coarser in the deepest layer, which could also be observed by the shifting of the PSD curve towards coarser sizes and slightly lower Fe contents. The decrease of grain size in the upward sense of a core is a characteristic of clastic sediments, where sediments gradually settle (finest particles settle last). In the case of Beth sediments, the particles are not really clastic, rather they are fine steelmaking wastes. Nonetheless, they were mixed with detrital suspended matter before deposition (diatom skeletons and clay minerals). The apparent decrease of D_{50} from 113 to 98 cm might thus be

caused by a graded settling of the waterborne materials. Moreover, Fe and Si did not follow a clear trend, and slightly fluctuated in that zone, while Ca followed an opposite trend (i.e. coarser grains had lower Ca contents). This indicates that the variation in D_{50} might not be related to detrital materials, rather Ca might be introduced into the river from steelmaking wastes not containing, or poor in Fe, such as finely granulated slag. Due to the different contributions of steelmaking wastes that occurred in the Orne River during the last century, it is not possible to suggest a period that took the 98 – 113 cm deposits to settle. The sediments between 74 and 98 cm were rather similar in terms of PSD curves, D_{50} and major elements. That similarity is also shared with 113 – 128 cm layers, which suggest that the deposited materials in 74 – 98 cm and 113 – 128 cm depths are similar. The increase of grain sizes in the upward sense might be related to the variation in introduced materials, similar to the case of 59 – 74 cm deposits. Indeed, the PSD showed a shifting towards coarser particles, and D_{50}, Si and other lithogenic elements (of detrital origin, such as La, Ce, Pr and Na; see SM V-3) increased, while Fe and Ca contents decreased from 74 to 59 cm (Figure VI-2). It is important to note that 68 cm presents a critical depth in the BETH1402 core; with higher contents of Fe and Ca (and other metals related to steelmaking industries) inferior to that depth, and higher contents of Si (and other elements of lithogenic contribution, such as Al, Ti and light REEs) superior to that depth (see SM V-3 and Figure V-4). Therefore, the variation from 74 to 59 cm depth is caused by the increasing contribution of detrital materials, the decreasing contribution of steelmaking wastes, and/or a change in the deposited materials. Moreover, PSD curves were symmetrical for layers deeper than 68 cm (till ~ 90 cm), while layers above 68 cm were more skewed to fine grain sizes (computations and descriptive terminology are based on Blott and Pye (2001)). From the data of the recent floods and from the grain sizes, several layers of BETH1402 sediments could be suggested to have settled accordingly. The layer 59 – 62 cm is thought to have formed by the flood that occurred in October 1981. Even though D_{50} showed only slight variation for that layer, the PSD curve showed a protrusion of a 100 – 200 µm grain population, which is responsible for the coarser sizes (indicated by a dashed grey rectangle in Figure VI-2). Grangeon et al., (2012) also recorded a protrusion of a coarser grain population in small catchments (22 km^2) which was caused by flood events. Furthermore, for layers inferior to 62 cm, the increase of D_{50} was accompanied by the protrusion of coarser populations (such as layers 110 – 113 cm, 101 – 104 cm, 83 – 86 cm and 71 – 74 cm). The chemical composition of 59 – 62 cm layer was similar to the underlying sediments. On the other hand, the finer character of the overlying 53 – 59 cm sediments did not have an influence on Si, Ca and Fe contents. This suggests that the variation in grain size can be justified by the deposited

steelmaking materials, such as dust or blast furnace sludge. The layer 50 – 53 cm, which was assigned to the flood that took place in December 1982, also showed a protrusion of a 100 – 200 µm grain population. The same applies to the layers that are thought to have deposited in April 1983 and May 1983, i.e. layers 41 – 44 cm and 32 – 35 cm, respectively. Those layers showed a widely distributed PSD (with a leptokurtic distribution; while the others showed a more centered mesokurtic distribution), which possibly merged the fine and the coarse grain populations. Some of the layers that had formed after flood events showed relatively lower Fe contents, such as layers 50 – 53 cm and 41 – 44 cm. This indicates that Fe contribution was lessened due to the increasing contribution of detrital materials. Moreover, the detrital contribution could be followed by increasing Ca contents, but not by Si, probably due to the complex release of steel wastes (slag, sludge and dust) to the river. It should be noted that 44 – 68 cm and 11 – 44 cm deposits were considered as distinct units, as proven by the composition of major and trace elements (developed in the previous *chapter*). The decrease in D_{50} from 35 to 23 cm could be followed by more centered (less wide) PSD curves. That decrease could also be followed by a general increase of Fe contents, and a general decrease in detrital elements (Si and Ca contents). Therefore, the decrease in grain size might be explained by the increasing contribution of steelmaking wastes (due to increasing Fe contents) and/or the decreasing contribution of detrital materials (due to decreasing Si and Ca contents). The sediments between 23 – 35 cm might had settled during a year (more or less) period[xxxiv]. The most recent two floods are thought to have occurred in 1984 and 1986; the PSD curves were rather centered in comparison to other floods; only very small populations were shown in the coarser range. On the other hand, Fe (and other elements related to steelmaking) contents decreased, while Ca and Si (and other elements originated from lithogenic materials) contents increased for sediments that settled afterward. The variation is not directly caused by variation in grain size, rather it is caused by the different nature of deposits between the 0 – 11 cm and 11 – 44 cm units.

Regarding the PSD curves, coarse particle populations were slightly noticeable when put next to the finer ones; therefore, the two populations were sometimes observed as one broad curve (e.g. 32 – 35 cm and 41 – 44 cm), while other layers showed centered populations. Indeed,

[xxxiv] Again, due to the complexity of the sediments (contribution of lithogenic and wastes from steelmaking facilities) and due to the possibility or remobilization of sediments, it is not certain that the mentioned layers had deposited during a specific period.

many riverine sediments display multimodal distributions (Bagnold and Barndorff-Nielsen, 1980; Di Francesco et al., 2016; Remo et al., 2016; Sun et al., 2002), which show overlapping particle size distribution curves (i.e. appearing as one broad population). The surficial 11 cm layer could hardly be associated with past flood events since more than 11 floods were recorded between 1986 and 2014 (Table VI-1). In addition, the grain size showed an increasing trend and PSD showed broader sizes (towards bimodal grain populations) from 11 cm depth towards the surface. It is therefore suggested that sedimentation was not continuous, and erosion/remobilization of sediments occurred.

4. Why didn't ^{137}Cs and ^{210}Pb data provide the age of Beth sediments?

A notion is raised here; since some sediments might have deposited after 1981, why didn't the ^{137}Cs peak caused by the Chernobyl nuclear accident (in 1986) show up in Beth sediments? First, and as mentioned earlier, the deposits between 11 and 131 cm depth had settled before the steelmaking facilities stopped in 1988; thus, either the top layers of the 11 – 131 cm unit, or the surficial 11 cm deposits, should contain the ^{137}Cs peak. For the former case, Beth sediments are majorly composed of materials that were deposited from industrial facilities, such as blast furnaces (dust and sludge), and not watershed surface run-off, therefore, the ^{137}Cs peak might not be evidenced. For the latter case, ^{137}Cs fallout from the atmosphere are readily fixed to fine soil particles, especially clays (Lepage et al., 2015; Sawhney, 1972); those particles are then translocated, as surface leaching, to nearby water systems where they settle. The surface 11 cm sediments had formed after 1986, therefore, sediments enriched with ^{137}Cs might had settled upstream the Beth dam, but were remobilized, possibly due to a flood that occurred after 1988 (see Table VI-1).

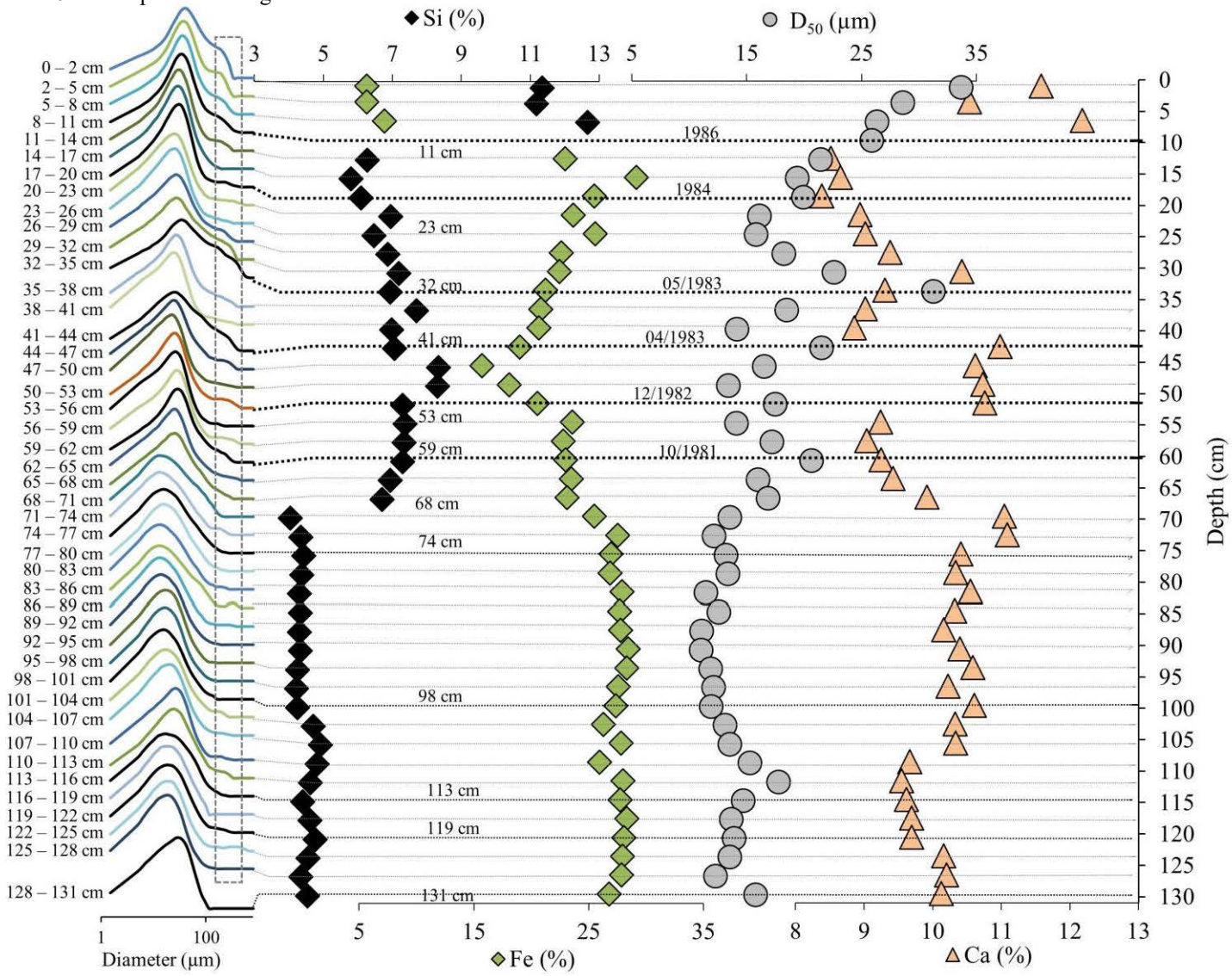

Figure VI-2: The particle size distribution (PSD) curves, the contents of Si (%), Fe (%) and Ca (%), and D_{50} values of BETH1402 sediment layers. The PSD curves follow the same depths as the metal contents and D_{50}, which are directed by dotted grey lines. The dashed and grey rectangle in the PSD figure shows the relatively coarser populations. The plotted metal contents are based on XRF data. The dates indicated near the D_{50} values represent the possible flood event (marked by black dotted lines).

5. Conclusion

The heterogeneity in the riverbed profile of the upstream zone of the Beth dam was seen at a meter scale. Therefore, settling and remobilization could vary between sediments, depending on their location. This explains the variation in the depths of the lithogenic surficial deposits of BETH1302 and BETH1402 (28 and 11 cm, respectively). Due to the highly complex nature of the Beth sediments, the contribution of lithogenic materials and steelmaking wastes, the role of the dam on modifying river hydrodynamics, and consequent sediment settling and remobilization, the proposed age model for the sediments remains a speculation. However, past flood events were linked to sediments with coarser grains and spread populations. In most cases, flood events could also be followed by increasing contents of elements that come from lithogenic sources (e.g. Si) and a decrease in metals that are originated from steelmaking waste (Fe in our case). On the other hand, the variation in grain size and chemical composition could also be caused by variation in waste materials that partly formed the settled sediments.

References

Bagnold, R.A., Barndorff-Nielsen, O., 1980. The pattern of natural size distributions. Sedimentology 27, 199–207. doi:10.1111/j.1365-3091.1980.tb01170.x

Bertrand, O., Mansuy-Huault, L., Montargès-Pelletier, E., Losson, B., Argant, J., Ruffaldi, P., Etienne, D., Garnier, E., Dezileau, L., Faure, P., Michels, R., 2012. Molecular evidence for recent land use change from a swampy environment to a pond (Lorraine, France). Org. Geochem. 50, 1–10. doi:10.1016/j.orggeochem.2012.06.004

Blott, S.J., Pye, K., 2001. GRADISTAT: A grain size distribution and statistics package for the analysis of unconsolidated sediments. Earth Surf. Process. Landforms 26, 1237–1248. doi:10.1002/esp.261

Di Francesco, S., Biscarini, C., Manciola, P., 2016. Characterization of a flood event through a sediment analysis: The tescio river case study. Water 8, 308. doi:10.3390/w8070308

EauFrance, 2016. Banque Hydro [WWW Document]. Le Serv. public d'information sur l'eau. Ministère l'Ecologie, du Développement Durable l'Energie. URL http://www.hydro.eaufrance.fr/ (accessed 5.28.16).

Freyssenet, M., 1979. La sidérurgie française : 1945 – 1979, l'histoire d'une faillite, les solutions qui s'affrontent. Savilli, <halshs-00165640>, Paris.

Grangeon, T., Legout, C., Esteves, M., Gratiot, N., Navratil, O., 2012. Variability of the particle size of suspended sediment during highly concentrated flood events in a small mountainous catchment. J. Soils Sediments 12, 1549–1558. doi:10.1007/s11368-012-0562-5

Lepage, H., Evrard, O., Onda, Y., Lefèvre, I., Laceby, J.P., Ayrault, S., 2015. Depth distribution of cesium-137 in paddy fields across the Fukushima pollution plume in 2013. J. Environ. Radioact. 147, 157–164. doi:10.1016/j.jenvrad.2015.05.003

Passega, R., 1964. Grain size representation by CM patterns as a geological tool. J. Sediment. Res. 34, 830–847.

Passega, R., 1957. Texture as characteristic of clastic deposition. Am. Assoc. Pet. Geol. Bull. 41, 1952–1984.

Remo, J.W.F., Heine, R.A., Ickes, B.S., 2016. Particle size distribution of main-channel-bed sediments along the upper Mississippi River. Geomorphology 264, 118–131. doi:10.1016/j.geomorph.2016.04.012

Robert, A., 2014. Fluvial Sediments: Processes of Erosion and Transport, in: River Processes: An Introduction to Fluvial Dynamics. Routledge, London, pp. 51–90.

Sawhney, B.L., 1972. Selective sorption and fixation of cations by clay minerals: a review. Clays Clay Miner. 20, 93–100. doi:10.1346/CCMN.1972.0200208

Sun, D., Bloemendal, J., Rea, D.K., Vandenberghe, J., Jiang, F., An, Z., Su, R., 2002. Grain-size distribution function of polymodal sediments in hydraulic and aeolian environments, and numerical partitioning of the sedimentary components. Sediment. Geol. 152, 263–277. doi:10.1016/S0037-0738(02)00082-9

Thouvenin, M., 1981. De Wendel-Sidélor à Sacilor-Sollac : 1968-1980. 13 années de mutations difficiles en Lorraine. Rev. Geogr. Est. 21, 37–63. doi:10.3406/rgest.1981.1483

VII. CHAPTER 5: ZINC SPECIATION IN SUBMERGED RIVER SEDIMENTS MIXED WITH STEELMAKING WASTES IN THE ORNE RIVER, NORTHEASTERN FRANCE

This chapter shows complementary data on the BETH1402 sediment core described and characterized in the previous chapter (chapter *V*). The previous chapter focused on Fe mineralogy at bulk, micrometric and sub-micrometric scales, which could reveal the possible fate of steelmaking wastes and by-products in the metal-laden sediments. Also, the variation between recent deposits of lithogenic materials and others originating from steel wastes or by-products was visible by various parameters, such as color, particle size, chemical composition and mineralogical phases (using XRD, SEM and TEM). However, in this part, the focus is made on the speciation of the "trace" metal Zn using microscopic (SEM and TEM) and spectroscopic techniques (XANES).

Abstract

Submerged river sediments were cored upstream of a dam that was shown to be highly influenced by past steelmaking industries, in the Orne River, northeastern France. This study focuses on the distribution, origin, fate and speciation of zinc in those sediments. The sediment layers were analyzed (chapter *V*), here the discussion will mainly revolve around Zn mineralogy and speciation in the metal-laden deposits. Due to the high amorphous character of Zn minerals, scanning and transmission electron microscopies and X ray absorption spectroscopy were used to reveal Zn speciation. First, it should be noted that the sediments below 11 cm revealed aspects of steelmaking wastes, while the layers superior to 11 cm showed more of a lithogenic character. The predominant Zn species detected in the sediments were sulfides (amorphous and crystalline), which counted for 60 to 80% in the contaminated sediments, other Zn species were franklinite, Zn into and onto clay and calcite, and adsorbed onto ferrihydrites, Fe oxy-hydroxides and Fe-aluminosilicates. Fe-aluminosilicates that were proven to be the fingerprint of former steelmaking facilities were main Zn carriers as well, sometimes as sulfides. Furthermore, polymorphic Zn (or polymetallic) sulfides precipitated in the submerged sediments, and were detected as amorphous or poorly crystalline phases. XANES spectra at the Zn Kedge and linear combination fitting showed a detectable trend of

Abstract
Zn species in the vertical profile, something which could not be seen by SEM nor by TEM. Indeed, franklinite, ZnS and Zn in clays were evident for distinct units of BETH1402 sediments. The heterogeneous nature of the sediments demonstrates that different weathering conditions occurred to the settled materials, which could form different species of Zn. Finally, since Zn sulfides were majorly encountered as nanometric particles, their transport and dissolution due to sediment remobilization, possibly caused by dam removal or floods for example, will cause the release of high metal concentrations to the river water.

Keywords: *Orne*, *Sediment, zinc speciation, mineralogy, zinc sulfides, TEM, XANES.*

1. Introduction

The development of mining and smelting activities has increased metal input into the environment for the last hundred years (e.g. Boughriet et al., 2007; Ettler, 2016; Nriagu, 1996, 1990; Van Damme et al., 2010). This is the case of the north and northeastern regions in France, which witnessed intense mining and metallurgical activities, especially in the XIXth and XXth centuries. The Lorraine region was famous for coal, salt and iron mining, and mainly steelmaking. Without proper management of wastes and by-products of such facilities, nearby soils and sediments become highly enriched with metals, such as As, Cd, Cr, Cu, Fe, Pb and Zn (Boughriet et al., 2007; Lesven et al., 2010; Lourino-Cabana et al., 2010; Montargès-Pelletier et al., 2014, 2007, Sterckeman et al., 2006, 2002, 2000). In the process of steel making, the main Zn sources originate not only from the pristine and raw materials, such as iron ore (or sinter) and coke, but also from the surface treatment applied to steel wires (Besta et al., 2013; Trinkel et al., 2015). Blast furnace sludge (BFS) is formed by wet scrubbing (or wet cleaning) of smokes collected on top of Blast furnaces (BFs). BFS is commonly composed of Zn, Pb, Ni, Cr, Fe and Cd (Das et al., 2007; Mansfeldt and Dohrmann, 2004; Trinkel et al., 2016, 2015). Moreover, the chemical composition of BFS depends on the pristine materials used and on the undergoing processes in BFs. Steelmaking facilities were installed near rivers, since the processes consume great volumes of water (Garcier, 2007; Rogé and Walterspieler, 1982). Caused by lack of regulations, sludge was mainly pumped into nearby landfills, collected in settling or sedimentation ponds, or released into rivers (Garcier, 2007; Kretzschmar et al., 2012; Mansfeldt and Dohrmann, 2004). As a result, sludge and contaminated waters, particularly enriched in Fe and trace metals (such as Zn and Pb), were quasi-continuously discharged into rivers, strongly degrading river water quality (Rogé and Walterspieler, 1982). Consequently, distinct Zn containing minerals are expected to reach sediments, such as Zn-phyllosilicates, Zn-ferrocyanide, hydrozincite, zincite, franklinite and smithsonite (e.g. Kretzschmar et al., 2012; Scheinost et al., 2002; Van Damme et al., 2010). Secondary minerals, such as zinc sulfides, would then form once those minerals reach matrices of different physicochemical conditions, such as the case of submerged sediments.

The previous chapter evidenced highly contaminated sediments in the Orne River (chapter *V*). The mineralogical investigations and chemical analyses of the sediments strongly suggested multiple sources of the materials including (i) iron ore (fingerprinted by goethite nanoparticles and few debris of oolites), (ii) blast furnace sludge (fingerprinted by fly ashes,

fine grain sizes, and high Fe, Zn and Pb contents), and (iii) a detrital contribution (fingerprinted by quartz, clay minerals, diatom frustules and a group of elements that were strongly correlated to each other (Si, Al, K, Ti, Na and light lanthanides)). The presence of this latter natural contribution suggested that the contaminated materials were simultaneously settled along with detrital minerals, which were naturally transported by the Orne River. Few studies had brought to our attention the mineralogy of steelmaking sludge, including those on Zn speciation (Huot et al., 2013; Kretzschmar et al., 2012; Mansfeldt and Dohrmann, 2004). They evidenced that in many cases, Zn and Pb were majorly scavenged by amorphous phases and that only a minor part of Zn or Pb-bearing phases could be identified with X-ray diffraction. It should be noted that transformation of mineral phases (including Zn phases) occur throughout different stages; i.e. upon the introduction of raw materials into BFs and exposure to elevated temperatures, during wet scrubbing of furnace smokes, upon waste stacking and exposure to humidity and the atmosphere (oxidative conditions), upon release into water systems, and after they settle as sediments where anoxic conditions might dominate. Using microscopic and spectroscopic techniques, namely SEM, TEM and XAS, the fate and speciation of Zn were described in BFS landfills (Mansfeldt and Dohrmann, 2004), sedimentation ponds (Kretzschmar et al., 2012) and smelter contaminated riverbank sediments (Van Damme et al., 2010). However, in the precise case of Orne River sediments, Zn speciation might have evolved differently due to the reductive conditions inherited by the submerged river sediments. Also, another unique feature is the presence of detrital and natural particles, including natural organic matter, clay minerals, and also living organisms (particularly micro-organisms). The mixed lithogenic-anthropogenic deposits have aged for more than 30 years, and the rise of new formed Zn species is highly anticipated.

The study site is located a few meters upstream a dam (named Beth dam), where great loads of metal-laden sediments had settled. However, the fate of the dam is on debate and should be modified or even removed in the coming decade. The removal of this dam will surely result in the remobilization of the contaminated sediments. Indeed, river sediment resuspension was shown to cause metal release, mainly due to oxidation; furthermore, the remobilization might be selective, where only distinct phases or certain species are remobilized (Boughriet et al., 2007; Montargès-Pelletier et al., 2014; Simpson et al., 2000; Vdović et al., 2006). As a result, Zn speciation in the sediments upstream of the Beth dam must be determined. The aims of this study are to report the mineralogy of Zn in the metal enriched sediments, using scanning and transmission electron microscopies (SEM and TEM) and X-ray absorption spectroscopy

(XAS), namely X-ray absorption near edge structure (XANES), to show the possible transformations that might have taken place in the water saturated river sediments.

2. Materials and Methods

2.1. Study area

The sampling site was described in the previous chapter (chapter *V*, section *2.1*). As a reminder, this area was filled with iron mining, coke production, and steelmaking factories during the end of the XIXth century and during most of the XXth century. The former facilities that were installed along the river are shown in Figure VII-1 and SM V-1. The sediment core described here was collected in Moyeuvre-Grande, which is located a few tens of meters upstream the Beth dam (Figure VII-1 b). During the period when the facilities were still active, waste materials were deposited into the river, and dams were built as water reservoirs for cooling of BFs, as well as to enhance the deposition of materials discarded by the facilities. Indeed, sediments in the upstream part of the Beth dam contains wastes originated from the steelmaking industries. In addition, other materials were deposited as a result of dredging in the upstream sites of the Beth dam, which occurred between the 60s and 80s.

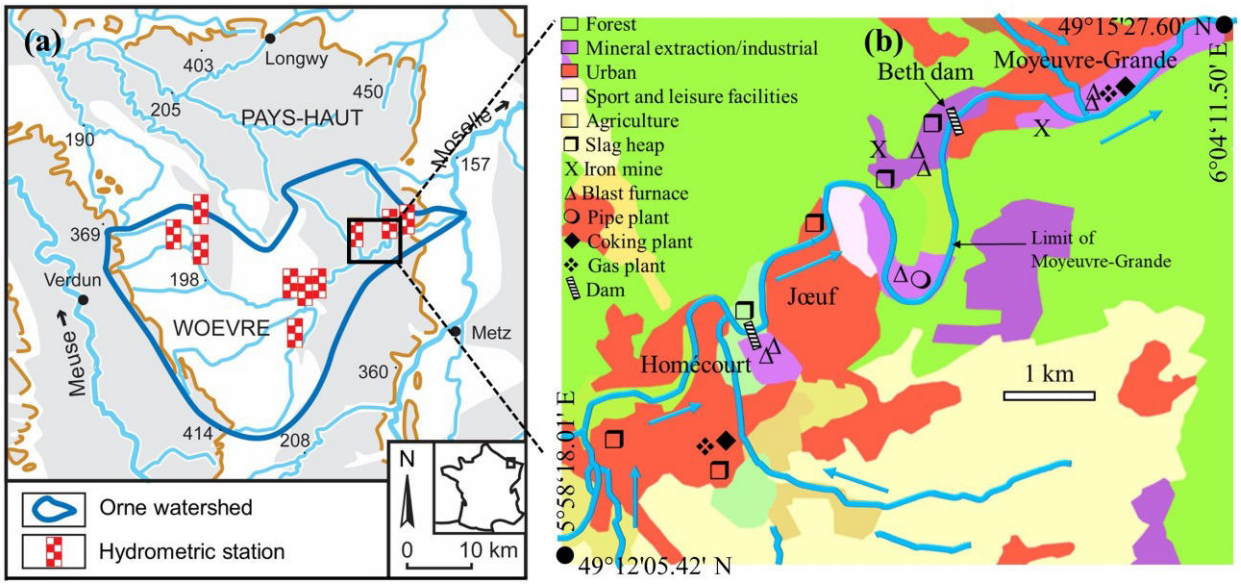

Figure VII-1: a: The Orne watershed located northeastern France and land cover.
a: map created by Benoit Losson, on the basis of data provided by the French National Institute of Geography IGN, www.geoportail.gouv.fr. b: The studied section of the Orne River, with the land use (Corine Land Cover 2006), the former locations of industrial facilities and the location of the Beth dam where the core was collected.

2.2. Sediment Coring

Sediment cores were collected upstream of the Beth dam. The collection of BETH cores was described before (see chapter *V*, section *2.2*). Here, tools that were not included before will be presented, especially XANES; also, only the BETH1402 sediment core will be concerned.

2.3. Sample preparation for analyses

The collected sediment core was sealed from air and transported back to the laboratory in a vertical position. Although limited compaction might occur during vertical transport (due to vibration), the disturbance of interstitial water (porewater) is limited. The sediment core was then divided into layers of various thicknesses, according to visual inspections, mainly color, grain size and plant debris. After the sectioning of the profile, a small aliquot of each layer was frozen at -80°C for microscopic (TEM) and spectroscopic (XAS) analyses. Each sediment layer was then divided into two fractions, the first one was put in pre-weighed glass containers, frozen, freeze-dried and a part was ground using an agate mortar and pestle; the second part was centrifuged at 12,000 g for 20 minutes to extract interstitial water. Consequently, pH and electric conductivity (EC) were measured on the resulting solutions. The solutions were then filtered using a 0.22 µm filter (cellulose acetate membrane filters, Sartorius), acidified using HNO_3 and the chemical concentrations were quantified by inductively coupled plasma optical emission spectrometry (ICP-OES; iCap 6500 ThermoFisher) and inductively coupled plasma mass spectrometry (ICP-MS, X7 ThermoFisher) for major and trace elements, respectively (Service d'Analyse des Roches et des Minéraux – CRPG Vandœuvre-lès-Nancy).

2.4. Chemical composition of sediments

The freeze-dried and ground sediment layers were quantified for total chemical composition according to the procedures developed at the SARM (Service d'Analyse des Roches et des Minéraux – CRPG Vandœuvre-lès-Nancy, France) by Carignan et al., (2001), and described elsewhere (see chapter *III*, section *2.4*). Only selected elements will be presented here, namely Zn, Pb, Si, Fe and S.

2.5. Mineralogical composition of sediments

X-ray diffraction (XRD) analyses were performed on the bulk sediment layers to determine the major crystalline phases of the freeze-dried and ground samples (see chapter *V*, section *2.7.1* for more info). In addition, micrometric particles were characterized and identified by scanning electron microscope (SEM, at GeoRessources laboratory, Vandœuvre-lès-Nancy, France), while poorly crystalline and amorphous phases at a sub-micrometric scale were identified using transmission electron microscope (TEM Philips CM200, at Department of Microscopy, University of Lorraine, Nancy, France). More information is found in chapter *V*, section *2.7.2*.

2.6. X ray absorption spectroscopy at the Zn K-edge

Zn K-edge (9659 eV) X-ray absorption spectroscopy (XANES and EXAFS) experiments were performed at XAS beamline at Elettra Synchrotron facilities (Trieste, Italy), and at SAMBA beamline at SOLEIL synchrotron facilities (Gif sur Yvette, France). X-ray beam was monochromatized using an Si(111) double crystal monochromator. Energy was calibrated by setting to 9659 eV the position in energy of the first inflection point of the K-edge spectrum of a Zn foil placed behind the sample. In order to reduce the possible modification of Zn status, sediment samples that were frozen at -80°C were dried under neutral atmosphere (N_2) and pellets were prepared in an N_2 filled glove bag installed at the beamlines. Sediment layers were prepared as pellets with a low weight percentage of polymer (cellulose; between 8 and 10%) to ensure pellet cohesion. For samples with relatively high Zn contents (higher than 2000 mg/kg), the transmission mode was preferred. For the other samples, including reference samples, the XAS spectra were collected in fluorescence mode using the 36 Ge elements fluorescence detector available at the SAMBA beamline. To avoid beam damage on samples and to reduce the oscillations dumping at high energy, the measurements were performed at low temperatures (-192°C) using the N_2 cryostat available on both beamlines. For each sample, 3 to 20 spectra were recorded, aligned in energy and merged using the software ATHENA (Ravel and Newville, 2005). The spectra were normalized and EXAFS oscillations were extracted using the same software. Pseudo radial distribution functions around Zn atoms were obtained by applying a Fourier Transform with an apodization window (Hanning, with a shape parameter τ fixed at 1).

Several reference samples were recorded, including zincite (ZnO), sphalerite (crystalline ZnS or ZnS_cryst), franklinite ($ZnFe_2O_4$), a spinel-type mineral, synthetic amorphous zinc sulfide, natural illite (purified and size-sorted) as a clay mineral containing 180 mg/kg Zn located in the octahedral layer (Znclay), Zn adsorbed onto different minerals, i.e. calcite, apatite, goethite, ferrihydrite and illite with various Zn loadings (H for high and L for low), and Zn complexed with citrate molecules (low molecular weight organic acid). The reference spectra, obtained on standard samples were selected on the basis of previous publications dealing with Zn speciation in BFS and in contaminated soils and sediments on one hand (Roberts et al., 2002; Kretzschmar et al., 2012; Panfili et al., 2005; Van Damme et al., 2010; Vanaecker et al., 2014), and on the basis of TEM and XRD findings on BETH1402 sediment samples on the other (Kanbar et al., 2017). All reference spectra were recorded at SAMBA beamline in fluorescence mode, except for amorphous ZnS and crystalline ZnO that were analyzed in

transmission mode. Franklinite spectrum was provided by Geraldine SARRET (ISTERRE, Grenoble, France). The XANES spectra at the Zn K-edge were fitted by linear combination (LCF) of reference spectra. The number of components was fixed to three, and combination fits were run to evidence the main components. It must be noted that fitting of XANES spectra using the aforementioned standards does not completely prove their percentage of occurrence since EXAFS spectra were not fitted. Final fitting result was selected on the basis of fit quality parameter (R-factor). In several cases the number of components was reduced to 2 as it was shown that the introduction of a third component did not improve the fit quality. R-factor is defined as the sum over all N measured points of the squared difference between each data point and the fit, normalized by the sum over all squared measured points of the data (Eq. VII-1).

Eq. VII-1: R-factor formula

$$R = \frac{\sum_{i=1}^{N}(data_i - fit_i)^2}{\sum_{i=1}^{N}(data_i)^2}$$

Alternatively, Chi squared (χ^2) is another common method that is used to quantify fit mismatch (Eq. VII-2)

Eq. VII-2: χ^2 formula

$$\chi^2 = \sum_{i=1}^{N_{ind}} \frac{(data_i - fit_i)^2}{\varepsilon_i^2}$$

where ε_i is the measurement uncertainty associated with point i and the points i are taken so as to make $data_i$ represent N_{ind} independent measurements. In Athena software the uncertainty values are set to 1, so from a statistical point of view, χ^2 is not very different from R-factor.

3. Results

3.1. Interstitial waters of BETH1402 sediments

The pH and EC of the interstitial waters along the vertical profile of BETH1402 are plotted in Figure VII-2. These two parameters generally decreased from the surface till 30 cm depth. Afterwards, the pH remained relatively constant (in the range of 7.5 to 7.8), while EC decreased till 68 cm, was quasi-stable till 110 cm (between 450 and 550 µS/cm), and then showed slight variations in the deepest layers. As for Zn concentrations, there was no clear trend along the profile (Figure VII-2). However, few distinctions can be made. The top 11 cm showed relatively low Zn concentrations (average 5.5 ± 1.2 µg/L); the 11 – 14 cm layer showed higher Zn concentration (~ 18 µg/L). That same layer also showed higher pH and EC with respect to the surface unit (i.e. 0 – 11 cm), which partially shows the variation in

physicochemical parameters between the upper 11 cm layers and the deeper ones. For deeper layers, Zn concentrations fluctuated, and the highest values were recorded for 74 – 77 cm, 95 – 98 cm and 104 – 107 cm layers (42, 37 and 84 µg/L, respectively). The variations of EC, pH and Zn concentrations were somehow expected, due to the variation between the recent 11 cm deposits of brown and loose materials, and the highly contaminated sediments for the deeper layers (i.e. 11 – 131 cm) (see chapter *V*, Figure V-4).

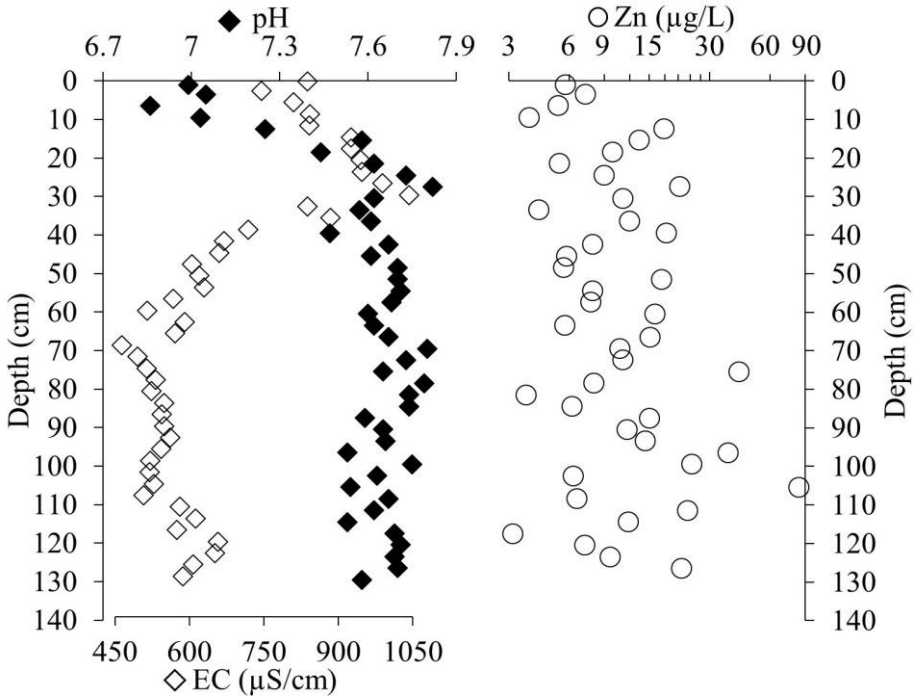

Figure VII-2: pH, EC (µS/cm) and dissolved Zn concentrations (µg/L) of BETH1402 interstitial waters.

3.2. Chemical composition of BETH1402 sediments

According to the chemical composition of BETH1402 sediment layers, four units were suggested, which are 0 – 11 cm, 11 – 44 cm, 47 – 68 cm, and 68 – 131 cm (termed units I, II, III and IV, respectively), while the 44 – 47 cm layer was taken as a distinct layer since it showed striking discontinuity for most elements (Figure VII-3). The first unit displayed rather lithogenic deposits, while the other units showed highly anthropogenic materials related to different steelmaking activities or modified nature of waste introduced into the river. The focus will be made on Zn, since some of the other elements were already discussed in the former chapter (mainly Fe, Si, Ca and V, chapter *V*, Figure V-4).

In river sediments, Zn is found in trace amounts, ranging between several tens till a few hundreds of mg/kg, depending on the nature of the parent rock (Mertens and Smolders, 2013

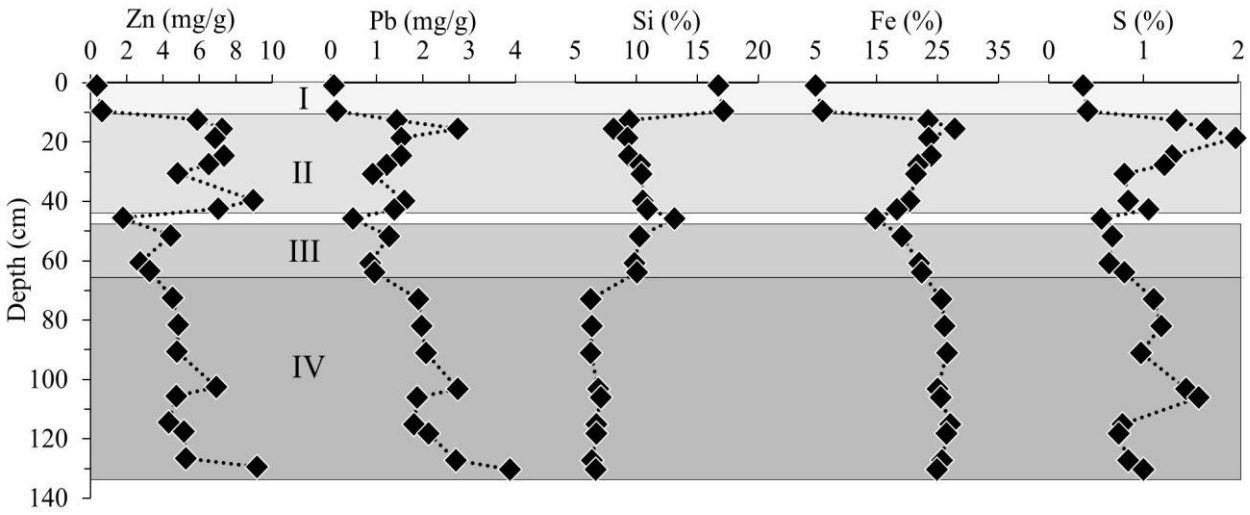

Figure VII-3: Variation of Zn (mg/g), Pb (mg/g), Si (%), Fe (%) and S (%) contents as a function of depth for BETH1402 sediments.

and references cited therein). At a regional scale, i.e. the French part of the Moselle watershed, the average Zn contents of surface sediments was 351 ± 338 mg/kg (with 1st and 3rd quartiles between 85 and 482 mg/Kg; see Table IV-1 of section *IV*), while the average SPM content was 334 ± 86 mg/kg (with 1st and 3rd quartiles between 279 and 401 mg/Kg) (Le Meur et al., 2016). For sediments collected in the upstream zone of the Beth dam, the Zn contents were in the range of 0.1 – 0.9% for layers inferior to 11 cm (Figure VII-3), and the enrichment factor reached as much as 35; moreover, Pb contents ranged between 0.1 and 0.4%, and the enrichment factor was as much as 77. Therefore, the degree of contamination is well established, without the need for enrichment factor calculations. It should be noted that the surface layer was used for the calculation of the enrichment factors (i.e. 349 mg/kg for Zn and 68 mg/kg for Pb). The grain sizes were fine along the vertical profile of BETH1402; in addition, Al (and other elements that are generally considered as conservative elements) drastically decreased with depth. Consequently, it was not relevant to normalize the metal contents. Zn, Pb, Fe and S followed a similar trend in the sediment profile (Figure VII-3). Sediments with high Zn and Pb contents are commonly found in river sediments near mining and metallurgical sites, such as the Geul in Belgium (Van Damme et al., 2010), Scarpe and Deûle in north France, and Fensch in northeastern France (Boughriet et al., 2007; Gabelle, 2006; Lesven et al., 2010; Montargès-Pelletier et al., 2007; Vdović et al., 2006; Zebracki, 2008). Some examples are presented in Table VII-1.

Table VII-1: Zn, Pb and Fe contents in sediments impacted by industrial activities.
The metal contents represented in the table are not representative of the entire river, rather they indicate spot locations. This is further seen by different metal contents for sediments collected from the Deûle River. The values in the table are the maxima from each cited study.

Location	Zn (mg/kg)	Pb (mg/kg)	Fe (%)	Reference
Deûle	3800	7300	2.0	(Vdović et al., 2006)
Deûle	19600	19900	4.1	(Gabelle, 2006)
Deûle	7170	12870	2.4	(Lesven et al., 2010)
Deûle	13000	10000	-	(Boughriet et al., 2007)
Scarpe	13000	2400	-	(Zebracki, 2008)
Fensch	4521	727	26.4	(Montargès-Pelletier et al., 2007)
Moselle after Fensch confluence	6413	1646	29.1	(Montargès-Pelletier et al., 2007)

3.3. Zn bearing phases revealed by SEM and TEM

First, it should be noted that even though Zn contents (and Pb as well) were elevated in the sediment layers of the 11 – 131 cm units (in the range of 0.2 – 0.9% and 0.1 – 0.3% for Zn and Pb, respectively), XRD on the bulk samples did not reveal any Zn and Pb containing minerals. The absence of Zn or Pb minerals in XRD patterns might be explained by the amorphous character of Zn and Pb minerals on one hand, and by the relatively low contents of crystalline phases (roughly less than 1%) on the other. Nevertheless, micrometric and sub-micrometric SEM and TEM analyses revealed Zn rich phases, since the latter techniques have lower detection limits and can reveal poorly crystalline and amorphous phases. Furthermore, SEM and TEM did not reveal detectable variations in Zn phases at a depth-dependent scale, unless indicated otherwise, therefore the following paragraphs treat various Zn phases, independent of depth.

Micrometric SEM investigations evidenced a few Zn containing phases. Zinc was found in small quantities (i.e. small atomic percentages) in calcium carbonates (Figure VII-4 a). Due to the sensitivity of SEM (detection level of 0.2 – 0.3%), Zn is surely found in the structure of carbonates (calcite in this case), and not sorbed onto the mineral surface. Zn was also noticed in Fe rich particles (Figure VII-4 b, particle 2). Additionally, polymetallic (Zn-Fe) sulfides were evidenced (Figure VII-4 c, particle 5). In the previous cases, Zn containing particles were either poor in Zn and micrometric (e.g. ~ 5 µm in Figure VII-4 a), or Zn was found in relatively high percentages (~ 10%) and sub-micrometric size (e.g. Figure VII-4 c). Furthermore, SEM elemental mapping was performed on two large-scale views of the 125 – 128 cm layer (Zn = 5265 mg/kg). Elemental mapping clearly demonstrated that the main components were Si, Al, Ca and Fe, while Zn could hardly be detected (Figure VII-5); additionally, the bulk view showed that the particles are relatively fine. This indicates that Zn is hardly, if any, carried by

those particles. Therefore, and due to the high Zn contents (Figure VII-3), Zn bearing minerals must be found at scales beyond the limits of XRD and SEM, such as at the sub-micrometric or molecular scales of TEM and XANES, respectively.

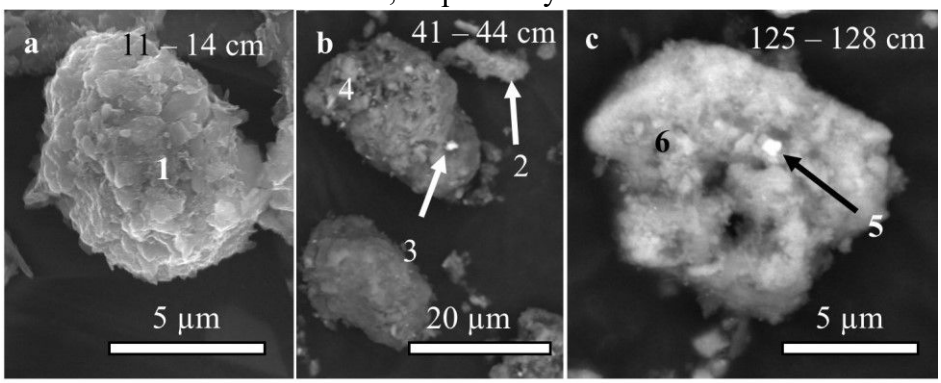

A%	1
O	52.4
Mg	0.9
Al	3.8
Si	1.2
P	0.3
S	0.5
Ca	**36.7**
Mn	0.6
Fe	2.4
Zn	1.2

A%	2
O	57.7
Al	0.4
Si	0.8
Ca	2.2
Ti	0.7
Fe	**27.6**
Ni	0.7
Zn	9.9

A%	5
O	67.2
Mg	1.2
Al	2.7
Si	3.6
P	0.5
S	8.8
Ca	0.7
Mn	0.2
Fe	4.4
Ni	0.4
Zn	**10.3**

Figure VII-4: SEM micro-images of Zn containing particles.
a: Secondary electron (SE) micro-image showing 1: calcium carbonate phase containing traces of Zn (11 – 14 cm), b: back-scattered electrons (BSE) micro-image of a Zn containing Fe rich mineral (2) and an Fe rich particle (3) in a calcium carbonate phase (4) (41 – 44 cm), and c: BSE micro-image of a polymetallic (Zn-Fe or Zn-Fe-Ni) sulfide (5) and an Fe rich clay (6) (125 – 128 cm). Under each figure, the atomic percentages generated by EDXS are included.

TEM investigations revealed hairy Fe-rich aluminosilicates in sediment inferior to 11 cm (Figure VII-6 a), hereafter termed Fe-aluminosilicates. The predominance of the hairy Fe-aluminosilicates and the characterization and possible origin of those phases were discussed in the previous chapter (chapter V, Figure V-8). Fe-aluminosilicates were detected throughout the contaminated sediments layers. The detected Fe-aluminosilicates represented ~ 13% of the TEM analyzed particles (51 out of 379). 24 out of those 51 particles contained Zn; most particles contained only traces of Zn (11/24 had Zn inferior to 2%), while 2 – 5% and 5 – 10% of Zn were detected for 9 and 4 particles, respectively. It should be noted that there was no visual distinction on the TEM micro-images between Fe-aluminosilicates containing or excluding Zn, and including or excluding S. Zn was also found as sulfides (Figure VII-6: b – f). Those phases were mainly composed of Zn and S, but also contained Fe and traces of Pb; thus, the phases might be considered as polymetallic sulfides. The circular polymetallic sulfides

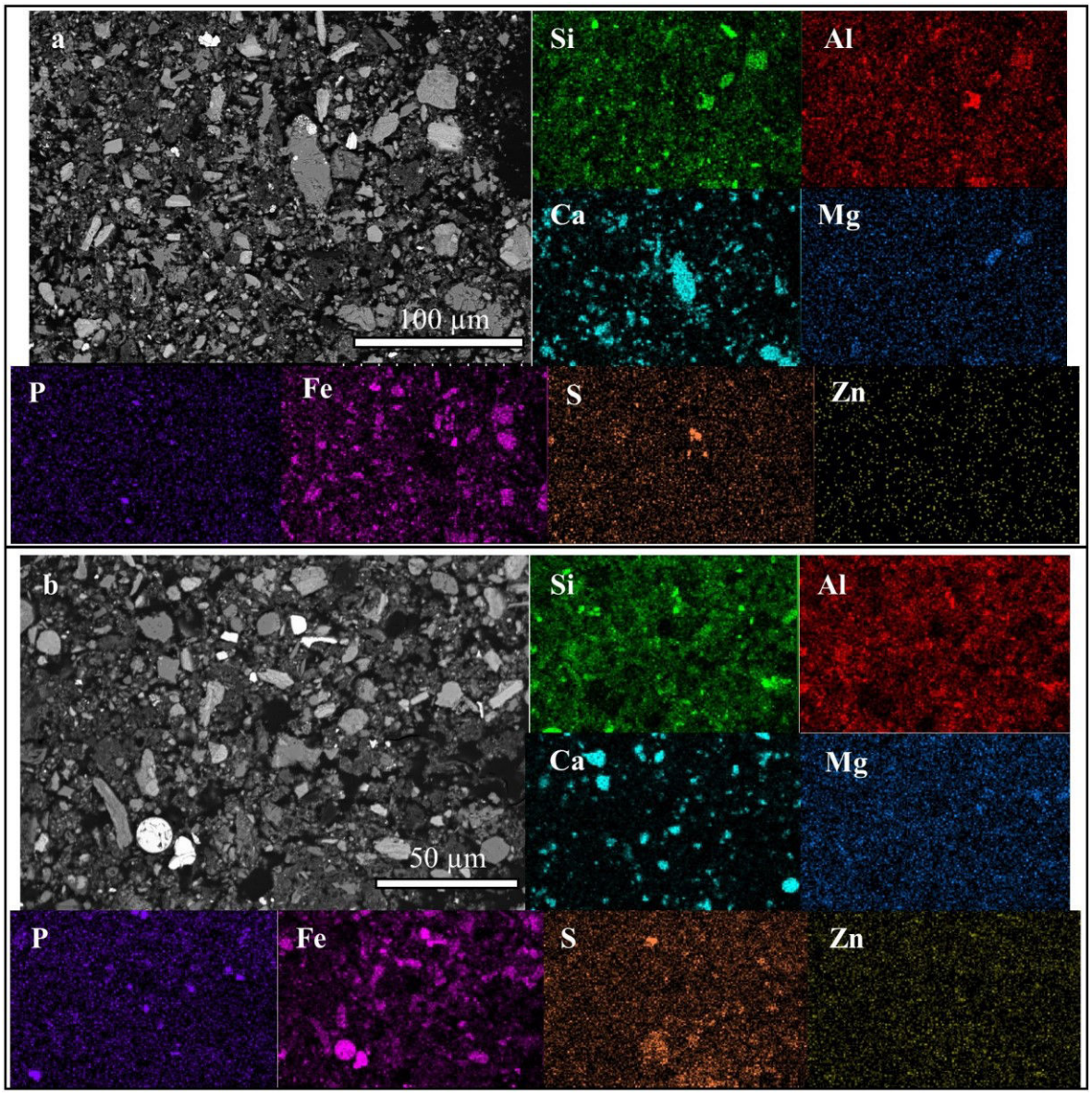

Figure VII-5: BSE micro-images and elemental dot maps for 125 - 128 cm layer (BETH1402).
a and b belong to the same layer, but focus on different zones (with different scales). More intense colors indicate higher contribution of an element.

ranged in diameters between a few tens to a couple of hundreds of nanometers (Figure VII-6: b and c). Those structures were mainly composed of Zn, S, Fe and to a lesser extent P (A% up to 3.5%) and Pb. However, lead might be underestimated, due to the relatively low contents of Pb and the interference between the emission lines of S (K_α) and Pb (M_α). It should be noted that elliptical structures of similar composition were also seen in sediments mainly composed of industrial sludge (data not shown). Another Zn species was poorly defined circular and non-defined ZnS (Figure VII-6 d and e, respectively). The detected phases were a few tens of nanometers in size. The latter phase was associated to clay particles (Figure VII-6 e). More defined Zn sulfides were detected as dense, fluffy and circular or spherical structures (Figure VII-6 f). Those sulfides were mainly composed of Zn, Fe and Pb. From the evidenced dense

circular structures, the average diameter was 92 ± 34 nm (n = 25). Finally, and due to the polymorphism of ZnS (defined, poorly defined and non-defined) and different levels of

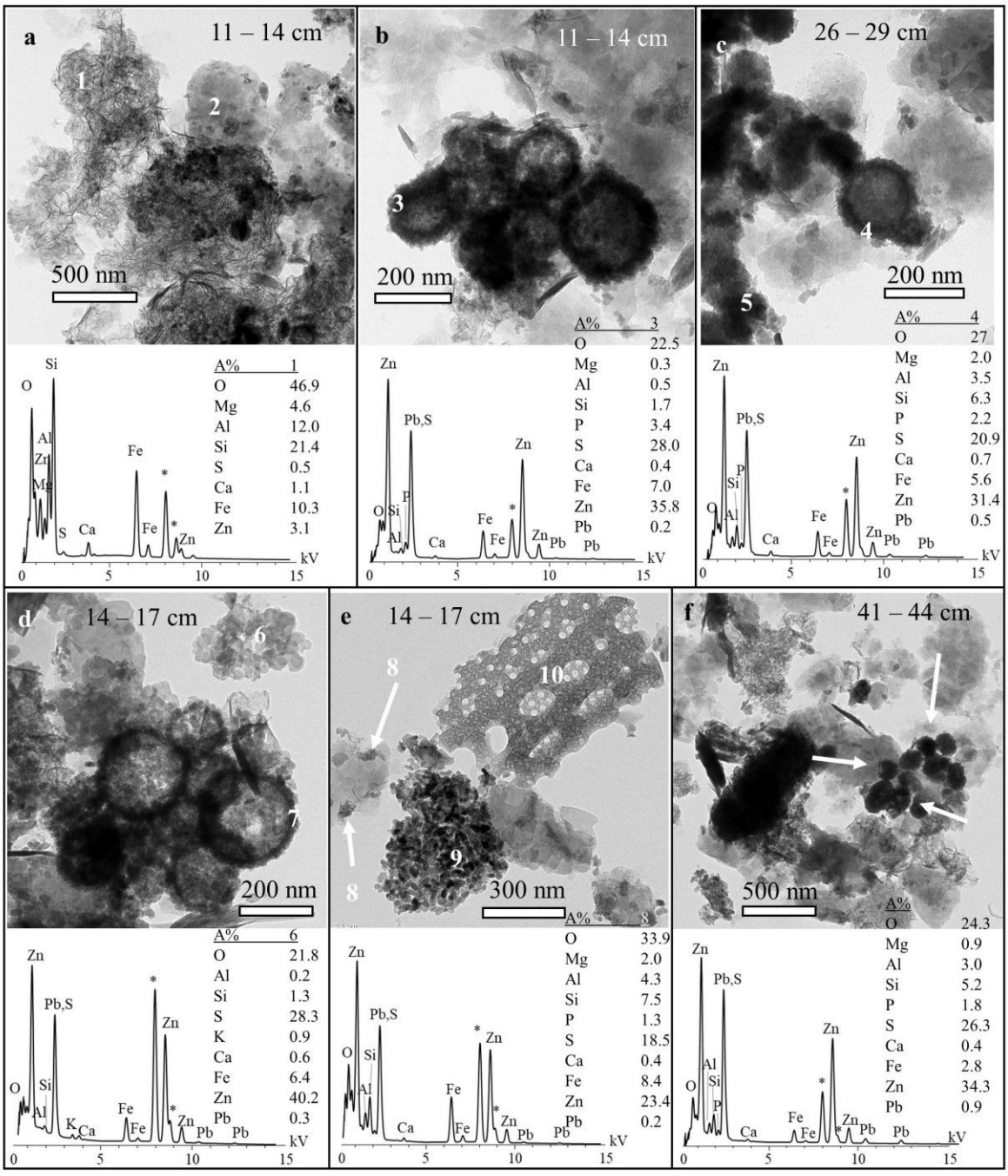

Figure VII-6: TEM micro-images of BETH1402 sediment layers mainly showing Zn bearing phases.
a: Hairy Fe-aluminosilicate phases containing Zn (1) and Fe containing smectite (2) (A% of Fe ~ 6.8 and Si/Al ~ 1.4) (11 – 14 cm), b: aggregates of circular structures mainly composed of ZnS (3) and also contain other metals (Fe and Pb) (11 – 14 cm), c: circular ZnS structures (4 and 5) similar to point 2 (26 – 29 cm), d: circular, more or less defined, polymetallic (Zn-Fe-Pb) sulfides (6) and circular ZnS (7) (14 – 17 cm), e: poorly defined polymetallic (Zn-Fe-Pb) sulfides on a clay phase identified as smectite (8), goethite nanoparticles (9) and weathered diatom frustule (10) (14 – 17 cm), and f: spherical polymetallic (Zn-Fe-Pb) sulfides (41 – 44 cm). The atomic percentages and EDX spectra of certain readings are show under the images. Asterisks on the EDX spectra indicate the emission lines of copper, which are due to the contribution of the TEM grid, a carbon coated copper grid.

crystallinity, several Zn species might be proposed. However, the Zn/S ratios were rather similar for the different sulfides (average 1.3 ± 0.2).

3.4. Zn solid speciation using X-ray absorption spectroscopy at the Zn K-edge

3.4.1. Introductory data about XANES spectra and references

XANES spectra are particularly sensitive to the oxidation state, the coordination of absorbing atom (Zn in our case) and the nature of the first neighbors (such as O and S). XANES spectra are the sum of three-dimensional scattering paths, and aim to reveal the global structure of the phase bearing the absorbing atom (i.e. Zn in our case). TEM can reveal Zn speciation of the finest particles only, while XANES provides exhaustive information on Zn speciation. Contrary to TEM results, XANES data could reveal the variation of Zn species at a depth-dependent scale.

The XANES spectra in Figure VII-7 are divided as minerals containing Zn in their structure (a) and minerals with sorbed Zn species onto mineral surface (b). In illite (ZnClay), zinc is included in the octahedral layer of the clay mineral sheets. This particular Zn status results in different resonances on the XANES spectra at 9666, 9668.4, 9673 and 9686.6 eV (Figure VII-7 a). Those resonances are also visible on the spectrum of Zn sorbed onto illite (Zn_clay L, Figure VII-7 b). For the four other standard samples plotted in Figure VII-7 (a), Zn is tetrahedrally coordinated. This is the case of franklinite, a normal spinel $^{[4]}Zn^{2+[6]}Fe_2^{3+}O_4$, in which Zn^{2+} occupy tetrahedral sites. The franklinite edge is characteristic of Zn-ferrites, with three distinct peaks at 9664.5, 9668.5 and 9673 eV, and with a shoulder at 9678.5 eV. Those structures are relatively well-defined and are assigned to multiple-scattering paths, enhanced by the high level of symmetry of the Zn-ferrites (cubic spinel phases). Their relative intensity can be modified due to the inversion of the spinel and the relative increase of Zn in octahedral sites (Stewart et al., 2007; Szczerba et al., 2016; Waychunas et al., 2003). Indeed, the peak at 9668.5 eV relatively increases in intensity when the proportion of octahedral zinc increases. Franklinite was often evidenced in Zn smelter soils and sediments, and in metal slag deposits (e.g. Panfili et al., 2005; Roberts et al., 2002; Vanaecker et al., 2014). However, its presence was not systematically detected in the context of Zn smelter contamination (Kretzschmar et al., 2012; Van Damme et al., 2010). On the basis of XRD data, franklinite was shown to account for only a minor fraction in fresh BFS (Van Herck et al., 2000). Zincite (ZnO) was also expected as a possible bearing phase in the context of blast furnaces and smelters, even though it was not evidenced in fresh BFS (Kretzschmar et al., 2012; Van Herck et al., 2000). In zincite,

Zn is tetrahedrally coordinated, and the first peak of the absorption edge is positioned at 9663.7 eV. ZnO spectrum also displays a strong resonance at 9680 eV due to multiple scattering (Galoisy et al., 2001). The other standard samples are zinc sulfides (sphalerite β-ZnS), with decreasing crystallinity. For those spectra, the absorption edge is also shifted towards lower energies, due to the tetrahedral coordination of zinc in those compounds. The absorption edge displays a first shoulder at 9662.5 eV, followed by the main absorption peak at 9665 eV (Figure VII-7 a). The post-edge resonances are more intense for ZnS-cryst, which is directly influenced by the higher level of order in crystalline compounds. ZnS was evidenced in BFS and contaminated sediments (Kretzschmar et al., 2012; Van Damme et al., 2010). In the case of BETH1402 sediments, those references (ZnS cryst and ZnS amor) appear mandatory, due to clear evidences of nanometric ZnS particles (TEM data, Figure VII-6).

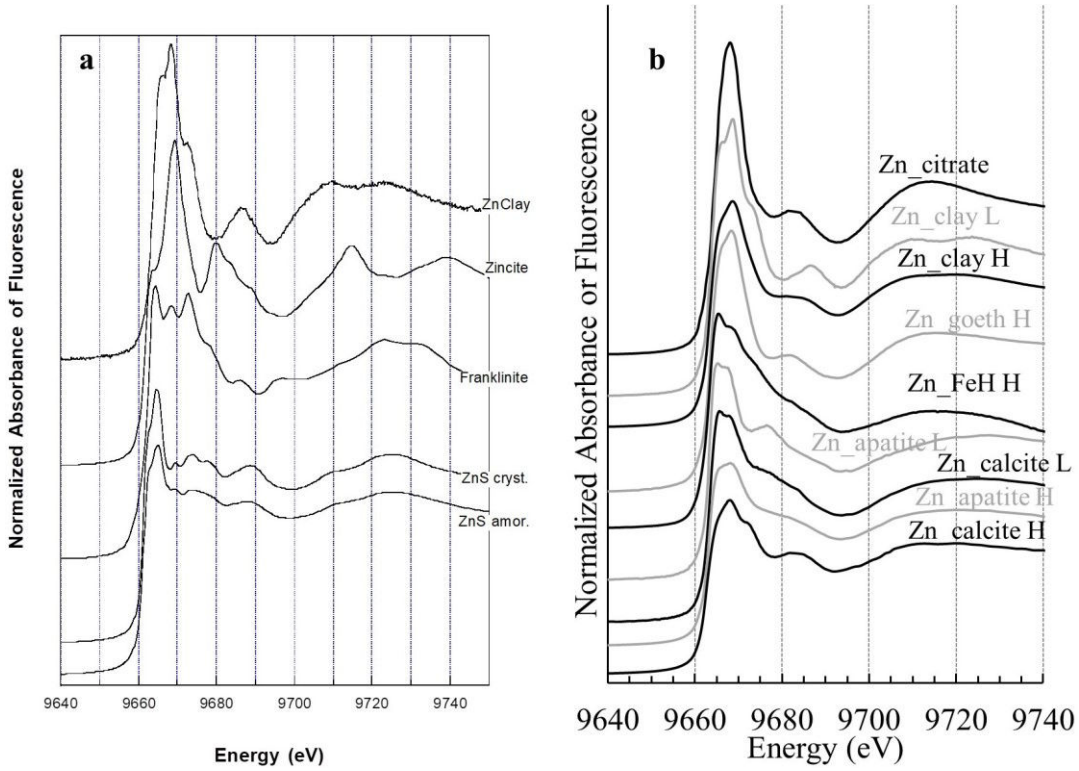

Figure VII-7: XANES spectra at the Zn K-edge for reference samples.
a: Mineral phases displaying Zn in their crystal structure, from the top of the graph: **ZnClay**, illite clay mineral containing Zn in the octahedral layer (171 mg/kg); **zincite** or ZnO (Carvalho et al., 2013); **franklinite** $ZnFe_2O_4$ (Van Damme et al., 2010); **ZnS_cryst** or sphalerite for crystalline zinc sulfide (with the courtesy of Valérie Briois) and **ZnS amor** for amorphous zinc sulfide (synthetic ZnS, (Le Meur, 2016)).
b: Zinc as a complex or sorbed species onto mineral surfaces, from the top of the graph: **Zn_citrate**, aqueous solution of zinc nitrate and citric acid; **Zn_clay L**, Zn sorbed onto illite at low sorption rate $[Zn]_{ads}$= 200 mg/kg; **Zn_clay H**, Zn sorbed onto illite at high sorption rate $[Zn]_{ads}$= 4600 mg/kg; **Zn_Goeth H**, Zn sorbed onto goethite $[Zn]_{ads}$= 3810 mg/kg; **Zn_FeH H**, Zn sorbed onto ferrihydrite $[Zn]_{ads}$= 3750 mg/kg; **Zn_apatite L**, Zn sorbed onto apatite at low sorption rate, $[Zn]_{ads}$= 120 mg/kg; **Zn_calcite L**, Zn sorbed onto calcite at low sorption rate $[Zn]_{ads}$= 190 mg/kg; **Zn_apatite H**, Zn sorbed onto apatite at high sorption rate $[Zn]_{ads}$= 23300 mg/kg; **Zn_calcite H**, Zn sorbed onto calcite at high sorption rate $[Zn]_{ads}$= 104.0 g/kg.

The XANES spectra of Zn sorbed onto different mineral surfaces, with different loadings, are shown in Figure VII-7 b. XANES spectra suggest that, in most cases, Zn is preferentially in octahedral coordination. Zn-citrate solution only contains octahedrally coordinated zinc, with a main absorption edge at 9668 eV, followed by a relatively flat feature centered around 9683-9684 eV. This spectrum is close in shape to the signal obtained for Zn as sorbed species onto clays at high sorption rate (Zn_clay H). In that case, Zn mainly occupies cation exchange sites of illite surfaces, and its local environment is fingerprinting, essentially the first shell of water molecules. In the case of Zn sorbed onto goethite, Zn appears mainly as octahedrally coordinated. The corresponding spectrum does not feature any particular structure, but resemble the relatively smooth spectrum of Zn-citrate and Zn_clay H. We will consider in the discussion of fitting results that those three spectra (i.e. Zn_goethite, Zn_clay H and Zn_citrate) represent octahedrally coordinated zinc involved in outer-sphere complexes. The spectrum obtained for Zn sorbed onto illite at low sorption rate (Zn_clay L) is quite close to that of pristine illite and can be assumed as a 1:1 mixture of Zn inserted in the phyllosilicate sheet structure and Zn sorbed onto the surface. Zn_FeH H spectrum, standing for Zn sorbed onto ferrihydrite, displays strong similarities with that reported by Waychunas et al., (2003). The energy positions of the different features at 9665.5 and 9668.3 eV suggest that a part of Zn is in tetrahedral coordination. This hypothesis was supported by EXAFS data (Zn-O at 1.96 Å (Juillot et al., 2008; Waychunas et al., 2002)). This assumption was found not only on theoretical calculations using FEFF code, but also on the comparison with franklinite spectrum. Identical resonances were observed for zinc sorbed onto substituted ferrihydrite (Cismasu et al., 2013).

Other standard samples included zinc sorbed onto apatite (calcium phosphate) and calcite (calcium carbonate), with two different loadings (low and high sorption rates). For low amount of sorbed Zn, the spectrum of Zn_apatite L displayed a first peak at 9665.2 eV, which suggests a partial tetrahedral coordination. The spectrum of Zn_calcite L shows a first peak at 9665.6 eV. It is well known that Zn forms monodentate complexes at the surface of calcite (inner-sphere complexes) with a tetrahedral coordination (Elzinga et al., 2006; Elzinga and Reeder, 2002). Finally, on apatite and calcite, Zn is supposed to sorb as tetrahedra forming inner-sphere complexes with surface groups (Bazin et al., 2009; Dessombz et al., 2013). For Zn sorbed onto calcite with high loadings, XANES spectrum presents a clear shift of the edge at 9668.2 eV as well as a post-edge structure at 9672 eV, and the first oscillation at 9683 eV is particularly well defined. In that latter case, Zn is expected to be octahedrally coordinated on calcite surface.

3.4.2. XANES spectra of BETH1402 sediments revealing Zn speciation

Linear combination fitting (LCF) on XANES spectra of BETH1402 sediments was performed using the reference spectra presented earlier (Figure VII-7) in order to quantify the evolution of Zn species along the vertical profile of the sediment core. The results of the LCF are reported in Figure VII-8, along with the XANES spectra for the selected BETH1402 sediment layers. In many cases, fitting was performed with two or three distinct components.

19 different layers were investigated. There is a clear distinction between the spectra of the surface layers (0 till 8 cm) and the deeper ones (Figure VII-8 a). Particular attention was brought to the top 17 cm sediments (Figure VII-8 b). Indeed, this zone displayed strong modifications in chemical contents and mineralogical composition (Figure VII-3; also see Figure V-4 and Figure V-5). In the downward sense, there was a clear modification of Zn status, as revealed by the features of XANES spectra at the Zn K-edge. The top layer 0 – 2 cm was characterized by an absorption edge with four main resonances at 9665.5, 9669, 9673 and 9686.8 eV. The following spectra, assigned to the deeper layers (2 to 32 cm), revealed the evolution of Zn status with depth. Furthermore, the edge is slightly shifted towards lower energies; the resonance at 9669 eV strongly decreased and the shoulder at 9662.5 (± 0.3 eV) is more obvious. Except for the apparent increase of the resonance centered at 9673 eV, XANES spectra at the Zn K-edge were rather similar from 8 to 128 cm. Quantification of the different Zn species was performed via LCF. Fit parameters are presented in Figure VII-8 and in Table VII-2. Four distinct components were used to fit the XANES spectra. The first sediment layer is highly heterogeneous as there is not really one predominant Zn species. Indeed, 38% of Zn is in ZnS (sphalerite or wurtzite), 31% of Zn is in the structure of clay, and about 30% of Zn is present as sorbed species (onto carbonate surfaces). For, the second layer (2 – 5 cm), ZnS clearly became the predominant species, accounted by 53%. For this layer, 24% Zn was in clay structure and about 22% of Zn was sorbed onto clays (17.4%) and iron-oxy-hydroxides (4.8%). The third layer from the top (5 – 8 cm) displayed even higher content in ZnS (65%), and only 15% in the octahedral layers of clays and 20% sorbed onto clay minerals and iron oxy-hydroxide (goethite). Reaching the depth of 8 cm, ZnS definitely became the major fraction of Zn in sediments, with a contribution of 80%. Zinc sulfide signal was reproduced by two ZnS spectra to improve the fit quality, including amorphous and crystalline spectra. We will not discuss the crystallinity of ZnS on the basis of XANES spectra at the Zn K-edge, since fitting of EXAFS spectra at the Zn K-edge would be necessary to defend this notion. Besides ZnS, Zn appears as sorbed species, mainly on iron oxy-hydroxide and ferrihydrite. XANES spectra at

the Zn K-edge evidenced, in a quantitative way, that ZnS was the predominant species very early in the vertical profile. There was a slight decrease of ZnS contribution in deeper layers of the core. Indeed, ZnS accounted for approximately 80, 72 and 63% for the 8 – 41, 44 – 65 and 68 – 128 cm layers, respectively. The evolution of ZnS (amorphous and crystalline), Zn in clay,

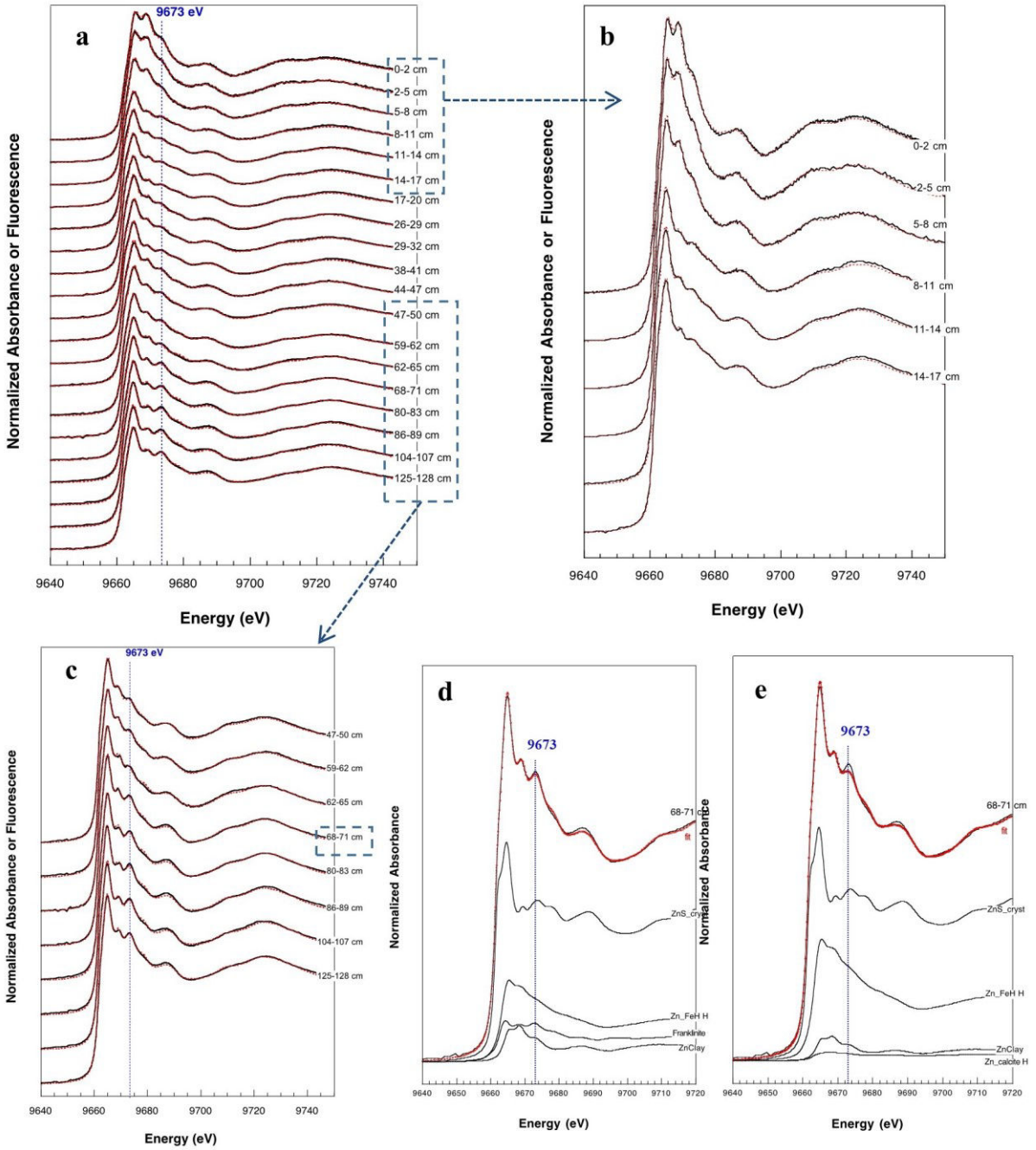

Figure VII-8: XANES spectra at the Zn K-edge on bulk BETH1402 samples.
The depth of sediment layers is indicated on the side of the graphs. The experimental spectra are plotted as black plain lines; the fitting curves are plotted as red dashed or dotted lines. a: XANES spectra collected from 19 sediment layers along the BETH1401 core, b: a zoom on the six first layers from the top of the core (0 to 17 cm), c: a focus on the deep layers of the core (47 to 128 cm) to evidence the occurrence of a new Zn-bearing phase with increasing depth, and d and e: comparison of fitting the 68 – 71 cm layer including (d) and excluding (e) one reference, which is franklinite. All the spectra were normalized using ATHENA software. E0 was fixed as the maximum of the first derivative, pre-edge background was fitted.

and sorbed species (onto surfaces of calcite, clay, ferrihydrite and goethite) contribution with depth is better shown in Figure VII-9. For Zn_illite L spectrum, we decided not to assign this contribution as sorbed species because the signal is strongly influenced by structural Zn. For the deepest layers (62 – 128 cm), a few percent of Zn were found in the structure of clay (< 10%), sorbed species on iron oxy-hydroxides (9 to 18%), and in franklinite (13 to 20%).

The main modifications of the spectra shape are due to the increase of sulfide species. However, the increase of the peak at 9673 eV could not be reproduced without the introduction of franklinite in the list of possible references (Figure VII-8: d and e). Franklinite was not revealed though the XRD analysis of BETH1402 sediments, and other analyses (SEM, TEM) could not confirm the presence of this mineral. Nonetheless, due to the context of pig iron furnace, franklinite is one the most expected phases. The feature at 9673.5 eV remains incompletely reproduced without franklinite as a reference spectrum (Figure VII-8 e). It can be assigned to another Zn-bearing phase not present in our set of reference spectra. Also, amorphous and crystalline ZnS were used to fit the XANES spectra at the Zn K-edge, even though the polymetallic sulfides detected with TEM were highly amorphous (Figure VII-6). Those sulfides were shown to contain traces of Pb and Fe. Despite the fact that iron might not considerably modify the local environment around Zn (their atomic numbers are very close), Pb displays a higher atomic number, higher number of electrons and depending on its position in the sulfides structure, it might generate specific back-scattering paths resulting in the apparition of features in the XANES region.

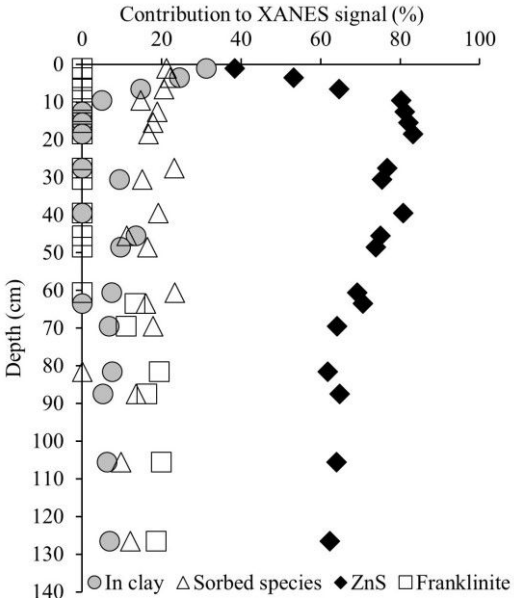

Figure VII-9: Contribution of XANES signals based on Zn species in clay, sorbed onto mineral surfaces, sulfides and franklinite.

Table VII-2: Quantified Zn species of BETH1402 sediments using linear combination fitting of the XANES spectra at the Zn K-edge.

	Sulfides		Spinel	Zn in clay structure		Sorbed species						
Layer	ZnS am	ZnS cryst	Franklinite	Znclay	Zn_clay L	Zn_calcite L	Zn_clay H	Zn_calcite H	Zn_FeH H	Zn_Goet H	Fitted sum (%)	R-factor ($x10^3$)
0-2 cm		38.4			31.2	9.0		21.3			99.9	0.8479
2-5 cm		53.2			24.5		17.4		4.8		99.9	0.8544
5-8 cm		64.7			14.8		12.5			8.1	100.1	0.8048
8-11 cm	58.0	22.3		5.0					14.8		100.1	0.8915
11-14 cm	13.2	67.9							8.4	10.5	100.0	0.9473
14-17 cm	28.8	53.3							10.6	7.3	100.0	0.7055
17-20 cm	25.3	57.9							9.6	7.1	99.9	0.7956
26-29 cm	13.4	63.3							11.0	12.3	100.0	0.7758
29-32 cm	39.0	36.5		9.4					15.1		100.0	0.8220
38-41 cm	16.6	64.2							12.1	7.1	100.0	0.6283
44-47 cm	22.9	52.2			13.6				11.2		99.9	0.8006
47-50 cm	42.5	31.4		9.7					16.4		100.0	0.6618
59-62 cm	40.0	29.2		7.5					23.3		100.0	0.6212
62-65 cm	16.2	54.4	13.3							16.1	100.0	0.7702
68-71 cm		64.2	11.1	6.8					17.9		100.0	0.5840
80-83 cm		61.8	19.4	7.6		11.2					100.0	1.1179
86-89 cm		64.8	16.3	5.3					13.6		100.0	1.1707
104-107 cm		64.0	19.9	6.3					9.8		100.0	1.0855
125-128 cm		62.3	18.6	6.9					12.2		100.0	0.8357

4. Discussion

4.1. An insight about the sources and fate of Zn in blast furnaces

The possible sources of metals (mainly Fe, but also Zn and Pb) and nature of the sediment layers were discussed in the previous *chapter* (section *4.1*). Steel industries and machineries were constructed near the Orne River in the last century (Figure VII-1 b and also SM V-1), and their activities stopped in the late 80s. River water was used for wet scrubbing of smokes (or dust) from the top of BFs. In general, coarse particles collected by dust bags are removed via gas cleaning or settling, while finer particles are removed via wet scrubbing (or wet cleaning), which results in the formation of BFS (e.g. Kiventerä et al., 2016; Korpa and Mudron, 2006). As a result, a great part of the settled materials in the upstream area of dams, including Beth dam, is partially composed of BFS released from facilities located in the upstream region. Indeed, BETH1402 sediments below 11 cm were characterized by high Fe, Pb and Zn contents (Figure VII-3), which are comparable with BFS produced in similar contexts of steelmaking (Das et al., 2007, 2002; Kretzschmar et al., 2012; Mansfeldt and Dohrmann, 2004). Nonetheless, BETH1402 sediments are clearly a mixture of BFS and lithogenic materials, as indicated by the mineralogical composition (see chapter *V*).

In the steelmaking facilities located between Jœuf and Moyeuvre-Grande (in the Orne basin), the local "Minette" iron ore was used for pig iron and steel production. The minette is a ferri-arenite, composed of goethite ooids, Fe phyllosilicates (chamosite and berthierine), Fe-carbonates and calcite (Dagallier et al., 2002). The Zn content in minette ranges between 100 and 240 mg/kg, depending on the age and position of the ironstone in the Earth (James, 1966). The exact Zn species are not known. Yet, the possible Zn species found in iron ores are ferrites, silicates and carbonates, as indicated by chemical composition of the iron ore; sulfides are completely absent, or only slightly present. In coal, however, Zn mainly occurs as ZnS, since coking reactions occur under anoxic conditions. In BFs, iron ore (or sinter) is the main Zn contributor (Trinkel et al., 2015 and references cited therein). In case ZnS was introduced into the furnace, either from the iron ore (or sinter) or coal, the high temperatures (500 to 870°C) cause ZnS oxidation and ZnO production. Therefore, the input and fate of ZnO and ZnS into BFs need to be argued (according to Trinkel et al., (2015) and references cited therein). In the case of Zn oxide, Zn is reduced by means of carbon monoxide at temperatures between 800 and 1000°C (Eq. VII-3). Zn might also be reduced by carbon at temperatures between 900 and 1300°C (Eq. VII-4). In both cases, molten Zn is produced (melting and boiling points of Zn are

420 and 910°C, respectively), which vaporizes (forms $Zn_{(g)}$) and moves to the top of BFs, where the temperature is lower.

Eq. VII-3: Reduction of metallic Zn by CO $$ZnO_{(s)} + CO_{(g)} \rightarrow Zn_{(g)} + CO_{2\,(g)}$$

Eq. VII-4: Reduction of metallic Zn by C $$ZnO_{(s)} + C_{(s)} \rightarrow Zn_{(g)} + CO_{(g)}$$

Vapor Zn then condenses at lower temperatures, possibly in the upper zones of BFs (Eq. VII-5) to form ZnO. The cycle of vaporization and condensation then continues.

Eq. VII-5: Oxidation of Zn vapor by CO_2 $$Zn_{(g)} + CO_{2\,(g)} \rightarrow ZnO_{(s)} + CO_{(g)}$$

Alternatively, Zn might condense onto dust/smoke particles that are eventually collected in filters. Sulfur, which mainly originates from coke, is also found as vapor in the BFs (Zhukova et al., 1976). Vapor Zn might react with S to form ZnS (Eq. VII-6); ZnS might also form from ZnO (Eq. VII-7).

Eq. VII-6: Formation of ZnS from Zn $$2Zn + \frac{1}{4}S_8 \rightarrow 2ZnS$$

Eq. VII-7: Formation of ZnS from ZnO $$ZnO + \frac{3}{16}S_8 \rightarrow ZnS + \frac{1}{2}SO_2$$

The formed ZnS then rises to the top of the BF. Upon reaching lower temperatures, ZnS condenses and solidifies (sublimation point of ZnS is ~ 1180°C). Therefore, the collected BF dusts are mainly made from zincite (ZnO), but also contain ZnS. Zincite and sphalerite were shown to form in the lining of BF as well (Zhukova et al., 1976 and references cited therein). In the case of BETH1402 sediments (lithogenic sediments mixed with sludge), crystalline Zn minerals could not be detected by bulk XRD. Even more, crystalline Zn minerals could not (or only in traces) be detected in BFS from steelmaking (Kretzschmar et al., 2012; Trung et al., 2011; Van Herck et al., 2000; Vereš et al., 2010), indicating their strong amorphous character, in addition to the relatively low Zn contents (up to 9 g/kg, i.e. < 1%, Figure VII-3). Some of the major Zn species found in BFS sedimentation ponds and soils influenced by steel and metalliferous activities were Zn sorbed onto calcite, ferrihydrite and goethite surfaces, incorporated in clay minerals, as carbonates (smithsonite), franklinite, and as Zn sulfides, such as sphalerite and wurtzite (Jacquat et al., 2009; Juillot et al., 2003; Kretzschmar et al., 2012). The latter minerals (sulfides) were proven to be dissolved under oxic conditions; which is not the case of the submerged Beth sediments.

4.2. Origin and fate of Zn in BETH1402 sediments

Zn speciation was revealed by microscopic and spectroscopic techniques of BETH1402 sediments. Zn was found sorbed onto and incorporated into clays, such as Fe-aluminosilicates, as sorbed species onto ferrihydrite, goethite and calcite, as franklinite, and mainly as sulfides (or polymetallic sulfides) (Figure VII-4, Figure VII-6, Figure VII-8, Figure VII-9 and Table VII-2). However, it is important to indicate the possible sources of Zn that are responsible for the aforementioned Zn species. Zn associated to phyllosilicates and sulfides, and found as zincite, smithsonite, ferrocyandide and hydrozincite are encountered in BFS (Kretzschmar et al., 2012; Mansfeldt and Dohrmann, 2004). Some of the minor phases that were detected in BFS are franklinite and sphalerite (Van Herck et al., 2000). Although not witnessed in BETH1402 sediments, we can assume, according to elevated metal contents (e.g. Fe, Zn and Pb) and distinct micrometric phases (such as ferrospheres and slag particles) that those minerals were present in the sediments before weathering (the classification of sediments as highly influenced by steelmaking wastes and weathering of phases was discussed in the previous chapter *V*, sections *4.1* and *4.2*). It is also highly anticipated that new Zn species form. As described previously, zincite breakdown requires high temperatures (Eq. VII-3 and Eq. VII-4); nonetheless, ZnO dissolution was proven to occur in soils after a period of ~ 9 months, and the new Zn species were Zn-layered double hydroxide and Zn-phyllosilicates (Voegelin et al., 2005). Still, the source of Zn from zincite dissolution is excluded in the case of the submerged sediments, due to the anoxic character. Smithsonite is readily dissolved under specific environmental conditions (Luxton et al., 2013), such as pH values inferior to 7 (Van Damme et al., 2010); smithsonite dissolution might occur as a buffering process triggered by pH decline (Isaure et al., 2005). The pH values of the top 10 cm sediments were close to 7 (Figure VII-2), the higher values in the deeper layers might had developed due to the protrusion of anoxic conditions (Ben-Yaakov, 1973; Lesven et al., 2010; Matijević et al., 2007). Furthermore, pH variations might be explained by the degradation of organic matter (Shaw et al., 1990) and dissolution or precipitation of carbonates and sulfides. Therefore, dissolution of smithsonite, if initially present upon BFS deposition, might explain why this mineral was not detected in BETH1402 sediments. However, the dissolved Zn concentrations in the interstitial waters generally ranged between 5 and 25 µg/L, except for higher values (~ 35 – 84 µg/L) for the layers 74 – 77 cm, 95 – 98 cm and 104 – 107 cm (Figure VII-2). Those values are similar to interstitial waters of contaminated sediments (Lesven et al., 2010, 2008; Louriño-Cabana et al., 2011).

4.3. Zn speciation in BETH1402 sediments

Linear combination fitting of XANES spectra at the Zn K-edge revealed that Zn in the sediments were present as sulfides (amorphous and crystalline), in spinel, in clay and sorbed onto different minerals (calcite, clay, ferrihydrite and goethite). For the 8 cm lithogenic deposits, the Zn species were rather diverse, while for the deeper layers, the predominance of sulfides was clearly evidenced (Figure VII-9). Interestingly, the spectra chosen for LCF demonstrated complete fits, with fitted sums between 99.99 and 100.1 (Table VII-2).

4.3.1. Clays as Zn bearing minerals, with focus on Fe-aluminosilicates

Hairy Fe-aluminosilicates are predominant in BETH1402 sediments inferior to 11 cm, constituted the main phases of the fine fraction, and were proven to have formed after weathering of steel by-products and wastes after deposition in the Orne River (see Figure V-10 of the previous chapter). Similar phases were reported by several authors in the context of steelmaking wastes, by-products and iron ore weathering (e.g. Huot et al., 2014; Maitte et al., 2015; Montargès-Pelletier et al., 2014). Moreover, some of the Fe-aluminosilicates in BETH1402 included Zn, and trace amounts of S (and Pb) in some cases (Figure VII-6 a). Zn containing Fe-aluminosilicates were also seen in SPM of the Fensch River, which had active steelmaking facilities until 2006 (Montargès-Pelletier et al., 2014). Nonetheless, the latter phase contained higher Fe, Ca and P contents than the Fe-aluminosilicates observed in this study, partially related to the different raw materials that were used in the steel industries, as well as different weathering conditions between the two (i.e. between sediments in this study and SPM in the other). However, further weathering/transformations surely occured, mainly by the formation of zinc and polymetallic sulfides, since anoxic conditions are well established in the submerged sediments. Due to the varying and relatively low Zn atomic percentages in the Fe-aluminosilicates (with respect to Fe), Zn is thought to be sorbed by those phases, possibly onto the mineral surface. Indeed, the contribution of Zn sorption onto clay minerals and ferrihydrite was evidenced by XANES spectra at the Zn K-edge and quantified by LCF (Figure VII-8 and Table VII-2, respectively). The interaction between Zn and aluminosilicates might be explained by electrostatic interactions between the negative charges of the octahedral sheets of phyllosilicates and Zn cations, and/or by Zn binding to the hydroxyl edge sites (e.g. Manceau et al., 2004, 2000; Nachtegaal and Sparks, 2004; Schlegel, 2001; Schlegel et al., 2001). This suggests that the relation between Zn and Fe-aluminosilicates might commence as surface sorption, and is followed by incorporation into the structure with time. Indeed, Zn

surface sorption, nucleation and epitaxial growth on phyllosilicates (montmorillonite) was evidenced (Schlegel et al., 2001; Schlegel and Manceau, 2006). BETH1402 sediments showed that the contribution of Zn as sorbed species could not be neglected (Figure VII-9). Furthermore, Kretzschmar et al., (2012) showed that Zn was mainly found in phyllosilicates in fresh BFS; after deposition, secondary Zn species form. The weathered products in the submerged sediments of BETH1402 would consequently be sulfides.

It should be noted that LCF of XANES spectra at the Zn K-edge showed only minor Zn species sorbed onto or into clay particles, except for the surface 8 cm (Table VII-2). Indeed, that unit was identified as lithogenic, while the underlying deposits were highly unnatural (as indicated by mineralogical and chemical composition; see chapter *V*); this explains the higher contribution of Zn-clay species. BFS in sedimentation ponds were shown to be majorly found within the octahedral sheets of phyllosilicates (Kretzschmar et al., 2012) (such as Znclay in this study). However, phyllosilicates, whether natural (smectite for example) or anthropogenic, have been shown to sequester Zn in soils (Vespa et al., 2010). Therefore, the Zn containing Fe-aluminosilicates might be marker phases in sediments highly influenced by steelmaking waste. The particular anoxic conditions of the BETH1402 sediments would certainly favor other Zn species, which are, again, sulfides.

4.3.2. Sorption of Zn onto carbonates, ferrihydrite and oxy-hydroxide

Zn incorporated into carbonates (such as calcites) might occur as new Zn species in sediments. Furthermore, Zn rich carbonates were slightly detected by SEM and clearly evidenced by XANES spectra at the Zn K-edge and quantified by LCF (Figure VII-4, Figure VII-8 and Table VII-2). On the possibility of Zn sorption onto calcium carbonate, calcite was shown to scavenge Zn in laboratory experiments with controlled pH (~ 8.3) and metal concentrations (Elzinga and Reeder, 2002). The pH in the sediments inferior to 11 cm ranged between 7.5 – 7.8, and contained hydrated Zn species (Figure VII-2), suggesting that conditions might be suitable for Zn sorption onto calcium carbonates. Nonetheless, the anoxic character and the anthropogenic nature of the sediments can explain the rare presence of Zn sorbed onto carbonates on one hand, and the predominance of ZnS on the other. BETH1402 sediments are enriched with Fe, even in comparison to raw BFS (e.g. Mansfeldt and Dohrmann, 2004), which suggests that Zn association to Fe minerals would certainly be present; indeed, Zn sorbed onto goethite and ferrihydrite was proven in the 2 – 128 cm layers (Table VII-2 and Figure VII-8). Zn was shown to be present as tetrahedrally coordinated inner-sphere complexes in BFS;

furthermore, poorly crystalline ferrihydrites are important metal sorbents, especially in weathered sludge from steel industries (Buatier et al., 2001; Kretzschmar et al., 2012; Scheinost et al., 2002; Van Herck et al., 2000). Due to the high iron contents and the presence of iron minerals (poorly crystalline and amorphous) in BETH1402 sediments, Zn sorbed onto ferrihydrite is very plausible. Finally, those phases limit Zn mobility, and therefore are considered as important Zn scavengers. The presence of Zn as franklinite only in the deepest layers (i.e. 62 till 125 cm) could be explained by franklinite weathering in the other layers. Indeed, franklinite weathering and Zn incorporation into neoformed goethite precipitate was evidenced in soil covered by contaminated dredged sediments (Isaure et al., 2005). Nonetheless, due to the anoxic state of BETH1402 sediments, the protrusion of franklinite in the layers of 62 till 128 cm is probably related to the unique materials forming those deposits, rather than weathering or ageing. Among many Zn phases usually associated to metallurgy, spinel (including franklinite) was shown to be stable under weathering conditions (Vanaecker et al., 2014). It should be noted that the distinction of BETH1402 sediments were clearly demonstrated in the previous chapter (chapter *V*, also see the different units in Figure VII-3 of this chapter).

4.3.3. Zn sulfides: the predominant Zn species

The main Zn species introduced into the river are expected to be zincite or franklinite. Sulfidization consequently occurred in the submerged sediments. Indeed, this was clearly demonstrated by TEM, where polymorphic Zn sulfides (with Fe and traces of Pb) were detected (Figure VII-6). LCF of XANES spectra at the Zn K-edge quantified the Zn species, and the predominance of Zn sulfides started from only 2 cm depth (Table VII-2 and Figure VII-9). Even though TEM evidenced the presence of zinc sulfides as amorphous phases (or at least poorly crystalline), XANES confirmed that the predominant Zn species is sulfide. The LCF of XANES spectra at the Zn K-edge seemed to be successful fits, however, the crystallinity (or amorphous) character of Zn sulfides cannot be guaranteed, since we have yet to fit the reference spectra to the EXAFS spectra at the Zn K-edge. Therefore, “crystalline” ZnS indicated previously (in Figure VII-9 and Table VII-2) might not be completely crystalline. Zinc sulfides are common phases in contaminated sediments (Lesven et al., 2010; Montargès-Pelletier et al., 2014), and in weathered sludge (e.g. Kretzschmar et al., 2012). It was previously indicated that Zn reach river sediments mainly as oxides (section 4.1). The source of dissolved Zn was also discussed in a previous section (section 4.2). BETH1402 sediments are submerged in river water throughout the year, therefore anoxic conditions are well maintained, which promotes

sulfides formation, such as iron, zinc and polymetallic sulfides. In addition, the pH values of the interstitial waters at various depths were superior to 7 (Figure VII-2). As a result, the conditions are favorable for zinc (or polymetallic) sulfide formation (Du Laing et al., 2009; Sobanska, 1999). Reduction of sulfate is an expected and a significant mechanism that immobilizes metals in anoxic sediments (Yoon et al., 2012). It is worth mentioning that zinc (or polymetallic) sulfides were mainly seen (via TEM) in layers having total sulfur contents above 0.6%. Indeed, Kretzschmar et al., (2012) found that whenever total S contents were below 0.5%, ZnS particle detection was rather low, even at the scale of bulk EXAFS. Sediments of the second unit (i.e. 11 – 41 cm) were most enriched with S and Zn, especially in the 11 – 20 cm layers (Figure VII-3); those layers showed the highest contributions of ZnS via LCF of XANES spectra at the Zn K-edge (Figure VII-9 and Table VII-2). In the BETH1402 sediments, it was demonstrated that weathering of ferrospheres, from fly ashes, and circular slag particles took part in the formation of Fe-aluminosilicates, sometimes maintaining their circular structure (Kanbar et al., 2017); in addition, Brownfield et al., (1999, 1997) reported a nanometric layer of sulfate at the periphery of those phases. From those studies, we can make the assumption that the weathered ferrospheres and slag particles retained their circular structure after weathering, and further transformations occurred, mainly reduction, to form the circular polymetallic (Zn-Fe-Pb) sulfides seen by TEM (Figure VII-6: b and c). Indeed, this idea is further supported by the similar diameters between the circular structures of the Fe-aluminosilicates (Kanbar et al., 2017) and the circular polymetallic sulfides (Figure VII-6: b and c), which is in the range of a few hundreds of nanometers (~ 100 – 300 nm). Sulfides were seen to be the main Zn hotspots in sedimentation ponds of weathered BFS, in the form of spherical particles (Kretzschmar et al., 2012). The distinct Zn rich phases (Zn > 20%) were either sulfides or polymetallic sulfides (Figure VII-6: b – f). The shape of the polymetallic sulfides detected and the Zn:S ratio well above 1 suggest a biological origin of the newly formed phases, possibly as (co)-precipitation. Furthermore, polymorphic and defective ZnS nanoparticles were associated to bacterial biofilms (Labrenz et al., 2000; Moreau et al., 2004). In our case, several hypotheses can be suggested on the formation of ZnS phases. For example, microbial derived bio-mineralization is proposed by the formation of spheroidal aggregates, since extracellular proteins were shown to limit metal nanoparticle dispersion (Moreau et al., 2007). The association of bacterial biofilms with zinc sulfides was reported in Pb-Zn mining sites (Labrenz et al., 2000; Moreau et al., 2004). Also, zinc sulfides might form via dissimilatory bacterial sulfate reduction or abiotic precipitation (Xu et al., 2016; Yoon et al.,

2012). In either case, bacterial cells and metabolites have enhancing roles on zinc sulfide formation (Xu et al., 2016).

Fluffy Zn sulfides, witnessed in Figure VII-6 (f), were also detected in anoxic sediments (Clark Fork River); the SAED pattern of the latter was a match for sphalerite, and was suggested to be the result of sulfate reducing bacteria (Hochella et al., 2005), based on what is known from other studies (Druschel et al., 2002; Labrenz et al., 2000; Ledin and Pedersen, 1996). Nonetheless, sphalerite could not be distinguished from wurtzite via TEM or XANES spectra at the Zn K-edge, due to their polymorphism and similar EXAFS spectra (Kretzschmar et al., 2012); therefore, the witnessed amorphous ZnS clumps might be the precursors of either ZnS mineral. TEM clearly evidenced ZnS polymorphs (Figure VII-6: b – f). Moreover, some of the polymetallic sulfides could be seen in the 5 – 8 cm layer, which might have formed in that layer, or might have been translocated from the underlying layers, possibly due to overburden or as a result of coring. Indeed, fine metal sulfide phases were proven to be transported towards the surface via porewater (Huo et al., 2015). In the vertical profile of BETH1402 sediments, contents of sulfur and metals (Fe, Zn and Pb) were rather similar (similar trend), which might support the idea that these elements form common phases, which are the polymetallic sulfides detected by TEM (Figure VII-6), proven by XANES spectra at the Zn K-edge (Figure VII-9) and quantified by LCF of XANES spectra at the Zn K-edge (Table VII-2).

5. Conclusion

The sediment layers of BETH1402 core were differentiated between the lithogenic top 11 cm and the highly contaminated 11 – 131 cm layers. Indeed, Zn species could clearly be distinguished between those two divisions. The sources and possible fates of various Zn species are discussed. The surface sediments showed variable contributions of Zn species, such as clays and calcite (sorbed onto and in structure), as well as sulfides. XRD and SEM evidenced that Zn is not associated to relatively coarse particles nor are they found as major crystalline minerals; rather Zn is associated to fine particles and mainly as amorphous or poorly crystalline phases. The newly formed Fe-aluminosilicates in BETH1402 sediments were evidenced to be main Zn carriers at the sub-micrometer scale (TEM). Furthermore, evolution or weathering of those Fe-aluminosilicates could have formed circular polymetallic (Zn-Fe-Pb) sulfides, possibly by the aid of microbial communities. The most precise Zn species were revealed by XANES spectra at the Zn K-edge and quantified by LCF. Interestingly, variation of Zn bearing

minerals could not be distinguished in the vertical profile by SEM and TEM, as observed with the chemical composition; nonetheless, that was rather noticeable by LCF of XANES spectra at the Zn K-edge. A progressive decrease was seen for ZnS (amorphous and crystalline) from unit II to IV, and franklinite was mainly present in unit IV. Finally, sulfides were clearly the predominant Zn species, particularly as fine phases. Those sulfides formed in the submerged sediments with time and scavenged other metals (e.g. Fe and Pb). Unfortunately, disturbance of those phases might cause dissolution of the formed sulfides, especially since a great part is amorphous (or poorly crystalline), which consequently release bound Zn (and other metals) to the water compartment. As a perspective, EXAFS data at the Zn K-edge should give more detailed information about the crystallinity of Zn sulfides and other Zn species, precisely on the second and third neighbors.

References

Bazin, D., Carpentier, X., Brocheriou, I., Dorfmuller, P., Aubert, S., Chappard, C., Thiaudière, D., Reguer, S., Waychunas, G., Jungers, P., Daudon, M., 2009. Revisiting the localisation of Zn^{2+} cations sorbed on pathological apatite calcifications made through X-ray absorption spectroscopy. Biochimie 91, 1294–1300. doi:10.1016/j.biochi.2009.05.009

Ben-Yaakov, S., 1973. pH buffering of pore water of recent anoxic marine sediments. Limnol. Oceanogr. 18, 86–94. doi:10.4319/lo.1973.18.1.0086

Besta, P., Janovská, K., Samolejová, A., Beránková, A., Vozňáková, I., Hendrych, M., 2013. The cycle and effect of zinc in the blast-furnace process. Metalurgija 52, 197–200.

Boughriet, A., Proix, N., Billon, G., Recourt, P., Ouddane, B., 2007. Environmental impacts of heavy metal discharges from a smelter in Deûle-canal sediments (northern France): concentration levels and chemical fractionation. Water. Air. Soil Pollut. 180, 83–95. doi:10.1007/s11270-006-9252-5

Brownfield, M.E., Affolter, R.H., Cathcart, J.D., O'Connor, J.T., Brownfield, I.K., 1999. Characterization of Feed Coal and Coal Combustion Products from Power Plants in Indiana and Kentucky, in: 24th International Technical Conference on Coal Utilization and Fuel Systems. Coal and Slurry Technology Association, Washington, DC, pp. 989–1000.

Brownfield, M.E., Cathcart, J.D., Affolter, R.H., 1997. Characterization of Feed Coals and Waste Products from a Coalburning Power Plant in Kentucky, in: Proceedings of the 1997 International Ash Utilization Symposium. Lexington, Ky, pp. 780–784.

Buatier, M.D., Sobanska, S., Elsass, F., 2001. TEM-EDX investigation on Zn- and Pb-contaminated soils. Appl. Geochemistry 16, 1165–1177. doi:10.1016/S0883-2927(01)00015-4

Carignan, J., Hild, P., Mevelle, G., Morel, J., Yeghicheyan, D., 2001. Routine analyses of trace elements in geological samples using flow injection and low pressure on-line liquid chromatography coupled to ICP-MS: A study of geochemical reference materials BR, DR-N, UB-N, AN-G and GH. Geostand. Geoanalytical Res. 25, 187–198. doi:10.1111/j.1751-908X.2001.tb00595.x

Carvalho, H.W.P., Pulcinelli, S.H., Santilli, C. V., Leroux, F., Meneau, F., Briois, V., 2013. XAS/WAXS time-resolved phase speciation of chlorine LDH thermal transformation: emerging roles of isovalent metal substitution. Chem. Mater. 25, 2855–2867. doi:10.1021/cm401352t

Cismasu, A.C., Levard, C., Michel, F.M., Brown, G.E., 2013. Properties of impurity-bearing ferrihydrite II: Insights into the surface structure and composition of pure, Al- and Si-bearing ferrihydrite from Zn(II) sorption experiments and Zn K-edge X-ray absorption spectroscopy. Geochim. Cosmochim. Acta 119, 46–60. doi:10.1016/j.gca.2013.05.040

Dagallier, G., Grgic, D., Homand, F., 2002. Caractérisation minéralogique et microtexturale du vieillissement anthropique du minerai de fer lorrain. Comptes Rendus Geosci. 334, 455–462. doi:10.1016/S1631-0713(02)01783-2

Das, B., Prakash, S., Reddy, P.S.R., Biswal, S.K., Mohapatra, B.K., Misra, V.N., 2002. Effective utilization of blast furnace flue dust of integrated steel plants. Eur. J. Miner. Process. Environ. Prot. 2, 61–68.

Das, B., Prakash, S., Reddy, P.S.R., Misra, V.N., 2007. An overview of utilization of slag and sludge from steel industries. Resour. Conserv. Recycl. 50, 40–57. doi:10.1016/j.resconrec.2006.05.008

Dessombz, A., Nguyen, C., Ea, H.K., Rouzière, S., Foy, E., Hannouche, D., Réguer, S., Picca, F.E., Thiaudière, D., Lioté, F., Daudon, M., Bazin, D., 2013. Combining μX-ray fluorescence, μXANES and μXRD to shed light on Zn^{2+} cations in cartilage and meniscus calcifications. J. Trace Elem. Med. Biol. 27, 326–333. doi:10.1016/j.jtemb.2013.02.001

Druschel, G.K., Labrenz, M., Thomsen-Ebert, T., Fowle, D.A., Banfield, J.F., 2002. Geochemical modeling of ZnS in biofilms: an example of ore depositional processes. Econ. Geol. 97, 1319–1329. doi:10.2113/gsecongeo.97.6.1319

Du Laing, G., Rinklebe, J., Vandecasteele, B., Meers, E., Tack, F.M.G., 2009. Trace metal behaviour in estuarine and riverine floodplain soils and sediments: A review. Sci. Total Environ. 407, 3972–3985. doi:10.1016/j.scitotenv.2008.07.025

Elzinga, E.J., Reeder, R.J., 2002. X-ray absorption spectroscopy study of Cu^{2+} and Zn^{2+} adsorption complexes at the calcite surface: Implications for site-specific metal incorporation preferences during calcite crystal growth. Geochim. Cosmochim. Acta 66, 3943–3954. doi:10.1016/S0016-7037(02)00971-7

Elzinga, E.J., Rouff, A.A., Reeder, R.J., 2006. The long-term fate of Cu^{2+}, Zn^{2+}, and Pb^{2+} adsorption complexes at the calcite surface: an X-ray absorption spectroscopy study. Geochim. Cosmochim. Acta 70, 2715–2725. doi:10.1016/j.gca.2006.02.026

Ettler, V., 2016. Soil contamination near non-ferrous metal smelters: A review. Appl. Geochemistry 64, 56–74. doi:10.1016/j.apgeochem.2015.09.020

Gabelle, C., 2006. Etude de la contamination des sediments par les metaux dans les canaux et rivieres du nord de

References

la France. Ph.D. thesis. Ecole Doctorale des Sciences de la Matiere, du Rayonnement et de l'Environnement. Universite de Lille, France.

Galoisy, L., Cormier, L., Calas, G., Briois, V., 2001. Environment of Ni, Co and Zn in low alkali borate glasses: Information from EXAFS and XANES spectra. J. Non. Cryst. Solids 293–295, 105–111. doi:10.1016/S0022-3093(01)00659-7

Garcier, R.J., 2007. Rivers we can't bring ourselves to clean – historical insights into the pollution of the Moselle River (France), 1850–2000. Hydrol. Earth Syst. Sci. 11, 1731–1745. doi:10.5194/hess-11-1731-2007

Hochella, M.F., Moore, J.N., Putnis, C. V, Putnis, A., Kasama, T., Eberl, D.D., 2005. Direct observation of heavy metal-mineral association from the Clark Fork River Superfund Complex: implications for metal transport and bioavailability. Geochim. Cosmochim. Acta 69, 1651–1663. doi:10.1016/j.gca.2004.07.038

Huo, S., Zhang, J., Yeager, K.M., Xi, B., Qin, Y., He, Z., Wu, F., 2015. Mobility and sulfidization of heavy metals in sediments of a shallow eutrophic lake, Lake Taihu, China. J. Environ. Sci. 31, 1–11. doi:10.1016/j.jes.2014.12.003

Huot, H., Simonnot, M.-O., Marion, P., Yvon, J., De Donato, P., Morel, J.-L., 2013. Characteristics and potential pedogenetic processes of a Technosol developing on iron industry deposits. J. Soils Sediments 13, 555–568. doi:10.1007/s11368-012-0513-1

Huot, H., Simonnot, M.O., Watteau, F., Marion, P., Yvon, J., De Donato, P., Morel, J.-L., 2014. Early transformation and transfer processes in a Technosol developing on iron industry deposits. Eur. J. Soil Sci. 65, 470–484. doi:10.1111/ejss.12106

Isaure, M.-P., Manceau, A., Geoffroy, N., Laboudigue, A., Tamura, N., Marcus, M.A., 2005. Zinc mobility and speciation in soil covered by contaminated dredged sediment using micrometer-scale and bulk-averaging X-ray fluorescence, absorption and diffraction techniques. Geochim. Cosmochim. Acta 69, 1173–1198. doi:10.1016/j.gca.2004.08.024

Jacquat, O., Voegelin, A., Juillot, F., Kretzschmar, R., 2009. Changes in Zn speciation during soil formation from Zn-rich limestones. Geochim. Cosmochim. Acta 73, 5554–5571. doi:10.1016/j.gca.2009.05.069

James, H.L., 1966. Chemistry of the Iron-Rich Sedimentary Rocks, in: Fleisher, M. (Ed.), Data of Geochemistry. US Government Printing Office, Washington, pp. W1–W61.

Juillot, F., Maréchal, C., Ponthieu, M., Cacaly, S., Morin, G., Benedetti, M., Hazemann, J.L., Proux, O., Guyot, F., 2008. Zn isotopic fractionation caused by sorption on goethite and 2-Lines ferrihydrite. Geochim. Cosmochim. Acta 72, 4886–4900. doi:10.1016/j.gca.2008.07.007

Juillot, F., Morin, G., Ildefonse, P., Trainor, T.P., Benedetti, M., Galoisy, L., Calas, G., Brown, G.E., 2003. Occurrence of Zn/Al hydrotalcite in smelter-impacted soils from northern France: Evidence from EXAFS spectroscopy and chemical extractions. Am. Mineral. 88, 509–526. doi:10.2138/am-2003-0405

Kanbar, H.J., Montargès-Pelletier, E., Losson, B., Bihannic, I., Gley, R., Bauer, A., Villieras, F., Manceau, L., El Samrani, A.G., Kazpard, V., Mansuy-Huault, L., 2017. Iron mineralogy as a fingerprint of former steelmaking activities in river sediments. Sci. Total Environ. 599–600, 540–553. doi:10.1016/j.scitotenv.2017.04.156

Kiventerä, J., Leiviskä, T., Keski-Ruismäki, K., Tanskanen, J., 2016. Characteristics and settling behaviour of particles from blast furnace flue gas washing. J. Environ. Manage. 172, 162–170. doi:10.1016/j.jenvman.2016.02.037

Korpa, L., Mudron', Y., 2006. System for cleaning blast-furnace gas in the blast-furnace shop at the VSZh Koshitse combine. Metallurgist 50, 379–383. doi:10.1007/s11015-006-0092-8

Kretzschmar, R., Mansfeldt, T., Mandaliev, P.N., Barmettler, K., Marcus, M.A., Voegelin, A., 2012. Speciation of Zn in blast furnace sludge from former sedimentation ponds using synchrotron X-ray diffraction, fluorescence, and absorption spectroscopy. Environ. Sci. Technol. 46, 12381–12390. doi:10.1021/es302981v

Labrenz, M., Druschel, G.K., Thomsen-Ebert, T., Gilbert, B., Welch, S.A., Kemner, K.M., Logan, G.A., Summons, R.E., Stasio, G. De, Bond, P.L., Lai, B., Kelly, S.D., Banfield, J.F., 2000. Formation of sphalerite (ZnS) deposits in natural biofilms of sulfate-reducing bacteria. Science (80-.). 290, 1744–1747. doi:10.1126/science.290.5497.1744

Le Meur, M., 2016. Matières en suspension de la Moselle (Lorraine, France) : caractérisation minérale et organique et réactivité vis à visdes contaminants métalliques. Ph.D. thesis. Geosciences. Lorraine University.

Le Meur, M., Montargès-Pelletier, E., Bauer, A., Gley, R., Migot, S., Barres, O., Delus, C., Villiéras, F., 2016. Characterization of suspended particulate matter in the Moselle River (Lorraine, France): evolution along the course of the river and in different hydrologic regimes. J. Soils Sediments 16, 1625–1642. doi:10.1007/s11368-015-1335-8

Ledin, M., Pedersen, K., 1996. The environmental impact of mine wastes — Roles of microorganisms and their significance in treatment of mine wastes. Earth-Science Rev. 41, 67–108. doi:10.1016/0012-8252(96)00016-5

Lesven, L., Gao, Y., Billon, G., Leermakers, M., Ouddane, B., Fischer, J.-C., Baeyens, W., 2008. Early diagenetic processes aspects controlling the mobility of dissolved trace metals in three riverine sediment columns. Sci. Total Environ. 407, 447–459. doi:10.1016/j.scitotenv.2008.08.033

References

Lesven, L., Lourino-Cabana, B., Billon, G., Recourt, P., Ouddane, B., Mikkelsen, O., Boughriet, A., 2010. On metal diagenesis in contaminated sediments of the Deûle river (northern France). Appl. Geochemistry 25, 1361–1373. doi:10.1016/j.apgeochem.2010.06.007

Lourino-Cabana, B., Lesven, L., Billon, G., Proix, N., Recourt, P., Ouddane, B., Fischer, J.C., Boughriet, A., 2010. Impacts of metal contamination in calcareous waters of Deûle River (France): Water quality and thermodynamic studies on metallic mobility. Water. Air. Soil Pollut. 206, 187–201. doi:10.1007/s11270-009-0095-8

Louriño-Cabana, B., Lesven, L., Charriau, A., Billon, G., Ouddane, B., Boughriet, A., 2011. Potential risks of metal toxicity in contaminated sediments of Deûle river in Northern France. J. Hazard. Mater. 186, 2129–2137. doi:10.1016/j.jhazmat.2010.12.124

Luxton, T.P., Miller, B.W., Scheckel, K.G., 2013. Zinc Speciation Studies in Soil, Sediment and Environmental Samples, in: Bakirdere, S. (Ed.), Speciation Studies in Soil, Sediment and Environmental Samples. CRC Press, Taylor & Francis Groups, New York, pp. 433–477. doi:doi:10.1201/b15501-12

Maitte, B., Jorand, F.P.A., Grgic, D., Abdelmoula, M., Carteret, C., 2015. Remineralization of ferrous carbonate from bioreduction of natural goethite in the Lorraine iron ore (Minette) by *Shewanella putrefaciens*. Chem. Geol. 412, 48–58. doi:10.1016/j.chemgeo.2015.07.024

Manceau, A., Lanson, B., Schlegel, M.L., Hargé, J.C., Musso, M., Eybert-Bérard, L., Hazemann, J.-L., Chateigner, D., Lamble, G.M., 2000. Quantitative Zn speciation in smelter-contaminated soils by EXAFS spectroscopy. Am. J. Sci. 300, 289–343. doi:10.2475/ajs.300.4.289

Manceau, A., Marcus, M.A., Tamura, N., Proux, O., Geoffroy, N., Lanson, B., 2004. Natural speciation of Zn at the micrometer scale in a clayey soil using X-ray fluorescence, absorption, and diffraction. Geochim. Cosmochim. Acta 68, 2467–2483. doi:10.1016/j.gca.2003.11.021

Mansfeldt, T., Dohrmann, R., 2004. Chemical and mineralogical characterization of blast-furnace sludge from an abandoned landfill. Environ. Sci. Technol. 38, 5977–5984. doi:10.1021/es040002+

Matijević, S., Kušpilić, G., Kljaković-Gašpić, Z., 2007. The redox potential of sediment from the Middle Adriatic region. Acta Adriat. 48, 191–204.

Mertens, J., Smolders, E., 2013. Zinc, in: Alloway, B.J. (Ed.), Heavy Metals in Soils: Trace Metals and Metalloids in Soils and Their Bioavailability. Springer Netherlands, pp. 465–493. doi:10.1007/978-94-007-4470-7_17

Montargès-Pelletier, E., Duriez, C., Ghanbaja, J., Jeanneau, L., Falkenberg, G., Michot, L.J., 2014. Microscale investigations of the fate of heavy metals associated to iron-bearing particles in a highly polluted stream. Environ. Sci. Pollut. Res. 21, 2744–2760. doi:10.1007/s11356-013-2192-x

Montargès-Pelletier, E., Jeanneau, L., Faure, P., Bihannic, I., Barres, O., Lartiges, B.S., 2007. The junction of Fensch and Moselle rivers, France; mineralogy and composition of river materials. Environ. Geol. 53, 85–102. doi:10.1007/s00254-006-0621-6

Moreau, J.W., Webb, R.I., Banfield, J.F., 2004. Ultrastructure, aggregation-state, and crystal growth of biogenic nanocrystalline sphalerite and wurtzite. Am. Mineral. 89, 950–960. doi:10.2138/am-2004-0704

Moreau, J.W., Weber, P.K., Martin, M.C., Gilbert, B., Hutcheon, I.D., Banfield, J.F., 2007. Extracellular proteins limit the dispersal of biogenic nanoparticles. Science (80-.). 316, 1600–1602. doi:10.1126/science.1141064

Nachtegaal, M., Sparks, D.L., 2004. Effect of iron oxide coatings on zinc sorption mechanisms at the clay-mineral/water interface. J. Colloid Interface Sci. 276, 13–23. doi:10.1016/j.jcis.2004.03.031

Nriagu, J.O., 1996. A history of global metal pollution. Science (80-.). 272, 223–224. doi:10.1126/science.272.5259.223

Nriagu, J.O., 1990. Global metal pollution: poisoning the biosphere? Environ. Sci. Policy Sustain. Dev. 32, 7–33. doi:10.1080/00139157.1990.9929037

Panfili, F., Manceau, A., Sarret, G., Spadini, L., Kirpichtchikova, T., Bert, V., Laboudigue, A., Marcus, M.A., Ahamdach, N., Libert, M.F., 2005. The effect of phytostabilization on Zn speciation in a dredged contaminated sediment using scanning electron microscopy, X-ray fluorescence, EXAFS spectroscopy, and principal components analysis. Geochim. Cosmochim. Acta 69, 2265–2284. doi:10.1016/j.gca.2004.10.017

Ravel, B., Newville, M., 2005. ATHENA, ARTEMIS, HEPHAESTUS: data analysis for X-ray absorption spectroscopy using IFEFFIT. J. Synchrotron Radiat. 12, 537–41. doi:10.1107/S0909049505012719

Roberts, D.R., Scheinost, A.C., Sparks, D.L., 2002. Zinc speciation in a smelter-contaminated soil profile using bulk and microspectroscopic techniques. Environ. Sci. Technol. 36, 1742–1750. doi:10.1021/es015516c

Rogé, M., Walterspieler, M., 1982. Chronique lorraine : L'eau et la sidérurgie en Lorraine. Le football lorrain. Rev. Geogr. Est. 22, 295–306. doi:10.3406/rgest.1982.1422

Scheinost, A.C., Kretzschmar, R., Pfister, S., Roberts, D.R., 2002. Combining selective sequential extractions, X-ray absorption spectroscopy, and principal component analysis for quantitative zinc speciation in soil. Environ. Sci. Technol. 36, 5021–5028. doi:10.1021/es025669f

Schlegel, M.L., 2001. Adsorption mechanisms of Zn on hectorite as a function of time, pH, and ionic strength. Am. J. Sci. 301, 798–830. doi:10.2475/ajs.301.9.798

Schlegel, M.L., Manceau, A., 2006. Evidence for the nucleation and epitaxial growth of Zn phyllosilicate on

References

montmorillonite. Geochim. Cosmochim. Acta 70, 901–917. doi:10.1016/j.gca.2005.10.021
Schlegel, M.L., Manceau, A., Charlet, L., Chateigner, D., Hazemann, J.-L., 2001. Sorption of metal ions on clay minerals. III. Nucleation and epitaxial growth of Zn phyllosilicate on the edges of hectorite. Geochim. Cosmochim. Acta 65, 4155–4170. doi:10.1016/S0016-7037(01)00700-1
Shaw, T.J., Gieskes, J.M., Jahnke, R.A., 1990. Early diagenesis in differing depositional environments: The response of transition metals in pore water. Geochim. Cosmochim. Acta 54, 1233–1246. doi:10.1016/0016-7037(90)90149-F
Simpson, S.L., Apte, S.C., Batley, G.E., 2000. Effect of short-term resuspension events on the oxidation of cadmium, lead, and zinc sulfide phases in anoxic estuarine sediments. Environ. Sci. Technol. 34, 4533–4537. doi:10.1021/es991440x
Sobanska, S., 1999. Etude de la spéciation du plomb et du zinc dans des poussières industrielles et dans un sol contaminé: Approche par méthodes spectroscopiques. Ph.D. thesis. Spectrochimie, molécules, solides, réactivités. University of Lille, France.
Sterckeman, T., Douay, F., Baize, D., Fourrier, H., Proix, N., Schvartz, C., 2006. Trace elements in soils developed in sedimentary materials from Northern France. Geoderma 136, 912–929. doi:10.1016/j.geoderma.2006.06.010
Sterckeman, T., Douay, F., Proix, N., Fourrier, H., 2000. Vertical distribution of Cd, Pb and Zn in soils near smelters in the North of France. Environ. Pollut. 107, 377–389. doi:10.1016/S0269-7491(99)00165-7
Sterckeman, T., Douay, F., Proix, N., Fourrier, H., Perdrix, E., 2002. Assessment of the contamination of cultivated soils by eighteen trace elements around smelters in the north of France. Water. Air. Soil Pollut. 135, 173–194. doi:10.1023/A:1014758811194
Stewart, S.J., Figueroa, S.J.A., Ramallo López, J.M., Marchetti, S.G., Bengoa, J.F., Prado, R.J., Requejo, F.G., 2007. Cationic exchange in nanosized ZnFe2O4 spinel revealed by experimental and simulated near-edge absorption structure. Phys. Rev. B - Condens. Matter Mater. Phys. 75, 3–6. doi:10.1103/PhysRevB.75.073408
Szczerba, W., Żukrowski, J., Przybylski, M., Sikora, M., Safonova, O., Shmeliov, A., Nicolosi, V., Schneider, M., Granath, T., Oppmann, M., Straßer, M., Mandel, K., 2016. Pushing up the magnetisation values for iron oxide nanoparticles via zinc doping: X-ray studies on the particle's sub-nano structure of different synthesis routes. Phys. Chem. Chem. Phys. 18, 25221–25229. doi:10.1039/C6CP04221J
Trinkel, V., Mallow, O., Aschenbrenner, P., Rechberger, H., Fellner, J., 2016. Characterization of blast furnace sludge with respect to heavy metal distribution. Ind. Eng. Chem. Res. 55, 5590–5597. doi:10.1021/acs.iecr.6b00617
Trinkel, V., Mallow, O., Thaler, C., Schenk, J., Rechberger, H., Fellner, J., 2015. Behavior of chromium, nickel, lead, zinc, cadmium, and mercury in the blast furnace — A critical review of literature data and plant investigations. Ind. Eng. Chem. Res. 54, 11759–11771. doi:10.1021/acs.iecr.5b03442
Trung, Z.H., Kukurugya, F., Takacova, Z., Orac, D., Laubertova, M., Miskufova, A., Havlik, T., 2011. Acidic leaching both of zinc and iron from basic oxygen furnace sludge. J. Hazard. Mater. 192, 1100–1107. doi:10.1016/j.jhazmat.2011.06.016
Van Damme, A., Degryse, F., Smolders, E., Sarret, G., Dewit, J., Swennen, R., Manceau, A., 2010. Zinc speciation in mining and smelter contaminated overbank sediments by EXAFS spectroscopy. Geochim. Cosmochim. Acta 74, 3707–3720. doi:10.1016/j.gca.2010.03.032
Vanaecker, M., Courtin-Nomade, A., Bril, H., Laureyns, J., Lenain, J.-F., 2014. Behavior of Zn-bearing phases in base metal slag from France and Poland: A mineralogical approach for environmental purposes. J. Geochemical Explor. 136, 1–13. doi:10.1016/j.gexplo.2013.09.001
Van Herck, P., Vandecasteele, C., Swennen, R., Mortier, R., 2000. Zinc and lead removal from blast furnace sludge with a hydrometallurgical process. Environ. Sci. Technol. 34, 3802–3808. doi:10.1021/es991033l
Vdović, N., Billon, G., Gabelle, C., Potdevin, J.-L., 2006. Remobilization of metals from slag and polluted sediments (Case Study: The canal of the Deûle River, northern France). Environ. Pollut. 141, 359–369. doi:10.1016/j.envpol.2005.08.034
Vereš, J., Jakabský, Š., Šepelák, V., 2010. Chemical, physical, morphological and structural characterization of blast furnace sludge. Diffus. Fundam. 12, 88–91.
Vespa, M., Lanson, M., Manceau, A., 2010. Natural attenuation of zinc pollution in smelter-affected soil. Environ. Sci. Technol. 44, 7814–7820. doi:10.1021/es101567u
Voegelin, A., Pfister, S., Scheinost, A.C., Marcus, M.A., Kretzschmar, R., 2005. Changes in zinc speciation in field soil after contamination with zinc oxide. Environ. Sci. Technol. 39, 6616–6623. doi:10.1021/es047962g
Waychunas, G.A., Fuller, C.C., Davis, J.A., 2002. Surface complexation and precipitate geometry for aqueous Zn(II) sorption on ferrihydrite I: X-ray absorption extended fine structure spectroscopy analysis. Geochim. Cosmochim. Acta 66, 1119–1137. doi:10.1016/S0016-7037(01)00853-5
Waychunas, G.A., Fuller, C.C., Davis, J.A., Rehr, J.J., 2003. Surface complexation and precipitate geometry for aqueous Zn(II) sorption on ferrihydrite: II. XANES analysis and simulation. Geochim. Cosmochim. Acta 67, 1031–1043. doi:10.1016/S0016-7037(02)01280-2

References

Xu, J., Murayama, M., Roco, C.M., Veeramani, H., Michel, F.M., Rimstidt, J.D., Winkler, C., Hochella, M.F., 2016. Highly-defective nanocrystals of ZnS formed via dissimilatory bacterial sulfate reduction: A comparative study with their abiogenic analogues. Geochim. Cosmochim. Acta 180, 1–14. doi:10.1016/j.gca.2016.02.007

Yoon, S., Yáñez, C., Bruns, M.A., Martínez-Villegas, N., Martínez, C.E., 2012. Natural zinc enrichment in peatlands: Biogeochemistry of ZnS formation. Geochim. Cosmochim. Acta 84, 165–176. doi:10.1016/j.gca.2012.01.022

Zebracki, M., 2008. Devenir des polluants métalliques associés aux sédiments contaminés dans un cours d'eau en relation avec la dynamique sédimentaire. Ph.D. thesis. Rayonnements et Environnement. Université Paris-Sud XI, France.

Zhukova, Z.D., Gul'ko, N. V., Tolstaya, V.Y., 1976. Formation of sphalerite in blast furnace lining. Refractories 17, 380–382. doi:10.1007/BF01281641

VIII. GENERAL DISCUSSION, CONCLUSION AND PERSPECTIVES

1. General discussion

This thesis is part of the ZAM/MOBISED project in which sediments along the Orne River were characterized, mainly in terms of geochemistry and mineralogy. Initially, surface sediments were collected from nine stations, with more than one sample per site in most cases. Along the 21 km river course, the surface sediments could be distinguished according to grain size parameters, chemical contents and mineralogical composition. The variations in the aforementioned features were attributed to land cover, land use, river hydrodynamics and former industrial activities that were installed in the Orne basin. The main mineralogical composition was similar for Orne River sediments; however, grain properties and chemical composition showed otherwise. The particle sizes of sediments were affected by river hydrodynamics, which showed to vary principally upstream the dams of Homécourt and Moyeuvre-Grande; moreover, the particularly fine deposits were also due to the nature of the sediments, which are thought to be waste materials originated from steelmaking, mainly sludge blast furnace sludge. Variation in chemical composition was seen for different grain sizes belonging to the same samples. The surface sediments were marked by detrital/lithogenic materials, which was followed by elements that originate from surface weathering, such as Si, Ca, Al and K, and by minerals that would be expected in Orne sediments (such as quartz, calcite and clays). The clays showed interlayered features, which showed to be stacked phyllosilicates, with varying contributions of interlayered cations (e.g. Na, K and Mg), as partially evidenced by TEM-EDXS. In addition, the anthropogenic contribution of the sediments could be followed by elevated metal contents as well as the presence of minerals with urban/domestic signature, such as Fe-aluminosilicates and apatite that might be sourced to weathered steelmaking wastes and WWTP effluents.

Steelmaking facilities were the main influencers of Orne sediment composition during the last two centuries. Even though the steelmaking facilities located in the study area stopped by the late 1980s, some of their features are still evidenced in surface, as well as subsurface, sediments. It is expected that sediments that had been impacted by former steelmaking facilities are not on the surface, since recent sediments certainly had settled after the facilities stopped. Nonetheless, sediment disturbance (e.g. due to flooding events) are expected to remobilize

some of the deposits that had settled during the last centuries. Some steel wastes (sludge) and by-products (slag) might have been piled near the river, settled in sedimentation ponds, or were deposited as overbank sediments. The surface leaching or remobilization of those particles might also explain the high metal contents and/or "steelmaking" feature of surface sediments, even if only slightly. Indeed, submerged and overbank sediments near the limit of Moyeuvre-Grande, where JOEP sediments were collected, showed to be mainly composed of metal enriched sludge. Although this idea is not included in the manuscript, the influence of those contaminated surface and overbank sediments will clearly affect water, SPM and sediment quality in the downstream reach, not forgetting the effect on biota. Settling of SPM is enhanced in upstream zones of dams; therefore, a great part of the deposits from the former steelmaking facilities had settled upstream of the Beth dam, which is located a little after JOEP (~ 1 km). Moreover, the river bed between JOEP and BETH, to our knowledge, had not been dredged; those sediments still hold the signature of the former steelmaking facilities, with the note that they had been submerged in the river for at least 25 years (from 1988 till the first sampling campaign in 2013). Those deposits could have been submerged since 1960 (i.e. 53 years ago), when the dam was built. As a result, those deposits had surely evolved, mainly due to anoxic state of the submerged sediments.

The sediments collected upstream of the Beth dam showed a relatively thin lithogenic layer, which was followed by metal laden deposits. Those deposits were detected starting from 3 cm depth at some locations, while they started at 28 cm depth at other locations. The variation in thickness of the lithogenic surface deposits were explained by the decametric variation of the riverbed profile. The lithogenic deposits were mainly composed of detrital materials (diatom skeletons, quartz, calcite and clay minerals). As for the contaminated sediments, they had settled in large amounts upstream of the Beth dam. Although we did not reach the deepest layers of the deposits, they could be found at depth below 200 cm at some points (BETH1701 core). Additionally, those metal rich deposits were evidenced in the horizontal section till approximately 200 m before the dam. The main metals that have been presented are Fe, Zn and Pb, which reached up to 27, 0.9 and 0.4%, respectively. Being trace elements, the significantly high Zn and Pb contents surely evidence anthropogenic contribution. The lithogenic character is still present in those samples, however, only slightly. Being the "major element" in the sediments of BETH1402, the mineralogy of Fe was studied. Fe mineralogy revealed that the deposits contained the fingerprint of the former steelmaking facilities. Sludge contribution was evidenced by high metal contents as well as the presence of Fe rich minerals, namely magnetite,

wuestite, pyrite and weathered Fe-aluminosilicates; iron ore contribution was revealed by Fe rich deposits and goethite nanoparticles, the latter being a major component of the minette iron ore. In the submerged sediments, the behavior of the metals has surely evolved differently than they would have on land (e.g. in settling ponds or landfills), due to anoxic conditions. Although the results for Fe and Zn were included in separate chapters, they have common fates and behaviors in the sediments; consequently, they will be partially described in a conjoint way.

One of the distinct features of the contaminated sediments was the hairy Fe-aluminosilicate structures. Even though similar Fe-aluminosilicates were evidenced in sediments and suspended matter in the context of steelmaking, fine yet important details about their composition and structure were unique. First, their chemical composition was distinctive in terms of Fe, Si and Al, in comparison to other similar structures. Secondly, the Fe-aluminosilicates displayed three dimensional aggregates of circles/spheres, which are thought to be the remains of the degraded/weathered ferrospheres. Thirdly, the borders or rings of the circular and hairy Fe-aluminosilicates showed fluffy polymetallic sulfides, mainly composed of Zn, but also contain Fe and slightly Pb. Interestingly, similar structures to those circular entities were seen, however, the hairy character was highly reduced to almost absent, the Fe content was lower, and the Zn and S contents were extremely higher; instead of a circular Fe-aluminosilicate with polymetallic sulfides on the rim, the phase is clearly identified as zinc sulfide. The polymetallic sulfides that rung the circular Fe-aluminosilicates are suggested to have evolved into zinc sulfides. Although we did not ascertain this transformation, this speculation is argued by similar sizes between the circular Fe-aluminosilicates and Zn-sulfides, by similar structures, and by the difference of the metal contents of the circular structures, which could be explained by different conditions of formation or different age. Even though we did not take into consideration the biological character in the formation of those phases, the microbial work, such as bio-mineralization or bio-precipitation is suggested by the circular shapes and aggregations, since extracellular proteins limit the dispersion of formed nanoparticles. Additionally, other structures of Zn sulfides were witnessed, such as fluffy deca-nanometric circular structures. Even though other Zn species were present in the contaminated sediments (in illite structure or sorbed by ferrihydrite for example), the predominance of Zn sulfides was revealed by LCF of XANES spectra at the Zn K-edge. It is important to note that Zn did not reach the sediments as sulfides, or only slightly, rather Zn is thought to have reached the sediments as oxides (zincite or franklinite) and carbonates (smithsonite), and sulfidization occurred with time.

2. General conclusion

The Orne River, being highly influenced by steelmaking facilities during the previous two centuries, is expected to retain some features of the wastes and by-products, mainly in the settled deposits. Therefore, an inventory of Orne surface sediments was made, in terms of particle size, chemical content and mineralogical composition. First, the heterogeneity of the Orne sediments was revealed by variable particle sizes on one hand, and by different fractionations of chemicals according to grain size (0 – 50 µm, 50 – 250 µm and 250 µm – 2 mm fractions) on the other. The correlation between chemical content and grain size was not consistent for all the collected sediments, meaning that the chemical composition is not only related to grain sizes. Indeed, complementary analyses and sample collection were necessary to unravel the cause(s) of that variation. Particle size distribution (PSD) data showed difference in grain sizes (D_i) as well as grain parameters (sorting, skewness and kurtosis). The results were used to roughly indicate the change in river hydrodynamics and consequent settling conditions, which were influenced by dams (at Homécourt and Moyeuvre-Grande). In addition, the chemical contents (quantified by ICP-MS and ICP-OES) varied for the sediments. Some sediments showed elevated metal contents (e.g. Fe, Zn and Pb), mainly in the direct upstream vicinity of dams (case of HOM and BETH), and sites further upstream, but still located in the influence zone of dams (case of JOEP). The elevated metal contents are indicators of anthropogenic contributions. Moreover, a variation in major and crystalline minerals was slightly observed using XRD, mainly by Fe minerals that were present in JOEP. The various clay minerals were identified by oriented slides; all surface sediments contained similar clay minerals, which are kaolinite, illite, chlorite, and swelling clays, such as smectites, chlorite and interlayered illite/smectite. At this stage, the resemblance of the mineralogy was quite obvious for the different samples, which required further identification at finer scales. Accordingly, scanning and transmission electron microscopies (SEM and TEM) were sought to identify crystalline, poorly crystalline and amorphous minerals on one hand, and to evidence the possible variations that might be related to multiple contributions (lithogenic and anthropogenic) on the other. Although SEM did not show significant variations among the scanned sediments, it was shown that the particles are generally fine and mainly composed of materials that are naturally found in river sediments (diatom skeletons and clays). At finer resolutions, TEM showed that the main minerals present in Orne sediments are interlayered clays, composed of various TOT phyllosilicates, with varying contribution of interlayered cations (e.g. Mg and K). TEM also evidenced that the sediments before the confluence with

the Moselle, i.e. RICH, had some features that were not evidenced in surface sediments of the upstream zone, such as hairy iron aluminosilicates, circular polymetallic sulfides and apatite. Although those phases were only vaguely detected, the fact that the site is located downstream a previously industrialized and current urbanized zone, and because the grain sizes and chemical contents were unique (in comparison to other sediments), the distinct TEM fingerprint could be anticipated. Finally, for the surface sediments, it was important to use various techniques and determine different parameters, in a conjoint way, to determine the nature of the sediments and the possible lithogenic and anthropogenic contributions.

Beth sediments represent a distinct case in the Orne river, which could be explained by the following: the surface sediments showed to be elevated with metallic elements, mainly Fe, but also Zn and Pb; TEM-EDXS showed that almost 50% of the analyzed particles contained significant amounts of Fe; the settled particles are relatively fine due to selective settling induced by the dam and due to the nature of the sediments; and finally, the location of the sediments upstream the Beth dam and downstream steelmaking industries that were active and had formerly released wastes and by-products. Being built in 1959/1960, the Beth dam stores deposits that were released until 1988, when the last facility stopped working in the upstream area. Therefore, Beth sediments have the tendency to reveal information about the wastes (e.g. sludge) and by-products (e.g. slag) that were released by the steelmaking facilities on one hand, and to reveal the fate of the chemical and mineralogical species after being submerged for more than a couple of decades on the other. For those reasons, several sediment cores upstream the Beth dam were collected. All the cores showed the same signatures, yet of various thicknesses of lithogenic and anthropogenic materials. The deposits were initially characterized according to color, eye-detectable grain variations, and in our case, a distinct odor possibly indicating fuel/oil. A change in color was seen between surface brown sediments (0 – 11 cm) and deeper black ones (11 – 131 cm) for BETH1402; the water content was distinct for certain units. The grain sizes of the sediment layers were really fine, especially for the deep deposits, yet some trends were observed. Interestingly, and from those bulk, easily obtained and inexpensive analyses (i.e. color, PSD and water content), the vertical profile of the BETH sediments could be divided into distinct units. At this point, the variation is clear, and more techniques that reveal sediment dating, chemical composition and mineralogy should be followed. ^{137}Cs and ^{210}Pb are usually used to reveal the date of settled materials. In the case of Beth sediments, the radionuclides evidenced that those deposits have not settled as conventional sediments would, and that the sediments had settled after 1954; i.e. they certainly had settled after the dam was

constructed. The chemical composition showed striking features with depth, notably between the brown and black colored deposits. The surface brown deposits showed “normal” contents that are mainly sourced from lithogenic contributions, such as Si, Al and lanthanides. Deeper layers were marked by deprivation of those elements; rather, they were highly enriched with Fe, Pb, Zn, V, As, Cd and other elements. The metal enriched deposits call for anthropogenic contribution(s), which is suggested to be sludge (formed from wet scrubbing of blast furnace smokes/gases), as indicated by their high metallic contents and fine character. Moreover, several distinct units could be proposed for the contaminated sediments (11 – 131 cm), not only by chemical composition, but also by grain size and water content; the color was the same. Due to the high metal contents and the unsuitability of sediment age detection by ^{137}Cs and ^{210}Pb, the main contribution of recent (after 1960) anthropogenic materials is clearly revealed. Nonetheless, the nature of those anthropogenic materials need to be unraveled in terms of mineralogy. The major and crystalline minerals detected by XRD clearly showed that the surface sediments hold lithogenic fingerprints, such as quartz, calcite and clay minerals, while the deeper layers evidenced Fe rich minerals (oxides, oxy-hydroxides and sulfides); the latter layers only showed slight contribution of lithogenic materials. For a better knowledge of the anthropogenic deposits, the mineralogy should be revealed, mainly Fe, since i) BETH sediments are highly enriched in Fe, ii) Fe minerals were detected by XRD, iii) Fe is one of the main elements that was released from the steelmaking facilities, and iv) Fe minerals, such as oxy-hydroxides, play a crucial role in the behavior and fate of other metals, including Zn. For those reasons, SEM and TEM-EDXS data were acquired. First, it should be noted that SEM and TEM further exhibited the variation between the lithogenic nature of the surface brown sediments and the anthropogenic nature of the deeper metal-rich deposits. Having different resolutions, SEM and TEM revealed Fe rich minerals at different scales, hence different phases and minerals. SEM evidenced ferrospheres, framboïdal pyrites, and distinct Fe minerals (oxides); TEM revealed more detailed features of the finer fraction, mainly the predominance of Fe-nanoparticles and hairy Fe-aluminosilicates with distinct three dimensional spherical aggregates; the latter having rings of fluffy polymetallic sulfides (mainly containing Zn). TEM-SAED was needed to identify the Fe-nanoparticles as goethite. Indeed, from XRD, TEM-EDXS and TEM-SAED patterns of the minette iron ore (which was used in the process of steelmaking in Lorraine), goethite nanoparticles were predominant. Therefore, high presence of goethite in the sediments is linked to the minette iron ore that was used as an iron source in the steelmaking facilities at Jœuf-Moyeuvre. Moreover, the contribution of slag is also demonstrated by a few slag particles that were detected by TEM. Collectively, the

contaminated sediments present before the Beth dam are mainly composed of sludge, but also contain slag and lithogenic materials (e.g. diatom skeletons and clays). Although we could not characterize the initial state of the sludge and slag that were generated from BFs, since the facilities closed and the materials are no longer present, the combined techniques of XRD, SEM and TEM-EDXS, and TEM-SAED could reveal some processes that had occurred in the submerged sediments. The proposed processes are not only linked to Beth sediments, but also to steelmaking wastes in rivers (as SPM) and settling ponds. Finally, on the Fe mineralogy, ageing of the phases present in the steelmaking wastes formed the circular structures of Fe-aluminosilicates which are rung by polymetallic (Zn-Pb) sulfides.

Since the Beth sediments were highly enriched with Zn, Zn speciation was targeted. In the case of zinc, XRD and SEM did not reveal possible Zn species or Zn bearing minerals. Nonetheless, XRD and SEM data were important to indicate that Zn bearing minerals might be present in quantities below the limits of XRD (in case the Zn bearing minerals were well crystalline), or that they are poorly crystalline or amorphous, and therefore undetectable via XRD. Additionally, since SEM could not reveal major Zn bearing minerals, finer particles are expected to hold Zn; consequently, the importance of using TEM and XAS (XANES and EXAFS) at the Zn K-edge arose. Using TEM-EDXS, Zn was found associated to the hairy Fe-aluminosilicates and as polymorphs of sulfides. Being found at relatively lower contents (in comparison to Fe), Zn speciation needs to be identified using more sensitive approaches, such as XAS at the Zn K-edge. It should be noted that XAS at the Fe K-edge is also crucial to reveal Fe speciation. XANES spectra at the Zn K-edge and linear combination fitting (LCF) revealed that, indeed, the predominant Zn carriers were sulfides, especially in the sediments deeper than 5 cm. Due to the heterogeneity of the sediments at Beth, many XANES reference spectra were collected in order to identify the possible Zn species. Although Zn speciation was revealed by XANES spectra at the Zn K-edge, and the fitting seemed to be successful, LCF of EXAFS spectra at the Zn K-edge are needed to ascertain Zn speciation; yet the predominance of ZnS is certainly demonstrated, as suggested by high Zn and S contents on one hand, and as witnessed by TEM and XANES-LCF on the other. Fe and Zn do not behave separately in the sediments. This might be further suggested by the circular ZnS structures similar in size to the circular Fe-aluminosilicates containing fluffy polymetallic sulfides on the rim. Indeed, with time, sulfidization occurred to form sulfides, and the structuring of the Fe-aluminosilicates into circular Zn sulfides might be expected.

Finally, that unique character of the contaminated Beth sediments might come in hand for revealing the fate of similar metal rich deposits; the unique character might also be used to track contaminated sediments upon remobilization/resuspension. Unfortunately, this might be the case in the near future, where the Beth dam is planned to be removed (in the coming decade). Having characterized the sediments, it is clear that the dam cannot be removed before creating a back-up plan for the contaminated sediments (i.e. a management plan). Otherwise, the metal rich particles will be remobilized to downstream sites, especially since they are fine, and because large masses were evident to be present upstream the dam. Furthermore, it is not only the concern of France, neither the Orne River or Lorraine authorities, but also the Moselle River in France, Luxembourg and Germany, the Rhine River in Germany and the Netherlands, and finally the North Sea. Therefore, the management plan should be of a regional interest. Due to the predominance of (poly)metallic sulfides, their oxidative dissolution and metal release upon remobilization and consequent oxidation is highly anticipated. Finally, a summarizing schema of the main Fe and Zn species of the sediments located upstream of the Beth dam is shown in Figure VIII-1.

3. Perspectives

For the detection of other unique sedimentary features along the Orne River, it is important to extend the inventory, especially between BETH and RICH, where the former industrialized/urbanized gradient might be shown. It should be noted that comparison of Orne sediments with Fensch and Moselle River sediments enhanced the interpretation of the data, especially in the context of steelmaking and natural weathering, respectively. This point should not be overlooked when a certain contribution is aimed to be seen at a larger scale or from other perspectives. Several sediment cores were collected along the Orne River, although not described in the manuscript, they showed unique features, namely HOM and JOEP. From the results already obtained on those sediments (PSD, XRD, SEM, TEM and chemical composition), those sediments hold distinct features, and were different among each other on one hand, and different from BETH on the other. Further analyses on HOM and JOEP sediments can reveal more information about the former steelmaking facilities, in a similar approach to what was done with Beth sediments. Surface, subsurface and deep sediments should be collected at various locations, especially where sedimentation is favored. Additionally, the horizontal and vertical reach of the contaminated sediments located upstream the Beth dam should be revealed. The hairy Fe-aluminosilicates presented in this study showed

to be interesting phases, especially since they presented variable contents of Si, Al and Fe (and traces of Zn). Although we demonstrated the predominance of Fe-aluminosilicates, the exact mode of association was not described. The latter can be studied using synchrotron based techniques, mainly XAS at the Fe K-edge (XANES and EXAFS), which can show the exact mode of interaction (e.g. as surface complex, in the interlayered phyllosilicates, to hydroxyl edge site, or others). Sorption experiments of Fe (as well as Zn) and aliquot collections at different times might help to understand the mechanism of formation and association. Indeed, thermodynamic experiments can reveal the kinetics of the association mechanisms. Additional information of Zn speciation, notably those associated to sulfides, will be revealed by EXAFS spectra at the Zn K-edge and LCF; the LCF of XANES spectra at the Zn-Kedge should be complemented with EXAFS spectra at the Zn K-edge for robust findings on those Zn sulfides (e.g. crystallinity of sulfides).

The geochemical identification of sediments is not sufficient for the overall characterization of those unique deposits. It is also important to reveal other features, such as microbial communities, especially since peculiar microbes are expected to be present in such metal rich sediments. Consequently, the possible roles of microbes on the reduction and oxidation processes, change in metal speciation, and breakdown and precipitation (mineralization) of phases might be explained. For example, the formation of the unique circular Fe-aluminosilicates, whether containing fluffy polymetallic sulfides on the rim or not, is surely dependent on microbial reactions that take place in the submerged sediments. Several questions are asked here. Could the microbes present in the anoxic and metal rich sediments cause the bio-mineralization of Fe-aluminosilicates from goethite nanoparticles (as indicated in the literature)? Are the circular structures of Fe-aluminosilicates formed after the alteration of ferrospheres and iron rich particles? If so, what is the period for that alteration? Did Si and Al come from the weathering of clays, diatoms or slag? In order to answer those questions, supplementary samples should be acquired, such as sludge and slag. The initial forms of mineralogical and elemental species, and their fate can ascertain the speculations that were made.

The microbial communities need a carbon source for their survival. This leads to the part where the organic geochemistry aspects are important. It is worth noting that organic geochemistry of Beth sediments, as well as other sediments (surface, subsurface and deep) and SPM along the Orne River course, are been studied, and have been the interest of other researchers (Laurence Mansuy-Huault et al.,). Even though it is not practical to include all

aspects in one manuscript, the data revealed by organic geochemistry can give unique and essential information, such as different organic compounds that were released from the steelmaking facilities (e.g. in sludge, slag, smokes and coal) or sourced from other industrial and urban sources, such as variable (oxygenated and nitrogen) polycyclic aromatic compounds. Part of those findings might also be revealed by Zn and Pb isotopic fingerprints of Beth sediments (as well as other Orne River sediments).

The same perspectives previously indicated for sediments need also to be applied on suspended matter of the Orne River, in addition to the dissolved phases that are present in the water column and interstitial water. The three compartments need to be included to have a clearer view, i.e. sediments, SPM and water/porewater. Since the Beth dam is planned to be modified or removed in the coming decade, remobilization experiments will be performed on the metal laden sediments, with an attempt to follow the fate of the minerals (such as Fe-aluminosilicates and polymetallic sulfides), and chemicals (such as Fe, Zn, Pb and S). Indeed, the last perspective is part of the MOBISED project that has recently started. Finally, the multidisciplinary work on Orne sediments, suspended particulate matter and river water will surely reveal the fate of chemical and mineralogical species caused by a complex and heterogeneous network of processes.

3.1. Recommendations on the management of metal rich sediments

It is important to address some of the adequate management strategies that can be implemented to prevent immobilization of the metal laden sediments, especially in the case of Beth sediments, that will be remobilized upon dam removal or modification. A lesson that could be learned regarding contaminated sediment remobilization and the consequences on fish and man can be seen in Maclin and Sicchio (1999). Briefly, the Ford Edward Dam in the Hudson River in New York held tons of polychlorinated biphenyl (PCB) contaminated sediments. Without prior adequate testing and analyses of the sediments stored upstream of the dam, it was removed in 1973. Consequently, the PCB-laden sediments were remobilized (over a period for more than a year) which affected water quality, navigation and threatened wildlife (mainly fish) and public health in the area further downstream. On the other hand, other case studies on removing dams and restoring natural sediment cascade were a success, and replenished the wildlife, solved sedimentation problems and restored natural water flow (e.g. Maclin and Sicchio, 1999 and references cited therein).

In the case of the sediments that had settled before the Beth dam, they are submerged in water throughout the year; therefore, the formed metal sulfides are retained in anoxic conditions (Fanning and Fanning, 1989). Nonetheless, metal sulfides might diffuse to the pore water and subsequently reach the water column, where oxidation and dissolution of sulfides might release metals (Huo et al., 2015; Van den Berg et al., 1998). Therefore, it is necessary not just to maintain the sulfide phases in stable anoxic environments, but also to form a barrier between the metal laden sediments and the water column. Indeed, *in-situ* capping of metal laden sediments in dynamic environments could be a solution. A clean sediment layer amended with metal scavengers added on top of metal rich sediments might halter their diffusion. Some of the common amendments that could be used in caps are phosphate compounds, lime, animal manure, metal oxy-hydroxides and biochar (e.g. Mahar et al., 2015 and references cited therein). However, the sediment should be characterized, from bulk to nano-scale, before implementation of management strategies.

At this stage, a quick plan should be proposed for Beth sediments. Indeed, it is important to avoid remobilization of Beth sediments, which will result in the dispersion of metal-rich deposits, and possible release of high metal contents into the water column. A proposed management strategy would be to redirect part of the Orne River, in particular the riverbed that contains metal rich sediments. According to the data collected so far, the river section between the limit of Moyeuvre-Grande city (see Figure V-1) till the Beth dam should be redirected. As a result, the river water would then flow in a dam free stream, as incited by the European parliament (EU Council, 2000), and the metal rich sediments can be dredged, disposed of, or re-used in a safe way. For example, the sediments can be used as road sub-base, or in construction materials after mixing with cement and steelmaking slag (e.g. Benzerzour et al., 2017; Rozière et al., 2015).

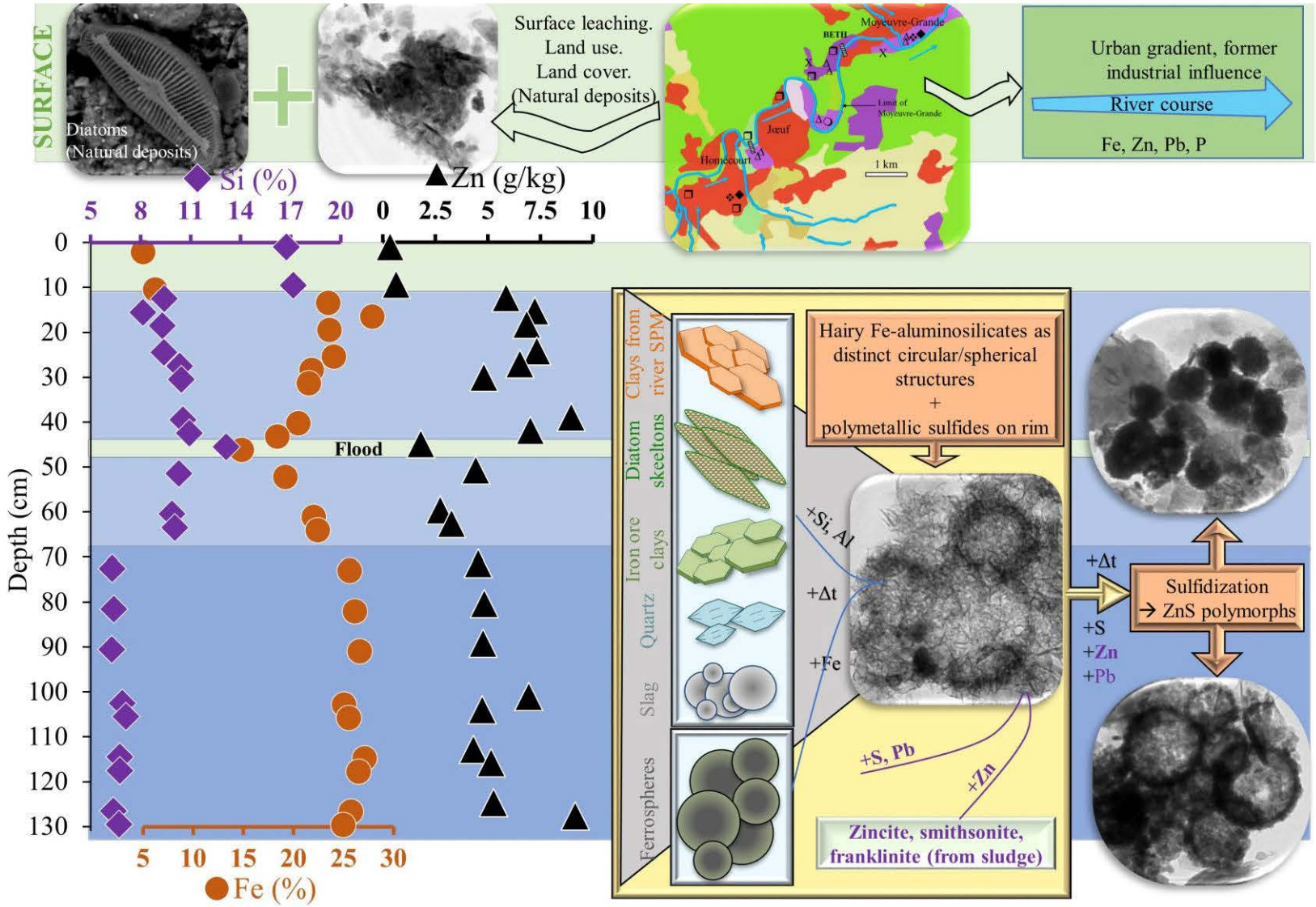

Figure VIII-1: Summarizing schema for the status of Beth sediments, showing the main and unique Fe and Zn phases.

References

Benzerzour, M., Amar, M., Abriak, N.-E., 2017. New experimental approach of the reuse of dredged sediments in a cement matrix by physical and heat treatment. Constr. Build. Mater. 140, 432–444. doi:10.1016/j.conbuildmat.2017.02.142

EU Council, 2000. Directive 2000/60/EC of the European Parliament and of the Council of 23 October 2000 on the establishing a framework for Community action in the field of water policy.

Fanning, D., Fanning, M., 1989. Sulfidization and Sulfuricization, in: Soil Morphology, Genesis and Classification. John Wiley and Sons Inc., New York, pp. 69–80.

Huo, S., Zhang, J., Yeager, K.M., Xi, B., Qin, Y., He, Z., Wu, F., 2015. Mobility and sulfidization of heavy metals in sediments of a shallow eutrophic lake, Lake Taihu, China. J. Environ. Sci. 31, 1–11. doi:10.1016/j.jes.2014.12.003

Maclin, E., Sicchio, M., 1999. Dam Removal Success Stories, Restoring Rivers through Selective Removal of Dams that Don't Make Sense. American Rivers, Friends of the Earth, & Trout Unlimited, Washington, DC.

Mahar, A., Wang, P., Li, R., Zhang, Z., 2015. Immobilization of lead and cadmium in contaminated soil using amendments: A review. Pedosphere 25, 555–568. doi:10.1016/S1002-0160(15)30036-9

Rozière, E., Samara, M., Loukili, A., Damidot, D., 2015. Valorisation of sediments in self-consolidating concrete: Mix-design and microstructure. Constr. Build. Mater. 81, 1–10. doi:10.1016/j.conbuildmat.2015.01.080

Van den Berg, G.A., Loch, J.P.G., Zwolsman, J.J.G., Heijdt, L.M. van der, 1998. Non-steady state behaviour of heavy metals in contaminated freshwater sediments. Water Sci. Technol. 37, 39–46.

ABSTRACT

The Orne River is a tributary of the Moselle River, located northeastern France. During the last two centuries, the Orne watershed was highly industrialized. The vicinity of the river was marked with mining and metallurgy for the purpose of steel making. Those facilities were constructed near the river to have cooling sources, especially for blast furnaces. The introduction of wastes or by-products into the water system is highly anticipated, such as the direct release or the indirect surface leaching of piled wastes and by-products. Based on the industrial needs, some Orne River courses were redirected, channels were constructed, artificial/cemented riverbeds and banks were created, and a few small dams were built. Dams created artificial water reservoirs for the well-functioning of the facilities on one hand, and promoted settling of suspended particulate matter on the other. However, the Directive 2000/60/EC of the European parliament and of the council strongly incite the European states to remove engineered structures (such as dams), and to restore the natural functions of rivers. The dams along the Orne River were built in the last century, and their functioning and maintenance are expensive; as a result, their removal is further advised. Nonetheless, this raises the question about the fate of contaminated sediment remobilization. The aims of this work are to identify the different sediment deposits along the Orne River, and to establish characteristics of recently settled sediments and those that had settled during the last decades; the latter being strongly fingerprinted by steelmaking activities. To realize the objectives, surface sediments and sediment cores were collected along the Orne River. The sediments were then analyzed for water content, grain size distribution, pH, semi-quantitative metal composition using XRF Niton gun (as preliminary Fe, Zn and Pb semi-quantifications), major and trace chemical composition using ICP-OES and ICP-MS, respectively, major crystalline minerals (XRD), micrometric (light microscope and SEM) and sub-micrometric (TEM) mineral identification, and Zn speciation at a molecular level (XANES). The chemical and mineralogical composition of the surface sediments revealed lithogenic contributions. Furthermore, the chemical composition showed a lithogenic nature and detrital minerals, such as quartz, calcite and clays (e.g. interlayered clays). Interestingly, the sediment layers of the core collected upstream the Beth dam showed distinct chemical and mineralogical composition, which are certainly related to the former steelmaking facilities on one hand, and their weathered or aged by-products or wastes on the other. Under a layer of lithogenic sediments lied deposits that were depleted with detrital elements and minerals. Those deposits were highly enriched in metals, mainly Fe, Zn and Pb, and were fingerprinted by crystalline iron minerals, such as goethite, magnetite, wuestite and pyrite, and by newly formed Fe-aluminosilicates. Those minerals could be used as fingerprints of the former steelmaking facilities, especially the predominant Fe-aluminosilicates of the contaminated sediments. Furthermore, TEM-EDXS and XANES at the Zn K-edge observations evidenced that Zn was mainly carried as sulfides (amorphous and crystalline), and to a lesser extent associated to Fe oxy-hydroxides and Fe-aluminosilicates. Finally, the mineral status of the aged steelmaking deposits and possible fingerprints are shown. The remobilization of the contaminated sediments can then be traced by the unique mineral composition; yet the imminent metal source of those sediments should not be overlooked, especially since the Beth dam is planned to be modified or removed in the near future.

Keywords: River sediments, Orne River, sediment core, steelmaking, Fe mineralogy, Zn speciation.

RESUME

En Lorraine, l'Orne et la Fensch, deux affluents de la Moselle, ont été affectés par une activité minière et industrielle qui s'est intensifiée depuis le milieu du XIXe siècle et au cours du XXe siècle. Le développement minier, sidérurgique et urbain de la vallée est accompagné de modifications du lit majeur (réduction de largeur par terrassements) et surtout du lit mineur (chenalisation, enrochement des berges, création de barrages). A ces changements morphologiques se sont ajoutées des perturbations hydro-sédimentaires et environnementales, liées aux exhaures minières, aux zones de remous à l'amont des barrages, à l'artificialisation du milieu fluvial et aux rejets industriels et domestiques non traités. Les barrages, créés pour les besoins en eau de l'industrie, ont favorisé l'accumulation de dépôts sédimentaires fortement contaminés en métaux (comme Fe, Pb et Zn) et produits organiques persistants (notamment des hydrocarbures aromatiques polycycliques ou HAPs). Suite à l'arrêt des activités sidérurgiques, un des enjeux majeurs pour l'Orne concerne sa renaturation, et notamment l'effacement des retenues d'eau dédiées au refroidissement des hauts-fourneaux. En effaçant les barrages qui ont perdu leur fonctionnalité première, le cours d'eau devrait retrouver une continuité écologique longitudinale et un fonctionnement hydrologique plus naturel, requis par la directive cadre européenne sur l'eau (DCE 2000/60/CE). Cet effacement doit prendre en compte également le devenir des sédiments et le potentiel toxique de leur remise en suspension lors des opérations de réaménagement du cours d'eau. Les travaux de recherche présentés ont mis en évidence les différents dépôts sédimentaires contaminés dans la partie d'aval de l'Orne. Des sédiments ont été prélevés en surface et carottés afin d'être précisément caractérisés d'un point de vue minéralogique et géochimique. Ces analyses ont permis de mettre en évidence le caractère fortement contaminé des dépôts sédimentaires en présents en amont des barrages. De plus, il a été possible, de distinguer les contributions industrielles et naturelles, ces dernières étant issues du lessivage des sols du bassin versant et amenant des composés minéraux originaires de l'érosion. Ces contributions industrielles sont plurielles, mettant en évidence la présence de minerai de fer extrait du sous-sol, mais aussi une forte contribution de boues sidérurgiques, issues du traitement en voie humide des fumées et cendres volantes émises par les hauts fourneaux, les convertisseurs, ou encore les fours d'agglomération du minerai. L'étude de la minéralogie du fer et de la spéciation du zinc a non seulement mis en évidence des marqueurs minéralogiques qui devraient permettre de tracer les sédiments contaminés au sein de la colonne d'eau lors de leur remise en suspension, mais elle a également mis à jour les modifications minéralogiques des déchets sidérurgiques au sein du compartiment sédimentaire. L'étude de la spéciation chimique du zinc a montré que cet élément était essentiellement stocké sous forme de sulfures (amorphes ou cristallisés). La prédominance de la taille nanométrique à sub-micrométrique de ces sulfures renforce leur probabilité de remobilisation lors d'opérations de réaménagement du cours d'eau ou lors d'évènements hydrologiques intenses (crues).

Mots clés : Sédiment de rivière, Rivière de l'Orne, carotte de sédiment, sidérurgie, minéralogie du fer, spéciation du Zn